ISSN: 2249-6645

International Journal of Modern Engineering Research (IJMER)

Volume 5 Issue 1 January 2015

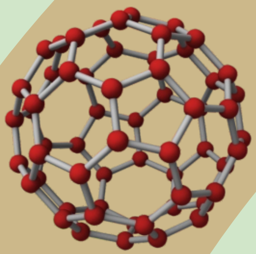

International Journal of Modern Engineering Research (IJMER)

Volume : 5 Issue : 1 (Version-1) ISSN : 2249-6645 January- 2015

Contents :

OPEN ACCESS

International
Journal
Of Modern Engineering Research (IJMER)

Stress Analysis of Functionally Graded Disc Brake Subjected To Mechanical Loading

Ch. Rajeswari[1], Ch. Rama Krishna[2], K. Rambabu[3]

[1]*Department of mechanical engineering, Sir C.R.Reddy College of Engineering, India*
[2]*Department of mechanical engineering, Sir C.R.Reddy College of Engineering, India*
[3]*Department of mechanical engineering, Sir C.R.Reddy College of Engineering, India*

ABSTRACT: *In this thesis, analytical investigation is to be done for functionally graded disc brake subjected to internal pressure. Different models of the disc brake are considered i.e. disc brake with 40, 50 and 60 holes. In this thesis, comparison is to be done by varying materials for disc brake, the materials are Cast Iron, FGM 1*(Al_2O_3-Al) *and FGM 2 (Zr-Al). FGM's are considered for material variation profile through the thickness for k =2, k =4 and k =6 .Theoretical calculations are done to calculate the material properties for each layer up to 10 layers for FGM's. Structural analysis and thermal analysis are done on the three models by varying materials. 3D modeling is to be done in Pro/Engineer and analysis is to be done in Ansys 14.5.*

Keywords: *Disc brake, Functionally graded material, Material variation Parameter.*

I. INTRODUCTION

Today technology is in need for speed, but at the same time, we need safety as well. For safety, we need deceleration to the maximum extent. These two things are moreover contradictory factors. For speed, we need engines of maximum efficiency and for keeping this speed in bounds, we need brakes of latest technology. For coping up with today's speed, new materials are introduced in the manufacture of disc brakes.

The disc brake is a device for slowing or stopping the rotation of a wheel while it is in motion. A disc brake is usually made of cast iron or ceramic composites (including carbon, Kevlar and silica). This is connected to the wheel and/or the axle.

Functionally graded structures are those in which the volume fractions of two or more materials are varied continuously as a function of position along certain dimension(s) of the structure to achieve a required function. Functionally graded materials are composite materials, which are microscopically in homogeneous, and the mechanical properties vary smoothly or continuously from one surface to the other. It is this continuous change that results in gradient properties in functionally graded materials.

Functionally graded materials are made from mixture of metals and ceramics or a combination of different metals. Unlike fiber-matrix composites, which have a strong mismatch of mechanical properties across the interface of two discrete materials, bonded together and may result in de-bonding at high temperatures.

Functionally graded materials have the advantage of being able to survive environment with high temperature gradient, while maintaining their structural integrity .The ceramic materials provides high temperature resistance due to its low thermal conductivity, while the ductile metal component prevents fracture due to thermal stresses.

The material property P is varied through the plate thickness in FGMs according to the expressions, (Power law)

$$P(z) = (P_t - P_b)\,V + P_b$$

$$\text{Where } V = \left(\frac{z}{h} + \frac{1}{2}\right)^k$$

Here P_t and P_b denote the property of the top and bottom faces of the plate, respectively, and k is a parameter that dictates the material variation profile through the thickness. Here it is assume that module E and G, density ρ, thermal coefficient of expansion α, and the thermal conductivity K vary according to the above equation.

Model calculation:
1) Young's Modulus:
Material properties for FGM 1 (Al_2O_3-Al):
Top material: Alumina, Al_2O_3 (E=380000 MPa)
Bottom material: Aluminium,Al (E=70000 MPa)
1) **For k = 2; z = 1**

$$E(z) = (E_t - E_b)\left(\frac{z}{h} + \frac{1}{2}\right)^k + E_b$$

$$= (380000 - 70000)\left(\frac{1}{10} + \frac{1}{2}\right)^2 + 70000$$

$$= (310000)\,(0.36) + 70000$$

$$= 181600 \text{ N/mm}^2$$

Above same procedure is repeated inorder to get different material properties for both FGM 1 (Al_2O_3-Al) and FGM 2(Zr-Al) at different layers.

Table 1.1: Material Input Values of FGM 1 (Al_2O_3-Al) For k = 2

Z	Young's modulus E (N/mm^2)	Density (Kg/mm^3)
+5	380000	3.96×10^{-6}
+4	321100	3.7206×10^{-6}
+3	268400	3.5064×10^{-6}
+2	221900	3.3174×10^{-6}
+1	181600	3.1536×10^{-6}
-1	119600	2.9016×10^{-6}
-2	97900	2.8134×10^{-6}
-3	82400	2.7504×10^{-6}
-4	73100	2.7126×10^{-6}
-5	70000	2.7×10^{-6}

II. DESIGN AND MODEING

Structural analysis for cast iron:
Element Type: Solid 20 node 95
Material Properties:
Young's Modulus: $103000 N/mm^2$
Poisson's Ratio: 0.3
Density: $0.0000071 kg/mm^3$

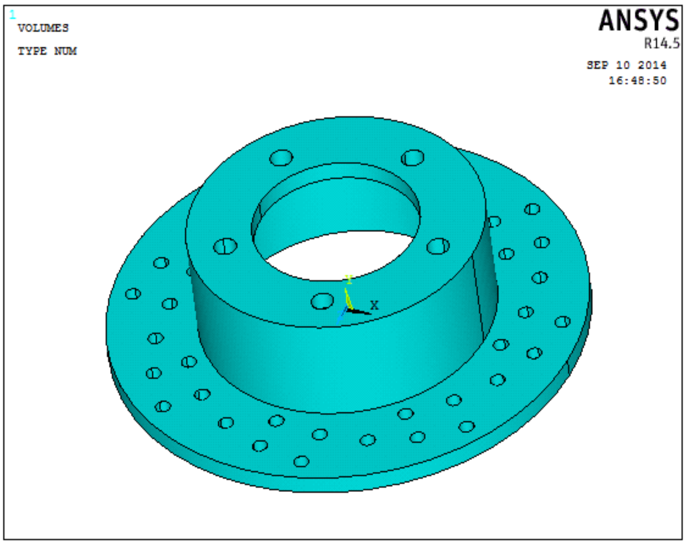

Fig 2.1 shows imported model from pro-e

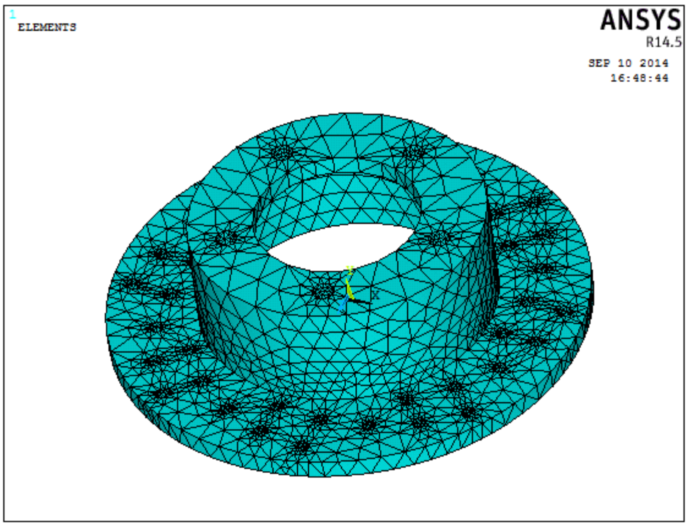

Fig 2.2 shows Meshed model of cast iron with 40 holes

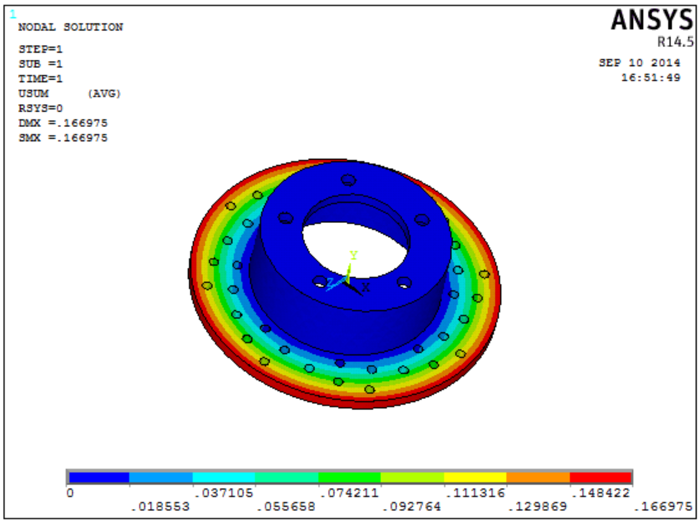

Fig 2.3 shows displacement vector sum

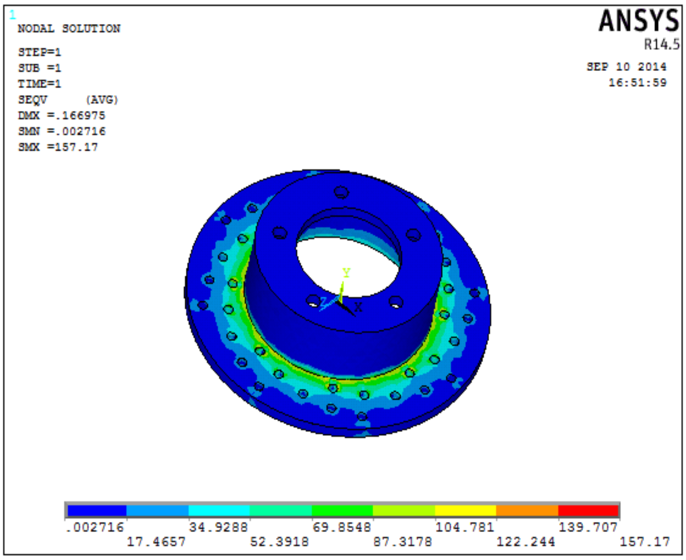

Fig 2.4 shows Von misses stress

Analysis of FGM 1 (Al_2O_3-Al) Disk Brake with 40 holes:

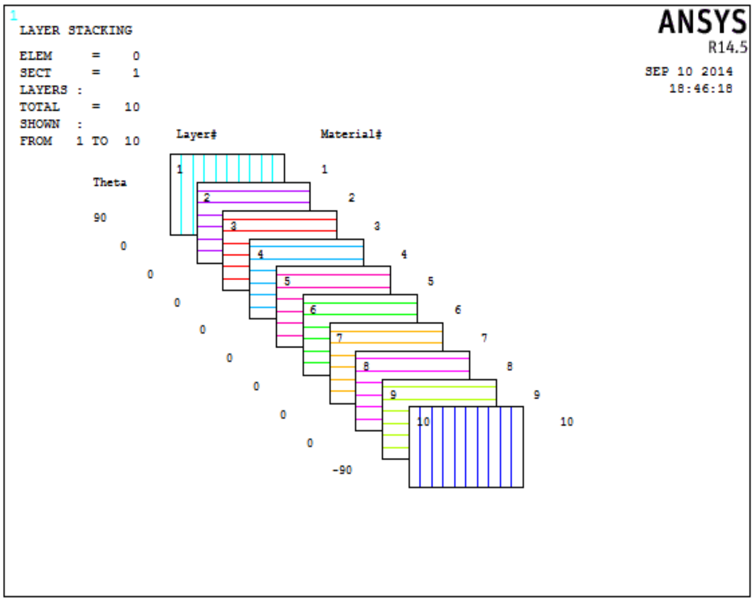

Fig 2.5 shows Layer Stacking method for FGM 1 (Al_2O_3-Al)

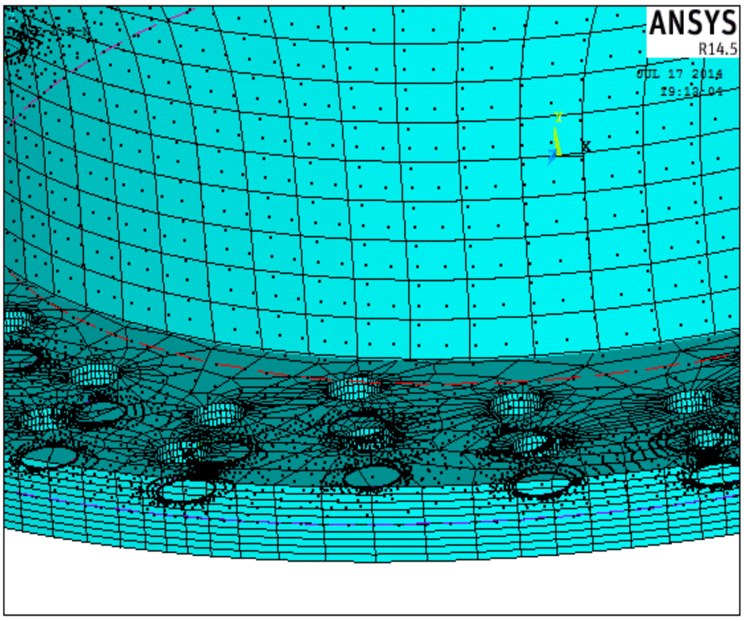

Fig 2.6 shows the layers of the FGM

STRUCTURAL ANALYSIS:

Table 2.1: Analytical results for Cast Iron Disc Brake

No of Holes	Displacement (mm)	Stress (N/mm^2)	Strain
40	0.521	157.17	0.675×10^{-3}
50	0.75	174.56	0.845×10^{-3}
60	0.88	182.56	0.902×10^{-3}

Table 2.2: Analysis results of FGM 1 (Al_2O_3-Al) For Material Variation Parameter k = 2

Number of Holes	Displacement (mm)	Stress (N/mm^2)	Strain
40	0.415	125.16	0.39×10^{-3}
50	0.734	162.24	0.83×10^{-3}
60	0.765	169.76	0.89×10^{-3}

Table 2.3: Analysis results of FGM 2(Zr-Al) For Material Variation Parameter k = 2

Number of Holes	Displacement (mm)	Stress (N/mm^2)	Strain
40	0.104	119.81	0.0010
50	0.111	121.33	0.0011
60	0.13	125.56	0.0015

THERMAL ANALYSIS:

Table 2.4: Thermal analysis results for Cast Iron Disc Brake

Number of holes	Thermal gradient	Thermal flux(W/m^2)
40	81.8071	9.2442
50	81.912	9.256
60	87.771	9.918

Table 2.5 :Thermal analysis of FGM 1(Al_2O_3-Al) for k = 2

Number of holes	Thermal gradient	Thermal flux(W/m^2)
40	10.526	0.315
50	11.617	0.3485
60	27.558	0.468

Table 2.6: Thermal analysis of FGM 2 (Zr-Al) for k=2

Number of holes	Thermal gradient	Thermal flux(W/m^2)
40	23.885	0.40
50	24.590	0.41
60	24.787	0.743

III. RESULTS AND DISCUSSIONS

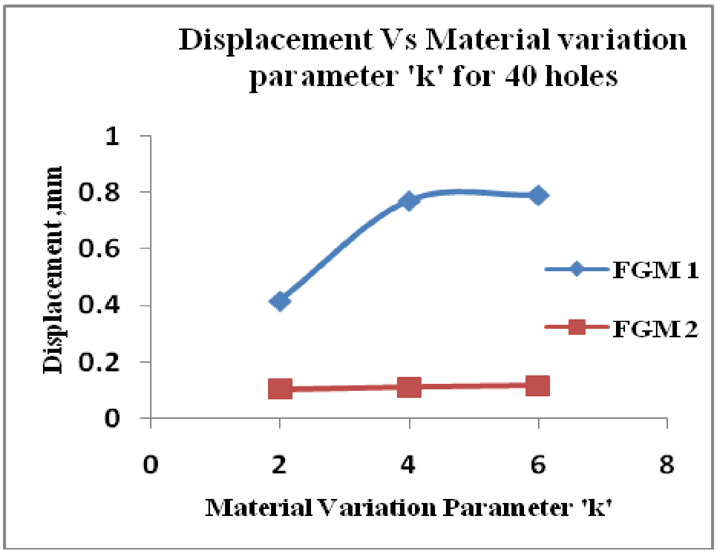

Fig 3.1: Displacement Vs material variation parameter ‘k’ for 40 holes

- Fig 3.1 shows the variation of displacement with respect to material variation parameter ‘k’ for FGM 1 (Al_2O_3-Al) and FGM 2 (Zr-Al) with number of holes 40 for disc brake.
- It can be observed with increase in material variation parameter ‘k’, displacement increases largely for FGM 1 and nominally for FGM 2.
- As material variation parameter ‘k’ increases, the volume fraction of ceramic decreases leading to an increase in the volume fraction of metal. So the material brittleness decreases leading to an increase in the deflection.
- FGM’s attain full metallic property with variation of ‘k’ from zero to infinity. Minimum to maximum k variations results in pure metallic behaviors there the above trend is justified when k = 2 the displacement is low where as it is high when k = 6.
- From the above graph it is observed that FGM 1 (Al_2O_3-Al) has shown higher displacement variations as compared to FGM 2 (Zr-Al).It can be predicted that FGM 1 (Al_2O_3-Al) has high modulus values as compared to FGM 2 (Zr-Al). Hence FGM 1 with high material variation parameter has shown higher displacement as compared to FGM 2 for the same value of k = 6.

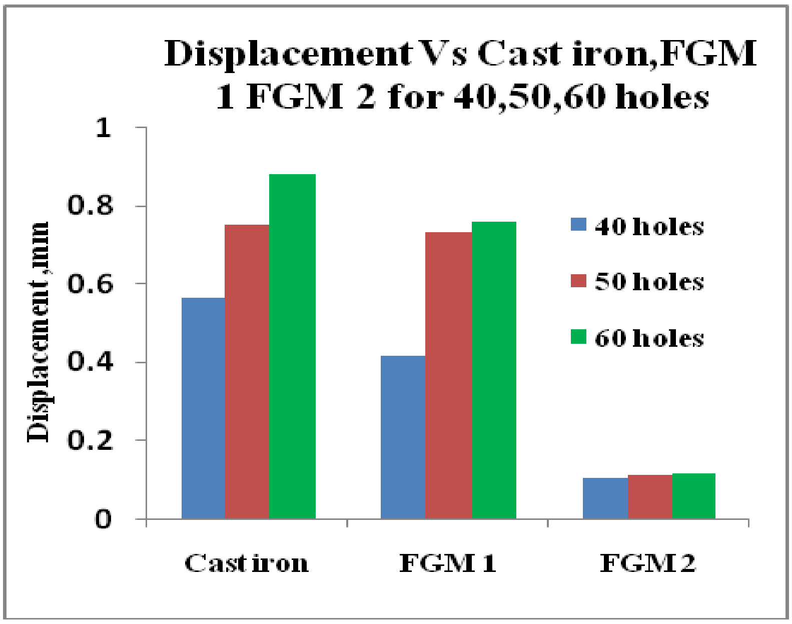

Fig 3.2: Displacement Vs cast iron, FGM 1, FGM 2

- Fig 3.2 shows the comparison of displacement for 40,50,60 holes with respect to cast iron, FGM 1 (Al_2O_3-Al),FGM 2 (Zr-Al).
- It can be observed that higher number of holes resulted in higher displacement.
- As the number of holes increases the disk may become weak due to reduction in load bearing area hence resulted in higher displacement. This is true for all cases of materials.
- The displacement variation is highest for cast iron as compared to FGM 1 and FGM 2.The reason for this behavior can be speculated in 2 ways. Cast iron being pure metal exhibited higher displacement upon load application. Whereas, FGM 1 (Al_2O_3-Al) and FGM 2 (Zr-Al) have shown poor response to displacement. Though cast iron is pure metal but brittle in nature, it’s response to displacement as compared to FGM 1 and FGM 2 is superior.
- It can also be explained that both FGM 1 and FGM 2 are rich in ceramic composition at k = 2,results in more brittle behavior as compared to cast iron. Hence, FGM’s produce lower displacement values as compared to cast iron.

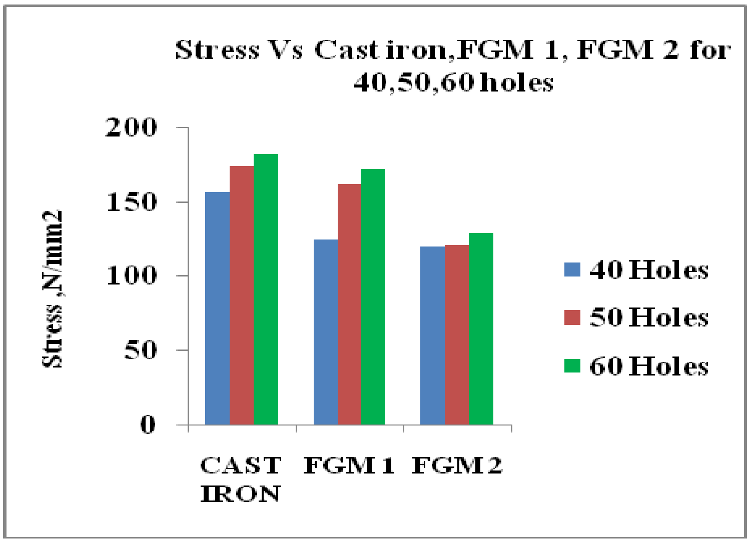

Fig 3.3: stress Vs cast iron, FGM 1(Al_2O_3-Al), FGM 2 (Zr-Al) for 40, 50, 60 holes.

- Fig 3.3 shows the stress variations for 40,50,60 holes. for cast iron ,FGM 1(Al_2O_3-Al) ,FGM 2(Zr-Al).
- It can be observed from the graph with increasing number of holes the stress generated are more. It is self explanatory upon increasing number of holes the surface area becomes less, thereby higher stresses will be developed. This is true for all cases of materials.
- From the above graph it can also be observed that FGM 1 (Al_2O_3-Al) generated higher stress as compared to FGM 2 (Zr-Al).As explained earlier FGM 2 is zirconium based which has got lower elastic modulus as compared to alumina based FGM 1.Further,it can be stated that the higher elastic modulus means higher capacity to bear the load as compared to the other.
- As compared to cast iron FGM 1 (Al_2O_3-Al) and FGM 2 (Zr-Al) showing low stresses. Though cast iron is brittle in nature, as it is metallic in general, the possibility of bearing the load and chances of early facilities are less as compared to FGM 1 and FGM 2 where they are rich in ceramic composition. Hence, the results are comparable.

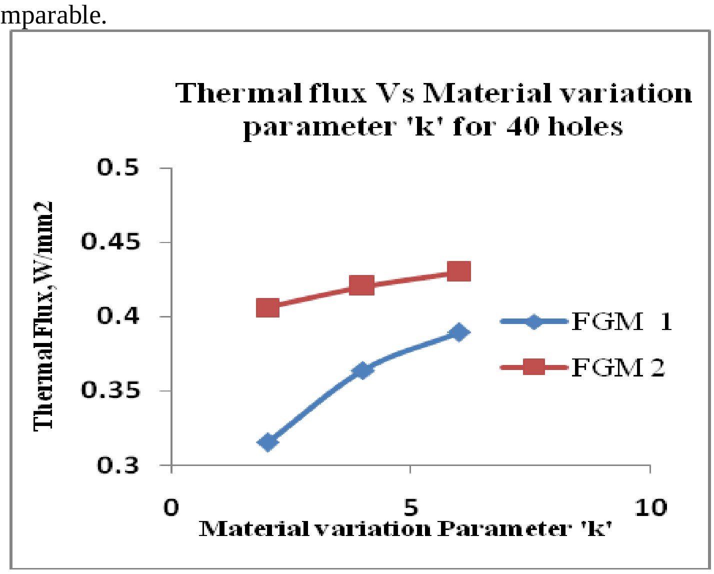

Fig 3.4: Thermal Flux Vs Material variation parameter ‘K’ for 40 holes

- Fig 3.4 shows the variation of thermal flux with respect to material variation parameter ‘k’ for disc brake with 40 holes.
- It is observed that with increase in material variation parameter ‘k’, thermal flux values are found to be increasing.
- It is true because as ‘k’ increases, the FGM’s attain near metallic properties, there by their behavior becomes more conductive. Hence, higher flux values have been observed for higher ‘k’ values.

- In addition it can also be observed that FGM 2 (Zr-Al) possess higher thermal flux as compared to FGM 1 (Al_2O_3-Al).as FGM 2 is zirconium based which has got higher conductivity value as compared to alumina based FGM .The results obtained are superior for FGM 2 compared to FGM 1 .As thermal flux is also one of the important parameter, higher thermal flux values are encouraged.

IV. CONCLUSIONS

- The proposed FGM 1 (Al_2O_3-Al) and FGM 2(Zr-Al) are found to be superior as compared to cast iron from generated stress point of view.
- FGM 2 can be preferred over FGM 1 because of less stress generation.
- Increment in stress values has been observed with increasing material variation parameter 'k'.
- Higher is the number of holes, higher is the stress produced irrespective of materials i.e. Cast Iron, FGM 1, FGM 2.
- Higher displacement values and variation in displacement with increasing 'k' is superior for FGM 1as compared to FGM 2.
- The proposed FGM 2 exhibited higher thermal flux values compared to FGM 1, which is very much essential from heat dissipation point of view.

REFERENCES

[1] Reddy, J.N. ''Analysis of functionally graded plates'', International Journal for Numerical Methods in Engineering, 47, pp. 663–684 (2000).

[2] Koizumi, M. ''The concept of FGM'', Ceramic Transactions, Functionally Gradient Materials, 34, pp. 3–10 (1993).

[3] Timoshenko, S.P. and Woinowsky-Krieger, S., Theory of Plates and Shells, McGraw-Hill, New York (1959).

[4] J.suresh kumar, ''Geometrically non linear analysis of functionally graded material plates using higher order theory'' Vol. 3, No. 1, 2011, pp. 279-288.

[5] M.A. Maleque, S.Dyuti and M.M. Rahman, "Material Selection Method in Design of Automotive Brake Disc", Proceedings of the World Congress on Engineering 2010 Vol III, WCE 2010, June 30 - July 2, 2010, London, U.K.

[6] Guru Murthy Nathi, K. Gowtham and Satish Reddy, "Coupled Structual / Thermal Analysis of Disc Brake", IJRET 2012, Vol.1, pp.539-553.

[7] Dr. Ramesha, Santhosh Kumar and Bharath Shekar, "Temperature Distribution Analysis of Aluminum Composite and Cast Iron Brake Drum Using Ansys", 'International Journal of Emerging trends in Engineering and Development', 2012, Vol. 3, Issn 2249-6149, pp 281- 292.

[8] V. M. Thilak, R. Krishnara Deepan & R.Palani ,"Transient Thermal and Structural Analysis of the Rotor Disc of Disc Brake ", International Journal of Scientific & Engineering Research Volume 2, Issue 8, August-2011 Issn 229-551.

OPEN ACCESS

International
Journal
Of Modern Engineering Research (IJMER)

Experimental Investigation of the Residual Stress and calculate Average Fatigue Life and Improved Resistance To Stress Corrosion Cracking on Aluminium Alloy 7075-T6 Plates by Using Various Shots through Shot Peening Process

Ganapathy T.[1], Bhoopathy T.[2]
[1,2,]Mechanical (cad/cam), Sri Krishna College of Engineering and Technology, Coimbatore-641008, Tamilnadu, India,)

ABSTRACT: *Shot peening procedures developed over the ago in substantial improvements of fatigue properties and Fatigue life. The use of shot peening on aluminium 7075-T6 plates to improve fatigue properties and improve resistance to stress on the corrosion cracking with help of glass beads and various peening methods. When these components subsequently are loaded in tension or bending to a stress level in the range below the required for yield, the actual tensile stress at the surface is lower than that calculated on the basis of load and cross sectional area. Fatigue are major problem which normally start at or near the surface stressed in tension, thus processes that produce residual surface compressive stresses in components usually enhance the resistance to fatigue. The impact of glass shots which create resistance after the shot penning process carried out and also control the effects of failure on aluminium alloys*

Keywords: *fatigue properties, fatigue life, residual stresses, shot peening, aluminium alloys, aluminium*

I. INTRODUCTION

Benefits obtained due to cold working include work hardening and Peening having a larger shots which gives maximum compressive stress layer depends on the material surface which enhances ultimate strength and improved fatigue life. Both compressive stresses and cold worked effects are used in the application of shot peening in forming metal parts. The beneficial effects of shot peening are attributed primarily to the presence of residual compressive stresses at or near the surface. These compressive stresses can be very effective in prolonging fatigue life and in minimizing corrosion failures. Their effectiveness can be impaired considerably by (a) exposure to temperatures at which significant stress &relaxation can occur. (b) Fatigue cycling at R values minimum stress/maximum stress ratio approaching where the residual stress pattern tends to fade with increasing number of cycles, or (c) exposure to environments that chemically attack the surface, thereby changing the residual stress pattern in the surface of the materials.

II. SHOT PEENING EQUIPMENT

In commercial shot peening equipment, the shot is propelled by a high- pressure air stream in a nozzle or by a high speed rotating wheel. Factors that control the peening intensity are

1) Air pressure at the node or wheel speed
2) Distance of nozzle or wheel from the surfaces being peened
3) Angle between the shot path and the surface being peened
4) Rate of feed of shot to the nozzle or wheel
5) Type and size of shot or beads.
6) Time of exposure to the shot stream

Equipment of relatively small size may have one wheel or one nozzle, with some provision for moving the component in the shot stream or moving the nozzle to get uniform peening coverage of the component. Larger equipment may have multiple nozzle arrangements, with a mechanism for moving the components through the area subjected to the shot streams at a controlled speed to obtain the desired peening coverage. Shot peening with metallic shot is always performed in the dry condition, but for some glass bead peening of non-rusting materials the glass beads may be in a water slurry. The slurry is metered to a high pressure air nozzle which produces the blasting effects.

III. METHODS OF SHOT PEENING

Conventional (Mechanical) Shot Peening

Conventional shot peening is done by two methods. The First Method involves accelerating shot material with compressed air. Shot is introduced into a high velocity air stream that accelerates maximum of speeds up to 250 ft/s. The second method involves accelerating the shot with a wheel. The shot gets dropped onto the middle surface of the wheel and then it accelerates to the outer edge where it leaves on a tangential path.

Dual Peening

Dual peening further enhances the fatigue performance from a single shot peen operation by re-peening the same surface a second time which gives maximum coverage has been achieved and also its increasing the compressive stress at the outer surface of the compressive layer

Strain Peening

The Dual Peening increases compressive stress at the outer surface of the layer, whereas the strain peening increases the compressive stress over the entire compressive layer. This additional stress is created by preloading the part within its elastic limit prior to shot peening. When the peening media impacts the surface, layer which yields further in tension because of the preloading. This results in additional compressive stress when the metal’s surface attempts to restore itself.

Laser-shot Peening

Laser shot peening, or laser shock peening (LSP), is the process of hardening or peening metal using a powerful laser. Laser peening can impart a layer of residual compressive stress on a surface that is four times deeper than that attainable from conventional shot peening treatments.

IV. TYPES OF SHOTS USED

Shot for peening is usually chilled can iron, cart steel, pure nickel shots, high chrome nickel balls, cut wire, or glass beads etc.. In our paper we used glass beads as 0.018-inch diameter were used in peening, and chilled iron shot sizes. Basically Glass beads for peening are designated by nominal Screen size or diameter and also low cost for application. For special peening applications, malleable iron or non-ferrous shot of various composition like stainless steel and aluminum are used.

V. IMPACT OF SHOT PEENING EFFECTS

Each shot particle impacting a component’s surface has a kinetic energy, 1⁄2mv2. Approximately half of this energy is transferred to the surface. Ninety percent of that transferred energy is converted into heat and 10% into the stored energy of cold work. It follows that we can think of the effect as that of a miniature thermal bomb. The plastic deformation creating a dimple occurs in a few millionths’ of a second. Heat is generated around the dimple simultaneously being caused by the plastic deformation. This adiabatic heating is absorbed relatively slowly by the surrounding material, which acts as a heat sink.

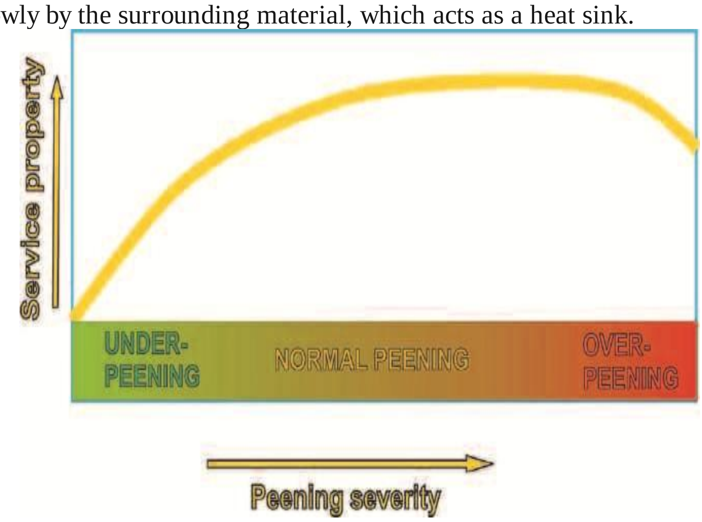

The maximum temperature in the heated zone will be at the surface and will be affected by multiple impacts which impart additive heat inputs. It is suggested that the temperature rise very near to the peened surface will be sufficient to cause a significant degree of stress-relief.

VI. STRUCTURAL CHANGES

Most metallic engineering components have a relatively-ductile matrix embedded with a variety of hard, relatively-brittle, strengthening, phases. Plastic strain on peening is then concentrated in the matrix. Some 90% of the energy absorbed from impacting shot particles is converted into heat energy. The remaining 10% is largely used to produce a vast increase in the dislocation population. This increase is from about 10^6 to about 10^{10} (ten billion) dislocation lines per square millimeter. Such an increase and such numbers are difficult to visualize. On a scale of a square micrometer the increase is by a factor of 1 to 10,000. This scale is used where in (a) there is just one dislocation (represented as a single dot) whereas in (b) there are 10,000.

The dislocation distribution is extremely non-uniform. High-strain deformation has generated a sub-grain structure. This is a characteristic feature of heavily worked metals. Peening changes the structure for each crystal from one of relative perfection to one where we have a ‘mashed up’ structure - regions of intense dislocation content (sub-grain boundaries) surrounding regions of merely high dislocation content (sub-grains). When plastic strain has induced maximum hardening the sub-grain size has reached its minimum. The dislocation density in the sub- grain boundaries is then so high that they are semi-amorphous. Further plastic strain does not thereafter increase the dislocation content. We have a situation, because peening is an intermittent process, where impact generated heat is softening some regions and hardening is occurring in other regions. These mechanisms balance to give a maximum average hardness.

VII. SHOT PEENING FOR IMPROVED FATIGUE RESISTANCE

The most effective improvement in fatigue resistance by shot peening is achieved in components that are subjected to tension-tension loading in service.

The improvement in fatigue resistance that peening provided made it feasible to use in application. Even though shot peening has effective in minimizing fatigue failures in many structural components, it is not necessary a cure for all structures that are subjected to fatigue failure. When such failure is observed in a components a complete review of the materials selection, processing specification, stress analysis, fracture appearance, metallographic structure, and components history should be considered in deciding what to do to the minimize the problem in future components of the same type.

If shot peening is recommended as a preventive measure to minimize further problems with fatigue failure, a testing program should be conducted to verify statistically the improvement in fatigue life that may be expected from the peening operation.

Because of the residual stresses produced by shot peening, yield strength of peened tensile specimen usually are lower than those of corresponding unpeened specimens. This occurs because bulk of the material in a peened tensile specimen at greater than 0.015 inch and the combination of tensile stress in the bulk with residual compressive stress in material near the surface, results in a low elastic modulus and yielding at gross stresses that are lower than those for unpeened specimens. The effect of the surface compressive stress is retained until general yielding occurs across the test section as the results of the tensile load. Beyond this point, results of the tensile test are the same as those for an unpeened specimen. The ultimate tensile strength of peened and unpeened specimens of the same material are the same.

VIII. SHOT PEENING ON ALUMINIUM ALLOYS

Peening of aluminum alloys for improved fatigue resistance is usually limited to the high –strength alloys that are used most often in aerospace application. Weight must be kept to a minimum in these application and service stresses are relatively high. The residual stress pattern near the surfaces of these specimens is shown in figures 3 for the curved marked 0.008A. Compressive residual stresses occur from the surface to a depth of about 0.009 inch. Longer peening to an intensity of 0.014 produces compressive stresses to a greater depth, about 0.013 inch. Beyond this depth, the residual stresses are in tension to compensate for the residual stresses are in tension to compensate for the residual compressive stresses near the surface. To avoid distortion of peened components, and particularly for components of sheet metal, if the edges are not peened, the surface, the surface residual stresses there will be in tension. Fatigue cracks will then start at the edges, if the service stresses are uniform across the stressed are of the component.

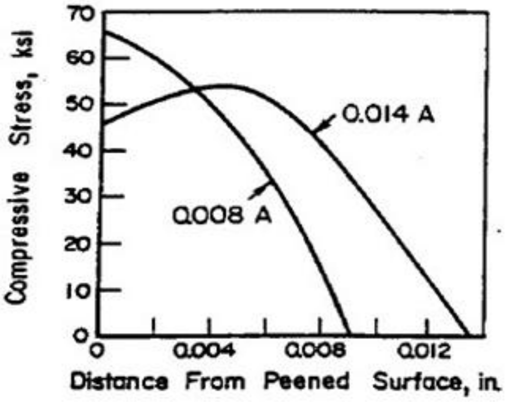

The test sections of the specimens were hand polished in the longitudinal direction with 180- grit emery paper, shot peened and subjected to axial fatigue loading.

Glass shot of 0.01Binch diameter also were used in peening additional specimen to intensities equivalent to 0.0035 and 0.0040 inch on the aluminum strips. An Almen gage war used in measuring curvature of the aluminum strips. Residual stress measurements were made on aluminum strips representing each peening condition. The fatigue - specimens were subjected to axial tensile loading at R = 0.1. Tests were made at maximum stress levels of both 55,000 and 70.000 pi. Cycling rate was 1800 cycles per minute. Average fatigue data for quadruplicate specimens peened with glass shots are shown in Table.

Data in the table show comparisons between intensity value for peened aluminum strips and the standard Amen Type A values. The data also show that the compressive surface stress and the maximum compressive stress in the peened layer near the surface increase as the peening intensity increases within the limits of these experiments. Results of the short-cycle fatigue tests indicate that the preferred shot size is P23 for 7075-T6 aluminum alloy at an intensity of 0.0124A. However, other combination of shot size and intensity develop nearly the same results for the fatigue tests.

TABLE 1: RESIDUAL STRESSES DATA AND AVERAGE FATIGUE LIFE FOR AXIALLY STRESSED SPECIMENS OF7075-T6 ALUMINIUM ALLOY

Parameter	Calculated Intensity		Residual Stresses From Peening			Average Fatigue Life, When Maximum Stress Is	
Shot	Aluminium Strip Intensity	Almen A Strip Intensity	Surface Stress Ksi	Maximum Stress Ksi	Maximum Stress Depth,In.	55,000 Psi, 10^3 Cycles	70,000 Psi, 10^3 Cycles
Glass	0.0035	0.008	--	--	--	99	43
Glass	0.0040	0.010	--	--	--	107	16
Glass	0.0040	0.010	-44.5	-56.4	0.0115	143	39
P23	0.0035	0.0085	-48.4	-62.5	0.004	165	55
P23	0.005	0.012	-59.8	-73.0	0.004	185	64
P55	0.0035	0.009	-49.8	-59.3	0.0055	150	68
P55	0.0055	0.015	-52.5	-74.5	0.0080	171	48
P55	0.0070	0.019	-64.4	-81.0	0.0105	179	43
P93	0.0035	0.005	-36.5	-58.5	0.008	170	47
P93	0.0055	0.0085	-54.4	-62.8	0.010	175	44
P93	0.0070	0.009	-62.7	-82.9	0.0085	141	35

The data for glass bead peening in Table, indicate that equivalent peening intensity with glass beads does not develop the same fatigue life as does peening others like chilled iron shot (P23,P55,P93).The various diameter of shot sizes used in chilled which are p23as 0.023 diameter and p55 as 0.055 diameter and p93 as 0.093 diameter used.

IX. Peening For Improved Resistance To Stress Corrosion Cracking On Aluminium Alloy

Stress corrosion tests have been conducted on specimen of aluminium alloys to determine the effect of shot peening. Ring type specimens were used of 7075-T6 alloy for these tests. Iron contamination is removed from peened aluminium alloy components by immersion in a 25 percent solution of nitric acid for about 25 minutes.

After rinsed, the peened surface are checked by means of a potassium ferrocyanide solution to insure the iron contamination has been removed.

Peening had a greater affect in retarding or preventing fracture of specimens in less severe environments. Examination of failed specimens indicated that attack of the peened surface occurs by pitting.as soon as the peened layer is penetrated, intergranular attack can occur, causing cracks and final failure.

Peening can be effective in reducing initiation of stress corrosion cracking only (1) if all exposed surfaces subjected to tensile stresses are peened and (2) the peened surface layer remains intact so the corroding media do not come in contact with the layers that are under tensile stresses. Various processing alternatives were considered to overcome the problem of stress corrosion cracking in aircraft structural forgings of 7075-T6 components. Localized areas of residual tensile stress in the machined components are a major contributor to the tendency for stress corrosion cracking of these components. Residual tensile stresses occur as a result of removal by machining of the surface layers which may have been in compression after heat treating. Distortion may result if the stresses are of sufficient magnitude. Straightening after machining increases the localized residual tensile stresses.

In addition, machining of the forgings may expose areas of short-transverse end grain, which are more susceptible to stress corrosion cracking than the other surface areas in a machined forging. Changing the design to avoid end grain exposure on machining is one alternative. But the cited references indicate that shot peening of these surfaces and all other surfaces of the machined forgings also will improve the stress corrosion resistance.

Experience gained with high-strength aluminum alloy forgings has indicated that shot peening without first establishing the most desirable peening conditions and without the required controls will not necessarily lead to improved stress-corrosion resistance. When peening aluminum forgings, use of the largest shot size and greater intensity that will not produce distortion is usually recommended. Table 2.explains the Typical shot sizes and intensities are as follows

Sections	Intensity	Shot Sizes
Sections 0.150 Inch And Over	0.010A - 0.014 A	0.025,0.028
Sections Under 0.150 Inch	0.006A - 0.0010A	0.017,0.019
Holes	0.003A - 0.005A	0.011,0.013

Surface roughness tolerances also should be considered when selecting shot sizes. The cited reference also indicates that all aluminum alloy components peened with metallic shot should be cleaned after peening by immersion in a nitric acid solution or by additional peening with glass beads. After cleaning, the forgings should be coated with a special oil supplied for this purpose until they are further protected by anodizing and painting.

X. PEENING FOR IMPROVED RESISTANCE TO STRESS CORROSION CRACKING IN 7075 –T6 ALUMINIUM ALLOYS

Table 3. Results Of Stress Corrosion Tests On Specimens Of 7075-T6 Aluminium Alloy With Glass Beads

Peening Methods	Peening Variables		Hours To Failures
	Intensity	Shot Or Beads Sizes	
Glass Beads Peening	0.003 To 0.005a	0.013	195.1 223.2 224.3
	0.006 TO 0.008 N	0.002 To 0.004	197.8 245.2 275.3
Shot Peening	0.003 TO 0.005A	110	139.8 180.7 192.8
	0.003 TO 0.005A Plus Glass Beads Cleaning	110	274.5 649.5 129.4
Control Penning	As Drilled And Reamed		219.4 219.4

Stress corrosion cracking trend to start at faster holes certain aluminium alloy components, since the holes usually represent stress raisers. Furthermore, the corroding medium tends to be retained around the fasteners. The stress corrosion can be reduced by shot peening in the holes but it is not always convenient to do this, for example, when the holes must be drilled and reamed during aircraft assembly.

A special tools was created and it moved axially through the hole, the hole, the steel balls are forced against the holes surface by a revolving hammer. To evaluate this effect, the specimens were peened on all surface with 280 shot too an intensity of 0.010 to 0.012A.they were then loaded in a testing fixture to a stress of 38,000psi (65%of yield strength) and subjected of yield strength1 and subjected to alternate immersion in a 3.5 percent solution of sodium chloride (10 minutes in and 50 minutes out of the solution per cycle). Results of these stress corrosion tests are presented in the table. Examination of control specimens (as drilled and reamed) indicated that the reaming process also developed residual compressive stresses in the holes. This account for the fact that the control specimens survived longer than some of the peened specimens. However results of this tests indicate equivalent effect of shot peening or glass bead peening reduce the stress corrosion cracking.

XI. CONCLUSION

Each shot materials is recommended for specific applications, the shots must be created a maximum stress to the materials which increase maximum of fatigue life to the material by using shot peening process. Glass beads peening also increase the endurance limit up to 30 percentage. Peening had a greater effect in retarding or preventing fracture of specimens in severe environments also peening had the benefits of protecting the materials from various efforts and also improved resistance to stress corrosion cracking

REFERANCES

[1]. Harish Kumar, Sehijpal Singh, Pardeep Kumar “Modified shot peening processes – a review”, International Journal of Engineering Sciences & Emerging Technologies, Apr. 2013. ISSN: 2231 – 6604 Volume 5, Issue 1, pp:12-19

[2]. A. Gariepy, S.Larose, C.Perron, P.Bocher, M.Levesqu “On the effect of the peening trajectory in shot peen forming”, Finite Elements in Analysis and Design 69 (2013) 48–61

[3]. X. Song, W.C. Liu,J.P. Belnoue, J. Dong “An eigenstrain-based finite element model and the evolution of shot peening residual stresses during fatigue of GW103 magnesium alloy”, International Journal of Fatigue 42 (2012) 284–295

[4]. S. Sathyajith, S. Kalainathan “Effect of laser shot peening on precipitation hardened aluminum alloy 6061-T6 using low energy laser”, Optics and Lasers in Engineering 50 (2012) 345–348

[5]. Kyun Taek Cho, Kyung Song, Sang Ho Oh “Surface hardening of aluminum alloy by shot peening treatment with Zn based ball”, Materials Science and Engineering A 543 (2012) 44– 49

[6]. Y. Fouad, Mostafa M, El Metwally “Effect of Shot Peening on High Cycling Fatigue of Al 2024-T4”, International Conference on Advanced Materials Engineering IPCSIT vol.15 (2011)

[7]. Y.K. Gao, X.R. Wu “Experimental investigation and fatigue life prediction for 7475-T7351 aluminum alloy with and without shot peening-induced residual stresses”, Acta Materialia 59 (2011) 3737–3747

[8]. Ivo Cerny “Growth and retardation of physically short fatigue cracks in an aircraft Al-alloy after shot peening”, Procedia Engineering 10 (2011) 3411–3416

[9]. Kazuyuki Oguri “Fatigue life enhancement of aluminum alloy for aircraft by Fine Particle Shot Peening (FPSP)”, Journal of Materials Processing Technology 211 (2011) 1395–1399

[10]. Jinxiang Liu, Huang Yuan. Ridong Liao “Prediction of fatigue crack growth and residual stress relaxations in shot-peened material”, Materials Science and Engineering A 527 (2010) 5962–5968

[11]. Harold Luong, Michael R. Hill “The effects of laser peening and shot peening on high cycle fatigue in 7050-T7451 aluminum alloy”, Materials Science and Engineering A 527 (2010) 699–707

[12]. Y.K. Gao “Improvement of fatigue property in 7050–T7451 aluminum alloy by laser peening and shot peening”, Materials Science and Engineering A 528 (2011) 3823–3828

[13]. Omar Hatamleh “A comprehensive investigation on the effects of laser and shot peening on fatigue crack growth in friction stir welded AA 2195 joints”, International Journal of Fatigue 31 (2009) 974–988

[14]. G.H. Majzoobi, K. Azadikhah, J. Nemati “The effects of deep rolling and shot peening on fretting fatigue resistance of Aluminum-7075-T6”, Materials Science and Engineering A 516 (2009) 235–247

[15]. M. Benedetti, V. Fontanari, P. Scardi “Reverse bending fatigue of shot peened 7075-T651 aluminium alloy: The role of residual stress relaxation”, International Journal of Fatigue 31 (2009) 1225–1236

[16]. A.Ali, X. An, C.A. Rodopoulos*, M.W. Brown, P. O’Hara,A. Levers , S. Gardiner “The effect of controlled shot peening on the fatigue behavior of 2024-T3 aluminium friction stir welds”, International Journal of Fatigue 29 (2007) 1531–1545

[17]. D.T. Asquith, A.L. Yerokhin, J.R. Yates, A. Matthews “Effect of combined shot-peening and PEO treatment on fatigue life of 2024 Al alloy”, Thin Solid Films 515 (2006) 1187 – 1191

OPEN ACCESS

International
Journal
Of Modern Engineering Research (IJMER)

Artificial Neural Networks (ANNS) For Prediction of California Bearing Ratio of Soils

Phani Kumar Vaddi[1], Ch. Manjula[2], P. Poornima[3]
[1]*Assistant Professor, Dept. of Civil Engineering, Gudlavalleru engineering College, Gudlavalleru, Krishna dt, A.P*
[2]*P.G student, Dept. of Civil Engineering, jntuk, kakinada, East Godavaridt, A.P*
[3]*Lecture, Dept. of Civil Engineering, A.A.N.M and V.V.R.S.R Polytechni, Gudlavalleru, Krishnadt, A.P*

ABSTRACT: *The behaviour of soil at the location of the project and interactions of the earth materials during and after construction has a major influence on the success, economy and safety of the work. Another complexity associated with some geotechnical engineering materials, such as sand and gravel, is the difficulty in obtaining undisturbed samples and time consuming involving skilled technician. Knowledge of California Bearing Ratio (C.B.R) is essential in finding the road thickness. To cope up with the difficulties involved, an attempt has been made to model C.B.R in terms of Fine Fraction, Liquid Limit, Plasticity Index, Maximum Dry density, and Optimum Moisture content. A multi-layer perceptron network with feed forward back propagation is used to model varying the number of hidden layers. For this purposes 50 soils test data was collected from the laboratory test results. Among the test data 30 soils data is used for training and remaining 20 soils for testing using 60-40 distribution. The architectures developed are 5-4-1, 5-5-1, and 5-6-1. Model with 5-6-1 architecture is found to be quite satisfactory in predicting C.B.R of soils. A graph is plotted between the predicted values and observed values of outputs for training and testing process, from the graph it is found that all the points are close to equality line, indicating predicted values are close to observed values.*

Keywords: *Artificial Neural Networks, California Bearing Ratio, Fine fraction, Liquid limit, Optimum Moisture content, Maximum Dry density and plasticity index.*

I. INTRODUCTION

The tests required for determination of California Bearing Ratio value are generally elaborate and time-consuming. Sometimes, the geotechnical engineer is interested to have some rough assessment of the C.B.R value without conducting elaborate tests. This is possible if index properties are determined. Simple tests which are required to determine the index properties are known as classification tests. The soils are classified and identified based on the index properties. The main index properties of course- grained soils are particle size and relative density. For fine- grained soils, the main index properties are Liquid limit and the Plasticity Index. In order to cope with the above complexities, traditional forms of engineering modeling approaches are justifiably simplified. An alternative approach, which has shown some promise in the field of geotechnical engineering, is Artificial Neural Networks (ANN).In these investigation the California Bearing Ratio (C.B.R) values for soils are predicted using Artificial Neural Networks (ANN). ANN model is developed using NN tool in MATLAB software (7.0.1).

In the paper an attempt has been made to model the California Bearing Ratio in terms of Fine Fraction (FF), Liquid Limit (WL), Plasticity Index (IP), Maximum Dry Density (MDD), and Optimum Moisture Content (OMC). A multi-layer perceptron network with feed forward back propagation is used to model the California Bearing Ratio varying the number of hidden layers. The best neural network model is identified by analyzing the performance of different models studied.

II. ARTIFICIAL NEURAL NETWORK MODELS DEVELOPMENT

Artificial neural networks (ANN) are developed by the structured arrangement of simple processing unit called “neurons”. Each neuron is a processing unit that performs a calculation on the input signal and outputs the result to the next neuron via “connections”. Connections indicate flow of information from one neuron to another. A weight is assigned to each connection and therefore, the resulting “weighted signal” is passed to the nextneurons. In a Multilayer Preceptron Network (MLP) the neurons are organized in the form of layers. It consists of an input layer, a hidden layer (or hidden layers), and an output layer, as shown in Fig. 1. In this type of network, each neuron has full connection to all neurons of the next layer but there is no connection between the neurons within the same layer. The neurons in the input layer represent number of input variables considered, while the output neurons identify the desired outputs. Each neuron in the network has an activation function, usually expressed by sigmoid function through other types of activation functions, such as linear and hyperbolic tangent functions, and may be used as well. Weights are assigned randomly to all of the connections inside the network so that optimum values of these are attained for minimizing the network error measure (the difference between the actual and computed outputs gives the error) which will be back propagated through hidden layers for all training sets until the actual and calculated outputs agree with some predetermined tolerance.

A multilayer perceptron neuron network is identified by its architecture, the way the neurons are arranged inside the network, and a learning rule. The learning rule is an algorithm used to determine the optimum values of the unknown weights that minimize the error measure of the network. A database is also required for training and testing the network. Feed-Forward-error-back-propagation network with supervised learning is currently used in applications relating to science and engineering. Fig.1. Shows typical three-layered network. In most of the neural networks the number of inputs, hidden nodes and the output in different layers has to be predetermined before feeding the data to the network based on the input considered and desired output from the model network. The number of hidden layers and neurons in each hidden layer are determined in contrast to the known output obtained from a known set of data used for training and this network topology can be generalized for prediction.

The objective of the present investigation is to develop a neural network model output being Compression index. The input parameters, for the networking should be those basic soil parameters, which has significant influence on Compression index. The details of the database used for training input parameters are presented in the following section.

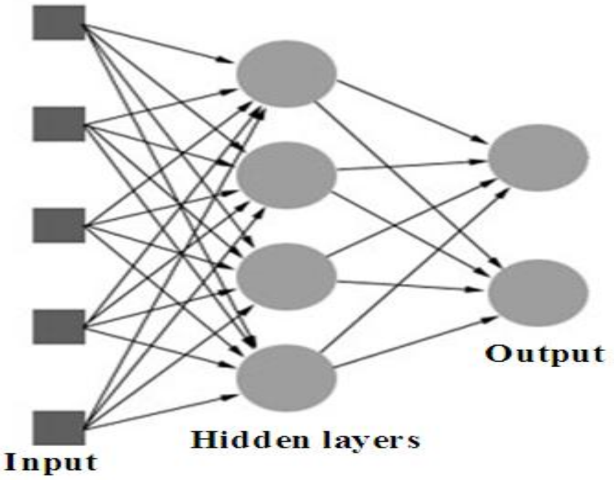

Fig. 1: The Architecture of Neural Network

A. Normalization of Data

Ideally a system designer wants the same range of values for each input feature in order to minimize bias within the neural network for one feature over another. Data normalization can also speed up training time by starting the training process for each feature within same scale. It is especially useful for modeling applications where the inputs are generally on widely different scales. The normalized data is determined by min-max normalization and is expressed as

$$X= 0.1+0.8*(x_i/x_{max})$$

Where

X = normalized value

x_i= input parameter

x_{max}= maximum in input parameter

B. Data used for Training and Testing

The soil test data is divided into 2 parts using 60:40 mode of distribution. A total of 50 soils which is obtained from different parts of chitter district with wide range of W_L from laboratory tests. Among 30 soils data is used for testing and remaining 20 soils data is used for training. The typical normalized data used for training phase is presented in Table 1 and inTable 2 presents the typical normalized data used for testing phase.

C. Network Training and Testing

30 soils test data was used for training the neuron, training data is presented in Table I. Remaining 20 soils test data was used for testing the network modeldeveloped for prediction of Compression index of soils. Testingdata ispresented in Table II. The feed forward back propagation training network models have been coded into a MATLAB program using neural network toolbox. The MATLAB software enables training with different convergence criteria, tolerance level, activation functions and number of epochs. The neural network models studied in this investigation uses transfer function 'LOGSIG' as activation function. A constant value of learning rate equals to 0.001 was assigned for all the models. The network training/learning halts automatically once the mean square error value converges to a tolerances value of 0.5 or the Number epochs become equal to 2000 whichever is earlier. After this the network model is ready for prediction of desired output.

Table I. Normalized Data for Training the Neural Network Models

S.No	FF	W_L	I_P	OMC	MDD	C.B.R
1	0.87	0.90	0.90	0.60	0.69	0.26
2	0.67	0.57	0.42	0.55	0.59	0.24
3	0.82	0.55	0.34	0.63	0.73	0.20
4	0.77	0.63	0.43	0.56	0.69	0.28
5	0.83	0.79	0.58	0.53	0.63	0.26
6	0.90	0.55	0.41	0.87	0.77	0.26
7	0.77	0.76	0.53	0.80	0.74	0.20
8	0.73	0.55	0.36	0.55	0.70	0.36
9	0.71	0.46	0.30	0.42	0.79	0.53
10	0.78	0.65	0.41	0.64	0.67	0.25
11	0.75	0.60	0.33	0.56	0.63	0.30
12	0.80	0.55	0.34	0.44	0.82	0.34
13	0.75	0.58	0.35	0.50	0.69	0.30
14	0.74	0.57	0.33	0.55	0.68	0.35
15	0.77	0.55	0.34	0.58	0.90	0.33
16	0.76	0.56	0.33	0.53	0.69	0.32
17	0.72	0.57	0.34	0.55	0.70	0.35
18	0.79	0.66	0.37	0.60	0.76	0.32
19	0.70	0.64	0.35	0.45	0.61	0.45
20	0.85	0.46	0.32	0.36	0.59	0.76
21	0.80	0.53	0.27	0.88	0.81	0.29
22	0.82	0.60	0.30	0.54	0.66	0.55
23	0.83	0.53	0.33	0.71	0.67	0.38
24	0.73	0.69	0.36	0.51	0.63	0.46
25	0.85	0.54	0.40	0.90	0.77	0.29
26	0.75	0.69	0.38	0.72	0.67	0.32
27	0.80	0.61	0.35	0.64	0.66	0.35
28	0.74	0.50	0.26	0.55	0.63	0.48
29	0.78	0.58	0.29	0.41	0.59	0.77
30	0.77	0.71	0.34	0.37	0.58	0.90

Table II. Typical Normalized Data for Testing the Neural Network Models

S.No	FF	W_L	I_P	OMC	MDD	C.B.R
1	0.80	0.90	0.90	0.75	0.77	0.16
2	0.83	0.60	0.31	0.90	0.79	0.22
3	0.89	0.84	0.68	0.71	0.74	0.20
4	0.88	0.59	0.48	0.68	0.69	0.22
5	0.90	0.44	0.23	0.78	0.72	0.25
6	0.84	0.54	0.56	0.73	0.81	0.22

7	0.89	0.42	0.33	0.66	0.67	0.18
8	0.71	0.50	0.34	0.48	0.82	0.37
9	0.78	0.54	0.32	0.55	0.81	0.33
10	0.74	0.45	0.35	0.46	0.83	0.47
11	0.77	0.47	0.34	0.59	0.73	0.31
12	0.81	0.32	0.31	0.38	0.87	0.66
13	0.72	0.39	0.34	0.42	0.90	0.62
14	0.89	0.51	0.43	0.63	0.76	0.27
15	0.71	0.47	0.36	0.53	0.79	0.29
16	0.68	0.59	0.43	0.71	0.71	0.18
17	0.86	0.48	0.40	0.52	0.79	0.35
18	0.76	0.34	0.27	0.34	0.75	0.90
19	0.82	0.36	0.28	0.40	0.83	0.57
20	0.88	0.50	0.30	0.57	0.77	0.33

III. VALIDATION AND COMPARISON OF NETWORK PREFORAMANCE

After training the ANN models were used to predict California Bearing Ratio value of soil of 20 soils reported in the literature. Data used for testing is shown in the Table II. The model developed for predicting the California Bearing Ratio value are 5-4-1(inputs-hidden layers-output), 5-5-1, and 5-6-1. Among these models the best model proposed is 5-6-1 network model. The CORR or (R^2) values for the developed models are presented in TableIII.The ratio normalized observed values to the normalizedpredicted values in training are shown in Table IV and testing values are shown in Table V. The model performance is given in Fig.3.1. Since graphical representation gives a clear idea, the same values are shown in Fig.3.2 during training and Fig.3.3 during testing respectively.

Table III ANN Model Statistical Parameter Performance Indices

Stastical parameter	Models	During training	During testing
		C.B.R	C.B.R
CORR	5-4-1	0.716	0.707
	5-5-1	0.924	0.881
	5-6-1	0.986	0.932

Table VIComparison of Normalized Observed and Normalized Predicted values of C.B.R for Trained Data

TRAINED DATA			
Observed C.B.R	Predicted C.B.R		
	No of Neurons		
	4	5	6
0.264	0.265	0.266	0.266
0.244	0.367	0.264	0.251
0.203	0.336	0.220	0.202
0.285	0.402	0.314	0.284
0.264	0.376	0.286	0.263
0.264	0.293	0.287	0.262
0.203	0.358	0.206	0.205
0.362	0.418	0.388	0.364
0.529	0.352	0.473	0.525
0.248	0.392	0.249	0.246
0.297	0.245	0.240	0.270
0.336	0.244	0.354	0.336
0.305	0.223	0.284	0.304
0.352	0.263	0.313	0.348
0.333	0.224	0.332	0.327

0.324	0.300	0.295	0.328
0.353	0.344	0.350	0.357
0.320	0.335	0.347	0.311
0.455	0.353	0.442	0.451
0.764	0.659	0.745	0.714
0.286	0.249	0.253	0.281
0.552	0.487	0.580	0.452
0.382	0.338	0.351	0.389
0.459	0.474	0.410	0.459
0.291	0.254	0.243	0.295
0.321	0.353	0.523	0.321
0.348	0.251	0.386	0.348
0.477	0.348	0.460	0.477
0.765	0.681	0.757	0.770
0.900	0.939	0.905	0.880

Table VComparison of Normalized Observed and Normalized Predicted values of C.B.R for Tested Data

TESTED DATA			
ObservedC.B.R	Predicted C.B.R		
	No of Neurons		
	4	5	6
0.159	0.222	0.217	0.155
0.218	0.104	0.290	0.227
0.204	0.259	0.283	0.215
0.218	0.289	0.227	0.238
0.247	0.275	0.209	0.229
0.218	0.341	0.192	0.214
0.183	0.071	0.168	0.292
0.372	0.486	0.416	0.280
0.329	0.426	0.314	0.331
0.471	0.331	0.464	0.487
0.309	0.488	0.383	0.343
0.658	0.688	0.547	0.678
0.619	0.438	0.728	0.528
0.270	0.325	0.312	0.255
0.292	0.115	0.301	0.320
0.182	0.249	0.119	0.288
0.353	0.349	0.267	0.285
0.900	0.847	0.811	0.850
0.565	0.700	0.447	0.564
0.329	0.493	0.374	0.322

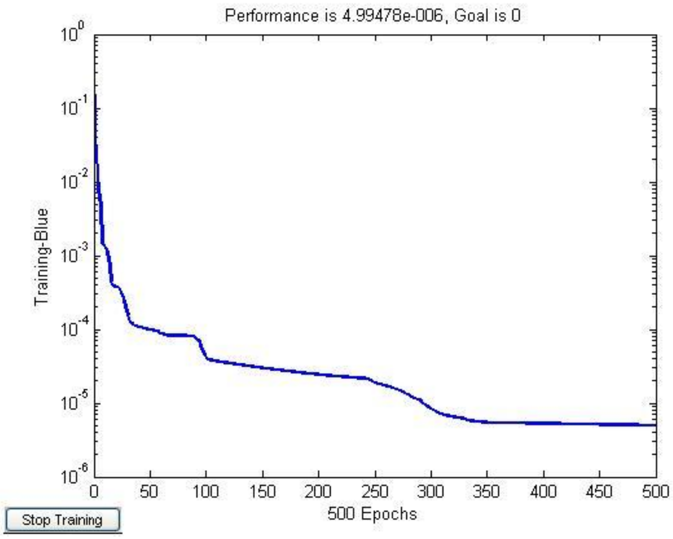

Fig.3.1 Model performance indication graph

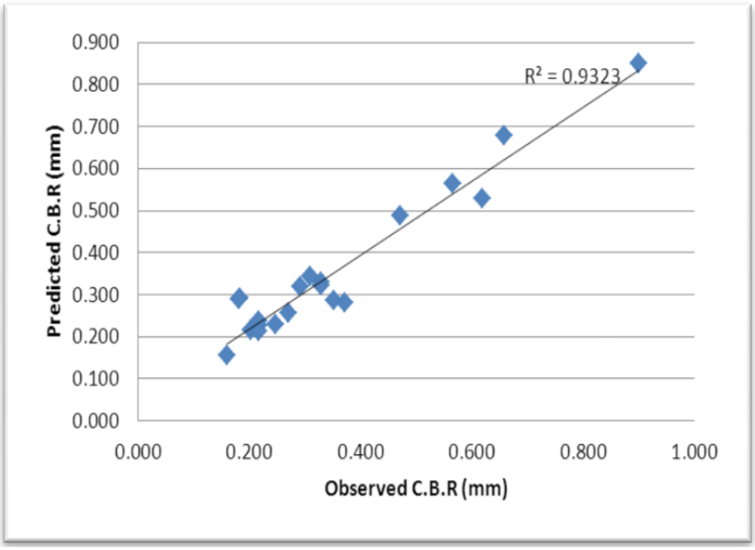

Fig.3.2Observed C.B.R Vs Predicted C.B.R during Training

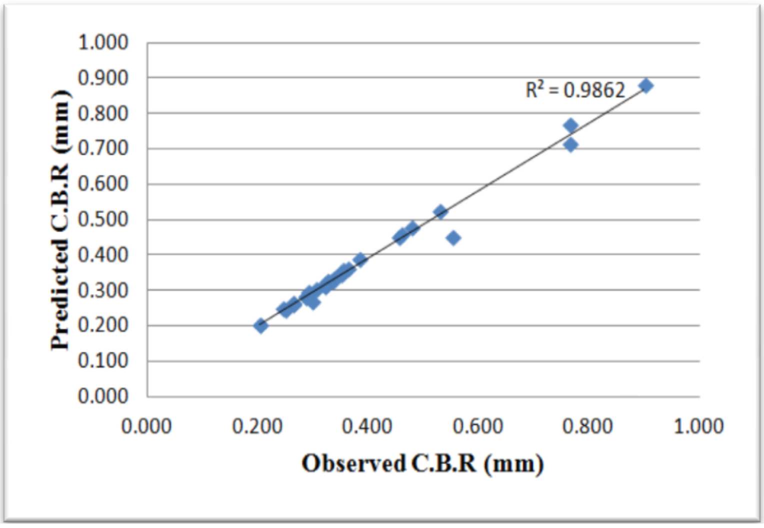

Fig.3.3Observed C.B.R Vs Predicted C.B.R during Testing

IV. CONCLUSIONS

Architecture of Proposed Model is shown in Ifig 4.1:

Inputs : 5
Neurons : 6
Outputs : 1
Transfer Function: Feed Forward Back Propagation
Activation Function: Log sigmoid

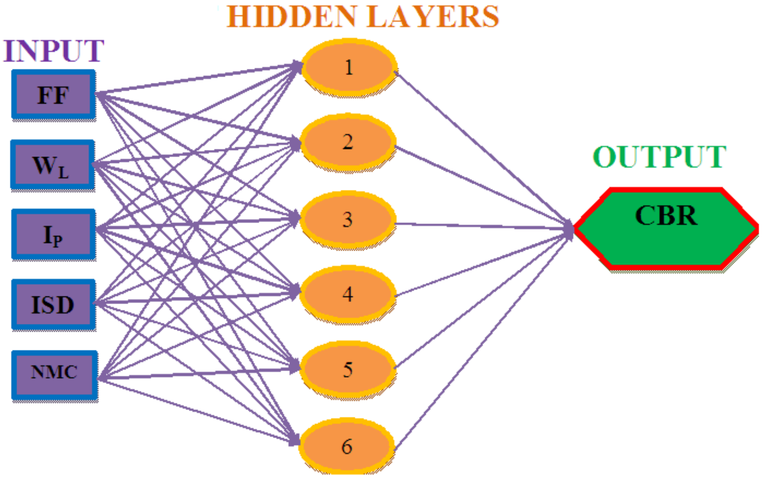

Fig.4.1. Architure of Proposed Model

An artificial neural network model with 5-6-1 architecture with a Feed Forward Back propagation using algorithm Log sigmoid activation function was developed to predictCalifornia Bearing Ratio value using basic soil properties FF(%),W_L(%),I_P(%), MDD and OMC as input parameters. The network is trained with 30 soils test data. The performance of the modal is verified for 20 soils test data. The proposed neural network model is found to be quite satisfactory in predicting desired output.

This is the foremost model for predicting the California Bearing Ratio of soils using Artificial Neural Network.

REFERENCES

[1]. **E.R. Levine, D.S. Kimes, V.G. Sigillito**, “Classifying soil structure using neural networks”, Ecological Modelling 92 (1996) 101-108.

[2]. **Ghabousi J, Garett JR, Wu X**, “Knowledge based modeling of material behavior with neural networks”, ASCE J EngMech 1991; 117(1):132–53.

[3]. **Hornik KM, Stinchcombe M, White H**, “Multi-layer feedforward networks are universal approximator”, Neural Networks, 1994; 2(5):359–66.

[4]. **Kwok, T.Y., Yeung, D.Y.**, “Constructive Algorithms for Structure Learning in Feedforward Neural Networks for Regression Problems”, IEEE Trans. Neural Networks, 1997, 8 (3), 630–645.

[5]. **Levine, E.R., Kimes, D.S., Sigillito, V.G**., “Classifying soil structure using neural networks”, Ecol. Model, 1996, 92 (1), 101–108.

[6]. **M.A. Shahin, M.B. Jaksa, H.R. Maier**, “Artificial neural network applications in geotechnical engineering”, Australian Geomechanics 36 (1) (2001) 49–62.

[7]. **M. Banimahd, S.S. Yasrobi, P.K. Woodward**, “Artificial neural network for stress–strain behavior of sandy soils: Knowledge based verification”, Computers and Geotechnics 32 (2005) 377–386.

[8]. **Pernot S, Lamarque CH**, “Application of neural networks to the modeling of some constitutive laws”, Neural Networks 1999;12:371–92.

[9]. **Rumelhart, D.E., Hinton, G.E. and Williams, R.J.,** “Learning representations by back-propagation errors”, Nature, 1986, 323: 533-536.

[10]. **S.K. Das, P.K. Basudhar**, “Prediction of coefficient of lateral earth pressure using artificial neural networks”, Electronic Journal of Geotechnical Engineering, 10—Bundle A (2005) paper 0506.

[11]. **Wang J, Rahman MS**, “A neural network model for liquefaction induced horizontal ground displacement”, Soil Dynamics and Earthquake Engineering 1999; 18(8):555-68.

[12]. **YushunZhai, J. Alex Thomassonb, Julian E, Boggess III, Ruixiu Sui**, “Soil texture classification with artificial neural networks operating on remote sensing data”, Computers and Electronics in Agriculture 54 (2006) 53–68.

OPEN ACCESS

International
Journal
Of Modern Engineering Research (IJMER)

Effects of Continuous Cooling On Impact and Micro Structural Properties of Low Carbon Steel Welded Plate

Aweda, E. O.[1], Dauda, M.[2], Dagwa, I. M[3]. , Dauda, E.T[4].

[1,2]Department of Mechanical Engineering Faculty of Engineering Ahmadu Bello University Zaria.
[3]Department of Mechanical Engineering Faculty of Engineering University of Abuja Abuja
[4]Department of Materials and Metallurgy Engineering Faculty of Engineering Ahmadu Bello University Zaria.

ABSTRACT: *Some mechanical properties and microstructural analysis were conducted on shielded metal arc weldments of low carbon steels in some simulated environments. Specimens were prepared and subjected to welding and continuous cooling at the same time at various positions. Results obtained for impact strength using Charpy impact testing machine showed that impact strength of water cooled samples were higher compared to salty water cooled samples. This is due to the increased formation of martensitic structure and finer pearlite grains. The microstructure of the samples was studied using photographic visual metallurgical microscope. For low cooling rate as in the air cooled sample, the austenite was observed to transform into ferrite and pearlite. Ferrite is a body-centred cubic crystal structure of iron alloys. For higher cooling rates of water and salt water cooled samples, low temperature transformation products like bainite (an acicular microstructure which is not a phase) or martensite (a very hard form of steel crystalline structure) were formed. The salt water cooled samples had more martensite regions because of the increased cooling rate.*

Keywords: Continuous cooling, impact strength, micro structural studies, low carbon steel

I. INTRODUCTION

The strength of steel is influenced by its microstructure (the type of crystal patterns). The microstructure is controlled by the arrangement of the atoms of the various elements in the steel. Heating and cooling of the steel influences this atomic arrangement.

In most welding procedures metal is melted to bridge the parts to be joined so that on solidification of the weld metal the parts become united. The common processes of this type are grouped as fusion welding. Heat must be supplied to cause the melting of the filler metal and the way in which this is achieved is the major point of distinction between the different processes. The method of protecting the hot metal from the attack by the atmosphere and the cleaning or fluxing away of contaminating surface films and oxides provide the second important distinguishing feature.

Welding operations that are done in offshore environments such as the construction, building, repair and maintenance of ships, the surrounding water which is salty serves as a cooling medium. Studies have shown that depending on the environment, welding can alter the carefully designed microstructure of steels as a result of heat affected zone thermal cycles that exceed the transformation temperature. (Shome et –al, 2004). Depending upon the heating and cooling cycles involved, different types of microstructures are obtained in weld bead and the heat affected zone (HAZ). However, from weldability stand point, one advantage that low carbon steels have over medium and high carbon steels is that heat may not drastically affect the materials strength, therefore preheat can be avoided entirely or only very low temperature preheat is required, saving cost in production.

The micro constituents that are evident in the weld metal and heat affected zone of ultra low carbon steel weldments were reported by Fonda (et – al, 2000), the precipitates could either be coarsen or dissolve in the steel matrix during heating cycle, which can lead to excessive austenite grain growth in the heat affected zone due to the absence of the pinning effect of precipitates on austenite grain boundaries. The coarse grain size decreases the nucleation sites for high temperature transformation products such as ferrite and pearlite, tending to suppress their formation. If cooling rate is sufficiently high, martensite could form in the heat affected zone. When parameters such as pre-heating temperature, cooling time after welding, post weld heat treatment were varied, the results showed that it is possible to get microstructures that do not contain any untempered martensite in the heat affected zone of hardenable steels (Hernandez, 2010).

During welding, molten metal consists of a mixture of the base metal, and substances from the coating of the electrode; this mixture forms the weld when it solidifies. The electrode coating deoxidizes the weld area and provides a shielding gas to protect it from oxygen, hydrogen and nitrogen in the environment.

The Shielded metal arc welding (SMAW) process is commonly used in general construction, shipbuilding, pipelines and maintenance work. The process is suited best for work piece thicknesses of 3 to 19 mm, although this range can be extended easily by skilled operators using multiple pass techniques.

Akselsen et al. (2009) conducted a research to assess the weldability of duplex stainless steel under hyperbaric (high pressure) conditions. This was achieved by horizontal welding with Inconel 625 (Nickel-Chromium-Molybdenum alloy) wire in V-grooves on plates in 2205 duplex steel in chamber pressures of 12 and 35 bar that is, welds 1 and 2 respectively. The results from all-weld-metal tensile testing showed average yield strengths of 491 and 468 MPa (mega pascal) for Welds 1 and 2, respectively. Weld metal yield strength was lower than that of the base metal which had yield strength of 518 MPa. The tensile strength is similar to that of the base metal. The tensile strength of the base metal was 744MPa. Welds 1 and 2 had tensile strengths of 739 and 735MPa respectively. For weld 1, the weld metal toughness exceeded 150 J, while weld 2 had values slightly below 150 J. Liu et al. (2011) observed that underwater friction stir welding (underwater FSW) has been demonstrated to be available for the strength improvement of normal FSW joints. A 2219 aluminium alloy was underwater friction stir welded at a fixed rotation speed of 800 rpm and various welding speeds ranging from 50 to 200 mm/min in order to clarify the effect of welding speed on the performance of underwater friction stir welded joint. The results revealed that the precipitate deterioration in the thermal mechanically affected zone and the heat affected zone is weakened with the increase of welding speed, leading to a narrowing of softening region and an increase in lowest hardness value. Tensile strength firstly increased with the welding speed but dramatically decreased at the welding speed of 200 mm/min owing to the occurrence of groove defect. Fukuoka et al (1994) welded steel plates of sizes 2mm, 8mm, 14mm, 16mm and 19mm using gas shielded arc welding for both air and underwater welding. Cooling rate was observed to increase with increase in plate thickness with air weld recording a more consistent increase. From the results, it was observed that the hardness for underwater welding is almost twice that of the welding in air around weld metal and heat affected zone (HAZ), and remarkable differences were not observed between both welding processes in the base metal away from the weld zone. According to Calik (2009), currently, there is a strong interest in studying the effect of cooling rate on the mechanical properties and microstructure of industrial processed steels. Calik (2009) has studied the effect of cooling rate on hardness and microstructure of AISI 1020, AISI 1040, and AISI 1060 steels and shown that the microstructure of these steels can be changed and significantly improved by varying the cooling rates. Adedayo and Oyatokun (2013) studied the effect of saline water cooling on service quality of a welded AISI 1013 Carbon steel plate by varying the coolant flow rates.

Therefore, in this study the effect of simultaneous cooling (using different cooling media such as air, water and salty water (3.5percent salty in water)) and welding at varying distances from the weld fusion line on the mechanical properties and the microstructures of low carbon steel plates was investigated.

II. EXPERIMENTAL PROCEDURE

The elemental composition of the low carbon steel is presented in Table 1 as determined using X-Ray Fluorescence (XRF) at the Universal Steels, Ikeja, Lagos. The cooling media used were: air, water and salty water (3.5 percent of sodium chloride in water). Using elemental values presented in Table 1, the Carbon equivalent of the low carbon steel was calculated thus;

$$\text{Carbon Equivalent (CE)} = C + \frac{Mn}{6} + \frac{Cr+Mo+V}{5} + \frac{Ni+Cu}{15}$$

When the values in Table 1 are substituted into the carbon equivalent formula, 0.2046 is obtained as the carbon equivalent for the material used for the research.

Table 1: Elemental composition of the material

Element	C	Si	Mn	S	P	Cr	Ni	Cu	Nb	Al	B	W	Mo	V	Ti	Fe
Average content	**0.146**	**0.297**	**0.285**	**0.027**	**0.021**	**0.040**	**0.018**	**0.028**	**0.0001**	**0.0001**	**0.0001**	**0.0001**	**0.0001**	**0.0001**	**0.007**	**99.131**

Specimen Preparation

A total number of 108 samples were prepared from a 5mm thick plate. 54 samples were used for impact test. Metallographic examination was carried out on another set of 54 samples. The effect of continuous cooling on their mechanical property was observed at eight(8) different positions. For each cooling position T1 to T8 (with an interval of 5mm between 10mm to 45mm from the fusion zone), three samples were produced in order to obtain average values. Six (6) of the samples were used as control or standard test samples. Before the

samples were butt joint welded, they were chamfered at angles 30^o creating a vee-groove and leaving a root face and a root gap as shown in Fig.1.
All the dimensions are in millimetres (mm).

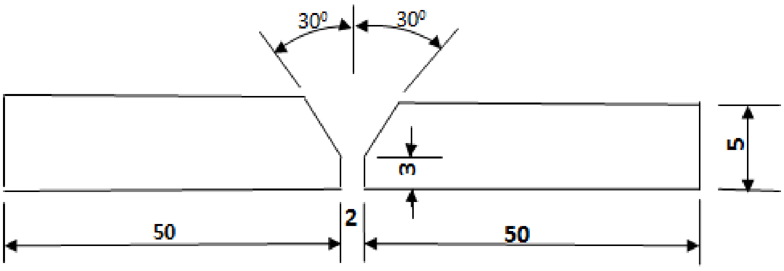

Figure 1: Sample preparation for butt (v- groove) welding

All the samples (both welded and unwelded) were cleaned from dirt and oil and a grinding machine was used to grind their surfaces before and after welding. Grinding of the surfaces was necessary to provide uniform thickness of the weld joint and other parts of the sample.

2.1 Mechanical Test

2.1.1 Impact Test

The Charpy (Balanced Impact Strength Tester) impact testing machine was utilized for impact tests of fifty-four samples. Charpy V-notches were prepared according to ASTM A370.

2.1.2 Welding Process

After sample cleaning and preparation, the samples were welded using shielded manual arc welding (SMAW) process. Core wire electrodes of standard wire gauge 12 were used. The cooling process was aided by coolant flow guide as shown in Figure 2. During the welding process, the samples were cooled simultaneously at different distances each from the fusion zone as shown in figure 3.4. The samples were cooled at distances (x) 10mm, 15mm, 20mm, and 25mm to 45mm length from the fusion zone. The accuracy of this cooling process is aided by using a coolant flow guide. Water, salt water (3.5percent sodium chloride) and air were used as cooling mediums. 72 samples were cooled with water and salt water, and nine samples in air. Temperatures at 10mm from the fusion zone were recorded for all the welded samples. After striking the electrode, it was held at an angle of 75-85 degrees to the plate and then moved steadily along the plate towards the operator and maintaining a constant height above the plate.
Welding parameters for the welding are shown it table 2.

Table 2: Welding parameters

Voltage	Current	Average Speed	Heat transfer efficiency factor f1 (for SMAW)	Heat Input	Mass Flow Rate of Coolant
18V	250A	3.1MM/S	0.65	1 453.06 J/mm	718.2 g/s

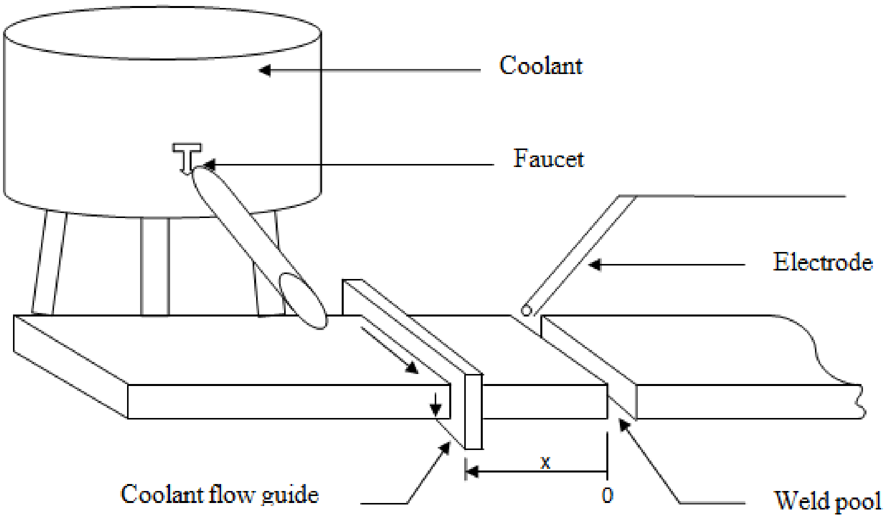

Figure 2: Experimental set-up

2.1.3 Metallurgical Examination

The sample surfaces were grinded using silicon carbide papers of various grits sizes. They are 120, 240, 320, 400 and 600. The finest grit size is 600 while the coarsest is 120. Coolant was applied simultaneously in order to avoid heating up the sample which can change its mechanical property by annealing the material. Secondly, the coolant provides a rinsing action to flush away the particles being removed from the surface.

Furthermore, the samples surfaces were polished giving rise to shiny surfaces. This was performed by applying a fine abrasive material such as synthetic alumina to a smooth, lint-free cloth polishing wheel mounted on a motor, and then robbing it on the work surface in a rotary action. During this process, the sample was rotated in a direction opposite the clockwise rotation of the wheel. Coolant was also used to keep the samples at low temperatures.

2.1.4 Etching and Microscopy

All the samples were etched using Nital. They were then examined under Photographic visual Metallurgical Microscope. The microscope was used to make visible the structural and metallographic characteristics of the samples under the different conditions of welding and cooling using a magnification of ×100.

III. RESULTS AND DISCUSSION

3.1 Cooling Curves

A typical arc weld thermal cycle consists of very rapid heating to a peak temperature, followed by relatively fast cooling to ambient temperature (Poorhaydari et al., 2005). This phenomenon is seen in the cooling curves shown below. The time it took to cool in air from 800°C to 500°C for weld was 12 seconds while for water cooled weld, it took 8 seconds. Salty water cooled welds took only 4 seconds to cool from 800^0C to 500^0C. Hence, it was observed that the cooling rate for salty water was higher than that of water then followed by air. This agrees with what Ibarra, et al, (1995) observed. The effect of these varying rates of cooling can be seen in the microstructures of the welded samples. The cooling curves were labeled from T1 to T8 representing temperatures recorded at intervals of 5mm from 45mm to 10mm towards the weld joint, respectively. The temperature at the weld zone and heat affected zone was observed to drop faster as cooling position was brought closer to the weld zone.

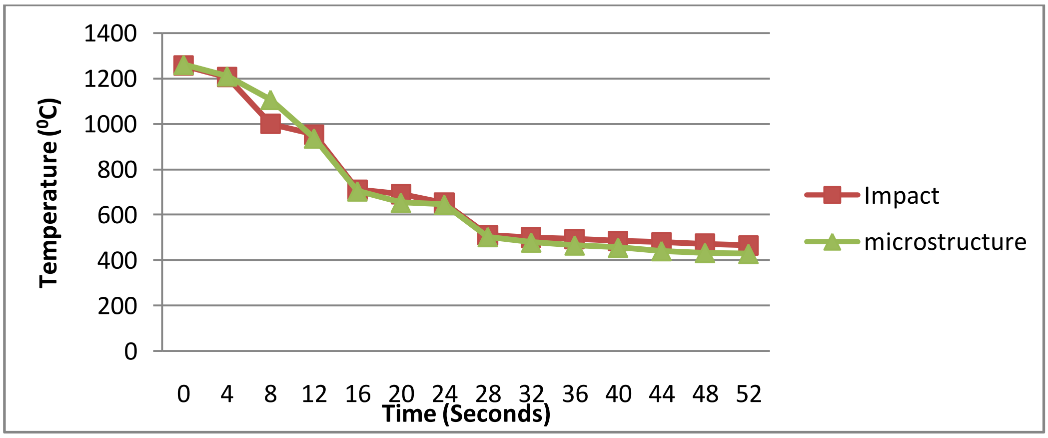

Figure 5: Air cooling curves for impact and microstructure test samples

Figure 5, presents the cooling curves of air cooled samples subjected to impact and and microstructure test. A rapid fall in temperature to about 1200^0C was observed followed by a gradual temperature fall to about 400^0C after 60 seconds.)

3.1.1 Cooling Curves for Water Cooled Samples

Water cooled: impact and microstructure test specimen cooling curves are shown in this section. It was observed in Figures 6 and 7 that temperature drops faster from curve T1 to T8. It took an average time of 8 seconds to cool the weld from 800^0C to 500^0C. It was again observed that the closer the cooling position is to the weld zone, the faster temperature drop increased because of the thermal gradient.

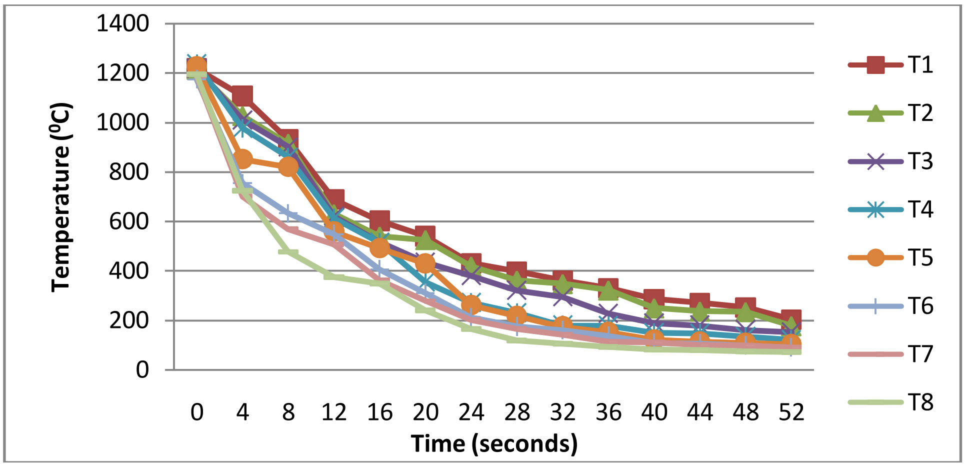

Figure 6: Impact test Curves for Water Cooled Samples

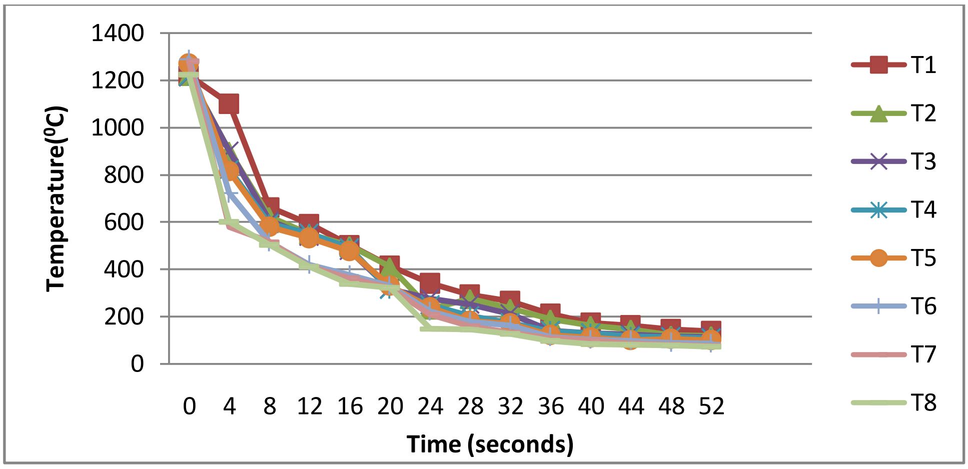

Figure 7: Microstructure Test Curves for Water Cooled Samples

The figures 6 and 7 also show that compared to air cooling curve, the temperature drop after 60 seconds was lower for the water cooled samples.

3.1.2 Cooling Curves for Salty Water Cooled Samples

In this section, salty-water cooled impact and microstructure test cooling curves are shown. It was observed from figure 8 that temperature dropped from 800^0C to 500^0C in 4 seconds. It was also observed that the closer the cooling position was to the weld zone, the faster the temperature dropped.

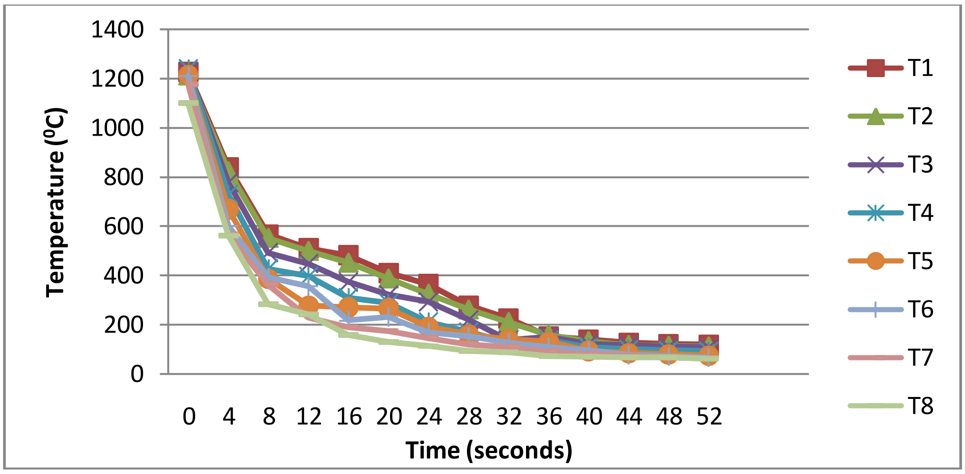

Figure 8: Impact test Curves for Salty Water Cooled Samples

From figure 8, it was observed that in about 60 seconds, the temperature dropped to about 100^{0}C and less. These cooling curves for salty-water cooling shows a more rapid cooling rate than air and water cooling. This rapid cooling resulted in a decrease in impact strength of the samples that were cooled with salty water. Calik (2009) has shown that the microhardness of steels increases with the cooling rate and also carbon content. Additionally, the microhardness increases with increasing pearlite percentage. Their microstructure also showed a decrease in the amount of ferrites.The cooling curves show that cooling distance from weld zone has minimal effect on peak temperature but it has influence on cooling rate.

3.2 Mechanical properties:

3.2.1 Impact Energy

Table 2 shows the impact test results for the air cooled sample and the control sample.
Impact energy values of water and salt water cooled samples are presented in Tables 2 and 3.

Table 2: Air Cooled Sample and Control sample

	Impact energy (Joules)
Air	**16.95**
Control Sample	**18.98**

Table 3: Impact Energy Values for Water Cooled samples

Distance from weld (mm)	Impact energy (Joules)
10	**12.88**
15	**13.56**
20	**14.92**
25	**18.31**
30	**19.26**
35	**21.70**
40	**21.70**
45	**25.09**

Table 4: Impact Energy Values for Salt Water Cooled Samples

Distance from weld (mm)	Impact energy (Joules)
10	**11.66**
15	**12.20**
20	**12.88**
25	**14.51**
30	**16.95**
35	**17.09**
40	**17.63**
45	**18.31**

Impact test results of water cooled samples and salty water cooled samples are presented in Figure 10.

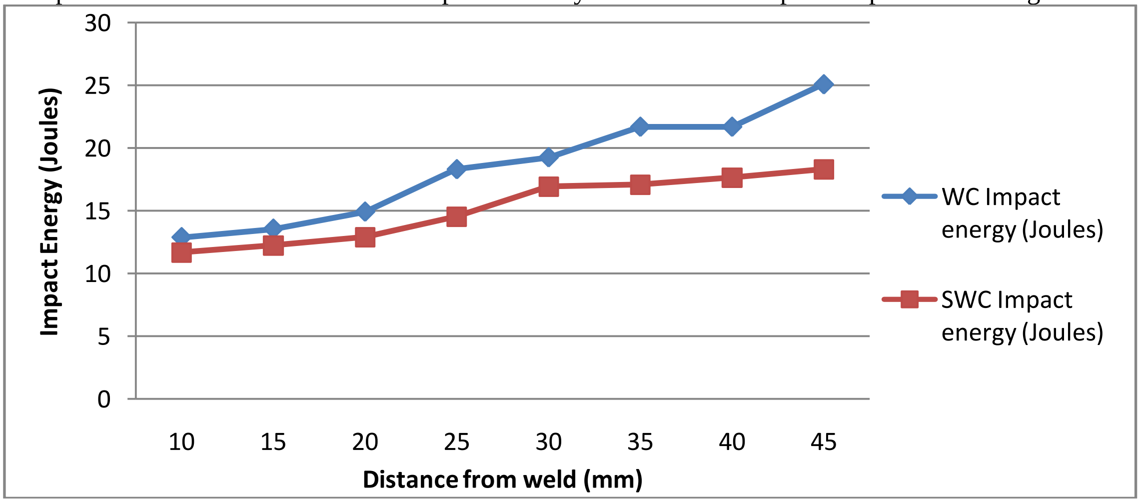

Figure 10: Variation of Impact Energy and Distance of Weld of Samples.

Figure 10 shows that increased rate of cooling has a negative effect on toughness of the low carbon steel. Toughness values of the water cooled samples are higher than the values of the samples that were cooled in salty water. This is due to the increased formation of martensitic structure and finer pearlite grains.

3.2.2 Microstructures

The microstructures of control, air, water and salty water cooled samples are presented in this section with a magnification of ×100.

Plate 1: Control sample

The control sample in plate 1 shows ferrite and pearlite layers because of the low carbon content in the material and the grain structure is coarse. The ferrites are the white areas while pearlites are the dark areas.

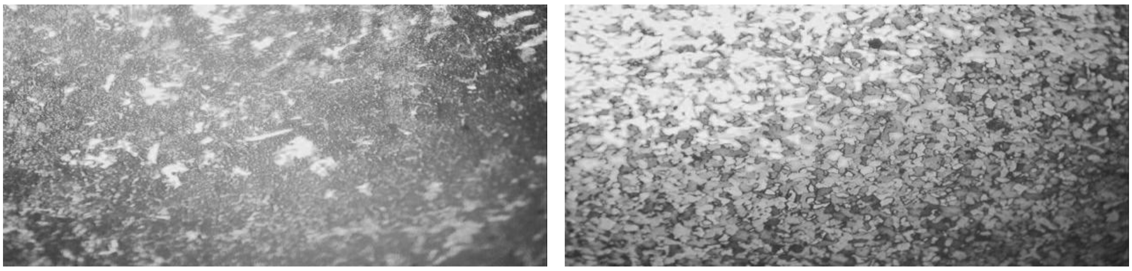

a, Air Weld **b, Air HAZ**

Plate 2: Weld zone and Heat Affected Zone (cooled under room temperature)

In plate 2, the weld zone has fine grains while the heat affected zone has coarse grains. This is because of the faster cooling rate at the weld zone. There is no sufficient time for grain growth and nucleation in the weld zone.

3.2.2.1 Heat Affected Zone (Water)

Ibarra, et al, (1995), observed in his work that due to the rapid cooling that occurs in wet weld, the heat affected zone of most welded mild steel are coarse-grained and martensitic. This was also observed in the heat affected zone micrographs shown in plate 3 and plate 4. The salty water cooled samples have more martensitic structures than water and air cooled samples.

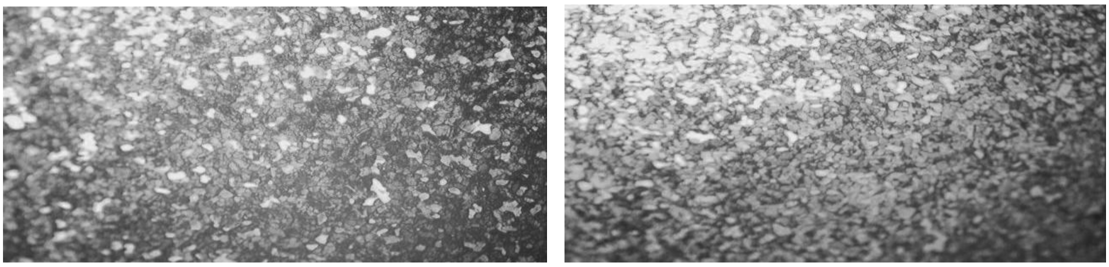

10mm **15mm**

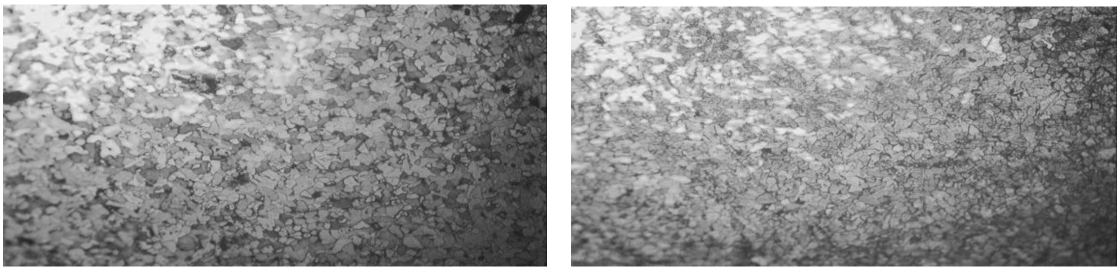

40mm **45mm**

Plate 3: Heat Affected Zone (Water Cooled)

From the micrographs presented in plate 3, at 45mm from the weld, ferrite structure is seen to be more and generally dispersed in the microstructure. The ferrite structures are the light-coloured regions of the structure.

The amount of pearlite was observed to increase as the cooling distance from the weld reduces (that is, as the material is cooled at a distance nearer to the weld zone).

3.2.2.2 Heat Affected Zone (salty water)

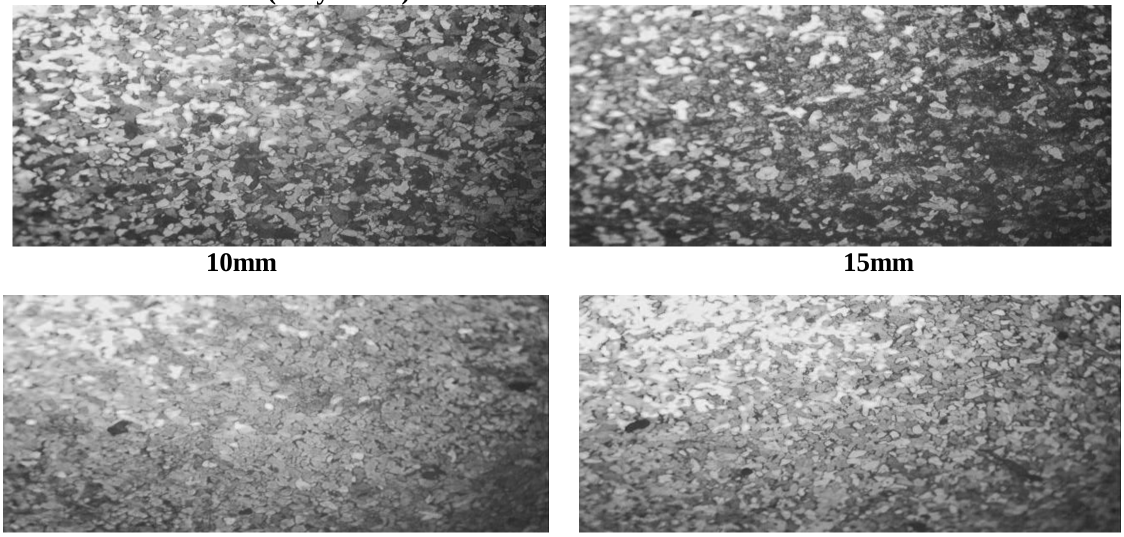

10mm **15mm**

40mm **45mm**

Plate 4: Heat Affected Zone (Salty Water Cooled)

The micrographs presented in this section show the samples cooled in 3.5percent salty in water. The cooling rate is faster than water cooling. The grains are also coarse but it was observed that there is an increase, though minimal, in the amount of pearlite layers. At 10mm and 15mm from the weld zone, martensitic structures were noticed.

3.2.2.3 Weld (water)

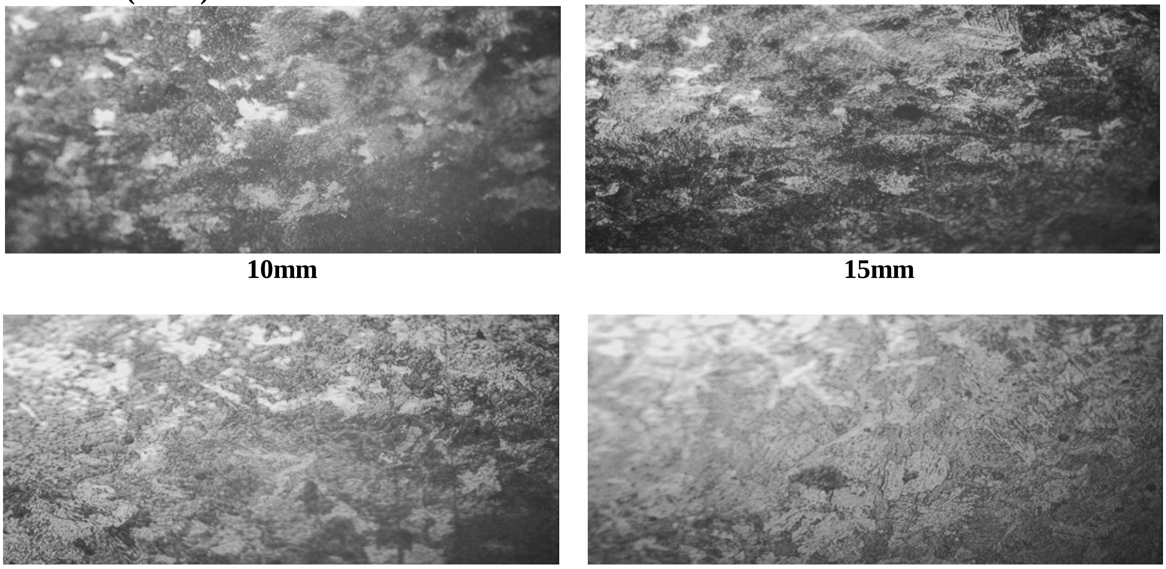

10mm **15mm**

40mm **45mm**

Plate 5: Weld Zone Microstructures (Water Cooled)

Weld zone microstructures when water cooled are presented in plate 5. The grain structures are fine and finger-like. This is because of the rapid cooling rate at the weld zone. The micrographs farther away from the weld show more ferrite structures and some few pearlite layers.

3.2.2.4 Weld (salty water)

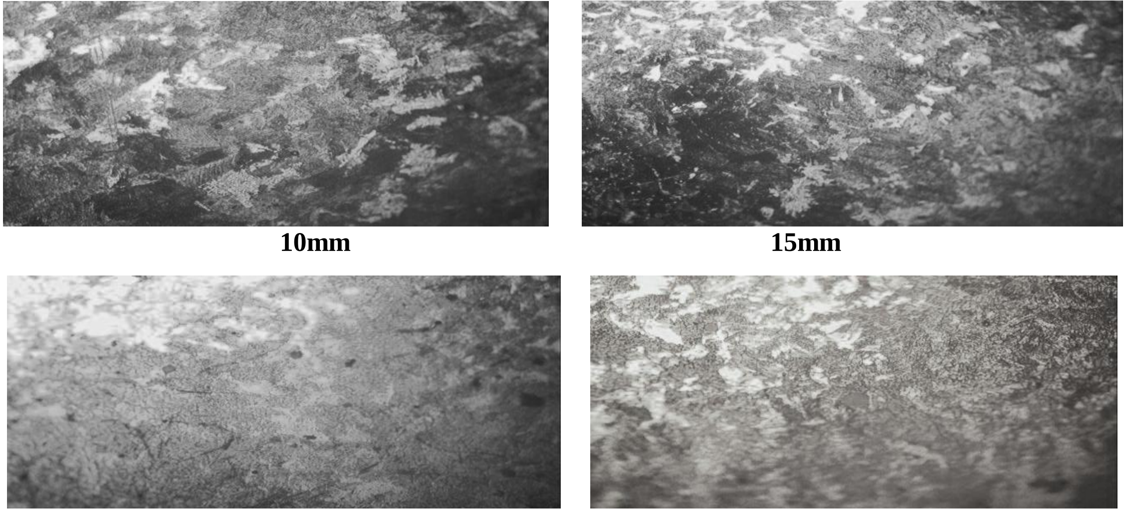

10mm 15mm

40mm 45mm

Plate 6: Weld Zone Microstructures (Salty Water Cooled)

The micrographs above (plate 6), are also fine grained. The microstructure of the 10mm and 15mm samples show some martensitic layers with some pearlite regions. It was observed that the martensite in the water cooled weld micrographs are more evenly dispersed than that of the salty water cooled weld zone micrographs. The microstructures of samples cooled far from the weld zone are also more ferritic. The increase in pearlite and martensite in the salty water cooled samples results in a decrease in their impact strength.

3.2.3 Comparison of Microstructure for the Different Cooling Media

The peak temperature of the weld zone and heat affected zone exceeds the lower critical temperature A_1 (723^0C) as shown in plate 1 to plate 6. Temperature readings were taken at 10mm from fusion zone of the weld. Ferrite, which has a body centred cubic (bcc) structure transforms into austenite (a high temperature phase with face centred cubic (fcc) crystal structure). During the cooling cycle, the austenite transforms back into ferrite or other metastable phases as seen in plate 2.

For low cooling rate as in the air cooled sample, the austenite was observed to transform into ferrite. For higher cooling rates of water and salty water cooled samples, low temperature transformation products like bainite or martensite were formed. The salty water cooled samples had more martensite regions because of the increased cooling rate (see plate 4 and 6). Temperature dropped from 800^0C to 500^0C in 4seconds in salty water cooling compared to 8 seconds for water cooling and 12 seconds in air cooling for the same temperature ranges of 800^0C to 500^0C. As the cooling rate in the weld zone and heat affected zone varied with cooling distance from the fusion zone of the weld, the phases formed from the transformation was observed to also vary with cooling distance. From the impact test results, the coarse grained heat affected zone (CGHAZ) had poor toughness properties compared to the rest of the heat affected zone (HAZ) and unaffected areas of the steel because of the large grain size and high cooling rate in the region.

IV. CONCLUSION

The following conclusions were drawn:

1. The samples cooled with salty water had lower impact strength values possibly due to the formation of martensitic structure after quenching, while, air cooled samples were mostly ferrite. Samples cooled with water had higher impact strength values. Improved toughness values were observed for water cooled samples between 30mm to 45mm cooling distance from the weld zone.
2. Cooling distance between 30mm to 35mm provided optimum impact strength.
3. It was observed that the variations in the microstructures were minimal. This was possibly due to the rapid heat input, very short soaking time during welding and the low carbon content of the material.
4. It was noticed that impact strength of the low carbon steel reduced with increasing cooling rate.
5. Furthermore, the closer the cooling position, the more the cooling effect and the more the mechanical and metallurgical properties were influenced.
6. Wet underwater welding should be avoided in environments containing high salty concentration because of their rapid cooling effect compared to ordinary water.

REFERENCES

[1]. Adedayo, S.M. and Oyatokun, V.O. (2013) Effect of saline water cooling on service quality of a welded AISI 1013 Carbon steel plate. Annals of faculty of engineering Hunedoara-International Journal of Engineering, Tome XI, Fascicule 2

[2]. Akselsen O. M., Fostervoll H. And Ahlen C. H. (2009), Hyperbaric GMA Welding of Duplex Stainless Steel at 12 and 35 bar, Supplement to the Welding Journal, American Welding Society and the Welding Research Council. PP 1-8.

[3]. Calik, A.(2009) Effect of cooling rates on the hardness and microstructure of AISI 1020, AISI 1040, and AISI 1060 steels, International Journal of Physical Sciences Vol.4(9),pp 514-518. Available online at hhtp://www.academicjournals.org/IJPS

[4]. Fonda R. W and Spanos. G (2000) Micrstructural evolution in ultra low carbon steel weldments-Part 1: Controlled thermal cycling and continuous cooling transformation diagram of weld metal. Metallurgical and Materials Transaction. A31A- Pp 2145- 2153

[5]. Fukuoka T. and Fukui S. (1994), Analysis for Cooling Process of Underwater Welding -Comparison with Welding in Air, Bulletin of the M.E.S.J., Vo1. 22, No.2. PP 88-92.

[6]. Ibarra S., Liu S. and Olson D.L., (1995), "Underwater Wet Welding of Steels", Welding Research Council Bulletin, no. 401, PP 1-39.

[7]. Keats D.J. (2009). Underwater Wet Welding Made Simple: Benefits of Hammerhead Wet-Spot Welding Process. International Journal of the Society for Underwater Technology. Vol 28, No 3. doi:10.3723/ut.28.115. PP 115-127.

[8]. Kou S. (2003). Welding Metallurgy. 2nd Edition, John Willey and Sons Inc., U.S.A. PP. 13-30

[9]. Liu H.J., Zhang H.J., and Yu L. (2011). Homogeneity of Mechanical Properties of Underwater Friction Stir Welded 2219-T6 Aluminum Alloy**.** Journal of Materials Engineering and Performance. Volume 20, Issue 8, pp 1419-1422.

[10]. Odusote,J.K., Ajiboye,T.K. and Rabiu,A.B. (2012)Evaluation of Mechanical Properties of Medium Carbon SteelQuenched in Water and Oil AU J.T. 15(4): 218-224 (Apr. 2012)

[11]. Oyetunji A. (2012) Effects of Microstructures and Process Variables on the Mechanical Properties of Rolled Ribbed Medium Carbon Steel Journal of Emerging Trends in Engineering and Applied Sciences (JETEAS) 3 (3):507-512 jeteas.scholarlinkresearch.org Assessed on 28/06/2013

[12]. Poorhaydari K, Patchett B. M., and Ivey D. G. (2005). Estimation of Cooling Rate in the Welding of Plates with Intermediate Thickness, supplement to the welding journal. PP. 4-10

[13]. Shome , M., Gupta, O. P andMohanty, O. N (2004) A modified anatytical approach for modelling grain growth in the coarse grain HAZ of HSLA teels. Scripta Materialla 50: Pp 1007- 1010

OPEN ACCESS

International
Journal
Of Modern Engineering Research (IJMER)

Mechanical Properties Of Sisal And Pineapple Fiber Hybrid Composites Reinforced With Epoxy Resin

Vikas Sahu[1], Keshav Singh Bisen[2], Murali Krishna[3]
[1&2]PG Student, Mechanical Engineering Department, GGITS,JBP
[3]Associate Professor, Mechanical Engineering Department, GGITS,JBP

ABSTRACT: *In this study, Work has been carried out to investigated tensile , bending and impact properties of hybrid composite of material constitutes sisal fiber and less discovered pineapple fiber. These composites are adhered using epoxy resin cosists HY951 resin and LY551 hardener suitably mixed in appropriate volume. Hybrid composites were prepared using sisal/pineapple fibers of 100/0, 70/30, 50/50, 30/70, and 0/100 Weight fraction ratios, while overall fiber weight fraction was fixed as 20gram. Here for preparing samples Hand lay up method is used , specimens are prepared , fibers are arrenged in unidirectional manner and tests are carried out , which shows tensile and bending strengths. The tensile & compressive test was applied on specimens of 300×50 & thickness varring from 4-6 mm in dimensions but in different proportions of sisal and pineapple by weight. The test result shows , the composite made by 50/50 fibers weight fraction of sisal & pineapple fiber has been shown best impact strenght 47.2 N/mm^2 as compare to other constitutes of sisal & pine fibers.this constitute have good tensile & bending strength & their density is also less than sisal fibers. These composites can be used in various purposes because of its unique features of recycleability, waste utilization, environment friendly, bio-degradibility, good strength and a good alternative to plastics.*

Keywords: *Composites, Bio-degradability, pine, sisal, resin, recyclability.*

I. INTRODUCTION

Now a day reinforced polymer composite become more popular for their variety of applications because of their high specific strength and light weight. Most of the materials are available in market which are made by the synthetic fiber .These fibers have serious drawbacks as high density, non-renewability, non-biodegradability, high energy consumption etc .Growing environmental awareness and societal concern, a high rate of depletion of petroleum resources, the concept of sustainability, and new environmental regulations have triggered the search for new products that are compatible with the environment. Due to that concern many of researchers are working on the field of natural fiber reinforced composite. The reason of attraction of that field over the traditionally using synthetic fiber is that, natural fibers having low density, high toughness, environment friendly, fully biodegradable , renewable, low cost. The biodegradability of plant fibers can contribute a healthy ecosystem while their low cost & high performance fulfils the economic interest of industries. India, endowed with an abundant availability of natural fibers such as jute, coir, sisal, pineapple, ramie, bamboo, banana etc., have focused on the development of natural fiber composites primarily to explore value-added application avenue.

One such fiber source known for a long time is pineapple leaves from which pineapple leaf fibers (PALF) may be extracted. Pineapple is the third most important tropical fruit in the world after banana and citrus. Due to development of fruit production industries like jam industries, production of pineapple fiber is increases. Earlier this pineapple fiber is residual waste in these industries, but now a days, due to its good appearance in color it is using in the textile industries .Sisal fiber is a promising reinforcement for use in composites on account of its low cost, low density, high specific strength and modulus, no health risk, easy availability in some countries and renewability. Sisal is a natural fiber is a yield, stiff fiber traditionally used in making twine and rope. It is a biodegradable and eco-friendly crop. Moreover, sisal is a strong, stable and versatile material and it has been recognized as an important source of fiber for composites. Sisal fiber made from the large spear shaped tropical leaves of the Agave Sisalana plant. In recent years, there has been an increasing interest in finding new applications for sisal-fiber reinforced composites that are traditionally used for making ropes, mats, carpets, fancy articles and others. Epoxy resin is a thermosetting resin , it is made of tightly linked adhesive polymer structure that are often used in surface coating. For the fiber reinforced polymer Epoxy resin is used as the matrix to efficiently hold the fiber in place.

In recent years researcher has shown their interest in the hybrid composite of natural & synthetic fibers. C. Grisha et al. (2012) investigate the tensile properties of hybrid composites made by reinforcing sisal, coconut spathe and ridge gourd as the new natural fibers into epoxy resin matrix. The composites fabricated consist of reinforcement in the hybrid combination like sisal-coconut spathe, sisal-ridge gourd and coconut spathe-ridge gourd with the weight fraction of fibers varying from 5% to 30%. The hybridization of the reinforcement in the composite shows greater tensile strength when compared to individual type of natural fibers reinforced. It is found that for the hybrid combination of ridge guard and sisal fibers there is 65% increase in the tensile strength. J Madhukiran et al (2013) investigated the mechanical properties like tensile & flexural strengths on the hybrid banana & pineapple fibers epoxy composite. Hybrid composites were prepared using banana/pineapple fibers in different weight ratio. The hybridization of these natural fibers has provided considerable improvement of flexural strength when compared to individual reinforcement. This work also demonstrates the potential of the hybrid natural fiber composite materials for use in a number of consumable goods.

To make further improvement in the field of natural fiber hybrid composites in this present investigation sisal & pineapple fiber hybrid composites of different fiber weight ratio has been prepared & evaluate the different mechanical properties of this hybrid composite.

II. LITERATURE REVIEW

Due to the world wide availability of sisal and pineapple fibers many researchers have begin to focus on these fibers. Some researchers are taking individual fibers for research & some had taken combinations of these fibers with other synthetic and natural fibers for the research work. N. Netrawali & S. Luo(1999) were prepared composite of pineapple fiber and PHBV resin of different fiber weight ratio wary from 20% to 30%. The tensile and flexural properties of these were tested & make a comparative study of these results with different types of wood specimens. Kuruvilla joseph et al.(1999) were make study of sisal reinforced polymer composites & they suggest, due to the low density & high specific properties sisal can be use in the automobile industries & sisal fiber composites can become good alternative material of wood in the building construction. JB Zhong et al.(2007) alkali treated sisal fibers were used for reinforcement & for the matrix phase urea-formaldehyde has been used for making composites. No. of specimen of different weight ratio of fiber has been prepared & different test impact, tensile & water absorption test has been performed over the specimens..V. Naga Prasad et al. (2011) were prepared sisal-glass fiber hybrid composites with the help of unsaturated polystyrene. The mechanical properties of like impact strength, compressive strength & tensile strength of sisal fiber, glass fiber & sisal-glass hybrid composite has been tested & made a comparative study between these properties of composites. The effect of chalk powder on compressive and impact strength of sisal/glass fiber hybrid composite has also been studied and it is observed. M. Boolan et al. (2012) were to investigate and compare the mechanical properties of raw jute and sisal fiber reinforced epoxy composites with sodium hydroxide treated jute and sisal fiber reinforced epoxy composites. The mechanical properties (tensile and flexural strength), water absorption and morphological changes were investigated for the composite samples. B Vinod & LJ Sukhdev (2013), were investigated the effect of orientation on the flexural strength of PALF reinforced bisphenol composite. Composites were made by using different fiber length . It was observed that the fiber length greatly influences the tensile properties of reinforced composites. A higher tensile strength of 36.36Mpa was obtained for the fiber length of 9mm compared to the fiber length of 3, 6 and 12mm. M.Sakthive & S.Ramesh (2013) were made a comparative study between banana, sisal & coir fiber. They prepared rectangular samples as per ASTM standard & then performed hardness test, impact charpy test & flexural test has been performed. From the testing results they suggest these fibers can be used in the automotive seat shell making.

III. MATERIALS AND EXPERIMENTAL METHODOLOGY

3.1 Materials

Two vegetable fibers were investigated: sisal and pineapple , For the matrix phase epoxy resin (Lapox HY 951) & Hardener (Lapox LY 556)is used for bonding the fibers .A mould of rectangular tube shape with 50 mm constant width and variable thickness is made in the college workshop. The sample piece obtained by this mould has constant 50 mm width & its thickness can be vary according to volume of fibers.

3.2 Sample Preparation

The testing samples are made by hand layup method. For sample preparation both sisal and pineapple fiber are cut into length of 28mm-30mm.these fiber are equally weighted into five groups i.e. sisal 100% with 0% pineapple ,sisal70% with pine30%, sisal50% with pine50%,sisal 30% with pine70% & 100 % pine apple fiber. Resin and hardener both mixed together in 4:5 respectively. Then mould is cleaned by brush and covered the mould by thin plastic film to avoid bonding between mould and sample pieces. After making the fiber straight resin and hardener mixture applied over the fibers layer to make the bunch of fibers. Fibers bunch is transfer to the mould and press that bunch with 20 kg load. The castings were allowed to cure for 24hrs at room temperature. The composite is released from mould and these composites are ready for testing. Then after composites releasing these composites are relief for 3-4 days then these was tested on computerized UTM & impact testing machine.

3(a) Pineapple fiber

3(b) Sisal fiber

3(d) Sisal & pine samples

3(d) Composite weight taking

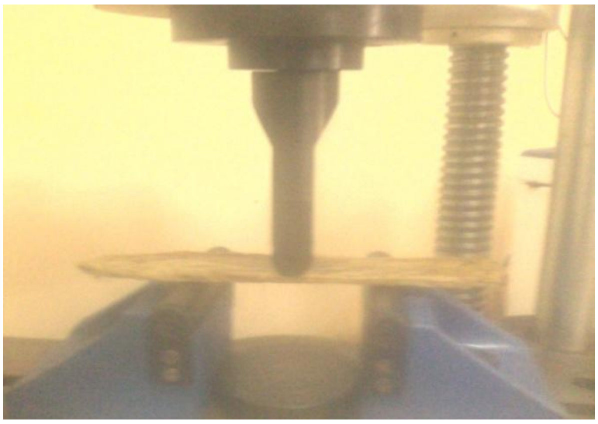

3(e) Bending test

3(f) Tensile test

3.3 Testing

3.3.1 Tensile test

Tensile test has been performed on tensile testing machine. Rectangular samples of size length 300 mm, width 50 mm & thickness 4-6 mm is used for tensile testing. The testing is done over 5 different types of sisal and pineapple fibers composite on the tensile testing machine. This tensile test is performed at load rate of 0.333KN per second. As shown in figure 100% sisal fiber weight composite shows maximum tensile strength while in case of pure pineapple samples the tensile strength is minimum. In the sisal and pineapple mix composites the tensile strength is increases with the increase in sisal fiber composition in the testing samples. But due to increase in sisal fiber percentage the density of the testing samples is also increased.

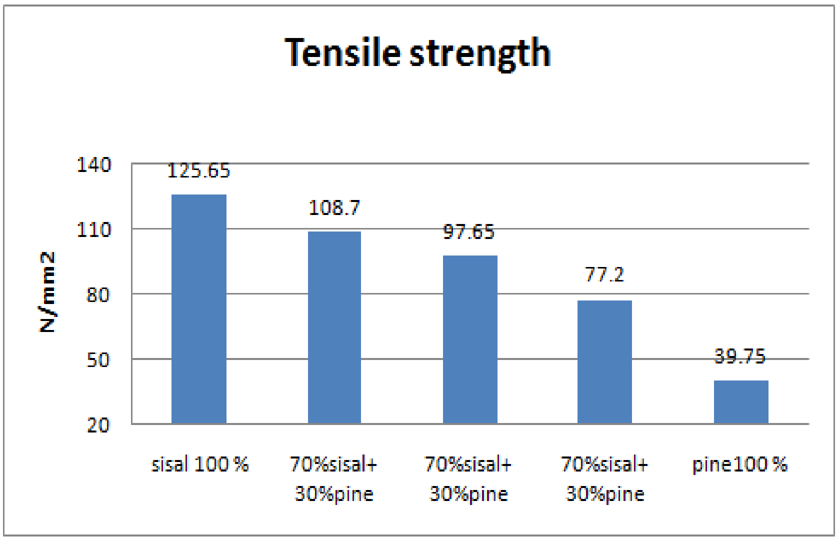

Fig.1 Tensile strength comparison graph

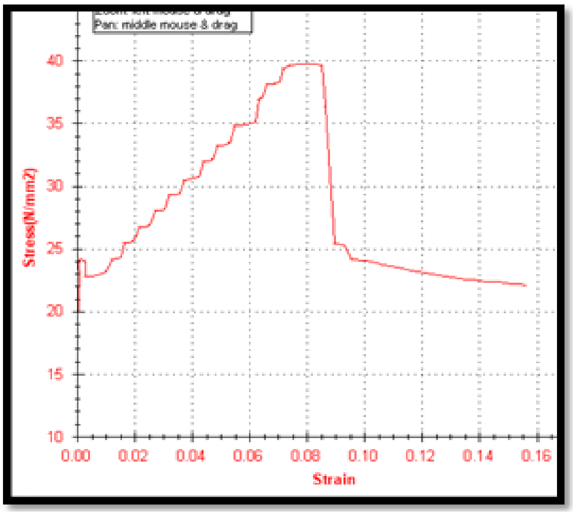

Fig2- Tensile test graph of Pure pine composite

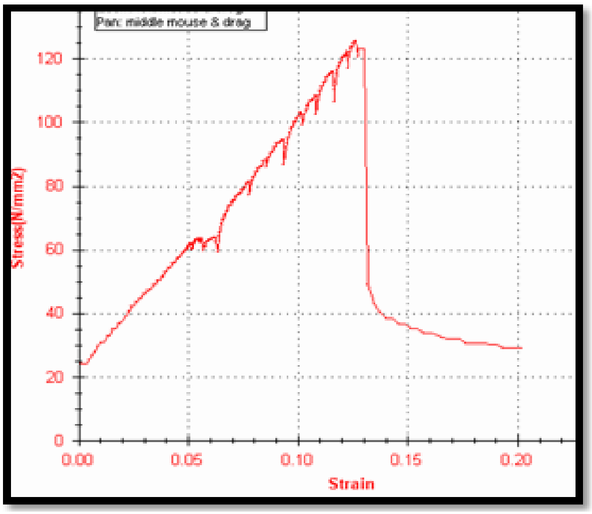

Fig 3-Tensile test graph of Pure sisal composite

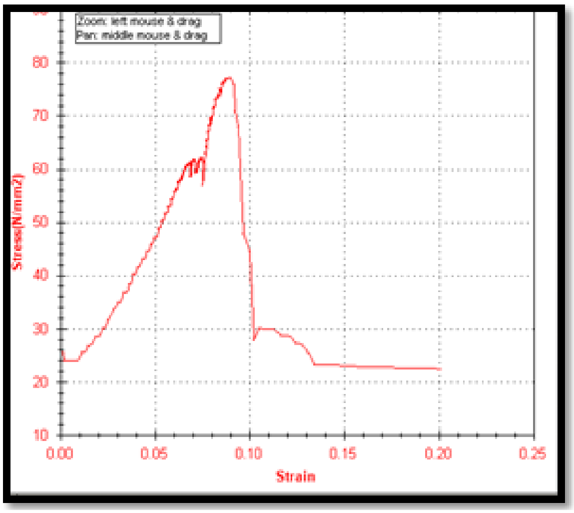

Fig 4- Tensile test graph of30% sisal+70% pine composite

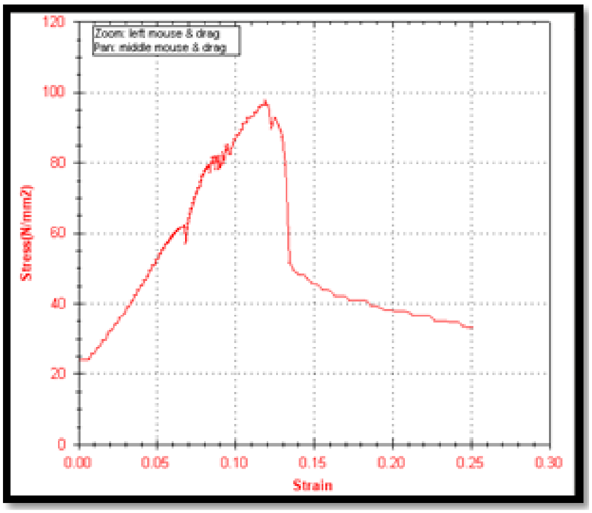

Fig 5- Tensile test graph of 50% sisal+50% pine composite

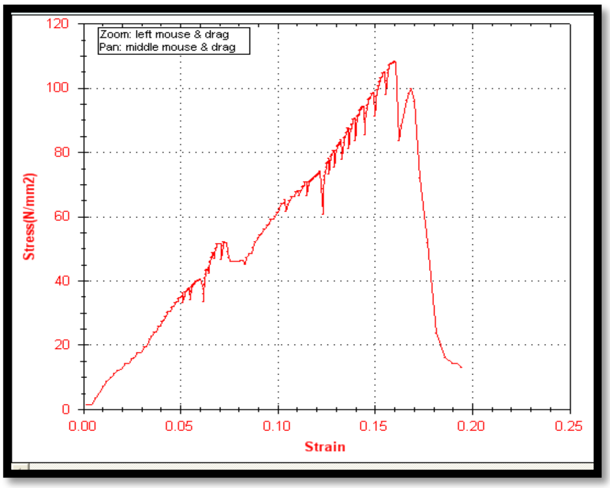

Fig 6- Tensile test graph of 70% sisal+30% pine composite

3.3.2 Bending test

Tensile test has been performed on computerized UTM .The long length rectangular flat composites have been tested. The composites had be hold over the two supports, the distance between supports had been maintain the twenty times of the width of the composites. Single point bending test is performed over the rectangular sample on the testing machine . A load rate of 0.333KN per second is applied for bending test. As the result it is observed that the sisal fiber composite has maximum bending strength with higher density and with the increase in the sisal fiber percentge the bending strength of fibers also increases.

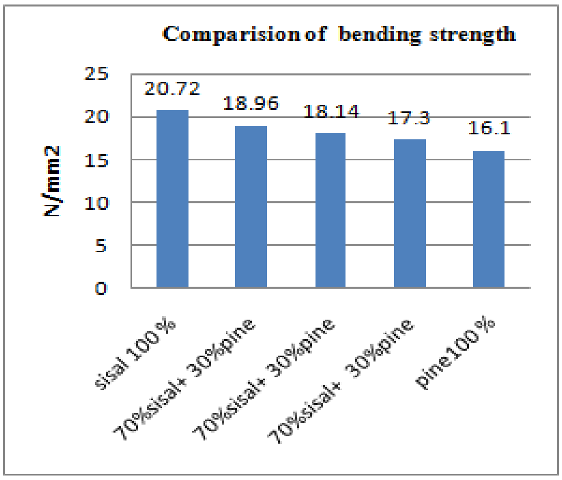

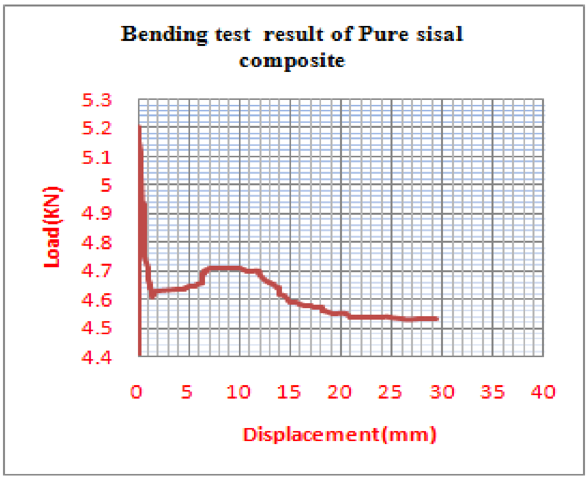

Fig. 7 **Fig. 8**

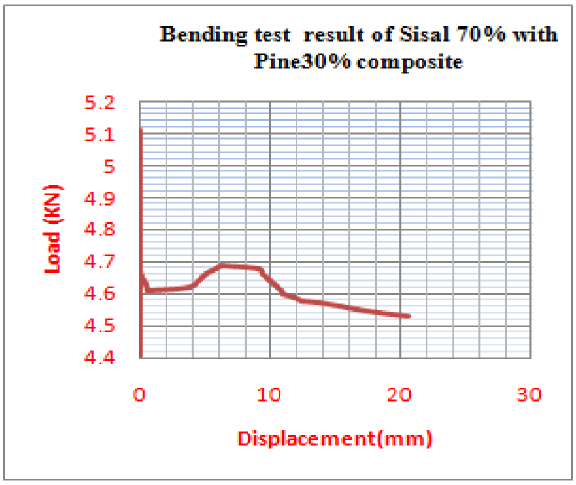

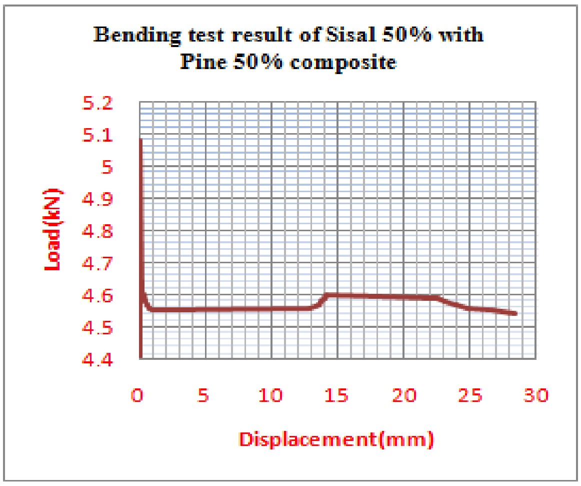

Fig. 9 **Fig. 10**

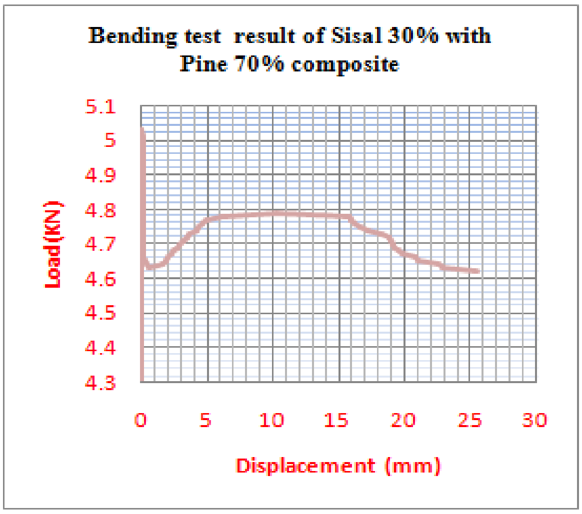

Fig. 11

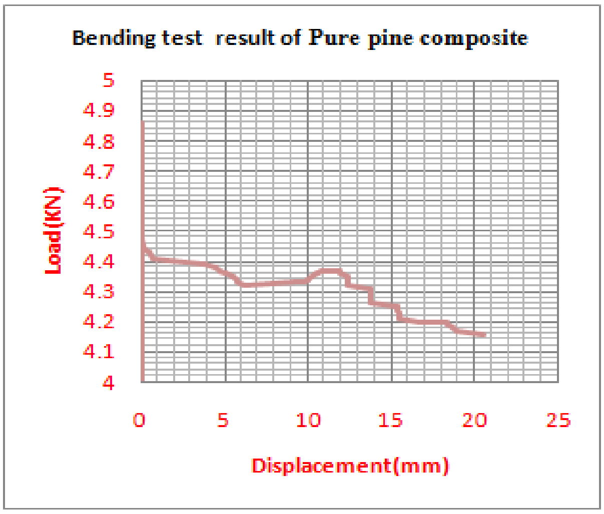

Fig. 12

3.3.3 Impact test

The impact test is performed over the samples of length 55 mm, width 10 mm & thickness is used 5.5 mm. Since fibers are arranged fibers longitudinally that's by Charpy test has been performed on the samples. Impact test had performed on manual impact machine. It has been observed that pure sisal composite is showing lower strength than the other composite & pure pine composite also showing also showing low strength as compare to sisal & pine mix composite. Sisal 50%+pine 50% mix composite is showing the maximum strength.

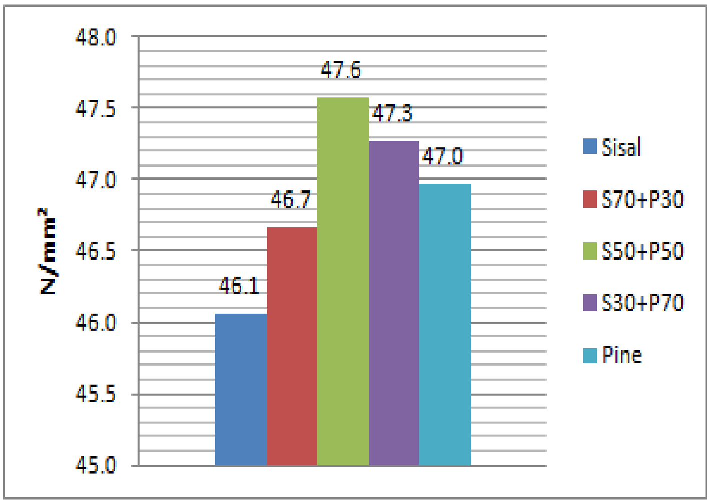

Fig. 13 Impact strength comparison graph

IV. Results and discussion

The mechanical properties like impact strength, bending strength & tensile strength has been tested on five different samples of sisal, pine & sisal-pine mix fiber composite. These results have been observed from the tensile, bending &impact testing.

S.No.	Reinforced Composites	Weight of composite (gm)	Length of composite (cm)	Width of composite (cm)	Thickness of composite (cm)	Density gm/cm³	Tensile strength (N/mm^2)	Bending strength (N/mm^2)	Impact strength (N/mm^2)
1	**Sisal 100 %**	**65**	**31.7**	**5**	**0.38**	**1.08**	**125.65**	**20.72**	**46.1**
2	**70%sisal + 30%pine**	**63**	**31**	**5**	**0.42**	**0.97**	**108.7**	**18.96**	**46.7**
3	**50%sisal + 50%pine**	**63**	**31.5**	**5**	**0.46**	**0.87**	**97.65**	**18.14**	**47.6**
4	**30%sisal + 70%pine**	**62**	**31**	**5**	**0.5**	**0.80**	**77.2**	**17.3**	**47.3**
5	**Pine100 %**	**60**	**30.5**	**5**	**0.55**	**0.72**	**39.75**	**16.1**	**47**

Table 1: Properties of composite

The composite made by sisal fiber having higher tensile & bending strength is maximum, but its Density also high. The composite made by pineapple fiber having lower tensile & bending strength, but its density is low. The composite made by mixing sisal & pineapple fiber, having tensile & bending strength is higher than the pineapple fiber, but lower than the composite made by sisal fiber. In which the percentage of sisal fiber is increase so that the tensile & bending strength are also high.

But in case of impact testing the impact strength of sisal fiber is lower as compare to the composite of pure pine & sisal- pine mix composites. The impact testing results shows that the sisal-pine mix composite showing more better impact strength as compare to the pure sisal & pure pine mix composite. The composite in which sisal & pine mix 50-50 percent that composite shows the maximum impact strength.

V. CONCLUSION

Polymer matrix composite contains the sisal & pine fibers as the reinforcement phase was successfully fabricated by different proportions of weight of fibers .The material properties of fabricated sisal & pine fibers reinforced composites were observed. It is found that

1. In increase of the percentage of sisal fibers increases the tensile & bending strength of sisal-pine fibers composite, but it also increases the density of composite.
2. In increase of the percentage of pine fiber help to reduce the density of the composite & by the addition of pine fiber the impact strength of the composites also improved.
3. The hybrid composite made by sisal & pine by using different weight ratio are showing the good strength to weight ratio as compare to their individual constituents composite.
4. These different hybrid composites can become good replacement of traditionally using synthetic fibers.
5. Composite made by 50% sisal with 50% pine have maximum impact strength (47.6 N/mm^2) & it is also shows good tensile & bending strength.

These composites can be use in the fabrication of polymer sheets, pipes, furniture & to make pallet box for storing goods in the industrial applications.

REFERENCES

[1]. J Madhukiran et al (2013), Fabrication and Testing of Natural Fiber Reinforced Hybrid Composites Banana/Pineapple, IJMER Vol.3.

[2]. M.Sakthive & S.Ramesh (2013), Mechanical Properties of Natural Fiber (Banana, Coir, Sisal) Polymer Composites, Science park Vol.1.

[3]. B Vinod & LJ Sukhdev (2013), Effect of Fiber Orientation on the Flexural Properties of PALF Reinforced Bisphenol Composites, IJEBEA Volume 2.

[4]. C. Grisha et al. (2012), Tensile properties of natural fiber-reinforced epoxy-hybrid composites, IJMER Vol. 2.

[5]. M. Boolan et al. (2012), A Comparative Study on the Mechanical Properties of Jute and Sisal Fiber Reinforced Polymer Composites, Springer Science.

[6]. V. Naga Prasad et al. (2011), Compressive & impact properties of sisal/glass fiber reinforced hybrid composites, International Journal of Fiber and Textile Research.

[7]. JB Zhong et al.(2007), Mechanical properties of sisal fibre reinforced ureaformaldehyde resin composites, eXPRESS Polymer Letters.

[8]. Kuruvilla joseph et al.(1999), A Review On Sisal Fiber Reinforced Polymer Composites, R. Bras. Eng. Agríc. Ambiental, Campina Grande, vol.3.

[9]. N. Netrawali & S. Luo(1999) ,Interfacial & mechanical properties of envoirment friendly “green composite” made from pineapple fibers, Journal of material science.

OPEN ACCESS

International
Journal
Of Modern Engineering Research (IJMER)

Between δ-I-closed sets and g-closed sets

M. Navaneethakrishnan[1], P. Periyasamy[2], S. Pious Missier[3]
[1]*Department of Mathematics, Kamaraj College, Thoothukudi, Tamilnadu, India.*
[2]*Department of Mathematics, Kamaraj College, Thoothukudi, Tamilnadu, India.*
[3]*Department of Mathematics, V.O.Chidambaram College, Thoothukudi, Tamilnadu, India.*

ABSTRACT: *In this paper we introduce a new class of sets known as* $\hat{\delta}_S$ *–closed sets in ideal topological spaces and we studied some of its basic properties and characterizations. This new class of sets lies between δ–I–closed [19] sets and g–closed sets, and its unique feature is it forms topology and it is independent of open sets.*

Keywords and Phrases: $\hat{\delta}_S$ *–closed,* $\hat{\delta}_S$ *–open,* $\hat{\delta}_S$ *–closure,* $\hat{\delta}_S$ *–interior.*

I. INTRODUCTION

An ideal I on a topological space (X,τ) is a non empty collection of subsets of X which satisfies (i) $A\in I$ and $B\subset A$ implies $B\in I$ and (ii) $A\in I$ and $B\in I$ implies $A\cup B\in I$. A topological space (X,τ) with an ideal I is called an ideal topological space and is denoted by the triplet (X, τ, I). In an ideal space if $P(X)$ is the set of all subsets of X, a set operator $(.)^*: P(X) \to P(X)$, called a local function [22] of a with respect to the topology τ and ideal I is defined as follows: for $A\subseteq X$, $A^*(X,\tau) = \{x\in X / U \cap A \notin I, \text{ for every } U\in\tau(x)\}$ where $\tau(x) = \{U\in\tau / x\in U\}$. A kuratowski closure operator $cl^*(.)$ for a topology $\tau^*(I,\tau)$, called the $*$–topology, finer than τ is defined by $cl^*(A)=A\cup A^*(I,\tau)$ [23]. Levine [5], velicko [13], Julian Dontchev and maximilian Ganster [3], Yuksel, Acikgoz and Noiri [14], M.K.R.S. Veerakumar [12] introduced and studied g–closed, δ–closed, δg–closed; δ-I–closed and $\hat{g}$ – closed sets respectively. In 1999, Dontchev [16] introduced Ig–closed sets and Navaneetha Krishnan and Joseph [26] further investigated and characterized Ig–closed sets. The purpose of this paper is to define a new class of closed sets known as $\hat{\delta}_S$–closed sets and also studied some of its basic properties and characterizations.

II. PRELIMINARIES

Definition 2.1. A subset A of a topological space (X, τ) is called a
(i) Semi-open set [10] if $A\subseteq cl(int(A))$
(ii) Pre-open set [13] if $A\subseteq int(cl(A))$
(iii) α - open set [1] if $A\subseteq int(cl(int(A)))$
(iv) regular open set[15] if $A = int(cl(A))$

The complement of a semi-open (resp. pre-open, α - open, regular open) set is called Semi-closed (resp. pre-closed, α - closed, regular closed). The semi-closure (resp. pre closure, α-closure) of a subset A of (X, τ) is the intersection of all semi-closed (resp. pre-closed α-closed) sets containing A and is denoted by $scl(A)$ (resp.$pcl(A)$, $\alpha cl(A)$). The intersection of all semi-open sets of (X,τ) contains A is called semi-kernel of A and is denoted by $sker(A)$.

Definition 2.2. [18] A subset A of (X,τ) is called δ - closed set in a topological space (X, τ) if $A = \delta cl(A)$, where $cl_\delta(A) = \delta cl(A) = \{x\in X : int(cl(U))\cap A\neq\phi, U\in\tau(x)\}$. The complement of δ - closed set in (x, τ) is called δ- open set in (X, τ).

Definition 2.3. [19] Let (X, τ, I) be an ideal topological space, A a subset of X and x a point of X.
(i) x is called a δ-I-cluster point of A if $A \cap int(cl^*(U)) \neq \phi$ for each open neighborhood of x.
(ii) The family of all δ-I-cluster points of A is called the δ-I-closure of A and is denoted by $[A]_{\delta\text{–}I}$ and
(iii) A subset A is said to be δ-I-closed if $[A]_{\delta\text{–}I} = A$. The complement of a δ-I - closed set of X is said to be δ-I - open.

Remark 2.4. From Definition 2.3 it is clear that $[A]_{\delta\text{–}I} = \{x\in X : int(cl^*(U)) \cap A\neq \phi, \text{ for each } U\in\tau(x)\}$

Notation 2.5. Throughout this paper $[A]_{\delta\text{–}I}$ is denoted by $\sigma cl(A)$.

Lemma 2.6. [19] Let A and B be subsets of an ideal topological space (x, τ, I). Then, the following properties hold.

(i) $A \subseteq \sigma cl(A)$

(ii) If $A \subset B$, then $\sigma cl(A) \subset \sigma cl(B)$

(iii) $\sigma cl(A) = \cap\{F \subset X \,/\, A \subset F$ and F is δ-I-closed$\}$

(iv) If A is δ-I-closed set of X for each $\alpha \in \Delta$, then $\cap\{A\alpha \,/\, \alpha \in \Delta\}$ is δ - I - closed

(v) $\sigma cl(A)$ is δ-I- Closed.

Lemma 2.7. [19] Let (X, τ, I) be an ideal topological space and $\tau_{\delta\text{-}I} = \{A \subset X \,/A$ is δ-I-open set of $(X, \tau ,I)\}$. Then $\tau_{\delta\text{-}I}$ is a topology such that $\tau_s \subset \tau_{\delta\text{-}I} \subset \tau$

Remark 2.8. [19] τ_s (resp. $\tau_{\delta\text{-}I}$) is the topology formed by the family of δ-open sets (resp. δ-I - open sets)

Lemma 2.9. Let (X, τ, I) be an ideal topological space and A a subset of X. Then $\sigma cl(A) = \{x \in X : int(cl^*(U)) \cap A \neq \phi, U \in \tau(x)\}$ is closed.

Proof: If $x \in cl(\sigma l(A))$ and $U \in \tau(x)$, then $U \cap \sigma cl(A) \neq \phi$. Then $y \in U \cap \sigma cl(A)$ for some $y \in X$. Since $U \in \tau(y)$ and $y \in \sigma cl(A)$, from the definition of $\sigma cl(A)$ we have $int(cl^*(U)) \cap A \neq \phi$.Therefore $x \in \sigma cl(A)$, and so $cl(\sigma cl(A)) \subset \sigma cl(A)$ and hence $\sigma cl(A)$ is closed.

Definition 2.10. A subset A of a topological space (X, τ) is called

(i) a generalized closed (briefly g-closed) set [9] if $cl(A) \subseteq U$ whenever $A \subseteq U$ and U is open in (X, τ).

(ii) a generalized semi-closed (briefly sg-closed) set [3] if $scl(A) \subseteq U$ whenever $A \subseteq U$ and U is semi-open in (X, τ).

(iii) a generalized semi-closed (briefly gs-closed) set [2] if $scl(A) \subseteq U$ whenever $A \subseteq U$ and U is open in (X, τ).

(iv) a generalized closed (briefly αg-closed) set [12] if $\alpha cl(A) \subseteq U$ whenever $A \subseteq U$ and U is open in (X, τ).

(v) a generalized α-closed (briefly gα-closed) set [12] if $\alpha cl(A) \subseteq U$ whenever $A \subseteq U$ and U is α- open in (X, τ).

(vi) a δ– generalized closed (briefly δg -closed) set [4] if $\delta cl(A)) \subseteq U$ whenever $A \subseteq U$ and U is open in (X, τ).

(vii) a $\hat{g}$ – closed set [17] is $cl(A) \subseteq U$ whenever $A \subseteq U$ and U is semi open.

(viii) a $\delta\hat{g}$ - closed set [8] if $cl_\delta(A) \subseteq U$, whenever $A \subseteq U$ and U is $\hat{g}$ -open set in (X, τ)

The complement of g–closed (resp. sg–closed, gs–closed, αg–closed, gα– closed, δg–closed, $\hat{g}$–closed, $\delta\hat{g}$–closed) set is called g–open (resp.sg – open, gs–open, αg–open, gα– open, δg–open, $\hat{g}$–open, $\delta\hat{g}$–open).

Definition 2.11. A subset A of an ideal space (X, τ, I) is called

(i) Ig-closed set [5] if $A^* \subseteq U$, whenever $A \subseteq U$ and U is open. The complement of Ig-closed set is called Ig-open set.

(ii) R-I-open [19] set if $int(cl^*(A)) = A$. The complement of R- I-open set is R-I-closed

III. $\hat{\delta}_S$ - CLOSED SETS

In this section we introduce the notion of $\hat{\delta}_s$ - closed sets in an ideal topological space (X, τ, I), and investigate their basic properties.

Definition 3.1. A subset A of an ideal topological space (X, τ, I) is called $\hat{\delta}_S$-closed if $\sigma cl(A) \subseteq U$, whenever $A \subseteq U$ and U is semi-open set in (X, τ, I). The complement of $\hat{\delta}_S$-closed set in (X, τ, I), is called $\hat{\delta}_S$-open set in (X, τ, I).

Theorem 3.2. Every δ-closed set is $\hat{\delta}_S$-closed set.

Proof: Let A be any δ-closed set and U be any semi-open set containing A. Since A is δ - closed, $cl_\delta(A) = A$. Always $\sigma cl(A) \subseteq cl_\delta(A)$. Therefore A is $\hat{\delta}_S$-closed set in (X, τ, I).

Remark 3.3. The converse is need not be true as shown in the following example.

Example 3.4. Let $X = \{a,b,c\}$, $\tau = \{X, \phi, \{b\}, \{a,b\}, \{b,c\}, \{a,b,c\}, \{a,b,d\}\}$ and $I = \{\phi, \{c\},\{d\}, \{c,d\}\}$. Let $A = \{a,c,d\}$ then A is $\hat{\delta}_S$-closed but not δ-closed.

Theorem 3.5. Every δ-I – closed set is $\hat{\delta}_S$-closed.

Proof: Let A be any δ - I-closed set and U be any semi-open set such that $A \subseteq U$. Since A is δ-I-closed, $\sigma cl(A)=A$ and hence A is $\hat{\delta}_S$-closed.

Remark 3.6. The following example shows that, the converse is not always true.

Example 3.7. Let $X=\{a,b,c,d\}$, $\tau=\{X, \phi, \{b\}, \{c\}, \{b,c\}\}$ and $I = \{\phi\}$. Let $A = \{a,c,d\}$. Then A is $\hat{\delta}_S$-closed set but not δ-I-closed.

Theorem 3.8. In an ideal topological space (X,τ,I), every $\hat{\delta}_S$-closed set is
(i) $\hat{g}$ - closed set in (X, τ)
(ii) g – closed (resp.gα, αg, sg, gs) – closed set in (X, τ).
(iii) Ig – closed set in (X,τ,I).

Proof. (i) Let A be a $\hat{\delta}_S$-closed set and U be any semi-open set in (X, τ, I) containing A. since A is $\hat{\delta}_S$-closed, $\sigma cl(A)\subseteq U$. Then $cl(A)\subset U$ and hence A is $\hat{g}$ - closed in (X, τ).
(ii) By [17], every $\hat{g}$ – closed set is g – closed (resp.gα – closed, αg – closed, sg – closed, gs – closed) set in (X, τ, I). Therefore it holds.
(iii) Since every g – closed set is Ig – closed, It holds.

Remark 3.9. The following example shows that the converse of (i) is not always true.

Example 3.10. Let $X = \{a,b,c,d\}$, $\tau = \{X, \phi,\{b\},\{a,b\},\{b,c\},\{a,b,c\},\{a,b,d\}\}$ and $I = \{\phi,\{b\}\}$. Let $A = \{c,d\}$, Then A is $\hat{g}$ – closed set but not $\hat{\delta}_S$-closed.

Remark 3.11. The following examples shows that the converse of (ii) is not true.

Example 3.12. Let $X = \{a,b,c,d\}$, $\tau = \{X, \phi,\{c\}, \{c,d,\}\}$ and $I = \{\phi,\{c\},\{d\},\{c,d\}\}$. Let $A = \{b,d\}$. Then A is g-closed, αg-closed, gα - closed but not $\hat{\delta}_S$-closed.

Example 3.13. Let $X = \{a,b,c,d\}$, $\tau = \{X, \phi, \{a\}, \{b\}, \{a,b\}, \{a,b,d\}\}$ and $I = \{\phi, \{a\}, \{c\}, \{a,c\}\}$. Let $A = \{a,d\}$. Then A is gs – closed and sg – closed but not $\hat{\delta}_S$-closed.

Remark 3.14. The following example shows that the converse of (iii) is not always true.

Example 3.15. Let $X = \{a,b,c,d\}$, $\tau = \{X, \phi, \{a\}, \{b\}, \{a,b\}\}$ and $I = \{\phi\}$. Let $A = \{a,b,c\}$. Then A is Ig - closed set but not $\hat{\delta}_S$-closed.

Remark 3.16. The following examples shows that $\hat{\delta}_S$-closed set is independent of closed, α-closed, semi-closed, δg – closed, $\delta\hat{g}$ – closed.

Example 3.17. Let $X = \{a,b,c,d\}$, $\tau = \{X, \phi,\{b\},\{a,b\},\{b,c\},\{a,b,c\},\{a,b,d\}\}$ and $I = \{\phi,\{a\},\{c\},\{a,c\}\}$. Let $A = \{a,d\}$. Then A is closed, semi-closed but not $\hat{\delta}_S$-closed.

Example 3.18. Let $X = \{a,b,c,d\}$, $\tau = \{X, \phi,\{a\},\{b,c\},\{a,b,c\}\}$ and $I = \{\phi,\{b\}\}$. Let $A = \{a,b,d\}$. Then A is $\hat{\delta}_S$-closed but not closed, semi-closed.

Example 3.19. Let $X=\{a,b,c,d\}$, $\tau = \{X,\phi, \{a\}, \{b\}, \{a,b\}\}$ and $I=\{\phi, \{c\}\}$. Let $A=\{b,d\}$. Then A is δg closed, $\delta\hat{g}$ - closed but not $\hat{\delta}_S$-closed.

Example 3.20. Let $X = \{a,b,c,d\}$, $\tau = \{X, \phi, \{c\}, \{a,c\}, \{b,c\}, \{a,b,c\}, \{a,c,d\}\}$ and $I = \{\phi, \{c\}\}$. Let $A=\{a,d\}$. Then A is $\hat{\delta}_S$-closed but not δg - closed, $\delta\hat{g}$ -closed.

Example 3.21. Let $X=\{a,b,c,d\}$, $\tau = \{X,\phi, \{b\},\{b,c\}\}$ and $I = \{\phi\}$. Let $A=\{c,d\}$. Then A is α-closed but not $\hat{\delta}_S$-closed.

Example 3.22. Let $X=\{a,b,c,\}$, $\tau = \{X,\phi, \{b,c\}\}$ and $I = \{\phi\}$. Let $A=\{a,c\}$. Then A is $\hat{\delta}_S$-closed but not α-closed.

IV. CHARACTERIZATIONS

In this section we characterize $\hat{\delta}_S$-closed sets by giving five necessary and sufficient conditions.

Theorem 4.1. Let (X, τ, I) be an ideal space and A a subset of X. Then $\sigma cl(A)$ is semi-closed.

Proof **:** Since $\sigma cl(A)$ is closed, it is semi-closed.

Theorem 4.2. Let (X, τ, I) be an ideal space and $A\subseteq X$. If $A\subseteq B\subseteq \sigma cl(A)$ then $\sigma cl(A)= \sigma cl(B)$.

Proof**:** Since $A\subseteq B$, $\sigma cl(A) \subseteq \sigma cl(B)$ and since $B\subseteq \sigma cl(A)$, then $\sigma cl(B) \subseteq \sigma cl(\sigma cl(A))= \sigma cl(A)$, By Lemma 2.6. Therefore $\sigma cl(A)= \sigma cl(B)$.

Theorem 4.3. Let (X, τ, I) be an ideal space and A be a subset of X. then $X–\sigma cl(X–A) = \sigma int(A)$.

Theorem 4.4. Let (X, τ, I) be an ideal topological space. then $\sigma cl(A)$ is always $\hat{\delta}_S$-closed for every subset A of X.

Proof**:** Let $\sigma cl(A)\subseteq U$, where U is semi-open. Always $\sigma cl(\sigma cl(A))=\sigma cl(A)$. Hence $\sigma cl(A)$ is $\hat{\delta}_S$-closed.

Theorem 4.5. Let (X, τ, I) be an ideal space and $A\subset X$. If sker(A) is $\hat{\delta}_S$-closed then A is also $\hat{\delta}_S$-closed.

Proof**:** Suppose that sker(A) is a $\hat{\delta}_S$-closed set. If $A\subseteq U$ and U is semi-open, then $sker(A)\subset U$. Since sker(A) is $\hat{\delta}_S$-closed $\sigma cl(sker(A))\subset U$. Always $\sigma cl(A)\subset \sigma cl(sker(A))$. Thus A is $\hat{\delta}_S$-closed.

Theorem 4.6. If A is $\hat{\delta}_S$-closed subset in (X, τ, I), then $\sigma cl(A) - A$ does not contain any non-empty closed set in (X, τ, I).

***Proof*:** Let F be any closed set in (X, τ, I) such that $F \subseteq \sigma cl(A) - A$ then $A \subseteq X - F$ and $X - F$ is open and hence semi-open in (X,τ,I). Since A is $\hat{\delta}_S$-closed, $\sigma cl(A) \subseteq X - F$. Hence $F \subseteq X - \sigma cl(A)$. Therefore $F \subseteq (\sigma cl(A) - A) \cap (X - \sigma cl(A)) = \phi$.

Remark 4.7. The converse is not always true as shown in the following example.

Example 4.8. Let $X=\{a,b,c\}$, $\tau = \{X, \phi, \{a\}\}$ and $I=\{\phi\}$. Let $A=\{b\}$. Then $\sigma cl(A) - A = X - \{b\} = \{a,c\}$ does not contain any non-empty closed set and A is not a $\hat{\delta}_S$-closed subset of (X, τ, I).

Theorem 4.9. Let (X, τ, I) be an ideal space. Then every subset of X is $\hat{\delta}_S$-closed if and only if every semi-open subset of X is δ-I-closed.

***Proof*:** Necessity - suppose every subset of X is $\hat{\delta}_S$-closed. If U is semi-open subset of X, then U is $\hat{\delta}_S$-closed and so $\sigma cl(U)=U$. Hence U is δ-I-closed.

Sufficiency - Suppose $A \subset U$ and U is semi-open. By hypothesis, U is δ-I-closed. Therefore $\sigma cl(A) \subset \sigma cl(U)=U$ and so A is $\hat{\delta}_S$-closed.

Theorem 4.10. Let (X, τ, I) be an ideal space. If every subset of X is $\hat{\delta}_S$-closed then every open subset of X is δ-I-closed.

***Proof*:** Suppose every subset of X is $\hat{\delta}_S$-closed. If U is open subset of X, then U is $\hat{\delta}_S$-closed and so $\sigma cl(U)=U$, since every open set is semi-open. Hence U is δ-I-closed.

Theorem 4.11. Intersection of a $\hat{\delta}_S$-closed set and a δ-I-closed set is always $\hat{\delta}_S$-closed.

***Proof*:** Let A be a $\hat{\delta}_S$-closed set and G be any δ-I-closed set of an ideal space (X, τ, I). Suppose $A \cap G \subseteq U$ and U is semi-open set in X. Then $A \subseteq U \cup (X - G)$. Now, $X - G$ is δ-I-open and hence open and so semi-open set. Therefore $U \cup (X - G)$ is a semi-open set containing A. But A is $\hat{\delta}_S$-closed and therefore $\sigma cl(A) \subset U \cup (X - G)$. Therefore $\sigma cl(A) \cap G \subset U$ which implies that, $\sigma cl(A \cap G) \subset U$. Hence $A \cap G$ is $\hat{\delta}_S$-closed.

Theorem 4.12. In an Ideal space (X, τ, I), for each $x \in X$, either $\{x\}$ is semi-closed or $\{x\}^c$ is $\hat{\delta}_S$-closed set in (X, τ, I).

***Proof*:** Suppose that $\{x\}$ is not a semi-closed set, then $\{x\}^c$ is not a semi-open set and then X is the only semi-open set containing $\{x\}^c$. Therefore $\sigma cl(\{x\}^c) \subseteq X$ and hence $\{x\}^c$ is $\hat{\delta}_S$-closed in (X, τ, I).

Theorem 4.13. Every $\hat{\delta}_S$-closed, semi-open set is δ-I-closed.

***Proof*:** Let A be a $\hat{\delta}_S$-closed, semi-open set in (X, τ, I). Since A is semi-open, it is semi-open such that $A \subseteq A$. Then $\sigma cl(A) \subseteq A$. Thus A is δ-I-closed.

Corollary 4.14. Every $\hat{\delta}_S$-closed and open set is δ-I-closed set.

Theorem 4.15. If A and B are $\hat{\delta}_S$-closed sets in an ideal topological space (X, τ, I) then $A \cup B$ is $\hat{\delta}_S$-closed set in (X, τ, I).

***Proof*:** Suppose that $A \cup B \subset U$, where U is any semi-open set in (X, τ, I). Then $A \subseteq U$ and $B \subseteq U$. Since A and B are $\hat{\delta}_S$-closed sets in (X, τ, I), $\sigma cl(A) \subseteq U$ and $\sigma cl(B) \subseteq U$. Always $\sigma cl(A \cup B) = \sigma cl(A) \cup \sigma cl(B)$. Therefore $\sigma cl(A \cup B) \subseteq U$ for U is semi-open. Hence A is $\hat{\delta}_S$-closed set in (X, τ, I).

Theorem 4.16. Let (X, τ, I) be an ideal space. If A is a $\hat{\delta}_S$-closed subset of X and $A \subseteq B \subseteq \sigma cl(A)$, then B is also $\hat{\delta}_S$-closed.

***Proof*:** since $\sigma cl(B) = \sigma cl(A)$, by Theorem 4.2. It holds.

Theorem 4.17. A subset A of an ideal space (X, τ, I) is $\hat{\delta}_S$-closed if and only if $\sigma cl(A) \subset sker(A)$.

***Proof*:** Necessity - suppose A is $\hat{\delta}_S$-closed and $x \in \sigma cl(A)$. If $x \notin sker(A)$ then there exists a semi-open set U such that $A \subset U$ but $x \notin U$. Since A is $\hat{\delta}_S$-closed, $\sigma cl(A) \subset U$ and so $x \notin \sigma cl(A)$, a contracdiction. Therefore $\sigma cl(A) \subset sker(A)$.

Sufficiency - suppose that $\sigma cl(A) \subset sker(A)$. If $A \subset U$ and U is semi-open. Then $sker(A) \subset U$ and so $\sigma cl(A) \subset U$. Therefore A is $\hat{\delta}_S$-closed.

Definition 4.18. A subset A of a topological space (X, τ) is said to be a semi$\wedge$ - set if $sker(A)=A$.

Theorem 4.19. Let A be a semi$\wedge$ - set of an ideal space (X, τ, I). Then A is $\hat{\delta}_S$-closed if and only if A is δ-I-closed.

***Proof*:** Necessity - suppose A is $\hat{\delta}_S$-closed. Then By Theorem 4.17, $\sigma cl(A) \subset sker(A) = A$, since A is semi$\wedge$ -set. Therefore A is δ - I – closed.

Sufficency - The proof follows from the fact that every δ-I-closed set is $\hat{\delta}_S$-closed.

Lemma 4.20. **[6]** Let x be any point in a topological space (X, τ). Then $\{x\}$ is either nowhere dense or pre-open in (X, τ). Also $X=X_1 \cup X_2$, where $X_1=\{x \in X:\{x\}$ is nowhere dense in $(X, \tau)\}$ and $X_2=\{x \in X:\{x\}$ is pre-open in $(X, \tau)\}$ is known as Jankovic – Reilly decomposition.

Theorem 4.21. In an ideal space (X, τ, I), $X_2 \cap \sigma cl(A) \subseteq sker(A)$ for any subset A of (X, τ, I).

***Proof*:** Suppose that $x \in X_2 \cap \sigma cl(A)$ and $x \notin sker(A)$. Since $x \in X_2$, $\{x\} \subset int(cl(\{x\}))$ and so $scl(\{x\}) = int(cl(\{x\}))$. Since $x \in \sigma cl(A)$, $A \cap int(cl^*(U)) \neq \phi$, for any open set U containing x. Choose $U = int(cl(\{x\}))$, Then $A \cap int(cl(\{x\})) \neq \phi$. Choose $y \in A \cap int(cl(\{x\}))$. Since $x \notin sker(A)$, there exists a semi-open set V such that $A \subseteq V$ and $x \notin V$. If $G = X–V$, then G is a semi-closed set such that $x \in G \subseteq X – A$. Also $scl(\{x\})=int(cl(\{x\})) \subseteq G$ and hence $y \in A \cap G$, a contradiction. Thus $x \in sker(A)$.

Theorem 4.22. A subset A is $\hat{\delta}_S$-closed set in an ideal topological space (X, τ, I). If and only if $X_1 \cap \sigma cl(A) \subseteq A$.

***Proof*:** Necessity - suppose A is $\hat{\delta}_S$-closed set in (X, τ, I) and $x \in X_1 \cap \sigma cl(A)$. Sppose $x \notin A$, then $X – \{x\}$ is a semi-open set containing A and so $\sigma cl(A) \subseteq X – \{x\}$. Which is impossible.

Sufficiency - Suppose $X_1 \cap \sigma cl(A) \subseteq A$. Since $A \subseteq sker(A)$, $X_1 \cap \sigma cl(A) \subseteq sker(A)$. By Theorem 4.21, $X_2 \cap \sigma cl(A) \subseteq sker(A)$. Therefore $\sigma cl(A) = (X_1 \cup X_2) \cap \sigma cl(A) = (X_1 \cap \sigma cl(A)) \cup (X_2 \cap \sigma cl(A)) \subseteq sker(A)$. By Theorem 4.17, A is $\hat{\delta}_S$-closed in (X, τ, I).

Theorem 4.23. Arbitrary intersection of $\hat{\delta}_S$-closed sets in an ideal space (X, τ, I) is $\hat{\delta}_S$-closed in (X, τ, I).

***Proof*:** Let $\{A_\alpha : \alpha \in \Delta\}$ be any family of $\hat{\delta}_S$-closed sets in (X, τ, I) and $A = \cap_{\alpha \in \Delta} A_\alpha$. Therefore $X_1 \cap \sigma cl(A_\alpha) \subseteq A_\alpha$ for each $\alpha \in \Delta$ and hence $X_1 \cap \sigma cl(A) \subseteq X_1 \cap \sigma cl(A_\alpha) \subseteq A_\alpha$, for each $\alpha \in \Delta$. Then $X_1 \cap \sigma cl(A) \subseteq \cap_{\alpha \in \Delta} A_\alpha = A$. By Theorem 4.22, A is $\hat{\delta}_S$-closed set in (X, τ, I). Thus arbitrary intersection of $\hat{\delta}_S$-closed sets in an ideal space (X, τ, I) is $\hat{\delta}_S$-closed in (X, τ, I).

Definition 4.24. A proper non-empty $\hat{\delta}_S$-closed subset A of an ideal space (X, τ, I) is said to be maximal $\hat{\delta}_S$-closed if any $\hat{\delta}_S$-closed set containing A is either X or A.

Examples 4.25. Let $X = \{a, b, c, d\}$, $\tau = \{X, \phi, \{c\}, \{d\}, \{c, d\}\}$ and $I = \{\phi\}$. Then $\{a, b, c\}$ is maximal $\hat{\delta}_S$-closed set.

Theorem 4.26. In an ideal space (X, τ, I), the following are true

(i) Let F be a maximal $\hat{\delta}_S$-closed set and G be a $\hat{\delta}_S$-closed set. Then $F \cup G = X$ or $G \subset F$.

(ii) Let F and G be maximal $\hat{\delta}_S$-closed sets. Then $F \cup G = X$ or $F = G$.

***Proof*:** (i) Let F be a maximal $\hat{\delta}_S$-closed set and G be a $\hat{\delta}_S$-closed set. If $F \cup G = X$. Then there is nothing to prove. Assume that $F \cup G \neq X$. Now, $F \subset F \cup G$. By Theorem 4.15, $F \cup G$ is a $\hat{\delta}_S$-closed set. Since F is maximal $\hat{\delta}_S$-closed set we have, $F \cup G = X$ or $F \cup G = F$. Hence $F \cup G = F$ and so $G \subset F$.

(ii) Let F and G be maximal $\hat{\delta}_S$-closed sets. If $F \cup G=X$, then there is nothing to prove. Assume that $F \cup G \neq X$. Then by (i) $F \subset G$ and $G \subset F$ which implies that $F = G$.

Theorem 4.27. A subset A of an ideal space (X,τ ,I) is $\hat{\delta}_S$-open if and only if $F \subseteq \sigma int(A)$ whenever F is semi-closed and $F \subseteq A$.

***Proof*:** Necessity - suppose A is $\hat{\delta}_S$-open and F be a semi-closed set contained in A. Then $X–A \subseteq X–F$ and hence $\sigma cl(X–A) \subset X – F$. Thus $F \subseteq X – \sigma cl(X–A) = \sigma int(A)$.

Sufficiency - suppose $X–A \subseteq U$, where U is semi-open. Then $X–U \subseteq A$ and $X–U$ is semi-closed. Then $X–U \subseteq \sigma int(A)$ which implies $\sigma cl(X –A) \subseteq U$. Therefore $X–A$ is $\hat{\delta}_S$-closed and so A is $\hat{\delta}_S$-open.

Theorem 4.28. If A is a $\hat{\delta}_S$-open set of an ideal space (X, τ, I) and $\sigma int(A) \subseteq B \subseteq A$. Then B is also a $\hat{\delta}_S$-open set of (X, τ, I).

***Proof*:** Suppose $F \subseteq B$ where F is semi-closed set. Then $F \subseteq A$. Since A is $\hat{\delta}_S$-open, $F \subseteq \sigma int(A)$. Since $\sigma int(A) \subseteq \sigma int(B)$, we have $F \subseteq \sigma int(B)$. By the above Theorem 4.27, B is $\hat{\delta}_S$-open.

V. $\hat{\delta}_S$–CLOSURE

In this section we define $\hat{\delta}_S$-closure of a subset of X and proved it is **"Kuratowski closure operator".**

Definition 5.1. Let A be a subset of an ideal topological space (X, τ, I) then the $\hat{\delta}_S$-closure of A is defined to be the intersection of all $\hat{\delta}_S$-closed sets containing A and it is denoted by $\hat{\delta}_S\mathrm{cl}(A)$. That is $\hat{\delta}_S\mathrm{cl}(A) = \cap\{F : A \subseteq F$ and F is $\hat{\delta}_S$-closed$\}$. Always $A \subseteq \hat{\delta}_S\mathrm{cl}(A)$.

Remark 5.2. From the definition of $\hat{\delta}_S$-closure and Theorem 4.23, $\hat{\delta}_S\mathrm{cl}(A)$ is the smallest $\hat{\delta}_S$-closed set containing A.

Theorem 5.3. Let A and B be subsets of an ideal space (X, τ, I). Then the following holds.

(i) $\hat{\delta}_S\mathrm{cl}(\phi) = \phi$ and $\hat{\delta}_S\mathrm{cl}(X) = X$

(ii) If $A \subseteq B$, then $\hat{\delta}_S\mathrm{cl}(A) \subseteq \hat{\delta}_S\mathrm{cl}(B)$

(iii) $\hat{\delta}_S\mathrm{cl}(A\cup B) = \hat{\delta}_S\mathrm{cl}(A) \cup \hat{\delta}_S\mathrm{cl}(B)$

(iv) $\hat{\delta}_S\mathrm{cl}(A\cap B) \subseteq \hat{\delta}_S\mathrm{cl}(A) \cap \hat{\delta}_S\mathrm{cl}(B)$

(v) A is a $\hat{\delta}_S$-closed set in (X, τ, I) if and only if $A = \hat{\delta}_S\mathrm{cl}(A)$

(vi) $\hat{\delta}_S\mathrm{cl}(A) \subseteq \sigma\mathrm{cl}(A)$

(vii) $\hat{\delta}_S\mathrm{cl}(\hat{\delta}_S\mathrm{cl}(A)) = \hat{\delta}_S\mathrm{cl}(A)$.

***Proof*:** (i) The proof is obvious.

(ii) $A \subseteq B \subseteq \hat{\delta}_S\mathrm{cl}(B)$. But $\hat{\delta}_S\mathrm{cl}(A)$ is the smallest $\hat{\delta}_S$-closed set containing A. Hence $\hat{\delta}_S\mathrm{cl}(A) \subseteq \hat{\delta}_S\mathrm{cl}(B)$.

(iii) $A \subseteq A\cup B$ and $B \subseteq A\cup B$. By (ii) $\hat{\delta}_S\mathrm{cl}(A) \subseteq \hat{\delta}_S\mathrm{cl}(A\cup B)$ and $\hat{\delta}_S\mathrm{cl}(B) \subseteq \hat{\delta}_S\mathrm{cl}(A\cup B)$. Hence $\hat{\delta}_S\mathrm{cl}(A) \cup \hat{\delta}_S\mathrm{cl}(B) \subseteq \hat{\delta}_S\mathrm{cl}(A\cup B)$. On the otherhand, $A \subseteq \hat{\delta}_S\mathrm{cl}(A)$ and $B \subseteq \hat{\delta}_S\mathrm{cl}(B)$ then $A\cup B \subseteq \hat{\delta}_S\mathrm{cl}(A) \cup \hat{\delta}_S\mathrm{cl}(B)$. But $\hat{\delta}_S\mathrm{cl}(A\cup B)$ is the smallest $\hat{\delta}_S\mathrm{cl}$-closed set containing $A\cup B$. Hence $\hat{\delta}_S\mathrm{cl}(A\cup B) \subseteq \hat{\delta}_S\mathrm{cl}(A) \cup \hat{\delta}_S\mathrm{cl}\ \mathrm{cl}(B)$. Therefore $\hat{\delta}_S\mathrm{cl}\ \mathrm{cl}(A\cup B) = \hat{\delta}_S\mathrm{cl}(A) \cup \hat{\delta}_S\mathrm{cl}(B)$.

(iv) $A\cap B\subseteq A$ and $A\cap B\subseteq B$. By (ii) $\hat{\delta}_S\mathrm{cl}(A\cap B)\subseteq \hat{\delta}_S\ \mathrm{cl}(A)$ and $\hat{\delta}_S\mathrm{cl}(A\cap B)\subset \hat{\delta}_S\mathrm{cl}(B)$. Hence $\hat{\delta}_S\mathrm{cl}(A\cap B) \subseteq \hat{\delta}_S\mathrm{cl}(A) \cap \hat{\delta}_S\mathrm{cl}(B)$.

(v) Necessity - Suppose A is $\hat{\delta}_S$-closed set in (X, τ, I). By Remark 5.2, $A\subseteq \hat{\delta}_S\mathrm{cl}(A)$. By the definition of $\hat{\delta}_S$-closure and hypothesis $\hat{\delta}_S\mathrm{cl}(A)\subseteq A$. Therefore $A=\hat{\delta}_S\mathrm{cl}(A)$.

Sufficiency - Suppose $A = \hat{\delta}_S\ \mathrm{cl}(A)$. By the definition of $\hat{\delta}_S$-closure, $\hat{\delta}_S\mathrm{cl}(A)$ is a $\hat{\delta}_S$ - closed set and hence A is a $\hat{\delta}_S$-closed set in (X, τ, I).

(vi) Suppose $x\notin\sigma\mathrm{cl}(A)$. Then there exists a δ-I-closed set G such that $A \subseteq G$ and $x \notin G$. Since every δ-I-closed set is $\hat{\delta}_S$-closed, $x\notin \hat{\delta}_S\mathrm{cl}(A)$. Thus $\hat{\delta}_S\mathrm{cl}(A) \subseteq \sigma\mathrm{cl}(A)$.

(vii) Since arbitrary intersection of $\hat{\delta}_S$-closed set in an ideal space (X, τ, I) is $\hat{\delta}_S$-closed, $\hat{\delta}_S\mathrm{cl}(A)$ is $\hat{\delta}_S$-closed. By (v) $\hat{\delta}_S\mathrm{cl}(\hat{\delta}_S\mathrm{cl}(A)) = \hat{\delta}_S\mathrm{cl}(A)$.

Remark 5.4. The converse of (iv) is not always true as shown in the following example.

Example 5.5. Let $X = \{a, b, c, d\}$, $\tau = \{X, \phi, \{a\}, \{c, d\}, \{a, c, d\}\}$ and $I = \{\phi, \{d\}\}$. Let $A = \{c\}$ and $B = \{d\}$. Then $\hat{\delta}_S\mathrm{cl}(A) = \{b, c\}$, $\hat{\delta}_S\mathrm{cl}(B) = \{b, d\}$. Since $A\cap B = \phi$, $\hat{\delta}_S\mathrm{cl}(A\cap B) = \phi$. But $\hat{\delta}_S\mathrm{cl}(A)\cap \hat{\delta}_S\mathrm{cl}(B) = \{b\}$.

Remark 5.6. From $\hat{\delta}_S\mathrm{cl}(\phi) = \phi$, $A \subseteq \hat{\delta}_S\mathrm{cl}(A)$, $\hat{\delta}_S\mathrm{cl}(A\cup B)= \hat{\delta}_S\mathrm{cl}(A)\cup\hat{\delta}_S\mathrm{cl}(B)$ and $\hat{\delta}_S\ \mathrm{cl}(\hat{\delta}_S\mathrm{cl}(A)) = \hat{\delta}_S\mathrm{cl}(A)$, we can say that $\hat{\delta}_S$ - closure is the "**Kuratowski Closure Operator**" on (X, τ, I).

Theorem 5.7. In an Ideal space (X, τ, I), for $x \in X$, $x \in \hat{\delta}_S\mathrm{cl}(A)$ if and only if $U\cap A\neq\phi$ for every $\hat{\delta}_S$-open set U containing x.

***Proof*:** Necessity - Suppose $x\in \hat{\delta}_S\mathrm{cl}(A)$ and suppose there exists a $\hat{\delta}_S$- open set U containing x such that $U\cap A=\phi$. Then $A\subset U^c$ is the $\hat{\delta}_S$-closed set. By Remark 5.2, $\hat{\delta}_S\mathrm{cl}(A)\subseteq U^c$. Therefore $x\notin \hat{\delta}_S\mathrm{cl}(A)$, a contradiction. Therefore $U\cap A\neq\phi$.

Sufficiency – Suppose $U\cap A\neq\phi$. for every $\hat{\delta}_S$-open set U containing x and suppose $x\notin \hat{\delta}_S\,cl(A)$. Then there exist a $\hat{\delta}_S$-closed set F containing A such that $x\notin F$. Hence F^c is $\hat{\delta}_S$-open set containing x such that $F^c\subseteq A^c$. Therefore $F^c\cap A=\phi$ which contradicts the hypothesis. Therefore $x \in \hat{\delta}_S cl(A)$.

Theorem 5.8. Let (X, τ, I) be an ideal space and $A \subseteq X$. If $A\subseteq B\subseteq \hat{\delta}_S cl(A)$ Then $\hat{\delta}_S cl\,(A) = \hat{\delta}_S cl(B)$.

***Proof*:** The Proof is follows from the fact that $\hat{\delta}_S cl(\hat{\delta}_S\,cl(A)) = \hat{\delta}_S cl(A)$.

Definition 5.9. Let A be a subset of a space (X, τ, I). A point x in an ideal space (X, τ, I) is said to be a $\hat{\delta}_S$-interior point of A. If there exist some $\hat{\delta}_S$-open set U containing x such that $U\subseteq A$. The set of all $\hat{\delta}_S$-interior points of A is called $\hat{\delta}_S$-interior of A and is denoted by $\hat{\delta}_S int(A)$.

Remark 5.10. $\hat{\delta}_S int(A)$ is the Union of all $\hat{\delta}_S$-open sets contained in A and by the Theorem 4.15, $\hat{\delta}_S int(A)$ is the largest $\hat{\delta}_S$-open set contained in A.

Theorem 5.11.

(i) $X - \hat{\delta}_S cl(A) = \hat{\delta}_S int(X - A)$.

(ii) $X - \hat{\delta}_S int(A) = \hat{\delta}_S cl(X - A)$.

(iii)

***Proof*:** (i) $\hat{\delta}_S int(A) \subseteq A \subseteq \hat{\delta}_S cl(A)$. Hence $X-\hat{\delta}_S cl(A) \subseteq X - A \subseteq X-\hat{\delta}_S int(A)$. Then $X - \hat{\delta}_S cl(A)$ is the $\hat{\delta}_S$-open set contained in $(X - A)$. But $\hat{\delta}_S int(X - A)$ is the largest $\hat{\delta}_S$-open set contained in $(X-A)$. Therefore $X-\hat{\delta}_S cl(A) \subseteq \hat{\delta}_S int(X - A)$. On the other hand if $x \in \hat{\delta}_S int(X-A)$ then there exist a $\hat{\delta}_S$-open set U containing x such that $U\subset X-A$ Hence $U\cap A=\phi$. Therefore $x \notin \hat{\delta}_S cl(A)$ and hence $x \in X-\hat{\delta}_S cl(A)$. Thus $\hat{\delta}_S int(X - A) \subseteq X - \hat{\delta}_S cl(A)$.

(ii) Similar to the proof of (i)

ACKNOWLEDGEMENTS

The authors thank the referees for their valuable suggestions and comments.

REFERENCES

[1]. Andrijevic, D. (1986) "Semipreopen Sets". Mat. Vesnik, 38, 24-32.
[2]. Arya, S.P. and T. Nour (1990) "Characterizations of S-normal Spaces", Indian J. Pure. Appl. Math. 21(8), 717-719.
[3]. Bhattacharya, P. and B.K. Lahiri (1987) "Semi-generalized closed sets in topology", Indian J. Math., 29, 375-382.
[4]. Dontchev, J. and M. Ganster (1996) "On δ-generalized closed sets and $T_{3/4}$-Spaces", Mem. Fac. Sci. Kochi Univ. Ser. A, Math., 17, 15-31.
[5]. Dontchev, J., M. Ganster and T. Noiri (1999) "Unified approach of generalized closed sets via topological ideals", Math. Japonica, 49, 395-401.
[6]. Jankovic, D., and Reilly, L. (1985) "On Semi-Separation Properties", Indian J.Pure Appl. Math, 16, 957-964.
[7]. Kuratowski, K. (1966) "Topology", Vol.1, Academic Press, New York, NY, USA.
[8]. Lellis Thivagar, M., B. Meera Devi and E. Hatir (2010) $\delta\hat{g}$ -closed sets in Topological spaces, Gen. Math. Notes, Vol.1, No.2, 17-25.
[9]. Levine, N. (1970) "Generalized closed sets in topology", Rend. Circ. Mat. Palermo, 19, 89-96.
[10]. Levine, N. (1963) "Semi-open sets and semi-continuity in topological spaces", Ameer Math. Monthly, 70, 36-41.
[11]. Maki, H., R. Devi and K. Balachandran (1993) "Generalized α-closed sets in topology", Bull.Fukuoka Uni.Ed Part III, 42, 13-21.
[12]. Maki, H., R. Devi and K. Balachandran (1994) "Associated topologies of generalized α-closed sets and α-generalized closed sets", Mem. Fac. Sci. Kochi Univ. Ser. A. Math., 15, 57-63.
[13]. Mashhour, A.S., M.E. Abdl El-Monsef and S.N. EI-Debb (1982) "On Precontinuous and Weak Precontinuous Mappings", Proc.Math. and Phys. Soc. Egypt 55, 47-53.
[14]. Njasted, O. (1965) "On some classes of nearly open sets", Pacific J. Math., 15, 961-970.
[15]. Stone, M. (1937) "Application of the theory of Boolian rings to general topology", Trans. Ameer. Math. Soc., 41, 374-481.
[16]. Vaidyanathaswamy, R. (1946) "Set topology", Chelas Publishing, New York, NY, USA.
[17]. Veera Kumar, M.K.R.S. (2003) " $\hat{g}$ -closed sets in topological spaces", Bull. Allah. Math.Soc, 18, 99-112.
[18]. Velicko, N.V. (1968) "H-closed topological spaces", Amer. Math. Soc. Transl., 78, 103-118.
[19]. Yuksel, S., A. Acikgoz and T. Noiri (2005) "On δ-I-continuous Functions", Turk J. Math., 29, 39-51.

OPEN ACCESS

International
Journal
Of Modern Engineering Research (IJMER)

The Impact of HIV/AIDS on Rural Household Welfare in Rukungiri District-Uganda

Robert Mugabe[1]
[1] *Consultant/Lecturer, Uganda Management Institute P.O. Box 20131, Kampala, Uganda*

ABSTRACT: *Many able bodied household members in Rukungiri district have died of HIV/AIDS. Consequently there are many house heads (often young and married) whose partners died. This study investigated the impact of HIV/AIDS on rural household welfare in Rukungiri district. A control group approach was used. Data was collected by the use of questionnaires and empirical observation from both the affected households and unaffected households. The study aimed at finding out how HIV/AIDS has led to depletion of households' productive assets. A binary logistic regression analysis was used to establish whether there is a significant difference in the sources of income for medical expenses between the affected households and unaffected households with the aim of finding out the extent to which HIV/AIDS has led to depletion of households' productive assets and consequent deterioration in households' welfare. The study has established that HIV/AIDS has led to deterioration in the welfare of the affected households through exhaustion of savings and increased borrowing, with the end result of depletion of productive assets leaving the survivors with minimal means of survival. Productive assets commonly depleted include; land, cattle, goats, chicken, sewing machines, wheelbarrows and bicycles. However, affected households have adopted many coping strategies including those that aim at improving food security, raising and supplementing their incomes so as to maintain their expenditure patterns, and coping with loss of labour. Since emergency traditional indigenous groups are already operating in all the communities in the district acting as a source of psychosocial support to individuals and communities affected by HIV/AIDS with their activities such as assisting with burial ceremonies, communal farming, supporting sick patients, rebuilding dwellings and rehabilitating farms, supporting survivors and creating income generating activities and providing material support, the study recommends government support in collaboration with donor agencies to provide them with training in HIV/AIDS home care support and enough funds to enable them meet their requirements. Government in collaboration with NGOs operating in the area should introduce short-term training courses in the affected areas to empower the survivors with practical skills and equip them with capital that can enable them create jobs for themselves. Further, improving agricultural yields through teaching them modern farming practices, provision of free anti-retroviral therapies by the government to all the affected households, accompanied by provision of food rations for boosting nutritional requirements would reduce the depletion of productive assets of these households.*

Key Words: *HIV/AIDS, Rural Household welfare, Affected, Unaffected and depletion of household assets*

I. INTRODUCTION

HIV/AIDS is a major impoverishing force and the leading cause of death in all age groups today. It is estimated that 39 million people are already dead since the first case of HIV/AIDS was identified in 1981, most of them from Eastern and Southern Africa. Today, it is estimated that 35 million people worldwide are living with HIV/AIDS of which over two-thirds are in sub-Saharan Africa (UNAIDS, 2014).

The effect of the disease has been pervasive, affecting all socio-demographic and economic categories of the population, with considerable short and long-term ramifications. As a result, it affects labour supply in all sectors of the economy especially in the rural households where labour intensive methods of production are mainly employed. Against this scenario, the causes and consequences of the HIV/AIDS pandemic are widely associated with wider challenges to household development, such as increase in expenditure, shortage of labour force, loss of income, selling of household assets, increase in borrowing, loss of employment and decline in savings. All these leading to rural poverty.

These growing linkages between the impact of HIV/AIDS and rural household welfare constitute a formidable challenge to development policy and practice.

In Uganda and other developing countries, past studies have shown that HIV/AIDS is significantly depleting the most productive human resource, both technically in terms of skilled personnel trained at a considerable cost, and physically in terms of household labour force, which is critical to a predominantly household agricultural economy. Against this, it is apparent that HIV/AIDS is directly and indirectly causing adverse social and economic effects to a significantly large number of households (Nalwadda, 1995) cited by Tumwine (2002).

This study considered a household to be a group of people that consists of all members of one family related by blood, marriage or adoption and including also other persons such as the house-keeper or farm labourers, where appropriate, who normally live together in one house or closely related premises who cook and eat together. In certain cases it also consists of only one member living alone. It also considered welfare to mean a state of well being of the households measured in terms of basic necessities that are enjoyed by the households such as food, clothing, beddings, shelter, basic health care, education, and land as a productive asset.

II. RESEARCH PROBLEM

Households face many disasters of which some call for the immediate coping mechanism to reverse the situation such as liquidating of savings accounts, borrowing from formal and informal institutions and selling some movable household assets. However, there is likelihood that HIV/AIDS as a long wave disaster has led to deterioration of households' welfare in Rukungiri district by causing permanent loss of employment. Labour is the rural households' most abundant asset. Illness due to HIV/AIDS directly affects labour benefits, leaving the household to resort to physical assets as a way to smooth consumption. This leads to depletion of productive assets such as, land, livestock, investment capital (sewing machines, bicycles, wheelbarrows), leaving households vulnerable. Little is known about the extent of the impact of HIV/AIDS on the households' physical assets.

III. OBJECTIVE OF THE STUDY

The objective of the study is to investigate the impact of HIV/AIDS on rural household welfare.

Scope of the study

This study was restricted to investigating the impact of HIV/AIDS on rural households welfare in Rukungiri district of western Uganda. Rukungiri district was chosen because few detailed studies (if any) have been carried out on the impact of HIV/AIDS on rural households' livelihoods.

The case study area

Rukungiri district is located in southwestern Uganda, bordering the districts of Ntungamo in the east, Kabale in the south, Bushenyi in the north and Kanungu to the west. It lies at an approximate altitudinal range of about 615 metres to 1864 metres above sea level. The administrative headquarters of the district are situated in Rukungiri Town Council about 400km from Kampala, the capital city of Uganda.

It has 69,010 numbers of households. Its population density is 220 persons per sq.km. It is the 16th district with the highest population density in the country and the third in the western region. It has a total population of 308,696, of which 144,875 are males and 163,821 are females.

Rukungiri district has two counties namely; Rujumbura and Rubabo with a total of 11 sub-counties including the Town council, 77 parishes and 825 villages. Its geographical location and its physical features especially Lake Edward where fishing takes place in Rwenshama fishing village, give it a peripheral district status.

The district in general is an agricultural area employing over 90 percent of the working population. Majority of the farmers are small holders using traditional agricultural techniques and keeping some animals. It is endowed with arable land and three lakes, namely; Edward, Kimbugu and Gambunda. But it is Lake Edward where many people fish for both food and trade. Crops like coffee, banana, Irish potatoes, tobacco, sorghum, beans, maize and groundnuts are the core crops for household incomes and food.

The problem of HIV/AIDS in Rukungiri district

Much as Uganda is regarded as a success story in reducing the sero-prevalence rate from 30.5 percent in 1990's to 6.1 percent in 2004, in Rukungiri district, according to District Director of Health Services, the infection rate is still high. In the age category of less than 15 years, 14.6 percent of males are infected, while 17 percent of the females are infected. In the age category of 15-24 years, 37.5 percent of males are infected by HIV/AIDS, while 40 percent of females are infected. In the age category of 25-49 years, 40.3 of males are infected, while 45 percent of females are infected. In the category of 50 years and above, 32.4 percent males are infected, while 24.1 percent of females are infected, making an overall HIV/AIDS sero-prevalence in the district as 30.4 percent, which is far higher than the national average (District profile report, 2004).

HIV/AIDS is by far much more than just a medical problem. Its effects extend to social, economic and political aspects of life. Economically, HIV/AIDS problem affects mainly the productive age. This results into a vicious cycle of poverty with low productivity and low income, beause when people contract the HIV/AIDS, they fall sick such that they are no longer as productive as before. They end up getting less income and therefore cannot get enough medical care, which further leads to even lower productivity, and the cycle continues. The HIV/AIDS scourge has also caused re-allocation of resources from economically viable projects to HIV/AIDS prevention and care.

Poverty situation in households that lost their household heads in the district

Poverty is reflected in the form of lack of basic necessities such as access to health units, good shelter, enough food, sufficient clothing, access to land, agricultural inputs, seeds and tools, inability to take children to schools and lack of security (LWF, 2000).

In devoting more time to taking care of sick person, land becomes over grown with weeds, coffee and banana plantations are left unattended. While the family's food supplies and incomes are falling, the need for money increases, especially to pay for medical treatment. To obtain cash, family savings are exhausted, family possessions for example livestock, furniture and even land are sold. This disables the households from meeting the basic necessities of life, leading to deterioration in their welfare.

Mention is also made of poverty in terms of educational needs. There is widespread lack of school-fees especially at the secondary level. There is also a failure to meet other school requirements like uniforms and building funds, making it hard for orphans to benefit from Universal Primary education and Universal secondary education that have been introduced by the government.

IV. LITERATURE REVIEW

HIV/AIDS and Household welfare

The detrimental impact that HIV/AIDS has on rural households productive capacity is felt in many ways. First, household labour quality and quantity are reduced initially in terms of productivity when the HIV/AIDS-infected person is ill, and later the supply of labour falls with the death of that person. Moreover, the probability that more than one adult per family being infected is high, given the heterosexual nature through which HIV/AIDS is transmitted, it affects negatively the levels of incomes in the household. A compound factor is that infection rates are higher among women who account for 70 percent of the agricultural labour force and 80 percent of food production. In addition, other household members will devote productive time to caring for the sick persons and traditional mourning customs, which can take a minimum of 40 days for some family members. This can adversely affect labour availability (UNAIDS, 2000).

Secondly illness of household members, means suffering loss of productive labour, loss of income, loss of food reserves, savings and assets which are diverted to meet healthcare and funeral costs. Additionally, educational opportunities are reduced, as children are withdrawn from school to care for the sick or to do odd jobs for extra income. Reduced levels of nutrition have been found in poor households (Tumwine et al, 2002).

Studies conducted by Tibaijuka (1997) and Rugalama (1998) in Tanzania, show that households that did not have enough income to buy food or to pay for healthcare, funeral expenses or education costs, sold assets in response to the crises although the amount and type of assets so disposed vary across households. The range of assets most commonly sold include; cattle, bicycles, chicken, furniture, carpentry tools, radios and wheelbarrows. However, in Chiang Mai, Thailand, 41 percent of households affected by HIV/AIDS reported having sold land. Once relieved of productive assets, the chances diminish that households can recover and rebuild their livelihoods. This leads to the threat of a terminal slide towards destitution and collapse. It is also noted that HIV/AIDS pushes people deeper into poverty as households lose their breadwinners, livelihoods are compromised and savings are consumed by the cost of health care and funerals.

Research shows that in two-thirds of Zambian families where the father died, monthly disposable income fell by more than 80 percent (UNAIDS, 2001). A study of three countries; Burkina Faso, Rwanda and Uganda, has calculated that HIV/AIDS will increase the percentage of people living in extreme poverty from 45 percent in 2000 to 51 percent in 2015 (UNAIDS, 2002). From all these studies, one concludes that HIV/AIDS epidemic has caused catastrophes in households' welfare and the crisis continues.

Women are also invariably left bearing even bigger burdens as workers, caregivers, educators and mothers. At the same time, their legal, social and political status often leave them more vulnerable to HIV/AIDS (UNAIDS, 2002).

HIV/AIDS has increased a number of orphans who are denied a chance of attending schools. A study carried out in Kampala, found that 47 percent of households with orphans did not have enough money to send the children to school, while only 10 percent of households without orphans did not have enough money (Muller and Abbas, 1990). The increasing number of HIV/AIDS orphans means that soon their needs will be beyond the capacity of the surviving guardians (TRAMADEC, 1993).

According to Booysen (2002), the incidence, depth and severity of poverty are relatively worse amongst households affected with HIV/AIDS, especially, those that have suffered illness or death in the recent past. The intensity of income mobility increases as the probability of households being affected by illness or death increases. Affected households, particularly those facing a greater burden of morbidity or mortality, are more likely to experience variations in income and to experience chronic poverty. Not only conventional determinants of poverty (human capital, access to labour market and physical capital), but also HIV/AIDS-related determinants (mortality and orphaned crisis) play a role in explaining why some households remain poor while other households are upwardly mobile and can escape poverty. Poverty, moreover, is likely to deepen as the epidemic takes its course.

The impact of HIV/AIDS combine to create a vicious cycle of poverty in which affected households are caught up. As adult members of the households become seriously sick, they are forced to give up their jobs leading to a fall in their income.

To cope with the change in income and the need to spend more on healthcare, children are often taken from school to assist in caring for the sick or to work so as to contribute to household income. Because expenditure on food comes under pressure, malnutrition often results, while access to other basic needs such as health care, housing and sanitation are also threatened. Consequently, the opportunities for children’s physical and mental development are impaired. This acts to further reduce the resistance of household members and children (particularly those that may also be infected) to opportunistic infections, given lower levels of immunity and knowledge, which in turn leads to increased mortality (World Bank, 1998; Bonnel, 2000 and Wekesa, 2000).

Households headed by HIV/AIDS widows are also particularly vulnerable, because women have limited economic opportunities and traditional norms and customs may see them severed from their extended family and denied access to an inheritance (UNDP, 1998).

V. METHODOLOGY

Study design

The study took a cross sectional design that included people from two different categories of households: the affected households and unaffected households. Unaffected households were used in comparative analysis. Both qualitative and quantitative methods of data collection and analysis were used. Information was collected on nature and form of effects of HIV/AIDS on rural household welfare, how households are coping and surviving in the face of the scourge.

Study Area

The study was conducted in Rujumbura County in Rukungiri district of Western Uganda. However, due to resource constraints, the whole county was not effectively covered. Out of seven sub-counties, only four were covered that is Kayunga, Nyakagyeme, Bugangari and Town Council. This is because according to district HIV/AIDS report (2000), these sub-counties are the most affected by HIV/AIDS.

Study Population

The population of the study included 80 households as key study respondents, 5 local leaders, 5 district administrators, 5 non-governmental organizations (NGOs), 5 community-based organizations operating in the area as key informants. Purposive sampling technique was used to select the required sampling frame in each category and then simple random sampling was used to select the required sample size.

Sample Selection

The study households were purposively selected and comprised of two categories of members of households; the affected by HIV/AIDS and unaffected neighbouring households. Affected household for this study is defined as all residents (members) of a dwelling in which at least one member is known to have HIV/AIDS at the start of the study, or to have had HIV/AIDS and/or have died. Affected households were got by identifying HIV/AIDS-infected individuals obtaining care from the local HIV/AIDS information centers (main community-based HIV/AIDS counseling and testing services). Eighty respondents were selected from the categories of affected households and unaffected households using simple random sampling technique.

Data Collection

The study combined both qualitative and quantitative data collection techniques. Participatory rural appraisal tools were used to collect data. These include focus group discussion, interviews and administered questionnaire.

Focus Group Discussion (FGD)

Three separate FGDs for women, men, and youth were organized to explore issues concerning HIV/AIDS epidemic and households' coping mechanisms. These provided diversified perceptions and opinions about the topic, generated information about households' structures (household dissolution, household mortality), economic changes (in school attendance, incomes and expenditures, savings and debts), household coping mechanisms, source of resilience and what people have relied on to make a living when struck by HIV/AIDS-linked death.

Questionnaires

Structured questionnaires were used to collect data from respondents after pre-testing them to check for their validity and reliability. The questionnaires for both the affected households and unaffected households were the same. One would only answer the relevant questions. Pre-testing the questionnaire was very helpful in determining whether the households who were going to be interviewed would understand the kind of questions put to them, and it also helped to know the kind of items to expect to find in their homes, such that the questionnaire was not over ambitious.

Interviewing

An interview schedule was used to collect information from the key informants that included local leaders, district administrators, NGOs and community-based organizations operating in the area. These provided the general information on the magnitude of HIV/AIDS morbidity and mortality in the area, how HIV/AIDS has affected the households' incomes, expenditure on healthcare, and the coping mechanisms/livelihood strategies adopted by the households.

Observations

The physical assets of the affected and unaffected households were observed.

Secondary data

The information on the magnitude of HIV/AIDS mortality, demographic structure, HIV/AIDS and household welfare were obtained from documents and records. This supplemented the findings of the study.

Data Analysis

Both qualitative and quantitative techniques were used. Survey questionnaires were edited before leaving the field in order to ensure consistency among the answers given. The edited data were classified into meaningful categories and then coded. Data were analysed using STATA package.

The impact of HIV/AIDS on household welfare was analyzed using logistic regression analysis. In a household where breadwinner falls sick, there is permanent loss of employment, which leads to loss of income and the alternative source could be exhaustion of savings or constant selling household assets, which were fitted in a logistic regression equation by assigning 1 and 0 to the dependent variable. Multivariate determinants were used because of dichotomous outcome of the variable indicating the source of income for household expenditure which can be either from household savings or from depleting household assets. In a logistic regression model, we assign the probability p; the household uses savings as the source of income to meet the house expenditures given by;

$$p=\frac{e^{z}}{1+e^{z}} \text{ --- } (1)$$

Therefore, the probability of household depleting household assets as a source of income to meet the household expenditures is;

$$1-p=\frac{1}{1+e^{z}} \text{ --- } (2)$$

Dividing equation (1) by (2), we obtain

$$\frac{p}{1-p}=e^{z} \text{ --- } (3)$$

Taking the natural log both sides, we obtain

$$\ln\left(\frac{p}{1-p}\right)=z, \text{ Where } z=X\beta+\varepsilon$$

$$\ln\left(\frac{p}{1-p}\right)=X\beta+\varepsilon$$

Where X is a vector comprising of explanatory variables, ε is a vector of the error term.

$\ln(\frac{p}{1-p})$ Is log of the odds ratio.

The estimated odds ratio was used to estimate the relative likelihood of occurrence of effect tested at 95 percent confidence interval. The marginal effects were used to find out the rate of change of probability of the occurrence of dependent variable per unit change in the independent variable.

Ethical considerations

The study being so sensitive, I sought permission and research clearance letter from Uganda National Council of Science and Technology (UNSCT) a body responsible for ethical clearance in Uganda as well an introductory letter from the Ministry of Health (MOH) which introduced me to the study sites to identify contact persons, key informants and appropriate stakeholders to participate in the study. In the study process, participants and other several research ethical issues were treated in accordance with research ethical guidelines of the UNSCT and MOH. For trust and confidence building to respondents, all rights and dignity of study participants, together with their personal experiences and any information offered for the study were respected and treated with confidentiality.

VI. RESULTS AND DISCUSSION

HIV/AIDS and the main areas of household expenditure

There was a need to establish the main areas of households' expenditure to ascertain the items that determine the households' welfare. This would help us determine whether HIV/AIDS has any effect on households' expenditure patterns and how this affects their welfare. Table 1 shows this.

Table 1: Main areas of household's expenditure

Areas of expenditure	Affected	Percent	Unaffected	Percent	Total	Percent
Health	50	26.9	30	16.8	80	21.9
Education	25	13.4	45	25.1	70	19.2
Food	35	18.8	35	19.6	70	19.2
Transport	35	18.8	20	11.1	55	15.1
Hired labour	10	5.4	2	1.1	12	3.3
Recreation	0	0.0	3	1.7	3	0.8
Clothing	30	16.1	40	22.3	70	19.2
Others	1	0.5	4	2.2	5	1.4
Total	186	100	179	100	365	100

Source: Survey

Table 1 shows that majority of the households spend their substantial amount of their income on healthcare, being 21.9 percent of all households' expenditures, followed by expenditure on food, clothing, education at 19.2 percent each, followed by transport at 15.1 percent. In the affected households, healthcare constitutes the major expenditure at 26.9 percent as compared to expenditure on it by unaffected households at 16.8 percent. Expenditure on education takes 13.4 percent of the income of affected households as compared to 25.1 percent of the unaffected. Expenditure on transport also takes a substantial amount of income in affected households at 18.8 percent as compared to 11.1 percent of the unaffected households. Whereas there was use of hired labour in affected households that constitute 3.4 percent of households, only 1.1 percent expenditure on hired labour was identified in the unaffected households.

The reason for increase in health expenditure in affected households is mainly as a result of sickness created by opportunistic infection due to HIV/AIDS weakening the immune system of the body. Therefore such expenditure cannot be attributed to improvement in welfare status of an individual.

The study also discovered that increase in expenditure is as a result of continuous transportation of patients to health-centers for treatment of opportunistic infections in the affected households. It was also discovered that affected households resort to hired labour because an HIV/AIDS patient who is already bedridden needs maximum attention. This reduces the labour force that should have been used in the gardens.

No recreational activities were identified in affected households yet in unaffected households, 1.7 percent of their expenditures are spent on recreational activities. This shows that unaffected households enjoy a better welfare as compared to affected households.

Distribution of the dead by sex and causes of death

The major causes of death in the households were identified. This was to find out the extent to which HIV/AIDS has claimed lives of individuals. This would help us in determining how HIV/AIDS is depleting the productive labour force in households and how this is related to welfare. Table 2 shows this.

Table 2: Causes and death distribution by sex

Sex	**Male**	**Percent**	**Female**	**Percent**	**Total**	**Percent**
Cause of death						
HIV/AIDS	47	56.7	36	43.3	83	62.4
Malaria	19	51.4	18	48.6	37	27.8
Others	5	38.5	8	61.5	13	9.8
Total	**71**	**5.4**	**62**	**46.6**	**133**	**100**

Source: Survey

Table 2 shows that 62.4 percent of deaths experienced in households are caused by HIV/AIDS, followed by malaria at 27.8 percent while other causes constitute only 9.8 Percent.

In the sex category, 56.7 percent of males have died of HIV/AIDS as compared to 43.3 percent of females. The reason for this could be that men who cannot abstain from sex and yet work far away from their homes tends to sleep with other women thereby increasing the chances of contracting HIV/AIDS. It was also discovered that males die of malaria more at 51.4 percent as compared to their counterpart females at 48.6 percent.

The study found out that in some households where HIV/AIDS has claimed husbands, all household assets including land were sold off to get money for treatment, leaving widows and children with minimal means of survival. On the other hand, households where HIV/AIDS has claimed a wife less household assets are depleted. This shows that men claim ownership of household assets and care for themselves more than their wives and children.

HIV/AIDS and the sources of income for healthcare treatment

The study sought to establish the sources of household income for healthcare treatment. This was to help find out whether there is significant difference in the sources of expenditure between the affected households and unaffected ones which would in turn help us determine the extent of HIV/AIDS impact on households expenditure patterns. Table 3 shows this.

Table 3: HIV/AIDS on the source of income for health care treatment

Source of medical care	**Affected**	**Percent**	**Unaffected**	**Percent**	**Total**	**Percent**
Savings	19	19.2	22	47.8	41	29.3
Borrowing	26	26.3	5	10.9	31	22.1
Sell of goats	5	5.1	8	17.4	13	9.3
Sell of cattle	20	20.1	5	10.9	25	17.9
Sell of land	28	28.3	1	2.2	29	20.7
Others	1	1.0	0	0.0	1	0.7
Total	**99**	**4100**	**46**	**100**	**140**	**100**

Source: Survey

Table 3 shows that majority of households used their main sources of income on medical treatment from savings being 29.3 percent, followed by borrowing at 22.1 percent, followed by sell of land at 20.7 percent and sell of cattle at 17.9 percent.

In the affected households, 28.3 percent meet their healthcare expenditures by selling land as compared to 2.2 percent in the unaffected households. This is followed by borrowing at 26.3 percent as compared to 10.9 percent in the unaffected households, then by sell of cattle at 20.1 percent as compared to 10.9 percent in the unaffected households. However, in the unaffected households, most of the healthcare expenditures are met through their savings being 47.8 percent as compared to 19.2 percent in the affected households.

In the affected households, HIV/AIDS has depleted the productive assets especially land which is the most productive asset sustaining the livelihoods of the rural population. The reason for this phenomenon could be that HIV/AIDS necessitates continuous expenditure to treat opportunistic infections as the immunity declines when somebody is infected with HIV.

It should also be noted that when a bread-winner falls sick of HIV/AIDS, he or she can no longer be able to continue working and therefore, this creates permanent loss of jobs that impairs the household source of survival. In the effort of sustaining their livelihoods, they embark on borrowing from formal and informal institutions, from friends and other sources. So in an effort to meet the burden of debts, accompanied by increasing expenditure on health care and meeting livelihood necessities, the productive assets are depleted. Yet depletion of productive assets where there are no chances of replacing them, leads to deterioration in the households welfare.

HIV/AIDS and the pattern of Asset holdings

The assets owned by various households were also analyzed by category to find out the present quantity and the depleted quantity of both affected and unaffected households. This would help us find out whether HIV/AIDS has had any effect on asset holdings or not and this would in turn help us to find out the extent to which HIV/AIDS has affected households welfare. Table 4 shows this.

Table 4: The pattern of Asset holdings

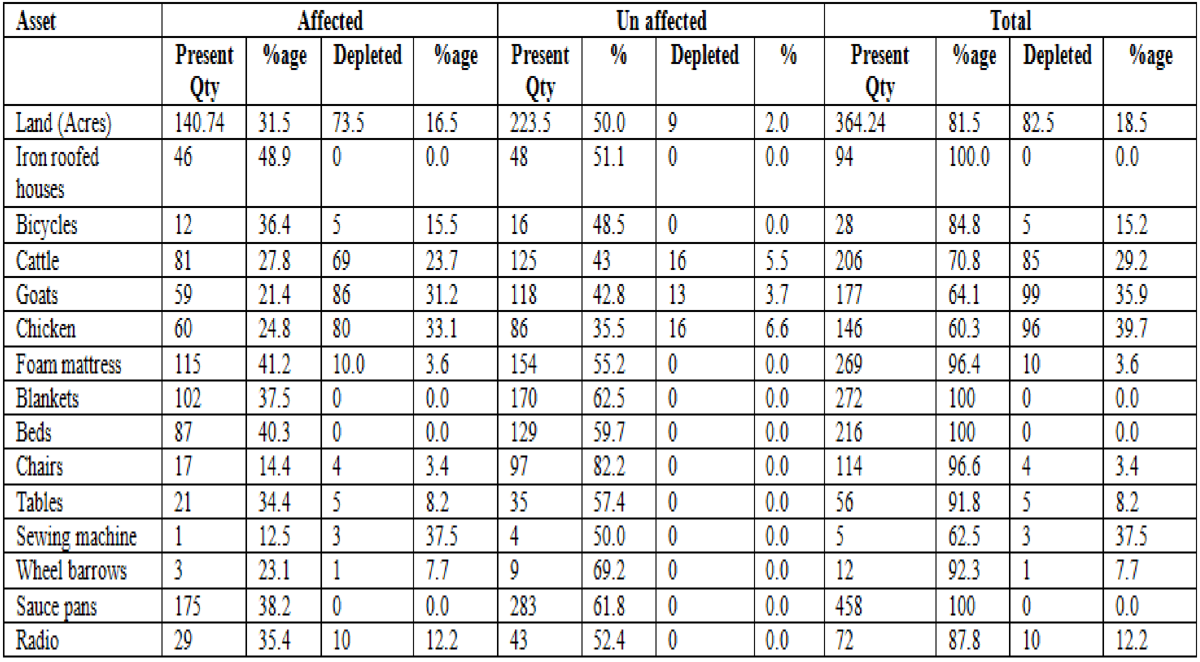

Asset	Affected				Un affected				Total			
	Present Qty	%age	Depleted	%age	Present Qty	%	Depleted	%	Present Qty	%age	Depleted	%age
Land (Acres)	140.74	31.5	73.5	16.5	223.5	50.0	9	2.0	364.24	81.5	82.5	18.5
Iron roofed houses	46	48.9	0	0.0	48	51.1	0	0.0	94	100.0	0	0.0
Bicycles	12	36.4	5	15.5	16	48.5	0	0.0	28	84.8	5	15.2
Cattle	81	27.8	69	23.7	125	43	16	5.5	206	70.8	85	29.2
Goats	59	21.4	86	31.2	118	42.8	13	3.7	177	64.1	99	35.9
Chicken	60	24.8	80	33.1	86	35.5	16	6.6	146	60.3	96	39.7
Foam mattress	115	41.2	10.0	3.6	154	55.2	0	0.0	269	96.4	10	3.6
Blankets	102	37.5	0	0.0	170	62.5	0	0.0	272	100	0	0.0
Beds	87	40.3	0	0.0	129	59.7	0	0.0	216	100	0	0.0
Chairs	17	14.4	4	3.4	97	82.2	0	0.0	114	96.6	4	3.4
Tables	21	34.4	5	8.2	35	57.4	0	0.0	56	91.8	5	8.2
Sewing machine	1	12.5	3	37.5	4	50.0	0	0.0	5	62.5	3	37.5
Wheel barrows	3	23.1	1	7.7	9	69.2	0	0.0	12	92.3	1	7.7
Sauce pans	175	38.2	0	0.0	283	61.8	0	0.0	458	100	0	0.0
Radio	29	35.4	10	12.2	43	52.4	0	0.0	72	87.8	10	12.2

Source: Survey

From the table (4) it can be seen that the present quantity of land was 364.24 acres of the total land owned by all households while 82.5 acres were depleted which constituted 18.5 percent.

In the affected households, 140.74 acres of land were presently owned being 31.5 percent and 73.5 acres were depleted being 16.5 percent. In the unaffected households, 223.5 acres were presently owned being 50 percent of all land owned by both affected and unaffected while only 9 acres were depleted being 2 percent. This therefore indicates that HIV/AIDS could be one of the major factors leading to depletion of land and yet land is the major productive asset in the rural areas. This therefore means that as the intensity of HIV/AIDS increases, land as a means of survival is likely to be depleted completely and this is likely to negatively affect the livelihoods of households.

Both the affected and unaffected households had iron-roofed houses though there was slight difference with 48.9 percent being owned by the affected and 51.1 percent being owned by unaffected households.

The easiest means of transport in the rural area of study was a bicycle, yet only 36.4 percent of the affected households had them while 15.5 percent of them had been sold off compared to unaffected households where 48.5 percent had bicycles and none of them had been sold off.

In terms of cattle, goats and chicken, the present quantities owned by affected households were 27.8 percent, 21.4 percent and 24.8 percent respectively as compared to 43 percent, 42.8 percent and 35.5 percent respectively present quantities owned by unaffected households.

Regarding beddings, like mattresses, blankets, and beds, still the unaffected households had more at 55.2 percent, 62.5 percent and 59.7 percent respectively as compared to 41.2 percent, 37.5 percent and 40.3 percent respectively for the affected households. And in terms of other household items like tables, chairs, saucepans and radios, still the unaffected households had more at 57.4 percent, 82.2 percent, 61.8 percent and 52.4 percent as compared to those owned by affected households at 34.4 percent, 14.4 percent, 38.2 percent and 35.4 percent respectively.

Other items considered as productive assets were sewing machines and wheelbarrows. In the affected households, only one sewing machine was still unsold being 12.5 percent and three were sold off being 37.5 percent. Three wheelbarrows were still presently owned being 23.1 percent while one had been sold being 7.7 percent. In the unaffected households, four sewing machines were still presently owned being 50 percent and none had been sold. It was also noted that nine wheelbarrows were recorded in the unaffected households being 69.2 percent of all the wheelbarrows owned by households and none had been sold.

The study discovered that the unaffected households buy most of the assets that have been sold by the affected households. This means HIV/AIDS has led to re-allocation of productive assets from affected households to unaffected households. Unfortunately, this has led to improvement in the welfare of unaffected households and deterioration in the welfare of affected households.

Results of binary logistic regression analysis

Exhaustion of household savings and depletion of productive assets as a source of income to cater for the needs of households' expenditures with; sex of household head, HIV/AIDS status of a household head, number of children attending school and length of sickness of a household head were fitted in the logistic equation. Results are in tables 5.10 and5.11. The table shows the logistic regression coefficients expressed as odds ratios to show the likelihood of the source of households' expenditures by each selected variable.

It should be noted that the effect caused by the presence of HIV/AIDS in the households is an added effect to what already existed before the coming of HIV/AIDS. Therefore, from the logistic regression analysis, whether the effect due to HIV/AIDS is greater or less, it remains an added effect, which increases the suffering of the affected households. The elicit responses are presented in table 5.

Table 5: Likelihood of source of household expenditures due to selected variables

Source	Odds ratio	Std. Err	z	$p >$ IzI	(95% conf. Interval
Sex	.9626156	.7317973	-.05	.960	.2169474 4.271213
HIV status	.123582	.0149177	-.364	.000	.00116 .1316587
Children in school	1.001801	.2177921	.01	.993	.6542289 1.534028
Length of sickness	1.015652	.0183758	.86	.391	.9802673 1.52314

Source: Survey

Table 5 shows that HIV/AIDS as cause for exhausting households' savings and depletion of productive assets was found to be highly significant at 0.05. HIV/AIDS was more likely to affect household expenditure than any other variable. The results show that the odds of exhausting the source of income for households' expenditure increases with a household head that gets infected by 0.12.

The marginal effects for each of the selected variables were also computed to find the rate of change of the probability of exhausting the source of income in a household with respect to each of the independent variable. Table 6 shows this.

Table 6: Marginal effects after logit

Variable	dy/dx	Std. Err	z	$p \succ$ IzI	(95% C.I)	x
Sex	-.0067294	.76022	-.01	.993	-1.49673 1.48327	.4125
HIV status	-.6963534	1.20711	-.58	.564	-3.06225 1.66954	.5
Children in school	.0003184	.003846	.01	.993	-.075071 .075707	2.937
Length of sickness	.002748	.00331	.83	.406	-.003733 .009229	22.32

Source: Survey

Table 6 shows that a unit change in HIV/AIDS infection leads to a decrease of 0.5 in the probability of retaining the source of income to maintain the households' expenditure.

This shows that as the gravity of HIV/AIDS increases in a household, savings are exhausted and the only alternative that remains available is the sell of productive assets that eventually lead to their depletion. And depletion of productive assets where there are no chances of replacing them has been responsible for deterioration of households' welfare in the affected households.

Coping mechanism of households affected by HIV/AIDS in the district

Households affected by HIV/AIDS have adopted many coping strategies. One of the strategies is aiming at improving food security. Under this strategy, households substitute cheaper commodities such as porridge instead of bread and they postpone some meals consumed in a day. They have also reduced consumption of the items that are used to sustain their daily lives. Some households have decided to reduce the number of people by sending some children to their relatives. Those without relatives or in cases where relatives are incapable of taking on extra childcare, children are forced to find their own survival elsewhere, leading many to become destitute.

Households have also adopted strategies aimed at rising and supplementing their incomes so as to maintain their expenditure patterns. As a result, they have exhausted their savings and accumulated a lot of debts from formal and informal institutions. Others have migrated in search for new jobs having sold their productive assets.

In an effort of coping with loss of labour when a member of the household falls sick, children are withdrawn from schools. Although children are not directly involved in care provision, they are involved indirectly by fulfilling mother’s and father’s roles in some domestic and agricultural activities such as harvesting crops, preparing food for the rest of the households, gathering of food, tending livestock and running errands.

Emotionally, some affected people have formed drama groups with the assistance of NGOs operating in the area to sensitize their communities to the dangers of HIV/AIDS but at the same time using the drama to mobilize income for their survival.

Spiritually, some affected members in the households have decided to join Born Again churches in the area by surrendering their lives to Jesus Christ with hope and faith of getting healed. This has created psychological satisfaction and comfort with the belief that they are healed of the disease.

The district has managed to cope with the problem in various ways. It has set up mitigation interventions, which are basically geared towards improving the lives of HIV/AIDS patients. Under the auspices of AIDS Information centre, HIV/AIDS testing and counseling facilities have been established in all major government health units within the district and the distribution of free ant-retroviral drugs. Some of the NGOs are also offering HIV/AIDS testing and counseling services, others have set up some income-generating activities like agricultural support programmes, youth skills training and micro-finance projects.

However, the universal awareness of HIV/AIDS transmission and the major preventive modes, the intensive health education, condom supply, HIV/AIDS sero-testing and counseling, HIV/AIDS-associated risky behaviours are still high. This coupled with the fact that HIV/AIDS has no cure or vaccine up to now, and the existing anti-retroviral drugs being unaffordable to the district population, the disease still poses a great challenge to the district and to the country as a whole.

VII. CONCLUSIONS AND POLICY RECOMMENDATIONS

Conclusions

Many able bodied household members in Rukungiri district have died of HIV/AIDS. One consequence of this has been the existence of many young widows and widowers. In the affected households, deterioration in the welfare was more noticed as compared to unaffected households. The objective of the study was to investigate the impact of HIV/AIDS on rural household welfare.

HIV/AIDS as a long wave disaster has led not only to permanent loss of jobs especially where the breadwinner falls sick and eventually dies but also to exhaustion of savings, increase in borrowing and eventually the depletion of productive assets leaving the survivors with no means of survival. Productive assets commonly depleted include, land, cattle, goats, chicken, sewing machines, wheelbarrows and bicycles.

Many children in the affected households were not attending school. This is because as the breadwinner falls sick, there is loss of permanent employment that creates sudden fall in income. This calls for the adjustment in the expenditure patterns that leads to withdrawal of children from schools. This is likely to create deterioration of their welfare in the future since their survival remains uncertain. In the unaffected households, many children were found to be attending school an indication that the future of these children is bright holding other factors constant as compared to those children from the affected households.

The health and living conditions of the affected households were also seen to be deteriorating. The numbers of households were not able to meet their medical expenses especially for treating opportunistic infections brought about by HIV/AIDS infection as well as sustainably buy the HIV and AIDS prolonging drugs. The situation worsens after exhausting their savings and selling their productive assets including land that provides food to households which has reduced the nutritional status of the affected households. However, the study revealed that the unaffected households are improving their welfare by buying the assets from the affected households who pay them less than the market price because of desperate, lack of money to cater for their needs at home. This has led to re-allocation of resources in favour of unaffected households and against affected households.

In the rural area of study, the means of transport is a bicycle, but in the affected households, most of them had been sold off. Land is the most productive asset in rural areas sustaining the livelihoods of many households, but in the affected households, it is being sold off as an alternative source of income having exhausted other assets such as cattle, goats, chicken, radios and others. However, the study discovered that asset holding in the unaffected households is increasing because they are the ones buying those of the affected households.

Policy Recommendation

Existence of traditional indigenous groups

Many organizations have been formed as a major emergency source of support to the people affected by HIV/AIDS in communities. They include; religious based hospitals, Aids Widows and Orphans Family Support and other traditional indigenous groups at micro level particularly the numerous local saving clubs, burial societies, grain saving schemes and labour sharing schemes (Tumwine, 2001 and Namusisi, 2003). These play a major role of helping households cope with the impact of HIV/AIDS. The major activities done by these emergency associations include; assisting with burial ceremonies, communal farming, supporting sick patients, rebuilding dwellings and rehabilitating farms, supporting the survivors and creation of income generating activities, as well as providing material support such as salt, soap, paraffin, food, blankets, clothing and other household necessities. Much as these informal groups are taken as source of psychosocial support, they still lack the capacity to deliver their services efficiently. Therefore the government in collaboration with donor agencies should strengthen their capacities by providing them with training in HIV/AIDS advocacy and home care support as well as providing them with enough funds to meet the requirements of their activities.

Improving on agricultural yields

Given the fact that agriculture is the backbone of this country, a lot of emphasis is needed to improve on welfare of the rural farmers. Most of the households interviewed admitted that they depend on peasant farming for survival. However, much as the government is undertaking the policy of modernizing agriculture, little progress is on the ground so far. The government should employ extension workers who should be moving into villages to mobilize households teaching them modern methods of agriculture. This should be accompanied by provision of better inputs like improved seeds, providing them with hoes and teaching them technologies that make optimal use of available resources, given labour and capital constraints. This is likely to improve productivity that will lead to improvement in the incomes of the affected households when they sell the surplus output and eventually these households can begin enjoying a better life.

Creation of jobs

Government in collaboration with NGOs operating in the area should introduce short-term training courses in the affected areas to empower the survivors with practical skills and equip them with capital that can enable them create jobs for themselves for the generation of income. For example, those who are taught tailoring could be provided with sewing machines and those who are taught carpentry could be provided with the necessary tools, those taught in handicrafts, bee-keeping, poultry farming and pig-farming could be assisted by providing them with initial capital and then later they can always access small loans from NGOs and micro-finance institutions for re-capitalizing their businesses. Also government and other development partners operating in the area should encourage households to form cooperatives that would help them market their products as well as using them for information dissemination in addition to using them to access loans from lending institutions. This would strengthen the productive capacity of the affected households which would enable them earn enough income, and sustain their livelihoods.

Health care provision

The study found that HIV/AIDS has led to depletion of households' most productive assets and subsequent depletion of productive assets has led to deterioration of household welfare. Most of these assets are sold to raise money in order to meet the expenses for medical treatment especially treating opportunistic infections due to immune suppression caused by HIV/AIDS infection. Since the government of Uganda is among the selected countries benefiting from the Global Fund for HIV/AIDS, it should build the capacity to ensure that free anti-retroviral therapy (ARVs) are distributed to all infected individuals. This should be accompanied by provision of food rations that supplement nutritional requirements to patients. This will reduce on demand for more money for treatment and will save the depletion of productive assets. However, this policy should be accompanied by massive sensitization of the general public on the dangers of getting infected with HIV such that individuals and communities do not become reckless knowing that when they get infected the government would cater for them such that they live longer. That means the policy should be adopted without over-stretching the government's budget such that even if Global Fund ceases, the exercise should remain within the reach of government.

Strengthening free education

The government of Uganda is already providing free education at primary and secondary levels by meeting the cost for school-fees, building classroom blocks, supplying scholastic materials such as textbooks, laboratory equipments as well as paying teachers, yet there is high drop-out rate especially children from affected households. Therefore the study recommends the provision of school uniform, books, pens and other school requirements as well as provision of free lunch in addition to what it is already available. This will retain the children from the affected households in schools and ensure they enjoy the same benefits enjoyed by children from unaffected households.

REFERENCES

[1]. Boonel, R (2000). Economic Analysis of HIV/AIDS: Apaper presented to the African Development Forum. Addis Ababa, 3-4 December.
[2]. Booysen,F. (2002). Poverty dynamics and HIV/AIDS-related morbidity and mortality in South Africa. Apaper presented at International Conference.”Emperical evidence for demographic and socio-economic impact of AIDS”, 26-28 march, 2003.
[3]. Lugalama G (1998). It is not only the loss of labour: HIV/AIDS,Loss of household assets and household livelihood in Bukoba district, Tanzania, paper presented at the East and Southern Africa. Regional Conference on Responding to HIV/AIDS: Development needs of African smallholder Agriculture, Harare (June 8-10).
[4]. Lutheran World Federation (LWF) (1998). Rakai Rehabilitation Annual report: Long-term DANIDA-funded assistance Programme.
[5]. Muller, O; Abbas N. (1990). “The impact of AIDS mortality on children’s education in Kampala (Uganda)”. AIDS CARE, Vol. 2 No. 1.
[6]. Namusisi (2003). NGO Assistance and poverty reduction in child-headed Households orphaned by HIV/AIDS in Rakai
[7]. Rukungiri District. (2004).District HIV/AIDS report. A health working paper.
[8]. Tibaijuka AK(1997). AIDS and Economic welfare in peasant-Agriculture,case studies from Kagabiro Village, Kagera Region, Tanzania. World Development, 25(6): 963-975.
[9]. Trans-Africa Management Development Consultants (TRAMADEC): “evaluation of Soci-economic impact of AIDs in Uganda”, Nairobi 1993; Mutolele Hospital (1996) “Coping strategies among AIDS affected people in Kisoro district, SouthWest Uganda” Feb.1996
[10]. Tumwine, J (2002). Assessment of the effects of HIV/AIDS on Rural Agricultural systems and the livelihoods that depend on it. Acomparison study of Rakai and Kabale districts.
[11]. Tumwine, J, Namusisisi, N and Musinguzi J. (2002). Report of the study on socio-economic impact of HIV/AIDS on household welfare and productivity. Un published.
[12]. Uganda AIDS Commission (UAC) (2004). Annual report. Uganda AIDS Commission, Kampala.
[13]. Uganda Demographic Health Survey (UDHS), (2001).Report on socio-economic Survey, Entebbe. Uganda Bureau of Statistics
[14]. UNAIDS (2014). Report on the Global AIDS Epidemic.
[15]. UNAIDS (1998). A review of household and community response to the HIV/AIDS epidemic in the rural areas of sub-Saharan Africa.
[16]. UNAIDS (2000). Report on global HIV/AIDS epidemic. Joint United Nations Program on HIV/AIDS, Geneva.
[17]. UNAIDS (2000). Report on the global HIV/AIDS epidemic. Joint program on HIV/AIDS and Rural Development, Rome and Geneva.
[18]. UNAIDS: Measuring the impact of HIV/AIDS on the Agricultural sector in Africa. Background paper. December 2000.
[19]. UNAIDS (2001). Report on global HIV/AIDS epidemic. UNAIDS, Geneva, Switzerland.
[20]. UNDP Kampala (1998). Uganda Human Development Report, Kampala
[21]. UNDP (1998), Human Development Report, Globalisation with a Human Face, New York and Oxford, Oxford University Press.
[22]. Wekesa, E. (2000). Impact of HIV/AIDS on Child Survival and Development in Kenya. AIDS analysis in Africa 10(4): 12-14.
[23]. World Bank (1998). Confronting AIDS. Washington, DC. World Bank

OPEN ACCESS

International
Journal
Of Modern Engineering Research (IJMER)

High Performance Germanium Double Gate N-MOSFET

Akshat Singh[1], Mr. Dhiraj Kapoor[2]
[1]Student, M.Tech (E.C.E), V.C.E, Rohtak, India
[2]Assistant Proffesor (E.C.E), V.C.E, Rohtak, India

ABSTRACT- *The current MOSFET technology supports scaling down to nanometer. To achieve enhanced transistor switching, it is difficult to keep the equivalent driver current at the same level since it changes by the certain restrictions like effective masses, density of states, uniaxial- and biaxial- strain; band structure, channel orientation, channel mobility, off-state leakage, switching delay in nano-scale and parasitic latch up. Current strained-Si is the ruling technology for intensifying the performance of MOSFET and development of strain can provide a better solution to the scaling. The future of nano-scale MOSFETs relies on exploration of novel higher mobility channel materials such as stained-Ge and strained III-V groups that might perform even better than very highly strained-Si. In addition, parameters such as injection velocity, short channel length effect and Band-to-Band Tunneling (BTBT) result in reduction of inversion charge, increase in leakage current, resulting in decrease in the drive current. While developing accurate model of MOSFETs all these complex effects should be captured. It is proposed to*

1. *Design high performance double gate n-MOSFET with channel material Ge.*
2. *Benchmarked & stimulate high performance double gate n-MOSFET by using the simulation techniques.*

Keywords- *Uniaxial strain, Strained Si, Strained Ge, Double-gate MOSFETs, Band To Band Tunneling.*

I. INTRODUCTION

The Si-based MOSFETs have been the most important building blocks of the Integrated Circuits (ICs), since they were first presented in 1960 *[1]*. Today's Integrated Circuits (ICs) use these MOSFETs as the basic switching element for digital logic applications and as an amplifier for analog applications. Even though the basic structure of the device has remained the same, the physical size has been continuously reduced by factor of two every 2-3 years using Moore’s Law (fig.1) *[2]* which results in faster and highly complex chips with lowered cost per transistor *[2]*.

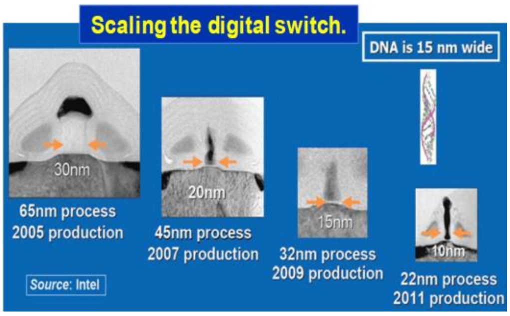

Fig.1: Scaling of bulk MOSFET using Moore’s Law *[2]*.

This trend has been the main driving force for electronics industry for putting large energy and budget into scaling device technologies. Currently, in the 32nm high performance processor technology, the physical gate length is scaled below 20nm, with effective gate oxide thinner than 0.8 nm. This exponential scaling of the physical feature size cannot continue forever, as beyond the 22nm node fundamental as well as practical limitations start restricting the performance of the conventional Si-based MOSFETs. Taking into consideration fig.2, after the development of 90nm device technology, enhanced drive currents were achieved with an exponential increase in the static, off state leakage of the device *[1]*.

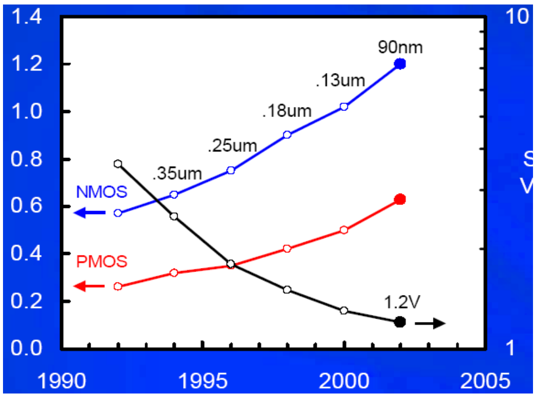

Fig.2: Need to maintain an increase in the drive current (Ion) even at reduced supply voltages (Vdd) in the future *[1]*.

Fig.3 defines the growth of static power dissipation (leakage) and active power dissipation as the devices are scaled down. The static power density on the chip has been exponentially increasing at the much faster rate than the active power density, which increases rather linearly with device scaling. The active power density arises due to the dissipative flow of charges between the transistor gates and ground terminals during switching of the device. The static power, also known as sub-threshold power, or standby power, is dissipated even though switching operation is absent. The major source of the static power dissipation is the sub-threshold leakage in the transistor since the MOSFET at below 50nm gate length scale does not behave as an ideal switch and allows the leakage current. The static power dissipation is relatively insignificant component of the total chip power just few generations back, but it is now comparable in magnitude to the active power.

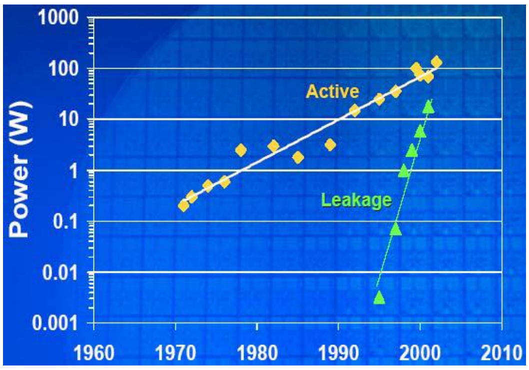

Fig.3: static power dissipation will cross the active power consumption (source: Intel) *[1]*.

When the scaling of the conventional bulk Si-MOSFET starts decreasing, it becomes necessary to insert performance boosters, such as novel materials and non-classical device structures, to enhance performance. In order to enhance the performance without sacrificing off state leakage power, strain technology was adopted to improve the drive current. Mechanically stressed Si has higher mobility than relaxed Si. However, for further scalability of the device, the materials with even higher mobility than strained Si are needed. The materials such as strained Ge, strained Si-Ge or even more futuristic carbon nanotubes and graphene have been actively investigated to study the possibility of substituting Si as a channel material in future as they exhibit 20 to 40 times larger mobility than Silicon, high mobility generally comes along with large dielectric constant and small band gap which are the basic properties of semiconductor materials which have weak bonding between atoms *[1]*.

II. MOTIVATION

Previous work laid stress on providing the explanation regarding the transport in uniaxial strained-Si MOSFETs through simple band structure and mobility calculations. However, as we scale down MOSFETs to very short channel lengths, the effect of the high-field transport, density of states (DOS), band structure, mobility and effective mass, in calculating the eventual drive current, we require expanded investigation *[3]*. Furthermore, strain modifies the band structure and changes the BTBT limited off-state leakage. Here in this work, the band structures are calculated using the non-local Empirical Pseudopotential method. Full-Band Monte-Carlo Simulations were used to evaluate the transport. 1-D Poisson-Schrodinger solver and detailed

BTBT simulations (including direct and indirect transitions) are used here to calculate the electrostatics and the off-state leakage. Then we will systematically compare and benchmark nano-scale (Ts=5nm, Lg=15nm) DG n-FETs, with different high mobility channel materials Si and Ge, in terms of their important performance metrics such as Drive Current, Intrinsic Delay and Off-state Leakage. Two standard channel directions, [100] and [110], on the (001) surface will be taken into consideration *[5]*.

III. UNIAXIAL STRAIN

We have considered uniaxially strained-Si and strained-Ge MOSFETs on a (001) wafer with channel direction in [100] and [110]. In addition, we have taken both tensile and compressive stresses from the –5GPa to +5GPa. Under this simulation study, we have extended our range of stress, however, it must be noted that for values of stress >3GPa, bulk materials are very close to their fracture point and may be impractical to achieve. The uniaxial stress was applied in the channel direction. Also we have considered that the channel direction is denoted ‘x’, the width direction ‘y’, and the direction perpendicular to the gate ‘z’ *[4]*.

IV. BAND STRUCTURE CALCULATION

The band structures are calculated using the non-local Empirical Pseudopotential method. Once we have the band structure of the material, complex movement of carriers in semiconductor can be simplified. The band structure of a semiconductor describes the range of energy and crystal momentum (k) whether an electron is “forbidden” or “allowed” to have. It is because of the diffraction of the quantum mechanical electron waves in the periodic crystal lattice. Also the band structure obtained in real 3-D crystal momentum (k) space gives us the information on carrier’s density of states, quantum quantization effective mass, transport effective mass. The band structure also can be expanded in complex k space where k space is no longer real number rather complex number. Band information in complex k-pace provides information on the decaying states coupling two bands *[5]*.

The Principles of Pseudo potential can express the complete Hamiltonian for the periodic semiconductor structure as *[1]*

“Equation 1 is . . .”

$$\mathbf{H} = \mathbf{H}_{\text{electrons}} + \mathbf{H}_{\text{nuclei}} + \mathbf{H}_{\text{nuclei-electron}}$$

where

“Equation 2 is . . .”

$\mathbf{H}_{\text{electrons}}=$

$$\sum_{\mu}\left(-\frac{\hbar^2}{2m_o}\nabla_\mu^2+\sum_{\lambda<\mu}\frac{e^2}{|\mathbf{r}_\lambda-\mathbf{r}_\mu|}\right)$$

where

$\mathbf{r}_\lambda$ is the position of the electron.

m_o is the mass.

“Equation 3 is . . .”

$\mathbf{H}_{\text{nuclei}}=$

$$\sum_{v}\left(-\frac{\hbar^2}{2M_v}\nabla_v^2+\sum_{\lambda<v}\frac{Z_\lambda Z_v e^2}{|\mathbf{R}_\lambda-\mathbf{R}_v|}\right)$$

where

$\mathbf{R}_v$ is the position.

Z_v is the atomic number.

M_v is the mass of the nuclei.

“Equation 4 is . . .”

$\mathbf{H}_{\text{nuclei-electron}}=$

$$-\sum_{\mu,\nu}\frac{Z_\nu e^2}{|\mathbf{R}_\nu - \mathbf{r}_\mu|}$$

There exists infinitely large numbers of electrons in a typical semiconductor, and hence it is almost impossible to track all these electrons. In addition, the strong Coulomb potential of the nucleus terms tend to go to negative infinity as an electron position gets close to the center of a nucleus, which needs very fine special gridding in numerical calculation of this system.

However, there are several approximations that allows one to achieve both acceptably accurate band structure and to reduce the computation complexity.

These are shown in fig.4 and includes *[1]*

1. Pseudopotential approximation under which, the electrons below the outer shell are tightly bound to the nucleus and the core states remain almost unchanged by interaction from electrons in outer shell (or valence bands).This permits us to replace the strong Coulomb potential of the nucleus and the effects of the tightly bound core electron by an effective ionic potential acting on the valence electrons.
2. The independent electron approximation replace the complicated electron-electron interactions with a time averaged potential.

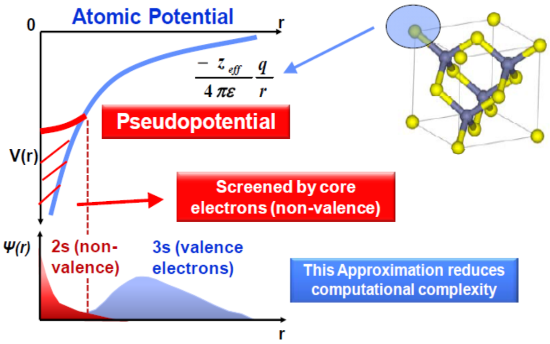

Fig.4: Pseudopotential approximation: The tightly bond inner electron shell can be effectively replaced by the pseudopotential *[1]*.

Thus, equation 4 can be expressed as
“Equation 5 is . . .”

H=

$$-\frac{\hbar^2}{2m_o}\nabla^2 + V_C$$

where

V_C is crystal potential that includes the interaction between the electrons and the nuclei and the interaction between the electrons.

V. EFFECTIVE MASS, DOS AND BAND GAP CALCULATION

The effective masses are depicted in figs. 5 (a) and (b). For Si [100] the effective mass reduces slightly for both tensile and compressive in all directions. For Si [110], compressive stress rapidly reduces the mass in the transport direction (x) while greatly increases the mass in the width direction (y), leading to a high density of states. For Ge, compressive stress allows a rapid reduction in the transport mass and in the [110] direction it behaves similar to Si *[5]*.

This allows the simultaneous increase in the DOS. Also, the relative positions of all the different valleys for Ge [110] are shown in fig. 6. The decrease in the band gap for compressive uniaxial stress along [100] for Si is always the X-valley. For Ge [110] it is the L-valley but for Ge [100], the lowest valley shifts from L- to X- for large values of stress, due to the rapid reduction in the X-valley band gap. As seen in the fig. 6, for compressive stress in Ge [110], the valley Γ - band gap increases, while for tensile it sharply reduces.

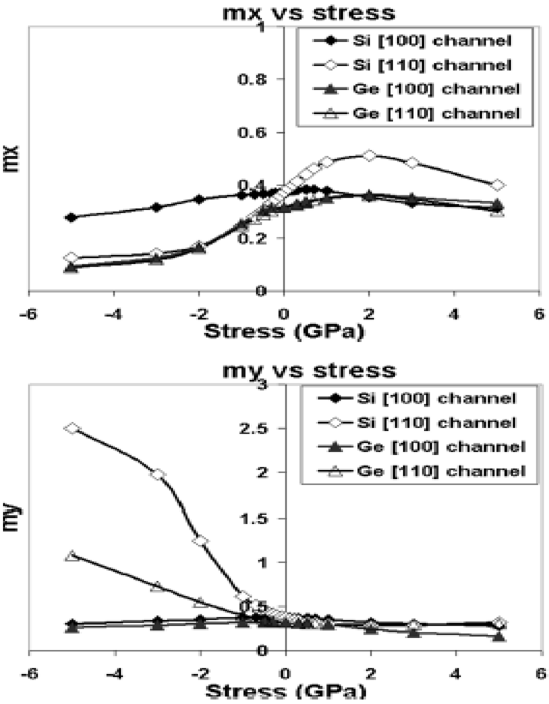

Fig.5 (a) and (b): The effective mass for Si and Ge as a function of uniaxial strain *[5]*.

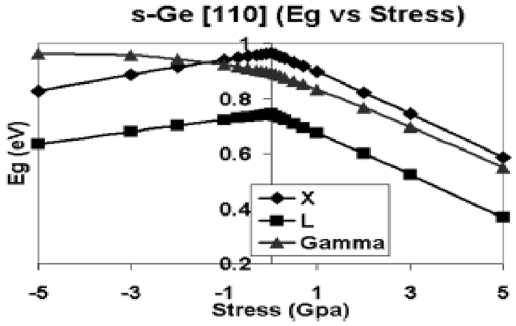

Fig.6: The lowest valley for Ge [110] is always L- and the band gap is relatively large even for large [110] uniaxial stress *[5]*.

VI. LOW-FIELD MOBILITY AND VELOCITY-FIELD CURVES CALCULATION

For a 2-D hole inversion carrier concentration of 1.8x10^{13}cm^{-2}, the effective, low driving field mobility in the channel transport direction is shown in fig.7. The mobility for compressively strained [110] strained-Ge is the highest in the channel direction, because of its lower mass and lifting of the band degeneracy. The mobility is ~6 times larger than for the relaxed-Ge and ~2 times larger than for [110] strained-Si. Thus mobility can be increased to ~12 times for strained-Ge [110], ~6 times for strained-Si [110] and ~2 times for relaxed-Ge, in comparison to the relaxed-Si *[5]*.

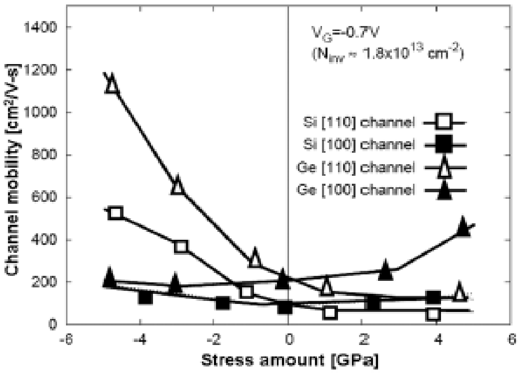

Fig.7: Low-field mobility vs uniaxial stress for Si and Ge *[5]*.

The bulk velocity-field curves for Si and Ge under uniaxial strain are depicted in figs. 8 (a), (b) and (c) (relaxed, compressive and tensile stress). The bulk velocities for compressive Si [110], and Ge [110] are extremely large and exhibit stationary velocity overshoot under bulk conditions. Si [110] shows an increase of ~50%, and Ge [110] exhibits an increase of ~40%, in comparison to their relaxed unstrained cases respectively.

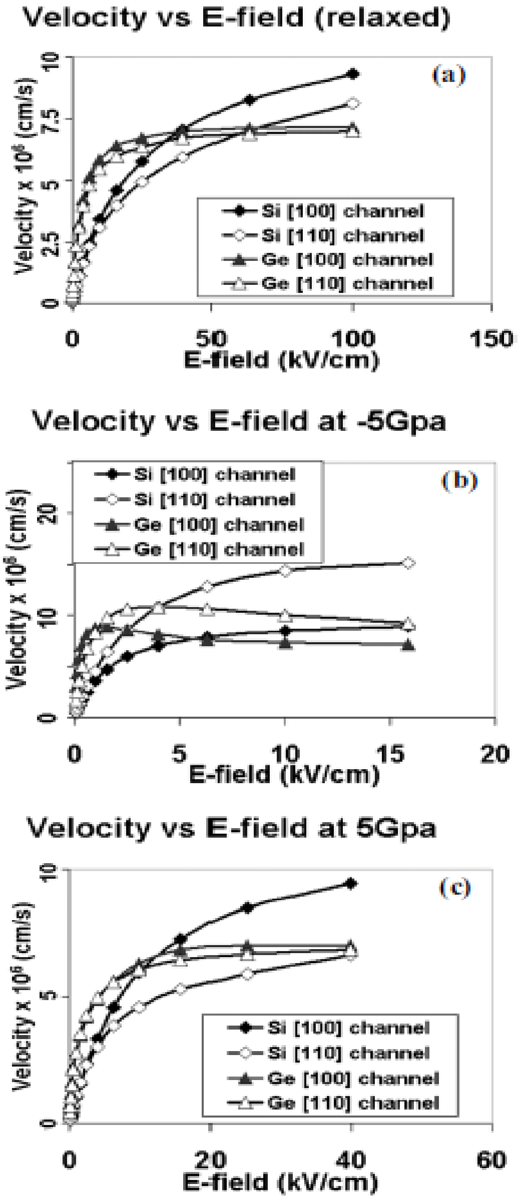

Fig.8 (a), (b) and (c): Velocity-field curves for the uniaxially strained Si and Ge in comparison to relaxed Substrates *[5]*.

VII. DRIVE CURRENT, DELAY AND OFF-STATE LEAKAGE CALCULATION

On studying fig.9, we find the large increase in the bulk velocity at high driving fields, in compressive Si [110], which leads to high drive currents. The higher mobility of compressively strained Ge [110] and the enhanced high driving field bulk velocity leads to a very high drive current, which is the highest among all the channels taken. The minimum off-state leakage in compressively strained-Ge [110] is an order of magnitude lower than in strained-Ge [100] due to the larger L- and Γ -valley band gaps (Fig. 10). Si [110] shows the lowest leakage, (100 times lower than Ge), because of its large indirect X-valley band gap *[5]*.

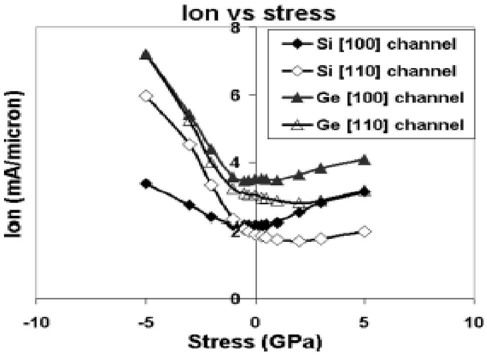

Fig. 9: The drive current for Ge [100] and Ge[110] under uniaxial compressive stress *[5]*.

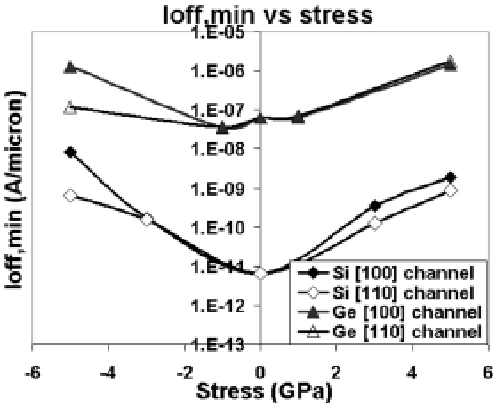

Fig.10: The minimum achievable off-state leakage under compressive stress *[5]*.

VIII. CONCLUSION

The parameters such as strain, channel orientation, band structure, DOS, effective mass, band gap, mobility and velocity helps us in calculating the performance n-MOSFETs. For the lower values of the uniaxial stress, compressively strained-Ge gives us the best performance in terms of the drive current, the delay reduction (~2 times in comparison to relaxed-Si). Although, the minimum off-state leakage because of BTBT is rather high (100nA/μm).

For the larger values of uniaxial strain, mainly because of the large increase in the bulk velocity at high driving fields, the anisotropic effective mass and large band gap, Si [110] strained compressively to >

-3GPa gives the best performance the in terms of the drive current ,delay reduction (~3 times) and very low off-state leakage (<1nA/μm). However, it should be keep in mind that the values of stress > +3GPa for bulk materials is very closer to their fracture point and may be impractical to achieve.

ACKNOWLEGMENT

I would like to acknowledge and extend my heartfelt gratitude to Mr. Dhiraj Kapoor (Assistant Professor, Department of E.C.E) and Mr. Naveen Goel (Associate Professor & Head Department of E.C.E) who supported me to complete this paper with proper guidance. I am heartily thankful to college for facilitating various means like material, which helped to accomplish the task.

REFERENCES

[1]. Donghyun Kim Thesis, "Theoretical Performance Evaluations of NMOS Double Gate FETs with High Mobility Materials: Strained III-V, Ge and Si", Stanford University, Nov 2009.
[2]. G. E. Moore, "Cramming more components onto integrated circuits (Reprinted from Electronics, pg 114- 117, April 19, 1965)," Proceedings of the IEEE, vol.86, no. 1, pp. 82-85, Jan, 1998.
[3]. Md. Imtiaz Alamgir et al., "Performance Analysis of Dg Mosfets with High-K Stack on Top & Bottom
[4]. Gate", International Journal of Scientific & Technology Research Volume 1, ISSUE 5, June 2012.
[5]. Rajni Gautam et al., **"**Analytic Model of Double Gate MOSFET for High Sensitivity Low Power Photosensor", Journal of Technology & Science Vol.13, No.5, October 2013.
[6]. T.Krishnamohan et al.,"High Performance, uniaxially-strained, si & ge, double-gate p- MOSFETs", Microelectronics Engineering 84 (2007) 2063–2066.

OPEN ACCESS

International
Journal
Of Modern Engineering Research (IJMER)

Effect of Nanoparticles on E-Glass Fiber Epoxy Resin Composites

Y. Haribabu[1], P. Devi Prasad[2]
[1]Mechanical department, AITAM college of engineering, AUTONOMOUS, INDIA
[2]Mechanical department, AITAM college of engineering, AUTONOMOUS, INDIA

ABSTRACT: *In the present work fabrication of composite material(E-Glass Fiber Epoxy Resin + NANO $CaCO_3$) was carried out and their tensile properties viz tensile strength, tensile strain(%),young's modulus, energy at maximum load and brihnall hardness number were found. Specimens of E-Glass Fiber Epoxy Resin) hybrid composites are prepared with four different compositions of nano-calcium carbonate ($CaCO_3$), viz., 0,3,5 and 7%.Each specimen consisting of 40%GF. The specimens are prepared by hand lay up method.. Tests are conducted on these specimens to determine the tensile strength, tensile strain, young's modulus energy at maximum load and hardness number at room temperature using universal testing machine and Brihnell hardness testing machine. The influence of the nano-$CaCO_3$ content on the mechanical properties tensile of hybrid composites was studied. It is found that the reinforcing and toughening effects of the E-Glass epoxy hybrid composites are increased by adding nano-$CaCO_3$.The tensile strength, tensile strain, young's modulus and energy at max load of these composites increased nonlinearly with the addition of the nano-$CaCO_3$.*

Keywords: *hybrid composites,Nano-$CaCo_3$, Epoxy resin, Tensile properties, hardness test, chopped strand mat E-glass fiber.*

I. INTRDUCTION

Fiber reinforced polymer composites are very widely used because of their favorable properties such as high specific tensile and compressive strength, controllable electrical conductivity, low coefficient of thermal expansion, good fatigue resistance and suitability for the production of complex shape materials. These materials have become the alternative of conventional structural materials such as steel, wood or metals in many applications. Typical areas of composite applications are car industry, aircraft fabrication, wind power plant, boats, ships, etc. During the human history, composites made occasionally large breakthroughs in construction and other materials. Among the composites, Chopped strand mat E-glass/ epoxy composite is emerging as a promising material for marine application due to their excellent superior strength, moisture resistance and electrical and fire insulation than that of other composites in making boat hulls, fiber glass boat. Bijesh1 , studied the mechanical properties of chopped strand mat E-glass / epoxy composite with different fiber wt%. He found that 50wt% fiber composite gave the high mechanical properties than that of (30 and 40wt %). They found that 5wt% nanoCaCo3 epoxy sample gave the highest tensile strength & Vickers hardness value among all remaining (0 to 8 wt %). Literature survey indicate that very limited work has been done on mechanical behavior of chopped strand mat E-glass fiber reinforced epoxy composite of varying fiber wt%. Various researchers have investigated the effect of Nano-inclusions on various polymers and also discussed the properties of polymers. The influence of adding Nano-inclusions to the polymers are studied. here the aim of this work is to fabricate the chopped strand mat E-glass / epoxy nanoCaCo3 composite of varying wt% using hand layup technique and to study the mechanical properties of the composites. Various other different methods of fabricating the polymer matrix composites are wet lay up (hand layup), resin transfer molding, filament winding and compression molding. Among the techniques mentioned above, Hand layup technique is used in this study since; it is effective, economic, good surface finish and easy fabrication.

II. EXPERIMENTAL ANALYSIS

Chopped strand mat (powder bonded) is formed by binding chopped glass fibers, using spraying powder binder. The density of the mat is 450g/m2 supplied by Binani Industries Limited (Glass Fibre Division). Initially (330x330) mm mat of four layers are cut for fabricating each composite. The fibre content in the three composites are 30 wt% of total weight of the composite. The type of epoxy resin used in the present investigation is Araldite LY556 and hardener is HY951. They are mixed in 10:1 weight ratio. The epoxy weight in the all composites are same wt% of total weight of the composite. Nano CaCo3 is added to all sheets.

Smectites have a unique morphology featuring one dimension in the nanometer range. Nonmaterial's can be defined as materials which have structured components with at least one dimension less than 100 nm.

III. COMPOSITES PREPARATION

The composite material used for this study is prepared by hand lay up method as shown in below fig. Mold release agent is applied to milar sheet of 75 micron. Epoxy resin and nano CaCo3are mixed and kept for one or two hours. Then, this mixture is mixed with the hardener, and applied to the milar sheet. Then the mat is kept and final mixture is applied to the mat. Now, roller is used to eliminate air bubbles. The same procedure is carried out for all four mats for each composite. Another milar sheet is kept on this and air bubbles are removed. Then the composites so prepared are cured at room temperature for 18 hours. The post curing is carried out in sun light for 4 hours on each side of the three composites. The stoppers are used for ensuring uniform thickness for the composites. Figures 2,3 and 4 show the composites prepared for this study.

Fig: Hand layup method

Instrument and Methodology

The tensile properties of E-Glass Fiber Epoxy Resin+*NANO* $CaCO_3$ hybrid composites are measured at room temperature by means of universal testing machine with extensometer .Tests were conducted according to ASTM D638 standard with cross-head descending speed of 2mm/min. The various properties are found from the experiment are tensile strength, tensile elongation at break point, young's modulus energy at maximum load. The mean values of polymer nano composites have been noted. The hardness test of the E-Glass Fiber Epoxy Resin+*NANO* $CaCO3_3$Ternary composites were measured at room temperature by means of a Brinell hardness testing machine. Hardness test is conducted according to ASTM E 10. All Brinell tests use a carbide ball indenter.

UNIVERSAL TESTING MACHINE

SPECIMANS FOR HARDNESS TEST

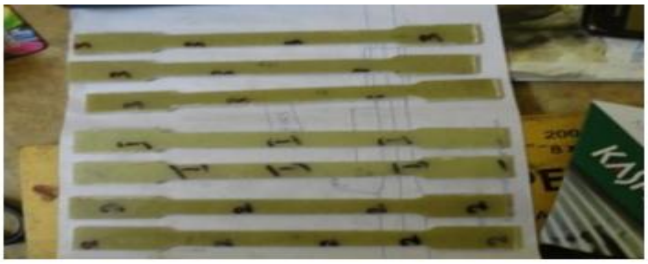

SPECIMANS FOR TENSILE TEST ASTM D638

IV. RESULTS AND DISCUSSION

This table shows the mean values of max load, tensile strength, tensile strain, young's modulus and energy at maximum load at different specimen labels.

S.NO	Specimen labels	Mean Tensile strength (MPa)	Mean Tensile strain at Break (%)	Mean value of Youngs Modulus (MPa)	Mean value of Energy at Maximum Load (J)
1	E-GF+ Epoxy Resin +0%NC	134	3.82	4091	10.90
2	E-GF+ Epoxy Resin +3%NC	146	4.04	5666	12.43
3	E-GF+ Epoxy Resin +5%NC	145	3.93	4572	12.03
4	E-GF+ Epoxy Resin +7%NC	145	3.86	4572	11.77

1. Tensile strength

Fig 1.1 shows the dependence of the tensile strength of the E-GF+ Epoxy Resin nano-$CaC0_3$ composites on the weight fraction of nano-$CaCO_3$ ($\varnothing_f$) particles. The value of tensile strength increased with the increase of addition of weight fraction of nano-$CaCO_3$ particles to the matrix E-GF+ Epoxy Resin. The graph varies non-linearly from base composite to the E-GF+ Epoxy Resin +7%nano-$CaCO_3$ Hybrid composite .The maximum increase of tensile strength observed when the addition of 3% of nano-$CaCO_3$ particles to matrix this increase observed as 8 compared to the base composite i.e. E-GlassFiber Epoxy nano-$CaCO_3$.

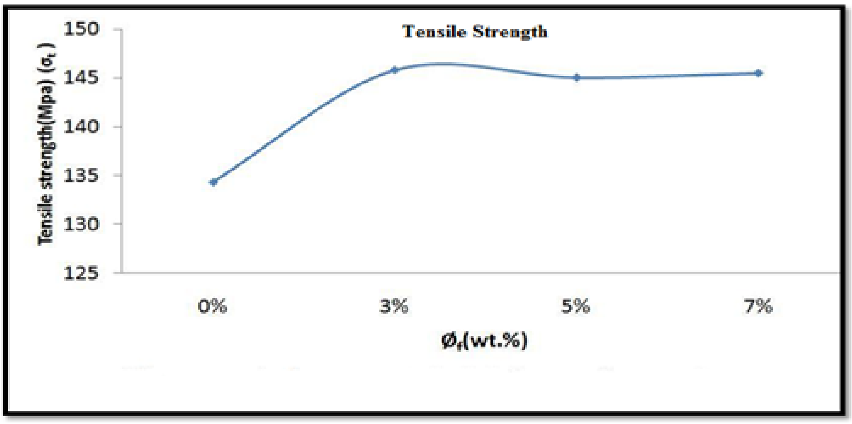

FIG 1.1 Effect of weight fraction of nano CaCO3 on tensile strength

2. Tensile strain

Fig 1.2 shows the dependence of the tensile strain of the E-GlassFiber Epoxy +Nano-$CaCO_3$ composites on the weight fraction of Nano-$CaCO_3$ particles.It can be seen that tensile strain increased non linearly with the addition of weight fraction of nano- $CaCO_3$.It means that the tensile strain of the E-GlassFiber Epoxy binary composite materials filled with the increasing nano-$CaCO_3$ concentration will be enhanced effectively. The Max increase of the tensile strain ($€_t$) is observed at $\varnothing_f$ =3% is 5.59% as compared to the weight fraction of nano-$CaCO_3$ at $\varnothing_f$ = 0%.

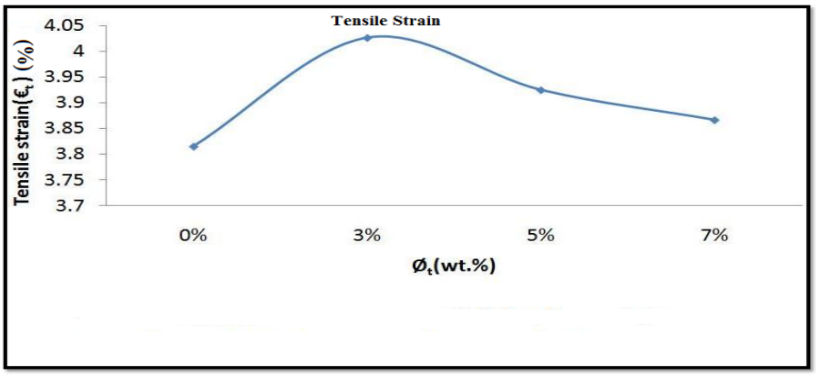

Fig 1.2: Effect of weight fraction of Nano-$CaCO_3$ ($\varnothing_f$) on Tensile Strain ($€_t$)

3. Young's modulus

Young's modulus is one major parameter for characterizing the tensile fracture toughness of materials. Fig 1.3 shows the effect of the weight fraction of the distribution of the particles in the matrix and the interfacial morphology between them are improved better. Consequently, the tensile fracture toughness of the E-Glass Fiber Epoxy +/nano-$CaCO_3$ hybrid composite was enhanced correspondingly. The maximum increase of the young's modulus (E_t) at $Ø_f$ =3% is 11.77% as compared to the weight fraction of nano-$CaCO_3$ at 0%.Here the young's modulus (E_t) increased non linearly up to $Ø_f$ =3% , with the addition of wt. fraction of nano-$CaCO_3$ particles then decreases up to $Ø_f$ =5% then slightly decreases up to $Ø_f$ =7%.

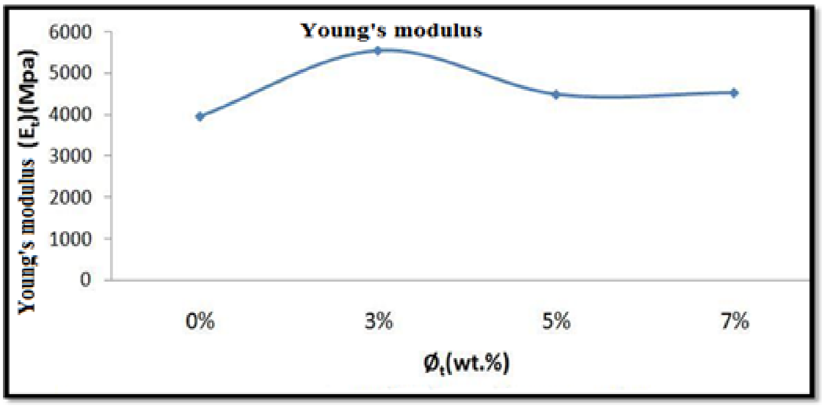

Fig 1.3: Effect of weight fraction of Nano-$CaCO_3$ ($Ø_f$) on young's modulus (E_t)

5. Hardness test results: Hardness is extensively used to characterize materials and to determine if they are suitable for their intended use. The most common uses for hardness tests is to verify the heat treatment of a part and to determine if a material has the properties necessary for its intended use. It can be seen that the maximum increase of hardness number is observed at $Ø_f$ =5% is3.14% compared to the weight fraction of nano-$CaCO_3$ at 0%. Here the hardness number increased up to $Ø_f$ =5%. With the addition of wt. fraction of nano-$CaCO_3$ particles then gradually decreases at $Ø_f$ =7%.

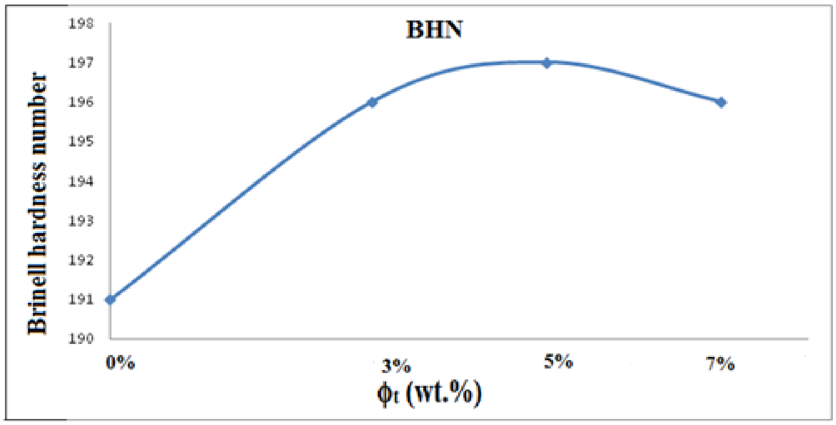

Fig.4.9 Effect of weight fraction of Nano-$CaCO_3$ ($Ø_f$) on Brinell hardness number (BHN**)**

V. CONCLUSIONS

The following conclusions are dragged from the experimental investigations

1. Reinforcing and toughening effects were found on E-GlassFiber Epoxy+nano-$CaCO_3$ composite materials.
2. It was found that when the weight fraction of the nano particles was equal to 3%, the tensile strength and young's modulus and tensile strain were increased non linearly with the weight fraction of nano-$CaCO_3$ ($Ø_f$).
3. The maximum increase of tensile strength observed when the addition of 3% of nano-$CaCO_3$ particles to matrix this increase observed as 8.78% compared to the base composite i.e., E-Glass Fiber Epoxy +nano-$CaCO_3$.
4. The maximum increase of the tensile strain (€$_t$) is observed at $Ø_f$ =3% is 5.59% compared to the weight fraction of nano-$CaCo_3$ at $Ø_f$ = 0%.
5. The maximum increase of the Young's Modulus (E_t) at $Ø_f$ =3% is 11.77% compared with the weight fraction of nano-$CaCO_3$ at 0%.Here the Young's Modulus (E_t) has been increased non linearly up to $Ø_f$

=3% with the addition of weight fraction of nano-$CaCO_3$ particles then decreases up to $Ø_f$ =5% then slightly decreases up to $Ø_f$ =7%.

6. The energy at maximum load (σ_E) is increased non linearly up to $Ø_f$=3%, with the addition of weight fraction of nano-$CaCO_3$ particles then gradually decreases up to $Ø_f$ =7%
7. It can be seen that the maximum increase of hardness number is observed at $Ø_f$ =5% is3.14% compared to the weight fraction of nano-$CaCO_3$ at 0%. Here the hardness number increased up to $Ø_f$ =5%, with the addition of wt. fraction of nano-$CaCO_3$ particles then gradually decreases at $Ø_f$ =7%.
8. The mechanical properties of tensile strength, tensile strain and young's modulus at 3% and hardness at 5% showed that there was a good.

REFERENCES

[1] Liang. and Li., “Mechanical Properties and Morphology of Glass Bead-Filled Polypropylene Composites, polymer composites” polymer composites,Vol.19 No. 6 December 1998.

[2] Ji-Zhao Lianga, Lia., “Brittle-ductile transition in polypropylene filled with glass blends” Elsevier polymer PP-3191-3195,1998.

[3] Kong Yang, Chaoyuan Wang, Jie Wei,“A study on biocomposite of nano apatite/poly(1,4-phenylene-sulfide)-poly (2,4-phenylene sulfide acid) science direct Composites: Part B 38,PP-306-310, 1st November 2006.

[4] Zhaobin Chen, Xujun Liu, Renguo Lu , Tongsheng Li,“Friction and Wear Mechanisms of PA66/PPS blend reinforced with Carbon Fiber ” Wiley Inter Science, DOI 10.1002/app.25999, 28thMarch 2007.

[5] Shimpi, Verma and Mishra, “Dispersion of nano $CaCO_3$ on PVC and its Influence on Mechanical and Thermal propetie” Journal of Composite Materials 2010 vol.44: 211 17th August 2009.

[6] Shimpi, Verma and Mishra, “Dispersion of nano $CaCO_3$ on PVC and its Influence on Mechanical and Thermal propetie” Journal of Composite Materials 2010 vol.44: 211 17th August 2009.

[7] Dan Lu, Shiwei Pan,“Effects of Ball Milling Dispersion of Nano-SiOx Particles on Impact Strength and Crystallization Behavior of nano-SiOx–poly(phenylene sulfide) Nanocomposites” Wiley InterScience,DOI 10.1002/pen.20547,2006.

[8] Knor,Walter,Haupert,“Mechanical and Thermal Properties of Nano-Titanium Dioxide-Reinforced Polyetheretherketone Produced by Optimized Twin Screw Extrusion” Journal of Thermoplastic Composite Materials 2011 vol.24: 185 ,2010.

[9] Rajendra Kumar Goyal and Amol Kadam, “Polyphenylene sulphide/graphite composites for EMI shielding applications” VBRI press Adv. Mat. Lett. 2010, 1(2), PP-143-147,27 July 2010.

[10] Hanim,Ahmad Fuad, Zarina, Mohd Ishak and Azman Hassa, “Properties and Structure of Polypropylene/ Polyethylene-Octene elastomer/nano $CaCO_3$ Composites” Journal of Thermoplastic Composite Materials vol.21: 123,2008.

[11] Qiyang, Limin, Guangxin and You“Preparation and Characterization of Acrylic/Nano-TiO2 Composite Latex High Performance Polymers”High Performance Polymers vol.14: 383,2002.

OPEN ACCESS

International
Journal
Of Modern Engineering Research (IJMER)

An Amalgamation-Based System for Micro aneurysm Detection and Diabetic Retinopathy Grading

Sudhir. S. Kanade[1], Tejashri. S. Bobade[2]
[1]*Head of Electronics&Telecommunication Department, TPCT'S college of engineering, Osmanabad, Maharashtra, India.*
[2]*Research scholar, Electronics&Telecommunications, TPCT'S college of engineering, Osmanabad, Maharashtra India.*

ABSTRACT: *We propose an ensemble-based framework to improve microaneurysm detection. Unlike the well-known approach of considering the output of multiple classifiers, we propose a combination of internal components of microaneurysm detectors, namely preprocessing methods and candidate extractors. We have evaluated our approach for microaneurysm detection in an online competition, where this algorithm is currently ranked as first, and also on two other databases.*

Keywords: *Diabetic retinopathy (DR) grading, ensemble-based systems, fundus image processing, microaneurysm (MA) detection.*

I. INTRODUCTION

Diabetic retinopathy (DR) is the most common cause of blindness in the developed countries. Microaneurysms (MAs) are early signs of this disease, so the detection of these lesions is essential in the screening process. DR can be prevented and its progression can be slowed down if diagnosed and treated early.. Microaneurysm appear as small circular dark spots on the surface of the retina .the most common appearance of microaneurysms is near thin vessels, but they cannot actually lie on the vessels. In some cases, microaneurysms are hard to distinguish from parts of the vessel system. A key feature to recognize DR is to detect microaneurysms (MAs) in the funduss of the eye. The importance of handling MAs are twofold. First, they are normally the earliest signs of DR; hence their timely and precise detection is essential.

II. OBJECTIVE

In this paper we use ensemble based frame work. This is used to choose the best combination of preprocessing methods and candidate extractors

III. EXISTING SYSTEM

DIABETIC retinopathy (DR) is a serious eye disease that originates from diabetes mellitus and is the most common cause of blindness in the developed countries. Therefore, much effort has been made to establish reliable computer aided screening systems based on color fund us images. In previous work "On combining computer-aided detection systems," showed that the fusion of the results of the several MA detectors leads to an increased average sensitivity measured at seven predefined false positive rate.

3.1 Existing System Disadvantages:

A. In our earlier research on combining MA detectors did not provide reassuring results
B. The low Sensitivity of MA detectors originates from the candidate extractor part.

IV. PROPOSED SYSTEM

In this paper, we propose an effective MA detector based on the combination of preprocessing methods and candidate extractors. We provide an ensemble creation framework to select the best combination. An exhaustive quantitative analysis is also given to prove the superiority of our approach over individual algorithms. We also investigate the grading performance of our method, which is proven to be competitive with other screening systems.

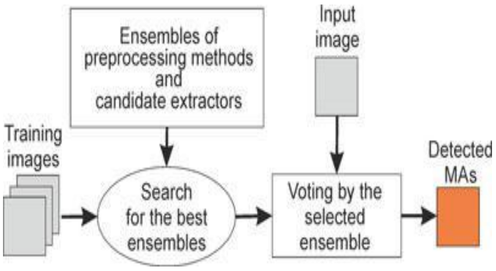

Fig- 1: Flow chart of the ensemble-based framework.

4.1. PROPOSED ADVANTAGES

A. The framework has high flexibility for different datasets.
B. The detector to provide sufficient sensitivity and specificity rate.

V. DIABETIC RETINOPATHY

Diabetes is a disease that occurs when the pancreas does not secrete enough insulin or the body is unable to process it properly. Insulin is the hormone that regulates the level of sugar (glucose) in the blood. Diabetes can affect children and adults . Patients with diabetes are more likely to develop eye problems such as cataracts and glaucoma, but the disease's affect on the retina is the main threat to vision. Most patients develop diabetic changes in the retina after approximately 20 years. The effect of diabetes on the eye is called diabetic retinopathy. Over time, diabetes affects the circulatory system of the retina. The earliest phase of the disease is known as background diabetic retinopathy. In this phase, the arteries in the retina become weakened and leak, forming small, dot-like hemorrhages. These leaking vessels often lead to swelling or edema in the retina and decreased vision.

The next stage is known as proliferative diabetic retinopathy. In this stage, circulation problems cause areas of the retina to become oxygen-deprived or ischemic. New, fragile, vessels develop as the circulatory system attempts to maintain adequate oxygen levels within the retina. This is called neovascularization. Unfortunately, these delicate vessels hemorrhage easily. Blood may leak into the retina and vitreous, causing spots or floaters, along with decreased vision.

In the later phases of the disease, continued abnormal vessel growth and scar tissue may cause serious problems such as retinal detachment and glaucoma.

The affect of diabetic retinopathy on vision varies widely, depending on the stage of the disease. Some common symptoms of diabetic retinopathy are listed below, however, diabetes may cause other eye symptoms.

A. Blurred vision (this is often linked to blood sugar levels
B. Floaters and flashes
C. Sudden loss of vision

Diabetic patients require routine eye examinations so related eye problems can be detected and treated as early as possible. Most diabetic patients are frequently examined by an internist or endocrinologist who in turn works closely with the ophthalmologist. The diagnosis of diabetic retinopathy is made following a detailed examination of the retina with an ophthalmoscope. Most patients with diabetic retinopathy are referred to vitreo-retinal surgeons who specialize in treating this disease. Diabetic retinopathy is treated in many ways depending on the stage of the disease and the specific problem that requires attention. The retinal surgeon relies on several tests to monitor the progression of the disease and to make decisions for the appropriate treatment. These include: fluorescein angiography, retinal photography, and ultrasound imaging of the eye

Fig-2: Influence Of Diabetes On Vision

5.1 CLASSIFICATION OF DIABETIC RETINOPATHY

Diabetic retinopathy occurs when the blood vessels of the retina in the posterior part of the eye are damaged. Damages due to small vessels would be known as microvascular disease while damages due to the arteries would be macrovascular disease. Generally, diabetic retinopathy is classified into two main stages, namely nonproliferative diabetes retinopathy (NPDR) and proliferative diabetes retinopathy (PDR).

5.1.1 NON-PROLIFERATIVE DIABETIC RETINOPATHY

In NPDR, depending on the presence and extent of the features such as hard exudates, microaneurysms or cotton wools spots due to leakage of fluid and blood from the blood vessels, can be classified to mild, moderate or severe stages as followings:

5.1.1.1. Mild NPDR:

This is the earliest stage of retinopathy and vision is usually normal except in some cases. However, deterioration of the blood vessels in the retina has already started. Blood vessels erupt when there is not enough oxygen in the blood because of high levels of glucose. Small swellings known as Micro-aneurysms or flame-shaped hemorrhages start to develop in the fundus quadrants.

5.1.1.2. Moderate NPDR:

As the disease progresses, some of the blood vessels that irrigate the retina become blocked. It is more than “mild” but less than “severe” stage. There will be micro-aneurysms or hemorrhages of greater severity in one to three quadrants and leakage might occur, resulting cotton wool spots and exudates etc to be present in the retina.

5.1.1.3. Severe NPDR:

As more blood vessels are blocked, those areas in the retina will be deprived of blood supply. Signals will then be sent to the body for the growth of new vessels in order to compensate for the lack of nourishment. The disease would be considered severe NPDR stage when any of the following criteria are met:

- Severe (more than 20) hemorrhages and micro-aneurysms in all four quadrants of the fundus
- Definite venous beading in at least two quadrants
- Severe damage to the small blood vessels in at least one quadrant but no signs of any proliferative diabetic retinopathy.

5.1.2 PROLIFERATIVE DIABETIC RETINOPATHY

PDR is the advanced stage whereby signals are sent by the retina to the body for the lack of blood supply and this triggered the growth of new blood vessels. These blood vessels can grow along the retina and the surface of the jelly-like substance (vitreous gel) which fills the centre of the eye. Although they are fragile and abnormal, they do not cause symptoms or vision loss. It is only when their thin and weak walls leak blood, severe visual loss or even irreversible blindness would occur.

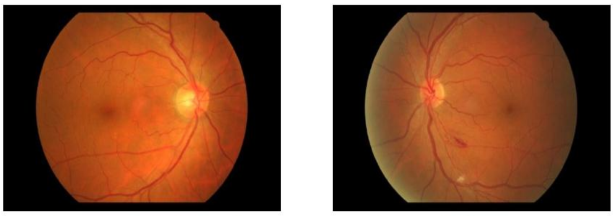

Mild Non-Proliferative Retinopathy   Moderate Non-Proliferative Retinopathy

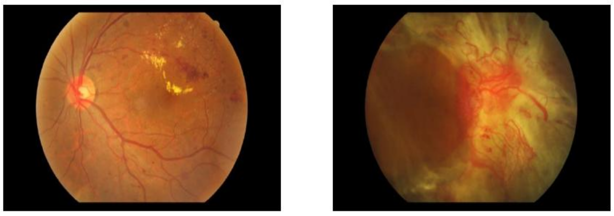

Severe Non-Proliferative Retinopathy   Proliferative Retinopathy

Fig-3: Retinal Images to Show The Different Stages Of Diabetic Retinopathy

VI. METHODOLOGIES

6.1 .PREPROCESSING METHODS

The selection of the preprocessing method and candidate extractor components for this framework is a challenging task. Comparison of preprocessing methods dedicated to MA detection has not been published yet. Since preprocessing methods need to be highly interchangeable, we must select algorithms that can be used before any candidate extractor and do not change the characteristics of the original images (unlike, e.g., shade correction. We also found some techniques to generate too noisy images for MA detection (histogram equalization adaptive histogram equalization or color normalization.

6.1.1.Walter–KleinContrast Enhancement

This preprocessing method aims to enhance the contrast of fundus images by applying a gray level transformation using the following operator,

$$f' = \begin{cases} \dfrac{\frac{1}{2}(f'_{\max} - f'_{\min})}{(\mu - f_{\min})^r} \cdot (f - f_{\min})^r + f'_{\min}, \ f \le \mu \\ -\dfrac{\frac{1}{2}(f'_{\max} - f'_{\min})}{(\mu - f_{\max})^r} \cdot (f - f_{\max})^r + f'_{\max}, \ f \ge \mu \end{cases}$$

Where {fmin, . . . , fmax}, {f_ min, . . . , f_ max} are the intensity levels of original and the enhanced image, respectively, μ is the mean value of the original grayscale image and r ∈ R is a transition parameter.

6.1.2. Contrast Limited Adaptive Histogram Equalization

Contrast limited adaptive histogram equalization (CLAHE) is a popular technique in biomedical image processing, since it is very effective in making the usually interesting salient parts more visible. The image is split into disjoint regions, and in each region local histogram equalization is applied. Then, the boundaries between the regions are eliminated with a bilinear interpolation.

6.1.3. Vessel Removal and Extrapolation

We investigate the effect of processing images with the complete vessel system being removed based on the idea proposed. We extrapolate the missing parts to fill in the holes caused by the removal using the inpainting algorithm presented. MAs appearing near vessels become more easily detectable in this way.

6.1.4. Illumination Equalization

This preprocessing method aims to reduce the vignetting effect caused by uneven illumination of retinal images. Each pixel intensity is set according to the following formula:

$$f' = f + \mu_d - \mu_l$$

Where f, f' are the original and the new pixel intensity values, respectively, μ_d is the desired average intensity, and μ_l is the local average intensity. MAs appearing on the border of the retina are enhanced by this step.

6.1.5. No Preprocessing

We also consider the results of the candidate extractors obtained for the original images without any preprocessing. That is, we formally consider a “no preprocessing” operation, as well.

6.2 MA CANDIDATE EXTRACTORS:

Candidate extraction is a process that aims to spot any objects in the image showing MA-like characteristics. Individual MA detectors consider different principles to extract MA candidates. In this section, we provide a brief overview of the candidate extractors involved in our analysis. Again, just as for preprocessing methods, adding new MA candidate extractors may lead to further improvement in the future. A summary on the key differences of the candidate extractor algorithms and their performance measured in the Retinopathy online challenge (ROC) training dataset

6.2.1. Walter et al.

In our approach, color images input from the fundus camera are initially resized to a standard size of 768 × 576 pixels while maintaining the original aspect ratio. We select the green channel for all our operations because retinal images are almost always saturated in the red channel and have very low contrast in the blue channel. A closing operation is performed on the green channel image using two different sizes of a structuring element (filter). Closing operation is defined as dilation (Max filter) followed by erosion (Min filter). The formulations of dilation and erosion for gray scale images are as follows.

Dilation:

$$A \oplus B = A_1(x, y) = \sup_{i,j\in b}\left(A(x-i, y-j) + B(i, j)\right)$$

Erosion:

$$A \ominus B = A_1(x, y) = \sup_{i,j\in b}\left(A(x-i, y-j) + B(i, j)\right)$$

Where A is the input image, B and B1 are the structuring elements or masks used for dilation and erosion respectively and b1 are grids over which the structuring elements are defined. Dilation in gray scale enlarges brighter regions and closes small dark regions. The erosion is necessary to shrink the dilated objects back to their original size and shape. The dark regions closed by dilation do not respond to erosion. Thus, the vessels being thin dark segments laid out on a brighter background are closed by such a closing operation. A subtraction of the closed images across two different scales (let S1 and S2 be the sizes of the structuring elements B1 and B2) will thus give the blood vessel segments of the green channel image. The operation is as follows:

We use a disk shaped structuring element for morphological operations. The radius of the larger disk (S2) is fixed at a high value (we use 6 pixels for an image of size 768 × 576 pixels) so that all the vessels including the main blood vessel get closed. The size of the structuring element is chosen based on which describes the blood vessels to be ranging from 1.5-6 pixels in radius on an average. S1 is chosen adaptively as follows:

1. 1 or 2 pixels below S2 if we want to obtain only the thicker vessels emanating from the optic disk.
2. At least 4 pixels below S2 to obtain the entire blood vessel network. Criterion 1 is used for optic disk localization whereas criterion 2 is used in microaneurysms and hemorrhages detection.

The image C′ is threshold (90% of the maximum intensity) and median filtered to obtain the binary image of the blood vessels (U). Morphological thinning is then performed on U to obtain the skeleton of the blood vessel network. Thinning operation is implemented as $U - (U \ominus B1 - \overline{U} \ominus B2)$, where B1 and B2 are disjoint structuring elements and $\overline{U}$ is the complement of the image U. Noise can occur in the thinned image usually in the form of dots. A 2 × 2 median filtering operation is performed to remove the isolated specks of noise. The vessel segments being connected structures are unaffected by this operation. An additional source of noise in retinopathy images could be exudates, the removal.

6.2.2. Spencer et al.

From the input fundus image, the vascular map is extracted by applying 12 morphological top-hat transformations with 12 rotated linear structuring elements (with a radial resolution 15°). Then, the vascular map is subtracted from the input image, which is followed by the application of a Gaussian matched filter. The resulting image is then binarized with a fixed threshold. Since the extracted candidates are not precise representations of the actual lesions, a region growing step is also applied to them. While the original paper is written to detect MAs on fluorescein angiographic images, our implementation is based on the modified version published by Fleming et al.

6.2.3. Circular Hough-Transformation

Following the idea presented in, we established an approach based on the detection of small circular spots in the image. Candidates are obtained by detecting circles on the images using circular Hough transformation. With this technique, a set of circular objects can be extracted from the image.

6.2.4. Zhang et al.

In order to extract candidates, this method constructs a maximal correlation response image for the input retinal image. This is accomplished by considering the maximal correlation coefficient with five Gaussian masks with different standard deviations for each pixel. The maximal correlation response image is threshold with a fixed threshold value to obtain the candidates. Vessel detection and region growing is applied to reduce the number of candidates, and to determine their precise size, respectively.

6.2.5 Lazar et al

Pixel-wise cross-sectional profiles with multiple orientations are used to construct a multidirectional height map. This map assigns a set of height values that describe the distinction of the pixel from its surroundings in a particular direction. In a modified multilevel attribute opening step, a score map is constructed from which the MAs are extracted by thresholding.

6.3 ENSEMBLE CREATION:

In this section, we describe our ensemble creation approach. In our framework, an ensemble *E* is a set of *(*preprocessing method, candidate extractor) or shortly *(*PP, CE) pairs. The meaning of a *(*preprocessing method, candidate extractor) pair is that first we apply the preprocessing method to the input image and then we apply the candidate extractor to this result. That is, such a pair will extract a set of candidates *HE* from the original image. If an ensemble *E* contains more *(*preprocessing method, candidate extractor) pairs, their outputs are fused in the following way:

Take 10 training images (already disease affected images). Then we present the selected preprocessing methods, which we consider to be applied before executing MA candidate extraction. There may be around 5 methods present in Preprocessing. Candidate extraction is present next to preprocessing. Similar to preprocessing there are 5 techniques or methods present in Candidate extractors.

For a single image, 25 combinations of results are available. Since there are 5 methods available in both preprocessing and candidate extraction, for each method in preprocessing 5 candidate extraction methods are processed. Likewise it repeated for 5 methods in preprocessing. So there are 25 methods proceeded for a single image. Then we should calculate the entropy for all 25 results. Then after calculating the entropy for the 25 methods, we can predict the best technique, considering whose entropy is highest. For ex., If 3rd method's entropy is highest means we determine that 3rd one is the best technique.

Likewise, we should calculate for a set of 10 training images. By following the procedure mentioned above we can determine best techniques for 10 images.

For ex. the best techniques of 10 images are like this format mentioned below:

[3 2 4 3 6 3 8 3 4 3]

After analyzing the best techniques whose entropies are highest for 10 images, mentioned above, we can see that 3rd technique is repeated many times than other. So we can conclude that the 3rd technique is the best one

VII. EXPERIMENTATION

Orignal Image:

Grayscale Image

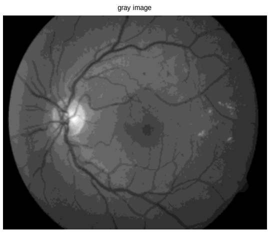

Histogram Equaliztion Image

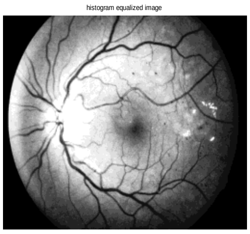

Walter-Klein Contrast Enhancement

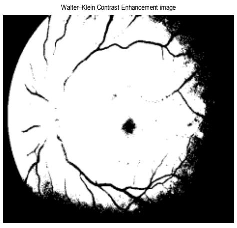

Contrast Limited Adaptive Histogram Equalization

Vessel Removal and Extrapolation

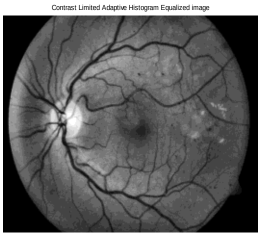

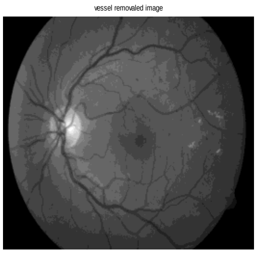

Illumination Equalization   Walter et al.

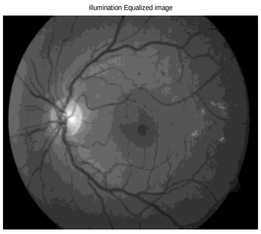

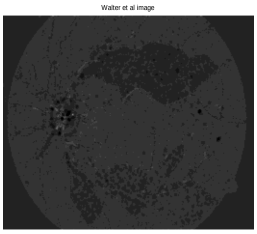

Circular
Hough-Transformation
Spencer et al

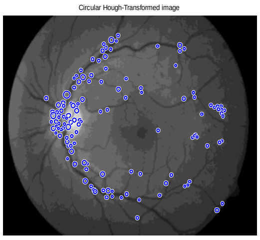

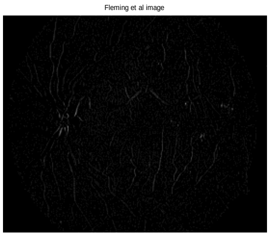

Zhang et al.   Lazar et al.

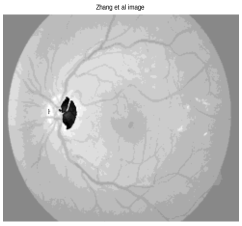

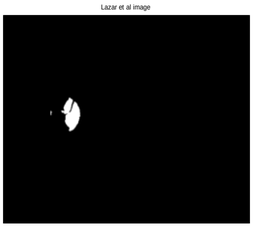

VIII. CONCLUSION

In this paper, we have proposed an ensemble-based MA detector that has proved its high efficiency in an open online challenge with its first position. Our novel framework relies on a set of⟨ preprocessing method, candidate extractor ⟩ pairs, from which a search algorithm selects an optimal combination. Since our approach is modular, we can expect further improvements by adding more preprocessing methods and candidate extractors. However, a proper screening system should contain other components, which is expected to increase the performance of this approach, as well.

ACKNOWLEDGEMENTS

I am grateful to my guide Dr. S.S.Kanade for providing me with invaluable guidance in this project.

REFERENCES

[1] M. Abramoff, M. Niemeijer, M. Suttorp-Schulten, M. A. Viergever, S. R. Russel, and B. van Ginneken, “Evaluation of a system for automatic detection of diabetic retinopathy from color fundus photographs n a large population of patients with diabetes,” Diabetes Care, vol. 31, pp. 193–198, 2008.

[2] A. D. Fleming, K. A. Goatman, S. Philip, G. J. Prescott, P. F. Sharp, and J. A. Olson, “Automated grading for diabetic retinopathy: A large-scale audit using arbitration by clinical experts,” Br. J. Ophthalmol., vol. 94, no. 12, pp. 1606–1610, 2010.

[3] H. J. Jelinek, M. J. Cree, D. Worsley, A. Luckie, and P. Nixon, “An automated microaneurysm detector as a tool for identification of diabetic retinopathy in rural optometric practice,” Clin. Exp. Optom., vol. 89, no. 5, pp. 299–305, 2006.

[4] M. Abramoff, J. Reinhardt, S. Russell, J. Folk, V. Mahajan, M. Niemeijer, and G. Quellec, “Automated early detection of diabetic retinopathy,” Ophthalmology, vol. 117, no. 6, pp. 1147–1154, 2010.

[5] M. Niemeijer, M. Loog, M. D. Abramoff, M. A. Viergever, M. Prokop, and B. van Ginneken, “On combining computer-aided detection systems,” IEEE Trans. Med. Imag., vol. 30, no. 2, pp. 215–223, Feb. 2011.

[6] B. Antal, I. Lazar, A. Hajdu, Z. Torok, A. Csutak, and T. Peto, “A multilevel ensemble-based system for detecting microaneurysms in fundus images,” in Proc. 4th IEEE Int.Workshop Soft Comput. Appl., 2010, pp. 137– 142.

[7] B. Antal and A. Hajdu, “Improving microaneurysm detection using an optimally selected subset of candidate extractors and preprocessing methods,” Pattern Recog., vol. 45, no. 1, pp. 264–270, 2012.

[8] A. A. A. Youssif, A. Z. Ghalwash, and A. S. Ghoneim, “Comparative study of contrast enhancement and illumination equalization methods for retinal vasculature segmentation,” in Proc. Cairo Int. Biomed. Eng. Conf., 2006, pp. 21–24.

[9] T. Walter and J. Klein, “Automatic detection of microaneurysm in color fundus images of the human retina by means of the bounding box closing,” Lecture Notes in Computer Science, vol. 2526. Berlin,Germany: Springer- Verlag, 2002, pp. 210–220.

[10] K. Zuiderveld, “Contrast limited adaptive histogram equalization,” Graphics Gems, vol. 4, pp. 474–485, 1994. [11] S. Ravishankar, A. Jain, and A. Mittal, “Automated feature extraction for early detection of diabetic retinopathy in fundus images,” in Proc. IEEE Conf. Comput. Vision Pattern Recog., 2009, pp. 210–217.

[12] A. Criminisi, P. Perez, and K. Toyama, “Object removal by exemplarbased inpainting,” in Proc. IEEE Conf. Comput. Vision Pattern Recog., vol. 2, 2003, pp. II-721–II-728.

[13] M. Niemeijer, B. van Ginneken, M. Cree, A. Mizutani, G. Quellec, C. Sanchez, B. Zhang, R. Hornero, M. Lamard, C. Muramatsu, X. Wu, G. Cazuguel, J. You, A. Mayo, Q. Li, Y. Hatanaka, B. Cochener, C. Roux, F. Karray, M. Garcia, H. Fujita, and M. Abramoff, “Retinopathy online challenge: Automatic detection of microaneurysms in digital color fundus photographs,” IEEE Trans. Med. Imag., vol. 29, no. 1, pp. 185–195, Jan. 2010.

[14] T. Walter, P. Massin, A. Arginay, R. Ordonez, C. Jeulin, and J. C. Klein, “Automatic detection of microaneurysms in color fundus images,” Med. Image Anal., vol. 11, pp. 555–566, 2007.

BIOGRAPHIES

Sudhir Sidheshwar Kanade received his B. E. (Electronics) degree in 1992 from Marathwada University, Aurangabad, (India) and M. E. (Electronics) degree in 1999 from Swami Ramanand Tirth Marathwada University, Nanded, (India). From 1993 to 2003 he worked as Lecturer and Senior Lecturer, from December 2003 to 2011 Assistant Professor and Associate Professor in department of Electronics and Telecommunication Engineering. Presently he is working as Professor and Head of Electronics and Telecommunication Engineering at College of Engineering, Osmanabad, (India). He received his Ph.D. degree in Electronics Engineering in 2013 at Dr. Babasaheb Ambedkar Marathwada University, Auranssgabad, (India). He is member of various professional bodies like IE, ISTE and IETE. His current research interests include content-based video retrieval and image processing. His work has been published in various international and national journals and conferences.

Tejashri. S. Bobade,
tejub35@gmail.com
Student of M.E.(E&TC)2nd Year,Terna College Of Engineering,Osmanabad,Maharashtra,India
B.E.(E&TC)from STB College of Engineering, Tuljapur, Maharashtra, India in 2011.

OPEN ACCESS

International
Journal
Of Modern Engineering Research (IJMER)

Voice over IP (VOIP) Security Research- A Research

Ashis Saklani[1], Rajni Nautiyal[2]
[1,]*Assistant Professor*, Dept. of CSE/MCA, *BTKIT(Kumaon Institute of Technology), Dwarahat, Almora*

ABSTRACT: *This is a work based on a survey of Voice over IP security research.Goal is to provide a roadmap for researchers seeking to understand existing capabilities and, and to identify gaps in addressing the numerous threats and vulnerabilities present in VoIP systems. We also briefly discuss the implications of our findings with respect to actual vulnerabilities reported in a variety VoIP products.*

I. INTRODUCTION

Voice over IP technologies are being increasingly adopted by consumers, enterprises, and telecoms operators due to their potential for higher flexibility, richer feature set, and reduced costs relative to their Public Switched Telephony Network (PSTN) coun- terparts. At their core, VoIP technologies enable the transmission of voice in any IP network, including the Internet. Because of the need to seamlessly interoperate with the existing telephony infrastructure, the new features, and the speed of development and deployment, VoIP protocols and products have been repeatedly found to contain numerous vulnerabilities [16] that have been exploited [19]. As a result, a fair amount of research has been directed towards addressing some of these issues. However, the effort is unbalanced, with little effort is spent on some highly deserving problem areas. We have conducted a comprehensive survey of VoIP security research, complement- ing our previous work that analyzed known vulnerabilities [16]. Our long-term goal is four-fold. First, to create a roadmap of existing work in securing VoIP, towards reducing the start-up effort required by other researchers to initiate research in this space. Second, to identify gaps in existing research, and to help inform the security community of challenges and opportunities for further work. Third, to provide an overall sanity check on the overall VoIP security research ecosystem, using known vulnerabilities as a form of ground truth. Finally, in the context of the VAMPIRE project [1] (which supported this work), to provide guidanceas to what further work in needed to better understand and analyze the activities of VoIP-system attackers. Naturally, such ambitious goals require significantly more space than is available in a single conference paper.

In this paper, we provide a representative sample of the research works we surveyed. We classify these works according to the class of threat they seek to address, using the VoIP Security Alliance (VoIPSA) [54] threat taxonomy. Although we were forced to omit a large number of related works (which we hope to present in a comprehensive form in due time), this survey should be a good starting point for anyone interested in conducting research on VoIP security. We also briefly discuss the implications of our findings with respect to actual vulnerabilities reported in a variety VoIP products. In the remainder of this paper, Section 2 gives a brief overview of SIP, one of the most popular VoIP technologies. Section 3 summarizes the threat model defined by the VoIP Security Alliance. We then present our survey of the research literature on VoIP security in Section 4, and discuss some of the implications in Section 5.

II. SIP OVERVIEW

SIP [42] is an application-layer protocol standardized by the Internet Engineering Task Force (IETF), and is designed to support the setup of bidirectional communication ses- sions including, but not limited to, VoIP calls. It is somewhat similar to HTTP, in that it is text-based, has a request-response structure, and uses a user authentication mech- anism based on the HTTP Digest Authentication. However, it is an inherently state- ful protocol that supports interaction with multiple network components (*e.g.*, PSTN bridges), and can operate over UDP, TCP, and SCTP. The main SIP entities are endpoints (softphones or physical devices), a proxy server, a registrar, a redirect server, and a location server. The registrar, proxy and redirect servers may be combined, or they may be independent entities. Endpoints communicate with a registrar to indicate their presence. This information is stored in the location server. A user may be registered via multiple endpoints simultaneously. During call setup, the endpoint communicates with the proxy, which uses the location server to de- termine where the call should be routed to. This may be another endpoint in the same network (*e.g.,* in the same enterprise), or another proxy server in another network. Alternatively, endpoints may use a redirect server to directly determine where a call should be directed to; redirect servers consult the location server in the same way that proxy servers operate during call setup. Once an end-to-end channel has been established (through one or more proxies) between the two endpoints, SIP negotiates the session parameters (codecs, RTP ports, *etc.*) using the Session Description Protocol (SDP). In a two-party call setup between Alice and Bob, Alice sends an INVITE message to her proxy server, optionally containing session parameter information encoded within SDP. The proxy forwards this message directly to Bob, if Alice and Bob are users of the same domain. If Bob is registered in a different domain, the message will be relayed to Bob's proxy, and thence to Bob. The message may be forwarded to several endpoints, if Bob is registered from multiple locations. While the call is being set up, Alice is sent RINGING messages. Once the call has been accepted, an OK message is sent to Alice, containing Bob's preferred parameters encoded within SDP. Alice responds with an ACK message. Alice's session parameter preferences may be encoded in the INVITE or the ACK message. Following this exchange, the two endpoints can begin transmitting voice, video or other content using the agreed-upon media transport protocol, typically RTP. While the signaling traffic may be relayed through a number of SIP proxies, the media traffic is exchanged directly between the two endpoints. When bridging different networks, *e.g.,* PSTN and SIP, media gateways may disrupt the end-to-end nature of the media transfer to translate content between the formats supported by these networks. There are many other protocol interactions supported by SIP, that cover a number of common (and uncommon) scenarios including call forwarding (manual or automatic), conference calling, voicemail, *etc.* Typically, this is done by semantically overloading SIP messages such that they can play various roles in different parts of the call. SIP can use S/MIME to carry complex authentication payloads, including public key certificates. When TCP is used as the transport protocol, TLS can be used to protect the SIP messages. TLS is required for communication among proxies, registrars and redirect servers, but only recommended between endpoints and proxies or registrars. IPsec may also be used to protect all communications, regardless of transport protocol.

III. VOIP THREATS

As a starting point, we use the taxonomy provided by the Voice over IP Security Alliance (VoIPSA) [54]. VoIPSA is a vendor-neutral, not for profit organization composed of VoIP and security vendors, organizations and individuals with an interest in securing VoIP protocols, products and installations. In addition, we place the surveyed vulnerabilities within the traditional threat space of confidentiality, integrity, availability (CIA). Finally, we consider whether the vulnerabilities exploit bugs in the protocol, implementation or system configuration.

In future work, we hope to expand the number of views to the surveyed vulnerabilities and to provide more in-depth analysis. The VoIPSA security threat taxonomy defines the security threats against VoIP deployments, services, and end users. The key elements of this taxonomy are:

1. Social threats are aimed directly against humans. For example, misconfigurations, bugs or bad protocol interactions in VoIP systems may enable or facilitate attacks that misrepresent the identity of malicious parties to users. Such attacks may then act as stepping stones to further attacks such as phishing, theft of service, or unwanted contact (spam).

2. Eavesdropping, interception, and modification threats cover situations where an adversary can unlawfully and without authorization from the parties concerned listen in on the signaling (call setup) or the content of a VoIP session, and possibly modify aspects of that session while avoiding detection. Examples of such attacks include call re-routing and interception of unencrypted RTP sessions.

3. Denial of service threats have the potential to deny users access to VoIP services. This may be particularly problematic in the case of emergencies, or when a DoS attack affects all of a user's or organization's communication capabilities (*i.e.,* when all VoIP and data communications are multiplexed over the same network which can be targeted through a DoS attack). Such attacks may be VoIP-specific (exploiting flaws in the call setup or the implementation of services), or VoIP-agnostic (*e.g.,* generic traffic flooding attacks). They may also involve attacks with physical components (*e.g.,* physically disconnecting or severing a cable) or through computing or other infrastructures (*e.g.,* disabling the DNS server, or shutting down power).

4. Service abuse threats covers the improper use of VoIP services, especially (but not exclusively) in situations where such services are offered in a commercial setting. Examples of such threats include toll fraud and billing avoidance [51,52].

5. Physical access threats refer to inappropriate/unauthorized physical access to VoIP equipment, or to the physical layer of the network.

6. Interruption of services threats refer to non-intentional problems that may nonetheless cause VoIP services to become unusable or inaccessible. Examples of such threats include loss of power due to inclement weather, resource exhaustion due to over-subscription, and performance issues that degrade call quality.

IV. SURVEY OF VOIP SECURITY RESEARCH

In the this section, we classify various research papers across the first four elements of the VoIPSA taxonomy (the last two relate to physical and non-security issues). We also include a *cross-cutting* category, which includes work that covers multiple areas (*e.g.,* proposing a security architecture), and an *overviews* category that includes works that survey vulnerabilities, threats, and security mechanisms. We give an indication as to how many total pieces of related work (including those described in the text) could be classified in that category but were omitted due to space limitations. The works that are discussed offer a representative view of the type of research activity in these problem areas.

Overviews (36 items) Persky gives a very detailed description of several VoIP vulnerabilities [32]. A long discussion of threats and security solutions is given by Thermos and Takanen [53]. Cao and Malik [8] examine the vulnerabilities that arise from introducing VoIP technologies into the communications systems in critical infrastructure applications. They examine the usual threats and vulnerabilities, and discuss mitigation techniques. They conclude by providing some recommendations and best practices to operators of such systems. Butcher *et al.* [7] overview security issues and mechanisms for VoIP systems, focusing on security-oriented operational practices by VoIP providers and operators. Such practices include the separation of VoIP and data traffic by using VLANs and similar techniques, the use of integrity and authentication for configuration bootstrapping of VoIP devices, authentication of signaling via TLS or IPsec, and the use of media encryption. They briefly describe how two specific commercial systems implement such practices, and propose some directions for future research.

Adelsbach *et al.* [2] provide a comprehensive description of SIP and H.323, a list of threats across all networking layers, and various protection mechanisms. A similar analysis was published by the US National Institute of Standards and Technology (NIST) [20]. Anwar *et al.* [3] identify some areas where the NIST report remains incomplete: counter-intuitive results with respect to the relative performance of encryption and hash algorithms, the non-use of the standardized Mean Opinion Score to evaluate call quality, and the lack of anticipation of RTP-based denial of service. They then propose the use of design patterns to address the problems of secure traversal of firewalls and NAT boxes, detecting and mitigating DoS attacks in VoIP, and securing VoIP against eavesdropping. Seedorf [45] overviews the security challenges in peer-to-peer (P2P) SIP. Threats specific to P2P-SIP include subversion of the identity-mapping scheme (which is specific to the overlay network used as a substrate), attacks on the overlay network routing scheme, bootstrapping communications in the presence of malicious first-contact nodes, identity enforcement (Sybil attacks), traffic analysis and privacy violation by intermediate nodes, and free riding by nodes that refuse to route calls or otherwise participate in the protocol other than to obtain service for themselves (selfish behavior).

Addressing social threats (49 items) Niccolini [29] discusses the difficulties in protecting against IP telephony spam (SPIT) and overviews the various approaches for blocking such calls, identifying the technical and operational problems with each. Possible building blocks for SPIT prevention include black/whitelists combined with strong identity verification to provide a reliable CallerID system, referral-based systems among trusted SIP domains, pattern or anomaly detection techniques to discriminate SPIT based on training data, multi-level grey-listing of calls based on caller behavior (similar to throttling), computational puzzles and CAPTCHAs, explicit callee consent (a form of capability, required to actually place a call), content filtering on voicemail spam, callee feedback to indicate whether a call was SPIT or legitimate (typically com- bined with white/blacklisting, and requiring strong identity), changing one's SIP address as soon as SPIT messages arrive, requiring a monetary fee for the first contact, and legal action. Niccolini argues that none of these methods by itself is likely to succeed, promotes a modular and extensible approach to SPIT prevention, and presents a high-level architecture that was designed for use in a commercial SIP router. Mathieu *et al.* [27] describe SDRS, an anti-SPIT system that combines several of these detection schemes and takes into consideration user and operator preferences.

The SPIDER project (SPam over Internet telephony Detection sERvice) released a public project report [38] providing an overview of SPIT threats and the relevant European legal framework (both on an EU and national basis). The second public project report [25] focuses on SPIT detection and prevention, summarizing some of the work done in this space and defining criteria for evaluating the efficiency of anti- SPIT mechanisms. They then classify prior work according to fulfillment of these criteria, expanding on the relative strengths and weaknesses of each approach. The third public project report [37] builds on the previous two reports, describing an anti-SPIT architectural framework. Elements of this architecture include improved authentication,white/blacklisting, behavior analysis, the use of computational puzzles for challenge/response, reputation management, and audio content analysis.

P¨orschmann and Knospe [34] propose a SPIT detection mechanism based on apply-ing spectral analysis to the audio data of VoIP calls to create acoustic fingerprints. SPIT is identified by detecting several fingerprints across a large number of different calls.Schlegel *et al.* [44] describe a framework for preventing SPIT. They argue for a modular approach to identifying SPIT, using hints from both signaling and media transfer. The first stage of their system looks at information that is available prior to accepting the call, while the second stage interacts with a caller (possibly prior to passing on the call to the callee). The various components integrated in their system include white/blacklists, call statistics, IP/domain correlation, and Turing tests. Their system also allows for feedback from the callee to be integrated into the scoring mechanism, for use in screening future calls. The evaluation focuses on scalability, by measuring the response time to calls as call volumes increase.

Quittek *et al.* [35] propose the use of *hidden* Turing tests to identify SPIT callers.As a concrete approach, they leverage the interaction model in human conversation minimizes the amount of simultaneous ("double") talk by the participants, and the fact that there is a short pause at the beginning of an answered call, followed by a statement by the callee that initiates the conversation. By looking for signs of violation of such norms, it is possible to identify na¨ıve automated SPIT callers. The authors implement their scheme and integrated it with a VoIP firewall.

Dantu and Kolan [17] describe the Voice Spam Detector (VSD), a multi-stage SPIT filter based on trust, reputation, and feedback among the various filter stages. The pri- mary filter stages are call pattern and volume analysis, black and white lists of callers, per-caller behavior profile based on Bayesian classification and prior history, and reputation information from the callee's contacts and social network. They provide a formal model for trust and reputation in a voice network, based on intuitive human behavior. They evaluate their system in a laboratory experiment using a small number of real users and injected SPIT calls.

Kolan *et al.* [18] use traces of voice calls in a university environment to validate a mathematical model for computing the nuisance level of an incoming call, using feed-back from the receivers. The model is intended to be used in predicting SPIT calls in VoIP environments, and is based on the history of prior communications between the two parties involved, which includes explicit feedback from the receiver indicating that a call is unwanted (at a particular point in time).

Balasubramaniyan *et al.* [4] propose to use call duration and social network graphs to establish a measure of reputation for callers. Their intuition is that users whose call graph has a relatively small fan-out and whose call durations are relatively long are less likely to be spammers. Conversely, users who place a lot of very short calls are likely to be engaging in SPIT. Furthermore, spammers will receive few (if any) calls. Their system works both when the parties in a call have a social network link between them, and when such a link does not exist by assigning global reputation scores. Users that are mistakenly categorized as spammers are redirected to a Turing test, allowing them to complete the call if the answer correctly. In a simulation-based evaluation, the authors determine that their system can achieve a false negative rate of 10% and a false positive rate of 3%, even in the presence of large numbers of spammers.

Addressing eavesdropping, interception, and modification threats (34 items) Wang *et al.* [55] evaluate the resilience of three commercial VoIP services (AT&T, Vonage and Gizmo) against man-in-the-middle adversaries. They show that it is possible for an attacker to divert and redirect calls in the first two services by modifying the RTP endpoint information included in the SDP exchange (which is not protected by the SIP Digest Authentication), and to manipulate a user's call forwarding settings in the latter two systems. These vulnerabilities permit for large-scale voice pharming, where unsus- pecting users are directed to fake interactive voice response systems or human repre- sentatives. The authors argue for the need for TLS or IPsec protection of the signaling. Zhang *et al.* show that, by exploiting DNS and VoIP implementation vulnerabilities, it is possible for attackers to perform man-in-the-middle attacks even when they are not on the direct communication path of the parties involved. They demonstrate their attack against Vonage, requiring that the attacker only knows the phone number and the IP address of the target phone. Such attacks can be used to eavesdrop and hijack the victims' VoIP calls. The authors recommend that users and operators use signaling and media protection, conduct fuzzing and testing of VoIP implementations, and develop a lightweight VoIP intrusion detection system to be deployed on the VoIP phone. Salsano *et al.* give an overview of the various SIP security mechanisms (as of 2002), focusing particularly on the authentication component. They conduct an eval-uation of the processing costs of SIP calls that involve authentication, under different transport, authentication and encryption scenarios. They show that a call using TLS and authentication is 2.56 times more expensive than the simplest possible SIP configuration (UDP, no security). However, a fully-protected a call takes only 54% longer to complete than a configuration that is more representative than the basic one but still offers no security; the same fully-protected call and has the same processing cost if the transport is TCP without any encryption (TLS). Of the overhead, approximately 70% is attributed to message parsing and 30% to cryptographic processing. With the advent of

Datagram TLS (DTLS), it \ is possible that encryption and integrity for SIP can be had for all configurations (UDP or TCP) at no additional cost. A similar conclusion is reached by Bilien *et al.* [6], who study the overhead in SIP call setup latency when using end-to-end and hop-by-hop security mechanisms. They consider protocols such as MIKEY, S/MIME, SRTP, TLS, and IPsec, concluding that the overall penalty of using full-strength cryptography is low. Barbieri *et al.* [5] had found earlier that when using VoIP over IPsec, performance can drop by up to 63%; however, it is questionable whether these results still hold, given the use of hardware accelerators and the more efficient AES algorithm in IPsec. Rebahi *et al.* analyze the performance of RSA as used in SIP for authentication and identity management (via public-key certificates and digital signatures), and describe the use of Elliptic Curve DSA (ECDSA) within this context to improve performance. Using ECDSA, their prototype can handle from 2 to 8 times as many call setup requests per second, with the gap widening as key sizes increase.

Guo *et al.* [14] propose a new scheme for protecting voice content that provides strong confidentiality guarantees while allowing for graceful voice degradation in the presence of packet loss. They evaluate their scheme via simulation and micro-benchmarks. However, Li *et al.* [23] show that the scheme is insecure. Kuntze *et al.* [21] propose a mechanism for providing non-repudiation of voice content by using digital signatures. Seedorf also proposes the use of cryptographically generated SIP URIs to protect the integrity of content in P2P SIP. Specifically, he uses self-certifying SIP URIs that encode a public key (or, more compactly, the hash of a public key). The owner of the corresponding private key can then post signed location binding information on the peer-to-peer network (*e.g.*, Chord) that is used by call initiators to perform call routing.

Petraschek *et al.* examine the usability and security of ZRTP, a key agreement protocol based on the Diffie Hellman key exchange, designed for use in VoIP environments that lack pre-established secret keys among users or a public key infrastructure (PKI). ZRTP is intended to be used with SRTP, which performs the actual content en-cryption and transfer. Because of the lack of a solid basis for authentication, which makes active man-in-the-middle attacks easy to launch, ZRTP uses Short Authentication Strings (SAS) to allow two users to verbally confirm that they have established the same secret key. The verbal communication serves as a weak form of authentication at the human level. The authors identify a relay attack in ZRTP, wherein a man-in-the- middle adversary can influence the SAS read by two legitimate users with who he has established independent calls and ZRTP exchanges. The attacker can use one of the legitimate users as an oracle to pronounce the desired SAS string through a number of means, including social engineering. The authors point out that SAS does not offer any security in some communication scenarios with high security requirements, *e.g.*, a user calling (or being called by) their bank. The authors implement their attack and demonstrate it in a lab environment. Wright *et al.* apply machine learning techniques to determine the language spoken in a VoIP conversation, when a variable bit rate (VBR) voice codec is used based on the length of the encrypted voice frame. As a countermeasure, they propose the use of block ciphers for encrypting the voice. In follow-on work [57], they use profile Hidden Markov Models to identify specific phrases in the encrypted voice stream with a 50% average accuracy, rising to 90% for certain phrases.

Addressing denial of service threats (19 items) Rafique *et al.* analyze the ro- bustness and reliability of SIP servers under DoS attacks. They launch a number of synthesized attacks against four well-known SIP proxy servers (OpenSER, PartySIP, OpenSBC, and MjServer). Their results demonstrate the ease with which SIP servers can be overloaded with call requests, causing such performance metrics as Call Completion Rate, Call Establishment Latency, Call Rejection Ration and Number of Retransmitted Requests to deteriorate rapidly as attack volume increases, sometimes with as few as 1,000 packets/second. As an extreme case of such attacks large volumes of IN- VITE messages can even cause certain implementations to crash. While documenting the susceptibility to such attacks, this work proposes no defense strategies or directions. Reynolds and Ghosal describe a multi-layer protection scheme against flood-based application- and transport-layer denial of service (DoS) attacks in VoIP. They use a combination of sensors located across the enterprise network, continuously estimating the deviation from the long-term average of the number of call setup requests and successfully completed handshakes. Similar techniques have been used in detecting TCP SYN flood attacks, with good results. The authors evaluate their scheme via simulation, considering several different types of DoS attacks and recovery models. Ormazabal *et al.* describe the design and implementation of a SIP-aware, rule- based application-layer firewall that can handle denial of service (and other) attacks in the signaling and media protocols. They use hardware acceleration for the rule matching component, allowing them to achieving filtering rates on the order of hundreds of transactions per second. The SIP-specific rules, combined with state validation of the endpoints, allow the firewall to open precisely the ports needed for only the local and remote addresses involved in a specific session, by decomposing and analyzing the con-tent and meaning of SIP signaling message headers. They experimentally evaluate and validate the behavior of their prototype with a distributed testbed involving synthetic benign and attack traffic generation. Larson *et al.* experimentally analyzed the impact of distributed denial of service (DDoS) attacks on VoIP call quality. They also established the effectiveness of low-rate denial of service attacks that target specific vulnerabilities and implementa- tion artifacts to cause equipment crashes and reboots. They discuss some of the possible defenses against such attacks and describe Sprint's approach, which uses regional "cleaning centers" which divert suspected attack traffic to a centralized location with numerous screening and mitigation mechanisms available. They recommend that critical VoIP traffic stay on private networks, the use of general DDoS mechanisms as a front-line defense, VoIP-aware DDoS detection and mitigation mechanisms, traffic policing and rate-limiting mechanisms, the use of TCP for VoIP signaling, extended protocol compliance checking by VoIP network elements, and the use of authentication mechanisms where possible.Sengar *et al.* describe vFDS, an anomaly detection system that seeks to identify flooding denial of service attacks in VoIP. The approach taken is to measure abnormal variations in the relationships between related packet streams using the Hellinger distance, a measure of the deviation between two probability measures. Using synthetic attacks, they show that vFDS can detect flooding attacks that use SYN, SIP, or RTP packets within approximately 1 second of the commencement of an attack, with small impact on call setup latency and voice quality. Conner and Nahrstedt [9] describe a semantic-level attack that causes resource exhaustion on stateful SIP proxies by calling parties that (legitimately or in collusion) do not respond.

This attack does not require network flooding or other high traffic volume attacks, making it difficult to detect with simple, network-based heuristics used against other types of denial of service attacks. They propose a simple algorithm, called *Random EarlyTermination* (RET) for releasing reserved resources based on the current state of the proxy (overloaded or not) and the duration of each call's ringing. They implement and evaluate their proposed scheme on a SIP proxy running in a local testbed, showing that it reduces the number of benign call failures when under attack, without incurring measurable overheads when no attack is underway. Zhang *et al.* describe a denial of service attack wherein adversaries flood SIP servers with calls involving URIs with DNS names that do not exist. Servers attempting to resolve them will then have to wait until the request times out (either locally or at their DNS server), before they can continue processing the same or another call. This attack works against servers that perform synchronous DNS resolution and only maintain a limited number of execution threads. They experimentally show that as few as 1,000 messages per second can cause a well provisioned synchronous resolution server to exhibit very high call drops, while simple, single-threaded servers can be starved with even 1 message per second. As a countermeasure, they propose the use of non-blocking DNS caches, which they prototype and evaluate. Luo *et al.* experimentally evaluate the susceptibility of SIP to CPU-based denial of service attacks. They use an open-source SIP server in four attack scenarios: basic request flooding, spoofed-nonce flooding (wherein the target server is forced to validate the authenticator in a received message), adaptive-nonce flooding (where the nonce is refreshed periodically by obtaining a new one from the server), and adaptive- nonce flooding with IP spoofing. Their measurements show that these attacks can have a large impact on the quality of service provided by the servers. They propose several countermeasures to mitigate against such attacks, indicating that authentication by itself cannot solve the problem and that, in some circumstances, it can exacerbate its sever- ity. These mitigation mechanisms include lightweight authentication and whitelisting, proper choice of authentication parameters, and binding nonces to client IP addresses.

Addressing service abuse threats (8 items) Zhang *et al.* present a number of exploitable vulnerabilities in SIP that can manipulate billing records in a number of ways, showing their applicability against real commercial VoIP providers. Their focus is primarily on attacks that create billing inconsistencies, *e.g.*, customers being charged for service they did not receive, or over-charged for service received. Some of these attacks require a man-in-the-middle capability, while others only require some prior interaction with the target (*e.g.*, receiving a call from the victim SIP phone device).

Abdelnur *et al.* [1] use AVISPA to identify a protocol-level vulnerability in the way SIP handles authentication [50]. AVISPA is a model checker for validating security protocols and applications using a high-level protocol specification and security-goals language that gets compiler into an intermediate format that can be consumed by a number of lower-level checkers. The attack is possible with the SIP Digest Authentication, whereby an adversary can reuse another party's credentials to obtain unautho- rized access to SIP or PSTN services (such as calling a premium or international phone line). This attack is possible because authentication may be requested in response to an INVITE message at any time during a call, and the responder may issue an INVITE message during a call either automatically (because of timer expirations) or through a user action (*e.g.*, placing the caller on hold in order to do a call transfer). While the solution is simple, it requires changes possibly to all end-device SIP implementations. This work is part of a bigger effort to apply testing and fuzzing toward identifying vulnerabilities in SIP protocols, implementations, and deployed systems. It is worth noting that this work has resulted in a number of vulnerability disclosures in the Common Vulnerabilities and Exposures (CVE) database and elsewhere.

Cross-cutting efforts (51 items) Wieser *et al.* [56] extend the PROTOS testsuite with a SIP-specific analysis fuzzing module. They then test their system against a number of commercial SIP implementations, finding critical vulnerabilities in all of them.

Gupta and Shmatikov [15] formally analyze the security of the VoIP protocol stack, including SIP, SDP, ZRTP, MIKEY, SDES, and SRTP. Their analysis uncovers a num- ber of flaws, most of which derive from subtle inconsistencies in the assumptions made in designing the different protocols. These include a replay attack in SDES that com- pletely break content protection, a man-in-the-middle attack in ZRTP, and a (perhaps theoretical) weakness in the key derivation process used in MIKEY. They also show several minor weaknesses and vulnerabilities in all protocols that enable DoS attacks. Dantu *et al.* [12] describe a comprehensive VoIP security architecture, composed of components distributed across the media gateway controller, the proxy server(s), the IP PBX, and end-user equipment. These components explicitly exchange information toward better training of filters, and creating and maintaining white/blacklists. Implicit feedback is also provided through statistical analysis of interactions (*e.g.*, call frequency and duration). The architecture also provisions for a recovery mechanism that incorporates explicit feedback and quarantining.

Wu *et al.* design an intrusion detection system, called SCIDIVE, that is specific to VoIP environments. SCIDIVE aims to detect different classes of intrusions, can operate with different viewpoints (on clients, proxies, or servers), and takes into consideration both signaling (*i.e.,* SIP) and media-transfer protocols (*e.g.,* RTP). SCIDIVE's ability to correlate cross-protocol behavior, theoretically allows for detection of more complex attacks. However, the system is rules-based, which limits its effectiveness against new/unknown attacks. In follow-on work, Wu *et al.* [60] develop SPACEDIVE, a VoIP-specific intrusion detection system that allows for correlation of events among distributed rules-based detectors.

They demonstrate the ability of SPACEDIVE to detect certain classes of attacks using a simple SIP environment with two domains, and compare it with SCIDIVE. Niccolini *et al.* design an intrusion detection/intrusion prevention system archi- tecture for use with SIP. Their system uses both knowledge-based and behavior-based detection, arranged as a series in that order. They develop a prototype implementation using the open-source Snort IDS. They evaluate the effectiveness of their system in an attack scenario by measuring the mean end-to-end delay of legitimate SIP traffic in the presence of increasing volumes of malformed SIP INVITE messages. Nassar *et al.* advocate the use of SIP-specific honeypots to catch attacks targeting the Internet telephony systems, protocols and applications. They design and implement such a honeypot system, and explore the use of a statistical engine for identifying attacks and other misbehavior, based on training on legitimate traces of SIP traffic. The engine is based on their prior work that uses Bayesian-based inference. The resulting SIP honeypot effort is largely exploratory, with performance and effectiveness evaluations left for future work.

Rieck *et al.* apply machine learning techniques to detecting anomalous SIP messages, incorporating a "self-learning" component by allowing for periodic re-training of the anomaly detector using traffic that has been flagged as normal. The features used for clustering are based on n-grams and on tokenization of theSIP protocol. To prevent training attacks, wherein an adversary "trains" the anomaly detector to accept malicious inputs are legitimate, they employ randomization (choosing random samples for the training set),sanitization [10], and verification (by comparing the output of the new and old training models). Their experimental prototype was shown to handle 70 Mbps of SIP traffic, while providing a 99% detection rate with no false positives. SNOCER, a project funded by the European Union, is "investigating approaches for overcoming temporal network, hardware and software failures and ensuring the high availability of the offered VoIP services based on low cost distributed concepts." The first public project report [48] provides an overview of VoIP infrastructure components and the threats that must be addressed (staying primarily at the protocol and network level, and avoiding implementation issues with the exception of SQL injection), along with possible defense mechanisms.

There is also discussion on scalable service provisioning (replication, redundancy, backups *etc.*), toward providing reliability and fault tolerance. The second public project report [11] describes an architecture for protecting against malformed messages and related attacks using specification-based intrusion detection, protocol message verification, and redundancy. They use ontologies to describe SIP vulnerabilities, to allow for easy updating of the monitoring components (IDS) [13]. Marshall *et al.* describe the AT&T VoIP security architecture. They divide VoIP equipment into three classes: trusted, trusted-but-vulnerable, and untrusted. The latter consists of the customer premises equipment, which is outside the control of the carrier. The trusted domain includes all the servers necessary to provide VoIP service. Between the two sit various border and security elements, that are responsible for protecting the trusted devices while permitting legitimate communications to proceed. They describe the interactions among the various components, and the security mechanisms used in protecting these interactions.

V. DISCUSSION

In our previous work [16], we surveyed over 200 vulnerabilities in SIP implementations that had been disclosed in the CVE database from 1999 to 2009. We classified these vulnerabilities along several dimensions, including the VoIPSA threat taxonomy, the traditional Confidentiality, Integrity, Availability concerns, and a Protocol, Implementation, Configuration axis. We found that the various types of denial of service attacks constitute the majority of disclosed vulnerabilities, over 90% of which were due to implementation problems and 7% due to configuration. Considering the research work we have surveyed (some of which was discussed in this paper), we can see that out of a total of 197 publications, 18% concern themselves with an overview of the problem space and of solutions — a figure we believe is reasonable, considering the enormity of the problem space and the speed of change in the protocols, standards, and implementations. We also see a considerable amount of effort (roughly 25%) going toward addressing SPIT. While SPIT is not a major issue at this point, our experience with email spam and telemarketing seems to provide sufficient motivation for research in this area. Much of the work is focused on identifying SPIT calls and callers based on behavioral traits, although a number of other approaches are under exploration (*e.g.,* real-time content analysis). One of the problems is the lack of a good corpus of data for experimentation and validation of the proposed techniques.We were also not surprised to see a sizable portion of research (17%) directed at design, analysis (both security- and performance-oriented), and attacking of cryptographic protocols as used in VoIP. The cryptographic research community appears to be reasonably comfortable in proposing tweaks and minor improvements to the basic au-thentication mechanisms, and the systems community appears content with analyzing the performance of different protocol configurations (*e.g.,* TLS *vs.* IPsec). With a few notable exceptions, much of the work lacks "ambition."

Most distressing, however, is the fact that comparatively little research (9.6%) is go- ing toward addressing the problem of denial of service. Given the numerical dominance of SIP-specific DoS vulnerabilities (as described earlier) and the ease of launching such attacks, it is clear that significantly more work is needed here. What work is being done seems to primarily focus on the server and infrastructure side, despite our finding that half of DoS-related vulnerabilities are present on endpoints. Furthermore, much of the existing work focuses on network-observable attacks (*e.g.,* "obviously" malformed SIP messages), whereas the majority of VoIP DoS vulnerabilities are the result of implemen- tation failures. More generally, additional work is needed in strengthening implemen- tations, rather than introducing middleboxes and network intrusion detection systems, whose effectiveness has been shown to be limited in other domains; taking a black box approach in securing VoIP systems is, in our opinion, not going to be sufficient. Also disconcerting is the lack of research (4%) in addressing service abuse threats, considering the high visibility of large fraud incidents [19,51,52]. In general, we found little work that took a "big picture" view of the VoIP security problem. What cross cutting architectures have been proposed focus primarily on intrusion detection. Work is desperately needed to address cross-implementation and cross-protocol problems, above and beyond the few efforts along those lines in the intrusion detection space. Finally, we note that none of the surveyed works addressed the problem of configu- ration management. While such problems represent only 7% of known vulnerabilities, configuration issues are easy to overlook and are likely under-represented in our previ- ous analysis due to the nature of vulnerability reporting.

VI. CONCLUSIONS

We have presented a survey of VoIP security research. While space restrictions prevent us from discussing all surveyed works, we have discussed a representative subset of these. We presented an initial classification using the VoIPSA threat taxonomy, and juxtaposed this against our previous analysis on VoIP security vulnerabilities. We iden- tified two specific areas (denial of service and service abuse) as being under-represented in terms of research efforts directed at them (relative to their importance in the vulnerability survey), and called for additional effort at securing implementations and configurations, rather than taking a black-box approach of VoIP systems. We intend to expand on this work and offer a more comprehensive analysis in the near future.

REFERENCES

[1]. H. Abdelnur, T. Avanesov, M. Rusinowitch, and R. State. Abusing SIP Authentication. In Proceedings of the 4th International Conference on Information Assurance and Security (ISIAS, pages 237-242, September 2008.

[2]. A. Adelsbach, A. Alkassar, K.-H. Garbe, M. Luzaic, M. Manulis, E. Scherer, J. Schwenk, and E. Siemens. Voice over IP: Sichere Umstellung der Sprachkommunikation auf IP- Technologie. Bundesanzeiger Verlag, 2005.

[3]. Z. Anwar, W. Yurcik, R. E. Johnson, M. Hafiz, and R. H. Campbell. Multiple Design Patterns for Voice over IP (VoIP) Security.

[4]. In Proceedings of the IEEE Workshop on Informational Assurance (WIA), held in conjunction with the 25th IEEE International Performance Com- puting and Communications Conference, (IPCCC), April 2006.

[5]. V. Balasubramaniyan, M. Ahamad, and H. Park. CallRank: Combating SPIT Using Call Duration, Social Networks and Global Reputation. In Proceedings of the 4th Email and Anti-Spam (CEAS), August 2007.

[6]. R. Barbieri, D. Bruschi, and E. Rosti. Voice over IPsec: Analysis and Solutions. In Proceedings of the 18th Annual Computer Security Applications Conference (ACSAC), pages 261-270, December 2002.

[7]. J. Bilien, E. Eliasson, J. Orrblad, and J.-O. Vatn. Secure VoIP: Call Establishment and Media Protection. In Proceedings of the 2nd Workshop on Securing Voice over IP, June 2005.

[8]. D. Butcher, X. Li, and J. Guo. Security Challenge and Defense in VoIP Infrastructures. IEEE Transactions on Systems, Man, and Cybernetics, Part C: Applications and Reviews, 37(6):1152-1162, November 2007.

[9]. F. Cao and S. Malik. Vulnerability Analysis and Best Practices for Adopting IP Telephony in Critical Infrastructure Sectors. IEEE Communications Magazine, 44(4):138-145, April 2006.

[10]. W. Conner and K. Nahrstedt. Protecting SIP Proxy Servers from Ringing-based Denial-of- Service Attacks. In Proceedings of the 10th (ISM), pages 340-347, December 2008.

[11]. G. F. Cretu, A. Stavrou, M. E. Locasto, S. J. Stolfo, and A. D. Keromytis. Casting out Demons: Sanitizing Training Data for Anomaly Sensors. In Proceedings of the IEEE Security and Privacy Symposium, pages 81-95, May 2008.

[12]. T. Dagiuklas, D. Geneiatakis, G. Kambourakis, D. Sisalem, S. Ehlert, J. Fiedler, J. Markl, M. Rokis, O. Botron, J. Rodriguez, and J. Liu. General Reliability and Security Framework for VoIP Infrastructures. Technical Report Deliverable D2.2, SNOCER COOP-005892, September 2005.

[13]. R. Dantu, S. Fahmy, H. Schulzrinne, and J. Cangussu. Issues and Challenges in Securing VoIP. Computers & Security (to appear), 2009.

[14]. D. Geneiatakis and C. Lambrinoudakis. An Ontology Description for SIP Security Flaws.Computer Communications, 30(6):1367-1374, April 2007.

[15]. J.-I. Guo, J.-C. Yen, and H.-F. Pai. New Voice over Internet Protocol Technique with Hierarchical Data Security Protection. IEE Proceedings — Vision, Image and Signal Processing, 149(4):237-243, August 2002.

[16]. P. Gupta and V. Shmatikov. Security Analysis of Voice-over-IP Protocols. In Proceedings of the 20th 2007. IEEE Computer Security Foundations Symposium (CSFW), pages 49-63, July D. Keromytis. Voice over IP: Risks, Threats and Vulnerabilities. In Proceedings of the Cyber Infrastructure Protection (CIP) Conference, June 2009.

[17]. P. Kolan and R. Dantu. Socio-technical Defense Against Voice Spamming. ACM Transactions on Autonomous and Adaptive Systems (TAAS), 2(1), March 2007.

[18]. P. Kolan, R. Dantu, and J. W. Cangussu. Nuisance of a Voice Call. ACM Transactions on Multimedia Computing, Communications and Applications (TOMCCAP), 5(1):6:1-6:22, October 2008.

[19]. B. Krebs. Security Fix: Default Passwords Led to $55 Million in Bogus Phone Charges, June 2009.

[20]. D. R. Kuhn, T. J. Walsh, and S. Fries. Security Considerations for Voice Over IP Systems.US National Institute of Standards and Technology (NIST) Special Publication SP 800-58, January 2005.

International Journal of Modern Engineering Research (IJMER)

Volume : 5 Issue : 1 (Version-2) ISSN : 2249-6645 January- 2015

Contents :

OPEN ACCESS

International
Journal
Of Modern Engineering Research (IJMER)

Enhancement of Power System Dynamics Using a Novel Series Compensation Scheme

G. Gopal[1], Dr. A. Jaya Laxmi[2]
[1]*Electrical and Electronics Engineering, Mahatma Gandhi Institute of Technology, Hyderabad, India*
[2]*Professor and Coordinator, Centre for Energy studies, JNTUH College of Engineering, Hyderabad, India*

ABSTRACT: *Phase imbalanced capacitive compensation is a "hybrid" series compensation scheme, where the series capacitive compensation in one phase is created using a single-phase TCSC in series with a fixed capacitor (Cc), and the other two phases are compensated by fixed series capacitors (C). The TCSC control is initially set such that its equivalent compensations at the power frequency combined with the fixed capacitor yield a resultant compensation equal to the other two phases. Thus, the phase balance is maintained at the power frequency while at any other frequency, a phase imbalance is created. The effectiveness of the scheme in damping power system oscillations for various network conditions, namely different system faults and tie-line power flows is evaluated using the MATLAB/SIMULINK Software.*

Keywords: *Power system oscillation, POD Controller, STATCOM, TCSC, Phase imbalance capacitor*

I. INTRODUCTION

Many electric utilities world-wide are experiencing increased loadings on portions of their transmission systems, which can, and sometimes do, lead to poorly damped, low- frequency oscillations (0.5 – 2 Hz). These oscillations can severely restrict system operation by requiring the curtailment of electric power transfers as an operational measure. They can also lead to widespread system disturbances if cascading outages of transmission lines occur due to oscillatory power swings, like the blackout in Western North America on August 10, 1996 [6]. The damping energy is obtained by the modulation of load or generation for a period of time, typically in the range of five to ten seconds. The damping energy must have the correct phase shift relative to the accelerated/decelerated system as incorrect phase angles can excite the oscillations. FACTS controllers are power electronic based controllers which can influence transmission system voltages, currents, impedances and/or phase angles rapidly [8], [9]. These controllers have the flexibility of controlling both real and reactive power, which could provide an excellent capability for improving power system dynamics. FACTS technology provides an unprecedented way for controlling transmission grids and increasing transmission capacity. FACTS controllers may be based on thyristor devices with no gate turn-off (only with gate turn-on), or with power devices with gate turn-off capability. In the studies conducted in this paper, a series FACTS controller based on thyristor switches as well as a shunt FACTS controller based on power devices with gate turn-off capability are considered. The series FACTS controller is called a Thyristor Controlled Series Capacitor (TCSC) whereas the shunt FACTS controller is called Static Synchronous Compensator (STATCOM) [8], [9].

II. THE HYBRID SINGLE-PHASE-TCSC COMPENSATION SCHEME

Figure 1 shows a phase imbalanced hybrid series capacitive compensation scheme using a TCSC. In such a scheme, the series capacitive compensation in one phase is created using a single-phase TCSC in series with a fixed capacitor (Cc) and the other two phases are compensated by fixed series capacitors (C). The TCSC control is initially set such that its equivalent compensation at the power frequency combined with the fixed capacitor Cc yield a resultant compensation equal to the other two phases. Thus, the phase balance is maintained at the power frequency while at any other frequency, a phase imbalance is created. Mathematically, this can be explained as follows:

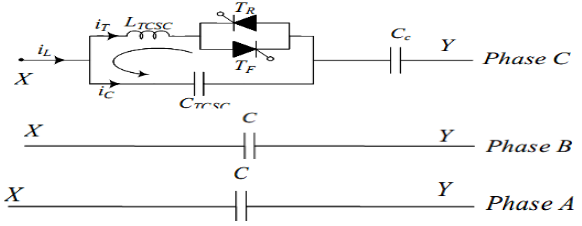

Figure 1: Hybrid single-phase TCSC compensation scheme

At the power frequency, the series reactance between buses X and Y in Figure1 in phases a, b and c are given by:

$$X_a = X_b = \frac{1}{j\omega_o C}$$

$$X_c = \frac{1}{j\omega_o C_c} - jX_{TCSCo}$$

Where $-j\, X_{TCSCo}$ is the effective capacitive reactance of the TCSC at the power frequency such that $X_a = X_b = X_c$.The control offered by the TCSC is an impedance type control, i.e. the inserted voltage is proportional to the line current. This type of control normally is best suited to applications in power flow corridors, where a well-defined phase angle difference exists between the ends of the transmission line to be compensated and controlled. In addition, the STATCOM can offer voltage regulation by functioning as a very fast variable reactive power generation source. As a result, transient stability improvement and the increase in the maximum real power transmitted can be achieved. TCSC and STATCOM can also be used, however, to provide additional damping to the electromechanical (0.5 - 2Hz) power oscillations as they provide fast speed of response and executes any switching patterns without such restrictions that might apply for mechanical switches.

In this paper, the effectiveness of the STATCOM and the hybrid single-phase-TCSC compensation scheme (Scheme I) supplemental controllers in damping power system oscillations is investigated. The test benchmark is shown in figure 2. The two load centers S1 and S2 are supplied by three large generating stations G1,G2 and G3 through five 500KV transmission lines. L1 and L2 are the two double circuit transmission lines and are series compensated with fixed capacitor banks located at the middle of the lines. The degree of compensation is 50%. The degree of compensation for fixed capacitor is $(X_C/X_L)*100\%$ and for hybrid compensated line is $(X_{Ce}+X_{TCSC})/X_L*100\%$. In order to maintain the voltages within 1±0.05 p.u. shunt capacitors are installed at buses 4and 5. Installed capacity is 4500MVA and peak load of the system is 3833MVA. The scheme is assumed to be installed in one or more circuits of lines L_1 and L_2 replacing the fixed series capacitor compensations as well as in the uncompensated line L3. The performance of the Scheme I and the STATCOM supplemental controllers is compared to the case with only fixed capacitor compensation in L1 and L2 (Fixed C) as well as to the case when the STATCOM supplemental controller is not activated (TCSC supplemental controller only).

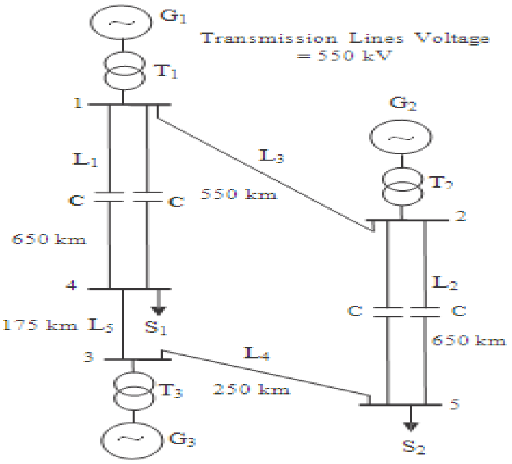

Figure 2: Test Benchmark.

III. TCSC AND STATCOM POWER OSCILLATION DAMPING CONTROLLERS

The TCSC can be made to vary the series-compensation level dynamically in response to the controller-input signal so that the resulting changes in the power flow enhance the system damping. The STATCOM controller consists of two loops which are: outer regulation loop and inner current loop. They work together to regulate the voltage at the connecting point with the system.

Voltage regulation improves the system damping. The traditional type of controller for Power Oscillations Damping (POD) uses cascade- connected washout filters and linear lead-lag compensators to generate the desired reactance modulation signal. The purpose of the wash-out filters is to eliminate the average and extract the oscillating part of the input signal. The lead-lag compensators provide the desired phase shift at the oscillating frequency. Such a controller is illustrated in Figure 2. In some situations, a simple controller consists of only the washout filters which can have a better performance than that of the lead-lag controller. Such a controller, shown in Figure 3 can be considered as a proportional type controller.

Figure 3: Structure of a lead-lag POD controller

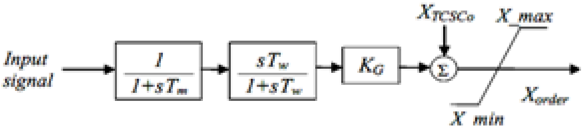

Figure 4 : Structure of a simple POD controller.

The selection of the appropriate input (stabilizing) signal is an important issue in the design of an effective and robust controller. The selected input signal must yield correct control action when a severe fault occurs in the system. As an example, it was reported that if the real power is used as input signal of a pure derivative controller, the output control signal may cause negative damping effects in the presence of disturbances involving large changes in the generator power angles.

The input signals could be local (e.g. real power flows) or remote (e.g. load angles or speed deviations of remote generators). If a wide-area network of Synchronized Phasor Measurement (SPM) units is available, then the remote signals can be downloaded at the controller in real time without delay. In the studies conducted in this thesis, the generator load angles and speeds, measured with respect to the load angle and speed of a reference generator are used as input signals.

It is worth noting here that due to the inherent imbalance nature of hybrid single-phase-TCSC compensation scheme during transients, the design of the TCSC supplemental controller using classical linear control techniques would be very difficult, if not, virtually impossible to achieve. However, nonlinear control theories for STATCOM and TCSC applications have been found to have a significant potential in recent years. Some of the examples are: Variable-Structure Controllers (VSCs), model reference adaptive controllers and self-tuning controllers. VSCs are capable of maintaining a desired response characteristic almost independently of the system structure. In the studies conducted in this paper, the supplemental controller parameters are determined by performing multiple time domain simulations with the aim of improving the transient responses of the system. In the case of multiple controllers, simultaneous tuning of the parameters of the controllers is performed to ensure that satisfactory dynamic and steady-state performances are met whilst minimizing or preventing undesirable interactions among controllers.

IV. THE HYBRID SINGLE-PHASE-TCSC COMPENSATION SCHEME IS INSTALLED IN DIFFERENT FORMATS

A. CASE STUDY A: Load Profile I

The best system transient time responses of four different combinations of stabilizing signals are examined in this case.

The final results of the time domain controllers tuning are shown in Figure 5. The transfer functions for the four combinations of the TCSC supplemental controllers are given in Table II.

In Figure 5, it is seen that the power swing damping controller effectively damps the system oscillations. The responses of the fixed series capacitor compensation and the hybrid TCSC compensation are shown in figure 5. The positive contribution of the proposed hybrid scheme to the damping of the system oscillations is very clear. The best damping of the relative load angle responses are achieved with the δ_{21}-δ_{21} combination and the δ_{31}-δ_{21} combination is the second best damped response. With P_{L1}- δ_{21} combination the worst damped response is obtained and also results in the increase of the first swings.

TABLE I

The Four Examined Combinations of Stabilizing Signals for Case Study I

Combination	Each TCSC in L_1	Each TCSC in L_2
1	$□_{21}$	$□_{21}$
2	$□_{31}$	$□_{21}$
3	$□_{31}$	$\mathbf{P_{L2}}$
4	$\mathbf{P_{L1}}$	$□_{21}$

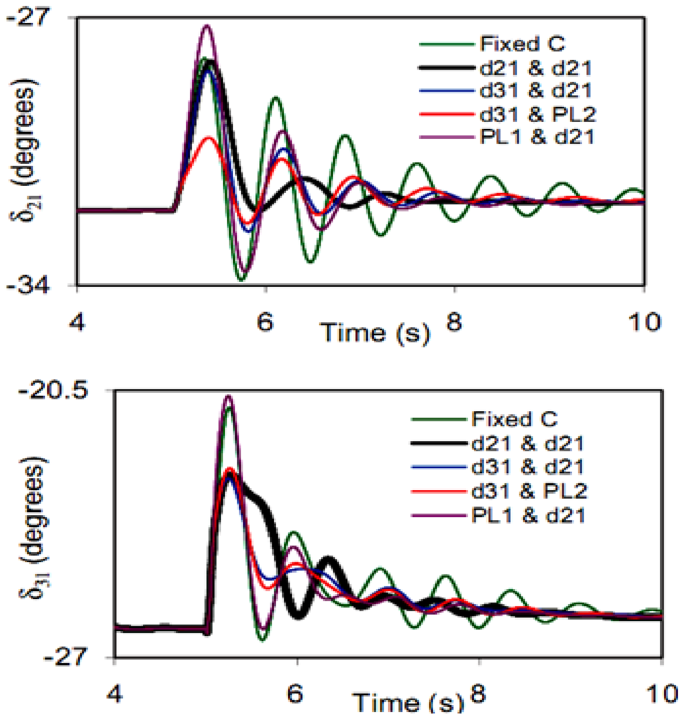

Figure 5: Generator load angles, measured with respect to generator 1 load angle, during and after clearing a three-phase fault at bus 4 (Load Profile I).

B. CASE STUDY B: Load Profile II

The stabilizing signal of the supplementary controllers is $\delta_{21.}$ In this case and the transfer functions are given in Table III. Compared to fixed capacitor compensation, the hybrid single phase TCSC scheme provides a better damping performance to the system oscillations, but there is a slight increase in the first swing of δ_{21} as shown in Figure 6.

TABLE II

Transfer Functions of the TCSC Supplemental Controllers for Case Study A

C	Each TCSC in L_1	Each TCSC in L_2
1	G(s)=0.25 (10/S+10)(3S/3S+1)	G(s)= -0.15 (10/S+10)(3S/3S+1)
2	G(s)=0.05 (10/S+10)(3S/3S+1)	G(s)= -0.15 (10/S+10)(3S/3S+1)
3	G(s)=0.1 (10/S+10)(3S/3S+1)	G(s)=-0.4 (10/S+10)(3S/3S+1)
4	G(s)= -0.25 (10/S+10)(3S/3S+1)	G(s)= -0.25 (10/S+10)(3S/3S+1)

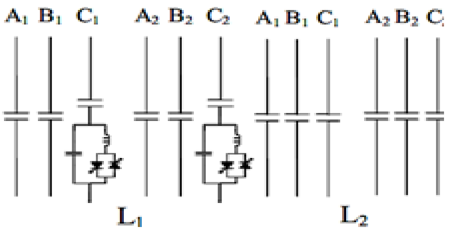

TABLE III

Transfer Functions of the TCSC Supplemental Controllers for Case Study II

Each TCSC in L_1	G(s)=0.3 (10/S+10)(3S/3S+1)
Each TCSC in L_2	G(s)=-0.15 (10/S+10)(3S/3S+1)

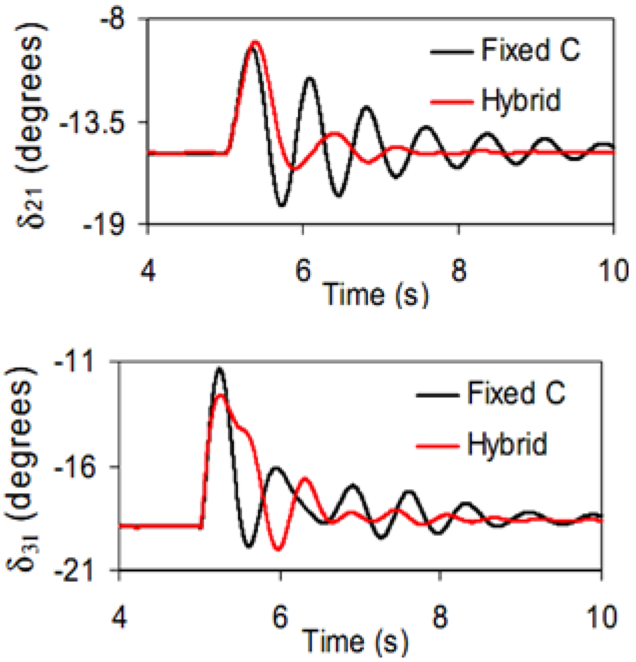

Figure 6: Generator load angles, measured with respect to generator 1 load angle, during and after clearing a three-phase fault at bus 4 (Load Profile II).

C. CASE STUDY C: A Dual-Channel Controller

Two natural modes of oscillations can be observed in any of the four signals δ_{21}, δ_{31}, PL1 and PL2 and these are used to add damping as in case study A. More effective damping will be resulted when two properly selected signals are added. The two natural modes of oscillations are not in phase in general. A dual-channel controller would adjust separately the gain and phase of each mode of oscillations and thus provides a better damping.

TABLE IV

The Six Examined Combinations of Stabilizing Signals for Case Study III

Pair number	Each TCSC (input signal 1 - input signal 2)
1	δ_{21}-δ_{21}
2	δ_{21} - P_{L1}
3	δ_{21} - P_{L2}
4	δ_{31} - P_{L1}
5	δ_{31} - P_{L2}
6	$P_{L1} - P_{L2}$

The dual channel TCSC supplemental damping power system oscillations using six pairs of signals is shown in figure 7.and are given in Table IV. The best and the second best damped responses are obtained with pairs 2 and 5, and the transfer functions of the TCSC supplemental controllers for the six pairs of signals are given in table V.

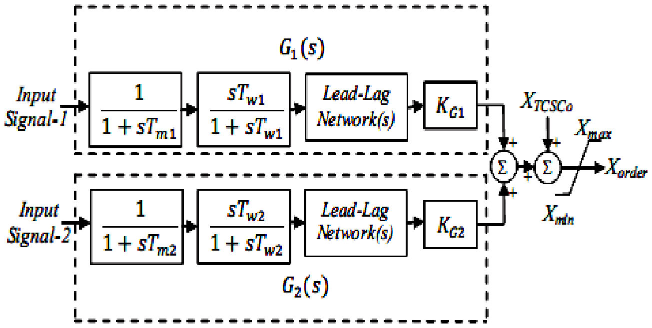

Figure 7: Structure of a dual-channel power oscillations damping controller.

TABLE V

Transfer Functions of the TCSC Supplemental Controllers

Pair 2 Each TCSC in L_1	G_1(s)=0.25 10/S+10)(0.5S/0.5S+1) G_2(s)=-0.5 /S+60)(0.01S/0.01S+1)
Pair 2 Each TCSC in L_1	G_1(s)=0.25 (10/S+10)(0.5S/0.5S+1) G_2(s)=-0.5 0/S+60)(0.01S/0.01S+1)
Pair 5 Each TCSC in L_1	G_1(s)=0.28 (10/S+10)(3S/3S+1) G_2(s)=-(60/S+60)(0.01S/0.01S+1)* ((S+0.1)/(S+0.2))((S+0.5)/(S+3))
Pair 5 Each TCSC in L_2	G_1(s)=0.26 (10/S+10)(S/S+1) G_2(s)=2.5(60/S+60)(0.01S/0.01S+1)* ((S+0.1)/(S+0.2))((S+0.5)/(S+3))

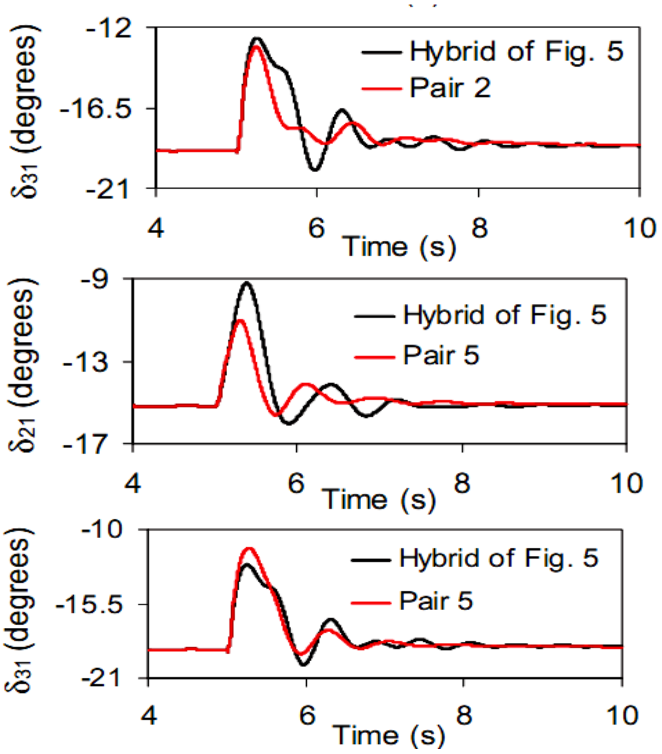

Figure 8: Generator load angles, measured with respect to generator 1 load angle, during and after clearing a three phase fault at bus 4 (Load Profile B, dual-channel controller).

Figure 9. Illustrates the three-phase voltages, VX-Y, across the hybrid single-phase-TCSC compensation scheme (installed in L1 and the controllers are Pair 2) during and after clearing the fault. The system phase imbalance during the disturbance is clearly noticeable especially in phase C.

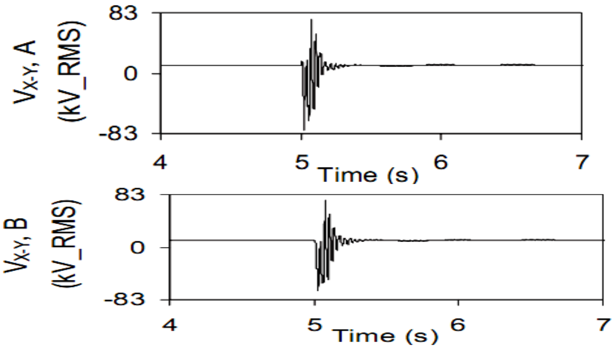

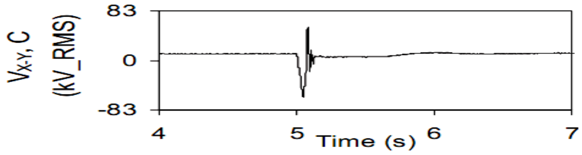

Figure 9: Phase voltages, $V_{X\text{-}Y}$ across the hybrid single-phase- TCSC scheme on L1 during and after clearing a three-phase fault at bus 4 (Load Profile B, dual-channel supplemental controllers, Pair 2).

V. CONCLUSION

Increasing the proportion of the single-phase-TCSC to the fixed capacitor of its phase results in improving the damping of system oscillations. Increasing the proportion of the hybrid single-phase-TCSC compensation scheme to the total fixed capacitor compensation (i.e. Installing the scheme in more transmission line circuits replacing fixed capacitor compensation) enhances significantly the damping of system oscillations. Choosing the values of such two proportion options can be considered as an optimization task between dynamic stability improvements and economical and reliability advantages of fixed series capacitors. In all case studies adequate power system oscillation damping is obtained with proportional type TCSC and STATCOM supplemental controllers. Overall the best damping of the relative load angle responses are achieved when the hybrid single-phase TCSC is installed in line L3 as well as in the two circuits of line L1.

REFERENCES

[1] D.N. Kosterev, C.W. Taylor, W.A. Mittelstadt, “Model Validation for the August 10, 996 WSCC System Outage,” IEEE Transactions on Power Systems, Vol. 14, No. 3, August 1999, pp. 967-979.
[2] Y.H. Song and A.T. Johns, Flexible AC Transmission Systems (FACTS), London, Institution of Electrical Engineers, 1999.
[3] N.G. Hingorani and L. Gyugyi, Understanding FACTS: Concepts and Technology of Flexible AC Transmission Systems, New York, IEEE Press, 2000.
[4] X. R. Chen, N.C. Pahalawaththa, U.D. Annakkage and C.S. Kumble, “Design of Decentralised output Feedback TCSC Damping Controllers by Using Simulated 86 Annealing,” IEE Proceedings, Generation, Transmission and Distribution, Vol. 145, No. 5, September 1998, pp. 553-558.
[5] D. Rai, S.O. Faried, G. Ramakrishna, and A. Edris, “Hybrid Series Compensation Scheme Capable of Damping Subsynchronous Resonance,” IET Generation, Transmission and Distribution, Vol. 4, No. 3, March 2010, pp. 456-466.
[6] N. Yang, Q. Liu and J. McCalley, “TCSC Controller Design for Interarea Oscillations,” IEEE Transactions on Power Systems, Vol. 13, No. 4, November 1998, pp. 1304-1309.
[7] X. Chen, N. Pahalawaththa, U. Annakkage and C. Kumbe, “Output Feedback TCSC Controllers to Improve Damping of Meshed Multi-Machine Power Systems,” IEE Proceedings, Generation, Transmission and Distribution, Vol. 44, No. 3, May 1997, pp. 243-248.
[8] J. Machowski, S. Robak and J. Bialek, “Damping of Power Swings by Optimal Control of Series Compensators,” Proceedings of the 10th International Conference on Power System Automation and Control PSAC'97, Bled, Slovenia, October 1-3, 1997, pp. 39-44.
[9] J.F. Hauer, M.K. Donnelly, W.A. Mittelstadt, W. Litzenberger and D.J. Maratukulam, “Information Functions and Architecture for Networked Monitoring of Wide Area Power System Dynamics: Experience with the Evolving Western System Dynamic Information Network,” Proceedings of the Sixth Symposium of Specialists on Electric Operational and Expansion Planning (VI SEPOPE), Bahia, Brazil, May 24-29, 1998.
[10] B. Bhargava and A. Salazar, “Use of Synchronized Phasor Measurement System for Monitoring Power System Stability and System Dynamics in Real-Time,” Proceedings of the 2008 IEEE PES GM, Pittsburgh, PA,July 20 – 24, 2008, pp. 1-8.
[11] H. Ni, G.T. Heydt and L. Mili, “Power System Stability Agents using Robust Wide Area Control, “IEEE Transactions on Power Systems, Vol. 17, No. 4, November 2002, pp. 1123-1131.
[12] X Xie. J. Xiao, C. Lu and Y. Han, “Wide-Area Stability Control for Damping Interarea Oscillations of Interconnected Power Systems,” IEE Proceedings, Generation, Transmission and Distribution, Vol. 153, No.5, September 2006, pp. 507-514.
[13] C.W. Taylor, D.E. Erickson, K.E. Martin, R.E. Wilson and V. Venkatasubramanian,” WACS-Wide-Area Stability and Voltage Control System: R&D and Online Demonstration,” Proceedings of IEEE, Vol. 93, No. 5, May 2005, pp. 892-906.
[14] X. Zhou and J. Liang, “Overview of Control Schemes for TCSC to Enhance the Stability of Power Systems,“ IEE Proceedings, Generation, Transmission and Distribution, Vol. 146, No. 2, March 1999, pp. 125-130.

OPEN ACCESS

International
Journal
Of Modern Engineering Research (IJMER)

Security of Data in Cloud Environment Using DPaaS

Prabhleen Singh[1], Ketki Arora[2]
[1]Student Lovely Professional University India
[2]Department of Computer Science, Lovely Professional University India

ABSTRACT: *The rapid development of cloud computing is giving way to more cloud services, due to which security of services of cloud especially data confidentiality protection, becomes more critical. Cloud computing is an emerging computing style which provides dynamic services, scalable and pay-per-use. Although cloud computing provides numerous advantages, a key challenge is how to ensure and build confidence that the cloud can handle user data securely. This paper highlights some major security issues that exist in current cloud computing environments. The status of the development of cloud computing security, the data privacy analysis, security audit, information check and another challenges that the cloud computing security faces have been explored. The recent researches on data protection regarding security and privacy issues in cloud computing have partially addressed some issues. The best option is to build data-protection solutions at the platform layer. The growing appeal of data protection as a service is that it enables to access just the resources you need at minimal upfront expense while providing the benefits of enterprise-class data protection capabilities. The paper proposes a solution to make existing developed applications for simple cloud Systems compatible with DPaaS. The various security challenges have been highlighted and the various necessary metrics required for designing DPaaS have been investigated.*

Keywords: *Cloud Computing, data security, privacy protection.*

I. INTRODUCTION

Over the past few years, cloud computing has become significant research topic of the scientific and industrial communities. The Cloud computing has emerged as a new computing model which aims to provide reliable, customized, scalable, pay-per-use and dynamic computing environments for end-users. Numerous organizations have started realizing the benefits by putting their applications and data into the cloud. Cloud computing is not new to Information Technology. Unlike other computing models, cloud computing possess some additional features that make it distinguishable such as service-driven, resource pooling, and data hosting in outsourcing storage. Pooling resource makes the hardware performance be used more efficient and provides economic benefits for users to reduce the capital cost and additional expenditure. The biggest benefit is that developers no longer require the large capital outlays in hardware to deploy the innovative ideas for new Internet services service and hence cutting the human expense to operate it.

Defining cloud computing actually becomes a difficult task with many definitions. Since recent past, several efforts have been made to provide the exact definition of “cloud computing”. The definition provided by U.S. NIST (National Institute of Standards and Technology) appears to include key common elements widely used in the Cloud Computing community as it says that: "Cloud computing is a model for enabling convenient, on-demand network access to a shared pool of configurable computing resources that can be rapidly provisioned and released with minimal management effort or service provider interaction [3].

The cloud computing offers numerous potential advantages comparatively traditional IT model. Yet the major barrier for the adoption of cloud computing are the security concerns. Security control measures in cloud are similar to ones in traditional IT environment. Traditional security issues are still present in cloud computing environments. But as enterprise boundaries have been extended to the cloud, traditional security mechanisms are no longer able to go with applications and data in cloud. Due to the openness and multi-tenant characteristic of the cloud, cloud computing is bringing tremendous impact on information security field [4].

II. CHARACTERISTICS OF CLOUD COMPUTING

Cloud computing provides several compelling characteristics which differentiate it from other computing paradigms. Some of them are:

- **Broad network access range:** System capacities are available to customers through a network and can be accessed from different devices such as desktop computers, mobile phones, smartphones and tablet devices.

- **Pay- per use model:** Cloud computing uses a pay-as you-go-pricing model. Resources in a cloud environment can be allocated and de-allocated on demand. So a service provider does not need to invest in the infrastructure to start gaining benefit from cloud computing. It simply rents resources from the cloud according to its own needs and pay for the usage.
- **Service provisioning on demand:** Computer services such as email, applications, network or server service can be provided without requiring human interaction with each service provider. Cloud service providers providing on demand self-service include Amazon Web Services, Microsoft, Google, IBM and Salesforce.com.
- **Sharing of resources:** The computing resources are pooled together to serve multiple consumers using multiple-tenant model, with different physical and virtual resources dynamically assigned according to consumer demand. The resources include storage, processing, memory, network bandwidth, virtual machines and email services.
- **Rapid elasticity:** The cloud is flexible and scalable to suit your immediate business needs. You can quickly and easily add or remove users, software features, and other resources.

III. CLOUD SERVICES

Cloud service delivery is divided among three service models. The three fundamental classifications are often referred to as the “SPI Model” where ‘SPI’ refers to software, platform, and infrastructure as defined below:

1. Software as a Service (SaaS)
2. Platform as a Service (PaaS)
3. Infrastructure as a Service (IaaS)

1.3.1 Software as a Service (SaaS)

Unlike the traditional model of one application per desktop, Software as a Service (SaaS) makes use of a cloud computing infrastructure to deliver one application to many users, regardless of their location. It allows activities to be managed from central locations in a one-to-many model, including architecture, pricing, partnering, and management characteristics. Some examples are Google Apps (mail, docs, and etc.) and Salesforce.com

1.3.2 Platform as a Service (PaaS)

Platform as a Service (PaaS) is a software distribution model in which hosted software applications are made available to customers over the Internet. Service provider provides a specific cloud environment, some software tools and programming language to consumer for developing, testing, and hosting their applications. PaaS provides users with a high level of abstraction that allows them to focus on developing their applications without concerning about the underlying infrastructure. An example of PaaS is Google App engine.

1.3.3 Infrastructure as a Service (IaaS)

IaaS allows consumer to rent hardware include processors, storages, network, and other fundamental computing resources. In this service model, consumers do not control or manage the underlying cloud infrastructure directly. They control the computing resources through operating systems [6]. This service provides the required infrastructure as a service. The key advantage here is that customers need to pay only for the time duration they use the service. As a result customers can achieve a much faster service delivery with less cost.

IV. SECURITY OF DATA IN CLOUD

Security within cloud computing is a critical issue because the devices that provide services do not belong to the users themselves in actual. Although cloud computing promises lower costs, rapid scaling, easier maintenance, and service availability anywhere, anytime, a key challenge is how to ensure and build confidence that the cloud can handle user data securely. This is a great concern in cases when users have valuable and personal information stored in a cloud computing service. It is an increasingly important problem to protect the confidentiality of information manipulated by computing systems. There is little assurance that current computing systems protect data confidentiality and integrity. New security issues are raised at the same time due to the changing system environment.

The development of new services open doors for new opportunities and difficulties. By now, almost all IT enterprises are involved in cloud storage by services provision. But while provision of services, we must take into account the problems emerging from the storage operations in cloud. When the data store on personal devices, users have the highest privilege to operate on them and ensure its security. But once the users choose to put data into cloud, they lose their control over the data [7]. The user's authentication and authorization is needed to access the data so as to prevent stealing other user's data through service failure or intrusion.

The answer to data confidentiality is data encryption. The use of both encryption algorithm and key strength are needed to be considered in order to ensure the effect of encryption,. The major issue about data encryption is key management. The major issue considered in key management is as who will be responsible for key management. Ideally, the data owners are responsible for managing the key. But at present, because the users have not enough expertise to manage the keys, they usually entrust the key management to the cloud providers. As the cloud providers need to maintain keys for a large number of users, key management become more complex and difficult [4].

V. SECURITY CHALLENGES

Data security has consistently been a major issue in IT. There are complex data security challenges in the cloud:

- The need to protect confidential business, government, or regulatory data
- Cloud service models with multiple tenants sharing the same infrastructure
- Data mobility and legal issues relative to such government rules as the EU Data Privacy Directive
- Lack of standards about how cloud service providers securely recycle disk space and erase existing data
- Auditing, reporting, and compliance concerns
- Loss of visibility to key security and operational intelligence that no longer is available to feed enterprise IT security intelligence and risk management
- A new type of insider who does not even work for your company, but may have control and visibility into your data

VI. ENCRYPTION

A feasible solution for data protection is data encryption. Encryption algorithm offers the benefit of minimum reliance on cloud provider. The user data can migrate from one provider to another provider without limiting to the specific provider. Encryption algorithm protects data without considering their physical location. Unfortunately, when performing the encryption algorithm, it often consumes a lot of system resources, such as CPU utilization, and stronger algorithm that generates more significant impact to the system performance. The trade -off between security and system performance become an important issue when applying an encryption algorithm in cloud environment.

It's very important to understand what kinds of encryption are most important for a particular need. Two types of encryption algorithms have been considered in the study: FDE and FHE.

- Full Disk Encryption- FDE: As the name reveals, FDE encrypts entire physical disks with a symmetric key for simplicity and speed. Although FDE is effective in protecting private data in certain scenarios, the concern is that it can't fulfill data protection goals in the cloud, where physical theft isn't the main threat. FDE offers excellent performance and ease of development but it does little to protect privacy at the required granularity.
- Fully Homomorphic Encryption- FHE: Here, the server does the real work, but it doesn't know the data it's computing. It offers the promise of general computation on ciphertexts. Any function in plaintext can be transformed into an equivalent function in ciphertext. This property guarantees strong privacy when computing on private data, but the question of its practicality for general cloud applications still remains. FHE removies data visibility entirely from both the server and application developer [8].

VII. DATA PROTECTION AS A SERVICE- DPAAS

DPaaS is a suite of security primitives offered by a cloud platform, which enforces data security and privacy and offers evidence of privacy to data owners, even in the presence of potentially compromised or malicious applications.

A cloud platform helps the developers to write maintainable applications that protect user data in the cloud, hence providing the same economies of scale for security and privacy as for computation and storage; and enabling independent verification both of the platform's operation and the runtime state of applications on it. Hence users can gain confidence that their data is being handled properly.

Cloud-delivered services allow businesses to access enterprise-class resources and infrastructures at a lower price and with very little capital expenses. Cloud- delivered services also help to free IT resources and maximize administrator productivity. Many midsize businesses have already moved costly and administratively time-consuming applications to the cloud. The adoption of data protection as a service has gained momentum due to these reasons. The growing appeal of data protection as a service is that it enable the access of resources you need at minimal upfront expense as well as providing the benefits of enterprise-class data protection capabilities. Data protection as a service removes the complexity barriers for midsize businesses to meet enterprise-level recovery point and recovery time objectives.

VIII. MOTIVATION

One of the main concerns people and organizations have about putting data in the cloud is that they don't know what happens to it. Having a clear audit of when data is accessed, who access the data contributes to strengthen the confidence that data is being handled appropriately. Cloud storage offers an on-demand data outsourcing service model, and is gaining popularity due to its elasticity and low maintenance cost. However, security concerns arise when data storage is outsourced to third-party cloud storage providers. It is desirable to enable cloud clients to verify the integrity of their outsourced data in the cloud, in case their data has been accidentally corrupted or maliciously compromised [9].

With the growing popularity of cloud computing, the importance of security show gradual upward trend, become an important factor in the development of cloud computing. Encryption in the cloud is about preventing outside hackers and external partners from accessing a company's private data. The cloud offers little platform-level support or standardization for user data protection. A new cloud computing paradigm data protection as a service DPaaS has been proposed in the work which is defined as security primitives offered by a cloud platform, which enforces data security and privacy and offers evidence of privacy to data owners, even in the presence of potentially compromised or malicious applications.

IX. PROPOSED SCHEME

Cloud computing refers to a large number of computers connected by real-time network viz. internet. Cloud computing provides a way to execute applications on many computers at same time so it is also called as Distributed computing. Though IaaS promises cost efficient and high availability of service across the internet, there is a limitation of building a confident cloud system which can handle data securely and reliably. DPaaS provides secure cloud environment to save data. There are different techniques used for handling data security like – encryption and authentication in data access.

The major issue is that providing protection to user data while enabling rich computation requires both specialized expertise and resources that might not be readily available to most application developers. Building in data-protection solutions at the platform layer is an attractive option as the platform can achieve economies of scale by reducing expertise costs and distributing sophisticated security solutions across different applications and their developers.

Major problem in DPaas is to make existing developed applications for simple cloud Systems compatible with DPaaS as there are many changes in cloud implementation and security integrations. This leads to requirement of changing application architecture and also many changes will be required in application codes. We shall be listing all the necessary metrics required for designing DPaaS so that simpler cloud applications can be migrated to DPaaS with minimum cost and updates.

In our system, there is an administrator who can view data of the users, change the data in the web files and save them. In other words administrator has the control over the user data. The users can upload, view, and change the data in their created web file. They cannot view data or web files of other users. While the auditor is one who audits the overall performance of the system. He can track the transactions, upload of file, change of data and logins of users with correct time and date.

Whenever a user will upload a file and the file gets migrated onto the cloud. After that if the user make any changes to that file, those changes are made standards for further uploads. Here in our system, three types of web files are uploaded- .asp, .jsp and .php files. These formats are made standard formats for the upload. If any file other than this file format is uploaded, it will not get migrated to the cloud. Another advantage offered is that user gets the control over his data protection. If administrator or auditor has made any change to user's file, user will get to know all the details about that through a notification message. It adds a lot into the data security on cloud.

The proposed methodology is needed to be implemented in a tool. The proposed solution is to be implemented in java and CloudSim. CloudSim enables modeling, simulation, and experimenting on Cloud computing infrastructures. It is a self-contained platform used to model data centers, service brokers, scheduling and allocation policies of large scale Cloud platforms. It provides a virtualization engine with extensive features for modeling creation and life cycle management of virtual machines in a data center, including policies for provisioning of virtual machines to hosts, scheduling of resources of hosts among virtual machines, scheduling of tasks in virtual machines, and modeling of costs incurring in such operations.

X. CONCLUSION

In an emerging discipline, like cloud computing, security needs to be analyzed more frequently. With advancement in cloud technologies and increasing number of cloud users, data security dimensions will continuously increase. Cloud computing security needs consider both technology and strategy, including: audit, compliance and risk assessment. Both the Service providers and the clients must work together to ensure safety and security of cloud and data on clouds. Mutual understanding between service providers and users is extremely necessary for providing better cloud security. In our paper we are laying stress on the security issue in the cloud. In this paper, we propose an approach for applying DpaaS to the existing applications in cloud environment to secure the confidentiality of users' data without increasing system performance overhead too much.

ACKNOWLEDGMENT

The paper has been written with the kind assistance, guidance and active support of my department who have helped me in this work. I would like to thank all the individuals whose encouragement and support has made the completion of this work possible.

REFERENCES

[1] Sadie Creese, Paul Hopkins, Siani Pearson, Yun Shen, "Data Protection-Aware Design for Cloud Computing", HP Laboratories
[2] "Introduction to Cloud Computing", Dialogic Corporation
[3] Yashpalsinh Jadeja, Kirit Modi (2012), "Cloud Computing - Concepts, Architecture and Challenges", 2012 International Conference on Computing, Electronics and Electrical Technologies [ICCEET]
[4] Deyan Chen, Hong Zhao (2012), "Data Security and Privacy Protection Issues in Cloud Computing", International Conference on Computer Science and Electronics Engineering
[5] Hans-Dieter Wehle (2011), "Cloud billing service: An SOA-enabled billing service module for the cloud environment", IBM
[6] Ranjita Mishra, Sanjit Kumar Dash (2011), "A Privacy Preserving Repository for Securing Data across the Cloud", 978-1-4244-8679-3/11/2011 IEEE
[7] Ling Li Lin Xu Jing Li Changchun Zhang (2011), "Study on the Third-party Audit in Cloud Storage Service", International Conference on Cloud and Service Computing, -1-4577-1637-9/11/2011 IEEE
[8] Dawn Song, Elaine Shi, and Ian Fischer, Umesh Shankar (2012), "Cloud Data Protection for the Masses", 0018-9162/12/2012 IEEE
[9] Henry C. H. Chen and Patrick P. C. Lee (2012), "Enabling Data Integrity Protection in Regenerating-Coding-Based Cloud Storage", 2012 31st International Symposium on Reliable Distributed Systems, IEEE Computer Society
[10] Raghu Yeluri, Enrique Castro-Leon, Robert R. Harmon, James Greene (2012), "Building Trust and Compliance in the Cloud for Services", 2012 Service Research and Innovation Institute Global Conference, 978-0-7695-4770-1/12/2012 IEEE
[11] Lingfeng Chen and Doan B. Hoang (2011), "Novel data protection model in healthcare cloud", 2011 IEEE International Conference on High Performance Computing and Communications
[12] Engr: Farhan Bashir Shaikh and Sajjad Haider (2011), "Security Threats in Cloud Computing",IEEE
[13] I-Hsun Chuang, Syuan-Hao Li, Kuan-Chieh Huang, Yau-Hwang Kuo (2011), "An Effective Privacy Protection Scheme for Cloud Computing", ISBN 978-89-5519-155-4, Feb. 13~16, 2011 ICACT2011
[14] Pei-Yun Hsueh, Tyrone Grandison, Ci-Wei Lan, lenHao Hsiao, and Henry Chang (2012), "Privacy Protection for Personal Data Integration and Sharing in Care Coordination Services A Case Study on Wellness Cloud", International Journal of Scientific and Research Publications, Volume 3, Issue 6, June 2013 1ISSN 2250-3153
[15] Sunumol Cherian, Kavitha Murukezhan (2013), "Providing Data Protection as a Service in Cloud Computing", International Journal of Scientific and Research Publications, Volume 3, Issue 6, June 2013, ISSN 2250 -3153
[16] http://searchitchannel.techtarget.com/feature/Challenges-of-transitioning-to-cloud-data-protection-services
[17] http://www.applicure.com/blog/securing-cloud-data
[18] http://www.pcworld.com/article/164933/cloud_computing.html
[19] http://www.darkreading.com/services/protecting-data-in-the-cloud-withoutmak/240145260

OPEN ACCESS

International
Journal
Of Modern Engineering Research (IJMER)

Removal of Artefact from Shoe Print Image

Prof. (Dr.) Samir Kumar Bandyopadhyay[1], Ms. Nabanita Basu[2]
[1]*Professor, Department of Computer Science & Engineering, University of Calcutta*
[2]*Research Scholar, Department of Computer Science &Engineering, University of Calcutta*

ABSTRACT: *Shoe marks at the place of crime provide valuable forensic evidence. Many different artefacts can occur during processing of shoe print images. This paper proposed a methodology to remove the artefacts from shoe print images. The proposed methodology is very simple with the combination of statistical and computational geometric approach. Statistical methods like standard deviation are used to calculate the global threshold to binarize the image and computational geometry like convex hull is used to produce final output. It is possible to remove artefacts if it is present either in front side of the image or rear of the image.*

Kevwords: *Artefact. Standard Deviation. Global Thresholdina. and Convex Hull.*

I. INTRODUCTION

Locard [1] believed that no matter what a perpetrator does or where he goes ,by coming in contact with things at or around a crimescene he can leave all sorts of evidence , including DNA, fingerprints, footprints, hair , skin cells, blood, body fluids, pieces ofclothing fibers and more[1]. While the criminal leaves something at the crime scene he is also expected to take something awayfrom the scene with him[1]. On a very loose connect it might be said that when killing an individual with a hammer hit thecriminal might take away the murder weapon with him but at the same time he might end up leaving behind bloody stains of theblood bearing hammer at the crime scene . ‘A bloodstain resulting from contact between a blood-bearing surface and anothersurface’ has been termed as ‘Transfer Stain’ by the International Association of Bloodstain Pattern Analysts (IABPA)[2-4]. Thusthis work is particularly directed at studying hammer transfer stain patterns at a crime scene.Many image processing techniques have been developed over the past two decades to help forensicscientist in detection of footprint image boundary. Most studies conducted have proven that measurementof parameters may help detection of crime scenario. In this paper we present initially pre-processing offootprint image after digitization and then find out the artefacts present. Segmentation of Region of Interest (ROI) is used. Further we useDivide and Conquer Homogeneity algorithm, followed by edge detection. We obtain the image boundaryby using our proposed algorithm. A RGB image taken as an input, but here the methodsdeals with grayimage, thus input RGB image converted intogray image first. Binarization is very effective preprocessingmethodsfor most of the segmentation. Due to largevariation on background and foreground ofshoe print imagesmaximum binarization fails but here a binarization methodhas been proposed and a globalthreshold value has beenselected by standard deviation of the image. Globalthresholding using standarddeviation gives very goodresults and binarize each component of the image.Shoeprint is the mark made by the outside surface of the soleof a shoe (consist of distinctive geometric patterns) found atcrime scenes. Shoe marks can be broadly classified into twoclasses: 1) shoe impressions which contain 3-dimensionalinformation (e.g. shoe impression at the beach) and 2) shoeprints which contain 2-dimensional information (e.g.shoeprint on a floor). Probability of occurrence of shoe marksat the place of crime is higher than that of fingerprints since ahigh proportion of burglars wear gloves [1]. In severaljurisdictions of Switzerland it was revealed that 35 percent ofcrime scenes had shoeprints usable in forensic science, andfound that 30 percent of all burglaries provide usableshoeprints [2, 3]. It is known that majority of the crimes arecommitted by repeat offenders. It is common for burglars tocommit a number of offences on the same day. As it would beunusual for offenders to discard their footwear betweencommitting different crimes [4]; timely identification andmatching of shoeprints helps in linking various crime scenes.

Often it is the case when number of crimes has beencommitted; the investigating officers have an idea of who hascommitted the crime(s). Indeed, they have suspect in custodywhose modus operandi fits the crime.

II. BRIEF REVIEW

In the IABPA Conference held in Tucson, Arizona, 2004, Peter Lamb presented the investigation report of the late night assault of a young man who was intoxicated at the time of attack and could only recollect part of the savagery that he had been subjected to[5]. Due to rain drop that had soaked the garment at the time of the assault it was difficult to examine the bloodstains on the soaked garment and shoe print image on the floor[5]. However there was evidence of kicking and stomping[5]. Based on the evidence the case finally proceeded for trial and the accused was proved guilty and hence imprisoned [5]. In his review of the Windsor city homicide case Scott Lamont pointed out that barefoot transfer impressions and footwear transfer impressions were found on the floor[6]. Foot morphology confirmed that the prints were left by the suspect who was wearing boots[6]. In the words of LeeAnnSingley, in the murder case of 2 women (74 year old mother and her 48 year old daughter) in their holiday home in a small town in Pennsylvania, while DNA evidence answered 'who ?' in identifying the perpetrator at the trial, the bloodstain pattern evidence proved to be valuable to the jury in answering the 'how?'[7]. To add to the list, in the case of Regina vs. Sion Jenkins, expirated and other bloodstains on clothing were used as relevant evidence within the legal setting to acquit Sion Jenkins of the murder of his 13 year old daughter Billie Jo[8]. In the case presented by Paul Treudson, at a particular crime scene bloody transfer impressions of an apparent right hand holding a knife was found on top of a sheet that lay at the foot of the bed [9]. The impressions included knuckles and a blade [9]. As Erin Sims puts it, for one particular case the evidence particularly the bloodstain pattern evidence was the only honest teller of the course of events that had led to the victim's injury[10]. Initially, the Birkett system of coding shoeprint patterns wasdevised by John Birkett of the metropolitan Police ForensicScience Laboratory by allocating alphanumerical values tovarious pattern elements. This system failed uniquely toidentify a pattern because of the multitude of new patternsfrom manufacturers in the late 1980s. The major problemwith the Birkett system was the volume of new patterns, whichthen addressed by prefixing the coding elements with twonumerical digits for the year and a 3 digit numerical suffix in1993. Again, as per the Federal Bureau of Investigation (FBI) Chart reports each year more people are killed by hammer, club or blunt ended object hit as compared to the number of people killed wt rifle or shotgun[11]. In this respect it might be interesting to mention that, in a case reviewed by Stuart H. James at the 2008 IABPA Annual Training conference, he reiterated that bodies of 4 Mexican construction workers were found in a rented apartment at Ohio [12]. The bodies of the victims remained undiscovered for almost a week [12]. When examined the victims were found to have suffered blunt and sharp force injuries [12-14]. The highlight of the case review were the interesting bloodstain patterns found at the crime scene which were studied in conjunction with the wounds suffered/sustained by the victims[12]. In their study, the authors came across many such cases where victims suffered blunt force injuries. Given the large possibility of instruments that can be easily obtained and hence deliver blunt force injuries to the human skull, the authors decided to particularly focus on the possible Transfer and Saturation stain patterns formed at a crime scene as a result of assault particularly with blunt ended objects.

III. METHODOLOGY USED

A statistical method i.e.standarddeviation is used to calculate the threshold value. In this processing statistical descriptions separate foreground images and background images. A digitized image I[m,n] and *h* is the intensity of each pixel of the gray image. Here Quickhull Algorithm for Convex Hulls is used. Quickhull Algorithm for Convex Hulls runs faster when the input contains non-extreme points and it uses merged facets to guarantee that the output is clearly convex.

IV. ALGORITHM (PSEUDO CODE)

Step 1. Grayscale shoe print image is taken as input.

Step 2. Threshold value of the image is calculated using the standard deviation technique described above.

Step 3. The image is binarized using the threshold value. i.e. pixels having value greater than the threshold is set to 1 and pixels less than the threshold are set to 0.

```
/* [A B]=size(I);
BI =zeros(a,b);
STD = std2(I);
FORi = 1 to A DO
FOR j=1 to B DO
IF I(i,j) > STD THEN
Set BI(i,j)=1
END IF
END FOR
END FOR*/
```

Step 4. The binarized image is labelled and areas of connected components are calculated using equivalence classes.

Step 5. The connected component with the maximum area and the connected component with the second highest area are found out.

Step 6. The ratio of the maximumarea to that of second maximum area are calculated if the ratio is high and if ratio is low

Step 7. On the basis of the ratio if ratio is high only the component with highest area is kept and all others are removed otherwise if ratio is low the component with the highest and second highest area are kept and all others are removed.

Step 8. A convex hull is calculated for the one pixel in the image and all regions within the convexhull are set to one.

Step 9.Now the above obtained image matrix is multiplied to the original image matrix to obtain an image consisting of only shoe print without any artefact.

V. CORRECTNESS

Loop invariant: At start of every iteration of outer loop, each row of image i = 1, 2, ... , A and inner loop , each column j = 1, 2, ... , B; in the end of the iteration it follows same process.

Initialization: Since i = 1 i.e. it is at first row of the image before the first iteration of the outer loop, so, the invariant is initially true and is same for the inner loop; some variable are initialize with the image size and dimension which is finite.

Maintenance: In each successive iteration loop invariant moves to next row by incrementing loop variable. Loop works by moving Image [i + 1][j], Image [i + 2][j], Image [i + 3][j] and so on.

Termination: The outer loop ends when outer loop >height, i.e. all the row of the image is already traversed.

Complexity Analysis

Assuming the height = width =n, the running time for both for loop is $O(n \times n)$ for all cases;At each level of the recursion, partitioning requires $O(n)$ time. If *partitions* were guaranteed to havea size equal to a fixed portion, and this held at each level, the worst case time would be $O(n \log n)$. However, those criteria do not apply; Partitions may have size in $O(n)$ (they are not balanced). Hence the worst case running time is $O(n2)$. Thus if we consider worst case time: $O(n\ 2)$ and expected time: $O(n \log n)$. To calculate the area of each component it requires $O(n \times n)$ running time.**T(n)**= $O(n2) + O(n \log n) + O(n2) = O(n2)$.

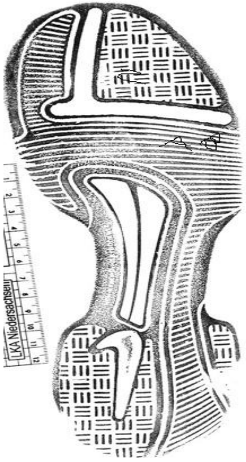

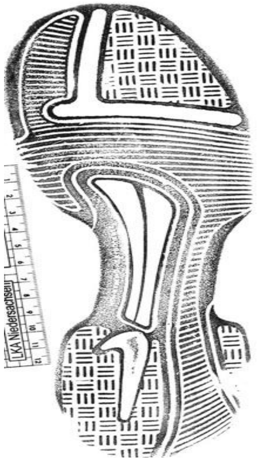

Figure 1(a) Shoe Print with artefact **Figure 1(b) Shoe Print without artefact**

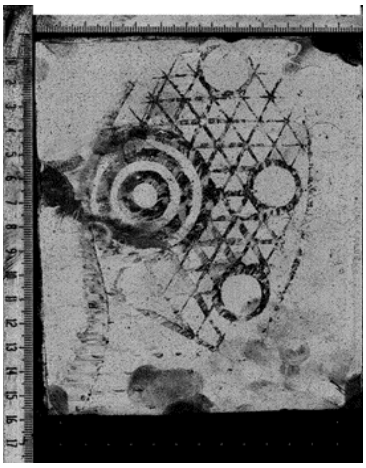

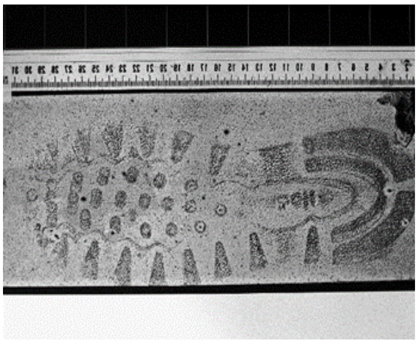

Figure 2(a) Shoe Print with artefact **Figure 2(b) Shoe Print without artefact(45 Degree rotation)**

VI. CONCLUSIONS

Removing artefact by calculating each component and the binarized output is shown in figure1 (b) and 2 (b). Maximum number of artefacts (mainly letter) removed from this step but if any metal or Gibbs artefact are present then those are removed by applying Quickhull convex hull and shown in figure 2(b). In figure 1(b) no artefact present i.e. all artefacts are removed by proposed algorithms. Artefact removal from shoe print is a pre-processing step. Here intelligence system for artefact removal on shoe print has been implemented. The automated system remove artefact using low time complexity. Proposed methods are based on a combination of statistical and geometric methods and it give very good results for different kinds of shoe print images.

REFERENCES

[1]. Welding, S. (2012, 12). Locard's Exchange Principle - Forensic HandbookForensic Handbook. Retrieved October 22, 2014, from http://www.forensichandbook.com/locards-exchange-principle/
[2]. Nordby, J. J. (2006). Final Analysis Forensics. Retrieved from http://www.finalanalysisforensics.com/media/pdfs/BasicBloodstainPatternAnalysisTEXT.pdf
[3]. Scientific Working Group On Bloodstain Pattern Analysis. (2009, April). FBI — Standards and Guidelines - Scientific Working Group on Bloodstain Pattern Analysis: Recommended Terminology - April 2009. Retrieved from http://www.fbi.gov/about-us/lab/forensic-science-communications/fsc/april2009/standards/2009_04_standards01.htm
[4]. http://www.iabpa.org/journal
[5]. December News 2004, The Use of BPA Modeling in Investigations, Peter Lamb,Page 8
[6]. December News 2004, City of Windsor Homicide Case, Scott Lamont, Page 11
[7]. December News 2006, We Got Our Man (in more ways than one), LeeAnnSingley,Page 23
[8]. December News 2007, Regina v. Sion Jenkins, Joe Slemko, Page 8-9
[9]. December News 2007, Case Presentation, Paul Treudson, Page 12
[10]. December News 2008, Bloodstain Patterns Help Tell the Story When the Victim Can't… or Won't, Erin Sims Page 19
[11]. Toplikar, D. (2010, December 13). Blood stain with hammer imprint shown in ex-FBI agent's murder trial - Las Vegas Sun News. Retrieved from http://www.lasvegassun.com/news/2010/dec/13/blood-stain-showed-imprint-hammer-says-analyst-ex-/
[12]. December News 2008 Page 17
[13]. December News 2005 Page 4
[14]. December News 2005 Page 11

OPEN ACCESS

International
Journal
Of Modern Engineering Research (IJMER)

Value Chain Bankrolling: Strategy towards enhancing growth in Agriculture sector in India

Sushil D. Yeole[1], Shailesh B. Wahulkar[2], Amol A. Parihar[3], Pankaj G. Dhoble[4]
Nandkishor D. Bankar[5], Bhalchandra D. Bhalekar[6]
[1,2,3,4,5,6]*Department of Mechanical Engineering, MGM Polytechnic, Aurangabad, India*

ABSTRACT: *Value chain has been an important concept in management offering improvement over the traditional supply or distribution chain, with an aim to optimize the chain and reduce it to limited links with each one performing an activity to enhance the value of the product and not merely the cost. Further, management of such value chain network should focus on cohesively taking the stake-holders along and sharing / spreading the benefits among them, such that the network becomes symbiotic and sustainable, and the process of value-addition & delivery gets ethical. The main objective of this research paper is to highlight the key value chain activities in context to agricultural products and suggests the importance of value chain financing which requires due attention from National and Regional level financing corporations.*

Keywords: *Value Chain, Value Chain Financing.*

I. INTRODUCTION

Today, the world is in the midst of a consumer revolution. The lifestyles, eating habits and the taste for the goods are changing drastically. The consumers in many countries are very conscious of what they eat and how they eat. People are not simply accepting the traditional lifestyle or the traditional eateries. Income levels have risen further influencing the tastes, choices and consumption patterns. This creates a new paradigm where the entire food system is driving the growth in agriculture and agribusiness, with better prospects for stakeholders. The choices, tastes are the driving factors for the value addition in agricultural supply chain.

A supply chain in agriculture can be thought of as a "farm to fork" process – from the inputs to production to processing, marketing and the consumer. Each level has one or numerous linkages. The unit value is increased as a product moves along the supply chain. Therefore, the value chain consists of a series of activities and relationships that add value to a final product, beginning with the production, continuing with the processing or elaborating of the final product, and ending with the marketing and sale to the consumer or end user. The interdependent linkages of the chain and the security of a market-driven demand of the final product provide the producers and processors with an assured market for their products. This reduces risk, thus making it easier to obtain financing and at lower cost from banks and other financiers. The linkages also allow financing to flow up and down the chain.

In fact, Value chain finance is not new, but is older than many forms of finance, especially in agriculture. What is new are the numerous new ways of providing such financing as well as the convergence and inter-linking of agribusiness and finance. It is receiving a lot of attention today. Business leaders in both finance and agriculture have come to realize that with the new innovations in communication technology, information management, etc., there is a wealth of new opportunities for them to profitably work together. It can be a win-win situation to reduce transaction costs and reduce risks. Many of these innovations are quite new, which is why we need to learn these innovations.

II. UNDERSTANDING SUPPLY CHAIN

The supply chain is an innovative management practice which insists on cooperative relationship between different players in the chain. Networking of farmers with suppliers of inputs and the processors is essential. It is nothing but a group organization which is connected to each other by flow of Products, Services, Finance and Information. The benefits of an integrated supply chain are:

1) Gives feedback to the farmer “to grow what sells."
2) Better price discovery.
3) Availability of best farming practices for ensuring good yield and quality.
4) Better post-harvest technologies to arrest deterioration.
5) Higher price due to sorting, grading etc.
6) Partial disintermediation by eliminating middlemen.

7) Extended shelf life of commodity due to processing / packaging etc.
8) It helps Indian farmers who lack market orientation.
9) It gives opportunity to have Industry – farmer Linkage.

III. VALUE CHAIN

Now, comes the concept of 'Value Chain' A value chain is a sequence of activities that a product passes through, with value added in each stage - from design, to the transforming of inputs, to the final market. These activities are carried out by a series of actors, who set rules and relate to each other in different ways, depending on the value chain. In chains dominated by the increasing concentration and power of retailers, value is increasingly derived by product differentiation and innovation that reduces cost and enhances the importance of reliable supply.

4.1 Developing the Fresh Produce Value Chain

Area	Present Scenario	Moving towards Future Scenario
Production	• Low yields • Production scattered over many Small farms • Outdated harvesting technologies • Inadequate information about prices, trends and customer needs	• Significantly higher yields • Use of modern technology • Better linkages with the market, more awareness about prices, trends and customer needs
Procurement / Transportation	• Traditional, agent driven procurement system • Extremely poor transportation infrastructure • Very limited cold storage facilities • High degree of wastage	• Improved post-harvest technologies available to most farmers • Efficient procurement system with few middle man • Reduced wastage due to better road / rail and refrigeration infrastructure.
Marketing / Distribution	• Produce is inconsistent in quality • Outdated, inadequate distribution infrastructure • Limited organized fresh produce • High degree of wastage	• Widespread organized fresh produce retailing, demanding high quality produce • Upgraded distribution export facilitated throughprovisions of adequate cold-storage/ pre-cooling infrastructure at ports/ airports

4.2 Value Chain Analysis

Value chain analysis helps us to identify key bottlenecks to economic growth, finds financial service gaps in terms of these key bottlenecks, and identifies and incorporates key actors in relevant value chains (such as those with the potential both for high growth and small enterprise participation). This tool can be useful in identifying financial services for which there is significant economic demand and interventions that can expand existing supply chain in efficient and sustainable ways. An analysis conducted by Kula and Farmer in 2004 (for USAID) included the following four steps:-

1) A cluster mapping of the region, starting with the key players in the identified commodity, and then layering on those entities providing services to the value chain – such as commercial agents, transporters, service providers, machinery repair businesses, insurance companies, and financial institutions.

2) An inventory of financial service providers – banks, finance, companies, NGOs, agribusinesses in the region, and the range and quantity of financial services they are currently providing; also the mutual finances / credit facilities provided among value chain partners.

3) Interviews of key stakeholders identified in the mapping and inventory exercises, focusing on three critical concerns:-
   a) The opportunities for and constraints to increased growth and competitiveness of the agribusiness sector in the region,
   b) the opportunities for and constraints to increased small holder participation in this growth, their benefit from it, and
   c) The role for improved financial services in contributing to this growth.

4) Identification of the critical constraints:-

As such, a banker has to work out the opportunities to finance different players in the chain covering various components. The Branches should consider the whole range of activities in a chain that would establish backward linkage i.e. networking with input suppliers and forward linkages i.e. covering processors who buy these products and marketers.

Till recently, Bankers were financing separately or in isolation to the suppliers, farmers, contract farming firms, distributors, transporters, etc. Most of the bank credit was limited to production and harvesting. Financing the whole chain is a paradigm shift called for in bankers' approach. The increased participation of private sector in agri - marketing and elimination of middle men would open up a host of opportunities for the banking sector from production to organized retailing.

In view of the above, promotion of value chain has been identified as one of the core initiatives of the Bank in Agri-business. This will help in:-

a) Financing the whole chain that can cover large quantum at lower cost.
b) All commercial activities in the chain getting finance.
c) Loan recovery efforts.
d) Giving momentum to our agri-exposure.

IV. STEPS FOR CONDUCTING A VALUE CHAIN STUDY

A detailed step-by-step guide to take up the value chain study is as under:-

A. Collection of Data:-

i) Area and production Taluka-wise.
ii) Potential clusters & Surplus.
iii) Branches in potential clusters.
iv) List of progressive farmers in potential clusters.
v) Cost of cultivation and Scale of Finance.
vi) Innovative methods.
vii) Major inputs and its suppliers.
viii) Flow of farm produce & Procurement structure.
ix) Post harvest technologies to be introduced.
x) Processing facilities.
xi) Marketing.
xii) Export.
xiii) Research institutes and agencies.

B. Scope for Finance:-

i) Crop production
ii) Crop Procurement
iii) Crop Post harvest
iv) Crop Processing
v) Crop Marketing
vi) Innovative Finance

V. THE THREE-PRONGED STRATEGY

1) Know the market

As a banker, we should not only finance parts of a value chain, but rather be involved from top to bottom. In that way we could really know the market from "inside out" and the weakest links could easily be exposed and addressed accordingly. Also, transaction costs could be reduced through the integration of knowledge and flow. A look at the leaders in the food industry brings out that they often have dedicated food and agribusiness research analysts whocontinuously accumulate knowledge in their major sectors and inform and advise clients on all relevant issues through-out the value chain. For small farmers, they may also need a catalyst and may require an intermediary to facilitate this market knowledge and linkage, but the principle holds – 'know the market'.

A) Suggestion:

As our Technical Officer (Farm Sector) strength is going up, we may think of ensuring a dedicated Officer in each Circle and identify some specific commodities (if not one for one commodity). He /she will collect all the relevant market information and pass it on to the branches / clients for increase in agri-business growth by way of value chain.

2) Financing along the Value Chain

Risk, return and repayment carry the same importance for value chain finance as with any conventional finance. For finance within the chain, credit risk is actually seen as a subset of the overall value chain business risk. The return, or profitability, is similar and often is embedded into the process in such a way as to not even be explicit. Repayment risk is also often not simply a function of a client going to the bank and repaying his/her loan but is payment through delivery of the product or payment when the processor or exporter delivers. If there is a "seamless" integration in the value chain system, this risk is minimized and the costs reduced.

3) Strategic partnerships

Value chain finance, like value chain systems, is all about strategic partnerships which link together the essential products and services. These are not just up and down the chain but in every direction. Strategic alliances can improve competitiveness in a win-win situation.

VI. CONCLUSION

By using value chain bankrolling strategy in agriculture sector a farmer can ensure higher yield with the use of modern technology and efficient procurement system with few middle man. Currently India has only 10% cold storage facility of the overall produce and because of this reason it leads to waste as agriculture products have short product life cycle and research shows that 20-40% of the food grown in India ends up spoiling before it ever reaches consumers, but with this funding strategy India can rise its cold storage capacity and undoubtedly be come food supplier of the world.

REFERENCES

[1] Porter, M. E. (1996), “What is strategy?” Harvard Business Review, Nov–Dec, The value chain, 61-78.

[2] Armand, Francoise. (2005), “Increasing Access to Affordable Hormonal Contraceptives: Can the Pool of Manufacturers Supplying the Developing World be Expanded?”.

[3] Goldmark& Barber (2005), “Trade, Micro and Small Enterprises and Global Value Chains”, DevelopmentAlternatives Inc, USAID MicroReport.

[4] Kula & Farmer (2004), “Mozambique Rural Financial Services Study”, AMAP, Microcase Study #1.

[5] USAID, AMAP (2005), “Value Chain Approach to Poverty Reduction: Equitable Growth in Today’s Global Economy”.

OPEN ACCESS

International
Journal
Of Modern Engineering Research (IJMER)

A flywheel energy storage system for an isolated micro-grid

Venkata Mahendra Chimmili

Studying B.Tech 4th year in department of electrical and electronic, NARASARAOPETA ENGG. COLLEGE,kotappakonda road yellamanda(p), narasaraopet- 22601,Gunturdistrict,A.P,INDIA.Affiliated to JNTU KAKINADA university, KAKINADA. ambedkar nagar 3rd line, kakaniroad,dr no;8-19/1-272,Guntur-1, pin code:522001,A.P,INDIA.

ABSTRACT: *The paper presents an investigation into the effects of integrating a Magnetically Loaded Composite (sMLC) flywheel to an isolated micro-grid. The Fair Isle is a small island located in northern Scotland, and supplied from two wind turbines and two diesel generators. The model of the micro-grid is developed and run on a real-time simulator with the physical MLC flywheel as a Hardware-In-the-Loop (HIL). Furthermore, a time-domain model of the MLC flywheel system is developed and its predictions are compared to measurements.*

I. INTRODUCTION

Isolated micro-grids, which include islands and remote communities, are generally characterised by high electricity generation costs and exhibit stability problems. High generation costs can be alleviated by maximising the usage of renewable sources, such as wind, solar and hydro powers, albeit at the expense of an increase in frequency and voltage fluctuations due to the varying environmental conditions. The introduction of short-term energy storage systems, such as flywheels, can improve the stability of a micro-grid and maximise the penetration of the renewable energy sources.For grid stabilisation applications, a high cycle life is normally required, typically 15 million cycles over a 20 year life span. The cycle life of battery systems is typically in the order of <10,000 cycles and therefore, would require frequent replacements, hence offsetting the potentially lower initial capital cost advantage . The cycle life of capacitor energy storage systems is significantly higher at approximately 1 million cycles. However, the life cycle of Magnetically Loaded Composite (MLC) flywheel systems is of the order of 10 million cycles, and combined with excellent power density and a wide temperature operating range, the MLC flywheel system is very suitable for frequency and voltage stabilisation applications.

The paper presents an investigation into the effects of integrating an MLC flywheel to an isolated micro-grid. The Fair Isle is a small island located in northern Scotland, it has around 80 residents living in 30 houses supplied from an isolated micro-grid, which consists of a heating network and a service network, which can be connected by two inductioncouplers, and supplied from two Wind Turbines (WT), rated at 60kW and 100KW, and two 32kW Diesel Generators (DG), as shown in Figure 1. The model of the micro- grid is developed and run on a real-time simulator connected to the physical MLC flywheel through a programmable power supply in a HIL set-up. The inputs to the model are power profiles measured on five selected nodes on the micro-grid, and sampled at 1 second intervals. Furthermore, a time-domain model of the flywheel is developed and experimentally validated.

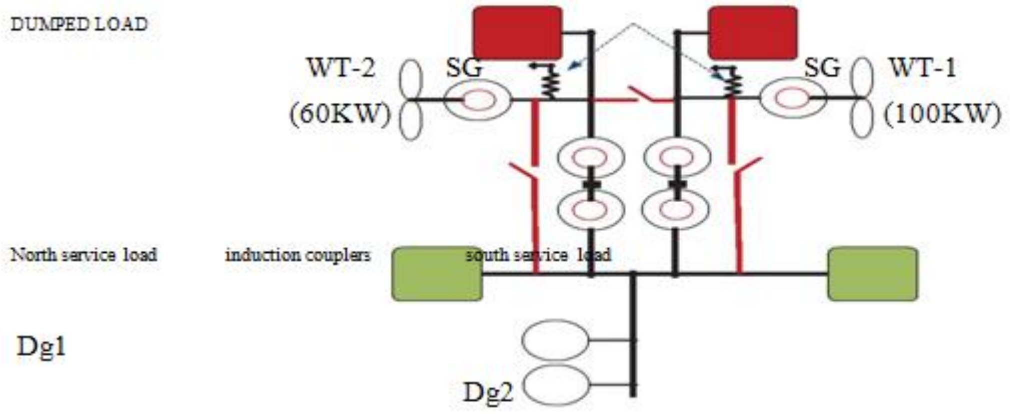

Figure1: Fair ISLE power system

Time-domain modelling of the MLC flywheel system:-A high-fidelity time-domain model of the MLC200 flywheel system, whose parameters are given in Table 1, has been developed and validated. The model includes the integrated permanent magnet motor/generator, the 3-phase power electronic converter and the low level controller for the power electronic switches and the high level controller for the flywheel Simulink and reproduces the behaviour of the flywheel system in its operating range.

Table 1 Parameters of the MLC200 Flywheel

Parameter	
Energy	14.3 MJ (4.0 kWh)
Power	200kW
Minimum speed	30,000rpm
Maximum speed	36,000rpm
Nominal dc-link voltage	700V

The functional schematic of the MLC200 flywheel system is shown in figure 2. The power electronic converter has been modelled using Simulink powerSystems toolbox and consists of a standard 3-phase converter, which provides the interface between the DC-link and the integrated permanent magnet motor/generator of the flywheel.

(a) MLC200 Flywheel

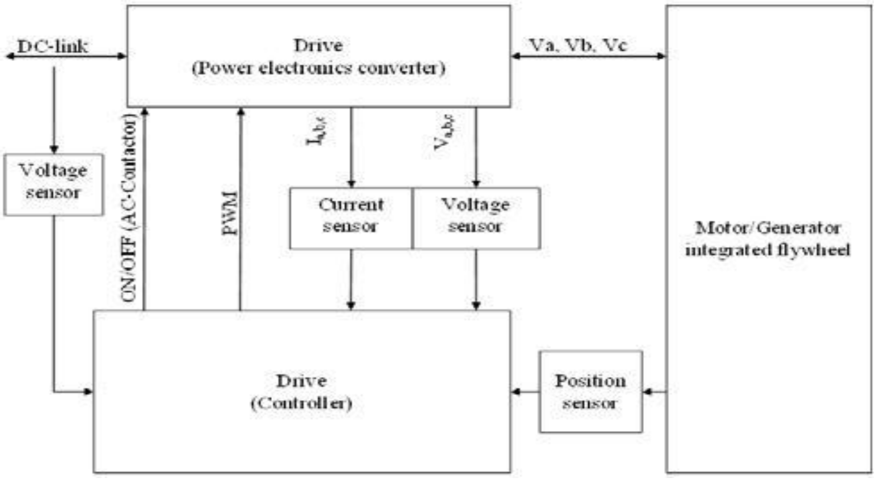

(b) Functional diagram

Figure 2: MLC200 flywheel system

The power demand of the flywheel is determined by the dc-link voltage level, as shown in Figure 3. Therefore, the controller monitors the DC link voltage and the speed of the flywheel, and generates the PWM signals for the IGBTs of the power electronic converter, in order for the flywheel to generate or absorb the required power. The controller aims to keep the DC- link level in the recovery region, adjustable between 570V and 900V.The controller has been modelled as a state machine using Simulink State-flow toolbox and was designed to reproduce the behaviour of the flywheel under various load conditions, i.e. various states of charge and DC-link voltages.

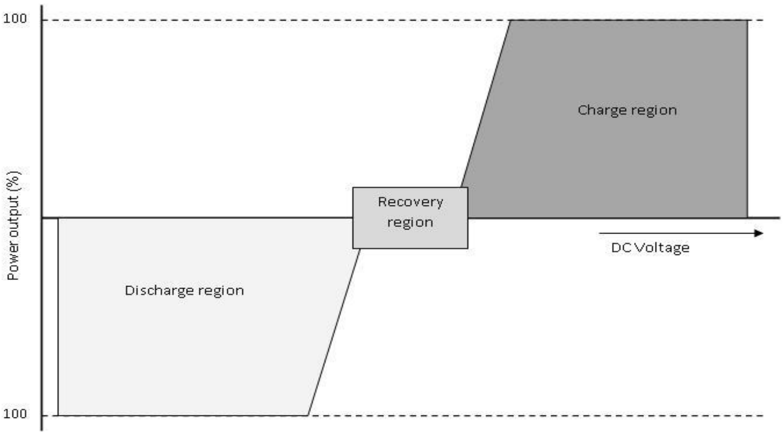

Figure 3: MLC200 power profile

II. EXPERIMENTAL VALIDATION

The MLC200 flywheel has been tested under different conditions, and the results have been compared to the predictions from the time-domain model, Figure 4 compares measured and predicted phase current waveforms for 40kW charge and discharge operations. It can be seen that the time-domain model predicts the phase current waveforms adequately Figure 5 shows charge and discharge cycles of the flywheel, where the recovery region has been set between 595V and 605V and the maximum power output was limited to 50kW. The DC-link was varied and the power of the flywheel was recorded. Again, it can be seen that the time-domain model represents the behaviour of the flywheel system adequately.

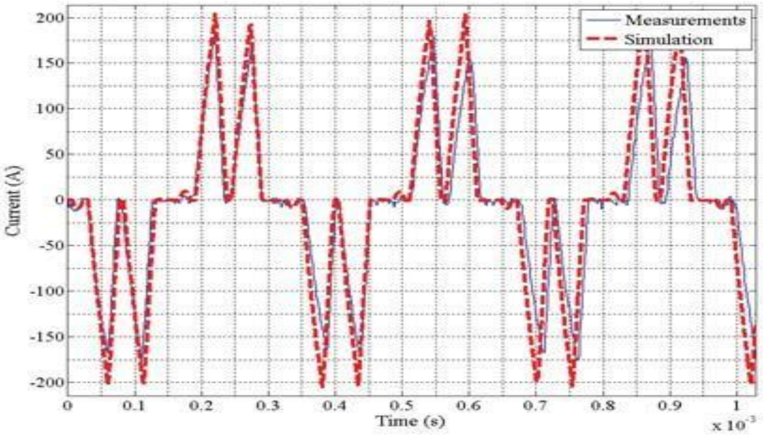

(a).40kW charging.

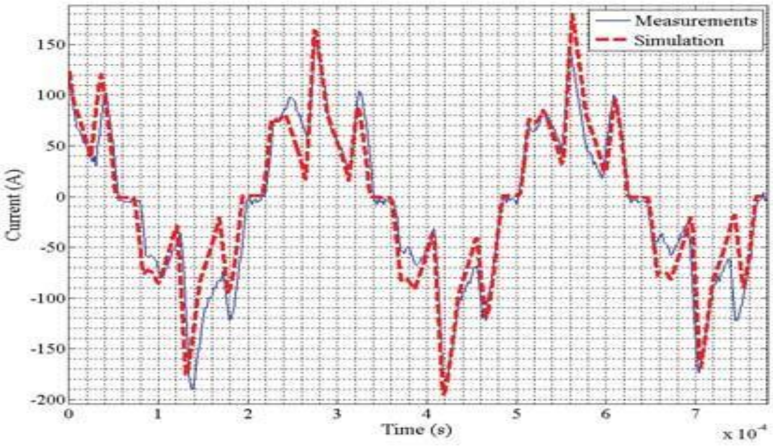

(b)40kW dis-charging.

Figure 4: Phase current waveforms

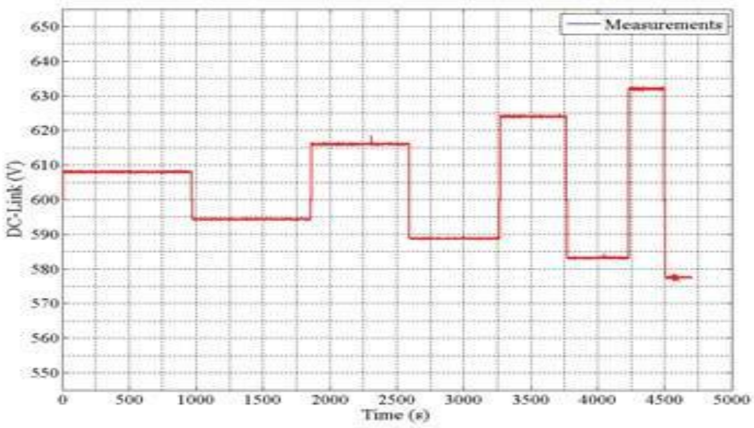

(a) DC-link voltage

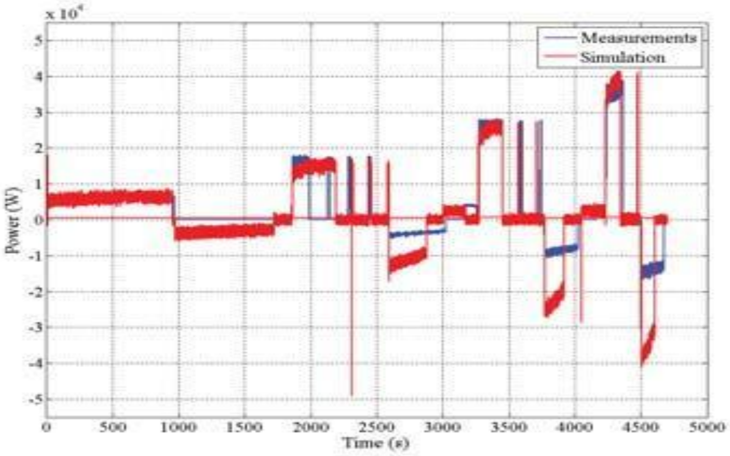

(b) Power of the flywheel

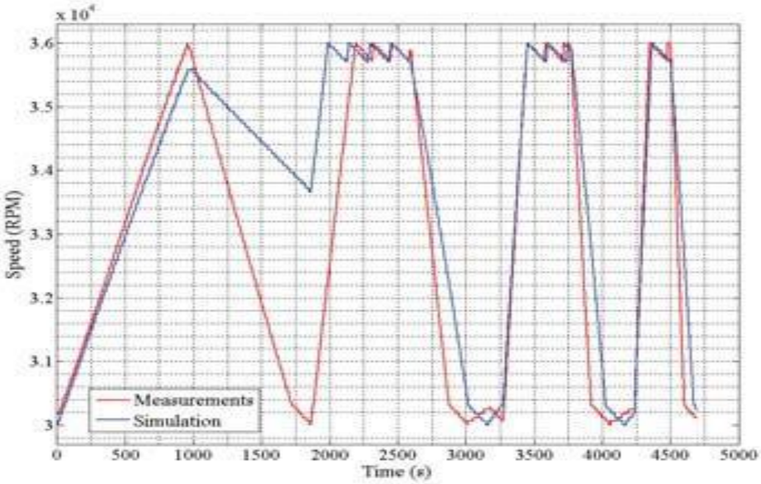

(c) Speed of the flywheel

Figure 5: Flywheel power flow for varying DC-link voltages

Fair Isle:-The Fair Isle is located in northern Scotland, lying around halfway between mainland Shetland and the Orkney Islands. There are around 80 residents living in 30 houses connected to an isolated micro- grid, and relies heavily on wind power . In fact, the Fair Isle is the first place in Europe which commercially operated a wind energy scheme, supported by council and government development agencies. The average daily energy consumption is typically 1,100kWh with a peak energy consumption of 50,692 kWh recorded in November 2012.

The micro -grid consists of two networks, a heating network where two wind turbines, WT1 and WT2 rated at 100kW and 60kW, respectively, are connected, and a service network where two diesel generators, rated at 32kW each, are connected, as can be seen in Figure 1. The two networks can be directly connected when sufficient power is produced by the wind turbines, or connected through induction couplers when the diesel generators are required. Dump loads are also connected to the heating network, in order to ensure the frequency doesn't exceed 52.4Hz under high wind conditions. The heating load is controlled by frequency relays located at each house to consume the remainder of the power of the WTs.

III. MICRO-GRID CONTROL METHODOLOGY:-

There are two modes of operation in the Fair Isle micro-grid. The first one is called guarantee hours where the power supply to the service load is guaranteed and it starts from 06:30 AM to 11:30 PM. The second one is a non-guarantee hours where the power supply can be discontinued depending on the availability of power from the wind turbines. The minimum allowed supply frequency is 45Hz below which power is turned off.

The control methodology can be summarised as follows:

- In guarantee hours, when the output power from one of the WTs is higher than the service load plus a manually set power margin of 0 kW, 3 kW, 6 kW, 10 kW, 15 kW or 20kW, for more than 8.0 minutes, the controller disconnects the DG and directly connects the WTs to the service network. Although electrically disconnected, the DG will remain running at no load for a while and then turned off.
- Outside the guarantee hours, there is no measurement of the service load demand. The controller compares the output powers of the WTs. If the power output of a WT is sustained for more than 2 minutes between 28kW and 36kW, it will take up the service load, if both satisfy the condition, WT1 will be connected to the service network
- In light winds where the lead WT1 is unable to provide enough power to the service network a soft induction coupler is energized to also connect the second WT.
- If the WTs cannot supply the service load, the power to the heating network is reduced, until the service frequency reaches 45Hz, when the WTs are disconnected from the service network. If this happens during guarantee hours, the DG is connected to supply the service network and the WTs will supply the heating network. During non-guarantee hours, the WTs are reconnected after each 2 minutes to supply the service loads, and this process is repeated until the WTs are capable of supplying the service network or the guarantee hours start.

IV. SIMULATION AND EXPERIMENTAL RESULTS

Five loggers are installed to measure the power, frequency and voltages of the service loads, the heating loads, the WTs and the DGs, as can be seen in Figure 1. Figure 6 shows the

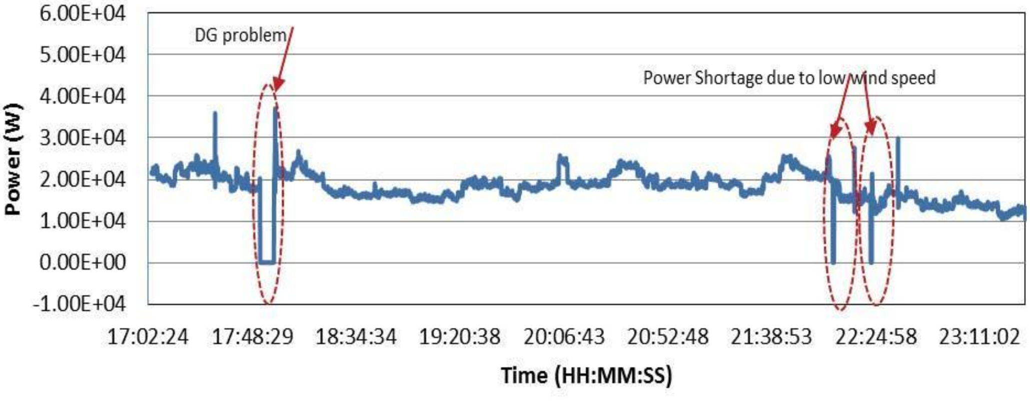

Figure 6: Measured service load power during the guarantee hours

Measured variation of the service load power during guarantee hours of a day in November 2013, where it can clearly be seen several power shortage events occurred due to reduced wind speed or DG issues. Figure 7 shows the measured variation of the service load frequency during guarantee hours. Again, frequency reached the minimum threshold of 45Hz several times. It may also be seen that there are two frequency ranges, when the WTs are supplying the service load, the frequency is between 50.7Hz and 52.1Hz, and when the DG is supplying the service load, the frequency is between 49.75Hz and 50.25Hz.

In order to assess the benefits of connecting a MLC200 flywheel to the Fair Isle micro-grid, a HIL set up is adopted, as shown in Figure 8. In the set-up, the model of the Fair Isle micro-grid and the grid-tie inverter are run on the real-time simulator, while the physical flywheel is connected to a programmable power supply. The power demand from the flywheel is achieved through the control of the power supply voltage, as shown in Figure 3, and a droop control methodology is employed in order to smooth the service load frequency. The power demand of the flywheel is given by:

Pdc=Kd*(Fd-FS)

Where P_{de} is the power demand from the flywheel, f_d is the demand frequency, f_s is the service load frequency, and Kd is a constant.

Two cases are considered, the first one is concerned with the smoothing of the service load frequency and the second is concerned with reducing the DG operating hours and guarantee to supply the service load.

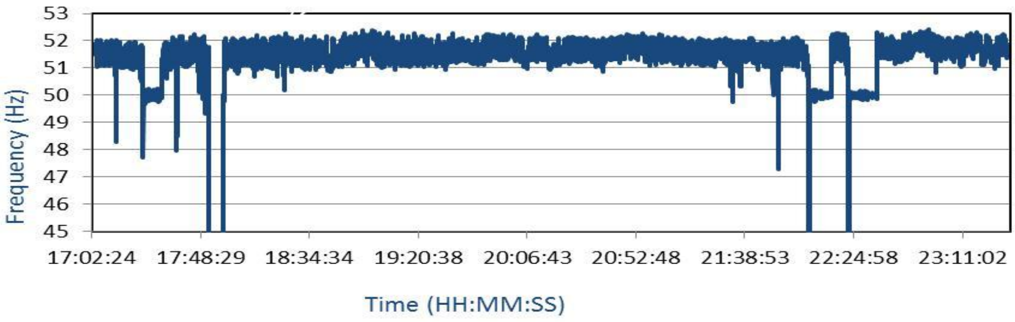

Figure 7: Measured service load frequency during the guarantee hours

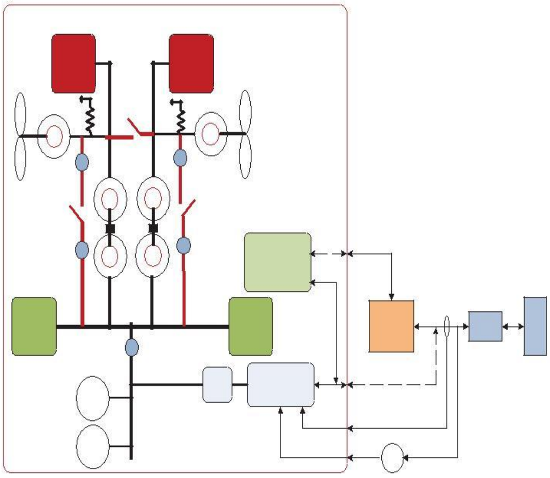

Figure 8: Schematic of the HIL set-up

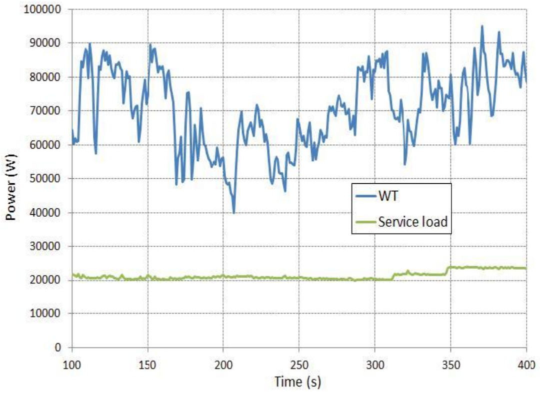

Figure 9: Measured WT and service load power

Case 1: smoothing of service load frequency

In this case the WTs supply the entire Fair Isle loads (Heating and service) as shown in Figure 9. The main purpose of the Flywheel is to smooth the service load frequency. Figure 10 shows the variation of the service load frequency, with and without the flywheel. The frequency variation without the flywheel is measured on the micro-grid at the Fair Isle, while the frequency variation with the flywheel is predicted by model of the Fair Isle, with the flywheel as hardware in the loop and as a model in the loop, when the powers measured on the Fair Isle are used as inputs. It can be seen that the introduction of the flywheel has resulted in reduced frequency fluctuations. Over the time interval of Figure 10, the average frequency is not affected by the introduction of the flywheel, being 51.48Hz for the Fair Isle measurements, and 51.43Hz and 51.48Hz, for the cases of flywheel in the loop and the flywheel model in the loop, respectively. However, the introduction of the flywheel has a significant impact on frequency fluctuation, with the standard deviation being 0.32Hz for the Fair Isle measurements and 0.19Hz and 0.2Hz for the cases of flywheel in the loop and the flywheel model in the loop, respectively

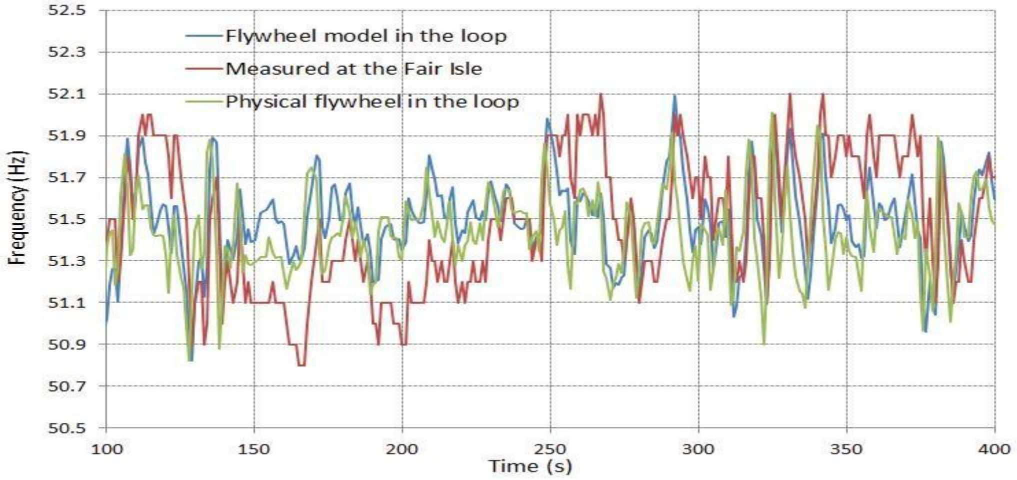

Figure 10: Service load frequency with and without Flywheel

Case 2:- Guarantee of supplying service load and reducing DG operating hours

In this case a changeover from WT to DG due to low wind speed is considered as shown in Figure 11. This results in a power cut lasting 26 seconds. The main purpose of the flywheel is to supply the power in order to keep the service load frequency higher than 45Hz, and avoid the power cut.

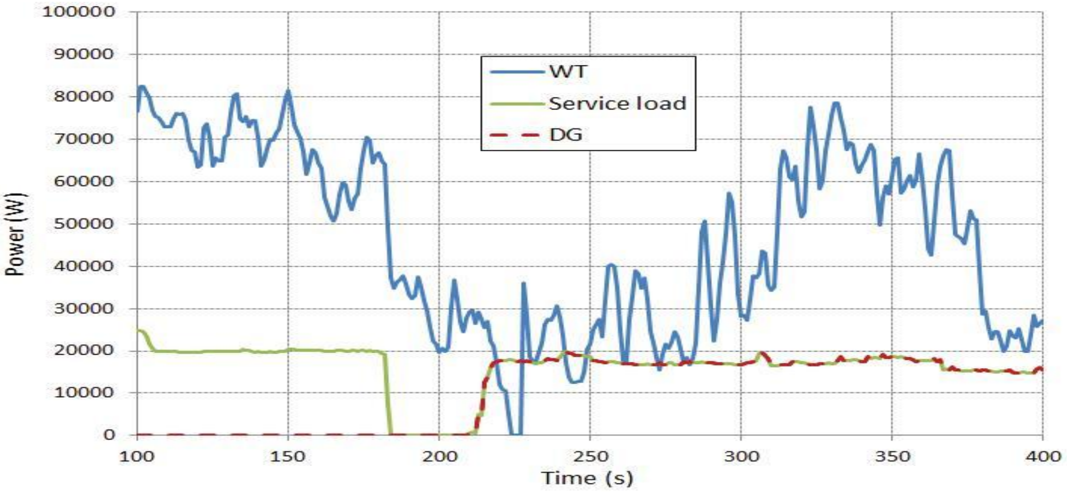

Figure 11: Measured DG, service load and WTG power

Figure 12, shows the variation of the service load frequency with and without the flywheel. It can be seen that the introduction of the flywheel maintains the service load frequency above 45Hz during the changeover between the WT and the DG, and hence, the power cut is avoided. As a result, the DG operating hours will be reduced, and the start and stop cycle will be minimised which should help extend the life of the DG and it components. Furthermore, it can also be seen that the flywheel model in the loop predicted adequately the behaviour of the physical flywheel.A model of the micro-grid is developed and run on a real time simulator with the physical flywheel being the hardware in the loop. The inputs to the micro -grid model are powers measured using loggers installed at specific locations of the micro-grid. It has been shown, that the flywheel can reduce frequency fluctuations and minimise the number of events when the diesel generators have to be called upon during temporary low winds.

Furthermore, a time-domain model for the flywheel system is also developed and experimentally validated. It has been shown, that when the Fair Isle micro -grid model is run with the developed flywheel model in the loop, similar results as those with the physical flywheel in the loop are achieved. Therefore, the developed model can be confidently employed to assess the benefits of the MLC200 flywheel systems.

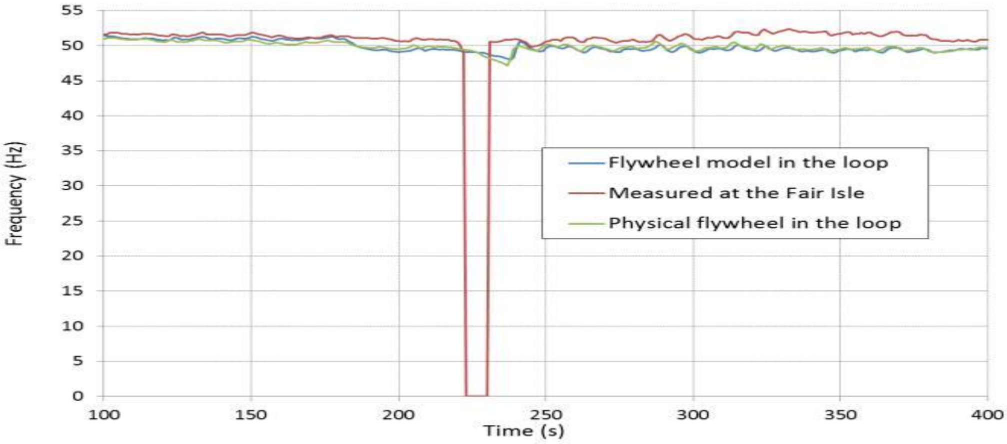

Figure 12: Service load frequency

V. CONCLUSIONS

The Fair Isle micro-grid is selected in order to demonstrate the benefits of employing a flywheel (MLC200) to improve the power quality, through frequency stabilisation, and increase the penetration of renewable sources, by minimising the need for diesel generation during temporary low winds.

REFERENCES

[1] Arghandeh, R., M. Pipattanasomporn, and S. Rahman, Flywheel Energy Storage Systems for Ride-through Applications in a Facility Micro grid. Smart Grid, IEEETransactions on, 2012. **3**(4): p. 1955-1962.

[2] Jayawarna, N., et al. Stability of a microgrid. in PowerElectronics, Machines and Drives, 2006. PEMD 2006. The 3rd IET International Conference on. 2006.

[3] McGroarty, J., et al. Flywheel energy storage system forelectric start and an all-electric ship. in Electric Ship Technologies Symposium, 2005 IEEE. 2005.

[4] Vracar, V., Modular High-Power Electronics for a High-Speed MLC Flywheel Energy Storage System. Journal ofEnergy and Power Engineering, 2012. **6**: p. 6.

[5] http://www.fairisle.org.uk/FIECo/index.htm.

OPEN ACCESS

International
Journal
Of Modern Engineering Research (IJMER)

Implementation of Multiple Touch Gesture Using Depth Information

Soon-kak Kwon[1], Dong-seok Lee[2]

[1,2]Department of Computer Software Engineering, Dongeui University, Korea

ABSTRACT: *In this paper, we propose a method of implementing a multiple touch gesture using the depth information. We obtain the depth information using depth camera and determine gesture type using it. Using this method, it is possible to provide an event according to this gesture and to implement the application supporting multiple touch gesture at low costs. In addition, user can control unit instinctively in shooting game by applying this method to the screen of large size.*

Keywords: *Touch, Gesture, Depth Information, Shooting game*

I. INTRODUCTION

Recent, the interests in touch technology are increasing by advances in smart IT technology and the applications using touch gesture are also increasing [1, 2]. Accordingly, there are many developments of shooting game with touch events in smart phone. However, it is difficult to apply to touch function in medium and large-screen due to high cost of applying it. For this reason, it is difficult to develop a shooting game that supports touch gestures in large screen.

In this paper, we propose a method to recognize the gestures by a touch sensor using optical type and apply for shooting game using it. First, the proposed method recognizes whether touch by this touch information, then traces the touch point until touch is released and determines gesture type through tracked path. Through this method, it is possible to be applied to recognize touch gesture in screen using optical touch sensor. And we can develop a shooting game that supports gesture by applying the above method.

II. IMPLEMENTATION OF SHOOTING GAME USING MULTIPLE TOUCH GESTURE

The touch sensor is composed almost the resistive type, the capacitive type, and the optical type [3]. Recently the optical sensing methods have been used for the large size of the touch screen. The optical methods detect a pointer over the touch screen from the outside camera without using the physical touch sensor.

In this paper, we use direction gesture because this gesture can be used simply and intuitively so users can play this game easy. Using direction gesture, gesture type is determined by straight line determined by start and end points of touch, and events is prevented according to this gesture type.

There is method of determining the touch gesture type. First, it draws a straight line from the touch point to the end point of the trace pointer and measures the angle formed by the line. Then it determines to the nearest one of the gestures by comparison with the pre-registered direction. After that, the method provides an event that is assigned to a gesture. Fig. 1 shows a method of determining gesture type and Fig. 2 shows an event flowchart of this method.

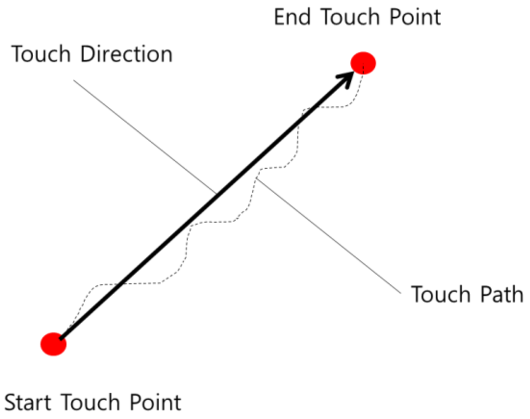

Fig. 1. Determining touch gesture type with start and end points

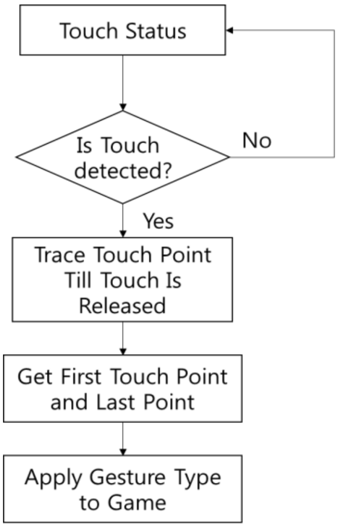

Fig. 2. Flowchart of determining the touch gesture type

In many shooting game, user controls a unit to move it or shots something like missile to enemy. Previously, user controls this unit through a joystick or a keyboard, mouse, etc. However, using these to control a unit in shooting game is uncomfortable because this controller is not intuitive. So user has to learn how to control this unit to play this shooting game. If the proposed method is applied to this shooting game, user can control this unit instinctively through touch gesture and play this shooting game in a wide screen at low cost.

Fig. 3 shows the class diagram of this shooting game using above touch gesture. Unit class is the role of storing unit information. GameController class is getting gesture information from TouchGesture class and controlling each unit to move it or to shot missile. TouchGesture class is the role of getting touch information from touch sensor and determines touch gesture type using this information through above method.

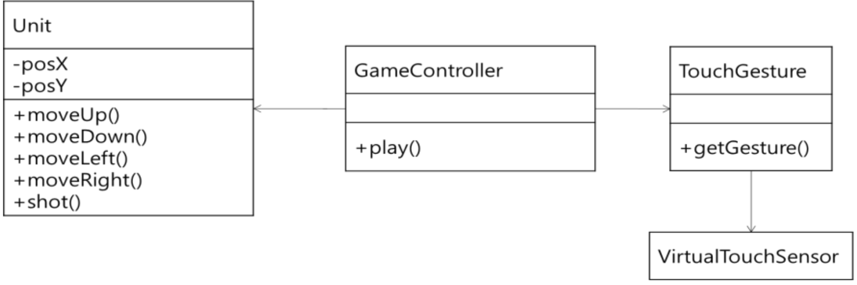

Fig. 3. Class diagram of the shooting game

Supporting direction gesture in this shooting game, it is important that intuitive and suitable events are provided. So if user drags to the left or right with touch, unit is moved in a direction of drag. Or if user drags to the top or bottom with touch, shooting angle is increased or decreased. If user wants to shot missile, user just touch and not drag to increase shooting power. And user keeps his touch until shooting power reaches the value user wants. Fig. 4 shows this direction gesture.

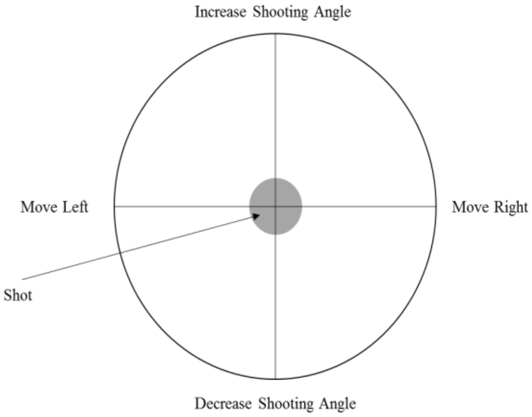

Fig. 4. Direction gesture in this shooting game

Fig. 4 is a prototype of the implemented game directly, using the class diagram of Fig. 3. A unit and another enemy are presented in Fig. 5(a). Fig. 5(b) and Fig. 5(c) shows that this unit is moved by touch gesture and its angle is increased. Fig. 5(d) indicates that this unit shoots to enemy unit through keeping and releasing touch.

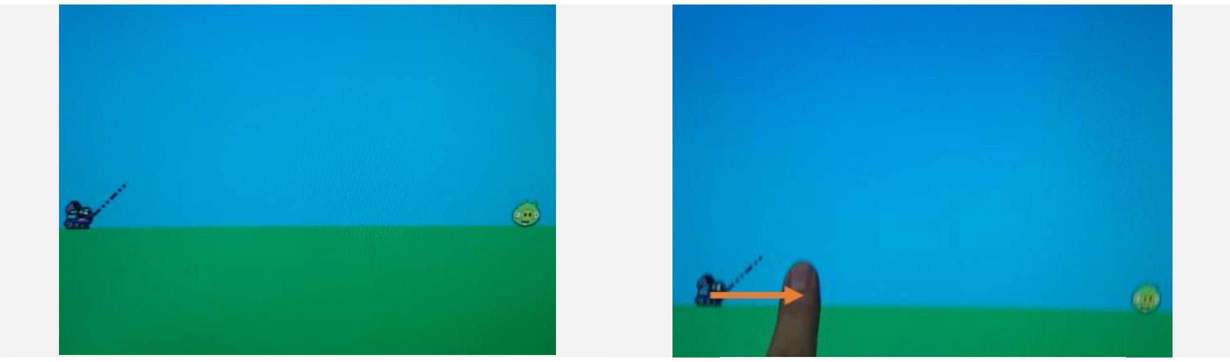

(a) 'A' Alphabet touch (b) Move a unit through touch gesture

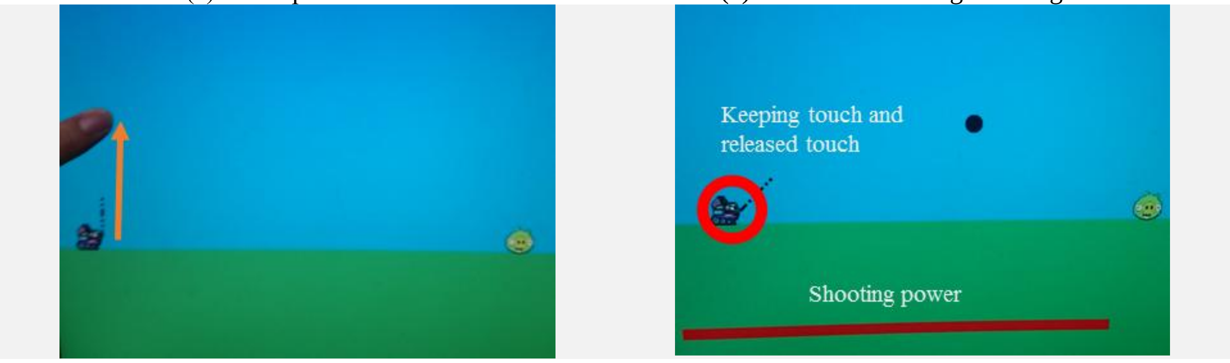

(d) Increase angle through touch (d) Shoot to enemy through touch

Fig. 5. Implementation of shooting game using touch gesture

III. CONCLUSION

In this paper, we propose method of touch recognition using optical touch information and method of determining to gesture type in touching using the direction. By using this method, it is cheaper than the existing methods and makes it easy to build a touch gesture environment. By providing suitable event for gesture with the proposed method, it is expected to be applied to touch gesture on shooting game that is used with big screen at low costs. And it is also expected that many gamers will have fun playing this.

IV. ACKNOWLEDGEMENTS

This work (Grants No. C0248402) was supported by Business for Cooperative R&D between Industry, Academy, and Research Institute funded Korea Small and Medium Business Administration in 2014. Corresponding author: Soon-kak Kwon (skkwon@deu.ac.kr).

REFERENCES

[1] R. Munoz-Salinas, R. Medina-Carnicer, F.J. Madrid-Cuevas, and A. Carmona-Poyato, "Depth silhouettes for gesture recognition", Pattern Recognition Letters, vol.29, no.3, pp.319-329, 2008.
[2] P. Suryanarayan, A. Subramanian, and D. Mandalapu, "Dynamic hand pose recognition using depth data", In International Conference on Pattern Recognition, 2010.
[3] S.K. Kwon, "Puzzle game in touch pad", IOSR Journal of Engineering, Vol. 4, No. 11, pp.14-17, 2014.

OPEN ACCESS

International
Journal
Of Modern Engineering Research (IJMER)

Experimental Investigation of Silica Fume and Steel Slag in Concrete

D. Karthik[1], J. Doraikkannan[2]

[1]*Departmentof civil engineering,N.S.N College of engineering and technology,Tamilnadu,India*
[2]*Department of civil engineering,N.S.N College of engineering and technology,tamilnadu,India*

ABSTRACT: *This paper gives a review on replacements in concrete made out of various industrial by-products like silica fume and steel slag in concrete Through my study a combined replacement of steel slag and silica fume in (40, 50, 60, and 70) % and (10, 15, 20, and 25) % and conduct a detailed experimental study on Compressive strength, split tensile strength, flexural strength at age of (7, 28, 56 and 90) days and durability study on acid attack was also determinedand investigates the potential use and optimum usage of steel slag and silica fume in the production of concrete.*

Keywords: *Compressive strength,Flexural strength, Silica fume,Steel slag,Split tensile strength*

I. INTRODUCTION

The use of concrete is increasing day by day, so our natural resources get depleted due to the production of concrete. In order to reduce this environmental problem we should find out materials that can substitute the natural resources, steel slag is an industrial by-product formed during the manufacturing of steel and silica fume are also one of the industrial by-product formed during the production of alloys of silicon. Various studies were carried out for the replacement of cement and aggregate and some of the literatures are have been discussed briefly, many studies have been carried out in this area from early 1980's.

Many steel plants have been set up in our country. However, production of iron and steel is associated with the generation of solid waste materials like slag. Big steel plants in India generate about 29 million tonnes of waste material annually. In addition, there are several medium and small plants all over the country. Slag reduces the porosity and permeability of soil, thus increasing the water logging problem.. Industrial area around major cities there are several small and large scale industries wasting nearly thousands of metric tonne steel slag daily. Problem of disposing this slag is very serious which can be reduced by utilizing steel slag for concrete construction. The final properties of concrete, such as strength, durability and serviceability depend mainly on the properties and the quality of the materials used. Steel slag can be used in conventional concrete to improve its mechanical, physical, and chemical properties.

Steel slag is generated as a melt at about 1600°C during steelmaking from hot metal in the amount of 15%–20% per equivalent unit of steel. The function of this slag is to refine the steel of sulphur and to absorb the oxides formed as a result of deoxidation during steel production. Steelmaking slags are composed principally of calcium silicates, calcium aluminoferrites, and fused calcium oxides, iron, magnesium, and manganese.

More recently strict environmental pollution controls and regulates have produced an increase in the industrial wastes and sub graded by-products which can be used as (supplementary cementitious material) SCMs such as fly ash, silica fume,ground granulated blast furnace slag etc. The use of SCMs in concrete constructions not only prevents these materials to check the pollution but also to enhance the properties of concrete in fresh and hydrated states. The SCMs can be divided in two categories based on their type of reaction: hydraulic and pozzolanic. Hydraulic materials react directly with water to form cementitious compound like ground granulated blast furnace slag (GGBS). Pozzolanic materials like fly ash, silica fume...etc. Do not have any cementitious property but when used with cement or lime react with calcium hydroxide to form products possessing cementitious properties.

STEEL SLAG

Steel slag, a by-product of steel making, is produced during the separation of the molten steel from impurities in steel-making furnaces. The slag occurs as a molten liquid melt and is a complex solution of silicates and oxides that solidifies upon cooling. Virtually all steel is now made in integrated steel plants using a version of the basic oxygen process or in specialty steel plants (mini-mills) using an electric arc furnace process. The open hearth furnace process is no longer used. Steel slag is produced in large quantities during the steel-making operations which utilize Electric Arc Furnaces (EAF). Steel slag can also be produced by smelting iron ore in the Basic Oxygen Furnace (BOF). Steel slag can be used in the construction industry as aggregates in concrete by replacing natural aggregates.

SILICA FUME

Silica fume, also known as microsilica, It is an amorphous (non-crystalline) polymorph of silicon dioxide, silica. It is an ultrafine powder collected as a by-product of the silicon and ferrosilicon alloy production and consists of spherical particles with an average particle diameter of 150 nm. The main field of application is as pozzolanic material for high performance concrete. Addition of silica fume to concrete has many advantages like high strength, durability and reduction in cement production. When pozzolanic materials are incorporated to concrete, the silica present in these materials react with the calcium hydroxide released during the hydration of cement and formsadditional calcium silicate hydrate (C – S – H), which improve durability and the mechanical properties of concrete.

II. EXPERIMENTAL INVESTIGATIONS

MIX COMBINATIONS

In this study various mix combinations of steel slag and silica fume was prepared under various mix ratios. Each mix is denoted by ‘M’ and M1 denotes the conventional mix ‘M_{30}’ and from M2 to M5 cement is replaced by 10% of silica fume and sand is replaced by 40-70 % of steel slag. The combinations are shown in table1

Table .1 Mix combinations

SI NO	SAMPLE DESIGNATION	PERCENTAGE OF REPLACEMENT	
		SILICA FUME	STEEL SLAG
1	M1	0	0
2	M2	10	40
3	M3	10	50
4	M4	10	60
5	M5	10	70
6	M6	15	40
7	M7	15	50
8	M8	15	60
9	M9	15	70
10	M10	20	40
11	M11	20	50
12	M12	20	60
13	M13	20	70
14	M14	25	40
15	M15	25	50
16	M16	25	60
17	M17	25	70

TEST RESULTS

In the experimental study mainly the mechanical strength of the concrete was found out forall mix combinations. Mechanical strength deals with compression, tension and flexural strength of concrete specimens and also durability studies are done to find, the most efficient combination of silica fume and steel slag.

Compressive strength test results

Through my study I have been found that, due to the presence of silica content in steel slag and silica fume,there is a great increase in the silica content in concrete and it reduces the strength of concrete, but the effective usage of both the materials, improve the strength of concrete.By considering the strength aspects the best combination is M8 ie, silica fume 15% and steel slag 60% and for optimum replacent level of steel slag content the best combination is M9 ie,silica fume 15% and steel slag 70%.

Table.2 Compressive strength test results for M1 - M5 mix

Sample designation	Compressive strength (N/mm^2)			
	7th day	28th day	56th day	90th day
M1	18.6	32	35.2	37.76
M2	26.2	34.1	37.16	39.55
M3	27.3	35.6	37.38	[1] 42
M4	30.4	36.4	40.40	[2] 41.86
M5	26	32.2	34.77	[3] 37.35

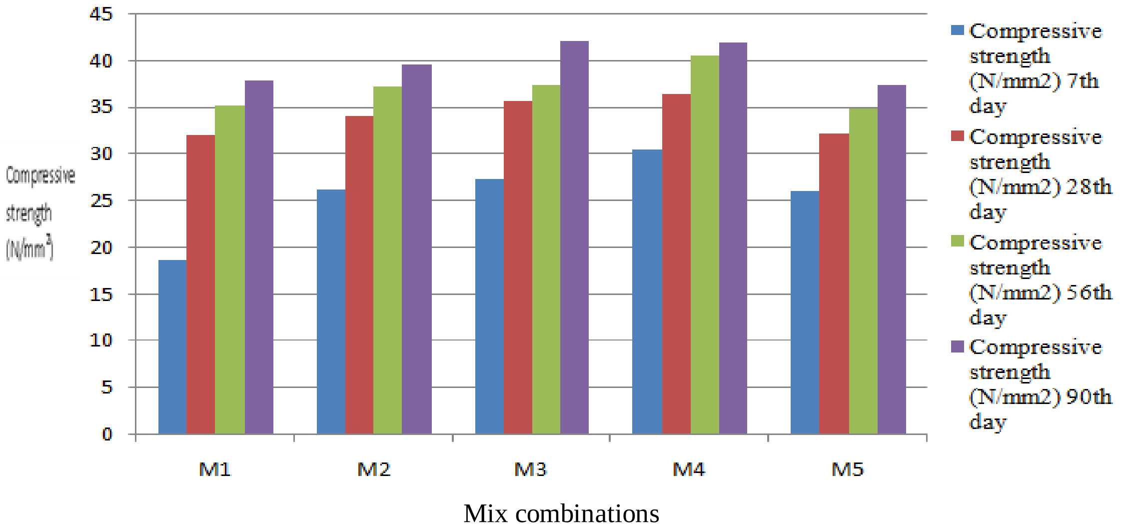

Graph showing compressive strength of mixes M1 –M5

As per the study, for the third set of combination ie, silica fume 20% and steel slag 40 - 70% maximum strength obtained is M12 mix ie, silica fume 20% and steel slag 60% and by compairing it with conventional mix it shows an increase in strength upto 10 % and obtained maximum replacement of steel slag in M12 mix ie, steel slag 60%.

Table 3 Compressive strength test results for M6 – M9 mix

Sample designation	Compressive strength (N/mm^2)			
	7th day	28th day	56th day	90th day
M6	24.5	33.4	36.74	38.41
M7	28.4	36.2	38.01	42
M8	34.35	41	43.46	48.38
M9	33.5	36.4	40.04	42.22

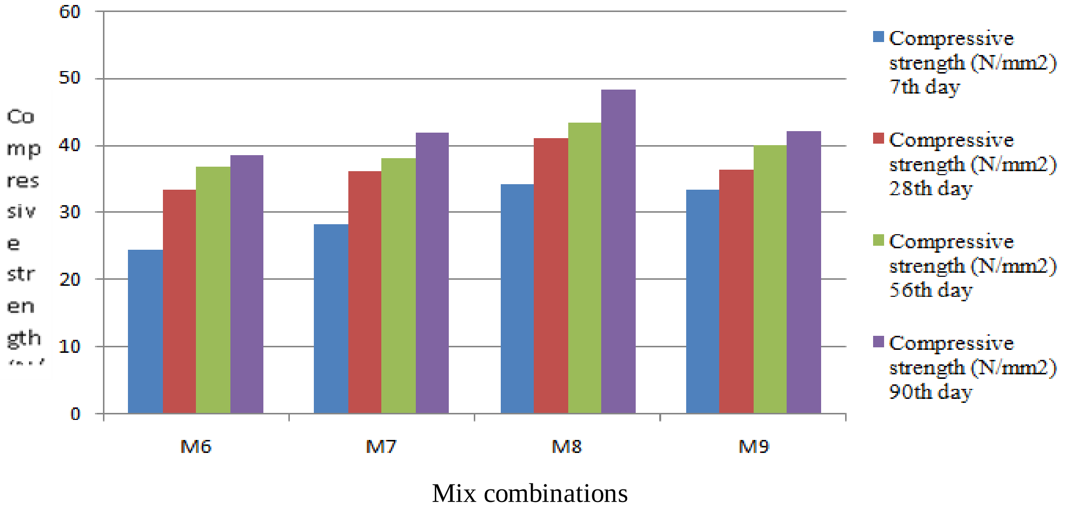

Graph showing Compressive strength of mixes M6-M9

As per the study, for the third set of combination ie, silica fume 20% and steel slag 40 - 70% maximum strength obtained is M12 mix ie, silica fume 20% and steel slag 60% and by compairing it with conventional mix it shows an increase in strength upto 10 % and obtained maximum replacement of steel slag in M12 mix ie, steel slag 60%.

Table. 5 Compressive strength test results for M14 – M17 mix

Sample designation	Compressive strength (N/mm^2)			
	7th day	28th day	56th day	90th day
M14	16.3	24.5	26.95	28.42
M15	20.2	30.6	33.05	36.12
M16	18.6	27.2	29.92	31.01
M17	17.2	24.5	26.22	28.66

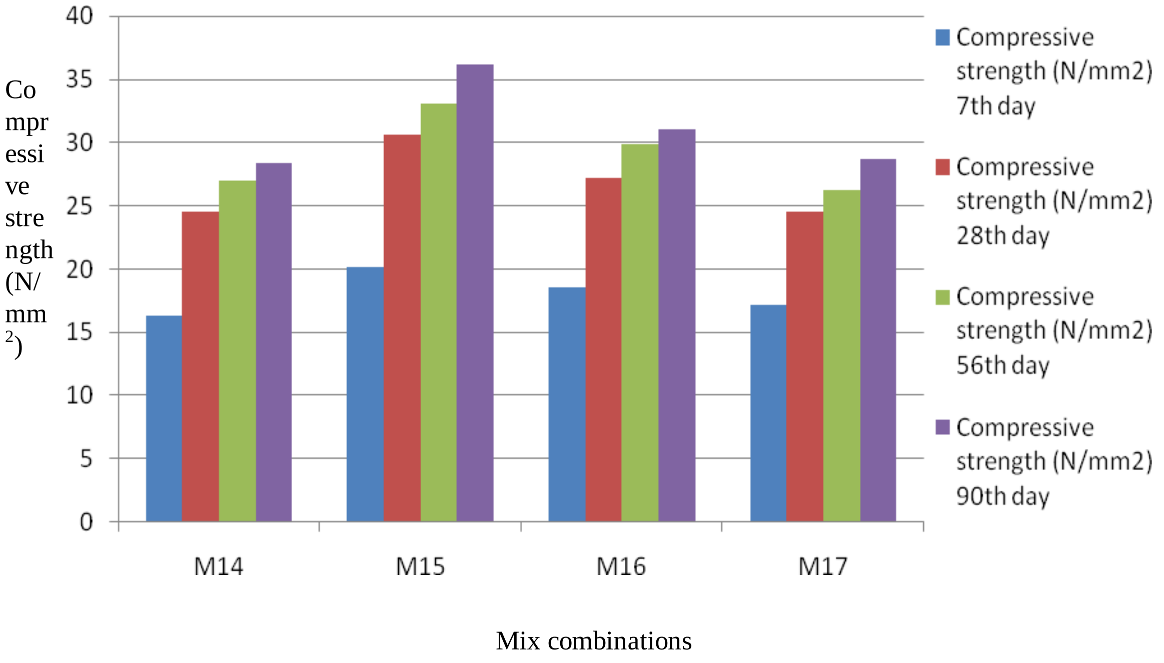

Graph showing Compressive strength of mixes M14 - M17

As per the study, for the last set of combinationsie, silica fume 25% and steel slag 40 - 70% the 'M15' mix shows a similar strength as conventional mix,there is no increase in strength but the maximum replacement of steel slag is 50%.

Split tensile strength test results

Table. 6 Split tensile strength test results for M1 - M5 mix

Sample designation	Split tensile strength(N/mm^2)			
	7th day	28th day	56th day	90th day
M1	2.551	4.47	4.69	5.09
M2	3.24	3.94	4.33	4.53
M3	3.34	3.91	4.22	4.53
M4	3.32	3.7	4.07	4.33
M5	2.8	3.22	3.54	3.67

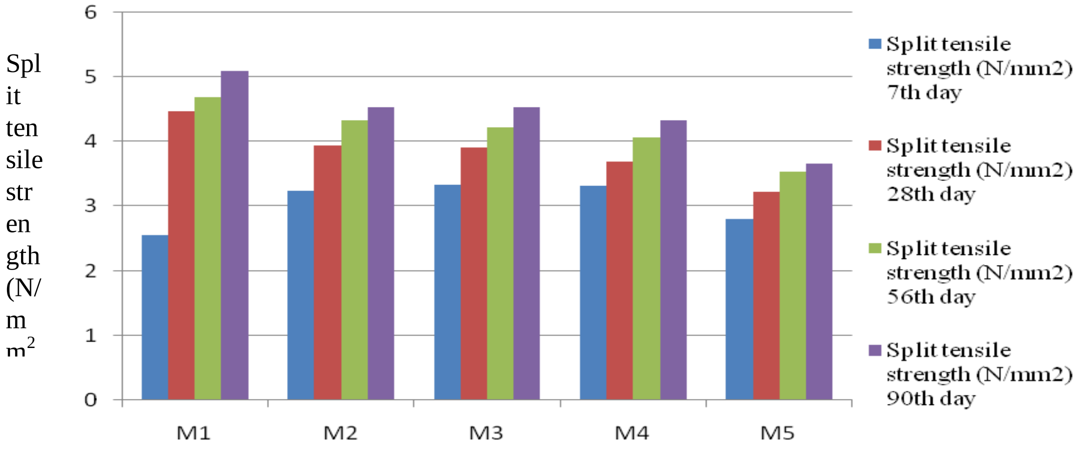

Graph showing Split tensile strength of mixes M1 –M5

According to the studies there is no increase in the split tensile strength and for the first set of combinations there is a small reduction in split tensile strength by comparing with the conventional mix and from these 'M2' mix shows high strength ie, 10% silica fume and 40% steel slag.

Table. 7 Split tensile strength test results for M6 – M9 mix

Sample designation	Split tensile strength(N/mm^2)			
	7th day	28th day	56th day	90th day
M6	3.21	4.12	4.44	4.73
M7	3.55	4.32	4.75	5.01
M8	3.91	4.65	5.06	5.30
M9	3.62	4.12	4.41	4.65

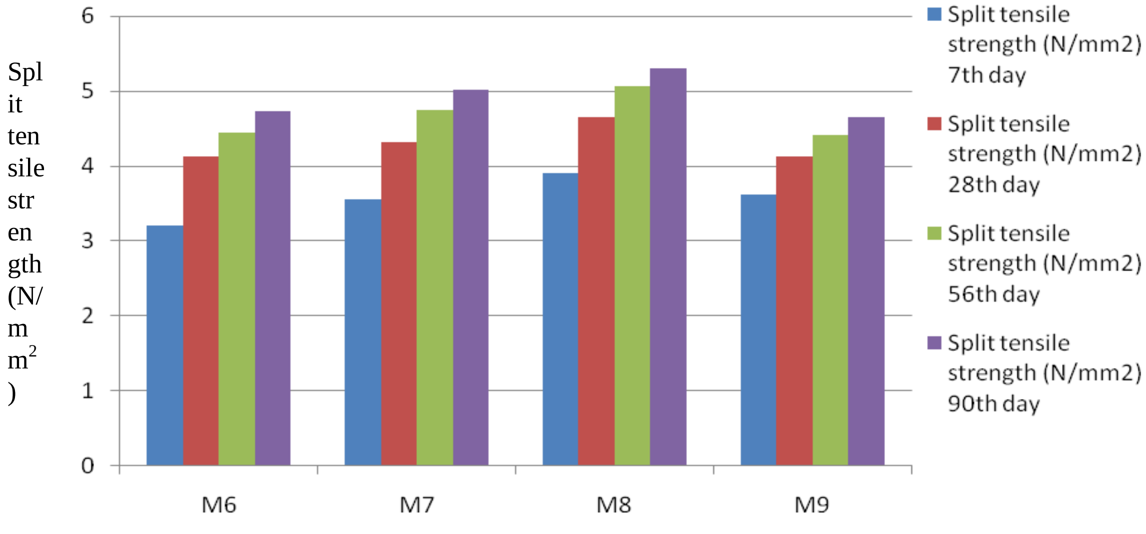

Mix combinations

Graph showing Split tensile strength of mixes M6 –M9

As per the study, for the second set of combination ie, silica fume 15% and steel slag 40 - 70% maximum strength obtained is M8 mix ie, silica fume 10% and steel slag 60% and by compairing it with conventional mix it shows an increase in split tensile strength upto 15 % and also obtained maximum replacement of steel slag in M9 mix ie, steel slag 70%.

Table. 8 Split tensile strength test results for M10 – M13 mix

Sample designation	Split tensile strength(N/mm^2)			
	7th day	28th day	56th day	90th day
10	2.68	3.14	3.45	3.64
M11	3.14	3.84	4.03	4.53
M12	2.96	4.11	4.47	4.81
M13	2.11	3.36	3.69	3.86

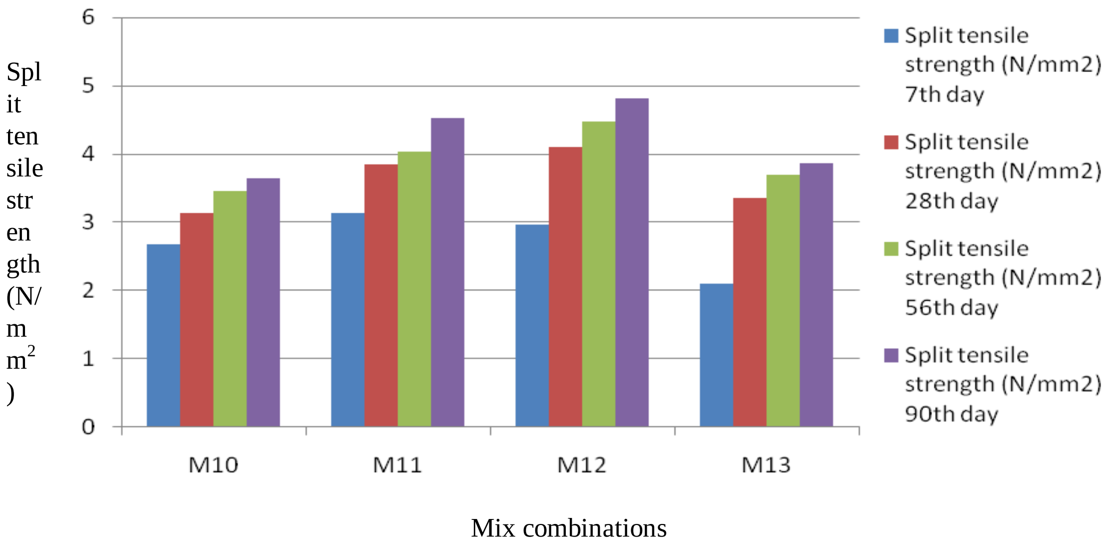

Graph showing Split tensile strength of mixes M10 –M13

According to the studies there is no increase in the split tensile strength and for the third set of combinations there is a small reduction in split tensile strength by comparing with the conventional mix and from these ‘M12’ mix shows high strength ie, 20% silica fume and 60% steel slag.

Table 9 Split tensile strength test results for M14 – M17 mix

Sample designation	Split tensile strength(N/mm^2)			
	7th day	28th day	56th day	90th day
M14	2.34	2.94	3.12	3.46
M15	2.54	3.12	3.43	3.48
M16	2.19	2.88	3.08	3.42
17	2.11	2.32	2.51	2.73

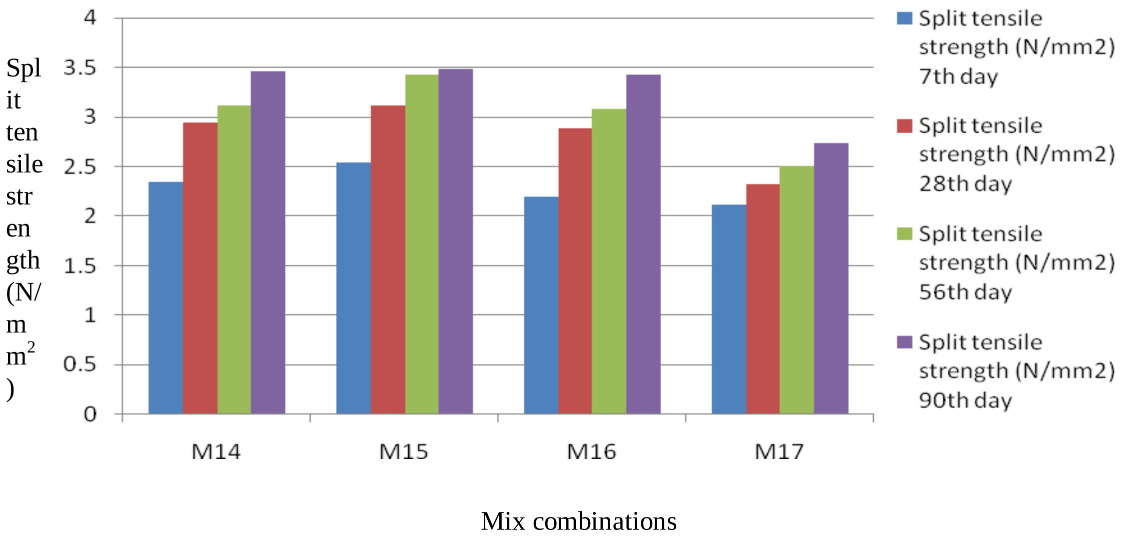

Graph showing Split tensile strength of mixes M14 –M17

According to the studies there is no increase in the split tensile strength and for the last set of combinations there is a small reduction in split tensile strength by comparing with the conventional mix, and from these 'M15' mix shows high strength ie, 25% silica fume and 50% steel slag.

Flexural strength test results

Table.10 Flexural strength test results for M1 - M5 mix

Sample designation	**Flexural strength (N/mm²)**			
	7th day	**28th day**	**56th day**	**90th day**
M1	3.89	3.92	4.12	4.46
M2	4.28	5.32	5.85	6.06
M3	4.76	5.50	5.94	6.43
M4	4.86	5.87	6.16	6.63
M5	4.29	5.55	5.77	6.82

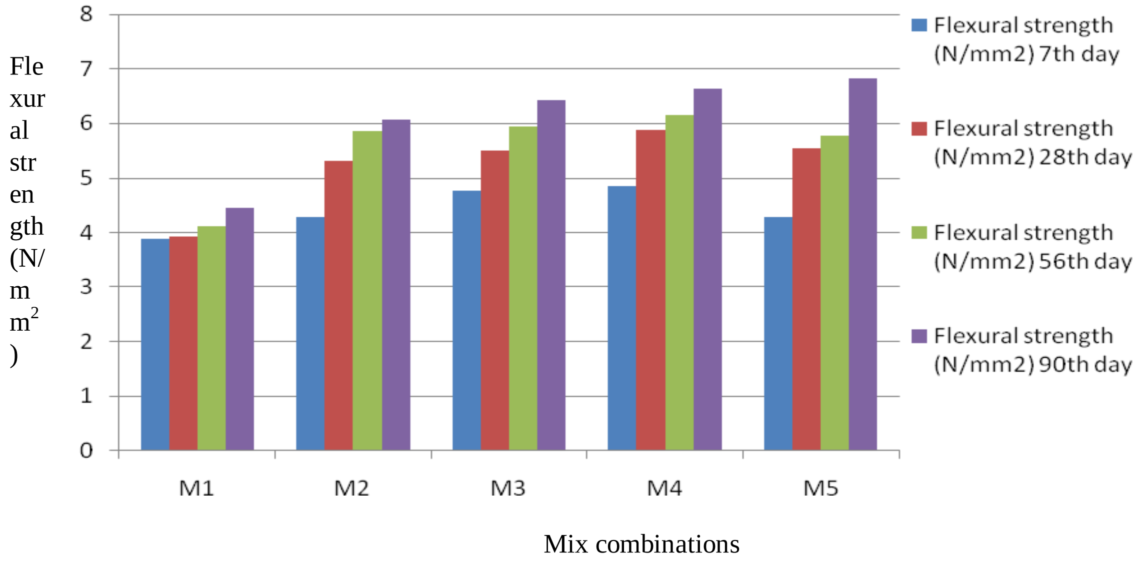

Graph showing flexural strength of mixes M1 –M5

As per the study, for the first set of combination ie, silica fume 10% and steel slag 40 - 70% maximum flexural strength obtained is M4 mix ie, silica fume 10% and steel slag 60% and by compairing it with conventional mix it shows an increase in flexural tensile strength upto 33 % and also obtained maximum replacement of steel slag in M5 mix ie, steel slag 70%.

Table.11 Flexural strength test results for M6 – M9 mix

Sample designation	**Flexural strength (N/mm²)**			
	7th day	**28th day**	**56th day**	**90th day**
M6	4.18	5.33	5.86	6.18
M7	4.60	5.86	6.09	6.68
M8	5.07	5.12	5.63	5.78
M9	4.08	5.01	5.41	5.81

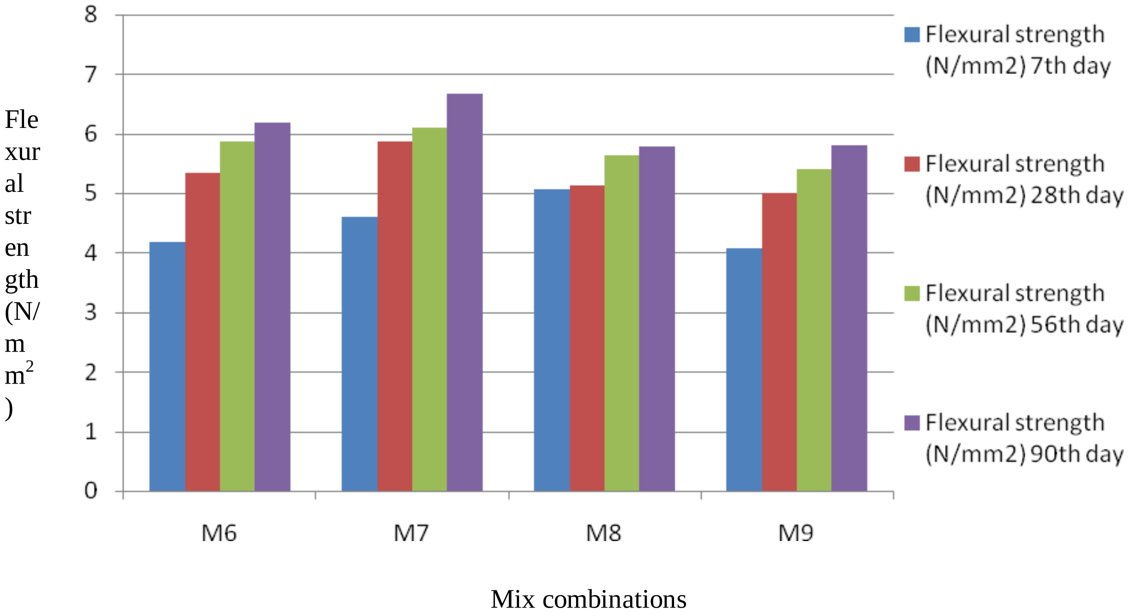

Graph showing Flexural strength of mixes M6 –M9

According to the studies there is no increase in the flexural strength and for the second set of combinations there is a small reduction in flexural strength by comparing with the conventional mix, and from these ‘M7’ mix shows high strength ie, 15% silica fume and 50% steel slag.

Table.12 Flexural strength test results for M10 – M13 mix

Sample designation	**Flexural strength (N/mm^2)**			
	7th day	**28th day**	**56th day**	**90th day**
M10	3.82	3.12	3.43	3.68
M11	4.23	3.63	3.92	4.24
M12	3.87	3.86	4.05	4.59
M13	3.56	3.25	3.64	3.83

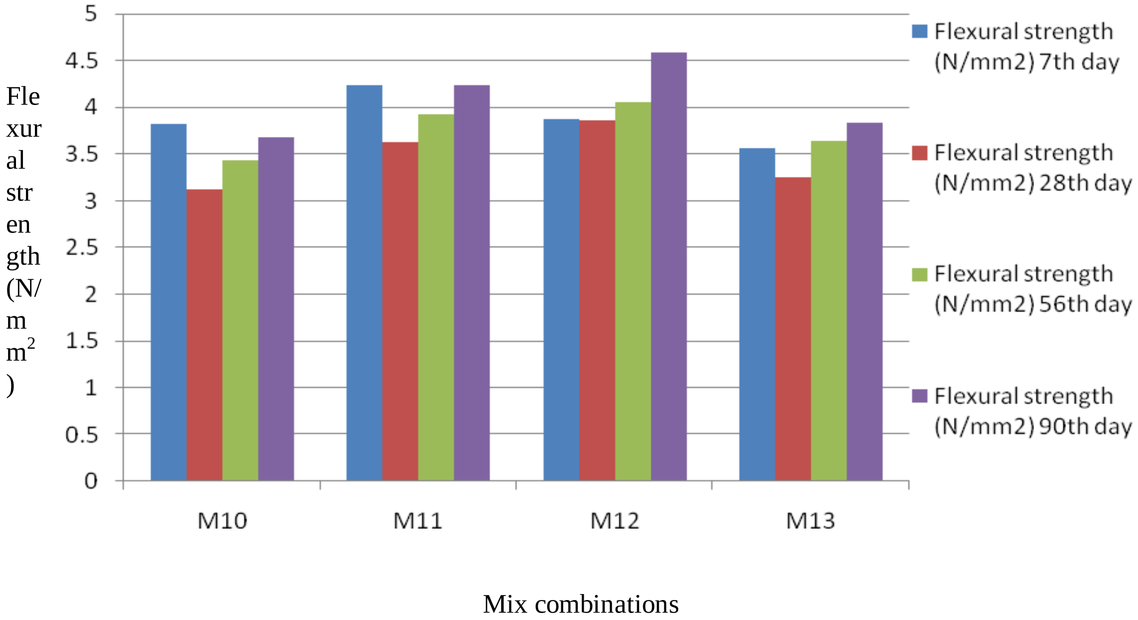

Figure 4.16 Graph showing flexural strength of mixes M10 –M13

According to the studies there is no increase in the flexural strength and for the third set of combinations there is a small reduction in flexural strength by comparing with the conventional mix, and from these ‘M12’ mix shows high strength ie, 20% silica fume and 60% steel slag.

Table.13 Flexural strength test results for M14 – M17 mix

Sample designation	Flexural strength (N/mm^2)			
	7th day	28th day	56th day	90th day
M14	2.81	3.17	3.55	3.71
M15	3.43	4.33	4.84	5.02
M16	3.11	2.98	3.13	3.4
M17	2.73	3.22	3.54	3.83

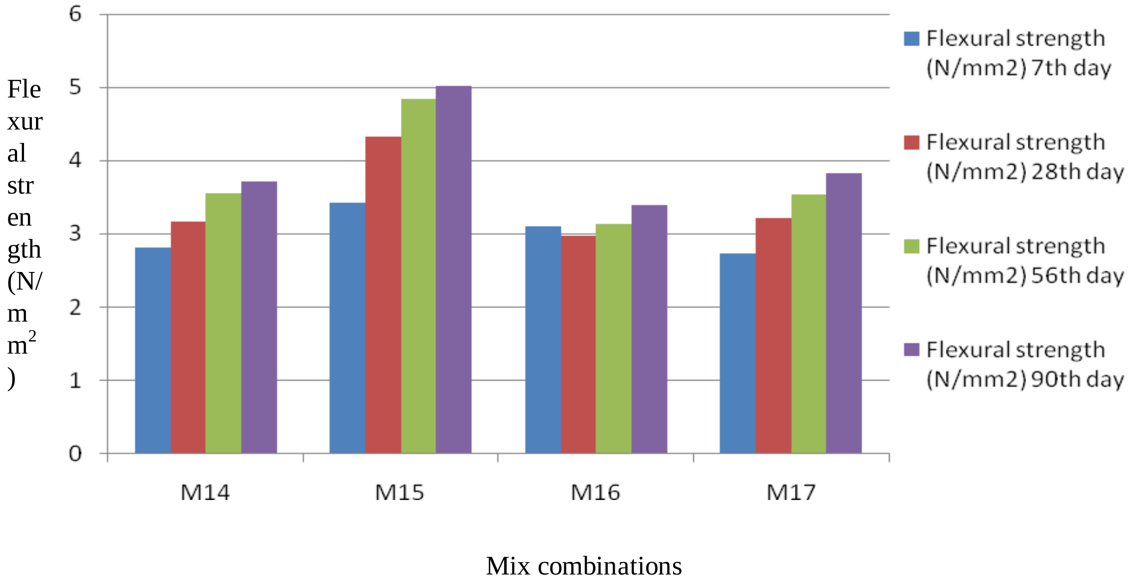

Graph showing flexural strength of mixes M14 –M17

As per the study, for the last set of combination ie, silica fume 25% and steel slag 40 - 70% maximum flexural strength obtained is M15 mix ie, silica fume 20% and steel slag 50% and by compairing it with conventional mix it shows an increase in flexural tensile strength upto 10 % and also obtained maximum replacement of steel slag in M15 mix ie, steel slag 50%.

Test result for durability studies

For the durability studies we consider the percentage of weight loss for every concrete mix and also loss in strength to find optimum mix. According to the durability studies we have been found that the optimum mix combination is M7 ie,silica fume 15% and steel slag 50%. Apart from the strength aspect of concrete mixes, the steel slag replacement level reduced upto 10%.

Table.14 Durability test results for M1 - M5 mix

Sample designation	Loss in Weight (%) At 30 Days	[4] Loss in Compressive strength (%) At 30 days
M1	4.34	11.29
M2	3.80	9.8
M3	3.12	8.72
M4	2.80	8.11
M5	2.94	8.72

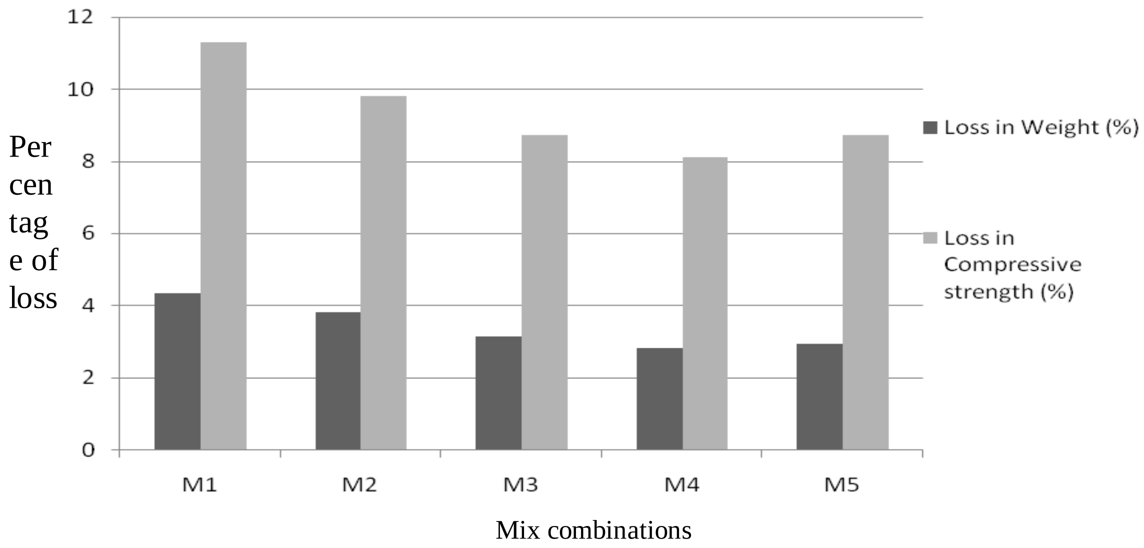

Figure 4.18Graph showing durability studies for M1-M5 mix

As per the study, for the first set of combinations mix M4 ie, silica fume 10% and steel slag 60% shows the least weight loss and it is more durable than the conventional mix.

Table.15 Durability test results for M6 – M9 mix

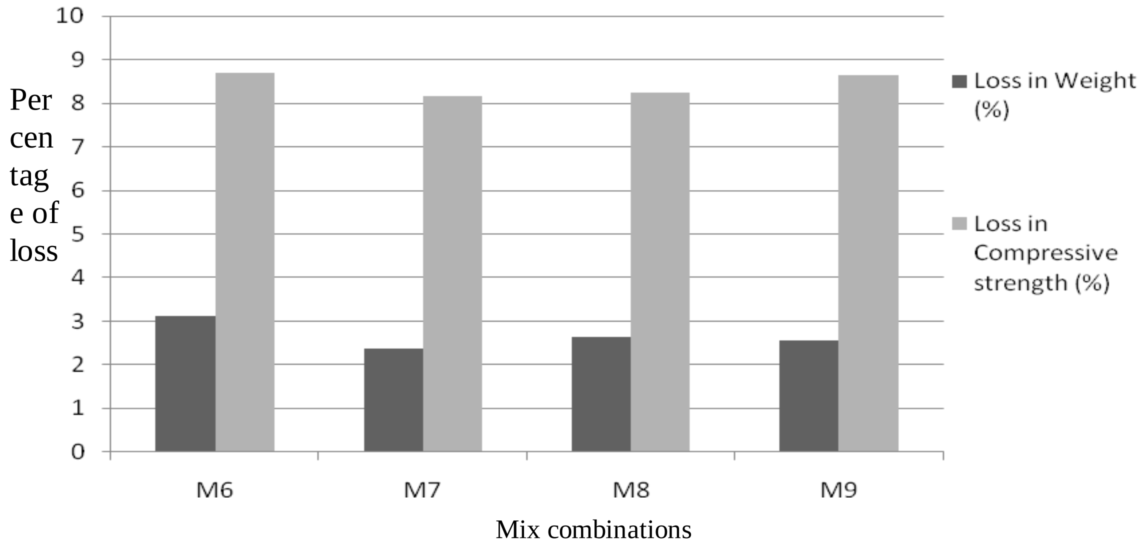

Figure 4.19Graph showing durability studies for M6-M9mix

As per the study, for the second set of combinations mix M7 ie, silica fume 15% and steel slag 50% shows the least weight loss and it is more durable than the conventional mix.

Table.16 Durability test results for M10 – M13 mix

Sample designation	Loss in Weight (%) At 30 Days	Loss in Compressive strength (%) At 30 days
M10	4.15	11.32
M11	3.86	9.78
M12	3.92	9.99
M13	4.17	11.22

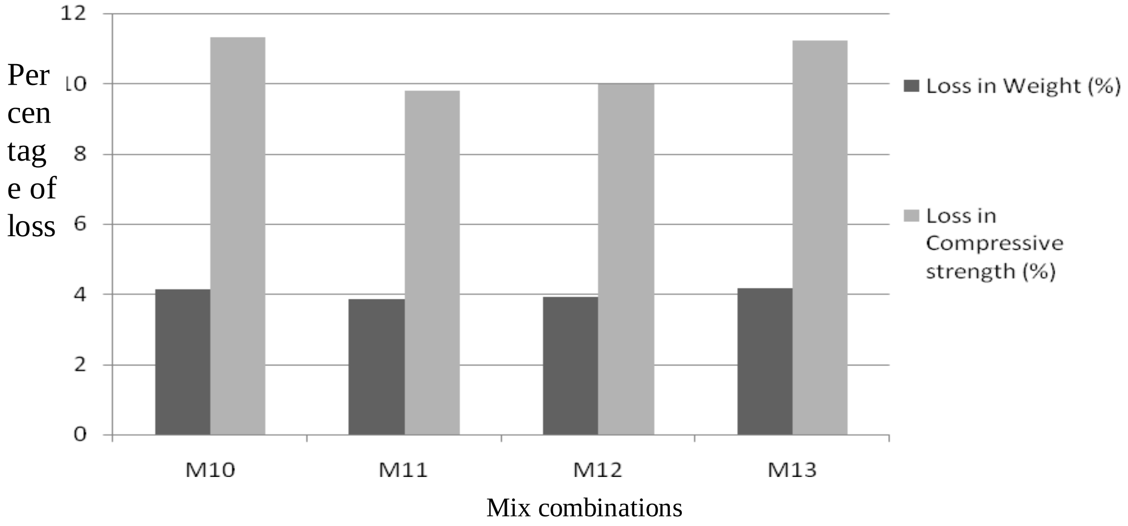

Figure 4.20Graph showing durability studies for M10-M13 mix

As per the study, for the third set of combinations mix M11 ie, silica fume 20% and steel slag 50% shows the least weight loss and it is more durable than the conventional mix. When we consider the other mixes the increase in silica fume content reduces the durability property of concrete.

Table.17 Durability test results for M14 – M17 mix

Sample designation	**Loss in Weight (%)** **At 30 Days**	**Loss in Compressive strength (%)** **At 30 days**
M14	4.72	12.01
M15	4.14	11.95
M16	3.94	9.13
M17	4.18	11.83

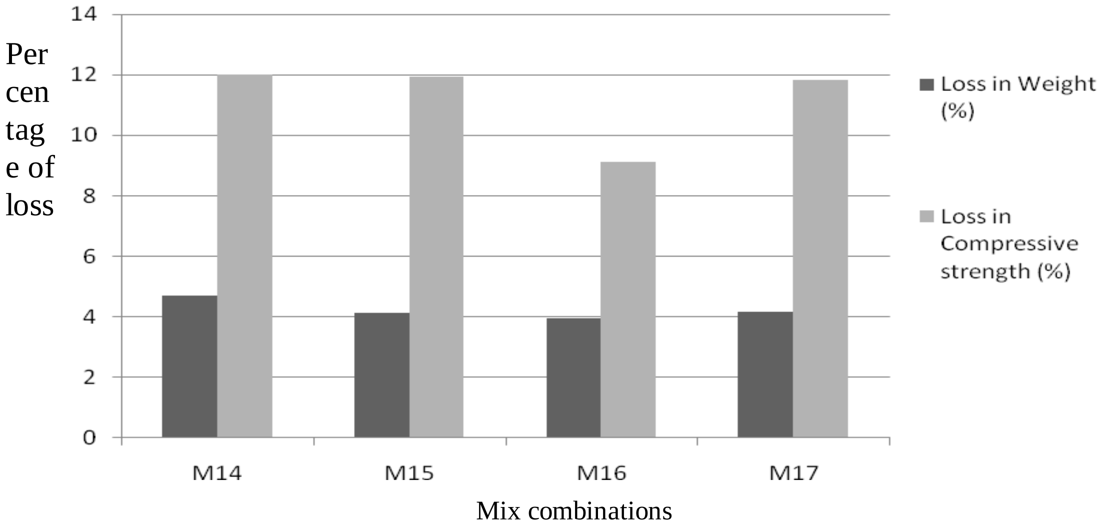

Figure 4.21Graph showing durability studies for M14-M17 mix

As per the study, for the last set of combinations mix M16 ie, silica fume 25% and steel slag 60% shows the least weight loss and it is shows almost same durability property as conventional mix. When we consider the other mixes the increase in silica fume content reduces the durability property of concrete. Throughout the study the optimum mix combination is found to be the mix M7 ie,silica fume 15% and steel slag 50%.

III. CONCLUSION

- As the steel slag content increases, the strength and durability of concrete decreases.
- The increase in amount of silica fume affect the optimum replacement level of steel slag.
- While comparing the results with conventional mix there is no significant improvement in the split tensile strength but the flexural strength is improved by 30%.
- The increase in steel slag content above 50% reduces the durability of concrete.Durability of concrete get reduced due to the porous nature of steel slag.
- The increase in silica fume content above 15% reduces the durability of concrete.
- The silica fume and steel slag content do not affect the long term strength of concrete.
- While comparing the results with conventional mix the best combination obtained is silica fume 15 % and steel slag 50%.
- Moreover with 15% replacement of cement by silica fume and 50% of sand by steel slag the performance of concrete get improved and also it will help to reduce the construction cost and the environmental pollution caused by industrial by products.

REFERENCES

Journal Papers

[1]. Han Young Moon, Jung HoonYoo and SeongSoo Kim, A fundamental study on the steel slag aggregate for concrete, GeosystemEng.,Volume 5, Issue 2, 38-45, (June 2002).

[2]. G. AppaRao, investigations on the performance of silica fume-incorporated cement pastes and mortars, cement and concrete research,Volume 33(2003) 1765-1770.

[3]. M mazloom , A ARamezanian Pool, and J J Brooks, Effect of silica fume on mechanical properties of high-strength concrete, cement &concrete composites 26(2004) 347-357.

[4]. S Banja and B Senguptha, influence of silica fume on the tensile strength of concrete, cement and concrete research,Volume 35(2005) 743-747.

[5]. Juan M Manso, Juan A Polanco, Milagros Losanez, Javir and J Gonzalez, Durability of concrete made with EAF slag as aggregate, cement and concrete composites,Volume 28(2006) 528-534.

[6]. HishamQasrawi, FisalShalbi and Ibrahim Asi, Use of low CaO unprocessed steel slag in concrete as fine aggregate, construction and building materials,Volume 23(2009) 1118-1125.

[7]. Carlo Pellergino and Vittorio Gaddo, Mechanical and durability characteristics of concrete containing EAF slag, cement and concrete composites,Volume 31(2009) 663-671.

[8]. H. Katkhuda, B. Hanayneh and N. Shatarat Influence of Silica Fume on High Strength Lightweight Concrete World Academy of Science, Engineering and Technology ,Volume 34 2009**.** Bouikni , R.N. Swamy, A. Bali, Durability properties of concrete containing 50% and 65% slag, Construction and Building Materials, Volume 23 (2009) 2836–2845.

[9]. N K Amudhavalli and JeenaMathew(2012),Effect of silica fume on strength and durability parameters of concrete ,ISSN,August 2012 , 2231-6604- Volume 3 issue 1 pp:28-35 @IJESET.

[10]. Dilip Kumar Singha Roy1, AmitavaSil Effect of Partial Replacement of Cement by Silica Fume on Hardened Concrete .ISSN 2250-2459, Volume 2, Issue 8, August 2012.

[11]. K.Chinnaraju,V.R.Ramkumar, K.Lineesh, S.Nithya, V.Sathish , study on concrete using steel slag as coarse aggregate replacement and ecosand as fineaggregate replacement, IJREAT International Journal of Research in Engineering & Advanced Technology, Volume 1, Issue 3, June-July, 2013.

Books:

[1]. IS : 12269 -1987 – reaffirmed 1989, Indian Standard Specification for 53 Grade Ordinary Portland Cement.

[2]. IS 383-1970 (Reaffirmed 1997) Indian Standard Specification

[3]. IS 10262:2009 Indian Standard Specification for concrete mix proportionin

OPEN ACCESS

International
Journal
Of Modern Engineering Research (IJMER)

The Effects of Vehicle Speeds on Accident Frequency within Settlements along Trunk Roads

Daniel Atuah Obeng
(Department of Civil Engineering, Kwame Nkrumah University of Science and Technology, Ghana)

ABSTRACT: *Literature provides overwhelming evidence that a strong relationship exist between vehicle speed and accident risk, and an outcome severity in the event of an accident. Excessive speed is said to be a major causal factor of road accidents on trunk roads; contributing 60% of all vehicular accidents. However, speed rationalization measures implemented on a number of trunk roads in Ghana have realized very little success. This study therefore investigated the effects of vehicle speeds on accident frequency within settlements along trunk roads. Data was collected on accidents, vehicle speeds and other road and environment-related features for ninety-nine (99) settlements delineated from four (4) trunk roads. Correlation analysis was employed to establish useful relationships and provided insight into the contributions of relevant road and environmental-related variables to the occurrence of road traffic accidents. Using the Negative Binomial error structure within the Generalized Linear Model framework, core (flow-based) models were formulated based on accident data and exposure variables (vehicle mileage, daily pedestrian flow and travel speed). Incremental addition of relevant explanatory variables further expanded the core models into comprehensive models. Findings indicate the main risk factors are number of accesses, daily pedestrian flow and total vehicle kilometers driven, as vehicle speed did not appear to influence the occurrence of road traffic accidents within settlements along trunk roads. In settlement corridors, mitigating accident risks should not focus only on traffic calming but rather on measures that reduce pedestrian and vehicular conflict situations as well as improve conspicuity around junctions.*

Key words**:** *Accident frequency, Settlements, Conspicuity, Speed, Trunk road.*

I. INTRODUCTION

The National Road Safety Commission reports that non-urban environments in Ghana are the most accident-prone as they account for two-thirds of all road traffic fatalities (***Road Traffic Crashes in Ghana, 2010***). It is said that excessive speed is a major causal factor of road accidents on trunk roads; contributing 60% of all vehicular accidents (***Wikipedia***). However, a number of speed rationalization measures implemented on trunk roads in Ghana have realized very little success. This is attributed to the little knowledge about the exact relationship between vehicle speed and road traffic accidents. Speed is generally considered a major risk factor in road traffic accident occurrence though there may be other intervening factors (***Wegman and Aarts, 2006***). Literature has provided overwhelming evidence that a strong relationship exist between travel speed and accident risk, and an outcome severity in the event of an accident (***Nilsson, 2004***). Therefore, this study attempted to develop a relationship between travel speed and road traffic accidents within settlements along trunk roads in order to gain insight into the effects of speeds on the frequency of road traffic accidents. Thus, effective intervention strategies and measures are elicited to address the menace of road traffic accidents within settlements on trunk roads.

II. STUDY'S APPROACH AND METHODOLOGY

In the event of a traffic accident, it is assumed that kinetic energy of the two colliding entities will be converted at an instant to some form of heat, sound and material distortion. The masses of the colliding entities are therefore significant to the severity outcome as occupants of the lighter entity are normally worse off than occupants of the heavier entity. From the mathematical relationship, the contribution of the entities' speeds in the accident incidence and injury outcomes becomes a significant issue of concern.

Thus, in an EU-funded project known as MASTER, a vehicle speed and road traffic accident relationship (the EURO model) was derived for European rural single-carriageway roads. The emerged Power Model was based on the empirical evaluation of the different changes in speed limits against road traffic accidents. It was established that the percentage change in the number of injury accidents was proportional to the square of the relative speed change. This applied both to increases and decreases in mean speed (***Elvik R et***

al, 2004). However, data availability limitations for the Master study necessitated the Transport Research Laboratory (TRL) to carry out a more extensive investigation of the relationship on rural single carriageway roads in England. The selected sites were roads with the 60 miles/h speed limit and the sample was stratified to cover all road classes. Provision was also made for road, traffic and environmental-related data. These data were included in the model development so as to establish their various contributions in road traffic accident causation. The TRL approach and methodology was adopted for this study. Data were collected for vehicle speeds and road traffic accidents on settlements along trunk roads. Additionally, other road and environment-related data were collected for the study road sections. Employing scatter diagrams, the nature of relationships between the dependent variable (road accident counts) and each of the independent variables (road section length, traffic and pedestrian flows, speed, and other road and environment-related features) were examined. Following the correlation analyses, the Generalized Linear Model (GLM), a sub-model in the Stata Software Package Version 12, was employed since all the relationships were non-linear. In developing the models however road traffic accident counts and vehicle travel speeds were used as the main variable inputs with vehicle mileage and pedestrian flows as exposure variables. Additionally, appropriate road and other environment-related variables were considered in the model development. Relevant tests were then conducted to assess the goodness of the relationships based on logic and statistics. Study findings thus provided an insight into strategies required for effective speed rationalization measures on trunk roads in Ghana.

III. DATA COLLECTION

3.1 Introduction

Data was collected from two main sources, primary and secondary, for 99 settlement corridors located on 4 trunk roads classified as national and inter-regional roads. The data requirements for the study included:

- Accident data (for a defined 3 year period);
- Vehicular flow data;
- Pedestrian flow data;
- Vehicle speed data; and
- Road geometric characteristics.

The length of the study sections ranged between 0.2km and 8.2km with a mean length of 1.8km. National and inter-regional roads featured road widths of 7.5m and 7.3m with corresponding shoulder widths of 2.0m and 1.5m respectively. There is no variability in the presence of shoulder as all the road sections had paved shoulders.

3.2 Accident Data

Details of road traffic accidents were solicited from the national accident database centre at the Building and Road Research Institute (BRRI) in Kumasi. Following the manipulation of the TRL Micro-computer Accident Analysis Package (MAAP 5) software, synthesized accident data were obtained from 2005 to 2007 for the study roads. The number of accidents was disaggregated by 3 accident types, namely; general accidents, pedestrian-only accidents and non-pedestrian accidents. Table 3.1 illustrates the distribution of injury accident by type on the study road sections. Out of a total of 958 road traffic accidents recorded, 346 were pedestrian-only accidents. This represents 36% of the total injury accidents which is below the annual national average of 42% of all accidents. In terms of accident severity, the proportion of pedestrian death and serious disability on trunk roads is significant as it remains the single most dominant road user at risk.

Table 3.1 – Distribution of Injury Accidents by Type

Accident Type	**Injury Accidents**	
	Nr	**(%)**
Pedestrian Accidents	346	36
Non-Pedestrian Accidents	612	64
General Accidents	**958**	100

Source: National Accident Data, 2005 – 2007, BRRI

3.3 Vehicle Flow Data

Manual classified counts on selected census stations on the study roads were complemented by historical traffic data obtained from the Ghana Highway Authority (GHA). The observed daily traffic flows were converted to average daily traffic (ADT) by the application of appropriate variation factors. Table 3.2 shows the vehicular traffic flows recorded for the study roads.

Table 3.2 – Traffic Flows on Study Roads

Road Type	**Daily Traffic Flow (vpd)**		
	Average	**Minimum**	**Maximum**
National Road	7,147	3,482	15,012
Inter-Regional Road	4,069	1,920	7,887
Total	5,406	1,920	15,012

Source: Field Surveys, 2008

It is evident that the national roads experienced the highest vehicular traffic and accounted for 60% of the total cumulative traffic. With respect to the minimum and maximum flows, the huge variations are attributed to the influence of substantial "local" traffic recorded in some of the "big" settlements (towns) along the study road corridors.

3.4 Pedestrian Flow Data

Limited pedestrian volume counts were conducted at crosswalks and along locations of major activity centers. Pedestrian volumes were counted at 15-minute intervals for durations of 12 hours between the hours of 06:00 and 18:00. Additional four-hour counts were conducted between 18:00 and 22:00 at locations where pedestrian activities were more pronounced at night. Daily pedestrian flows were determined for the study roads. Table 3.3 presents the average, minimum and maximum daily pedestrian flows estimated for the study roads.

Table 3.3 – Daily Pedestrian Flows on Study Roads

Road Type	**Daily Pedestrian Flow**		
	Average	**Minimum**	**Maximum**
National Road	2,586	62	32,816
Inter-Regional Road	933	26	9,445

Source: Field Surveys, 2008

A prominent feature observed was the intensity of roadside activities within settlement corridors and this was reflected in the different levels and spread of human activities captured by the pedestrian flow counts.

3.5 Vehicle Speed Data

Using the "floating car method", the average speed of a vehicle passing a study road section was computed. Travel times over a road section were recorded directly for 3 runs per direction for 2 days. The section mean speeds were estimated by dividing the section distance by the travel time for the run. Section mean speeds computed for the road sections were then averaged to obtain the average section mean speeds. Table 3.4 presents the space mean speed estimated for the study roads.

Table 3.4 – Space Mean Speeds on Study Roads

Road Type	**Space Mean Speed (km/h)**		
	Average	**Minimum**	**Maximum**
National Road	66	25	127
Inter-Regional Road	81	27	132

Source: Field Surveys, 2008

It is evident that the national road corridors experienced slightly lower speeds than the inter-regional road corridors. While an average of 66km/h was recorded in settlements located on national roads, an average of 81km/h was realized for those on the inter-regional roads. This is not surprising because most of the settlements along national roads are densely populated than settlements along inter-regional roads. Drivers are therefore constrained by human activities and interactions, thus, reducing their vehicle operating speeds. The average speeds recorded in settlements are still high on the inter-regional and national roads.

3.6 Road Geometric Characteristics

Apart from traffic flow and vehicle speed, other road alignment features were also identified to be relevant to the incidence of road traffic accidents. For this study, data was collected for three geometric characteristics, namely; horizontal curvature, number of accesses and terrain type. The features were described as continuous or categorical and presented as physically measured or based on the features' options.

IV. CORRELATION ANALYSIS

From the correlation analysis, the relationships between accident count and vehicle speed as well as other possible risk factors; namely; traffic flow, pedestrian flow, road section length, road type, number of horizontal curve, horizontal curve density, and number of access, access density and terrain type were established.

As in exploratory studies, the correlation coefficient (r), which indicates the strength of relationships between variables are assessed based on some thresholds (***Okoko, 2001***). For this study, the following thresholds were adopted:

- Weak correlation, $0 < r < 0.3$;
- Fairly strong correlation, $0.3 < r < 0.6$;
- Strong correlation, $0.6 < r < 0.8$; and
- Very strong correlation, $0.8 < r < 1.0$

Details of the analyses between accident counts (all accidents, pedestrian-only and non-pedestrian accidents) and traffic flow and road geometry features along the study roads are presented. Tables 4.1, 4.2 and 4.3 provide summaries of correlations coefficients estimated for the analyses between accident counts and the independent variables considered to influence accidents.

Table 4.1 - Correlation Coefficient of Variables influencing All Accidents

Variable	Correlation Coefficient (r)	Remarks
Travel Speed	-0.204	Weak relationship
Horizontal Curves	0.302	Weak relationship
Average Daily Traffic	0.457	Fairly strong relationship
Road Section Length	0.605	Strong relationship
Number of Accesses	0.751	Strong relationship
Daily Pedestrian Flow	0.783	Strong relationship

Source: Field Surveys, 2008

Table 4.2 - Correlation Coefficients of Variables influencing Pedestrian Accidents

Variable	Correlation Coefficient (r)	Remarks
Travel Speed	-0.292	Weak relationship
Horizontal Curves	0.297	Weak relationship
Road Section Length	0.477	Fairly strong relationship
Average Daily Traffic	0.488	Fairly strong relationship
Number of Accesses	0.718	Strong relationship
Daily Pedestrian Flow	0.806	Very strong relationship

Source: Field Surveys, 2008

Table 4.3 - Correlation Coefficients of Variables influencing Non-Pedestrian Accidents

Variable	Correlation Coefficient (r)	Remarks
Travel Speed	-0.143	Weak relationship
Horizontal Curves	0.284	Weak relationship
Average Daily Traffic	0.431	Fairly strong relationship
Road Section Length	0.637	Strong relationship
Daily Pedestrian Flow	0.714	Strong relationship
Number of Accesses	0.717	Strong relationship

Source: Field Surveys, 2008

4.1 Correlation of Accidents with Significant Study Variables

For the three accident data sets, namely, all accidents, pedestrian-only accidents and non-pedestrian accidents, the risk variables showed positive correlations with accident counts except travel speed. The exposure variables (average daily traffic, daily pedestrian flow and road section length) showed significant relationships, from fairly strong to strong relationships with the three accident data sets. Road geometric characteristics represented by number of horizontal curves and road accesses contributed to the occurrence of road traffic accidents. The nature of relationships is mixed though with horizontal curvature showing weak relationships whilst number of accesses indicated strong relationships. Travel speed has weak relationships with the three accident data sets but it is still critical in determining the safety of users of road space.

The environs of the study corridors showed continuous exposure of people to road accident due to intense roadside activities. Another conspicuity problem is the presence of obstructive billboards, trees and shrubs at major road intersections and accesses. Generally, the road space lacked adequate facilities for pedestrians and the interactions among various users of the roads are of immense safety concern.

4.2 Correlations of Travel Speed with Other Risk Variables

The study focus is on establishing a relationship between travel speeds and road traffic accidents. Knowing however the significant contributions of other road and environmental-related factors to road accidents, the strength of relationships between travel speed and other potential risk variables was estimated. This was to assess the masking influence by some other risk variables on travel speed in the development of "model" relationships with accident counts. In all of the accident types under consideration, travel speed showed a fair relationship with average daily traffic (-0.4) but a weak relationship with daily pedestrian flow (-0.2). Another exposure variable, vehicle mileage, representing the combination of road section length and average daily traffic showed no relationship with travel speed. Table 4.4 presents the correlation coefficients of relationships between travel speed and other risk variables for the three accident data sets.

Table 4.4 - Correlations Coefficients of Other Risk Variables with Travel Speed

Correlates	**Coefficient (r)**		
	All Accidents	**Pedestrian**	**Non-Pedestrian**
Daily Pedestrian Flow	-0.253	-0.257	-0.253
Average Daily Traffic	-0.439	-0.457	-0.439
Road Section Length	0.070	0.091	0.070
Number of Accesses	-0.143	-0.149	-0.143
Horizontal Curves	-0.086	-0.040	-0.086
Terrain Type	0.025	0.040	0.025

Source: Field Surveys, 2008

4.3 Summary of Correlation Analysis

This section established useful relationships and provided insights into the contributions of some road and environment-related factors to road traffic accidents. Road traffic accidents increase with the risk variables of average daily traffic, daily pedestrian flow, road section length, horizontal curvature and number of accesses except travel speed. Generally, the nature of the relationships is mixed, as daily pedestrian flow and number of accesses consistently showed strong to very strong relationships with road accidents compared to the fair relationships between road accidents with road section length, average daily traffic and horizontal curvature.

On relationships between travel speed and the other study variables, it was established that travel speed has a fair relationship with average daily traffic (0.4) and a weak relationship with daily pedestrian flow (0.2). Another exposure variable, vehicle mileage showed no relationship with travel speed. Thus, provide indication to possible relevant and significant variables to be considered in developing the models. The requirement of retaining the exposure variables in the model development therefore made it necessary to consider only daily pedestrian flow and vehicle mileage as well as the other road and environmental-related variables as relevant and significant in the development of the model equations.

V. MODEL DEVELOPMENT

5.1 Introduction

Modeling was conducted within the framework of the Generalized Linear Models (GLM) using the Stata Software Package Version 12. A two-stage process was employed and included development of the core (flow-based) model and further expansion into the comprehensive (full variable) model. The core model included exposure variables only which were daily pedestrian flow and vehicle mileage as well as travel speeds. It was expanded into a comprehensive model by the addition of other explanatory variables, namely; horizontal curvature, number of accesses and terrain type. Based on previous work gleaned from literature, the core and comprehensive models are mathematically expressed as below:

For the core model,

$$E(Y) = a_0 P^{a_1} T^{a_2} V^{a_3} \ldots\ldots\ldots\ldots\ldots\ldots\ldots\ldots\ldots\ldots\ldots (5.1)$$

For the comprehensive model,

$$E(Y) = a_0 P^{a_1} T^{a_2} V^{a_3} \exp \sum_{j=1}^{n} b_j X_j \ldots\ldots\ldots\ldots\ldots\ldots\ldots\ldots\ldots\ldots\ldots\ldots (5.2)$$

where,

E (Y) = predicted accident frequency,

P = daily pedestrian flow (per day),
T = vehicle mileage (veh-km),
V = travel speed (km/hr),
X_j = any variable additional to P, T and V,
exp = exponential function, e = 2.7183, and
a_0, a_1, a_2, a_3, b_j = model parameters.

In conformity with the GLM framework, equations 5.1 and 5.2 were transformed into the prediction mode using a log-link function as follows:
For the core model,

$$\ln[E(Y)] = \ln(a_0) + a_1 \ln(P) + a_2 \ln(T) + a_3 \ln(V) \ldots\ldots (5.3)$$

For the comprehensive model,

$$\ln[E(Y)] = \ln(a_0) + a_1 \ln(P) + a_2 \ln(T) + a_3 \ln(V) + \sum_{j=1}^{n} b_j X_j \ldots\ldots (5.4)$$

5.2 Modeling Procedure

The accident data sets were over-dispersed thus the Negative Binomial error structure was adopted as the most appropriate distribution and within the GLM framework to estimate the model coefficients (***Miaou and Lum, 1993***). By specifying the dependent variable, the explanatory variables, the error structure and the link function, the models were fitted. Model parameters (coefficients) were estimated using the maximum likelihood approach. The procedure adopted in the model development was the forward procedure in which the variables were added to the model in a stepwise manner.

In accordance with previous studies on accident prediction models, the decision on which variables should be retained in the model was based on two criteria. The first criterion was whether the t-ratio of the estimated parameter was significant at the 95% confidence level (p-value less than 5%) and the second criterion was whether the addition of the variable to the model causes a significant drop in the scaled deviance at 95% confidence level. Two statistical measures were used in assessing the validity of the model developed. These were the Pearson Chi square statistic and the Deviance statistic. The coefficient of determination (R^2) was also employed to determine the amount of variability in the response variable explained by the variation in the selected set of explanatory variables. The R-squared estimation was carried out by the method recommended by *Miaou (1996).*

5.3 Model Results

The results of the developed prediction models for the accident data sets, namely, all accidents, pedestrian-only and non-pedestrian accidents captured the differences in accident patterns and risk factors. From the best fit models, the differences in the model variables for all, pedestrian-only and non-pedestrian accidents were presented to enable comparisons to be made.

5.3.1 Core Models

The parameter estimations for the log-linear equation of the core (flow-based) model using the Negative Binomial distribution are as presented in Table 5.1.

Table 5.1 - Parameter Estimation of Core Model for All Accidents

No. of Observations = 99
Residual df = 96
Log likelihood = -271.82
Deviance (1/df) = 1.196
Pearson (1/df) = 1.014
AIC = 5.55
BIC = -326.34

Notation	Parameter	Coefficient	Standard Error	z
T	Mileage	0.5655	0.1018	5.55
P	Daily Pedestrian Flow	0.3511	0.0557	6.30
a_o	Constant	-5.3129	0.7721	-6.88

The resulting core model developed for all accidents is as follows:

$$E(Y) = 4.9 \times 10^{-3} \times T^{0.6} P^{0.4} \ldots\ldots (5.5)$$

where,
E (Y) = expected accidents along road section for 3 years,
T = vehicle mileage (veh-km), and
P = daily pedestrian flow (per day).

The goodness-of -fit statistic for the model shows that the model fits reasonably well with the data. Table 5.1 presents the Pearson Chi-square divided by its degrees of freedom and the deviance statistic divided by its degrees of freedom, and the two statistics were estimated to be 1.01 and 1.19 respectively. The values are within the permissible range of 0.8 and 1.2 (***Dissanayake and Ratnayake, 2006***) indicating that the Negative Binomial error structure assumption is therefore acceptable. The important variables were vehicle mileage and daily pedestrian flow. They were statistically significant ($p<0.05$) with positive estimated model parameters in the core model. Vehicle mileage and daily pedestrian flow are measures of exposure and had direct proportional relationships with road accident occurrence. Travel speed was not significant in the core modeling process of the three accident datasets, namely; all accidents, pedestrian-only and non-pedestrian accidents. Table 5.2 presents the coefficients in the core models for the different accident types.

Table 5.2 - Coefficients in the Core Models for Different Accident Types

Parameter	**All Accidents**	**Pedestrian Accidents**	**Non-Pedestrian Accidents**
T	0.5655	0.3640	0.6320
P	0.3511	0.5000	0.2683
a_o	-5.3129	-5.5507	-5.8118

Using the R-squared value, the variables in the core model, namely; vehicle mileage and daily pedestrian flow could explain 53% of the total variation in the all accidents data. The core model is regarded as relatively coarse and rough estimator of accident frequency (***Salifu, 2004***). However, the estimated coefficient of determination of 0.53 is good enough measure to substantially explain the variation in the accident data by the exposure variables. ***Dissanayeke and Ratnayeke (2006)*** said that the coefficient of determination is significant if found to be greater than 0.45. For the pedestrian-only and non-pedestrian accidents, the exposure variables could explain 51% and 48% respectively of the total variations in the accident datasets.

5.3.2 Comprehensive Models

In expanding the core models, relevant explanatory variables including speed were introduced. The parameter estimations for the log-linear equation of the comprehensive models using the Negative Binomial distribution are as presented in Tables 5.3, 5.4 and 5.5.

Table 5.3 - Parameter Estimation of Comprehensive Model for All Accidents

No. of Observations = 99
Residual df = 96
Log likelihood = -284.29

Deviance (1/df) = 1.19
Pearson (1/df) = 1.01
AIC = 5.80
BIC = -327.04

Notation	**Parameter**	**Coefficient**	**Standard Error**	**z**
T	Mileage	0.7900	0.1183	6.68
A	Number of Accesses	0.0268	0.0101	2.67
a_o	Constant	-5.3008	1.0187	-5.20

The resulting comprehensive model developed for all accidents is as follows:

$$E(Y) = 4.9 \, x \, 10^{-3} \, x \, T^{0.8} x \, EXP^{\left(0.03A\right)} ......(5.6)$$

where,
E (Y) = expected accidents along road section for 3 years,
T = vehicle mileage (veh-km), and
A = number of accesses, and
EXP = Exponential function, e = 2.718282.

Table 5.4 - Parameter Estimation of Comprehensive Model for Pedestrian Accidents

No. of Observations = 99
Residual df = 96
Log likelihood = -186.6

Deviance (1/df) = 1.07
Pearson (1/df) = 0.83
AIC = 3.83
BIC = -338.16

Notation	**Parameter**	**Coefficient**	**Standard Error**	**z**
T	Mileage	0.3644	0.1351	2.70
P	Daily Pedestrian Flow	0.5033	0.0737	6.82
a_o	Constant	-5.5507	1.0230	-5.43

The resulting comprehensive model developed for pedestrian accidents is as follows:

$$E(Y) = 3.9 \times 10^{-3} \times T^{0.4} P^{0.5} \ldots\ldots\ldots\ldots\ldots\ldots\ldots\ldots(5.7)$$

where,

E (Y) = expected accidents along road section for 3 years,
T = vehicle mileage (veh-km), and
P = daily pedestrian flow (per day).

Table 5.5 - Parameter Estimation of Comprehensive Model for Non-Pedestrian Accidents

No. of Observations = 99
Residual df = 96
Log likelihood = -245.22
Deviance (1/df) = 1.19
Pearson (1/df) = 1.09
AIC = 5.01
BIC = -326.62

Notation	Parameter	Coefficient	Standard Error	z
T	Mileage	0.7543	0.1172	6.44
A	Number of Accesses	0.0258	0.0099	2.60
a_o	Constant	-5.4120	1.0133	-5.34

The resulting comprehensive model developed for non-pedestrian accidents is as follows:

$$E(Y) = 4.5 \times 10^{-3} \times T^{0.8} \times EXP^{(0.03A)} \ldots\ldots(5.7)$$

where,

E (Y) = expected accidents along road section for 3 years,
T = vehicle mileage (veh-km), and
A = number of accesses, and
EXP = Exponential function, e = 2.718282.

The goodness-of -fit statistic for the models show reasonably fits with the accident datasets. The Pearson Chi-square and deviance statistic divided by its degrees of freedom were within the permissible range of 0.8 and 1.2, indicating the Negative Binomial error structure to be an acceptable assumption. The computed coefficient of determination, R-squared values for all accidents, pedestrian accidents and non-pedestrian accidents are 0.64, 0.51 and 0.60 respectively.

This implies the comprehensive models could explain 64%, 51% and 60% of the systematic variation in the accident data. Suggesting that, there are still some important variables that could not be captured. For example, factors relating to weather, environment and human behaviour were not possible to be considered in the models and they could have contributed to accident occurrence. Following the model results, these significant risk variables were identified and their contributions to accident occurrence have been explained:

Vehicle Mileage

Vehicle mileage is an important exposure variable because of its influence in all the accident types. It shows a direct proportionality with accident frequency. In all and non-pedestrian accidents, especially, a 10% increase in vehicle mileage is expected to increase road traffic accidents by 8%. For pedestrian accidents, the influence of vehicle mileage was halved as a 10% increase in vehicle mileage will result in a 4% increase in pedestrian accidents.

Daily Pedestrian Flow

As exposure variable, the contribution of daily pedestrian flow was pronounced in pedestrian-only accidents. It shows a direct proportionality with accident frequency and a 10% increase in daily pedestrian flow will result in a 5% increase in pedestrian accidents.

Number of Accesses

The number of accesses was the only explanatory variable that featured in the all and non-pedestrian accidents. The predicted effect of this variable is such that, an additional access (junction) to a road section will be expected to increase the accident frequency by about 3%. It is not surprising because of the conspicuity problems motorists faced at junctions as the presence of overbearing billboards obstruct their lines of vision.

Travel Speed

Travel speed did not feature in any of the accident types either as an exposure variable or explanatory variable. Following the correlation analysis however it was established that travel speed was weakly related to average daily traffic and daily pedestrian flow. It is evident that vehicle speed did not contribute significantly to road traffic accident within settlements along trunk roads.

VI. CONCLUSION

The objective of this study was to investigate the effects of vehicle speed on accident frequency within settlements along trunk roads and from the analysis of gathered data, the following specific findings were made:

- The major risk factors that influence road traffic accidents within settlements along trunk roads are vehicle mileage, daily pedestrian flow and number of accesses. In the case of all accidents, the variables explained 64% of the systematic variation in the accident data confirming some earlier findings of ***Caliendo et al, (2006)*** and ***Stamatiadis et al (2008)*** on risk factors that influence road traffic accidents on highways (trunk roads);
- Mean speeds of vehicles appear not to influence the occurrence of road traffic accidents within settlements along trunk roads. In modeling the three accident types, it came out to be insignificant either as an exposure variable or explanatory variable. However, it only showed a weak relationship with average daily traffic and daily pedestrian flow in the correlation analysis and could not have been considered "masked" by other influential variable(s);
- In mitigating accident risks, therefore, intervention measures should not necessarily focus mainly on speed rationalization measures such as traffic calming but a more effective solution will be to segregate facilities for pedestrians and vehicles to eliminate conflict situations. The need to improve conspicuity at junctions became clear as overbearing billboards obstructed lines of vision of motorists; and
- A wider scope of studying the effectiveness of the application of traffic calming measures within rural settlements along trunk roads will provide the needed insight into the relevance of its continuous use. For instance, a "Before and After" study will help assess the impacts of such measures on the safety of road users.

The unique character of rural settlements and its emerging socio-economic circumstances pose enormous traffic safety challenges to practitioners. It is important that appropriate diagnosis of the road traffic accidents issues are conducted before proffering intervention strategies and measures. This should be done within the context of the rural setting dynamics that features a highway and the peculiarities of its environment.

REFERENCES

[1]. Caliendo, C., Guida, M., and Parisi, A., **A Crash-Prediction Model for Multilane Roads**, Accident Analysis and Prevention Vol 39, 2006, pp. 657 – 670.

[2]. Dissanayeke, S., and Ratnayake, I., **Statistical Modeling of Crash Frequency on Rural Freeways and Two-Lane Highways using Negative Binomial Distribution**, Advance in Transportation Studies, International Journal, Section B.9, 2006, .

[3]. Elvik, R., Christensen, R., and Amundsen, A., **Speed and Road Accidents: An Evaluation of the Power Model**, Institute of Transport Economics, TOI Report 740, 2004, pp. i - v.

[4]. http://en.wikipedia.org/wiki/Speed_limits

[5]. Miaou, S. P. and Lum, H., **Modeling Vehicle Accidents and Highway Geometric Design Relationships**, Accident Analysis and Prevention, Vol. 25, No.6, 1993, pp. 689-703.

[6]. Miaou, S. –P., **Measuring the Goodness-of-Fit of Accident Prediction Models**, FHWA-RD-96-040, Federal Highway Administration, Washinghton, D. C., 1996.

[7]. National Road Safety Commission, 2010 Road Traffic Crashes in Ghana Annual Report, 2010.

[8]. Nilsson, G., **Traffic Safety Dimensions and the Power Model to describe the Effect of Speed on Safety**, Bulletin 221, University of Lund, Lund, Sweden, 2004.

[9]. Okoko E., Quantitative Techniques in Urban Analysis, 2001, pp. 116 – 117.

[10]. Salifu, M., **Accident Prediction Models for Un-signalized Urban Junctions in Ghana**, IATSS Research Vol. 28 No. 1, 2004, pp. 68 - 80.

[11]. Stamatiadis, N., Pigman, J., Lord, D,. Sacksteder, J., and Ruff, W., **Safety Impacts of Design Element Trade-offs**, A Paper prepared for 2009 Annual Meeting of the Transportation Research Board, 2008.

[12]. Wegman, F.C.M. and Aarts, L.T., Advancing Sustainable Safety - A National Exploration of Traffic Safety for the Years 2005 – 2020., 2005.

OPEN ACCESS

International
Journal
Of Modern Engineering Research (IJMER)

Optimization of Skin Condenser Using Bundy Tube In Place Of Copper Tube

D. Sasidhar Reddy[1], Dr. K. Hemachandra Reddy[2], Kumari D. Jyothi[3]

[1]*Department of Mechanical Engg., JNTUA College of Engineering, Anantapur - 515002, Andhra Pradesh, India.*

[2]*Professor&Registrari/c, Department of Mechanical Engg., JNTUA College of Engineering, Anantapur – 515002, Andhra Pradesh, India.*

[3]*Lecturer, Department of Mechanical Engg., JNTUA College of Engineering, Anantapur-515002, Andhra Pradesh, India.*

ABSTRACT: *The condenser is an important device used in the high pressure side of a refrigeration system. Its function is to remove heat of the hot vapour refrigerant discharged from the compressor. The main objective of this work is to carryout experimental investigation on Bundy Condenser coil used in Skin Condenser for a Deep Freezer of 425 liters capacity; it is proposed to optimize the length of the condenser coil. R – 134A will be used as refrigerant for the proposed investigation.*

I. INTRODUCTION

CHEST-TYPE FEEZERS:

A chest freezer is nothing but a storage unit for frozen food such as meat, poultry, fish, prawns, some vegetables and some frits. The chest type freezer has certain advantages. Since cold air is heavier than warm air, the very cold air in a chest-type freezer does not spill out each time the lid is opened. This stops a considerable amount of moisture from entering the cabinet.

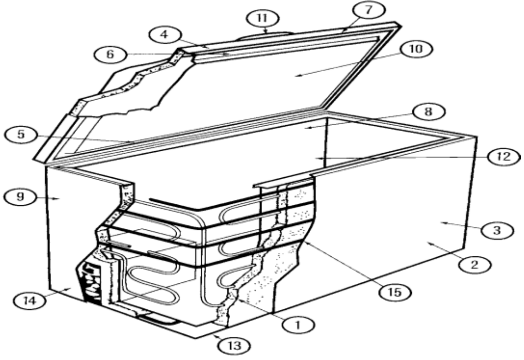

Fig 4.1 CHEST FREEZER 425L

Fig. 4.1 The parts of a chest-type freezer: 1—polyurethane foam insulation, 2—wrap-around steel cabinet, 3—baked-on enamel finish, 4— self-adjusting lid, 5—spring-loaded hinges, 6—vinyl lid gasket, 7—safety lock and self-ejecting key, 8—lift-out wire baskets, 9—temperature-control knob, 10—automatic interior light, 11—power-on light, 12—vertical cabinet divider, 13—defrost water drain, 13—sealed compressor, and 15—wrap-around condenser.

There is little air change when the cabinet opened. To make chest-type freezers more convenient to use, they are usually fitted with baskets that maybe lifted out to provide access to frozen food packages near the bottom. Also, the lids usually have a counterbalancing mechanism, which makes them easy to open. The chest-type freezer provides the most economical type of food freezing mechanism. Chest-type freezers require a manual defrost.

Defrosting may be accomplished best by unplugging the condensing unit. Then remove the stored food and place either an electric space heater or a pail or two of hot water in the cabinet. With the cabinet closed, the ice will soon drop water from the evaporator surface and will be easy to remove. These freezers have a drain, which makes removing the moisture from the cabinet quite easy. Remaining moisture must be wiped out of the cabinet. Cabinets are available in various capacities. Height and width are quite uniform. However, the length will vary with the capacity of the freezer k.

II. EXPERIMENTAL SETUP

In vapor compression refrigerating system basically there are two heat exchangers. One is to absorb the heat which is done by evaporator and another is to remove heat absorbed by refrigerant in the evaporator and the heat of compression added in the compressor and condenses it back to liquid which is done by condenser. This project focuses on heat rejection in the condenser this is only possible either by providing a fan. The rate of heat rejection in the condenser depends upon the length of Bundy copper coil attached to the condenser.

This project investigated the performance of condenser using Bundy Tube condenser in the present 425 L chest freezer.

III. BUNDY TUBE CONDENSER COIL

It is a type of double walled low – carbon steel tube manufactured by rolling a copper coated steel strip through 720 degrees resistance brazing. The performance of the condenser will also help to increase COP of the system as the sub cooling region.

Specifications of selected Domestic refrigerator
Refrigerant used: R-134a
Capacity of The Refrigerator: 425 liters
Compressor capacity: 933Btu/hr =273.435W

Bundy Tube Condenser Sizes
Length - 97.44 feet = 29.71 m
Diameter - 6.35*0.7mm

Evaporator
Length - 7.62 m
Diameter - 6.4 mm

Capillary
Length - 2.428 m
Diameter - 0.8 mm

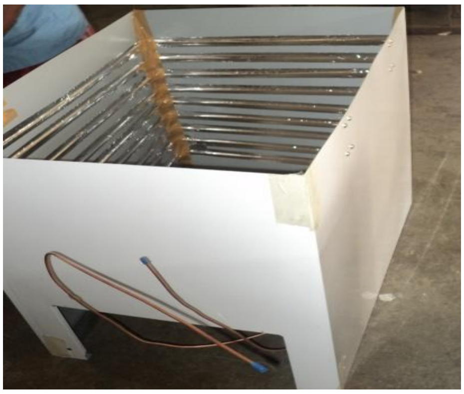

Fig. 2Bundy Coil Skin condenser arrangement

Fig.3 425 LITRES CAPACITY FREEZER OUTER

Fig.4 Freezer connected with Pressure gauges and Thermocouples

IV. CALCULATIONS

EXISTING SYSTEM

Compressor Suction Temperature, $T_1 = 5^oC$
Compressor Discharge Temperature, $T_2 = 82.2\ ^oC$
Condensing Temperature, $T_3 = 42.8\ ^oC$
Evaporator Temperature, $T_4 = -19\ ^oC$

Pressures

Suction Pressure, $P_1 = 1.5$ bar
Discharge Pressure, $P_2 = 12.5$ bar
Condenser pressure, $P_3 = 12.2$ bar
Evaporator pressure, $P_4 = 1.65$ bar

Enthalpies From P-H chart for R-134a, enthalpy values at state points1, 2, 3, and 4.

h_1 = 610 kJ/kg
h_2 = 660 kJ/kg
h_3 = 465 kJ/kg
h_4 = 465 kJ/kg

V. OPTIMUM DESIGN OF A CONDENSER COIL

The function of the condenser is to remove heat from the superheated high pressure refrigerant vapor and to condense the vapor into a sub cooled high pressure refrigerant. Since the condensing unit capacity depends on the capacity of the compressor, methods of designing condensing units are based on the saturated suction temperature and on the quantity and temperature of the condensing medium. Since the heat given up by the refrigerant vapor includes both the heat absorbed in the evaporator and the heat of compression, the heat load on the condenser always exceeds that on the evaporator an amount equal to refrigeration load.

Let U = overall heat transfer coefficient, W/ m^2 K
X_a = thickness of inner wall, $(0.7/3)x10^{-3}$ m
X_i = thickness of insulation, 0.04 m
K_c = thermal conductivity of copper, 386 W/m K
K_l = thermal conductivity of low carbon steel, 36.3 W/m K
K_i = thermal conductivity of insulation, 0.025 W/m K
h_o = outside heat transfer coefficient, 20 W/ m^2 K
h_i = inside heat transfer coefficient, 9 W/ m^2 K

Optimization of length of condenser coil

Q=U x A x LMTD
Let the diameter of coil=d=3/16"=0.00775 m
Properties of Bundy type material:
h_O =20 W/m²K
h_i =9 W/m²k
$x_1 = x_2 = x_3 = (0.7/3) \times 10^{-3}$ m
$x_{insul} = 0.04$ m

$k_1 = k_3 = 386$ W/m k
$k_2 = 36.3$ W/mk
$k_{insul} = 0.025$ W/mk

For air – cooled condensers, the quantity of air passing over the condenser is fixed by the fan selection, the only variable determining the capacity of the condensing unit, other than the suction temperature, is the ambient air temperature. The surface area and the value of U, and the capacity of condenser depend on the mean effective temperature difference between the air and the condensing refrigerant. The coils are made of double walled low carbon steel tube by rolling a copper coated steel strip.

Hence, the overall heat transfer coefficient of the Bundy Coil,

$$U= [1/(1/h_O)+(1/h_i)+(x_1/k_1)+(x_1/k_2)+(x_3/k_3)+(x_{insul}/k_{insul})]$$

$$U= [1/ (1/20) + (1/9) + (2.3x10^{-4}/386) + (2.3x10^{-4}/ 36.3) + (2.3x10^{-4}/386) + (0.04/0.025)]$$

$U=8.189$ W/m²k

From Table .1,

load (Q)=103 W
Condenser inlet Temperature $= T_1=83°C=356K$
Condenser outlet Temperature $= T_2=48.5°C=321.5K$
Condenser coil Temperature $= T_C=43°C=316K$
$td_1=T_1-T_C=40K$
$td_2=T_2-T_C=5.5K$
$LMTD = (td_1-td_2) / \log (td_1/td_2)$
$=17.387$ K

we have,
Area (A) = Q / (U x LMTD) = (3.14 x d x L)
=0.72 m²
we know that $A = \pi dL \Rightarrow L = A/ \pi d$
= 0.72 / (3.14x0.00775) m
= 29.71m

Hence,
Optimized length of Evaporator coil= L=A / (3.14 x d)
L= 97.44 feet = 29.71 m

Calculation Performance Parameters

Net Refrigerating Effect (NRE) = h_1-h_4
= 610-465 = 145 kJ /kg
Heat of Compression = $h_2- h_1$
=660-610 = 50 kJ/kg
Coefficient of Performance (COP) = NRE/Heat of Compression
= 145/50 =2.9

VI. GRAPHS

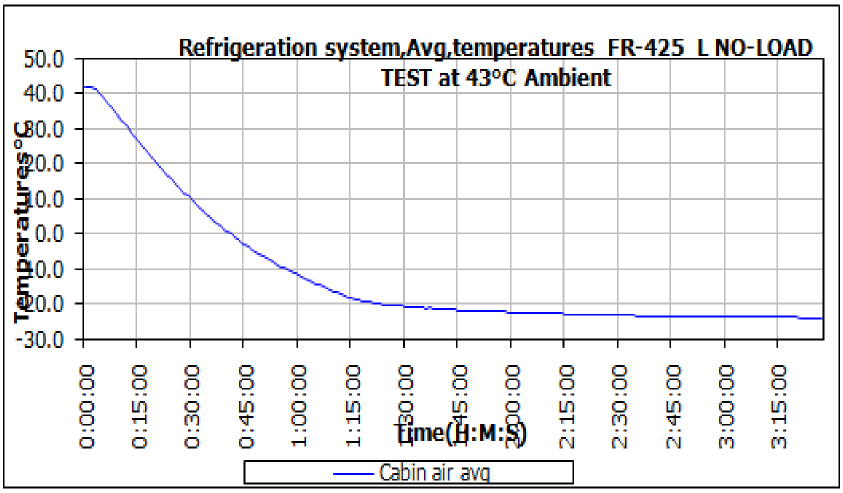

Graph.1. Temperature (Cabin air avg.) Vs Time

From the graph.1 it is observed that the cabin air average temperature decreased linearly with time in the first 1 hour, decreased till 1 hour 45 minutes and there after the variation is almost constant with time. The temperature at the end of the test is found to be -22.5^{0}C.

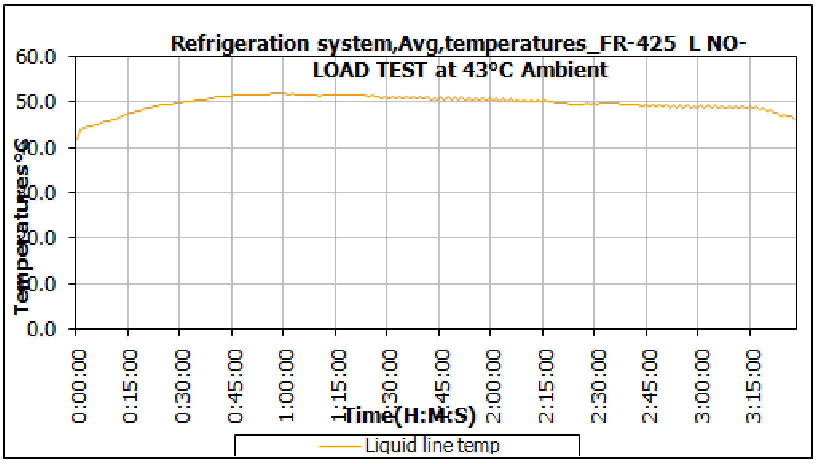

Graph.2. Temperature (Liquid line) Vs Time

From the graph.2 it is observed that the liquid line temperature increased initially in the first hour of operation there after the variation is almost constant till 3hours 15 minutes, and then sloped downwards at the end. The temperature at the end of the test is found to be 48.5^{0}C.

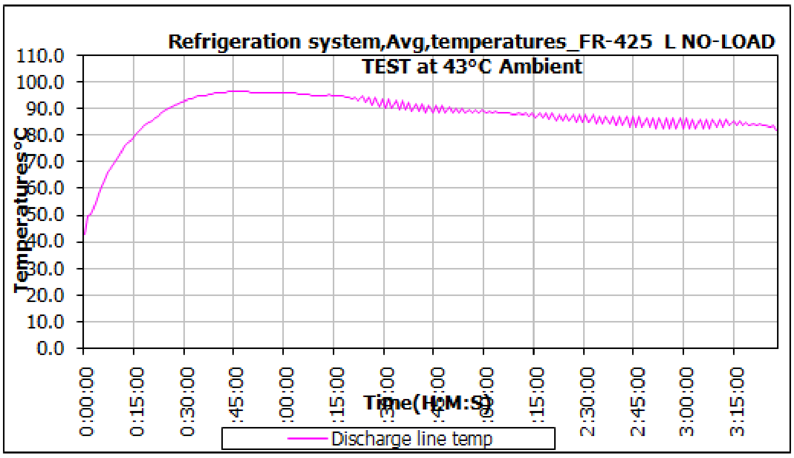

Graph.3. Temperature Vs Discharge line temperature

From the graph.3 it is observed that the discharge line temperature increased with time till 45 minutes decreased slightly and there after the variation is zigzag sloping slightly downwards. The temperature at the end of the test is found to be 82.2^{0}C.

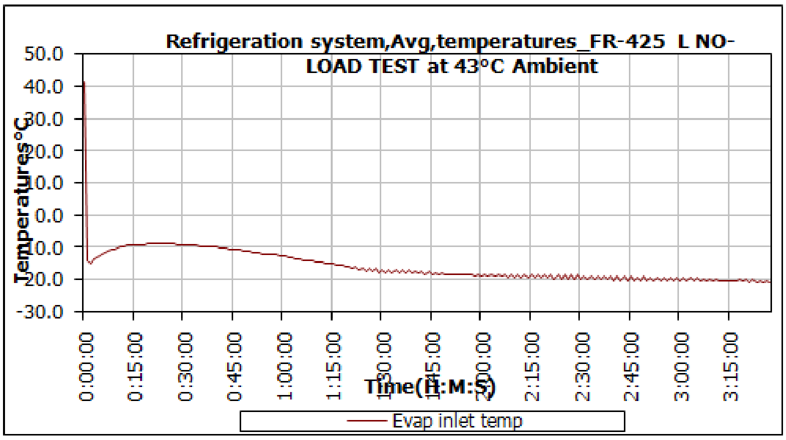

Graph.4. Temperature Vs Evaporator inlet temperature

From the graph.4 it is observed that the Evaporator inlet temperature decreased suddenly initially, then the variation is curvy till 1hour 30 minutes and there after the variation is zigzag. The temperature at the end of the test is found to be -19^{0}C.

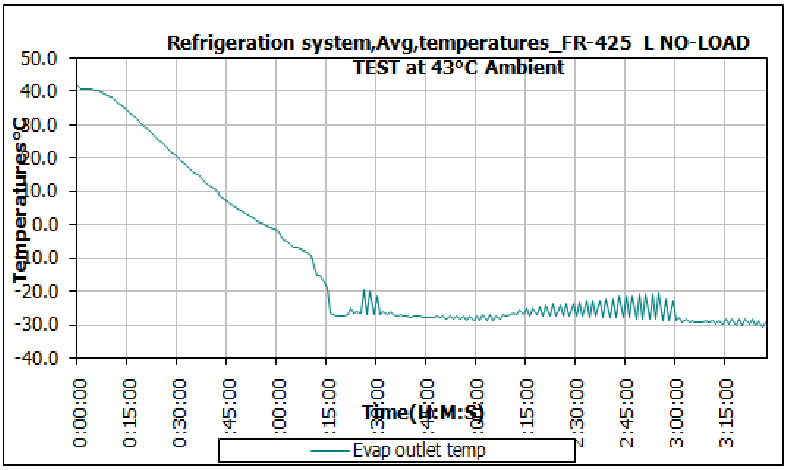

Graph.5. Temperature Vs Evaporator outlet temperature

From the graph.5 it is observed that the evaporator outlet temperature decreased initially till 1hour 15 minutes, and there after the variation is zigzag with slight change in temperature. The temperature at the end of the test is found to be 5^{0}C.

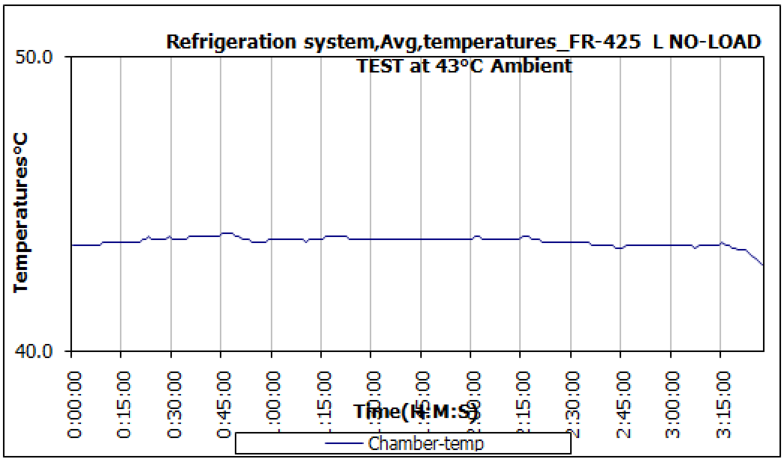

Graph.6. Temperature Vs Chamber Temperature

From the graph.6 it is observed that the variation of chamber temperature slightly deviated from the constant relationship with time. The temperature at the end of the test is found to be 44^{0}C.

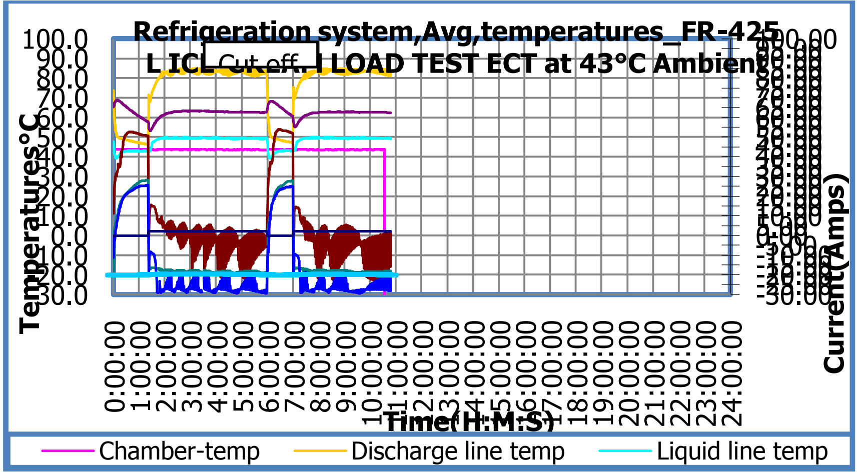

Graph.7. for Load Test

VII. RESULTS AND DISCUSSIONS

- From the graph.7 the cut off thermostat position of 2.5, it is observed that compressor shell temperature decreased initially and there after remain constant with time, the variation is found to be repeatable. The cycle time is found to be 6 hours.
- From the graph.7 the cut off thermostat position of 2.5, it is observed that discharge line temperature decreased in the first hour of operation, increased till 2hours, and then remained constant with time till 6 hours. The variation is found to be repeatable. The temperature at the end of the cycle time is 83^0C.
- From the graph.7 the cut off thermostat position of 2.5, it is observed that evaporator outlet temperature increased initially till 1 hour, decreased up to 2 hours and there after the variation is wavy and the cycle is repeatable.
- From the graph.7 the cut off thermostat position of 2.5, it is observed that evaporator inlet temperature increased in first hour, decreased suddenly and then remained constant with time there after the variation is repeatable.

Table1. Results

Properties	R-134a
ODP	0
GWP	0.27
Outer cabinet	Cold rolled carbon steel(thkn=0.40mm)
Insulation	Polyol, isocyanate and cyclopentane
Condenser Fan	Plastic
Condenser coil	Bundy Tube
During power-off / Breakdown condition	8 hrs
Net refrigerating effect	145kJ/kg
Work done	50kJ/kg
COP	2.9

VIII. CONCLUSIONS

In the design of the refrigeration system for a freezer, rigid standards are maintained so as not to have any compromise with the quality and flexibility of the system. The system design is in such a way that it has optimum efficiency with moderate costs. Hence, efficient equipment design will result in conservation of energy, which reduces the running cost. Placement of the freezer also plays a major role in reducing the load on the system. The more it is exposed to the higher temperature the more will be the capacity requirement and power requirement.

On low temperature applications like Freezers, Skin type Condensers is often preferred. In this design the outer causing of the cabinet is equipped with a tube on the inside surface, so that the outer causing act as plate type heat transfer surface. Until now copper tube is used in Skin Condenser, copper has excellent heat transfer properties, but as the length increases the cost of the copper tube also increases. There by the vapor compression refrigeration system cost also increases.

The experimental investigation on Bundy Condenser Coil used in Skin Condenser for a Deep Freezer of 425 ltrs. capacity is done. Through the experiments, the length of the condenser coil is optimized. R–134A is used as refrigerant for the proposed investigation and the results are tabulated in table1. Experimental work is done using Bundy Tube for optimizing Skin Condenser.

The results infer that

1. COP of the proposed system decreased by 0.1(3.3%) compared to the existing system for optimized length.
2. Also cost of the Bundy Tube is less than the cost of copper coil.

REFERENCES

[1] Akintunde, M.A. 2004b. Experimental Investigation of the performance of Vapor Compression Refrigeration Systems. Federal University of Technology, Akure, Nigeria.

[2] Performance enhancement of a household refrigerator by addition of latent heat storage International Journal of Refrigeration, Volume 31, Issue 5, August 2008, *Pages 892-901* Azzouz, K.; Leducq, D.; Gobin, D.

[3] Seshimo Y, Fujii M. An experimental study of the performance of plate fin and tube heat exchangers at low Reynolds numbers. ASME/JSME Thermal Engineering. Proceedings, ASME 1991; 4:449–54.

[4] Refrigeration and air conditioning by C P Arora

[5] Refrigeration and air conditioning by R S Khurmi and J K Guptha

[6] Refrigeration and Air Conditioning by MANOHAR PRASAD.

[7] Refrigeration and Air Conditioning by C.P.ARORA.

[8] Basic Refrigeration and Air Conditioning by P.N.ANANTHANARAYANA, Tata Mc.Grew Hill Publishing Company Ltd.,

[9] Refrigeration and Air Conditioning by P.L.BALLENY.

[10] Refrigeration and Air Conditioning by R.S.KHURMI, S.Chand & Company Ltd.

[11] Refrigeration and Air Conditioning by ARORA AND DOMKUNDWAR (Dhanapat Rai & Co).

[12] Refrigeration and Air Conditioning by Prof.P.S.DESAI.

[13] Refrigeration and Air Conditioning by RAMESH CHANDRA ARORA

[14] Rockwell Manual

OPEN ACCESS

International
Journal
Of Modern Engineering Research (IJMER)

Integration by Parts for D_K Integral

T. K. Garai[1], S. Ray[2]

[1]Department of Mathematics, Raghunathpur College, Raghunathpur-723133, Purulia, West Bengal, India
[2]Department of Mathematics, Siksha Bhavan, Visva-Bharati, Santiniketan West Bengal,India

ABSTRACT: *In this paper we have defined* D_k *integral and proved the integration by parts formula.*

Key Words and phrases: Absolutely Continuous function, Generalised absolutely continuous function, Denjoy integration. 2000 Mathematics subject Classification: Primary 26A24 Secondary 26A21, 26A48, 44A10.

I. PRELIMINERIES

Let f be a real valued function defined on a set E. Let $c,d \in E, c<d$, and $k \geq 2$ the oscillation of f on $[c,d] \cap E$ of order k is defined to be

$$O_k(f,[c,d]\cap E) = \sup\left|(d-c)[f,c,x_1,x_2,\ldots x_{k-1},d]\right|$$

where the sup is taken over all points $x_1,x_2,\ldots x_{k-1}$ on $[c,d]\cap E$ and $[f,c,x_1,\ldots,x_{k-1},d]$ represents the k^{th} order divided difference of f at the $k+1$ points $c,x_1,\ldots,x_{k-1},d$.

The weak variation of f of order k is defined as follows,

$$V_k(f,E) = \sup\sum_i O_k(f,[c_i,d_i]\cap E)$$

where the sup is taken over all sequences $\{(c_i,d_i)\}$ of non overlapping intervals with end points on E. Then f is said to be of k^{th} variation in the wide sense if $V_k(f,E)<\infty$ and it is written as $f \in BV_k(E)$. The function f is said to be k^{th} absolutely continuous on E if for any $\varepsilon>0$ there is $\delta>0$ such that for every sequence of non overlapping intervals (c_i,d_i) with end points on E and with $\sum_i(d_i-c_i)<\delta$ we have $\sum_i O_k(f,[c_i,d_i]\cap E)<\varepsilon$ and we write it as $f\in AC_k(E)$.

The function F is said to be generalised absolutely k^{th} continuous (resp. of generalised bounded k^{th} variation) on E if $E=\bigcup E_i$ where each E_i is closed and $f\in AC_k(E_i)$ (resp. $f\in BV_k(E_i)$ for each i and we write it as $f\in AC_kG(E)$ (resp. $f\in BV_kG(E)$)

II. AUXILIARY RESULT

Following result will be needed which are proved in [2]

Lemma 2.1 *Let E be a closed set. Then* $f\in AC_kG(E)$ *(resp.* $f\in BV_kG(E)$) *if and only if every closed subset of E has a portion on which f is* AC_k*(resp.*BV_k*.)*

Lemma 2.2 *The classes of functions* $AC_k(E), BV_k(E), AC_kG(E), BV_kG(E)$ *are all linear spaces.*

Theorem 2.3 *If* $f\in BV_k(E_i)$ *then* $f_{ap}^{(k)}$ *exists finitely a.e on E, where* $f_{ap}^{(k)}$ *is repeated approximate derivative of* f.

Theorem 2.4 *Let* $k\geq 2$ *and* $f:[a,b]\to R$ *be such that*

---

[1] The research work of first author is financially supported by UGC, MRP.
[2] Corresponding auther.

i) $f \in AC_k G([a,b]) \bigcap D[a,b]$

ii) $f_{ap}^{(k-2)}$ *exists in [a,b]*

iii) if for r=0,1,...,k-2 and $x \in (a,b)$ *one of* $(f_{ap}^{(r)})_{+}'(x)$ *and* $(f_{ap}^{(r)})_{-}'(x)$ *exists then* $(f_{ap}^{(r)})'(x)$ *exists.(this condition is weaker than the smoothness condition of* $f_{ap}^{(r)}$*).*

iv) $f_{ap}^{(k)} \geq 0$ *a.e*

Then $f^{(k-1)}$ *exists and is nondecreasing in [a,b] and.* $f^{(k-1)} \in AC_1([a,b])$

The following theorem is proved for *k*=2 in Theorem-4 of [2], and similarly can be proved any *k*.

Theorem 2.5 *Let F and G be* AC_k *(resp.*BV_k*) on E . Then FG is* AC_k *(resp.*BV_k*) on E. Then FG is* AC_k *(resp.*BV_k*) on E .*

Corollary 2.6 *If F and G are* $AC_k G$ *(resp.*$BV_k G$*) on [a,b] then FG is so in [a,b]*

The proof is similar of the corollary of Theorem-4 of [2].

III. THE D_k INTEGRAL

A function $f:[a,b] \to R$ is said to be D_k integrable on [*a*,*b*] if there exists a continuous function $\phi:[a,b] \to R$ such that

i) $f \in AC_k G([a,b])$

ii) $\phi_{ap}^{(k-2)}$ exists in [*a*,*b*]

iii) $\phi_{ap}^{(r)}$ is smooth in (*a*,*b*) for *r*=0,1,...,*k*-2.

iv) $\phi_{ap}^{(k-1),+}(a)$, $\phi_{ap}^{(k-1),-}(b)$ exists and $\phi_{ap}^{(k)} = f$ a.e in [*a*,*b*]. Where $\phi_{ap}^{(k-1),+}(a)$ and $\phi_{ap}^{(k-1),-}(b)$ denote right hand approximate derivative of ϕ at *a* of order *k*-1 and left hand approximate derivative of ϕ at *b* of order *k*-1. (The existence of $\phi_{ap}^{(k)}$ a.e in [*a*,*b*] is guaranteed by Theorem-2.3)

The function ϕ if exists is called k^{th} primitive of *f* on [*a*,*b*]. If $F = \phi_{ap}^{(k-1)}$ we call *F* to be an indefinite D_k integral of *f* and

$$\phi_{ap}^{(k-1),-}(b) - \phi_{ap}^{(k-1),+}(a) = F(b) - F(a)$$

is called the definite D_k integral of *f* over [*a*,*b*]and is denoted by

$$(D_k) \int_a^b f(t)dt.$$

The definite D_k integral is unique by Theorem-2.4. The indefinite D_k integral is unique upto an additive constant and the k^{th} primitive is unique upto an addition of polynomial of degree *k*-1.

Theorem 3.1 *Let f be* D_k *integrable on [a,b] and on [b,c] and let* ϕ *and* ψ *be* k^{th} *primitives of f in [a,b] and [b,c] respectively. If* $\phi^{(k-1),-}(b)$ *and* $\psi^{(k-1),+}(b)$ *exists then f is* D_k *integrable in [a,c] and*

$$(D_k) \int_a^b f + (D_k) \int_b^c f = (D_k) \int_a^c f.$$

Proof: Since $\phi_{ap}^{(k-1),-}(b)$ and $\psi_{ap}^{(k-1),+}(b)$ exists, the previous derivative exists in some left and right neighbourhood of b . Let

$$H(x) = \begin{cases} \phi(x)+\psi(b)+(x-b)\psi^{(1),+}(b)+\ldots+\dfrac{(x-b)^{(k-1)(}}{(k-1)!}(x-b)\psi^{(k-1),+}(b) if, x\in[a,b], \\ \psi(x)+\phi(b)+(x-b)\phi^{(1),-}(b)+\ldots+\dfrac{(x-b)^{(k-1)(}}{(k-1)!}(x-b)\phi^{(k-1),-}(b) if, x\in[b,c]. \end{cases}$$

Then *H* is continuous in [a,c]. We show that *H* is the k^th primitive of *f* in [a,c]. Clearly $H \in AC_k G([a,c])$. Also for $0 \le r \le k-2,$

$$H_{ap}^{(r)}(x) = \begin{cases} \phi_{ap}^{(r)}(x)+\psi^{(r),+}(b)+(x-b)\psi^{(r+1),+}(b)+\ldots+\dfrac{(x-b)^{(k-r-1)}}{(k-r-1)!}\psi^{(k-1),+}(b), if, x\in[a,b), \\ \psi_{ap}^{(r)}(x)+\phi^{(r),-}(b)+(x-b)\phi^{(r+1),-}(b)+\ldots+\dfrac{(x-b)^{(k-r-1)}}{(k-r-1)!}\phi^{(k-1),-}(b), if, x\in(b,c], \\ \psi^{(r),+}(b)+\phi^{(r),-}(b), if, x=b \end{cases}$$

And hence $H_{ap}^{(k-2)}$ exists in [a,c]. We are to show that $H_{ap}^{(r)}$ is smooth at *b* for $0 \le r \le k-2.$ Let $h > 0$ and $0 \le r \le k-2.$ Then

$$\frac{H_{ap}^{(r)}(b+h)+H_{ap}^{(r)}(b-h)-2H_{ap}^{(r)}(b)}{h} = \frac{H_{ap}^{(r)}(b+h)-H_{ap}^{(r)}(b)}{h} + \frac{H_{ap}^{(r)}(b-h)-H_{ap}^{(r)}(b)}{h}$$

$$= \frac{\psi_{ap}^{(r)}(b+h)-\psi^{(r),+}(b)+h\phi^{(r+1),-}(b)}{h} + \frac{\phi_{ap}^{(r)}(b-h)-\phi^{(r),-}(b)-h\psi^{(r+1),+}(b)}{h} + O(h)$$

The first term tends to $\phi^{(r+1),-}(b)+\psi^{(r+1),+}(b)$ and the second term tends to $-\phi^{(r+1),-}(b)-\psi^{(r+1),+}(b)$ as $h \to 0.$ So $H_{ap}^{(r)}$ is smooth at b for $0 \le r \le k-2.$ Hence $H_{ap}^{(r)}(x)$ is smooth on (a,c) for $0 \le r \le k-2.$ The proof of other properties of k^th primitive are easy. Hence H is the k^th primitive of *f* on [a,c]. So *f* is D_k integrable on [a,c]. Also

$$\begin{aligned} (D_k)\int_a^c f &= H_{ap}^{(k-1),-}(c) - H_{ap}^{(k-1),-}(a) \\ &= \{\phi^{(k-1),-}(b)+\psi^{(k-1),-}(c)\} - \{\phi^{(k-1),+}(a)+\psi^{(k-1),+}(b)\} \\ &= \{\phi^{(k-1),-}(b)-\phi^{(k-1),+}(a)\} + \{\psi^{(k-1),-}(c)-\psi^{(k-1),+}(b)\} \\ &= (D_k)\int_a^b f + (D_k)\int_b^c f \end{aligned}$$

Theorem 3.2 *Let f be* D_k *integrable in [a,b] and let a<c<b. Let* ϕ *the* k^{th} *primitive of f in [a,b]. If* $\phi_{ap}^{(k-1)}(c)$ *exists then f is* D_k *integrable on [a,c] and on [c,b] and*

$$(D_k)\int_a^b f + (D_k)\int_b^c f = (D_k)\int_a^c f.$$

The proof is immediate.

Theorem 3.3 *Let f and g be* D_k *integrable in [a,b] and* α, β *are constants then* $\alpha f + \beta g$ *is* D_k *integrable in [a,b] and*

$$(D_k)\int_a^b (\alpha f + \beta g) = \alpha (D_k)\int_a^b f + \beta (D_k)\int_a^b g$$

The proof follows from the definition of the integral and Lemma 2.2.

Theorem 3.4 *If f be D_k integrable on [a,b], then f is measurable and finite a.e on [a,b].*

Proof: Since *f* is D_k integrable on [a,b], there is a continuous function $\phi \in AC_kG([a,b])$ such that $\phi_{ap}^{(r)}$ is smooth for $r = 1,2,...k-2$ and $\phi_{ap}^{(r)} = f, a.e$ on [a,b]. Let [a,b]=$\bigcup E_n$, where E_n is closed and ϕ is AC_k on E_n for each n. Let $E_n = P_n \cap D_n$ where P_n is perfect and D_n is countable. Since $\phi \in AC_kG(E_n)$, $\phi \in AC_kG(D_n)$ and so by Theorem-6(i) of [3], $\phi^{(k-1)}$ is AC_1 on P_n where the derivative $\phi^{(k-1)}$ is taken with respect to P_n . Let $\psi_n(x) = \phi^{(k-1)}(x)$ for $x \in P_n$ and ψ_n be linear in the closure of all intervals contiguous to P_n . Then $\psi_n \in BV_1[a,b]$ and so ψ_n' exists *a.e* on [a,b]. Also $f = \phi_{ap}^{(k)}(x) = \psi_n'(x)$ *a.e* in E_n . Since derivative of a function of bounded variation is finite *a.e* and measurable, *f* is finite *a.e* and is measurable on E_n for each *n*. The rest is clear.

Theorem 3.5 *If f is D_k integrable and f≥0 in [a,b], then f is Lebesgue integrable and the integrals are equal.*

Proof: Let ϕ be the k^th^ primitive of *f*. So $\phi_{ap}^{(k)} = f \geq 0$ *a.e* in [a,b]. Then from Theorem-2.4, $\phi^{(k-1)}$ exists and is nondecreasing in [a,b] and $\phi^{(k-1)} \in AC_1([a,b])$. Hence $\phi^{(k)}$ exists *a.e* in [a,b] and is Lebesgue integrable in [a,b]. Hence *f* is Lebesgue integrable in [a,b].

Theorem 3.6 *(Integration by parts). Let $f:[a,b] \to R$ is D_k integrable in[a,b], F be its indefinite D_k integral and F is D^* integrable. Let $G^{(k-1)}$ be absolutely continuous in [a,b], then fG is D_k integrable in [a,b] and*

$$(D_k)\int_a^b fG = [FG]_a^b - (D^*)\int_a^b FG'$$

Proof: Let ϕ be the k^th^ primitive of *f* in [a,b] .Let $\varphi(x) = \phi(x)G(x), x \in [a,b]$. Then since $\phi_{ap}{}^{(r)}$ is smooth for r=0,1,……,k-2 and $G^{(k-1)}$ exists finitely so $\psi_{ap}^{(r)}$ is smooth for r=0,1,…,k-2. Since $G^{(k-1)}$ is absolutely continuous ,G is AC_k in [a,b] and since ϕ is AC_kG in [a,b] . And a.e in [a,b]

$$\psi_{ap}{}^{(r)} = \phi G^{(k)} + {}^kc_1\phi' G^{(k-1)} + ... + k\phi^{(k-1)}G' + \phi_{ap}^{(k)}G$$
$$= \phi G^{(k)} + {}^kc_1\phi' G^{(k-1)} + ... + kFG' + fG$$

So $\phi G^{(k)} + {}^kc_1\phi' G^{(k-1)} + ... + kFG' + fG \text{ } is \text{ } D_k$ integrable in [a,b].

Let $H(x) = \phi G^{(k-1)} + {}^{k-1}c_1\phi' G^{(k-2)} + ... + (k-1)\phi^{(k-2)}G'$

Then in a similar way as that of Theorem-14 of [1] it can be proved that $H \in ACG^*([a,b])$.

Again since $\phi^{(k-1)}$ and $G^{(k)}$ exists a.e in [a,b],we have,

$$H'(x) = \phi G^{(k)} + ({}^{k-1}c_0 + {}^{k-1}c_1)\phi' G^{(k-1)} + ...(k-1)\phi^{(k-1)}G'$$
$$= \phi G^{(k)} + {}^kc_1\phi' G^{(k-1)} + ... + (k-1)FG'$$

So $\phi G^{(k)} + {}^kc_1\phi' G^{(k-1)} + ... + (k-1)FG'$ is D^* integrable in [a,b] and so D_k integrable and H is indefinite D_k integral. Since F is D^* integrable and G' is absolutely continuous in [a,b], FG' is D^* integrable by Theorem2.5(p.246) of [4] and hence FG' is D_k integrable in [a,b]. Again since, $(\phi G^{(k)} + {}^kc_1\phi' G^{(k-1)} + ... + kFG' + fG)$, $(\phi G^{(k)} + {}^kc_1\phi' G^{(k-1)} + ... + (k-1)FG')$ and FG' are D_k integrable, by Theorem3.3, *fG* is D_k integrable in [a,b] and

$$(D_k)\int_a^b fG = (D_k)\int_a^b (\phi G^{(k)} + {}^k c_1 \phi' G^{(k-1)} + \ldots\ldots\ldots + kFG' + fG)$$

$$-(D^*)\int_a^b (\phi G^{(k)} + {}^k c_1 \phi' G^{(k-1)} + \ldots\ldots\ldots + (k-1)FG') - (D^*)\int_a^b FG'$$

$$= [\psi_{ap}^{(k-1)}]_a^b - [H]_a^b - (D^*)\int_a^b FG'$$

$$= [\phi G^{(k-1)} + {}^{k-1} c_1 \phi' G^{(k-2)} + \ldots\ldots\ldots + (k-1)\phi^{(k-2)} G' + FG]_a^b$$

$$-[\phi G^{(k-1)} + {}^{k-1} c_1 \phi' G^{(k-2)} + \ldots\ldots\ldots + (k-1)\phi^{(k-2)} G']_a^b - (D^*)\int_a^b FG'$$

$$= [FG]_a^b - (D^*)\int_a^b FG'$$

REFERENCES

[1.] S.N.Mukhopadhyay and S.K.Mukhopadhyay,"A generalised integral with application to trignometric series". Analysis Math., **22**(1996) 125-146.

[2.] S. N. Mukhopadhyay and S. Ray, "Generalised Absolutely kth Continuous Function". Indian Journal of Mathematics, **Vol 53, No 3**(2011) 459-466.

[3.] S.K.Mukhopadhyay and S.N.Mukhopadhyay,"Functions of bounded kth variation and absolutely kth continuous functions". Bull.Austral.Math.Soc **46**(1992),91-106.

[4.] S.Saks,"Theory of the integral",Dover,Newyork(1937).

International Journal of Modern Engineering Research (IJMER)

Volume : 5 Issue : 1 (Version-3) ISSN : 2249-6645 January- 2015

Contents :

OPEN ACCESS

International
Journal
Of Modern Engineering Research (IJMER)

Spectroscopic and Thermal Characterization of Charge-Transfer Complexes Formed In the Reaction of 2-Amino-6-Ethylpyridine with Π-Electron Acceptors

Adel Mostafa[1], A. A. Bengali[2], Siham Y. AlQaradawi[3]

[1,2,] Department of Chemistry, Texas A&M University at Qatar, P.O.Box 23874, Doha, Qatar.

[3]Department of Chemistry and Earth Sciences, College of Arts and Sciences, Qatar University, P.O Box 2713, Doha, Qatar,

ABSTRACT: *The spectrophotometric characteristics of the solid charge-transfer molecular complexes (CT) formed in the reaction of the electron donor 2-amino-6-ethylpyridine (2A6EPy) with the π-acceptors tetracyanoethylene (TCNE), 2,3-dichloro-5,6-dicyano-1,4-benzoquinone (DDQ) and 2,4,4,6-tetrabromo-2,5-cyclohexadienone (TBCHD) have been studied in chloroform at 25* ^{0}*C. These were investigated through electronic, infrared, mass spectra and thermal studies as well as elemental analysis. The results show that the formed solid CT- complexes have the formulas* $[(2A6EPy)(TCNE)_2]$, $[(2A6EPy)_2(DDQ)]$, $[(2A6EPy)_4(TBCHD)]$ *for 2-amino-6-ethylpyridine in full agreement with the known reaction stoichiometries in solution as well as the elemental measurements. The formation constant* k_{CT}*, molar extinction coefficient* ε_{CT}*, free energy change* ΔG^0 *and CT energy* E_{CT} *have been calculated for the CT- complexes* $[(2A6EPy)(TCNE)_2]$, $[(2A6EPy)_2(DDQ)]$.

Keywords: *DDQ, TCNE, TBCHD, Spectra, Thermal.*

I. INTRODUCTION

The molecular interactions between electron donors and acceptors are generally associated in the formation of intensely colored charge-transfer (CT) complexes which absorb radiation in the visible region [1-8]. The photometric methods used to study these interactions are usually simple and convenient because of the rapid formation of the complexes. The chemical and physical properties of charge-transfer (CT) complexes formed by the reactions of π- and σ- electron acceptors with different donors like amines, crown ethers, polysulfur bases and oxygen-nitrogen mixed bases have been the subject of many studies both in solution and in the solid state [9-13]. It was found that the reaction stoichiometries as well as the structure of these CT-complexes depend strongly on the number of nitrogen donor atoms as well as on their terminal attached groups, hydrogen or donating groups like alkyl or withdrawing atoms like halogens. Electron donating alkyl groups were found to enhance the acceptor: donor stoichiometry. Interestingly, most of the CT- complexes have many applications in chemical analysis like quantitative drug estimation and some complexes have interesting physical properties like electrical conductivities [14-17].

In this paper, we report the formation of three new CT- complexes formed by the reaction of 2-amino-6-ethylpyridine with different types of π-electron acceptors. The π-acceptors are tetracyanoethylene (TCNE), 2,3-dichloro-5,6-dicyano-1,4-benzoquinone (DDQ) and 2,4,4,6-tetrabromo-2,5-cyclohexadienone (TBCHD). All reactions were carried out in $CHCl_3$ as a solvent. The obtained results enabled us to investigate the stoichiometries and structure of these new CT- complexes.

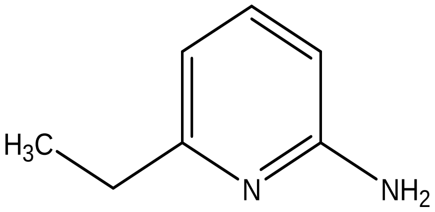

2-Amino-6-ethylpyridine
(2A6EPy)

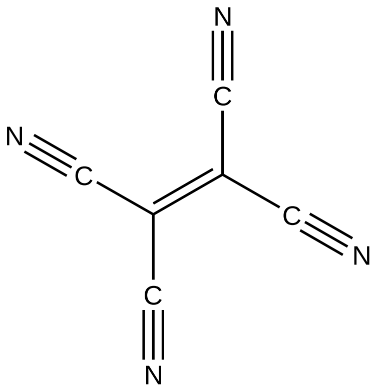

TCNE

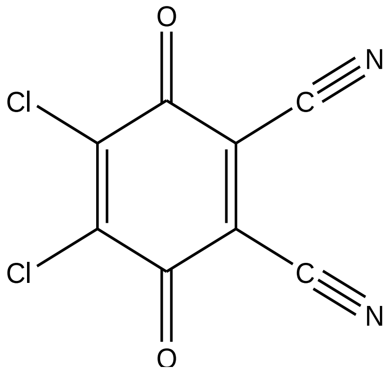

DDQ

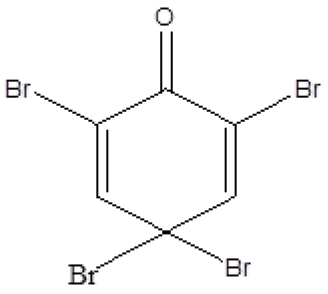

TBCHD

II. EXPERIMENTAL

1.1. Materials

All chemicals used in this study were of analytical reagent grade and obtained from Sigma-Aldrich, USA, and used without further purification.

1.2. Instrumentation

The UV/Vis electronic absorption spectra of the $CHCl_3$ solutions of the solid CT- complexes formed in the reactions of the donor 2-amino-6-ethylpyridine and the acceptors tetracyanoethylene (TCNE), 2,3-dichloro-5,6-dicyano-1,4-benzoquinone (DDQ) and 2,4,4,6-tetrabromo-2,5-cyclohexadienone (TBCHD) as well as the reaction products were checked in the region 320-1100 nm using a lambda 950 Perkin Elmer UV-Vis-NIR spectrometer with quartz cell of 1.0 cm path length. Elemental analysis was done using a Perkin Elmer CHNSO Elemental Analyzer model 2400 series II. The obtained CT – complexes have been checked using Agilent Triple Quad LC MS/MS model 6420.

The infrared spectra of the reactants, (2A6EPy), TCNE, DDQ, and TBCHD and the obtained CT-complexes (KBr pellets) were recorded on Perkin Elmer FTIR spectrometer model Spectrum one.

1.3. Photometric titration

Photometric titration measurements were performed for the reactions between the donor (2A6EPy) and each of the acceptors TCNE DDQ, and TBCHD in $CHCl_3$ at 25 ^{0}C in order to determine the reaction stoichiometries according to a literature method [3, 18]. The measurements were conducted under the conditions of fixed donor (2A6EPy), concentration while those of the acceptors TCNE, DDQ or TBCHD were changed over a wide range, to produce in each case reaction solutions where the molar ratio of donor: acceptor varies from 1: 0.25 to 1: 4. The peak absorbancies of the formed CT- complexes were measured for all solutions in each case and plotted as a function of the acceptor to donor molar ratio.

1.4. Preparation of the solid CT- complexes

The three solid CT- complexes formed in the reaction of (2A6EPy) with each of TCNE, DDQ and TBCHD were prepared in $CHCl_3$ by the drop wise addition of a saturated solution (70 ml) of the donor to a saturated solution (95 ml) of each of the acceptors. In each case the mixing of reactants was associated with a strong change in color. The resulting precipitate in each case was filtered off, washed with minimum amounts of $CHCl_3$ and dried in vacuum over P_2O_5. The complexes were characterized using spectroscopic techniques (FTIR, UV-vis and mass) and by elemental analysis: (theoretical values are shown in brackets):

2-amino-6-ethylpyridine CT complexes: [(2A6EPy)$(TCNE)_2$] dark blue complex (M/W: 378.3g); C, 60.18% (60.27%) H, 2.61% (2.64%); N, 37.11% (37.01%); [$(2A6EPy)_2$(DDQ)] dark brown complex (M/W: 471.29g); C, 56.11% (56.02%); H, 4.21% (4.24%); N, 17.79% (17.82%) and [$(2A6EPy)_4$(TBCHD)] dark brown complex (M/W: 898.26g); C, 45.38% (45.42%); H, 4.71% (4.68%); N, 12.44%(12.47%).

III. RESULTS & DISCUSSION

3.1. Electronic spectra studies

The electronic absorption spectrum of the reaction of tetracyanoethylene (TCNE) with the donor 2A6EPy is shown in Fig.1. While none of the reactant's spectra display any measurable absorption in the region 400 – 650 nm, the resulting CT- complex shows strong absorptions centered on 597, 555 and 524 nm for 2A6EPy-TCNE reaction. These absorptions are associated with the strong change in color observed upon mixing of reactants (dark blue from colorless solution for 2A6EPy-TCNE), and reflect the electronic transitions in the formed CT- complex.

Photometric titration measurements based on these absorptions were performed in order to determine the reaction stoichiometry in $CHCl_3$ (Fig. 2). The results showed that the donor: TCNE molar ratio was found to be 1:2 for the donor. This is in good agreement with the obtained elemental analysis of the solid CT- complex. On the basis of these experimental data, the complex obtained can be formulated as $[(2A6EPy)(TCNE)_2]$.

Interestingly, the reaction stoichiometry using TCNE as a π-acceptor is 1:2 for the donor and the alkyl group (ethyl group at position 6) is enhancing the electron donation in comparison with the reaction stoichiometry of 2-aminopyridine with TCNE which was 1:1 in our previous study [19].

Fig.3 shows the electronic spectra recorded in the region 400 – 1100 nm of the reaction of 2,3-dichloro-5,6-dicyano-1,4-benzoquinone (DDQ) with the donor (2A6EPy). Similar to the reaction with the previous acceptor, a strong change in color is observed upon mixing. A dark brown color indicated the formation of the 2A6EPy-DDQ charge-transfer complex and is associated with the electronic transitions at 716, 567, 501, and 460 nm. Photometric titration measurements were performed for 2A6EPy reaction in $CHCl_3$ as shown in Fig. 4. The results showed that the donor-DDQ molar ratio was 2:1. This is in good agreement with the obtained elemental analysis of the solid CT- complex which accordingly can be formulated as $[(2A6EPy)_2(DDQ)]$.

The reaction stoichiometry using DDQ as a π-acceptor is 2:1 because of the steric hindrance, the donation became less (2: 1) than that in case of 2-aminopyridine with DDQ which was 1:1 in our previous study [19] and the ethyl group in 2A6EPy isn't enhancing the donation as in the previous acceptor TCNE.

Fig.5 shows the electronic spectra recorded in the region 320-500 nm of the reaction of 2,4,4,6-tetrabromo-2,5-cyclohexadienone (TBCHD) with 2A6EPy. A strong change in color is observed upon mixing and a dark brown color indicated the formation of the 2A6EPy-TBCHD charge-transfer complex and is associated with an electronic transitions at 372 nm

The stoichiometry of the charge-transfer complex between 2A6EPy and TBCHD was obtained as 4:1. This was based on the elemental analysis of the isolated solid complex $[(2A6EPy)_4(TBCHD)]$. However, the use of photometric titration to determine the stoichiometry was unsuccessful and resulted in a straight line (Fig.6). Table 1 shows the spectroscopic data of the resulting CT- complexes.

These obtained UV/Vis spectra of the CT- complexes $[(2A6EPy)(TCNE)_2]$, $[(2A6EPy)_2(DDQ)]$ and $[(2A6EPy)_4(TBCHD)$ have clarified that the variation of the CT-absorptions of TCNE, DDQ and TBCHD should be related to the electron affinity of each acceptor with the donor 2A6EPy. These pronounced variations of CT- interaction stoichiometries are relatively complicated and need to be evaluated. It is definitely connected to many factors such as the donor molecular symmetry, the type of electron withdrawing groups or atoms Cl, Br or C≡N as well as the sterric hinderance between reactants. All of these factors are expected to play an important role on the electron donation process from the nitrogen electron pairs of the donor 2A6EPy and the aromatic ring of DDQ and TBCHD acceptors. The aromatic ring in TBCHD has lower electron accepting ability compared with that in DDQ, related to the lower electron withdrawing process of the substituent Br in TBCHD compared with C≡N in DDQ. This certainly, allows stronger electron donation from 2A6EPy base to DDQ compared with that with TBCHD.

3.2. Formation Constant and molar extinction coefficient

The formation constant (K_{CT}) and molar extinction coefficient (ε_{CT}) values for the formed CT-complexes of the donor 2-amino-6-ethylpyridine with the π-acceptors TCNE and DDQ in $CHCl_3$ at 25 ^{0}C were calculated.

The formation constant, K_{CT} ($lmol^{-1}$), and the molar extinction coefficient ε_T ($lmol^{-1}cm^{-1}$) have been calculated for the complexes $[(2A6EPy)(TCNE)_2]$ and $[(2A6EPy)_2(DDQ)]$ using the known [20] equation (1) of 1:2 complexes:

$$\frac{(A_0)^2 D_0 \ell}{A} = \frac{1}{k\varepsilon} + \frac{A_0(A_0 + 4D_0)}{\varepsilon} \qquad (1)$$

Here A_0 and D_0 are the initial concentrations of the acceptors and donor, respectively, while A is the absorbance at the mentioned CT bands and ℓ is the light path length (1cm). The data obtained throughout this calculation are given in Table 2. Plotting the values $(A_0)^2 D_0 \ell$ /A versus $A_0 (A_0 + 4D_0)$ values of equation (1), straight lines were obtained with a slop of 1/ ε_{CT} and intercept of 1/K_{CT} ε_{CT} as shown in Figures 7 and 8.

These complexes show high values of both the formation constant (K_C) and the molar extinction coefficient (ε_{CT}). The obtained values of K_{CT} are 14.51 x 10^5 and 31.39 x10^5 lmol^{-1}for (2A6EPy)(TCNE)$_2$] and [(2A6EPy)$_2$(DDQ)] and their respective values of ε_{CT} are 0.564 x 10^3 and 0.225 x 10^3 lmol^{-1}Cm^{-1}. These values confirm the expected high stabilities of the formed CT- complexes as a result of the expected high donation of 2-amino-6-ethylpyridine. The formation constants are strongly dependent on the nature of the used acceptors including the type of electron withdrawing substituent on it such as cyanide group in DDQ and TCNE. For the system 4:1 we are not aware for the equation to calculate those parameters. Identification of charge transfer bands can be illustrated as follows:

The color: of CT- complexes is reflective of the relative energy balance resulting from the transfer of electronic charge from donor to acceptor.

Solvatochromism: In solution, the transition energy and therefore the complex color varies with variation in solvent permittivity, indicating variation in shifts of electron density as a result of the transition. This distinguishes it from the ππ* transitions on the ligand. Intensity: CT absorptions bands are intense and often lie in the ultraviolet and visible portion of the spectrum.

3.3. Measurement of ΔG^0, E_{CT} and Ip

The free energy change ΔG^0 (cal mol^{-1}) values of the complexes [(2A6EPy)(TCNE)$_2$], and [(2A6EPy)$_2$(DDQ)] were calculated from Gibbs free energy of formation according to the equation (2) [21, 22]:

$$\Delta G^0 = - RT \ln K_{CT} \qquad (2)$$

Where ΔG^0 is the free energy for the formation of the charge transfer complexes; R the gas constant (1.987 cal mol^{-1} ^{0}C); T the temperature in Kelvin; K_{CT} the formation constant of donor-acceptor complexes (l mol^{-1}). The ΔG^0 values of the complexes [(2A6EPy)(TCNE)$_2$], and [(2A6EPy)$_2$(DDQ)] are -8.40 x 10^3 and -8.86 x 10^3 cal mol^{-1} respectively.

The obtained results of ΔG^0 reveal that the CT- complexes formation process is spontaneous. The results of ΔG^0 are generally more negative as the formation constants of the CT- complexes increase. The more negative the value for ΔG^0, the farther to the right the reaction will proceed in order to achieve equilibrium.

The charge - transfer energy E_{CT} of the formed solid CT- complexes is calculated using the following equation (3) [23, 24]:

$$E_{CT}(nm) = \frac{1243.667}{\lambda_{CT}} \qquad (3)$$

Where λ_{CT} is the wavelength of the band of the studied CT-complexes [(2A6EPy)(TCNE)$_2$] and [(2A6EPy)$_2$(DDQ)], The E_{CT} values calculated from equation (3) for both complexes are 2.24 and 1.74 eV respectively.

The ionization potential of the free donor was determined from the CT energies of the CT band of its complexes. In case of the acceptors TCNE and DDQ the relationship becomes the following equation (4) [25]:

$$E_{CT} = Ip - 5.2 + \frac{1.5}{Ip - 5.2} \qquad (4)$$

Where Ip is the ionization potential and E_{CT} is the charge transfer energy of the formed solid CT- complexes. The obtained values of Ip are 6.5 and 6.0 eV for the CT- complexes [(2A6EPy)(TCNE)$_2$] and [(2A6EPy)$_2$(DDQ)] respectively. It has been reported that the ionization potential of the electron donor may be correlated with the charge transfer transition energy of the complex [25].

These results in table 2 (KCT, ε_{CT}, ΔG^0 and E_{CT}) suggest that the solid CT-complexes formed in the reaction of the donor 2A6EPy with the π-acceptors TCNE and DDQ have high CT energy and formation constants K_{CT}. These high values confirm the expected high stabilities of the formed CT- complexes as a result of the expected high donation of 2A6EPy.

3.4. Mass Spectral studies

Mass spectral measurements were performed for the complexes [(2A6EPy)(TCNE)$_2$], [(2A6EPy)$_2$(DDQ)] and [(2A6EPy)$_4$(TBCHD)]. Fig.9 (A) shows the mass spectrum of [(2A6EPy)(TCNE)$_2$] in the region m/z = 100 – 380. The molecular ion M^+ is observed as a short peak at m/z = 377.2 in good agreement with the calculated value for the molecular weight of the CT- complex of 378.3 g. The found difference of about 1.1 between the observed and calculated molecular weight value is acceptable within the allowed experimental errors. The mass spectrum (Fig. 9 A) also shows a number of other peaks; the peak at m/z = 106.1 is for the donor 2A6EPy losing a methyl group (A), the peak at m/z 123.1 is for the mass of the donor (122.17 calculated) which is probably a protonated 2A6EPy. The peak at m/z 187.2 is for the fragment $C_{10}H_{10}N_4$ ($C_{19}H_{10}N_{10}$ / complex formula), the m/z 224.2 is the mass of fragment $C_{12}H_{12}N_5$ and the m/z 256.2 is the mass equivalent to two molecules of the acceptor TCNE (m/z 256.18 calculated) and m/z 315.2 is for the fragment $C_{16}H_{10}N_8$ ($C_{19}H_{10}N_{10}$ / complex formula).

The mass spectrum (Fig.9 B) for the complex [(2A6EPy)$_2$(DDQ)] in the region m/z = 100- 480 is showing the molecular ion M^+ as a short peak at m/z = 470.2.0 very close to the calculated value for the molecular weight of that complex of 471.29 g. The peak at m/z = 106.1 is for the donor 2A6EPy losing a methyl group (A), the peak at m/z 123.1 is for one molecule of donor (122.17 calculated), the peak at m/z 138.1 is for fragment $C_8H_{13}N_2$ ($C_{22}H_{20}N_6Cl_2O_2$ / complex formula), at m/z 200.1 is for the cation of 2,3-dichloro-6-cyano-1,4-benzoquinone (200 calculated) (B) and the peak at m/z 270.2 is for the fragment ($C_{15}H_{20}N_5$).

The mass spectrum (Fig.9 C) for the complex [(2A4EPy)$_2$(TBCHD)] in the region m/z = 100 – 900 is showing the molecular ion M^+ as a medium peak at m/z = 897.1 in a good agreement with the calculated value for the molecular weight of that complex of 898.26 g. The peak at m/z 106.1 is for the donor (2A4EPy) losing a methyl group (A), the peak at m/z 123.1is for one molecule of donor (122.17 calculated) (A), m/z 137.1 is for fragment ($C_8H_{13}N_2$), the peak at m/z 407.1 is for the acceptor cation $[TBCHD]^+$ (C) and m/z 506.9 is for the fragment $C_{28}H_{42}N_8O$ ($C_{34}H_{42}N_8Br_4O$ / complex formula).

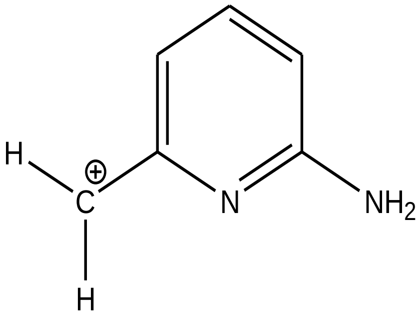

(A), m/z 106

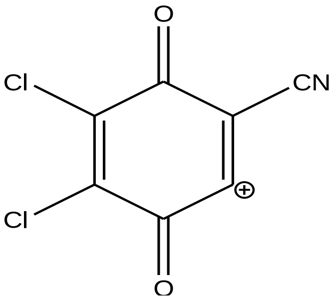

(B), m/z 200

n

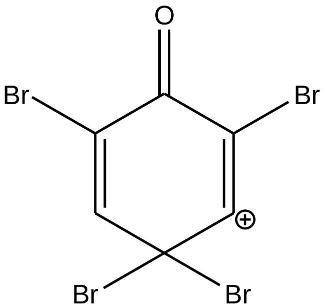

(C), m/z 407

3.5. IR spectral studies

The infrared absorption spectra of the donor 2-amino-6-ethylpyridine and the formed CT-complexes [(2A6EPy)(TCNE)$_2$], [(2A6EPy)$_2$(DDQ)] and [(2A6EPy)$_4$(TBCHD)] are shown in Fig.10. The infrared band assignments are given in Table 2. These assignments are based on the comparison of the spectra of the formed products with the spectra of the free reactants, the donor 2-amino-6-ethylpyridine and the acceptors TCNE, DDQ and TBCHD. Interestingly, the spectra of the reaction products contain the main infrared bands for both the reactants in each case.

This strongly supports the formation of the donor-acceptor CT- complexes. However, the absorptions of 2A6EPy and acceptors in the formed products show same changes in band intensities and in some cases small shifts in the frequency wavenumber values. These changes could be understood on the basis of the expected symmetry and electronic structure modifications in both donor and acceptor units in the formed products compared with those of the free molecules.

For example, the ν(N-H) vibrations of the free 2-amino-6-ethylpyridine in [(2A6EPy)$_2$ (DDQ)] has two strong absorptions at 3327 and 3181 cm^{-1} while in the [(2A6EPy) (TCNE)$_2$], one weak absorption is observed at 3192 cm^{-1} and in [(2A6EPy)$_4$(TBCHD)], two strong absorptions are observed at 3326 and 3181 cm$^{-1.}$

The outlined changes in ν (N-H) upon complexation clearly support the involvement of the nitrogen atoms of the donor 2A6EPy in the CT – interaction process.

It might also indicate here that ν(C≡N) vibrations of the acceptors TCNE and DDQ show some changes particularly in terms of band wavenumber values upon complexation. The ν(C≡N) vibrations for free TCNE are observed as a doublet at 2196 and 2182 cm^{-1} and for free DDQ at 2203 cm^{-1}. These vibrations occur at 2181, 2148 and 2132 cm^{-1} in the spectrum of [(2A6EPy)(TCNE)$_2$] and at 2202 cm^{-1} in the spectrum of [(2A6EPy)$_2$(DDQ)] complexes.

3.6. Thermal studies

Thermal analysis (TG and DTG) were carried out under a nitrogen gas flow (20 ml min^{-1}) within a temperature range 30 – 950 ^{0}C and heating rate 10 ^{0}C min^{-1} to confirm the proposed formula and structure for the obtained CT- complexes. Figs. 11 (A), (B) and (C) show the thermograms of [(2A6EPy)(TCNE)$_2$], [(2A6EPy)$_2$(DDQ)] and [(2A6EPy)$_4$(TBCHD)] respectively. The thermogravimetric data for these complexes are shown in Table 3. The obtained data support the calculated formulas and structures of the formed CT-complexes. The degradation steps and their associated temperatures vary from one complex to another depending on the type of constituents as well as on the stoichiometry in each case. Obviously, these two factors have pronounced effects on the type of bonding, relative complex stabilities and geometries. For the CT-complex [(2A6EPy)(TCNE)$_2$] shown in Fig.11 (A) two degradation steps at temperatures 138 and 224 ^{0}C correspond to the decomposition of the donor [2A6EPy] with a mass loss of 31.8 % very close to the calculated value of 32.3 %. This step is followed by another two degradation steps at temperatures 341 and 549 ^{0}C correspond to the decomposition of (C_5N_3) of mass loss of 28.8 % very close to the calculated value of 27 % and carbon residue of mass 39.4 %, Table 4. Accordingly, a proposed mechanism for the thermal decomposition of [(2A6MPy)(TCNE)$_2$] as follows:

(i) $[(\text{2A6EPy})(\text{TCNE})_2] \xrightarrow{138,\ 224\ ^0\text{C}} (\text{2A6EPy}) + 2[\text{TCNE}]$

(ii) $2[\text{TCNE}] \xrightarrow{341,\ 549\ ^0\text{C}} (C_5N_3)$ + Carbon residue of mass 39.4 %

The second complex [(2A6EPy)$_2$(DDQ)] is shown in Fig.11 (B); at 158 and 262 ^{0}C correspond to the loss of [2(2A6EPy) + CN] with total mass loss of 57.9 % (57.36 % calculated), at 328 and 344 ^{0}C correspond to the loss of (CN + Cl + O) with mass of 16.36 % (16.44 % calculated) and carbon residue of mass 25.74 %; the following proposed mechanism clarifies the thermal decomposition steps:

(i) $[(\text{2A6EPy})_2(\text{DDQ})] \xrightarrow{158,\ 214\ ^0\text{C}} 2(\text{2A6EPy}) + \text{CN} + [\text{DDQ}]$

(ii) $[\text{DDQ}] \xrightarrow{262,328,\ 344\ ^0\text{C}} (\text{CN} + \text{Cl} + \text{O})$ + Carbon residue of mass 25.74 %

The third complex [(2A6EPy)$_4$(TBCHD)] is shown in Figure 11 (C); at 220 and 310 ^{0}C correspond to the loss of the 4[2A6EPy] with a mass of 55.95 % very close to the calculated value of 54.4 %. The acceptor TBCHD decomposed at 366, 400 and 453 ^{0}C correspond to the loss of (2Br + CO) with mass loss of 21.96 % (20.91 % calculated) and remaining carbon residue with mass of 22.1 %; a proposed mechanism for the thermal decomposition of [(2A6EPy)$_4$(TBCHD)] as follows:

(i) $[(\text{2A6EPy})_4(\text{TBCHD})] \xrightarrow{220,\ 310\ ^0\text{C}} 4(\text{2A6EPy}) + [\text{TBCHD}]$

(ii) $[\text{TBCHD}] \xrightarrow{366,\ 400,\ 453\ ^0\text{C}} (2\text{Br} + \text{CO})$ + Carbon residue of mass 22.1 %

IV. CONCLUSION

Charge – transfer interactions between the donor 2-amino-6-ethylpyridine with the π- acceptors TCNE, DDQ and TBCHD were studied in $CHCl_3$ at 25 ^{0}C. We were able to show that the reaction stoichiometry is not the same for π-acceptors, TCNE, DDQ, TBCHD; the resulting CT – complexes were shown to have the formulas: [(2A6EPy)(TCNE)$_2$], [(2A6EPy)$_2$(DDQ)] and [(2A6EPy)$_4$(TBCHD)]. Our obtained results indicate that the nitrogen atom (>NH) of the donor is involved in the complexation with acceptors. Next studies will focus on using different donors with different substituent groups attached to the nitrogen atoms to further investigate the nature of such complexation.

REFERENCES

[1] A.S.N. Murthy, A.P. Bhardwaj, Spetrochim. Acta, 39A, 1983, 415.
[2] J. Casaszar, Acta Phys. Chim., 29, 1998, 34.
[3] R. Foster, Organic Charge -Transfer Complexes, Academic Press, New York, 1969.
[4] E.M. Abd-Alla, A.A.A. Boraei, M.R. Mahmoud, Can. J. Appl. Spectrosc., 39, 1994, 123.
[5] A. Mostafa, H.S. Bazzi, J. Mol. Struct., 983, 2010, 153 – 161.
[6] A. Mostafa, H.S. Bazzi, Spectrochim. Acta Part A, 79, 2011, 1613.
[7] H.S. Bazzi, A. Mostafa, S.Y. AlQaradawi and E.M. Nour, J. Mol. Struct., 842, 2007, 1.
[8] H.S. Bazzi, S.Y. AlQaradawi, A. Mostafa, and E.M. Nour, J. Mol. Struct., 879, 2008, 60.
[9] S.Y. AlQaradawi, A. Mostafa, H.S. Bazzi, J. Mol. Struct., 1037, 2013, 209.
[10] A. Mostafa, Nada El-Ghossein, S.Y. AlQaradawi, Spectrochim. Acta Part A, 118, 2014, 1012
[11] S.Y. AlQaradawi, H. S. Bazzi, A. Mostafa and E. M. Nour, J. Mol. Struct., 998, 2011, 126.
[12] A. Arslan, H. Duymus, Spectrochim. Acta Part A, 67, 2007, 573.
[13] S.Y. AlQaradawi, E.M. Nour, J. Mol. Struct. 794, 2006, 251.
[14] S.Y. AlQaradawi, E.M. Nour, Spectrochim. Acta Part A, 62, 2005, 578.
[15] P.J. Trotter, P.A. White, Appl. Spectrosc. 32, 1978, 323.

[16] H. Salem, J. Pharm. Biomed. Anal., 29, 2002, 527

[17] S. Licht, Sol. Energy Mater. Sol. Cells, 35, 1995, 305

[18] D.A. Skoog, F.J. Holler, T.A. Nieman, Principle of Instrumental Analysis, fifth ed., vol. 347, Saunders College Publishing, New York, 1992.

[19] A. Mostafa, H.S. Bazzi, Spectrochim. Acta Part A, 74, 2009, 180.

[20] A. El-Kourashy, Spectrochim. Acta Part A, 37, 1981, 399,

[21] M. Arslan, H. Duymus, Spectrochim. Acta A, 67, 2007, 573.

[22] A.A.A. Boraei, Spectrochim. Acta Part A, 58 (9), 2002, 1895.

[23] G. Briegleb, Z. Angew. Chem., 72, 1960, 401.

[24] G. Briegleb, Z. Angew. Chem., 76, 1964, 326.

[25] M. Pandeeswaran, K.P. Elango, Spectrochim. Acta Part A, 65, 2006, 1148.

Table 1

Spectroscopic data for the $CHCl_3$ solutions of solid CT- complexes of 2A6EPy with the acceptors TCNE, DDQ and TBCHD

Complex	**Color**	**Absorption ^{a} (nm)**	**Stoichiometry (Donor: acceptor)**
$[(2A6EPy)(TCNE)_2]$	Dark green	597s, 555s, 524sh	1:2
$[(2A6EPy)_2(DDQ)]$	Dark brown	716m, 567sh, 501sh, 460sh	2:1
$[(2A6EPy)_4(TBCHD)]$	Dark brown	372m	4:1

$^{(a)}$The reactants 2A6EPy, TCNE, DDQ and TBCHD have no measurable absorptions in the region of study with used concentrations; m, medium; s, strong; sh, shoulder.

TABLE 2

Infrared wavenumbers (cm^{-1}) and tentative band assignments for 2-amino-6-ethylpyridine (2A6EPy), $[(2A6EPy)(TCNE)_2]$, $[(2A6EPy)_2(DDQ)]$ and $[(2A6EPy)_4(TBCHD$

2A4EPy	**$[(2A4EPy)(TCNE)_2]$**	**$[(2A4EPy)_2(DDQ)]$**	**$[(2A4EPy)_2(TBCHD)]$**	***Assignments***
3460s	3439m	3429m	3412ms	ν (H_2O); KBr
3307ms,3153ms	3367ms	3328s	3296w	ν (NH); 2A4EPy
	3299ms, 3189ms	3180ms	3140m	ν (C-H); 2A4EPy
2967ms	2972m	2969ms	2967w	
	2214s	2201ms		ν (C$\equiv$N); DDQ
	2191w			and TCNE
		1638s	1668s	ν (C=O); DDQ, TBCHD
1613m	1567s	1624s	1628s	ν (C=C); DDQ,
1552s	1544w	1557ms	1563w	TBCHD, 2A4EPy
1393w	1377ms	1394w	1396w	Free and complexed 2A4EPy
1312m	1309ms	1355w	1372m	
1276m	1284ms	1233m	1276m	
1237m	1219s	1233m	1229m	ν (C-N); 2A4EPy
1181m	1153ms	1177m	1179m	
1132m	1153ms	1139w	1149w	ν (C-C); 2A4EPy
1054m	1056m	1069ms	1053m	
997m	985m	996ms	995m	δ (CH)deformation,

m,medium ; s,strong ; w,weak ; br,broad ; ν ,stretching ; δ ,bending

Table 3

Thermal decomposition data[a] for the [(2A6EPy)(TCNE)$_2$], [(2A6EPy)$_2$(DDQ)] and [(2A6EPy)$_4$(TBCHD)] CT-complexes.

mplex	Reaction stoichiometry	DTG max. (°C)	G% mass loss found / calc.	st species
A6EPy)(TCNE)$_2$]	1: 2	138, 224	31.8 / 32.3	6EPy]
		341, 549	28.8 / 27.0	N$_3$ .4 % Carbon sidue
A6EPy)$_2$(DDQ)]	2: 1	158, 262	57.9 / 57.36	vo [2A6EPy] CN (from DDQ) N + Cl + O)
		328, 344	16.36 / 16.44	.74 % Carbon sidue
A6EPy)$_4$(TBCHD)]	4: 1	220, 310	55.95 / 54.4	ur [2A6EPy]
		66, 400, 453	21.96 / 20.91	Br + CO) .1 % Carbon sidue

[a] Thermal measurements were carried out under N_2 flow rate at 20 ml.min^{-1}.

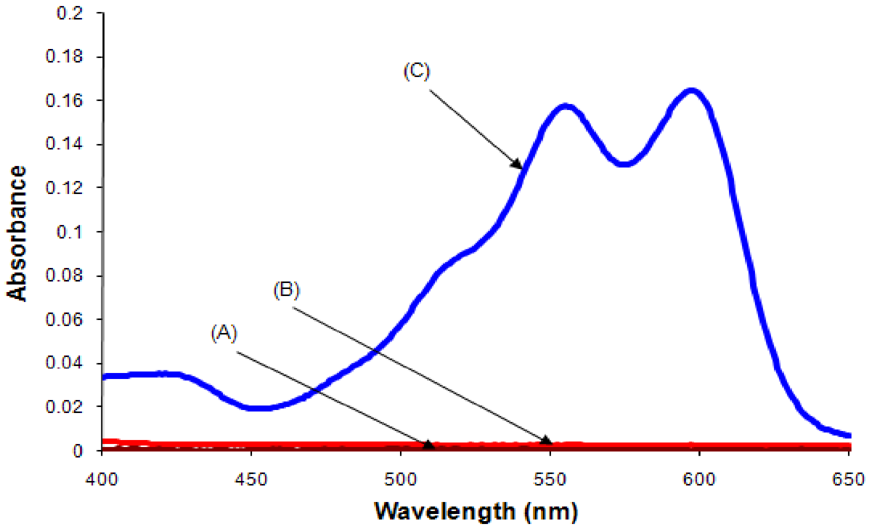

Figure 1. Electronic absorption spectra of 2-amino-6-ethylpyridine -TCNE reaction in $CHCl_3$. (A) [2A6EPy] =1x10^{-3}M; (B) [TCNE] =1x10^{-3}M; (C) 1:2 2A6EPy-TCNE mixture, [2A6EPy] = [TCNE] =1x10^{-3} M.

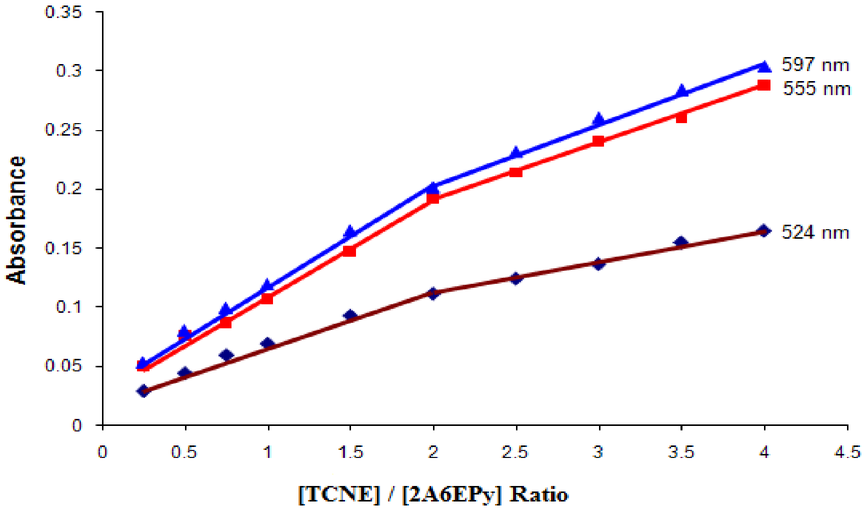

Figure 2. Photometric titration curves for 2A6EPy– TCNE reaction in $CHCl_3$ measured at the 597 nm, 555 nm and 524 nm absorptions.

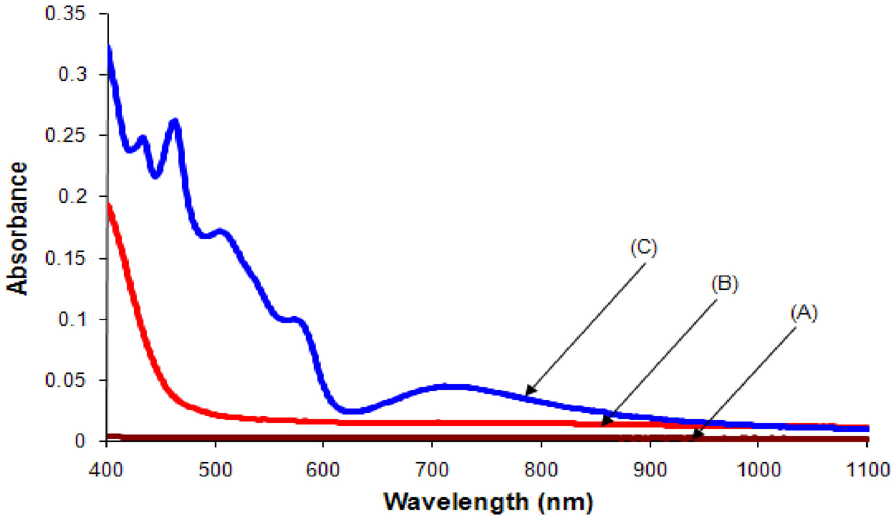

Figure 3. Electronic absorption spectra of 2-amino-6-ethylpyridine - DDQ reaction in $CHCl_3$. (A) [2A6EPy] = 1 $x10^{-3}$M; (B) [DDQ] = 5 $x10^{-3}$M; 2:1 2A6EP - DDQ mixture, [2A6EPy] = 1 $x10^{-3}$ M and [DDQ] = 5 $x10^{-3}$ M.

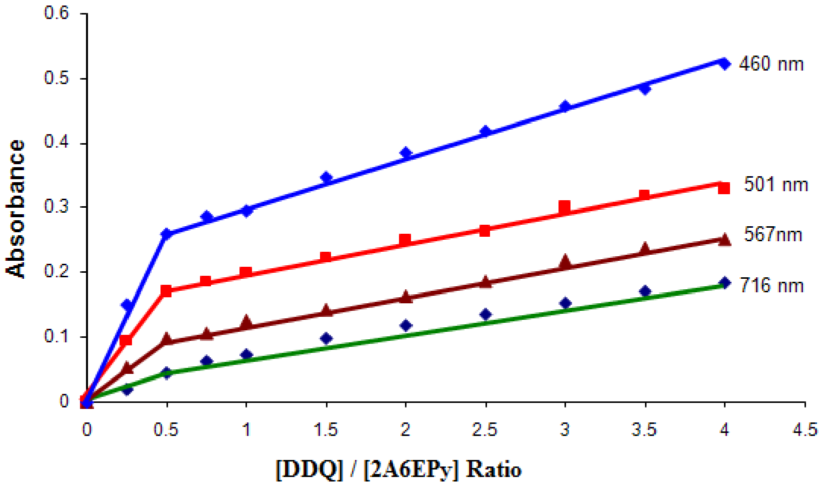

Figure 4. Photometric titration curves for 2A6EPy - DDQ reaction in $CHCl_3$ measured at the 716 nm, 567 nm, 501nm and 460 nm absorptions.

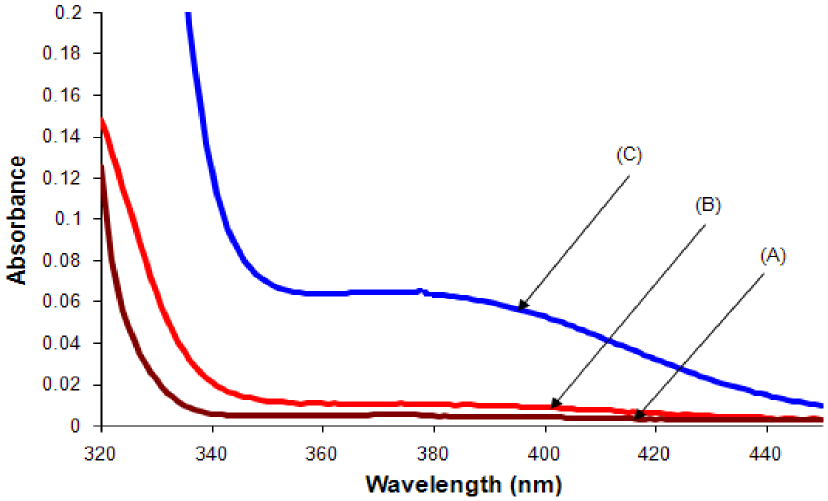

Figure 5. Electronic absorption spectra of 2-amino-6-ethylpyridine -TBCHD reaction in $CHCl_3$. (A) [2A6EPy] = 1 x10^{-3}M; (B) [TBCHD] = 5 x10^{-3}M; 4:1 2A6EPy-TBCHD mixture, [2A6EPy] = 1 x10^{-3} M and [TBCHD] = 5 x10^{-3} M.

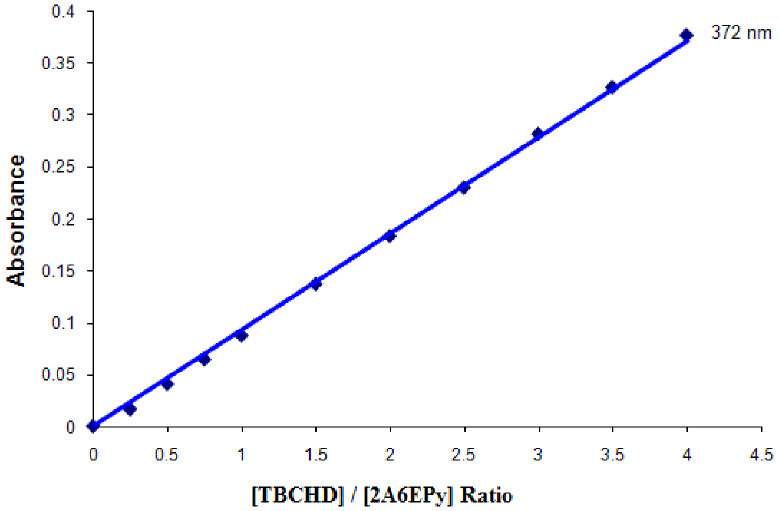

Figure 6. Photometric titration curve for 2A6EPy – TBCHD reaction in $CHCl_3$ measured at the 372 nm absorption.

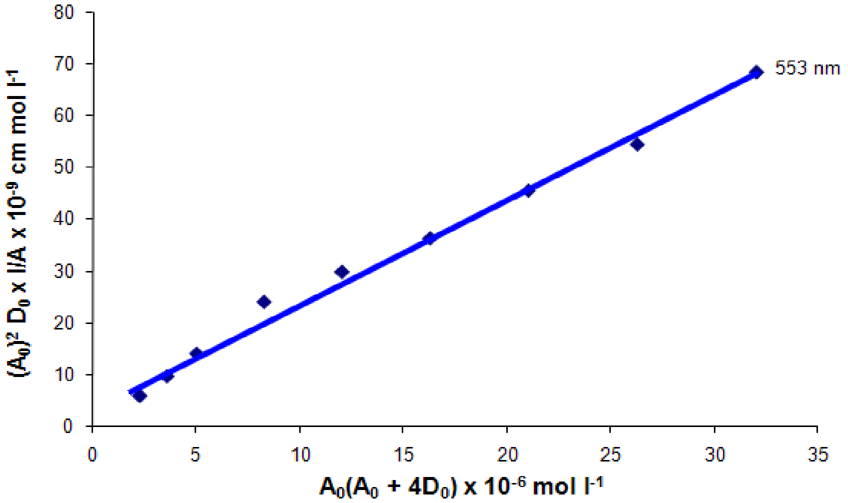

Figure 7. Spectral determination of formation constant and molar extinction coefficient of CT- complex $[(2A6EPy)(TCNE)_2]$ at 553 nm

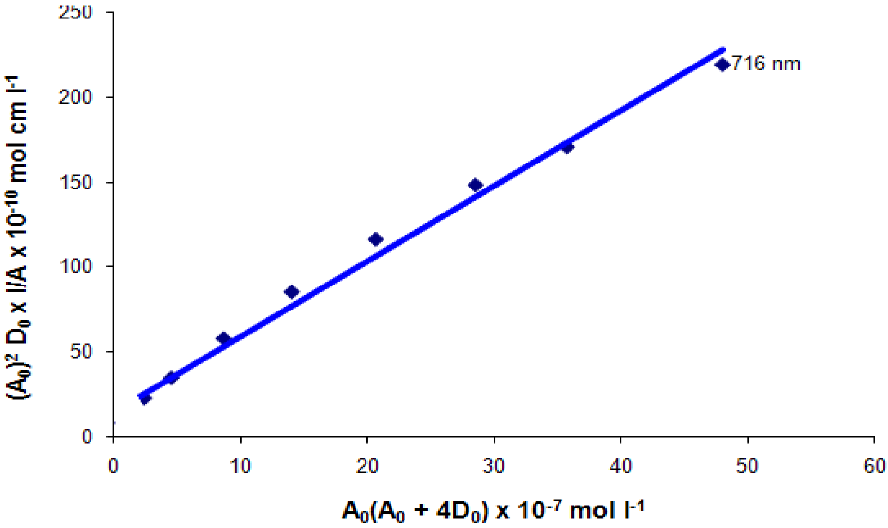

Figure 8. Spectral determination of formation constant and molar extinction coefficient of CT- complex [$(2A6EPy)_2(DDQ)$] at 716 nm.

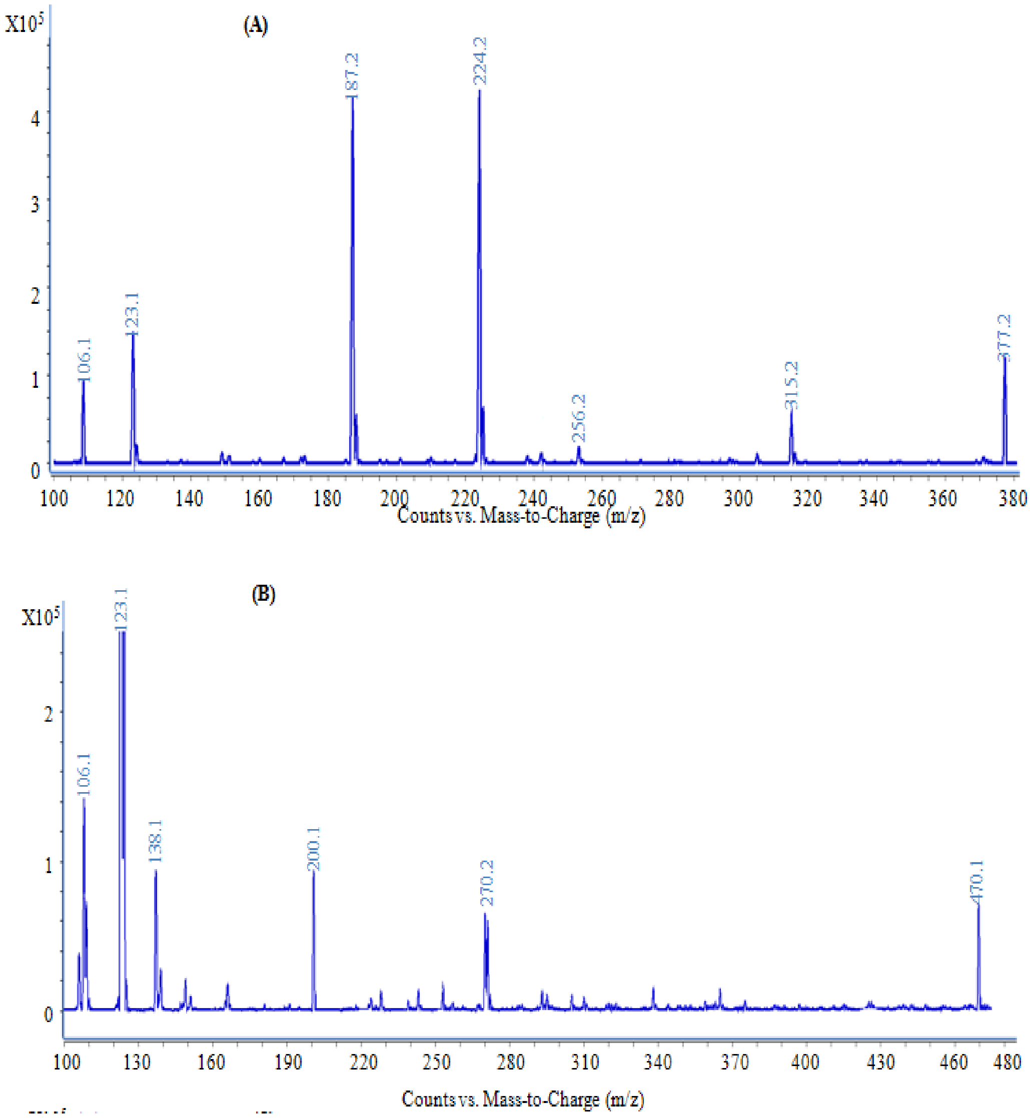

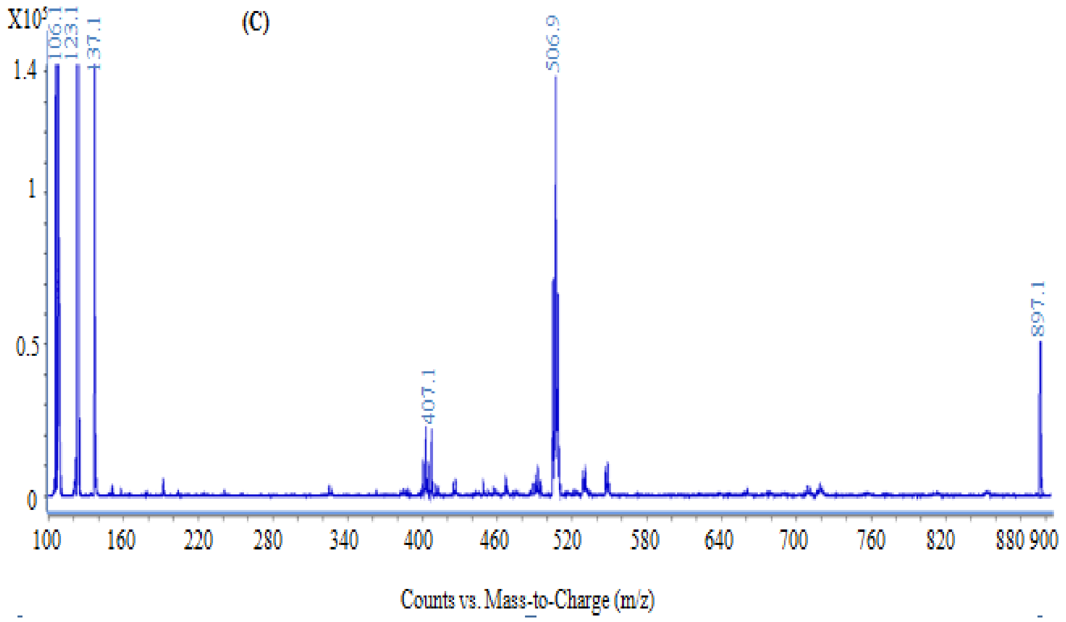

Figure 9. Mass spectra of CT- complexes: (A) $[(2A6EPy)(TCNE)_2]$, (B) $[(2A6EPy)_2(DDQ)]$ And (C) $[(2A6EPy)_4(TBCHD))]$.

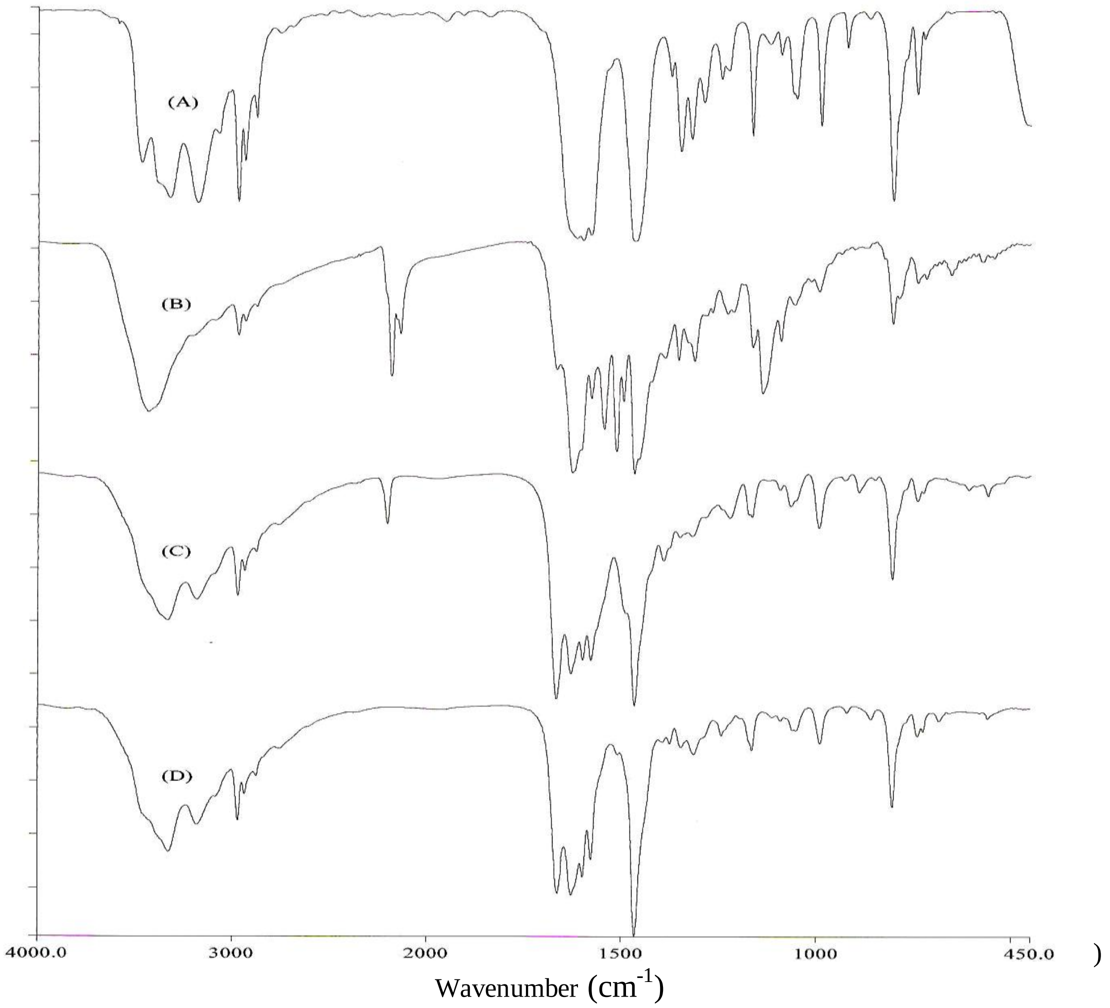

Figure 10. Infrared absorption spectra of: (A) 2-amino-6-ethylpyridine (2A6EPy); (B)$[(2A6EPy)(TCNE)_2]$; (C) $[(2A6EPy)_2(DDQ)]$ and (D) $[(2A6EPy)_4(TBCHD)]$.

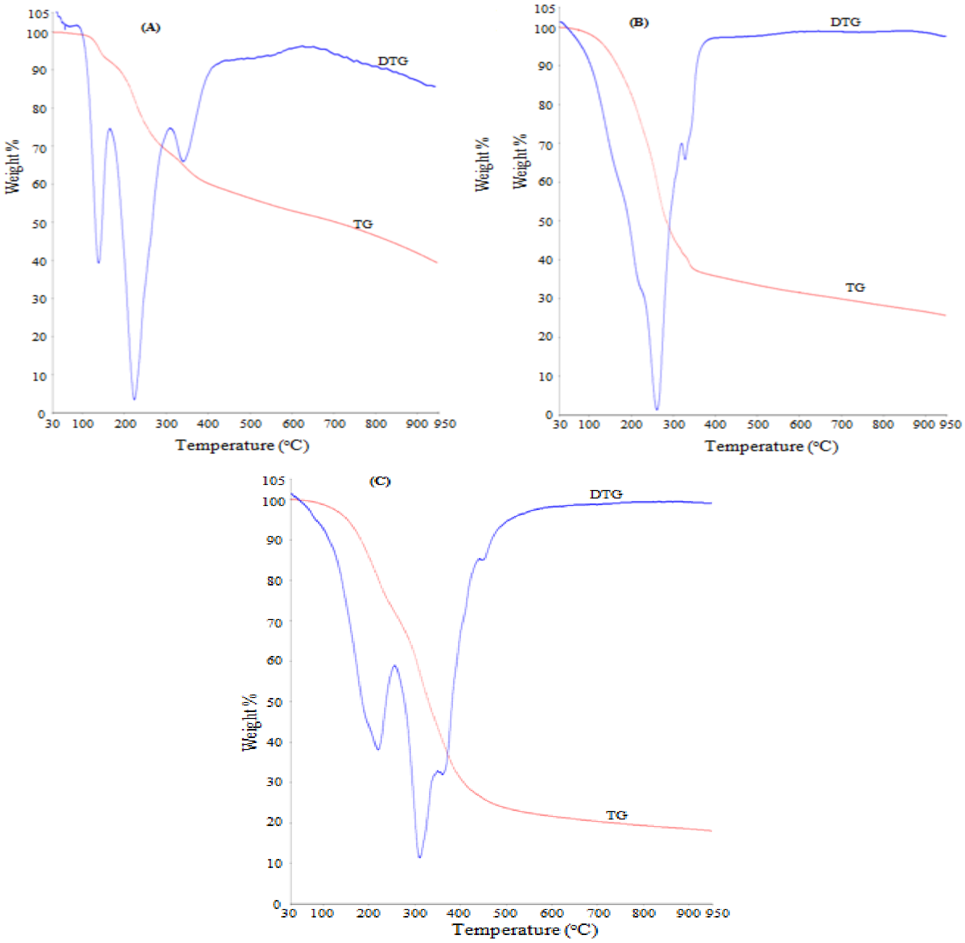

Figure11: Thermograms of: (A) $[(2A6EPy)(TCNE)_2]$; (B) $[(2A6EPy)_2(DDQ)]$ and (C) $[(2A6EPy)_4(TBCHD)]$.

Graphical abstract

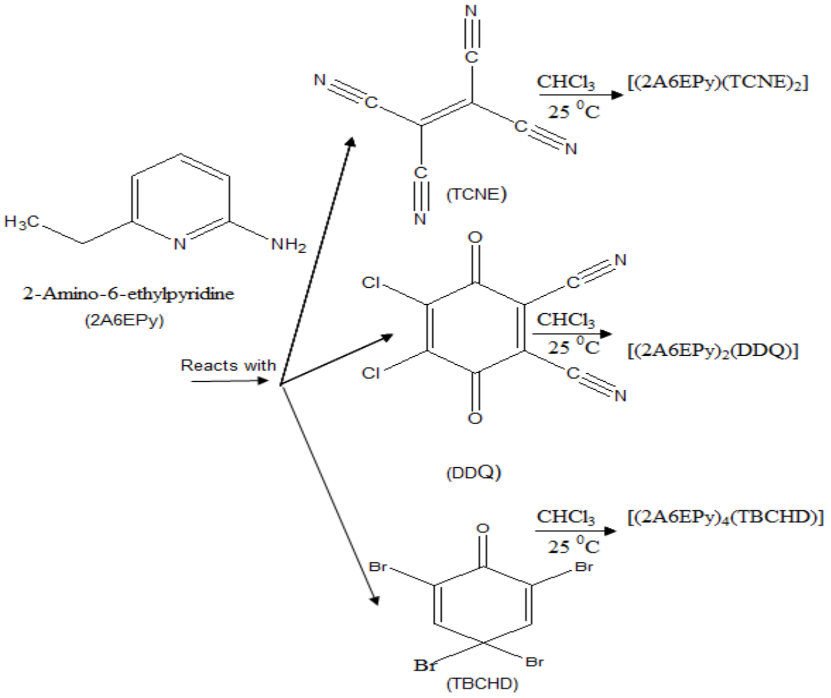

- TCNE : Tetracyanoethylene
- DDQ : 2,3-Dicchloro-5,6-dicyano-4-benzoqunone
- TBCHD: 2,4,4,6-Tetrabromo-2,5-cyclohexadienone

Highlights

- Three CT- complexes of donor 2A6EPy with the acceptors TCNE, DDQ and TBCHD are obtained.
- The CT- complexes are characterized through FTIR, UV– Vis, TGA, elemental analysis and LC MS/MS.
- The values of K_{CT}, ε_{CT}, E_{CT}, ΔG^0 and Ip are calculated

OPEN ACCESS

International
Journal
Of Modern Engineering Research (IJMER)

Experimental Study with Rotating Tool Electrode of EDM for Ni-Alloy

Sanjay Gaur[1], PK Bharti[2]
[1]Director General of Aeronautical Quality Assurance, Ministry of Defence, New Delhi, India
[2]Head of Mechanical Department, Integral University, Lucknow, India

ABSTRACT: *Conventional machining process has the limitation when desired surface finish and dimensional accuracy in geometry is required in difficult to machine aerospace materials especially for the cases of drilling holes. Non conventional advance machining processes (AMPs) are extensively used in the industry to machine for the complex geometrical dimension along with desired surface finish in hard materials. Electrical Discharge machining with modification for holding and rotating the electrode has been used in the present experiment for making holes in the Nimonic alloy. This paper investigate the influence of gap current, pulse on time, duty factor, tool electrode rpm and especially the polarity of the machine on Material Removal Rate (MRR) and surface roughness (R_a) for machining of Nimonic alloy. It is observed that with suitable control of input parameters of Electrical Discharge drilling (EDD), MRR and Ra both found to be improving together from 60 to 90 mg and 4.8 to 2.9 µm respectively which confirm the viability of using tool electrode rotation in EDM machining.*

Keywords: *Advance machining process, Average surface roughness, Material removal rate, Electrical discharge drilling*

I. INTRODUCTION

The ever increasing growth of aviation sector especially the fighter aircrafts has increased the demand for materials that have excellent mechanical and chemical characteristics along with high temperature resistance in comparison to originally employed various types of steels in aerospace applications. The developed materials, such as Ti-alloys, Nimonic super alloys, new ceramics, metal matrix composites, silicon infiltrated carbide (SiSiC), aluminium oxide,-titanium carbide etc. are usually employed in manufacturing of the components for aerospace application. Because these materials possess unique properties like high strength at elevated temperature, resistance to chemical degradation, wear resistance and low thermal conductivity etc. [1, 2]. However ability of these materials to retain their properties at elevated temperatures severely hampers its machinability. Such materials are referred as difficult-to-machine or advanced materials [3].

In conventional machining methods, the materials are removed from workpiece by shears which generate huge amount of heat at the interface of cutting edge of tool and workpiece [4, 5]. This results into the softening of cutting tools and reduces the strength of the cutting tool materials [6]. To address the difficulties faced in machining difficult to machine materials by conventional machining processes, researchers have developed many non-conventional machining processes which are used at increased rate in the industries. However its machining efficiency is very low in terms of material removal rate etc. These non-conventional machining processes are also known as AMP. Some of these AMPs are: Chemical Machining Processes, Ultrasonic Machining Processes, Electrical Discharge Machining, Beam Machining Processes, Electro Chemical Machining, and Jet Machining Processes etc.

In spite of all the efforts made to machine advanced material, still the challenges are not over especially for the machining of Ni-alloy and Ti-alloy. These alloys are extensively used in aeroengine because they are able to meet the characteristic requirements of aerospace materials such as high strength to weight ratio, high strength at elevated temperature, resistance to chemical degradation, high wear resistance and non corrosiveness etc. Ni-alloy specially nimonic alloy posses these aforesaid characteristics along with high resistance to mechanical and thermal fatigue, high resistance to mechanical and thermal shock and high resistance to creep and erosion at elevated temperature. Ni-alloy and Ti-alloy is used extensively in hotter section of aeroengine of aerospace vehicle in the form of turbine blades, compressor blades and liners etc as shown in Fig. 1 and Fig. 2.

Fig. 1 Photograph of a Turbine Blade

Fig. 2 Photograph of a Component used in Fuel System of aeroengine

Drilling of holes in difficult-to-cut aerospace materials specially nimonic alloy with desired surface finish and accurate geometry is beyond the capability of conventional machining such as drilling etc. In machining four basic factors are considered w. r. t. material, shape, size and quality of finish required etc. Problems of machining are associated with:-

- Frequent Tool failure due to poor heat conductivity.
- Difficult to machine because of their high hardness.
- Difficult to make intricate shapes in these materials.
- Difficult to make channel/cylindrical hole of miniature diameter in complex units
- Deformation of tool due high hardness.
- Poor surface finish and machining accuracy.
- Wear on the tool materials results from combination of dissolution /diffusion and attrition process.
- Localization of shear stress on cutting tool due to high dynamic shear strength.
- Notch formation at cutting tool due production of abrasive saw tooth.
- Rapid work hardening during machining especially in Ni-alloy.
- Abrasion based tool failure due to presence of abrasive carbides in Ni-alloys.
- Localization of temperature due to low thermal diffusivity.
- Welding of the work piece to the cutting tool edge resulting in poor surface finish.
- Reaction of the cutting tool with workpiece at elevated temperature, resulting in accelerated tool wear.

Non conventional machining methods are being used to machine the harder materials which have eased out the cutting difficulties to some extent. To overcome the problems of difficult to machine tough and high strength material by conventional machining, Advance machining methods are developed. Some of the of advance machining methods over conventional machining are:-

- Ease in Machining even with complex/intricate shapes and inaccessible areas
- Better surface integrity and high surface finishing.
- Precision & Ultra precision Machining (Micro & Nano Machining).
- Higher volumetric material removal rate
- With Adaptive control leading to unmanned and automated factories.
- Computer control of process result in better performance, higher reliability, better repeatability and higher accuracy.
- Drilling of holes with High Aspect ratio
- Material removal take places in the form of atoms/molecules or in group of these

In this paper authors have investigated the impact of the rotation of the tool electrode in Die sinking EDM on *MRR* and R_a of machined hole with the input parameters of current, pulse on time, duty factor and tool rpm. They have termed it as electrical discharge drilling (EDD) process. It is observed that both the parameters have improved while machining with rotating tool electrode EDM process.

II. LITERATURE REVIEW AND OBJECTIVE OF THE STUDY

Literature Review

Literature on research on EDM for last 10 years have been surveyed and found a very limited works related to EDD and particularly on high content nickel base superalloys. Jeswani [7] the first who was successful in drilling of small diameter holes between 0.19-0.71 mm in carbon steels using tool electrode of copper wires. Jain [8] used rotary EDM to drill precision blind holes in carbon steel and analyzed the effect of pulse time, tool electrode diameter and depth of penetration of precision blind hole drilling in high speed steel. Soni [9] used rotary EDM and sinking EDM both for drilling of holes in Ti-alloy with copper-tungsten electrode and compared the results of both machining. He reports that with rotary EDM, material removal rate (MRR) increases along with improvement in out of roundness in comparisons to hole made by sinking EDM. He supports his finding and credited the increase in *MRR* to improved flushing of eroded debris due to tool rotation. Mohan et al. [10] used hollow tubular electrode in rotary EDM and drilled holes in Al-SiC metal matrix composite and confirms improved *MRR*, R_a and low TEW. The author credited the improvement to improved flushing due to use of rotary EDM. Recently authors have reported for reduction in TEW by providing cooling effect on tool electrode. Suleiman et al. [11] conducted the experiments by providing cooling to tool electrode during machining of titanium alloy (Ti-6Al-4V) and reported for 27% reduction in TEW than that of sinking EDM. Kuppan et al. [12] has drilled holes in Inconel 718 with 99.9% tubular copper electrode. He finds that *MRR* increases with increase in peak current, duty factor, pulse on time and rpm of tool and substantially R_a also improves due to effective dielectric flushing. Addition of additives in dielectric a latest approach in EDM machining is also reported [13]. They have claimed that by using additives in dielectric, *MRR* and R_a both improves. And a latest journal reports for the use of water mixed dielectric in EDM to reduce the environmental hazards, which generates due to decomposition of dielectric [14]. Goswami et al. [15] studied the influence of machining parameters on cutting speed and MRR of Nimonic 80A using wire EDM. They have investigated that cutting speed (CS) and *MRR* increased with increase in pulse-on time and peak current. Yadav and Yadava [16] carried the parametric study on Electrical Discharge Drilling of Aerospace Nickel Alloy. They studied the effect of tool rotation on Average circularity (C_a) value on drilled hole by EDD process.

It is perceived from referred surveyed papers that *MRR* and R_a improve with rotary EDM due to effective flushing of eroded debris. However there is limited information available on Nimonic alloys with sinking EDM machine. Present authors have tried to highlight the issue related to *MRR* and R_a by controlling the input process parameter of EDM machine along with tool electrode rpm and to analyze the effects of selected input parameters for encouraging performance results.

Objectives of the Study

In the present experimental study, the main objective is to investigate the effect on machining performance of *MRR* and R_a with rotating tool electrode used in conventional Die sinking EDM on nimonic alloys aerospace material within the considered domain of selected input parameters.

III. EXPERIMENTAL PROCEDURE

3.1 Development of the Set-up

To conduct the experimental study an arrangement was made to rotate the tool electrode in the existing Die-sinking EDM machine with controlling of tool rpm as shown in Fig 3.

Fig. 3 Photograph of assembled setup on ZNC EDM machine

Since R_a requires a very precision machining and therefore all possible precautions were taken during manufacturing of the setup which was assembled on ZNC EDM machine. Prior to assembly on ZNC EDM machine, the setup was pre-tested with assembled tool electrode for the total indicating run out (TIR) by dial test indicator (DTI) and adjusted for maximum accuracy. An Electronic Automation Private Ltd (EAPL), India made portable digital tachometer (model: DT 200 1B) was used to measure and calibrate the tool rpm which was controlled by the variable speed controller.

3.2 Work piece and Tool Material

Ni-based superalloy of round bar 22 mm diameter is used as workpiece specimen. The chemical composition of the workpiece specimen is given in Table 1. The workpieces were sliced of 6 mm thickness disc by wire cut EDM machine. After measurement of MRR, the machined workpieces will be partitioned into two half to facilitate the accurate measurement of R_a.

Table 1. Composition of nickel alloy workpiece material (%)

Elements:	C	Al	Mn	Si	S	P	Cr	Fe	Ti	Ni
%age :	0.098	0.12	0.04	0.06	0.001	0.005	21.0	0.14	0.33	78

The tool electrode used was made of 99.9 % electrolytic copper having cylindrical diameter of 10 mm as shown in Fig 4.

Fig. 4 Photograph of tool electrode

The specification of dielectric fluid is given in Table 2 which has been used during EDM machining.

Table 2. Dielectric Specifications

Appearance	Bright and clear
Colour	0.0
Specific gravity @ 29.5 ° C	0.750 Min
Kinematic viscosity @ 40 ° C cSt	2.0-2.5
Flash point ° C	100 Min
Pour point ° C	< -3

3.3 Experimental condition

EDD process was performed using rotating tool electrode. The tool electrode was fed downwards under the control of servo system. The workpiece was connected to negative and tool was connected to positive terminal (referred as reverse polarity) of EDM machine power supply. All the experiments for desired output parameters of *MRR* and R_a were performed on reverse polarity.

3.4 Consideration of process parameters

Exhaustive pilot experiments were carried out to determine the range of input process parameters such as gap current, pulse on time, duty factor, and tool electrode rpm. Based on pilot experiments it was concluded to conduct the experiments in reverse polarity with constant pulse off time of 65 µs. The variation on *MRR* and R_a were observed by varying the input parameters one at a time, keeping other parameters constant known one parameter at a time (OPAT) study and ranges of input parameters were decided.

IV. RESULTS AND DISCUSSION

4.1 Average Surface Roughness

Effect of current

Figure 5 shows the variation of R_a with varying current at different duty factors. It is observed that on 800 rpm of tool electrode and at 60% duty factor, R_a increases by 31.03% (from 2.90 to 3.80 µm) with increasing of current from 16 to 24 A and similar trend is seen for all the considered duty factors at 800 rpm. This is due to reason that as the current increases, the intensity of the sparks increases. This lead to the increasing of higher energy of heat along with discharge power. This produces the large craters with appreciable depth at increased duty factor which has been observed in the form of higher Ra values on machined surface of work specimen.

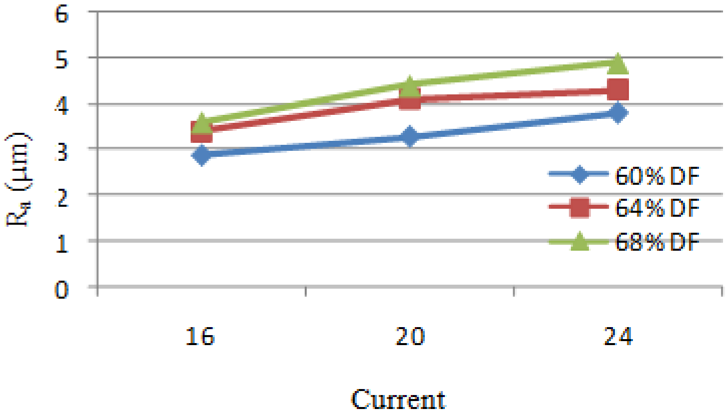

Fig. 5 Effect of current on R_a for different duty factor

Effect of Duty factor

Figure 6 shows the variation of R_a with duty factor at different tool rpm. It is observed that on 16 A current and at 800 rpm, R_a increases by 2.63 % (from 3.80 to 3.90 µm) with increasing of duty factor from 60 to 68%. The trend is found to be improving for all the considered rpm and the R_a values are found to be lower at increasing tool rpm. This is because of improved flushing of eroded debris from inter electrode gap (*IEG*) as a result the surface roughness improves along with increasing of tool rpm. The improvement of R_a at higher tool rpm is also due to the effect of improved melting of the materials from the machined surface at increased duty factor.

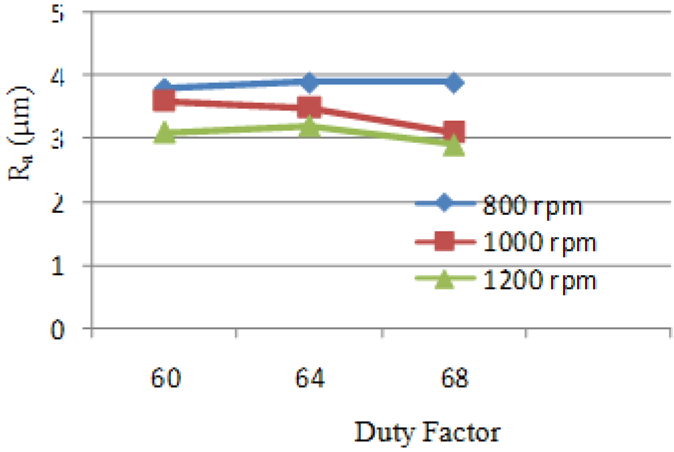

Fig. 6 Effect of duty factor on R_a for different tool rpm

Effect of Tool Rotation

Figure 7 shows the variation of R_a with tool rpm at different current and at 60% duty factor. It is observed that R_a almost improves or seems to be constant with the increase of tool rpm for all the current. It is noted that R_a has varied between 3 to 4 µm for all the current values. This is because of the effective melting of materials and improved flushing as a result of rotation of the tool electrode.

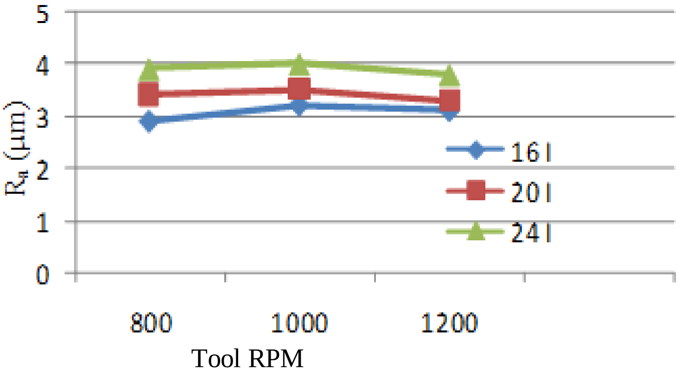

Fig. 7 Effect of tool rpm on R_a for different current

3.2 Material Removal Rate (MRR)

Effect of current

Figure 8 shows the variation of *MRR* with current at different duty factors and at 800 rpm. It is observed that at 60% duty factor, *MRR* increases by 14.56% (from 60.23 to 69.00 mg) with increasing of current from 16 to 24 A and increases by 20.98 % (from 73.21 to 88.57 mg) at 64% duty factor. The trend is found to be similar for 68% duty factor also. This is because of intensive heat generation with increasing of gap current and melting of the materials thereof.

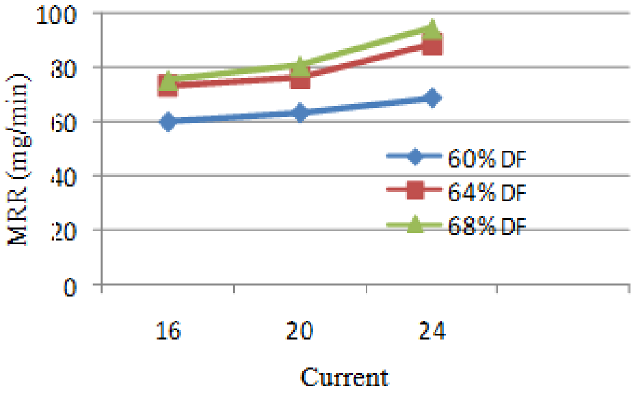

Fig. 8 Effect of gap current on MRR for different duty factor

Effect of Duty factor

Figure 9 shows the variation of *MRR* with duty factor at different tool rpm at 16 A current. It is observed that at 800 rpm, *MRR* increases by 16.31 % (from 60.00 to 69.79 mg) with increasing of duty factor from 60 to 68% and at 1200 rpm it has been increased by 5.15% (from 78.00 to 82.02 mg). This is also credited to the improved flushing of eroded debris from inter electrode gap (*IEG*) along with the increased heat energy due to the increased duty factor.

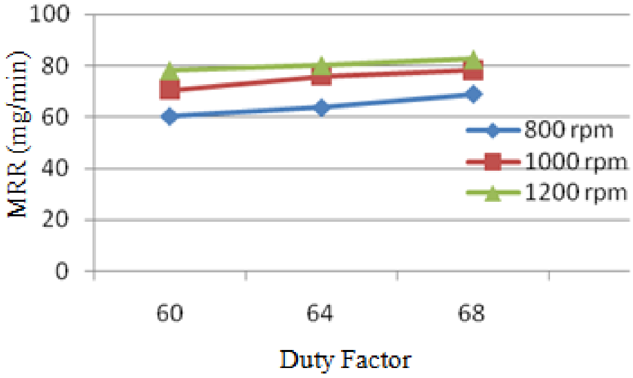

Fig. 9 Effect of duty factor on R_a for different tool rpm

Effect of Tool Rotation

Figure 10 shows the variation of *MRR* with tool rpm at different current and at 60% duty factor. It is observed that *MRR* increases with the increase of tool rpm for all the current. It is noted that at increased value of current (at 24 A), *MRR* has been found to be maximum which has varied from 74 to 81.23 mg. This is because of the effective melting of materials with increasing of current along with increasing of tool rpm. The increasing of tool rpm has certainly enhanced the flushing of eroded debris from the machined surface, as result *MRR* improved.

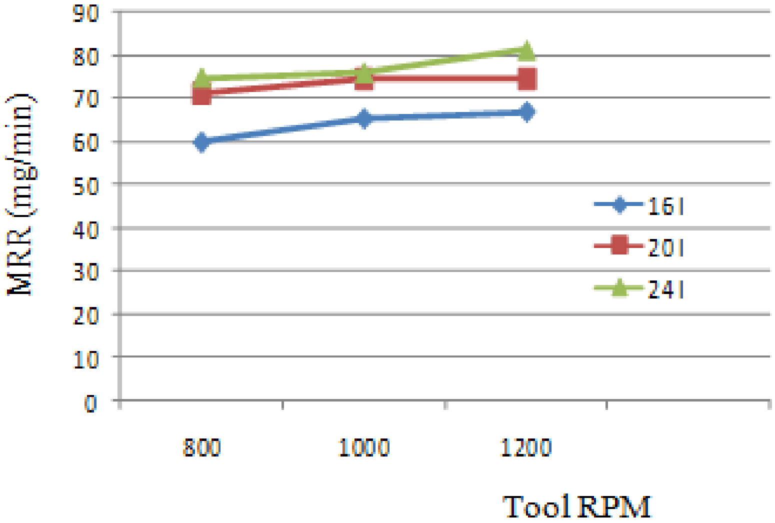

Fig. 10 Effect of tool rpm on R_a for different current

V. CONCLUSIONS

Following conclusions have been derived from the above study:

1. Materials have been developed to meet the challenges of ever increasing demand of high temperature resistance, light in weight along with enhanced strength materials, but the machining processes have to be developed for cheaper, reliable and easier machining processes.
2. The developed EDD process has been able to machine such difficult to cut materials with enhanced performances as this experimental study of nickel based super alloy confirms.
3. MRR has been increasing with the increasing of tool RPM and at the same time R_a has also been improved. The minimum MRR has found to be of 60 mg/min which is adequately enhanced. Also there has been an overall increase of 50% in MRR from 60 mg/min within the considered and controlled parameters of the present EDD process.
4. The observed R_a is found to be in between 3-4µm, which is very nominal for such superalloy materials, which can be further easily improved with light grade emery paper polishing.
5. Since the present experiment (EDD) has been very successful on high precipitation materials and hence authors confirm that future scope of EDD can be further explored for machining of ever developing such materials.

REFERENCES

[1]. Miller. S, Advanced materials means advanced engines. Interdisciplinary Science Review, 21 (2), 1996, 117-129.
[2]. Boyer. R. R, An overview on the use of titanium in the aerospace industry, Materials Science & engineering, A213, 1996. 103-104.
[3]. Ezugwu. E. O, Key improvement in the machining of difficult to-cut aerospace superalloys. International Journal of Machine Tools & Manufacturing, 45, 2005, 1353-1367.
[4]. Ezugwu. E. O, and Wang. Z. M., Titanium alloys and their machinability- A review. Journal of Materials Processing Technology, 68, 1997, 262-274.
[5]. Ezugwu. E.O, Bonney. J, and Yamane. Y, An overview of the machinability of aeroengine alloys. Journal of Material Processing Technology, 134, 2003, 233-253.
[6]. Kramer. B. M, On tool materials for high speed machining, Journal of Engineering for Industry, 109, 1987, 87-91.
[7]. Jeswani. M. L, Small hole drilling in EDM, International Journal of Machine tool Design and Research, 19, 1979, 165-169.
[8]. Jain. V. K, Analysis of electrical discharge drilling of a precision blind hole in HSS using bit type of tool, Microtechnic, 2, 1989, 34-40.
[9]. Soni, J.S., Machining of Titanium Alloy by Rotary EDM. Industrial products Finder, 1994, 253-260

[10]. Mohan. B, Rajadurai. A, and Satyanarayana. K.G, Electric discharge machining of Al-SiC metal matrix composites using rotary tube electrode, Journal of Materials Processing Technology, 153, 2002, 978-985.
[11]. Abdulkareem.Suleiman, Khan. Ahsan Ali, and Konneh. Mohammed, Cooling effect on electrode and process
[12]. parameters in EDM, Materials and Manufacturing Processes, 25, 2010, 462-466.
[13]. Kuppan. P, Rajadurai. A, and Narayanan. S, Influence of EDM process parameters in deep hole drilling of Inconel 718, International Journal of Advance Manufacturing Technology, 38, 2008, 74-84.
[14]. Kumar. anil, Maheshwari. Sachin, Sharma. Chitra, Beri. Naveen, Analysis of machining characteristics in
[15]. additive mixed electric discharge machining of nickel-based super alloy Inconel 718, Materials and
[16]. Manufacturing Processe,26, 2011, 1011-1018.
[17]. Liu. Younghong, Zhang. Yanzhen, Ji. Renjie, Cai. Baoping, Wang, Fei, Tian. Xiaojie, and Dong. Xin,
[18]. Experimental characterization of sinking electrical discharge machining using water in oil emulsion as
[19]. dielectric, Materials and Manufacturing Processe,28, 2013, 355-363.
[20]. Goswami. Amitesh, and Kumar. Jatinder, An Investigation into the Machining Characteristics of Nimonic 80A using CNC Wire-EDM, International Journal of Advanced Engineering Technology, III (I) 2012, 174-174.
[21]. Umacharan. Singh. yadav, and Vinod. Yadav, Parametric study on Electrical Discharge Drilling of Aerospace
[22]. Nickel Alloy, International Journal of Material and Manufacturing Processes, 29, 2014, 260-266.

OPEN ACCESS

International
Journal
Of Modern Engineering Research (IJMER)

Air Compression and Electricity Generation by Using Speed Breaker with Rack And Pinion Mechanism

Mr. Amol Sheshrao Fawade
M.Tech(Machine Design)

ABSTRACT: *On roads, speed breakers provided to control the speed of traffic in rushed areas. The potential energy in terms of weight of vehicle is loss on speed breaker can be utilized for useful purposes. This paper describes the potential energy of such type of energy available on roads and its utilization for useful work. The stages of development of a speed breaker device are described and the mechanism to generate electricity using rack, pinion and speed increasing gear box and generator and store compressed air with the help of piston cylinder compressor arrangement. Whenever the vehicle is allowed to pass over the speed breaker dome, it gets pressed downwards. As the springs are attached to the dome, they get compressed and the rack, which is attached to the bottom of the dome, moves down in reciprocating motion. Since rack has teeth connected to pinion there is conversion of reciprocating motion of rack in to rotary motion of pinion, but the two gears rotate in opposite direction. So that shafts will rotate with certain RPM these shafts are connected through a belt drive to the generators, which converts the mechanical energy into electrical energy. The rack is attached to piston rod of cylinder so downward stroke of rack we can use for air compression in reservoir, with help of piston cylinder arrangement. Simultaneously reciprocating piston cylinder arrangement compresses the air and stores it in the reservoir. We can use the generated electricity and compressed air for different purpose.*

Keywords- *Speed Breaker, Rack &Pinion, Gear, Air Compressor, Generator, Electricity Generation.*

I. INTRODUCTION

On road vehicles waste a tremendous amount of energy on speed breakers, where there is a necessity to provided speed breaker to control the speed of the vehicles. The annual rate of growth of motor vehicle population in India has been almost 20 percent during the last decade. There is tremendous vehicular growth in year by year. The increasing traffic and number speed breakers on roads motivate to manufacture an innovative device which can channelize the energy of vehicles that is wasted on speed breakers to some useful work. In this practical manufacturing processes and steps of speed breaker device for generation of compressed are described which can be used to generate compresses air on highways in remote areas. The reciprocating air compressors are used for pressurized air generation taking advantage of design simplicity and also these are the most common type of compressors found in various applications. This paper based on the principle of reciprocating air compressor in which compressor compresses the air by reducing the volume of air that has been isolated. we put our machine underground of road exactly below speed barker, the head of piston rod is bring up to level of road surface. When vehicles move on rack it will be pushed down. The piston is reciprocating in the cylinder. The piston and cylinder arrangement convert reciprocating motion in to air compression. The second part is specially planned to design and fabricate the conversion unit for utilizing the available unconventional energy source. That is tremendously available energy in low intensity with ample quantity can be utilized. This machine converts reciprocating motion in to rotary motion. The rotational power is converted into the electrical energy by using speed increasing gear box and generator that generate electricity. And this generated electricity is used in various applications.

II. SYSTEM REPRESENTATION

Block diagram of electricity generation and air compression by using speed breaker is shown in figure 2.1. First part is air compression by using speed breaker is shown as vertical block diagram and electricity generation is shown in horizontal block diagram. It indicates both electricity generation and air compression are occurs simultaneous when vehicle passes over speed breaker. It is main advantages of such arrangement of components.

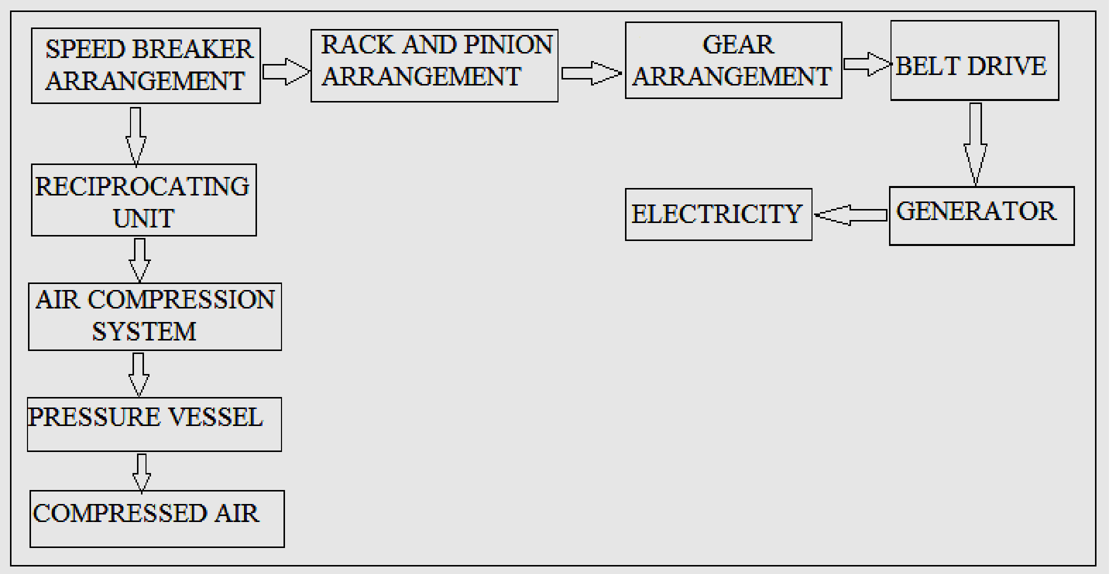

Figure 2.1: Block Diagram of Electricity Generation and Air Compressor by using Speed Breaker

III. CONSTRUCTION DETAILS

The following elements are used for construction of ‘speed breaker air compressor and energy generation’ model. Specification of this equipment is as per requirement amount of energy generation and air compression as shown in Table No.3.1.

The welding is used in fabricating the device is shielded metal arc welding by using the flux coated electrode. Another part welded on the bottom of the mild steel plate and in the middle of the plate. It is welded to give support and adjusts the reciprocating air compressor head.

Table3.1: Specification of Components

SR. NO	***COMPONENT***	***MATERIAL***	***SIZE***	***MATERIAL***
1	Piston	C-40	50mm x 25mm	EN34 with coating hard
2	Cylinder	C-40	80mm x100mm	Cast iron
3	Piston rod	C-40	20mm x 150mm	Plain carbon steel
4	Angles	C-25	25x 25 x 800mm in length	Plain carbon steel
5	Rack	C-30	20mm square	Plain carbon steel
6	Receiver tank	C-40	6 bar	EN8
7	Spring	C-40	4 x 20 x 140mm in length	Spring Steel
8	Nut bolts	C-25	10 x 5mm	Plain carbon steel
9	Washer	C-25	40 x 12 x 4mm	Plain carbon steel
10	Bearing	C-25	skf 6204, I.D 20mm	Plain carbon steel
11	Flexible pipes	_	Inner diameter 10mm	PVC rubber
12	Pinion gear	C-30	50mm diameter 22teeth	Plain carbon steel
13	Spur Gear	C-30	200mm diameter 70teeth	Plain carbon steel
14	Belt	Rubber	V belt	_

IV. PROPOSAL WORK

4.1 SPEED BREAKER AIR COMPRESSOR

4.1.1 WORKING PRINCIPLE

It works on the principle of reciprocating air compressor in which compressor compresses the air by reducing the volume of air that has been isolated. Here, first important point is how we get reciprocating motion, which is prime input in the system for that we use weight of moving vehicles that run on roads.

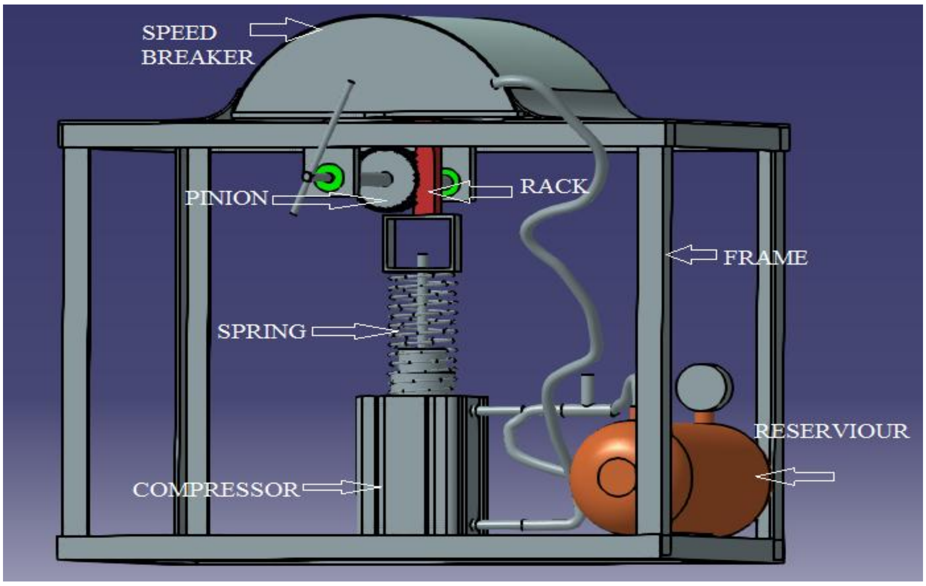

Figure 4.1: Speed Breaker Air Compressor

These machine unit kept underground of road exactly below speed breaker , the head of piston rod is bring up to level of road surface. When vehicles move on speed breaker it will be pushed down so rack move downward and rack is jointed to piston rodso the piston is reciprocating in the cylinder. The piston and cylinder arrangement convert reciprocating motion in to air compression. Now during the dome shaped part press stroke, the piston is coming towards or away direction pressing the already admitted air to be compressed. Thus the pressure or air increases due to compaction of air in the restricted air i.e. more amount of air packed in the low volume area caused by the sweeping of the piston inside the cylinder. The principle parts of kinetically operated reciprocating air compressor are same as that for the I.C. Engine. Inlet and delivery valves Automatic in their operation being spring loaded. They are operated and closed due to the difference of pressure created on either side and a spring provided to close the valve at its seat. [2]

In Working there are two strokes

1. Suction Stroke. **2. Delivery Stroke**

During the suction stroke, piston moves down ward due to which pressure in cylinder falls down below atmospheric pressure. Intake value opens and the atmospheric air is taken inside during the whole stroke. In delivery stroke the piston moves inward with the compression of air in cylinder. Both the inlet and delivery are closed and compression proceeds. At the end of compression strokes, the pressure increases above the receiver pressure. The high pressure air overcomes the spring force on delivery valve and the air is discharged to the receiver tank.

4.1.2COMPRESSED AIR

Compressed air a mixture of all gases contained in the atmosphere. In this paper compressed air is referred to a gas when it is used as a fluid medium. The unlimited supply of air and the ease of compression make compressed air the most widely used fluid for pneumatic system although moisture and solid particles must be removed from the air it does not require the extensive distillation or separation process required in the production of other gases. Compressed air has most of the desired properties and characteristics of a gas for pneumatic system. It is nonpoisonous and non –flammable but does contain oxygen, which supports combustion .One of the most undesirable qualities of compressed air as a fluid medium for pneumatic systems is moisture content. The atmosphere contains varying amount of moisture in vapor from. Changes in the temperature of compressed air will cause condensation of moisture in the pneumatic system. This condensed moisture can be very harmful to the system, as it increases corrosion, dilutes lubricants, and may freeze in lines and compressed air lines to minimize or eliminate moisture in systems where moisture would deteriorate system performance. The supply of compressed air at the required volume and pressure is providing by an air compressor.The normal type of compressor will be of the multi stage, reciprocating piston type (displacement of time the diver must carry with him a supply of breathing gas, usually compressed air. A single cylinder compressor capable of charging a scuba cylinder to 300bar would have compression ratio of 300:1 it would require massive construction and use colossal power to drive it.To simplify the compressor, improve efficiency and reduce power requirements manufacturers use a multi stage arrangement. The following theoretical example is a 3 stage (3 cylinders) compressor with a compression ratio of 1:9 or 1:7 per stage. This would provide us an output pressure of 441barin practice compressor manufactures may install four or more stages use different compressor ratios to arrive at the desired output pressure and will arrange for the air to be cooled as it passes from one stage to another. [5] The volume of gas contained within a diving cylinder can be calculated using Boyle's law e.g.: A 10 liter cylinder charged to 200bar contains 2000 liters. Notes that the amount of air that a cylinder will hold when charged to its working pressure is known as its working pressure is known as its free air capacity i.e. if discharged to atmospheric pressure the volume to which the compressed air would expand .The size of compressor will depend upon the desired duty. A scuba cylinder of 12 liter working capacity and 240 bar working pressure will hold 2880 liters when charged. A portable compressor of 2 cfm (60 1/ min) will take over 45 minutes to fill the cylinder from empty. It is obvious that a machine with such a slow delivery would be useless in a dive center. [5] When air is compressed considerable heat is generated. If no attempt is made to cool it, the air will contain all the heat generated. Air, which contains all the heat in this way, is said to have undergone adiabatic compression (sometimes termed isentropic).

4.2 SPEED BREAKER ELECTRICITY GENERATION

4.2.1 WORKING PRINCIPLE

Whenever the vehicle is allowed to pass over the dome shape speed breaker it gets pressed downwards. As the springs are attached to the dome, they get compressed and the rack, which is attached to the bottom of the dome, moves down in reciprocating motion. Since rack has teeth connected to gear there is conversion of reciprocating motion of rack in to rotary motion of gears, but the two gears rotate in opposite direction. Pinion and larger gear are mounted on same shaft and they rotate with same rpm larger gear is engaged to the small gear which is mounted on another shaft and which rotates with maximum rpm. So that shafts will rotate with certain rpm these shafts are connected through a belt drive to the generator, which converts the mechanical energy into electrical energy. The output of generator is given to the LED bulb which shows generation of electricity by blinking. For more simplification of working principle and construction the proposed model has been modeled using CATIA softwareas shown in figure 4.1 and 4.2.

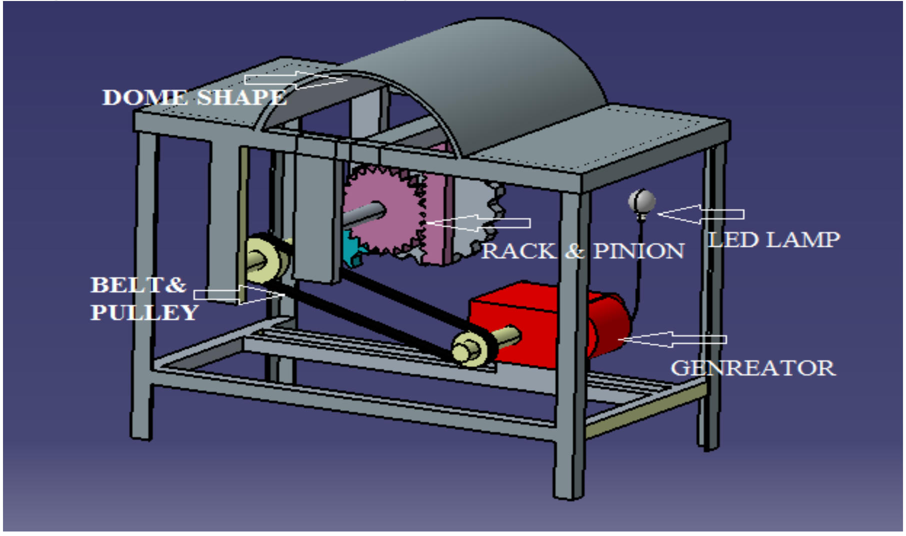

Figure 4.2: Electricity Generation by using Speed Breaker

4.2.2 MATHEMATICAL CALCULATION

Let consider,
The mass of a vehicle =400 Kg (Approximately)
Height of speed brake =8 cm
Work done=Force x Distance
But, here
Force =Weight of the Body
=400 Kg x 9.81
=3924 N
Distance traveled by the body = Height of the speed brake =8 m
Output power = Work done/Sec
= (3924 x 0.08)/60
= 5.232 W
Power developed for 1 vehicle passing over the speed breaker arrangement for one minute is 5.232 W,
Power developed for 60 minutes (1 hour) = 5.232 x60 =313.92

Power developed for 24 hours =313.92 x 24
=7.53408 KW

4.2.3 DC GENERATOR

The main function of Generator is to convert mechanical input energy into electrical output energy. A generator in basic form consists of a powerful field magnet between the poles of which a suitable conductor, usually in the form of a coil (armature), is rotated. The magnetic lines of force are cut by the rotating wire coil, which induces a current to flow through the wire.

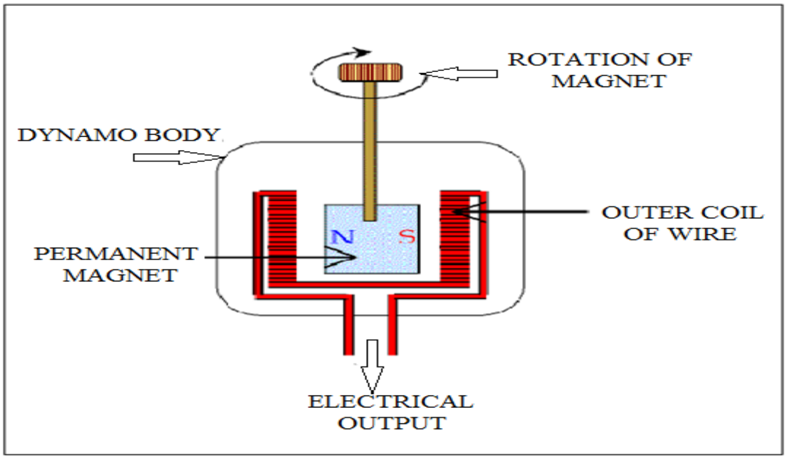

Figure 4.3: DC Generator

The mechanical energy of rotation is thus converted into an electric current in the armature. Present day generators work on the principles described by English physicist Michael Faraday in 1830, that an electromotive force is developed in a conductor when it is moved in a magnetic field. The generator that powers the lights on a bicycle is an example of an alternator, that is, it produces alternating current (AC).A generator produces direct current with the use of a commentator. Generators were the first electrical equipment, capable of delivering power for industry, and the foundation upon which many other later electric-power conversion devices were based, including the electric motor, the alternating-current alternator, and the rotary converter. They are rarely used for power generation now because of the dominance of alternating current, the disadvantages of the commentator, and the ease of converting alternating to direct current using solid state methods. [7].

V. MANUFACTURING AND SELECTION OF MATERIAL

The proper selection of material for the different part of a machine is the main objective in the fabrication of machine. For a design engineer it is must that he be familiar with the effect which the manufacturing process and heat treatment have on the properties of materials. The choice of material for engineering purpose depends upon the following factors.

1. Availability of the materials.
2. Suitability of materials for the working condition in service.
3. The cost of materials.
4. Physical and chemical properties of material.
5. Mechanical properties of material.

The mechanical properties of the metals are those, which are associated with the ability of the material to resist mechanical forces and load. We shall now discuss these prosperities as follows. Required properties for the selection of material are Strength, stress, stiffness, elasticity, plasticity, ductility, brittleness, toughness, resilience, creep, hardness. The science of the metal is a specialized and although it overflows in to realms of knowledge it tends to shut away from the general reader. The knowledge of material and their properties is of great significance for a design engineer. The machine elements should be a material which has properties suitable for the conditions of operations. In addition to this a design engineer must be familiar with the manufacturing processes and the heat treatments have on the properties of the materials. In designing the various part of the machine it is necessary to know how the material will function in service. For this certain characteristics or mechanical properties mostly used in mechanical engineering practice are commonly determined from standard tensile tests. In engineering practice, the machine parts are subjected to various forces which may be due to either one or more of the following. [4]

1. Energy transmitted
2. Weight of machine
3. Frictional resistance
4. Inertia of reciprocating parts
5. Change of temperature
6. Lack of balance of moving parts

The selection of the materials depends upon the various types of stresses that are set up during operation. The material selected should with stand it. Another criterion for selection of metal depends upon the type of load because a machine part resist load more easily than a live load and live more easily than a shock load. Selection of the material depends upon factor of safety which in turn depends upon the following factors. [3]

1. Reliabilities of properties.
2. Reliability of applied load.
3. The certainly as to exact mode of failure.
4. The extent of simplifying assumptions.
5. The extent of localized.
6. The extent of initial stresses set up during manufacturing.
7. The extent loss of life if failure occurs.
8. The extent of loss of property if failure occurs.
9. Materials selected in machine.

VI. ADVANTAGES

1. No fuel is required for its operation.
2. Uninterrupted power generation during day and night.
3. Easy for maintenance.
4. Nonpolluting energy sources.
5. Multipurpose.
6. It is cheap compared to the conventional power Generation units

VII. CONCLUSION

The growth of any nation depends on utilization of energy and this paper helps for that. It is successfully produced electricity and compressed air by using speed breaker. This electricity can store in battery in day time and we can use it in night time for high way illumination, signal system on road, tollbooth or any other useful work. And compressedair can use for cleaning purpose in tollbooth and refilling of air in tires. This paper helps for conservation of natural resources.

REFERENCES

[1] “S.K. HajraChoudhary”, “A.K. HajraChaudhary”, “Nirjhar Roy” *Workshop Technology.*

[2] “R.S.khurmi”, J.K. Gupta *Machine Design, S.Chand Publication.*

[3] “P.C.Sharma” *Production Technology S.Chand Publication.*

[4] “R.K.Jain” *EngineeringMetrology, khanna publication.*

[5] “PSG College” *Machine Design Data Book PSG Data Book.*

[6] “Ashok Kumar Sharma1”, “Omkar Trivedi2”, “Umesh Amberiya2”, “Vikas Sharma2” (2012) ‘Development of speed breaker device for generation of compressed Air on highways in remote areas’ ‘*International journal of recent research and review, vol. i’*

[7] “Aswathaman.V”, “Priyadharshini.M”(2011) ‘Every speed breaker is now a source of power’ *‘International conference on Biology, Environment and Chemistry IPCBEE, vol.IACSIT press Singapore’*.

OPEN ACCESS

International
Journal
Of Modern Engineering Research (IJMER)

An Enhance PSO Based Approach for Solving Economical Ordered Quantity (EOQ) Problem

Ashutosh Khare[1], Dr. B. B. Singh[2], Shalini khare[3]
(Department of Mathematics, SMS Govt. Science College, India
(Department of Computer Science Govt. K.R.G. College, India)
(Department of Electronics, Govt. polytechnic College, India)

ABSTRACT: *The Meta-heuristic approaches can provide a sufficiently good solution to an optimization problem, especially with incomplete or imperfect information and with lower computational complexity especially for numerical solutions. This paper presents an enhanced PSO (Particle Swarm Optimization) technique for solving the same problem. Through the PSO performs well but it may require some more iteration to converge or sometimes many repetitions for the complex problems. To overcome these problems an enhanced PSO is presented which utilizes the PSO with double chaotic maps to perform irregular velocity updates which forces the particles to search greater space for best global solution. Finally the comparison between both algorithms is performed for the EOQ problem considering deteriorating items, shortages and partially backlogging. The simulation results shows that the proposed enhanced PSO converges quickly and found much closer solution then PSO.*

Keywords: *PSO (Particle Swarm Optimization), Chaotic Maps, EOQ, Inventory, deteriorating items.*

I. INTRODUCTION

As of late more consideration is paid to the supply chain systems due to increasing expenses, globalization of assets, globalization of economy, expanded verities of items and prerequisites of lower reaction time. As a result of substantial variability in the impacting conditions, essential suppositions of the EOQ model obliges incessant changes as per the inventory. As of late the thoughtfulness regarding an alternate essential perspective known as decaying properties of things has been generally examines for the exact demonstrating of supply chain systems.

Since numerous other essential variables may be considered to more practical model arrangement. Numerous analysts have officially proposed the various types of EOQ models for diverse things, like no-shortage inventory model with constant speed decay, inventory model with Weibull-distributed deteriorating rate, inventory model with discount and partial backordering and so on.

Finally in this paper the enhanced PSO is tested for the EOQ problem considering inventory model with deteriorating items is taken [1], which considered that the demand function is exponentially decreasing and the backlogging rate is inversely proportional to the waiting time for the next replenishment. The objective of the problem is to minimize the total relevant cost by simultaneously optimizing the shortage point and the length of cycle. The rest of the paper is organized as the section 2 presents a brief literature review of related articles while in section 3 mathematical modeling for the considered EOQ problem is presented. The section 4 describes the PSO and the enhanced PSO algorithms followed by the simulation results in section 5. Finally in the section 6 the conclusion drawn on the basis of simulation results is presented.

II. LITERATURE REVIEW

This section presents some of the important literatures related to this work. Kai-Wayne Chuang et al. [2] studied pricing strategies in marketing, with objective to find the optimal inventory and pricing strategies for maximizing the net present value of total profit over the infinite horizon. The studied two variants of models: one without considering shortage, and the other with shortage. Lianxia Zhao [7] studied an inventory model with trapezoidal type demand rate and partially backlogging for Weibull-distributed deterioration items and derived an optimal inventory replenishment policy. Liang Yuh Ouyang et al. [1] presented an EOQ inventory mathematical model for deteriorating items with exponentially decreasing demand. Their model also handles the shortages and variable rate partial backordering which dependents on the waiting time for the next replenishment. Jonas C.P. Yu [4] developed a deteriorating inventory system with only one supplier and one buyer. The system considers the collaboration and trade credit between supplier and buyer. The objective is to maximize the total profit of the whole system when shortage is completely backordered. The literature also discuss the negotiation mechanism between supplier and buyer in case of shortages and payment delay. Kuo-Lung Hou et al. [10] presents an inventory model for deteriorating items considering the stock-dependent selling rate under inflation and time value of money over a finite planning horizon. The model allows shortages and partially backlogging at exponential rate. Ching-Fang Lee et al. Al [14], considered system dynamics to propose a new order system for integrated inventory model of supply chain for deteriorating items among a supplier, a producer and a buyer. The system covers the dynamics of complex relation due to time evolution. Michal Pluhacek et al [15] compared the performance of two popular evolutionary computational techniques (particle swarm optimization and differential evolution) is compared in the task of batch reactor geometry optimization. Both algorithms are enhanced with chaotic pseudo-random number generator (CPRNG) based on Lozi chaotic map. The application of Chaos Embedded Particle Swarm Optimization for PID Parameter Tuning is presented in [16]. Magnus Erik et al [17] gives a list of good choices of parameters for various optimization scenarios which should help the practitioner achieve better results with little effort.

III. MATHEMATICAL MODELING OF SYSTEM AND PROBLEM FORMULATION

The mathematical model in this paper is rendered from reference [1] with following notation and assumptions.

Notation:
c_1 : Holding cost, ($/per unit)/per unit time.
c_2 : Cost of the inventory item, $/per unit.
c_3 : Ordering cost of inventory, $/per order.
c_4 : Shortage cost, ($/per unit)/per unit time.
c_5 : Opportunity cost due to lost sales, $/per unit.
t_1 : Time at which shortages start.
T : Length of each ordering cycle.
W : The maximum inventory level for each ordering cycle.
S : The maximum amount of demand backlogged for each ordering cycle.
Q : The order quantity for each ordering cycle.
$Inv(t\,)$: The inventory level at time t.

Assumptions:
1. The inventory system involves only one item and the planning horizon is infinite.
2. The replenishment occurs instantaneously at an infinite rate.
3. The deteriorating rate, $\theta\ (0 < \theta < 1)$, is constant and there is no replacement or repair of deteriorated units during the period under consideration.
4. The demand rate $R(t)$, is known and decreases exponentially.

$$R(t) = \begin{cases} Ae^{-\lambda t}, I(t) > 0 \\ \quad D\,, I(t) \leq 0 \end{cases}$$

Where $A\ (> 0)$ is initial demand and $\lambda\ (0 < \lambda < \theta)$ is a constant governing the decreasing rate of the demand.
5. During the shortage period, the backlogging rate is variable and is dependent on the length of the waiting time for the next replenishment. The longer the waiting time is, the smaller the backlogging rate would be. Hence, the proportion of customers who would like to accept backlogging at time t is decreasing with the waiting time $(T - t)$ waiting for the next replenishment. To take care of this situation we have defined the backlogging rate to be $\frac{1}{1+\delta(T-t)}$ when inventory is negative. The backlogging parameter δ is a positive constant $t_1 < t < T$.

3.1 Model Formulation

Here, the replenishment policy of a deteriorating item with partial backlogging is considered. The objective of the inventory problem is to determine the optimal order quantity and the length of ordering cycle so as to keep the total relevant cost as low as possible. The behavior of inventory system at any time is depicted in Figure 1.

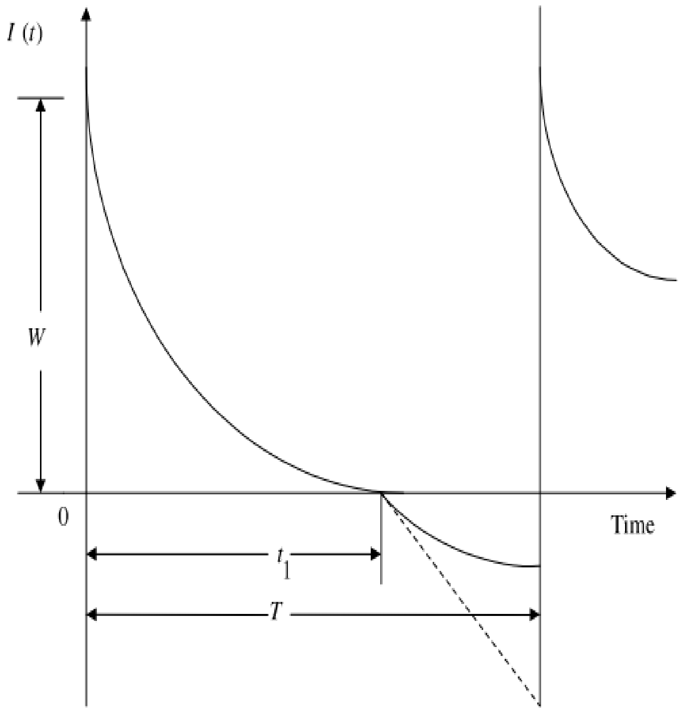

Figure 1: Inventory level $Inv(t\,) vs.\, t\ (time)$.

Replenishment is made at time $t = 0$ and the inventory level is at its maximum W. Due to both the market demand and deterioration of the item, the inventory level decreases during the period $[0, t_1]$, and ultimately falls to zero at $t = t_1$. Thereafter, shortages are allowed to occur during the time interval $[t_1, T]$ and all of the demand during the period $[t_1, T]$ is partially backlogged.

As described above, the inventory level decreases owing to demand rate as well as deterioration during inventory interval $[0, t_1]$. Hence, the differential equation representing the inventory status is given by

$$\frac{dInv(t)}{dt} + \theta Inv(t) = -Ae^{-\lambda t}, 0 \le t \le t_1 \dots\dots\dots.(3.1)$$

with the boundary condition $I(0) = W$. The solution of equation (1) is

$$Inv(t) = \frac{Ae^{-\lambda t}}{\theta - \lambda}\left[e^{(\theta-\lambda)(t_1-1)} - 1\right], 0 \le t \le t_1 \dots\dots\dots(3.2)$$

So the maximum inventory level for each cycle can be obtained as

$$W = Inv(0) = \frac{A}{\theta - \lambda}\left[e_1^{(\theta-\lambda)t} - 1\right] \dots\dots\dots\dots\dots\dots\dots..(3.3)$$

During the shortage interval $[t_1, T]$, the demand at time t is partly backlogged at the fraction $\frac{1}{1+\delta(T-t)}$ Thus, the differential equation governing the amount of demand backlogged is as below.

$$\frac{dInv(t)}{dt} = \frac{D}{1 + \delta(T - t)}, t_1 < t \le T \dots\dots\dots\dots\dots.(3.4)$$

with the boundary condition $I(t_1) = 0$. The solution of equation (3.4) can be given by

$$Inv(t) = \frac{D}{\delta}\{\ln[1 + \delta(T - t)] - \ln[1 + \delta(T - t_1)]\}, t_1 \le t \le T \dots\dots\dots.(3.5)$$

Let $t = T$ in (3.5), we obtain the maximum amount of demand backlogged per cycle as follows:

$$S = -Inv(T) = \frac{D}{\delta}\ln[1 + \delta(T - t_1)] \dots\dots\dots\dots\dots(3.6)$$

Hence, the order quantity per cycle is given by

$$Q = W + S = \frac{A}{\theta - \lambda}\left[e^{(\theta-\lambda)t_1} - 1\right] + \frac{D}{\lambda}\ln[1 + \delta(T - t_1)] \dots\dots\dots\dots..(3.7)$$

The inventory holding cost per cycle is

$$HC = \int_0^{t_1} c_1 Inv(t)dt = \frac{c_1 A}{\theta(\theta - \lambda)}e^{-\lambda t_1}\left[e^{\theta t_1} - 1 - \frac{\theta}{\lambda}\left(e^{\lambda t_1} - 1\right)\right] \dots\dots\dots..(3.8)$$

The deterioration cost per cycle is

$$DC = c_2[W - \int_0^{t_1} R(t)dt]$$
$$= c_2[W - \int_0^{t_1} Ae^{-\lambda t}]$$
$$= c_2 A\left\{\frac{1}{\theta-\lambda}\left(e^{(\theta-\lambda)t_1} - 1\right) - \frac{1}{\lambda}\left(1 - e^{-\lambda t_1}\right)\right\} \ldots\ldots.(3.9)$$

The shortage cost per cycle is

$$SC = c_4\left[-\int_{t_1}^{T} I(t)dt\right] = c_4 D\left\{\frac{T-t_1}{\delta} - \frac{1}{\delta^2}\ln[1+\delta(T-t_1)]\right\} \ldots.(3.10)$$

The opportunity cost due to lost sales per cycle is

$$BC = c_5\int_{t_1}^{T}\left[1 - \frac{1}{1+\delta(T-t)}\right]D\,dt = c_5 D\left\{(T-t_1) - \frac{1}{\delta}\ln[1+\delta(T-t_1)]\right\}\ldots(3.11)$$

Therefore, the average total cost per unit time per cycle is

$$TVC \equiv TVC(t_1, T)$$

= (holding cost + deterioration cost + ordering cost + shortage cost + opportunity cost due to lost sales)/ length of ordering cycle

$$TVC = \frac{1}{T}\left\{\frac{c_1 A}{\theta(\theta-\lambda)}e^{-\lambda t_1}\left[e^{\theta t_1} - 1 - \frac{\theta}{\lambda}\left(e^{\lambda t_1} - 1\right)\right] + c_2 A\left[\frac{e^{(\theta-\lambda)t_1} - 1}{\theta-\lambda} - \frac{1 - e^{-\lambda t_1}}{\lambda}\right]\right.$$
$$\left. + c_3 D\left(\frac{c_4}{\lambda} + c_5\right)\left[T - t_1 - \left(\frac{\ln[1+\delta(T-t_1)]}{\delta}\right)\right]\right\}$$

$$TVC = \frac{1}{T}\left\{\frac{A(c_1+\theta c_2)}{\theta(\theta-\lambda)}\left[e^{(\theta-\lambda)t_1} - (\theta-\lambda)t_1 - 1\right] - \frac{A(c_1+\theta c_2)}{\theta\lambda}\left[1 - \lambda t_1 - e^{-\lambda t_1}\right] + c_3\right.$$
$$\left. + \frac{D(c_4+\delta c_5)}{\delta}\left[T - t_1 - \frac{\ln[1+\delta(T-t_1)]}{\delta}\right]\right\}\ldots\ldots.\ldots(3.12)$$

The objective of the model is to determine the optimal values of t_1 and T in order to minimize the average total cost per unit time, TVC. The optimal solutions t_1^* and T^* need to satisfy the following equations:

$$\frac{\partial\, TVC}{\partial t_1} = \frac{1}{T}\left\{\frac{A(c_1+\theta c_2)}{\theta}\left[e^{(\theta-\lambda)t_1} - e^{-\lambda t_1}\right] - \frac{D(c_4+\delta c_5)}{\delta}\left[1 - \frac{1}{1+\delta(T-t_1)}\right]\right\} = 0 \ldots\ldots\ldots(3.13)$$

and

$$\frac{\partial\, TVC}{\partial T} = \frac{1}{T^2}\left\{\frac{D(c_4+\delta c_5)}{\delta}\left[\frac{(T-t_1)(\delta t_1 - 1)}{1+\delta(T-t_1)} + \frac{1}{\delta}\ln[1+\delta(T-t_1)]\right] - \frac{A(c_1+\theta c_2)}{\theta(\theta-\lambda)}\left[e^{(\theta-\lambda)t_1}\right] - c_3\right\}$$
$$= 0 \ldots(3.14)$$

IV. PARTICLE SWARM OPTIMIZATION (PSO)

The PSO algorithm is inspired by the natural swarm behavior of birds and fish. It was introduced by Eberhart and Kennedy in 1995 as an alternative to other ECTs, such as Ant Colony Optimization, Genetic Algorithms (GA) or Differential Evolution (DE). Each particle in the population represents a possible solution of the optimization problem, which is defined by its cost function. In each iteration, a new location (combination of cost function parameters) of the particle is calculated based on its previous location and velocity vector (velocity vector contains particle velocity for each dimension of the problem).

The PSO algorithm works by simultaneously maintaining several candidate solutions in the search space. During each iteration of the algorithm, each candidate solution is evaluated by the objective function being optimized, determining the fitness of that solution. Each candidate solution can be thought of as a particle "flying" through the fitness landscape finding the maximum or minimum of the objective function.

Initially, the PSO algorithm chooses candidate solutions randomly within the search space. It should be noted that the PSO algorithm has no knowledge of the underlying objective function, and thus has no way of knowing if any of the candidate solutions are near to or far away from a local or global maximum. The PSO algorithm simply uses the objective function to evaluate its candidate solutions, and operates upon the resultant fitness values.

Each particle maintains its position, composed of the candidate solution and its evaluated fitness and its velocity. Additionally, it remembers the best fitness value it has achieved thus far during the operation of the algorithm, referred to as the individual best fitness and the candidate solution that achieved this fitness, referred to as the individual best position or individual best candidate solution. Finally, the PSO algorithm maintains the best fitness value achieved among all particles in the swarm, called the global best fitness, and the candidate solution that achieved this fitness, called the global best position or global best candidate solution.

The PSO algorithm consists of just three steps, which are repeated until some stopping condition is met:

1. Evaluate the fitness of each particle
2. Update individual and global best fitness's and positions
3. Update velocity and position of each particle
4. Repeat the whole process till the

The first two steps are fairly trivial. Fitness evaluation is conducted by supplying the candidate solution to the objective function. Individual and global best fitness's and positions are updated by comparing the newly evaluated finesses against the previous individual and global best fitness's, and replacing the best fitness's and positions as necessary.

The velocity and position update step is responsible for the optimization ability of the PSO algorithm. The velocity of each particle in the swarm is updated using the following equation:

$$v(i+1) = w * v(i) + c_1 * (pBest - x(i)) + c_2 * \left(gBest - x(i)\right) \ldots\ldots\ldots (4.1)$$

$Where$:

$v(i+1)\ -\ New\ velocity\ of\ a\ particle.$

$v(i)\ -\ Current\ velocity\ of\ a\ particle.$

$c_1\ , c_2\ -\ Priority\ factors.$

$pBest\ -\ Best\ solution\ found\ by\ a\ particle.$

$gBest\ -\ Best\ solution\ found\ in\ a\ population.$

$x(i)\ -\ Current\ position\ of\ a\ particle.$

The new position of a particle is then given by (4.2), where $x(i\ +\ 1)$ is the new position:

$$x(i+1) = x(i) + v(i+1) \ldots\ldots\ldots\ldots..(4.2)$$

Each of the three terms $(w * v(i), c_1 * (pBest - x(i))\ and\ c_2 * \left(gBest - x(i)\right)$ of the velocity update equation have different roles in the PSO algorithm. The first term w is the inertia component, responsible for keeping the particle moving in the same direction it was originally heading. The value of the inertial coefficient w is typically between 0.8 and 1.2, which can either dampen the particle's inertia or accelerate the particle in its original direction. Generally, lower values of the inertial coefficient speed up the convergence of the swarm to optima, and higher values of the inertial coefficient encourage exploration of the entire search space.

The second term $c_1 * \left(pBest - x(i)\right)$ called the cognitive component, acts as the particle's memory, causing it to tend to return to the regions of the search space in which it has experienced high individual fitness.

The cognitive coefficient c_1 is usually close to 2, and affects the size of the step the particle takes toward its individual best candidate solution $pBest$.

The third term $c_2 * \left(gBest - x(i)\right)$, called the social component, causes the particle to move to the best region the swarm has found so far. The social coefficient c_2 is typically close to 2, and represents the size of the step the particle takes toward the global best candidate solution $gBest$ the swarm has found up until that point.

4.1 Enhanced PSO

In the Enhanced PSO direct output iterations of the chaotic map were used for the generation of real numbers for the main PSO formula that determines new velocity, thus the position of each particle in the next iteration (See $Rand$ in equation (4.1) in section 5). The concept of embedding chaotic dynamics into evolutionary algorithms is presented in [15][16]. The two different maps which are used here are

4.1.1 Logistic map

The logistic map is a polynomial mapping (equivalently, recurrence relation) of degree 2, shows the complex, chaotic behavior from very simple non-linear dynamical equations. Mathematically, the logistic map is written

$$X_{n+1} = \mu X_n(1 - X_n) \ldots\ldots\ldots\ldots\ldots (4.3)$$

4.1.2. lozi map

The Lozi map is a simple discrete two-dimensional chaotic map. The map equations are given in (17).

$$X_{n+1} = 1 - x|X_n| + bY_n \ \ldots\ldots\ldots\ldots.(4.4a)$$

$$Y_{n+1} = X_n \ldots\ldots\ldots\ldots\ldots\ldots.(4.4b)$$

V. SIMULATION AND RESULTS

To test the PSO and Enhanced PSO algorithms for finding the optimal solution of the problem as discussed in section (3), the equation (3.13) and (3.14) is taken as the fitness function, while the values of t_1 and T are to be searched for satisfying the fitness function. The other variables are taken as follows:

Table I

Variable Name	Variable Value
A	12
θ	0.08
δ	2
λ	0.03
c_1	0.5
c_2	1.5
c_3	10
c_4	2.5
c_5	2
D	8

The exact solution found analytically in [1] was $t_1 = 1.4775$ and $T = 1.8536$. Which provides the optimal maximum inventory level $W = 18.401$ units, the optimal order quantity $Q = 20.1183$ units and the minimum average total cost per unit time $TVC = \$11.1625$.

While the PSO based technique with following configuration-

Table II

Variable Name	Variable Value
c_1 (PSO Const.)	2
c_2 (PSO Const.)	1
w_{max}	0.9
w_{min}	0.1
Total Particles	100
Maximum Iterations	100
$\mu\ (Logistic\ Map)$	4 (Only For E-PSO)
$k\ (Logistic\ Map)$	0.63 (Only For E-PSO)
$a\ (Lozi\ Map)$	1.7 (Only For E-PSO)
$b\ (Lozi\ Map)$	0.5 (Only For E-PSO)

The equation (3.12) can be directly selected as objective function for the PSO algorithm hence it avoids the complex differentiations required for analytical methods.

Using the equation (3.12) as objective function the results obtained by all three PSO as listed below-

Table III:

Technique	t_1	T	TVC
PSO	1.4785	1.8550	11.1625
PSO1	1.4772	1.8532	11.1625
PSO2	1.4771	1.8531	11.1625
Analytical	1.4775	1.8536	11.1625

Every algorithm Provides the minimum value of $TVC = \$11.1625$, although at different t_1 and T.

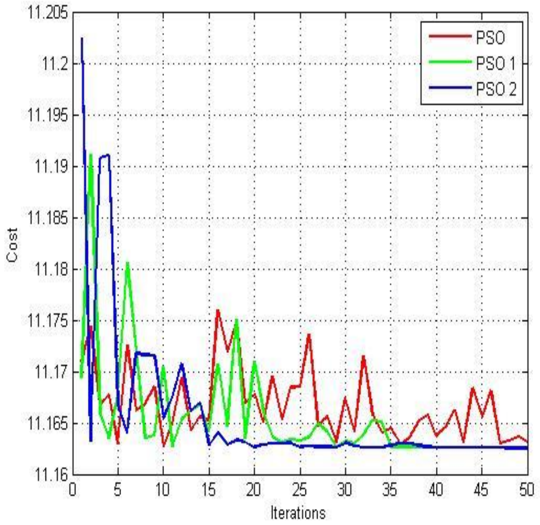

Figure 2: Comparison for the value of objective function (fitness value) at each iteration of all three PSO (PSO = standard PSO, PSO1 = PSO with Single Chaotic Map, PSO2 = PSO with Double Chaotic Map.

Also if we try to use the objective function by combining the equation (13) and (14)

$$objective\ function = abs\big(eq(13)\big) + abs(eq(14))$$

Using the above given equation as objective function the results obtained by all three PSO as listed below

Technique	t_1	T	obj
PSO	1.4776	1.8538	0.3417e-3
PSO1	1.4776	1.8537	0.4098e-3
PSO2	1.4775	1.8537	0.1943e-3
Analytical	1.4775	1.8536	0

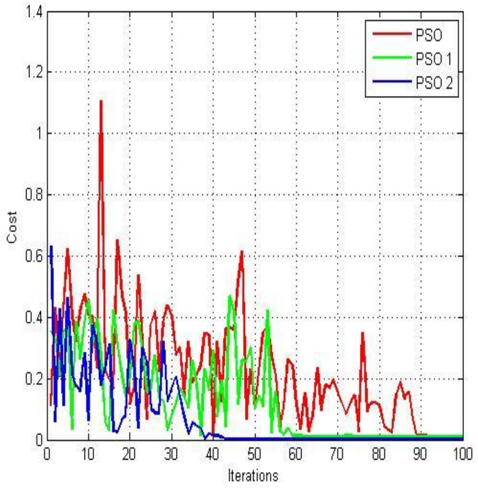

Figure 3: Comparison for the value of objective function (fitness value) at each iteration of all three PSO. The best fitness value achieved in the process is $1.943 * 10^{-04}$ by PSO2 which almost equal to 0.

VI. CONCLUSIONS

This paper presented an enhanced PSO algorithm for efficient solution of classical economic order quantity (EOQ) model problem. The simulation results shows that the enhanced PSO not only converges quickly about half of the iterations of standard PSO but also provides much closer solution. Hence the presented approach can solve the EOQ problem much efficiently than standard PSO and can be preferred for complex EOQ models where analytical solution required extensive analysis or normal PSO fails to produce required closeness to solution.

REFERENCE

[1] liang-yuh ouyang, kun-shan wu, mei-chuan cheng, “an inventory model for deteriorating items with exponential declining demand and partial backlogging”, yugoslav journal of operations research 15 (2005), number 2, 277-288.

[2] kai-wayne chuang, chien-nan lin, and chun-hsiung lan “order policy analysis for deteriorating inventory model with trapezoidal type demand rate”, journal of networks, vol. 8, no. 8, august 2013.

[3] g.p. samanta, ajanta roy “a production inventory model with deteriorating items and shortages”, yugoslav journal of operations research 14 (2004), number 2, 219-230.

[4] jonas c.p. yu “a collaborative strategy for deteriorating inventory system with imperfect items and supplier credits”, int. j. production economics 143 (2013) 403–409.

[5] s. kar, t. k. roy, m. maiti “multi-objective inventory model of deteriorating items with space constraint in a fuzzy environment”, tamsui oxford journal of mathematical sciences 24(1) (2008) 37-60 aletheia university.

[6] vinod kumar mishra , lal sahab singh “deteriorating inventory model with time dependent demand and partial backlogging”, applied mathematical sciences, vol. 4, 2010, no. 72, 3611 – 3619.

[7] lianxia zhao “an inventory model under trapezoidal type demand, weibull-distributed deterioration, and partial backlogging”, hindawi publishing corporation journal of applied mathematics volume 2014, article id 747419, 10 pages.

[8] xiaohui hu, russell eberhart “solving constrained nonlinear optimization problems with particle swarm optimization”,

[9] tetsuyuki takahama, setsuko sakai “constrained optimization by combining the α constrained method with particle swarm optimization”, soft computing as transdisciplinary science and technology advances in soft computing volume 29, 2005, pp 1019-1029.

[10] kuo-lung hou, yung-fu huang and li-chiao lin” an inventory model for deteriorating items with stock-dependent selling rate and partial backlogging under inflation” african journal of business management vol.5 (10), pp. 3834-3843, 18 may 2011.

[11] nita h. shah and munshi mohmmadraiyan m. “an order-level lot-size model for deteriorating items for two storage facilities when demand is exponentially declining”, revista investigación operacional vol., 31 , no. 3, 193-199 , 2010.

[12] hui-ling yang “a partial backlogging inventory model for deteriorating items with fluctuating selling price and purchasing cost”, hindawi publishing corporation advances in operations research volume 2012, article id 385371, 15 pages.

[13] ibraheem abdul and atsuo murata “an inventory model for deteriorating items with varying demand pattern and unknown time horizon”, international journal of industrial engineering computations 2 (2011) 61–86.

[14] ching-fang lee, chien-ping chung “an inventory model for deteriorating items in a supply chain with system dynamics analysis”, procedia - social and behavioral sciences 40 (2012) 41 – 51.

[15] michal pluhacek, roman senkerik, ivan zelinka and donald davendra “performance comparison of evolutionary techniques enhanced by lozi chaotic map in the task of reactor geometry optimization”, proceedings 28th european conference on modelling and simulation ©ecms.

[16] o.t. altinoz a.e. yilmaz g.w. weber “application of chaos embedded particle swarm optimization for pid parameter tuning”, int. j. of computers, communication and control (date of submission: november 24, 2008).

[17] magnus erik, hvass pedersen “good parameters for particle swarm optimization”, technical report no. hl1001 2010.

OPEN ACCESS

International
Journal
Of Modern Engineering Research (IJMER)

The Evolution of Traditional Urban Survey using Applicable Surveying Techniques

Ahmed E. Ragheb[1], Mohamed A. El-Fayoumi[2]
[1]*Assistant Professor, Public works Department, Faculty of Engineering, Ain Shams University*
[2] *Assistant Professor, Urban Planning and Design Department, Faculty of Engineering, Ain Shams University*

ABSTRACT*: This research deals with how to facilitate and manage surveying methods to accomplish modernized and cost effective urban survey with best achievable accuracy. This is done by replacing traditional surveying methods with modern methods from both theoretical and practical point of view. At first, a theoretical assessment process on a tradition urban planning project in Saudi Arabia is performed by replacing traditional urban planning techniques previously used with more applicable surveying techniques as total stations regarding different matters such as applicability, cost and accuracy. After approving the main idea of this modernization process, a practical urban planning case study is performed using total station, geodetic GPS receivers and GPS navigators, on a private settlement block consisting of 6 buildings in a crowded neighborhood of Cairo city. The applied surveying techniques showed high efficiency regarding cost and effort, while saving observation time reaching to 60%. Accordingly, the adopted practical application proved to be beneficial for all desired aspects, as well as being promising for more extensive study areas in future.*

Keywords: *GPS, Surveying techniques, Urban Survey*

I. INTRODUCTION

Various purposes of urban planning are of vital importance nowadays, basically [1] property documentation of formal and informal settlements, legalization and taxation are just few applications. However, initial stages of these applications in the form of urban survey have to be performed in a safe and economical manner along with social and environmental experience of the area under consideration to achieve adequate and high performance [2]. Undoubtedly, there is a strengthened relationship between urban survey procedures and surveying field, as the need for accurate and comprehensive urban survey parallel with efficient cost and time is a problematic phenomenon of traditional, primitive and detailed urban survey, hindering accuracy and inclusion of data [3]. Accordingly, urban field is firm depending on that of surveying to start its existing situation studies phase, followed by analysis and the upgrade process or even any other missions that must initially refer surveying, in order to know what will be used to upgrade or develop. See Fig.1.

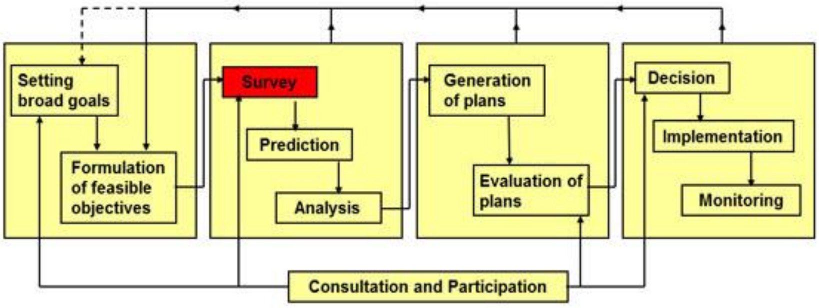

Fig. 1 Characteristic features of different stages in the physical planning process [4]

II. METHODOLOGY

The basic idea starts with illustrating both urban and surveying fields to pinpoint the main problematic issue that is the different urban surveying types and techniques and their reflections on traditional and modern surveying methods. Here by, the research penetrates deeply into its two main axes, the first is the theoretical part on a previously surveyed project using linear measurements and the simulation of other applicable surveying technique in the form of total station. Secondly, the practical part, with a comparative study through different traditional and more advanced surveying methods, in order to reach out and deduce how to facilitate and manage surveying methods to accomplish modernized and cost effective urban survey with best achievable accuracy.

III. URBAN SURVEY

Urban planning is the discipline of land use planning which explores several aspects of the built and social environments of municipalities and communities. Other professions deal in more detail with a smaller scale of development, namely architecture, landscape architecture and urban design. Regional planning deals with a still larger scale. In terms of its objectives, planning is the elaboration of a set of related programs designed to achieve certain goal, while the planning process itself is the set of interventions and other actions undertaken during the elaboration of a plan. On the other hand, in terms of future control, it is the ability to control the future by current acts [4].

3.1 Urban Survey Definition

The urban survey concerns with the existing situation studies for an urban fabric context, which is a preparatory phase for analysis studies for the location to start further upgrading phases. This mentioned preparatory phase is very important as the accuracy of the related studies after that depends totally on the accuracy of this initial step. Accordingly, it is clearly essential to study and compare between different types and methods of urban survey, as to be able to reach the most accurate and progressive method to be used as a starting step in the right way of this long phases work.

3.2 Urban Survey Types

Here we need to define and study different variable types and methods, then subsequently, give fairly comparative analysis to illustrate the most effective, accurate, short timing and cheapest method. Consequently, several methods can be used to obtain the same main results with some differences in quality, details, accuracy, data covering and many fields' usages. The first type is the ordinary method by using the satellite images maps then start to update it by visual observations and non-accurate measurements of lengths and dimensions, then merging these drawn information by filled applications for all observed data to obtain finally the named fundamental maps, using geographic information system (GIS). This can be summarized clearly in five basic drawing sheets namely; land-uses, building uses, buildings heights, building conditions and building construction. An example of some of those sheets is given in Fig. 2.

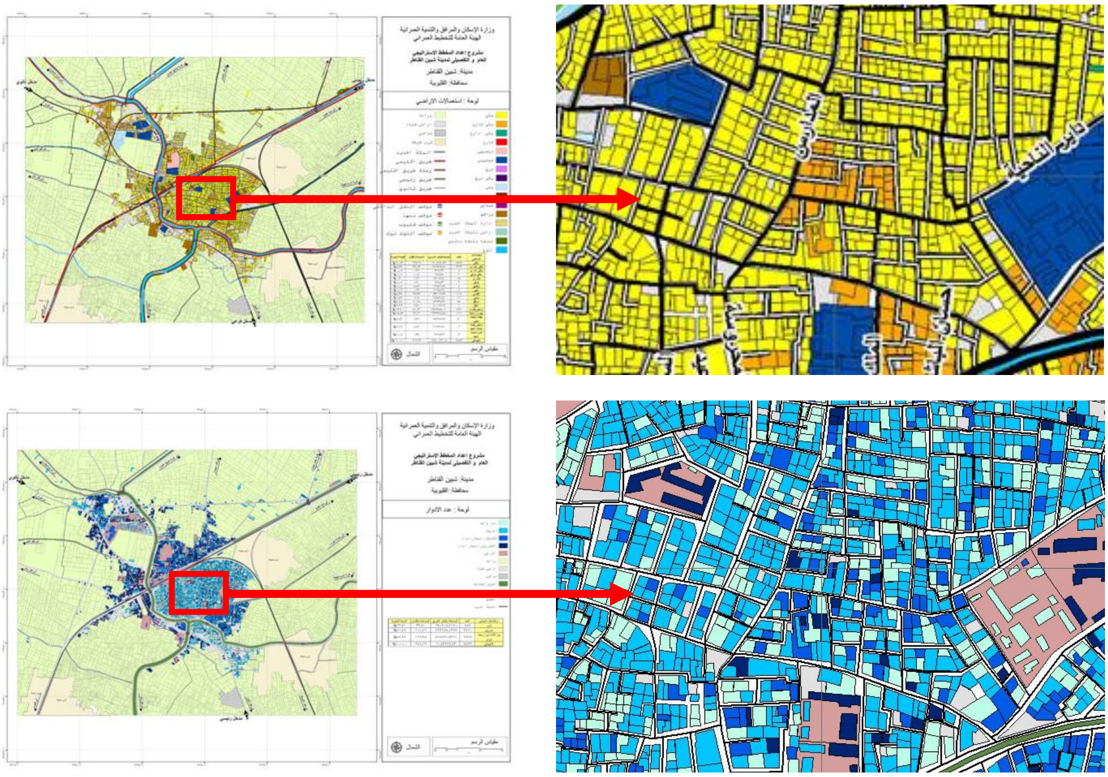

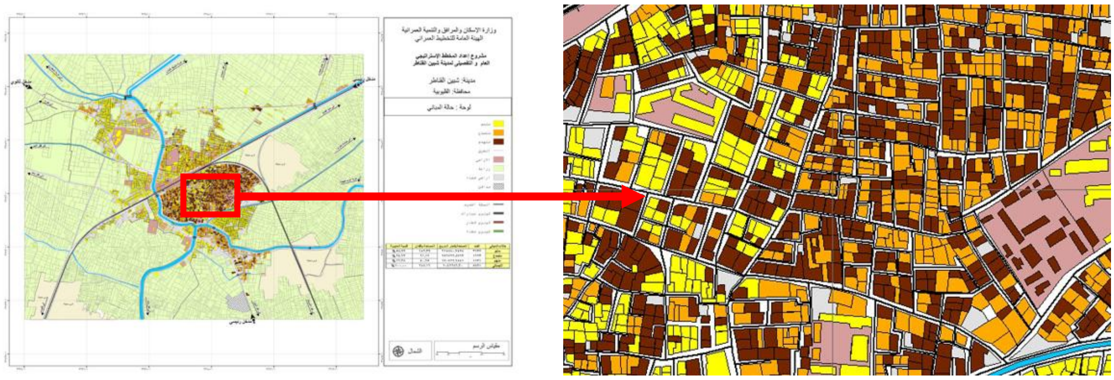

Fig. 2 Example for land-uses, buildings heights and conditions sheets [6]

The second type is detailing, which uses first sketches to draw, approximate the building outlines, this sometimes can be aided by total stations to give more accurate drawing for its outlines of the ground floor plan and the land edges. After that the survey engineers starts to measure the internal dimensions for the roof and its components and any missing dimensions not given by the total station, and then all observed data and obtained information are filled in applications. The overall product are cad drawings sheet for the collective map of the buildings, and every building is drawn in a different sheet as follows: land sheet, ground floor sheet, typical floor sheet, roof sheet, apartment sheet and any additional drawings sheet (such as shops,….etc), as given earlier in Fig. 2. Note that, this second type is used by both the urban field and that of surveying.

3.3 Urban Survey Results

Accordingly, as illustrated in the previous section, urban survey results are, in the first type; colored drawing sheets with areas and information which are not detailed and accurate enough and do not give full needed data, while in the second type, almost full detailed information are extracted, but takes longer time, more effort, expensive procedures, great number of manpower and variable work steps that gives accumulative errors.

IV. SURVEYING FIELD

As much known to many people in the engineering field, the surveying process is the base and start point for almost all projects. That is to say, prior, during or even after design, construction or field work, surveying measurements will be taken, whether for fixation of control reference points, setting out of previously determined points onsite or production of maps and quality control. Few examples of such applications include; water pipelines layout, establishment of residential complexes, excavation works, deformation monitoring…..etc. This can be done by different instruments and techniques varying in technology, price and application.

4.1 Traditional Surveying Methods

Previously, surveying application in urban survey projects included mainly the use of regular tapes distance measurements and optical theodolites for angular measurements. Different kind of tapes varying in length and material were used in measuring the boundaries and details of buildings and complexes. However, this technique –although its simplicity and cheap price of the used tool- has many disadvantages, starting with various errors accompanied with the tape, such as sagging especially in long distances, difference of nominal length and temperature effect….etc. Optical theodolites were quite handy and popular in angular and direction measurements in order to maintain building corners especially non right angle corners, but similar to the use of tapes, at the end large amount of data are required to be taken, displayed and then saved and copied, in addition to all this, the whole field operation being time consuming and executed using extensive manpower.

4.2 Modern Surveying Methods

Recently, many modern surveying instruments are used in various projects and applications, mainly total stations and GPS equipment. Total stations combine both distance measuring device (EDM) along with angular measuring equipment (Theodolite) together with processor and memory, in order to observe, calculate and save direct boundaries corners and features in their local or global coordinate (Easting, Northing, Height) format. GPS receivers wither geodetic precise ones or less accurate navigators, observe continuously rotating satellite signals from sky, and again determine the global coordinates of surveyed points relative to the Global datum. The wide use of the aforementioned instruments comes from their efficiency, or in other words easiness of data sampling, storage and display. This will of course lead to reduction in manpower needed as well as required field and even office work time. However, these advantages will surely be accompanied with slight disadvantages, which should be compared versus their benefit of usage.

Now speaking about disadvantages, price of used instruments here in is one good example, as total stations are minimum three time expensive than regular digital theodolites, while geodetic GPS receivers being at least 7 times more. However, regular navigators are cheap in price; quarter the price of digital theodolites, but they sure will propose degraded accuracy. Concerning GPS receivers, various errors will affect GPS positioning, either from satellites, atmosphere or receivers. However, most of these errors can be modeled and thus reduced by adopting several techniques such as differencing between two receivers, i.e. relative positioning, some errors will still evolve in the solution, especially the inevitable multipath error, caused by receiving signals from more than one path.

V. THEORETICAL ASSESSMENT PROCESS

After presentation of the different techniques to be adopted in the current research, the theoretical applied part in this research will be introduced, regarding the case study area, and surveying of the building complex using both traditional and modern instruments.

5.1 Case Description

The area under study consists of 9 buildings as a part of building complex in Madinah, KSA, which was already under investigation in a previous urban survey project. Three of these buildings are only one floor buildings and the others are multi-story buildings consisting of three to four floors. Fig. 3 shows a layout of these buildings along with surrounding streets [7].

Fig. 3 Madinah map, KSA showing Google maps hierarchy for case site [8]

5.2 Traditional Surveying Methods Application

Dimensions of all buildings in this case are surveyed using a tape and two persons. The required time intervals to survey each building are indicated in Table 1. Note that, all common points repeated among floors in each building have to be observed each time in order to find its relation and dimensions with respect to every point per each floor, which is considered a disadvantage when compared to surveying of such buildings using more advanced instruments.

5.3 Modern Surveying Methods Application

The application of reflectorless total station here is a theoretical application, meaning that it was not applied during the actual project. Herein, the time required for the surveying of buildings using a total station is investigated, which is shown as well in Table 1. Note that the application of GPS was not undertaken in the theoretical case because it was not applied during the actual project, basically due the variety of its usage according to the surrounding environment, mainly because the usage of GPS and its success will depend on the blockage of satellite signals, loss of lock and multipath. This will be highly variable near to buildings especially while surveying of buildings dimension from the outside. However, the usage of GPS will be taken into consideration in the practical applied case later on.

Also not here that, surveying of buildings using a total station in this case is done only using one surveyor only due to the unneccessity of another surveyor to hold the reflector, as the use of reflectorless total station is very beneficial here in and could be thought to be a must. This is backed by the fact that the cost of reflectorless total station is reasonable nowadays and very applicable here in by targeting buildings' points directly given that buildings are within few hundred meters from the instrument, which is the case here and originally during any urban survey project. Of course, the usage of only one surveyor during the whole process will definitely vastly decrease the overall cost of the urban survey work.

5.4 Theoretical case Results and Conclusions

After studies from different point of views such as shape, accessibility….etc, some important conclusions can be extracted, noting that some factors regarding the building such as building dimensions, current status, material….etc. is outside the scope of the current research as it will not affect the undertaken factors, such as time and cost among the comparison between techniques and thus can be considered non effective here. In addition, some of the shops within the buildings were identified without dimensions, due to accessibility, which could be solved easily using total station, as will be shown later.

From previous experience, the time required for one linear measurement is taken to be 15 seconds, and another 15 seconds for manipulation between one measurement and the other, while regarding total station measurements, the time for setting the instrument over any point for a regular surveyor with moderate experience is 3 minutes, taking 15 seconds for observing each point and targeting from one point to the other. A very powerful remark in the use of total station, is that when the building dimensions changes from the base to repeated floors, and since buildings usually are not entered from the inside and measured from the outside borders, in some cases mostly the dimensions of the buildings are obtained in an approximate way using the projection of a staff and mentioning the distance between such projection and the actual dimension of the base, or approximated from the previous or latter floor. This will surely affect the accuracy of these measurements. On the other hand, this can be simply resolved using reflector less total station.

In addition, a very important remark, is that number of setups of the total station instrument can be minimized (which considered the most time consuming step) if the dimensions of several buildings can be obtained from common setups of the instrument especially for adjacent buildings. This is very clear in the time saved, as shown in Table 1. From the shown table, it can be seen that the concept of common setups among different buildings has excluded seven required setups through the whole project saving around 62.5 minutes of the whole process, that is around 44 % of the total required time when using linear measurements. This of course will surely be highly multiplied for bigger projects having multiple of buildings' complexes. Based on the results obtained here from the theoretical case study, the efficiency of the applicable total station technique was well illustrated, in the form of time saving, less effort and manpower needed and of course leading to better accuracy. This was a main catalyst to apply such technique along with GPS positioning in the practical case study.

VI. PRACTICAL URBAN SURVEY CASE STUDY

6.1 Case Description

Following the conclusions obtained from the theoretical case study, it was essential to justify the results through an actual practical case applying traditional and more advanced surveying instruments. The chosen practical study area consists of six adjacent buildings as a part of a building complex in Nasr City area, Cairo, Egypt. These buildings had variable heights, different floors and accessibility around them, as two of these buildings are about 11 floor buildings and the others are intermediate height buildings consisting of five floors, as shown in Table 2. Fig. 4 and Fig. 5 show a layout of these buildings along with surrounding streets. These variable factors were the main reason behind the choice of this study area.

Table 1 Comparison on the usage of traditional and modern surveying techniques for the urban survey of the practical applied case (Ground: G, Repeated: R)

Building	Floors	Tape		Total Station (TS)					Time difference between TS and Tape (sec)	Remarks
		Measurements	Time required (sec)	Points	No. of setups	Setup Location	Time required (Setup & Observation) (sec)	Effective Required Time		
2610401	G	9	270	6	1	Roof	270	270	0	One common setup on roof for the three buildings
2610403	G	11	330	7	1	Roof	285	105	225	
267439	G	11	330	7	1	Roof	285	105	225	
268402	G	11	330	7	2	G	465	285	45	Setup A for 2 buildings
	R	23	690	11		G	165	165	525	
	Roof	8	240	4	1	Roof	240	240	0	---
268404	G	6	180	5	2	G	435	75	105	No new setup required
	R	9	270	5		G	75	75	195	
	Roof	5	150	3	1	Roof	225	225	-75	---
267440	G	17	510	10	2	G	510	330	180	Setup B for 4 buildings
	1	15	450	5		G	75	75	375	
	R	25	750	14		G	210	210	540	
	Roof	17	510	10	2	Roof	510	510	0	---
269402	G	11	330	7	2	G	465	285	45	Setup C for 3 buildings
	R	13	390	5		G	75	75	315	
	Roof	23	690	10	2	Roof	510	510	180	---
267441	G	7	210	5	2	G	435	255	-45	Setup D for 3 buildings
	R	14	420	7		G	105	105	315	
	Roof	16	480	8	2	Roof	480	480	0	---
269404	G	5	150	4	2	G	420	240	-90	Setup E for 2 buildings
	R	31	930	16		G	240	240	690	
	Roof	7	210	2	1	Roof	210	210	0	---

Fig. 4 Cairo map, Egypt showing practical case site [9]

Fig. 5 General layout of practical case site [9]

6.2 Surveying using Traditional methods

Herein, as a common linear surveying procedure, two tapes are going to be used for the planimetric surveying of the six buildings whether from the ground, the roof or any floor. From a practical point of view, several photos and sketches were taken for proper visualization and reliability of all surveyed buildings. Note that some measurements were taken on the roof as well, for the case where the plan of the building differs on the ground from that corresponding plan on the roof. This is a familiar case nowadays, especially with modern architecture design. Accordingly, the first part of Table 2 shows a detailed vision of the total linear measurements taken for each floor and building, along with the time taken for each process. This extensive time taken for the surveying process is accompanied with hard working paid labor, however on the contrary the whole process is executed using cheap surveying tools, such as the tape, along with moderate payments for regular not necessary skilled trained labor. Note that, in this case here, each floor should be entered in order get all relevant information for such floor, which is considered a major disadvantage of such technique regarding time, effort and privacy of such floor especially if it is occupied by civilian users. However, in such a case were details of any floor cannot be obtained directly, it is referenced with an approximation from the previous or latter floor, as mentioned earlier, which is always considered a disadvantage of this technique regarding accuracy and time.

6.3 Surveying using Modern Methods

A mixture of modern commonly used surveying instruments are utilized here, namely one total station, two geodetic receivers and one GPS navigator. The Trimble reflectorless total station is used for surveying of the outer perimeter of buildings from the ground. GPS receivers or navigators will be mainly used on the roof of the buildings, but not on the ground or of course inside the buildings due to the lack of clear sky and thus blockage of signals or loss of lock on satellites. The remaining part of Table 2 shows the whole procedure for the total station technique. Note that, surveying with the total station was done differently to what was performed in the practical theoretical case. Each building was surveyed relative to some control points for all its floors. Accordingly, the setup time is being considered only for the ground floor, in which any of these setups can be used then freely for all floors. In other words, in each setup, different points are observed for all sighted floors of nearby buildings.

The surveying of buildings was then performed first using two geodetic GPS receivers, where one base station is fixed on one of the previously known control points and the other rover kinematic receiver mounts on different points on the roof, and then using a GPS navigator, taking an observation time of 15 seconds on each point. However this was performed only on the roof of the buildings only, due to satellite blockage at the bottom of building or at any of its floors. This of course will lead to different analysis due the change of dimensions from the ground floor and repeated floors and roof as well, but will surely be beneficial where roof is similar to ground as well as similar multi-stories. Surveying using both GPS techniques will appear similar regarding number of surveyed points but will differ in the accuracy of the position of points, leading to higher accuracy in the case of using geodetic receivers. The whole process using GPS receivers and navigator is shown in Table 3.

6.4 Practical case Results and Conclusions

The comparison here between those three sets of measurement technique, is considered relative to the amount of data i.e. observed measurements, consumed time and manpower needed. However, another parameter here can be added regarding the format of data output from those latter three techniques, when compared to the output data using traditional surveying methods. This can be effective while considering the additive calculations required in order to output building coordinates to be exported to AutoCAD.

As well as, based on the results obtained from both the theoretical and practical cases, several comparisons can be extracted regarding several factors, mainly: accuracy, time and cost. Starting with accuracy, the total station and geodetic receivers possessed the best accuracy when compared to tapes and GPS navigators, as the used of tapes will degrade the accuracy due to the vast negative effect of human errors during measurements. The use of GPS navigators will implement point positioning technique which is full of errors affecting highly the accuracy of surveyed points. Now speaking about time management for each technique, and having a quick glance at Tables 1, 2 and 3, the use of modern surveying instruments especially the total station technique reduced the required time by 683 minutes, that is with 60%, due to the reduction of manpower and mainly the required time to survey each point. This proves that although the total station and GPS techniques seem to be more expensive due to the more advancement of the instrument used, but when compared to the manpower used and time required, as previously mentioned, the cost of the whole process is significantly reduced.

Table 2 Detailed report on the usage of total station technique for the urban survey of the practical case (Common Point: CP)

Building	Floors	Tape		Total Station (TS)					Time difference between TS and Tape (sec)	Remarks
		Measurements	Time required (sec)	Points	No. of setups	Setup Location	Time required (Setup & Observation) (sec)	Effective Required Time		
B1	G	18	540	8	3	G	320	320	220	
	1	29	870	24			360	360	510	
	2	51	1530	35			525	525	1005	
	3	52	1560	39			585	585	975	Similar to 8th Floor
	4	54	1620	39			585	585	1035	
	5	54	1620	39			585	585	1035	
	6	54	1620	44			660	660	960	
	7	54	1620	43			645	645	975	
	8	-	-	-			-	-	-	
	9	54	1620	47			705	705	915	
	10	54	1620	42			630	630	990	
	11	54	1620	38			570	570	1050	
	Roof	44	1320	36	2	Roof	900	900	420	
B6	G	22	660	16	4	G	960	960	-300	
	1	68	2040	44			660	660	1380	
	2	99	2970	70			1050	1050	1920	Similar to 3rd Floor
	3	-	-	-			-	-	-	
	4	52	1560	37			555	555	1005	
	5	99	2970	71			1065	1065	1905	
	6	123	3690	83			1245	1245	2445	
	7	62	1860	39			585	585	1275	
	8	71	2130	45			675	675	1455	
	9	62	1860	40			600	600	1260	
	10	71	2130	45			675	675	1455	
	11	62	1860	38			570	570	1290	
	Roof	83	2490	50	2	Roof	1110	1110	1380	

Building	Floors	Tape		Total Station (TS)					Time difference between TS and Tape (sec)	Remarks
		Measurements	Time required (sec)	Points	No. of setups	Setup Location	Time required (Setup & Observation) (sec)	Effective Required Time		
B2	G	10	300	4	4	G	780	240	60	3 common CP with B1 (1st and 3rd floor are similar)
	1	44	1320	24			360	360	960	
	2	67	2010	40			600	600	1410	
	3	-	-	-			-	-	-	
	4	60	1800	38			570	570	1230	Similar to 5th Floor
	5	-	-	-			-	-	-	
	Roof	36	1080	24	2	Roof	720	540	540	1 CP from B6
B3	G	10	300	4	3	G	600	420	-120	1 common CP with B2
	1	47	1410	29			435	435	975	
	2	70	2100	47			705	705	1395	
	3	63	1890	37			555	555	1335	
	4	63	1890	37			555	555	1335	
	5	63	1890	43			645	645	1245	
	Roof	65	1950	23	2	Roof	705	345	1605	2 CP from B1 and B6
B4	Ground	10	300	4	3	G	600	240	60	2 common CP with B3
	1	16	480	8			120	120	360	
	2	22	660	12			180	180	480	Similar to 3rd, 4th and 5th Floor
	3	-	-	-			-	-	-	
	4	-	-	-			-	-	-	
	5	-	-	-			-	-	-	
	Roof	46	1380	25	2	Roof	735	375	1005	2 CP from B1 and B6
B5	G	10	300	4	2	G	420	420	-120	2 common CP with B6
	1	16	480	12			180	180	300	Similar to 2nd, 3rd and 4th Floor
	2	-	-	-			-	-	-	
	3	-	-	-			-	-	-	
	4	-	-	-			-	-	-	
	5	22	660	12			180	180	480	
	Roof	44	1320	25	2	Roof	735	555	765	1 CP from B1

Table 3 Detailed report on the usage of GPS surveying techniques for the urban survey of the practical case

Building	No. of points	Geodetic Receivers		GPS Navigator	Time difference (sec)	Remarks
		Setup time of Base station (sec)	Time of surveyed points (sec)	Time of surveyed points (sec)		
B1	36	1800	540	540	1800	Setup time required for initialization on the reference point
B2	24	-	360	360	-	
B3	23	-	345	345	-	
B4	25	-	375	375	-	
B5	25	-	375	375	-	
B6	50	-	750	750	-	

It is worthwhile mentioning here that, although surveying using GPS is always hindered on the ground and repeated floors of all buildings, it can be merged efficiently with total station. This can be performed by surveying each building with both the total station and GPS techniques, by using the first on the ground and repeated floors, while using the latter on the roof. This will surely produce the most effective combined technique regarding applicability, cost and time.

VII. RESULTS AND RECOMMENDATIONS

The use of modern surveying equipment in the form of total stations and GPS receivers/ navigators, improved not only the accuracy of the surveying task, but as well as the efficiency of the survey due to the vast improvement in the form of reduction in number of manpower required to perform the same task in the traditional method using tapes, in addition to time saving in performing the survey and planning process. This of course can be easily proved by the large amount of data required to survey buildings' relations and dimensions using tapes. However, this large amount of data is reduced quite considerably using modern surveying by dealing with coordinates obtained from any of the aforementioned instruments, as well as the ability to control the amount of data that are essentially needed in urban planning purposes.

In addition, modern surveying is not only appreciated than traditional methods in this context only, but since the amount of data is known and easily formatted, and can be recognized easily, given the fact of proper reconnaissance of the site prior to surveying, field planning is considered advantageous in this case, since total number of instruments, manpower per day, number of days can all be set in advance before start of the survey, which offers a very powerful tool for modern surveying, as several factors and focal issues can be resolved accurately, not forgetting the pre-estimation of the surveying process cost in advance.

REFERENCES

[1] R. Wickramasuriya, L. Chisholm, M. Puotinen, N. Gill, and P. Klepeis, An automated land subdivision tool for urban and regional planning: Concepts, implementation and testing, Environmental Modeling and software, 26(12), 2011, 1675-1684.

[2] C. Freeman, Development of a simple method for site survey and assessment in urban areas, Landscape and Urban Planning, 44, 1999, 1-11.

[3] A. Burger, A. Grimm-pitzinger, and E. Thaler, A combination of modern and classic methods of surveying historical buildings – The church st. valentine in the South Tyrol, XXI International CIPA Symposium, Athens, Greece, 2007.

[4] P. Wathern, Environmental impact assessment: Theory and Practice, ISBN 0-203-40997-3, 1988, Master e-book ISBN.

[5] G. Smith, Impact Assessment and Sustainable Resource Management, London: Longman, 1993, 77-78.

[6] General Organization for Physical Planning (GOPP): Strategic planning for Shebin el Kanater city / Kaliobia governorate / Egypt, Urban survey phase, 2006.

[7] Urban survey and surveying project for the central area in Madinah, Kingdom of Saudi Arabia KSA, Dar El Salam office, Planning Organization in Madinah, KSA, 2011.

[8] Google Earth maps 2011.

[9] Google Earth maps 2013.

OPEN ACCESS

International
Journal
Of Modern Engineering Research (IJMER)

Developing a Programme for Engine Design Calculations of a Commercial Airliner

K. Suresh[1], K. Sai Sharath[2], Karrothu Vigneshwara[3], V.Rajiv[4]
[1]Asst. Professor, [2,3,4]Student, Aeronautical dept., Guru Nanak Eng. College(GNITC), Hyderabad, India

ABSTRACT: *This project leads to a path of understanding the necessary fundamental calculations that need to be done during an engine design of a commercial airliner. These calculations are hand based calculations that are done based on the parameters of the airframe data provided by the airline manufacturers. These calculations are a little tedious and require a paper and a pen to carry out the procedures. This project will enable the following outcomes for the students: providing a fundamental understanding of the aircraft engine design, more from the grounds up approach and an automated way (program) of doing the above, enabling faster iterations and making it easy to achieve the required parameters for designing an engine.*

Keywords: *Bypass ratio,Efficiency, Flow properties, HTML, PHP, Turbofan engine.*

I. INTRODUCTION

As we all know that an engine is the heart of any vehicle, without the engine there wouldn't be a vehicle. This heart in an aircraft is really big and there may be not one but four hearts. Designing these engines is really tricky and involves some serious work. Well it would basically require any engine designer to fill up this design sheet(fig 1.1).It is really a tedious work and requires a lot of time. This project basically allows any aeronautical engineering student to get acquainted with the theory behind designing of an aircraft engine and so as to save time with calculation a program for calculating has been developed.

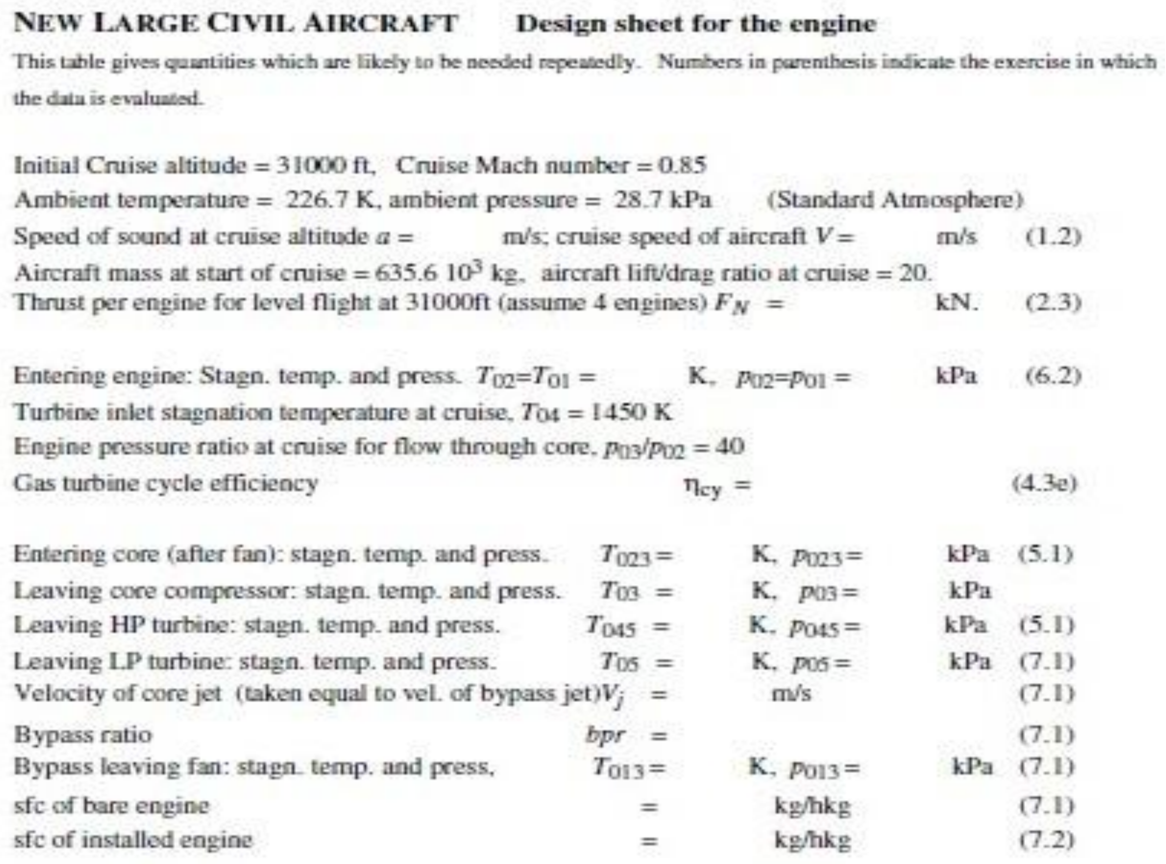

NEW LARGE CIVIL AIRCRAFT **Design sheet for the engine**

This table gives quantities which are likely to be needed repeatedly. Numbers in parenthesis indicate the exercise in which the data is evaluated.

Initial Cruise altitude = 31000 ft, Cruise Mach number = 0.85
Ambient temperature = 226.7 K, ambient pressure = 28.7 kPa (Standard Atmosphere)
Speed of sound at cruise altitude a = m/s; cruise speed of aircraft V = m/s (1.2)
Aircraft mass at start of cruise = 635.6 10^3 kg, aircraft lift/drag ratio at cruise = 20.
Thrust per engine for level flight at 31000ft (assume 4 engines) F_N = kN. (2.3)

Entering engine: Stagn. temp. and press. $T_{02}=T_{01}$ = K, $p_{02}=p_{01}$ = kPa (6.2)
Turbine inlet stagnation temperature at cruise, T_{04} = 1450 K
Engine pressure ratio at cruise for flow through core, p_{03}/p_{02} = 40
Gas turbine cycle efficiency η_{cy} = (4.3e)

Entering core (after fan): stagn. temp. and press. T_{023}= K, p_{023}= kPa (5.1)
Leaving core compressor: stagn. temp. and press. T_{03} = K, p_{03}= kPa
Leaving HP turbine: stagn. temp. and press. T_{045} = K, p_{045}= kPa (5.1)
Leaving LP turbine: stagn. temp. and press. T_{05} = K, p_{05}= kPa (7.1)
Velocity of core jet (taken equal to vel. of bypass jet) V_j = m/s (7.1)
Bypass ratio bpr = (7.1)
Bypass leaving fan: stagn. temp. and press, T_{013}= K, p_{013}= kPa (7.1)
sfc of bare engine = kg/hkg (7.1)
sfc of installed engine = kg/hkg (7.2)

II. LITERATURE SURVEY

The Boeing 747-400 was the largest civil aircraft that was introduced in service in the year 1989 but it is a derivative of the 747-100 which entered service in 1969. Presently Airbus A380 is the largest civil aircraft in this world. The 747-400 incorporated some aerodynamic improvements, including some improvements to the existing engines, but a much more radical redesign is needed to take the full advantage of the developments in aerodynamics and materials since 1969. Boeing and Airbus industries have separately and jointly discussed proposals for a much larger plane, with anywhere from about 600 to about 800 seats.

Boeing at that time had announced plans for a major derivative of the 747 to incorporate new wings and to be propelled by new engines. Two versions were proposed, the 747-500 and 747-600, with a common wing. The 747-600, which it is proposed should be produced first, was intended to carry 548 passengers over a range of up to 7890nm, whilst the 747-500 was to carry 462 passengers over a range of up to 8830nm. Airbus then proposed the A3XX with an expected capacity of 555 passengers for a range of up to 7450nm.

It takes several years to design, develop and certificate a new plane, though the length of time is becoming shorter. It seems to take even longer to develop the engines, but until the specifications of the plane are settled it is not clear what engine is needed. There are currently three major engine manufactures and they are, Rolls Royce in Britain, Pratt & Whitney and General Electrics in the USA and it is their aim to have an engine already for whatever new large aircraft is decided to build.

A specifications for the ‘paper’ airplanes alter, the ‘paper’ engine design to power them will also change; literally hundreds of potential engines will be tried to meet a large number of proposals for the new airplane before any company finally commits itself.

It is essential to realize that both the new plane, and the engines which power it, will depend heavily on the experience gained in earlier products. In Table 2.1 below, the proposed specifications for the New Large Aeroplane are therefore set beside those achieved for the 747-700.

Table 2.1 Comparison of some salient aircraft parameters

	New Large Aeroplane NLA	Boeing 747-400
No. of passengers	620	400
Range(nautical miles)	8000	7300
Payload at this range (a)	58.5tonne	38.5tonne
Max take-off weight (d = a + b + c)	635.6tonne	395.0tonne
Empty weight (b)	298.7tonne	185.7tonne
Fuel capacity (c)	275.4tonne	174.4tonne
Cruise Mach No.	0.85	0.85
Initial cruise Altitude	31000ft	31000ft
Cruise Lift/Drag	20	17.5
Wing Area	790m^2	511m^2

The atmosphere through which the plane flies depends on the altitude, with the pressure, temperature and density failing as altitude increases. At high altitude the variations with season, location and time of day is much less than at ground level and it is normal to use a standard atmosphere in considering aircraft and engine performance. According to International Civil Aviation Organization the values at altitudes are expressed as a ratio to the values at sea level. Standard sea-level atmospheric conditions are defined for a standard day: T_{sl} = 288.15K, P_{sl} = 101.3 kPa, ρ_{sl} = 1.225 kg/m3. In Standard atmosphere temperature is assumed to decrease linearly with altitude at 6.5K per 1000m below the tropopause, but to remain constant above this altitude at 216.65K. Cruise often begins at 31000ft, and the corridors are separated by 2000ft. below table (2.2) gives information about different conditions of standard atmosphere.

Table 2.2 Useful values of ICAO standard atmosphere

ALTITUDE		TEMPERATURE	PRESSURE	DENSITY
Feet	Km	K	10^5 Pa	Kg/m^3
0	0	288.15	1.013	1.225
31000	9.45	226.73	0.287	0.442
33000	10.05	222.28	0.260	0.336
35000	10.67	218.80	0.238	0.380
37000	11.28	216.65	0.214	0.285
39000	11.88	216.65	0.197	0.316
41000	12.50	216.65	0.179	0.287
51000	15.54	216.64	0.110	0.179

The below fig (2.1) gives the ICAO standard atmosphere:

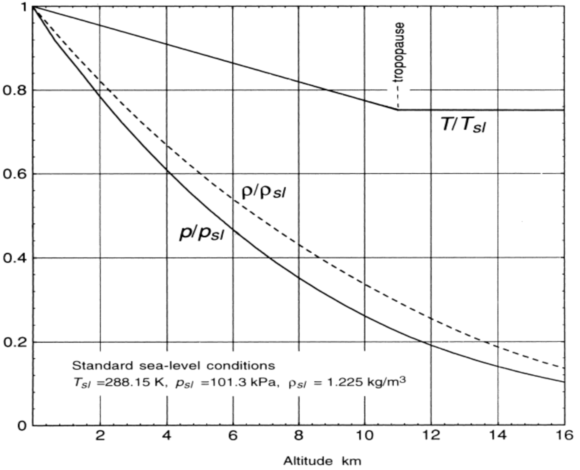

Fig 2.1: ICAO Standard Atmosphere

In order to calculate the speed of vehicle that is required for further calculation part is given by the formula;

$$\text{Mach no} = \frac{\text{SPEED OF VECHILE}}{\text{SPEED OF SOUND}} \qquad (1)$$

The speed of sound formula can be given by;

$$a=\sqrt{\gamma}\ RT \qquad (2)$$

Where: a = Speed of sound

$\gamma = 1.4$

R = 287 J/kg K

T = Temperature at given altitude (i.e. Ta)

Hence in order to find out the speed of the vehicle;

$$V = M \times a \qquad (3)$$

Where: V = speed of sound

M = Mach no

a = speed of sound

III. THEORY BEHINDTHE CALCULATION OF ESSENTIAL PARAMETERS

There are three main critical legs of a flight that affect the engine performance, they are: Take-off, Climb and Cruise. In any engine the first parameter to be fixed would be thrust. There has to be a compromise between a machine that can travel fast at cruise and relatively slow during take-off and landing. The lift co-efficient is given as;

$$C_L = L \,/\, \tfrac{1}{2}\rho A V^2 \qquad (4)$$

Where L is the lift force that acts perpendicular to the direction of travel.The figure below shows how the lift of the aircraft varies with angle of attack at low speeds such as take-off and it can be seen that the lift rises almost proportionally to the incidence until around the peak, beyond which it falls rapidly. The rapid fall in the lift is referred to as stall and in simple terms occurs when the boundary layer separates from the upper surface of the wing.

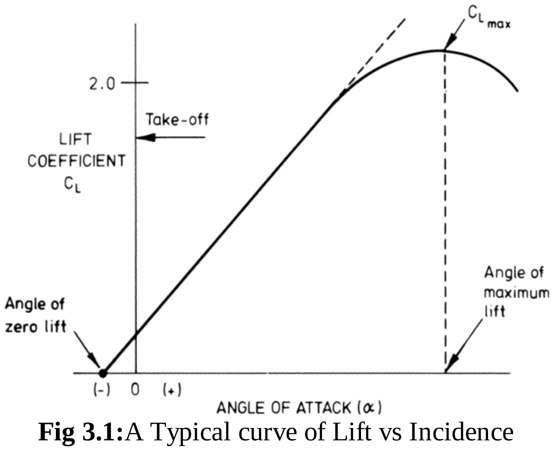

Fig 3.1:A Typical curve of Lift vs Incidence

It is an objective of a civil aircraft to lift as much as it can with the least possible drag. Reducing the drag for the same lift allows the aircraft to use less fuel and to travel further. For steady level flight at small incidence, as for cruise, two statements can be made on the basis of simple mechanics:

Lift = Weight and Drag = Thrust of the engines

To estimate the range we use Breguet's Range equation;

$$\frac{\mathrm{dw}}{\mathrm{dt}} = -\mathrm{g}(\mathrm{sfc} \times \text{net thrust}) = -\mathrm{g}(\mathrm{sfc} \times \text{drag}) = -\mathrm{g}\frac{\mathrm{sfc} \times \mathrm{w}}{\mathrm{l/d}} \qquad (5)$$

Where *L/D* ratio of lift to drag and we use W=L. Rearranging

$$\frac{\mathrm{dw}}{\mathrm{w}} = -\frac{\mathrm{g\ sfc\ dt}}{\mathrm{L/D}} \qquad (6)$$

This equation can then be rewritten in terms of distance travelled *s* as

$$\frac{\mathrm{dw}}{\mathrm{w}} = -\frac{\mathrm{g\ sfc\ ds}}{\mathrm{V\ L/D}} \qquad (7)$$

Keeping VL/D and sfc constant the above equation can be then integrated to give *Breguet's* range formula

$$\mathrm{s} = -\frac{\frac{\mathrm{VL}}{\mathrm{D}}}{\mathrm{g\ sfc}} \times \ln\left(\frac{\mathrm{wend}}{\mathrm{wstart}}\right) \qquad (8)$$

A flow of fuel m_f passes down the pylon, but its velocity is low and it conveys negligible momentum. A mass flow of air m_{air} enters the engine; m_{air} is typically two orders of magnitude greater than m_f. It is assumed for simplicity here that the jet is uniform as it crosses the control surface with velocity V_j. The thrust is calculated by considering the flux of momentum across the control surface around the engine – since the pressure is assumed uniform over the control surface the pressure creates no net force. Considering the flow which crosses the control surface and passes through the engine, we can write down two fluxes are;

Flux of momentum entering the engine = m_{air} x V. (9)

Flux of momentum leaving the engine = (m_{air}+m_f) x $\mathrm{V_j}$. (10)

The extra mass flow in the jet is included here for completeness, but this represents a small effect for high bypass ratio engine.

The net thrust F_N which is available in flight is given by the difference between the two momentum fluxes, that is;

$$F_N = (m_{air}+m_f) \times \mathrm{V_j} - m_{air} \times \mathrm{V} \qquad (11)$$

If the engine were being tested on a stationary test bed or before the aircraft started to move the thrust produced is known as the **gross** thrust, which, since V=0, is given by;

$$F_G = (m_{air}+m_f) \times \mathrm{V_j}. \qquad (12)$$

The difference between gross and net thrust is m_{air}V, often referred to as the **ram drag** or the **inlet-momentum drag**, so;

$$F_N = F_G - m_{air}\, x\mathrm{V_j}. \qquad (13)$$

Here we have ignored the drag on the outside of the engine nacelle drag, which leads to a ring of reduced relative velocity around the jet and consequent reduction in useful thrust. Unfortunately, nacelle drag is becoming a more significant factor as the engine becomes larger for the same thrust, i.e. as the bypass ratios go up. The Kinetic Energy of the engine can be given as;

$$\Delta KE = \frac{1}{2}[(mair + mf)Vj^2 - mairV^2] \qquad (14)$$

The power actually associated with propelling the aircraft is given by;

$$Power\ to\ the\ aircraft = flight\ speed \times net\ thrust = V \times Fn$$
$$= \mathrm{V}[(m_{air}+m_f) \times \mathrm{V_j} - m_{air} \times \mathrm{V}]. \qquad (15)$$

The propulsiveefficiency compares the power supplied to the aircraft with the rate of increase in kinetic energy of the air through the engine. Propulsive efficiency η_p is straightforward to define by;

$$\eta p = \frac{Power\ \ to\ aircra\ ft}{Power\ \ to\ jet} \qquad (16)$$

$$\eta p = \frac{\mathrm{V}[(mair + mf\ ) \mathrm{\ x\ Vj} - mair\ \mathrm{x\ V}]}{\frac{1}{2}[(mair + mf\ )Vj^2 - mair\ V^2]} \qquad (17)$$

Since, as already noted, the mass flow rate of fuel is very much less than that of air it is possible to write η_p with sufficient accuracy for our present purposes as;

$$\eta p = \frac{2V}{V+Vj} \tag{18}$$

The above equation is known as the *Froude* equation for propulsive efficiency.

The overall efficiency is given by;

$$\eta o = \frac{Useful\ work}{Thermal\ energy\ from\ fuel} = \eta p \times \eta th \tag{19}$$

From the first law of thermodynamics when applied to this steady flow process can be written as;

$$Qnet - Wnet = mair \times \Delta h \tag{20}$$

Where Δh is the enthalpy difference between the inlet air and the exhaust based on stagnation condition;

$$Qnet - Wnet = mair \times Cp \times (T5 - T2) \tag{21}$$

This can be written in terms of lower calorific value of the fuel;

$$mf \times lcv = mair \times Cp \times (T4 - T3) \tag{22}$$

These isentropic processes are those which ideal compressors and turbines would perform. As can be seen, the actual compression process involves a greater temperature rise than
That of the isentropic compressor for the same pressure rise;

$$T_3 - T_2 > T_{3is} - T_2 \tag{23}$$

And in the same way

$$T_4 - T_5 < T_4 - T_{5is} \tag{24}$$

For compressors and turbines it is normal to define efficiencies which relates actual work per unit mass flow to that of an ideal (i.e. loss free) machine with equivalent pressure change;

$$\eta comp = \frac{Ideal\ work}{Actual\ work} \text{ And } \eta turb = \frac{Actual\ work}{Ideal\ work} \tag{25}$$

Treating fluid as a perfect gas, for which $h = c_p T$.

$$\eta comp = \frac{T3is - T2}{T3 - T2}\ \ and\ \ \eta turb = \frac{T4 - T5}{T4 - T5is} \tag{26}$$

Nowadays the isentropic efficiencies in a high quality aircraft engine for use on a civil aircraft are likely to be around 90% for compressor and turbine and this round number will normally be used in this project.

$$\frac{p}{T^{\frac{\gamma}{\gamma-1}}} = constant \tag{27}$$

This means in the present cases,

$$\frac{T3is}{T2} = \left(\frac{p3}{pa}\right)^{(\gamma-1)/\gamma}\ \ and\ \ \frac{T4}{T5is} = \left(\frac{p4}{pa}\right)^{(\gamma-1)/\gamma}. \tag{28}$$

The power which must be supplied to the compressor is given by;

$$Wc = mair \times Cp \times (T3 - T2) \tag{29}$$

$$Wt = mair \times Cp \times (T4 - T5is) \tag{30}$$

The Thermal Efficiency of the cycle can be given as;

$$\eta cycle = \frac{Wnet}{mair \times Cp \times (T4 - T3)} \tag{31}$$

But the thermal efficiency can be given by;

$$\eta th = Wnet/mf \times LCV \tag{32}$$

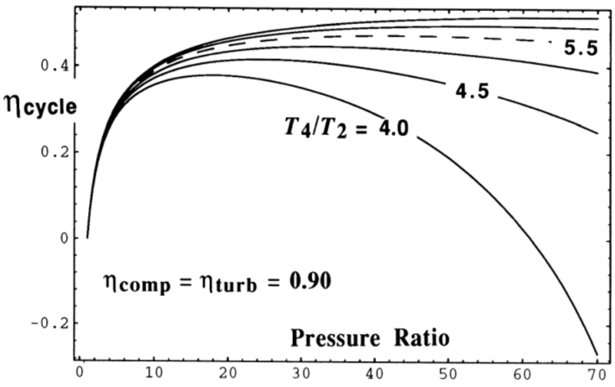

Fig 3.3: The Comparison between Efficiency of cycle and that of Pressure Ratio.

The blade cooling can be given by;

$$\varepsilon = (Tg - Tm)/(Tg - Tc) \qquad (33)$$

Turbine inlet temperature is important because increasing its value makes the pressure ratio across the core turbine smaller inrelation to the pressure rise of the core compressor and thereby increases the power available from the LP turbine. Increasing this temperature also increases the thermal efficiency, provided that the pressure ratio increases by an appropriate amount.

Table 3.1: Representing the Compressor and Turbine inlet temperatures

	T_2	T_4	T_4/T_2
Take-Off (Standard day, sea level)	288.15 K	1700 K	5.90
Top of Climb(31000ft, M=0.85)	259.5 K	1575 K	6.07
Start Of Cruise(31000ft, M=0.85)	259.5 K	1450 K	5.59

The steady flow energy equations for the flow of gas with no heat transfer and no external work transfer can be written as;

$$h1 + \frac{V1^2}{2} = h2 + V2^2/2 \qquad (34)$$

Where h is the enthalpy, which can be rewritten in a way more convenient for us;

$$Cp \times T + \frac{V^2}{2} = Cp \times To \qquad (35)$$

Where T_o is the *stagnation* temperature, being that temperature which the gas would attain if brought to rest without work and heat transfer, not necessarily in an ideal or loss-free manner. The specific heat can be rewritten as $Cp = \gamma R/(\gamma - 1)$ and on rearranging and inserting this into the above equation the stagnation temperature may be written as;

$$\frac{To}{T} = 1 + (\gamma - 1)/2 \times (\frac{V^2}{\gamma RT}) \qquad (36)$$

Again this equation between stagnation temperature T_0 and static temperature T does not imply ideal or loss-free acceleration or deceleration.

At this point we suppose that the acceleration or deceleration of the gas between the static state p and T and that at stagnation p_0 and T_0 is reversible and adiabatic, for which we know that;

$$\frac{P}{\rho^{\gamma}} = constant\ and \frac{p}{\frac{\gamma}{T^{\gamma-1}}} = constant \qquad (37)$$

It then immediately follows that;

$$\frac{p0}{p} = (\frac{T0}{T})^{\gamma/(\gamma-1)} \qquad (38)$$

The bypass ratio is defined as the mass flow of the air passing outside the core divided by the mass flow through the core;

$$bpr = mb/mc \qquad (39)$$

The choice of bypass ratio has a major effect on the efficiency, because for a given core the bypass ratio determines the jet velocity. The bypass ratio also greatly affects the appearance, size and weight of the engine: the pure turbojet has a small diameter relative to its length, whereas high bypass ratio engines have their overall diameter comparable to their length.Previous engines (the RB211, CF6 and JT9D generation) had bypass ratios of around 5 and we may assume that a bypass ratio at least as great as this will be employed in a new engine for the New Large Aircraft.

To achieve this it would probably be necessary to install a gear box between the LP turbine and the fan, to allow the turbine to run faster; this requires considerable development and will very probably be heavy. For a civil transport engine a major requirement is low fuel consumption, equivalent to high overall efficiency. The overall efficiency is the product of propulsive and thermal efficiency;

$$\eta 0 = \eta p \times \eta th \qquad (40)$$

The combination of constraints on ηcy and ηp give rise to the high bypass engine for subsonic propulsion. The constraints give rise to;

$$sfcinstalled = \{1.04 + 0.01(bpr - 1)\}sfcbare \qquad (41)$$

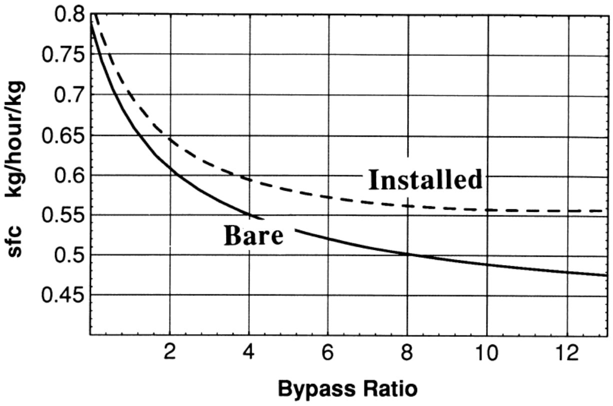

Fig 3.4: Prediction variation of sfc with bypass ratio for bare and installed engine

IV. PROBLEMS WITH SOLUTION

To find the engine thrust needed for steady flight at start of cruise, when the weight of the aircraft and wing area for the NLA at altitude 31000ft and Mach number of 0.85. Given;

Initial Cruise altitude: 31000ft Cruise Mach number: 0.85 Ambient Temperature= 226.7K
Ambient pressure= 28.7×10^3 Pa Speed of sound at cruise altitude a= 301.827 m/s
Cruise speed of the aircraft V= 256.5 m/s Aircraft mass at start of cruise = 635.6×10^3 Kg
Aircraft L/D ratio= 20
And thus;
L/D = 20
Lift/Drag = 20
Replacing Lift with Weight and Drag with Thrust,
Weight/Thrust = 20
W/T =20

$$635.6 \times 1000 \times 9.81/T = 20 \qquad T = 635.6 \times 1000 \times 9.81/20$$

T = 311.655 kN

Thrust per engine (Assuming the large aircraft to have 4 engines) = 77.914 kN/engine

Calculating the thermal efficiency and the net work per kg of air flowing in the engine. Assume isentropic efficiencies of compressor and turbine is 90%. For the following conditions;

T_2 = 259.5K, T_4 = 1450K, PR = 40.

Given:T_2 = 259.5K T_4 = 1450K PR = 40

$$T3is = \left(PR^{\frac{\gamma-1}{\gamma}}\right) \times T2 \tag{41}$$

T_{3is} = 716.63K on substitution of values in the above equation

.:

The work done by the compressor is,

$$Wc = Cp \times (T3is - T2)/\eta comp$$

$$W_c = 510.47 \text{ Kj/kg}$$

$$T5is = T4/(PR^{\frac{\gamma-1}{\gamma}}) \tag{42}$$

T_{5is} = 525.05K on substituting the values in the above equation

.:

The work done by the turbine is;

$$Wt = Cp \times (T4 - T5is) \times \eta turb \tag{43}$$

Wt = 836.61 Kj/kg

.:

$$Wnet = Wt - Wc = 326.14\ kJ/kg$$

$$\eta th = \frac{Wnet}{Cp} \times (T4 - T3) = 0.4754$$

Finding Temperature entering the core compressor and hence the temperature at exit from the core compressor and the temperature leave the H.P turbine and the pressure at the outlet from the turbine. The temperature and pressure at cruise is 259.5K and 46.0 KPa. Assume a pressure ratio of 1.6 for flow through the fan which enters the core and a pressure ratio of 25 in the core compressor itself. The temperature of the entry of H.P turbine is 1450K. Assume efficiency of compressor and turbine 90%.

$$\frac{Tfan}{Tair} = Pr^{(\gamma-1)/\gamma} = 1.143$$
$$Tfan = 296.79K$$
$$(Tfanis - T\,air) \times 100 = (Tfan - Tair) \times 90$$
$$Tfan = 300.9K$$
$$\Delta T = 41.4K$$

Now to find the Core temperatures:

$$\frac{Textcoreis}{Tentcore} = Pr2^{(\gamma-1)/\gamma}$$
$$Texcoreis = 754.80K$$
$$(Texcoreis - Tencore) \times 100 = (Texcore - Tencore) \times 90$$
$$Texcore = 805.2K$$
$$\Delta Tcorecomperssor = \Delta Tturbine$$
$$Texturb = 945.6K$$
$$(Tenturb - Texturb) \times 100 = (Tenturb - Texturbis) \times 90$$
$$Texturbis = 889.66K$$
$$Pfan = 1.6 \times 46 = 73.6 \quad Pcomp = 73.6 \times 25 = 1840$$
$$\frac{T5is}{T4}^{\gamma/(\gamma-1)} = \frac{P}{1840} = 332.82\,kPa$$

If the airplane cruises at Mach number of 0.85 at an altitude of 31000ft find the stagnation temperature and pressure of the flow perceived by the plane.
We know that;

$$\frac{T0}{T} = 1 + \frac{\gamma-1}{2} \times M^2 = 1.1445 \qquad (44)$$

$T0 = 1.1445 \times 226.73 = 259.5K$

$$\frac{p0}{pa} = \left(\frac{T0}{T}\right)^{\frac{\gamma}{\gamma-1}} = 1.603$$
$$p0 = 1.603 \times 28.7 = 46.0\,kPa$$

Using the results above to provide the inlet conditions into the LP turbine at a flight Mach number of 0.85 at 31000 ft. Assume equal velocity for the core and bypass jets. Assume thatthe inlet decelerates the flow isentropically and the nozzles expand the flow isentropically to ambient pressure. Take the isentropic efficiencies for the fan and for the LP turbine to be each 0.90. The following is calculated: The jet velocity, propulsive efficiency, gross thrust F_G and net thrust F_N and the Overall Efficiency.

For bpr = 10

We know that $$(bpr + 1) \times \Delta Tfan = \Delta Tlpturb$$
$$7 \times \Delta Tfan = \Delta Tlpturb = 376.2K$$

.:

$$T05 = 945.7 - 376.2 = 569.5K$$
$$T05is = 945.7 - \frac{\Delta Tlpturb}{0.90} = 527.7K$$

Temp ratio = 7.705

$$P05 = 43.2\,kPA$$
$$Pa = 28.7\,kPA$$

Pressure ratio = 0.889

$$Vj^2 = 2 \times 1004.5 \times 569.5 \times (1 - 0.889)$$
$$Vj = 355.3\,m/s$$
$$FG = \frac{Vj}{mair + mf} = 3.91\,kN\,kg^{-1}s$$
$$\eta p = \frac{2V}{V + Vj} = 0.839$$
$$\eta 0 = 0.428 \quad FN = 1.087\,kN\,kg^{-1}s \quad sfc = 0.492\frac{kg}{h/kg}$$

From the above results the following graphs are obtained:

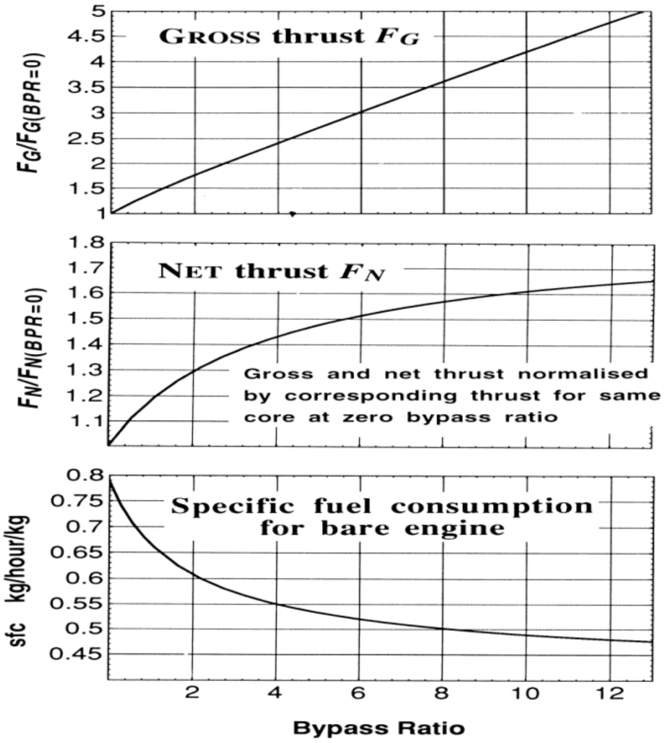

Fig 4.1: Prediction variations in Thrust and SFC with bypass ratio for constant core

V. RESULTS AND CONCLUSION

From the above we can say that the parameters are interdependent on each other and one must be careful in calculating the parameters involved in designing an engine for a new large aircraft. As one can see that there is a lot of work involved when one sits to design an engine, in order to simply the above process we developed a program using HTML and PHP 5 programing language. The result program looks like this:

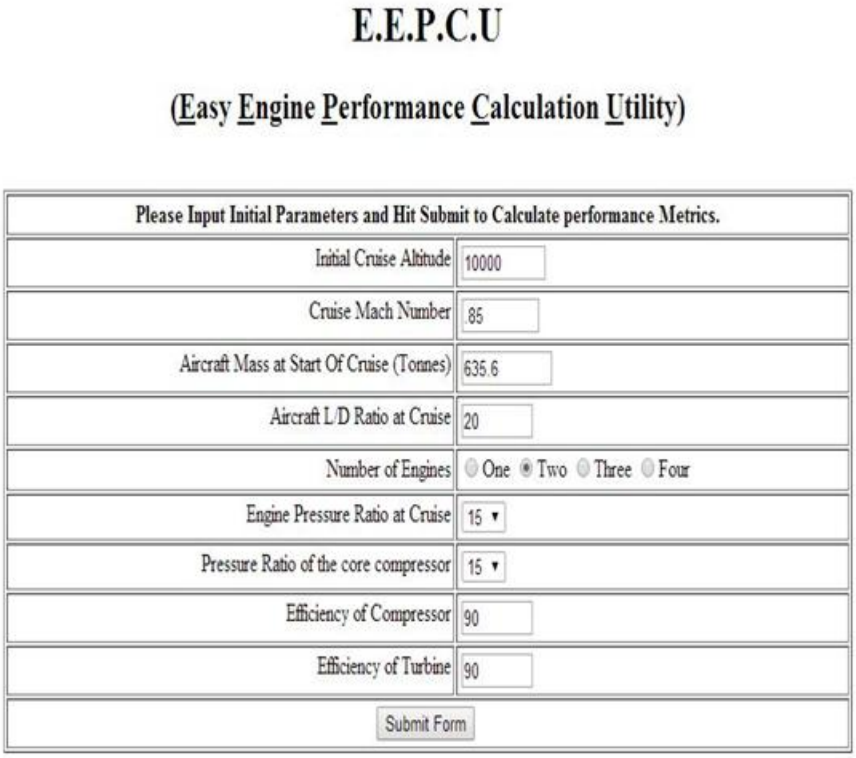

E.E.P.C.U

(Easy Engine Performance Calculation Utility)

Please Input Initial Parameters and Hit Submit to Calculate performance Metrics.	
Initial Cruise Altitude	10000
Cruise Mach Number	.85
Aircraft Mass at Start Of Cruise (Tonnes)	635.6
Aircraft L/D Ratio at Cruise	20
Number of Engines	○ One ● Two ○ Three ○ Four
Engine Pressure Ratio at Cruise	15 ▾
Pressure Ratio of the core compressor	15 ▾
Efficiency of Compressor	90
Efficiency of Turbine	90

Fig 5.1: The main page of the program with all the input variables

Hence one can just input all the variables required and then submit the form. The result when one submits the form looks like this:

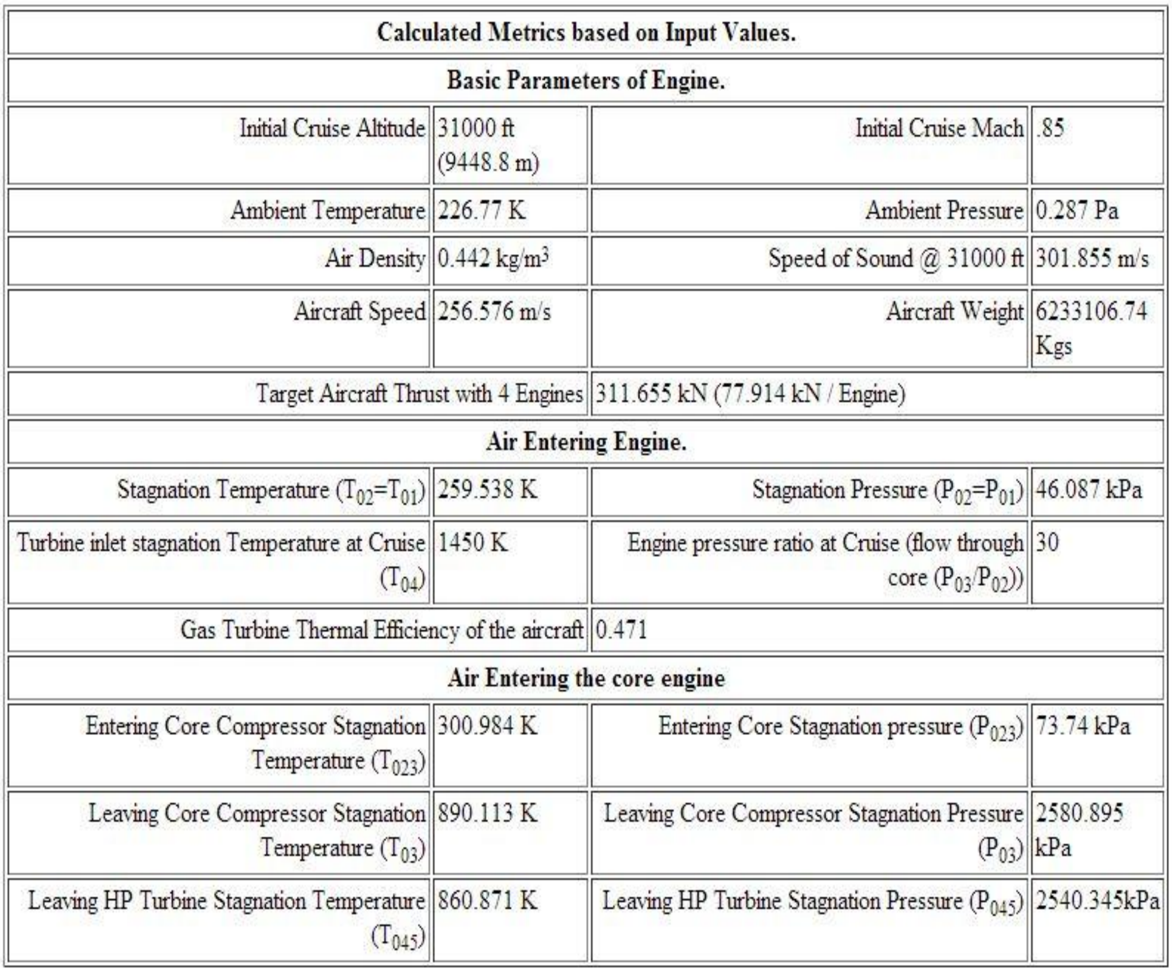

Calculated Metrics based on Input Values.			
Basic Parameters of Engine.			
Initial Cruise Altitude	31000 ft (9448.8 m)	Initial Cruise Mach	.85
Ambient Temperature	226.77 K	Ambient Pressure	0.287 Pa
Air Density	0.442 kg/m^3	Speed of Sound @ 31000 ft	301.855 m/s
Aircraft Speed	256.576 m/s	Aircraft Weight	6233106.74 Kgs
Target Aircraft Thrust with 4 Engines	311.655 kN (77.914 kN / Engine)		
Air Entering Engine.			
Stagnation Temperature (T_{02}=T_{01})	259.538 K	Stagnation Pressure (P_{02}=P_{01})	46.087 kPa
Turbine inlet stagnation Temperature at Cruise (T_{04})	1450 K	Engine pressure ratio at Cruise (flow through core (P_{03}/P_{02}))	30
Gas Turbine Thermal Efficiency of the aircraft	0.471		
Air Entering the core engine			
Entering Core Compressor Stagnation Temperature (T_{023})	300.984 K	Entering Core Stagnation pressure (P_{023})	73.74 kPa
Leaving Core Compressor Stagnation Temperature (T_{03})	890.113 K	Leaving Core Compressor Stagnation Pressure (P_{03})	2580.895 kPa
Leaving HP Turbine Stagnation Temperature (T_{045})	860.871 K	Leaving HP Turbine Stagnation Pressure (P_{045})	2540.345kPa

Fig 5.2: The output page of the program

The input page(fig 5.1) of the program is written in HTML, whereas the output page(fig 5.2) is written in PHP5 programming language.

The site on which the program is been uploaded is www.konidala.in/engine. The project as said is intended to help one learn about the engine designing and all reduce efforts. We have succeeded in making one understand the basics behind the theory of designing. The main objective as discussed in the introduction was to fill in the design sheet that is essential for designing an engine and thus:

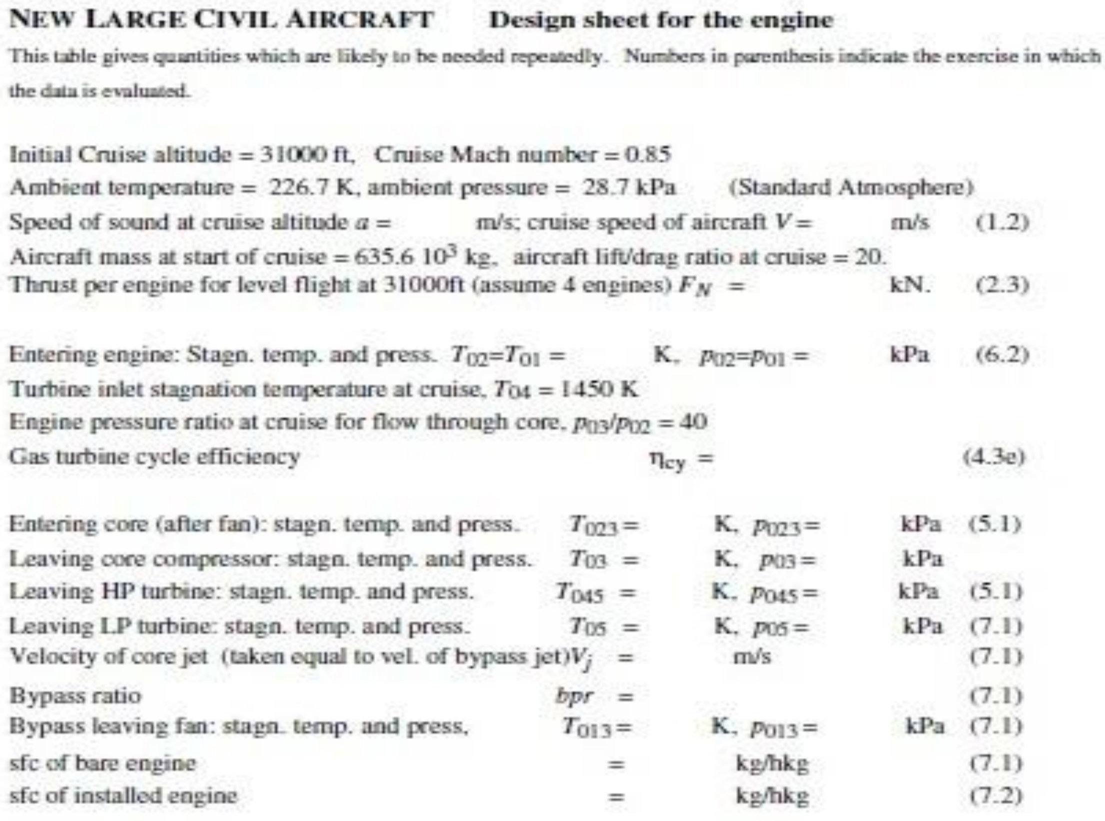

NEW LARGE CIVIL AIRCRAFT **Design sheet for the engine**

This table gives quantities which are likely to be needed repeatedly. Numbers in parenthesis indicate the exercise in which the data is evaluated.

Initial Cruise altitude = 31000 ft, Cruise Mach number = 0.85
Ambient temperature = 226.7 K, ambient pressure = 28.7 kPa (Standard Atmosphere)
Speed of sound at cruise altitude a = m/s; cruise speed of aircraft V = m/s (1.2)
Aircraft mass at start of cruise = 635.6 10^3 kg, aircraft lift/drag ratio at cruise = 20.
Thrust per engine for level flight at 31000ft (assume 4 engines) F_N = kN. (2.3)

Entering engine: Stagn. temp. and press. T_{02}=T_{01} = K, p_{02}=p_{01} = kPa (6.2)
Turbine inlet stagnation temperature at cruise, T_{04} = 1450 K
Engine pressure ratio at cruise for flow through core, p_{03}/p_{02} = 40
Gas turbine cycle efficiency η_{cy} = (4.3e)

Entering core (after fan): stagn. temp. and press. T_{023} = K, p_{023} = kPa (5.1)
Leaving core compressor: stagn. temp. and press. T_{03} = K, p_{03} = kPa
Leaving HP turbine: stagn. temp. and press. T_{045} = K, p_{045} = kPa (5.1)
Leaving LP turbine: stagn. temp. and press. T_{05} = K, p_{05} = kPa (7.1)
Velocity of core jet (taken equal to vel. of bypass jet) V_j = m/s (7.1)
Bypass ratio bpr = (7.1)
Bypass leaving fan: stagn. temp. and press, T_{013} = K, p_{013} = kPa (7.1)
sfc of bare engine = kg/hkg (7.1)
sfc of installed engine = kg/hkg (7.2)

Fig 5.3: Design sheet

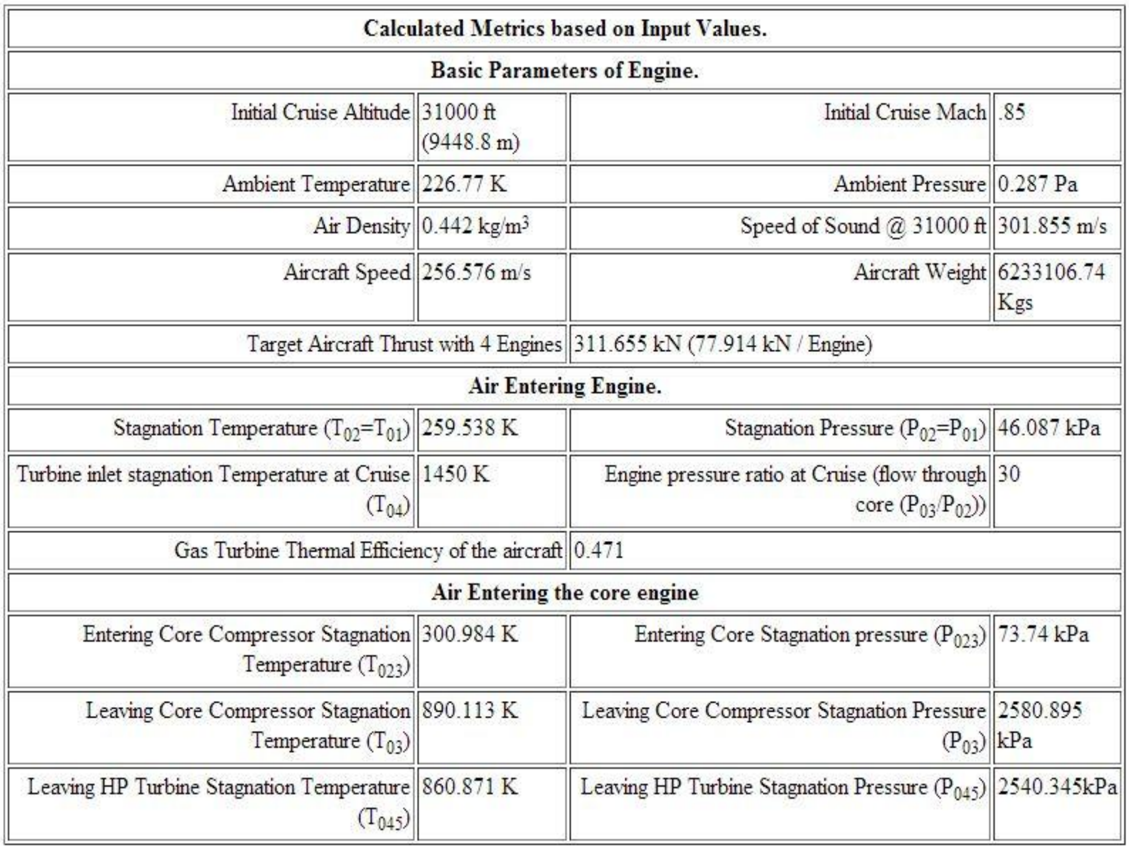

Calculated Metrics based on Input Values.			
Basic Parameters of Engine.			
Initial Cruise Altitude	31000 ft (9448.8 m)	Initial Cruise Mach	.85
Ambient Temperature	226.77 K	Ambient Pressure	0.287 Pa
Air Density	0.442 kg/m^3	Speed of Sound @ 31000 ft	301.855 m/s
Aircraft Speed	256.576 m/s	Aircraft Weight	6233106.74 Kgs
Target Aircraft Thrust with 4 Engines	311.655 kN (77.914 kN / Engine)		
Air Entering Engine.			
Stagnation Temperature (T_{02}=T_{01})	259.538 K	Stagnation Pressure (P_{02}=P_{01})	46.087 kPa
Turbine inlet stagnation Temperature at Cruise (T_{04})	1450 K	Engine pressure ratio at Cruise (flow through core (P_{03}/P_{02}))	30
Gas Turbine Thermal Efficiency of the aircraft	0.471		
Air Entering the core engine			
Entering Core Compressor Stagnation Temperature (T_{023})	300.984 K	Entering Core Stagnation pressure (P_{023})	73.74 kPa
Leaving Core Compressor Stagnation Temperature (T_{03})	890.113 K	Leaving Core Compressor Stagnation Pressure (P_{03})	2580.895 kPa
Leaving HP Turbine Stagnation Temperature (T_{045})	860.871 K	Leaving HP Turbine Stagnation Pressure (P_{045})	2540.345kPa

Fig 5.4: The completed design sheet.

REFERENCES

[1]. THE JET PROPULSION' by NICHOLAS CRAIG

[2]. ANDERSON J D. 'Introduction to Flight'. McGraw-Hill Book Co. Inc. 3rd Edition, 1989.

[3]. BAHR D W & DODDS W J. 'Design of Modern Turbine Combustors' Academic Press Inc., San Deigo C.A., 1990.

[4]. COHEN H, ROGERS G F C & SARAVANAMUTTOO H I H. 'Gas Turbine Theory' 5th Edition, 2001.

[5]. CUMPSTY N A. 'Compressor Aerodynamics' Longman, 1989.

[6]. DIXON S L. 'Fluid Mechanics, Thermodynamics of Turbomachinery'. Butterworth-Heinemann, 3rd Edition, 1995.

[7]. GREEN J E. 'Greener by Design - the technology challenge', The Aeronautical Journal, Vol. 106, pp57-113, 2002.

[8]. GUNSTON B. 'The Development of Jet and Turbine Aero Engines', Patrick Stephens Ltd., Spark ford, England, 2nd Edition, 1997.

[9]. HÜNECKE K. 'Jet Engines: Fundamentals of Theory, Design and Operation', England, 1997.

[10]. HILL P G & PETERSON C R. 'Mechanics and Thermodynamics of Propulsion'. Addison-Wesley, Second Edition, 1992.

[11] INTERGOVERNMENTAL PANEL ON CLIMATE CHANGE'. Aviation and the Global Atmoshpere,Special Report of IPCC Working Groups I& III. 1999 (Cambridge University Press).

[12]. ISO *Standard Atmosphere ISO 2533* International Standards Organization, Geneva 1975. [13]. 'THE JET ENGINE'. Rolls Royce, 4th Edition, 1986.

[14]. KERREBROCK J L. 'Aircraft Engines**'.**

OPEN ACCESS

International
Journal
Of Modern Engineering Research (IJMER)

Conventional Method For Ground Water Augmentation Of Panamaruthupatti Block, Salem District, Tamil Nadu, India - A Case Study

R. Neelakantan[1], C. T. Sivakumar[2]

[1] *Professor, Department of Industries and Earth Sciences, Tamil University, Thanjavur-613 010*
[2] *Research Scholar, Department of Geology, Periyar University, Salem -636 011*

ABSTRACT: *Artificial groundwater recharge is a process by which the groundwater reservoir is augmented at a rate exceeding the augmentation rate under natural conditions of replenishment. In some parts of India, due to over-exploitation of groundwater, decline in groundwater levels resulting in shortage of supply of water, and intrusion of saline water in coastal areas have been observed. In such areas, there is need for artificial recharge of groundwater by augmenting the natural infiltration of precipitation or surface-water into underground formations by methods such as water spreading, recharge through pits, shafts, wells et cetera The choice of a particular method is governed by local topographical, geological and soil conditions; the quantity and quality of water available for recharge; and the technological-economic viability and social acceptability of such schemes. In our project our study area is mainly comprised of hilly terrain with the maximum elevation at 1184m at Bodamalai(melur). With other hillocks and hills are Jarugu malai, Bodamalai, Jalluthumalai and Perumal malai, etc. In the north west of the study area, a lake is situated namely Panamaruthupatti Lake. It is a natural lake surrounded by hills by which it receives sources of water. Panamaruthupatti lake is about 3500 acres in area which provides water to Salem town before the supply of Cauvery water from Mettur. Now this source of water is used to meet the requirements in some parts of southern suburbs of Salem city and Northern part of Namakkal District upto Rasipuram Town. This source of water will support to enhance the over all augmentation of sub surface water in the study area. Now a days the supply of Cauvery water is not fulfilling the needs of people and its sub urban because of increase in population. Any improvement in ground water condition of study area will have the chance of additional supply of drinking water and also the possibility of increase in agricultural activity in and around the said village. Hence we plan to do research and propose the ideas for recharging the water to Panamarathupatti Block by using conventional method.*

Keywords: *Conventional Method, Ground Water Augmentation, Panamaruthupatti Block, Salem District, Case Study*

I. INTRODUCTION

Artificial recharge is the planned, human activity of augmenting the amount of groundwater available through works designed to increase the natural replenishment or percolation of surface waters into the groundwater aquifers, resulting in a corresponding increase in the amount of groundwater available for abstraction. Although the primary objective of this technology is to preserve or enhance groundwater resources, artificial recharge has been used for many other beneficial purposes. Some of these purposes include conservation or disposal of floodwaters, control of saltwater intrusion, storage of water to reduce pumping and piping costs, temporary regulation of groundwater abstraction, and water quality improvement by removal of suspended solids by filtration through the ground or by dilution by mixing with naturally-occurring ground waters (Asano, 1985). Artificial recharge also has application in wastewater disposal, waste treatment, secondary oil recovery, prevention of land subsidence, storage of freshwater within saline aquifers, crop development, and stream flow augmentation

Our nation with strong agricultural background mainly depends upon sub surface water and this subsurface water necessity is more in South India. In Tamil Nadu based on the availability of surface water and its geographic nature leads to the increase the need for the sub surface water for their multiple demands. The demand for water has increased over the years and this has led to water scarcity in many parts of our country.

The situation is aggravated by the problem of water pollution or contamination. India is heading towards a freshwater crisis mainly due to improper management of water resources and environmental degradation, which has lead to a lack of access to safe water supply to millions of people. This freshwater crisis is already evident in many parts of India, varying in scale and intensity depending mainly on the time of the year.

Groundwater crisis is not the result of natural factors; it has been caused by the action of mankind. During the past two decades, the water level in several parts of the country has been falling rapidly due to an increase in extraction. The number of wells drilled for irrigation of both food and cash crops have rapidly increased. India's rapidly rising population and changing lifestyles has also increased the domestic need for water. The water requirement for the industry also shows an overall increase. Intense competition among users (agriculture, industry, and domestic sectors) is driving the groundwater table lower. The quality of groundwater is getting severely affected because of the widespread pollution of surface water. Besides, discharge of untreated waste water through bores and leachate from unscientific disposal of solid wastes also contaminates groundwater (Biswas, 2007), thereby reducing the quality of fresh water resources.

Water harvesting is an ancient art practiced in the past in many parts of North America, Middle East, North Africa, China, and India (Oweis et al., 1999). Geographic Information systems (GIS) can be employed to identify the regions of good recharge in the region (Ramaswamy and Anbazhagan, 1997; Saraf and Choudhury, 1998; Shankar and Mohan, 2005; Ragul and Kumar, 2006; Rao and Roy, 2007). Artificial recharge is achieved by putting water on the land surface where it infiltrates into the soil and moves downward to underlying groundwater (Bouwer, 1997, 1999).

II. STUDY AREA

The present study area Panaimarathupatti Block is situated near the suburbs of Salem City. It is a Panchayat town in Salem District, Tamil nadu. It is bounded by the North Latitudes between 11^{0}39’ south latitutde 11^{0} 31’and East Longitudes 78^{0}10’ and West longitude 78^{0}14’ and falls in parts of survey of India topo sheets 58I/2 and 58I/6 as per the version,C44A2 and C44A6 of 2005 updated topo sheet. It covers an area of 180 Sq. Kms.(Figure.2.1)

This study area is bounded by Mallur at west, Kamalapatti and other villages at East, Salem Taluk towards North , Rasipuram Taluk towards South. The over all climate at the study area is warm and dry. The average temperature of the area is around 30°C and it receives the rain fall during SW and NE mansoon periods. The following villages are in the Panamarathupatti Block are benefitted if the lake get recharged

- Kammalapatti
- Kuralnatham
- Kullappanayakannur
- Thippampatty
- Thumbalpatti
- Vedapatti
- Naliyam Pudur
- Melur
- Kitchipalayam
- Unjakattupudur

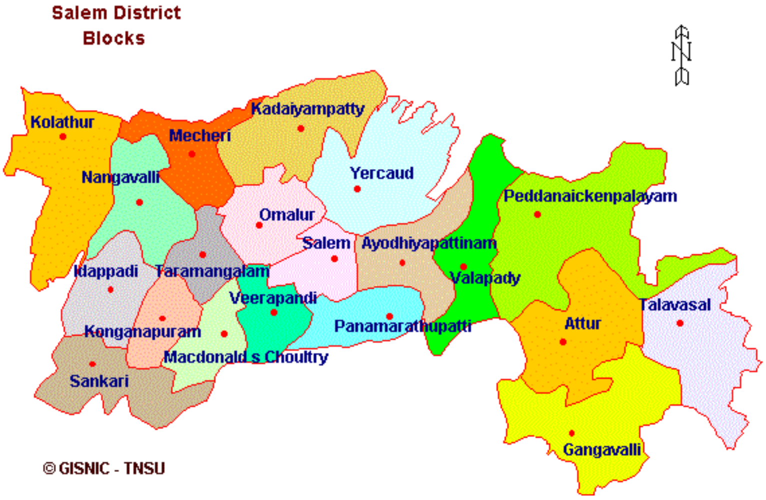

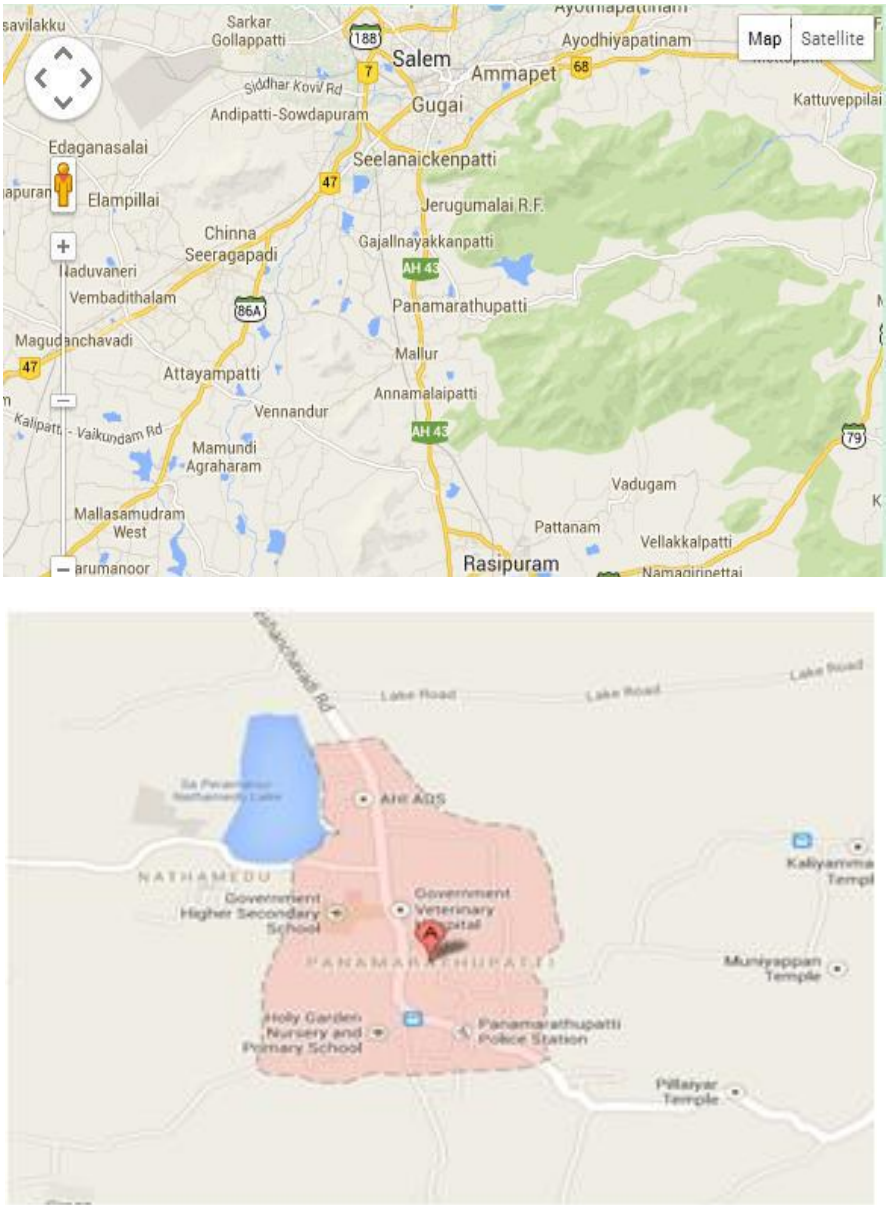

Figure.2.1. Location of the study area

Geology of the study area

Our study area is located on the high grade Precambrian terrain of south India with a network of shear zones of Neo to Early Proteorozoic age.The Salem-Attur shear zone, an extension of Moyar-Bhavani shear zone passes through this area. Charnockite, pyroxene granulite, Magnetite quartzite, Khondalite, calc granulite and younger granitoid are other rock units exposed in the area of our study is fully comprised with charnockit rock and lateritic soil. Geologically interesting nearby our study area:

- Ultramafics of Sitampundi Complex
- Iron ore deposits of Kanjamalai
- Magnesite deposit-Salem

2.1 IDENTIFICATION OF AREAS FOR RECHARGE

The first step in planning a recharge scheme is to demarcate the area of recharge. Such an area should, as far as possible, be a micro-watershed (2,000-4,000 ha) or a mini-watershed (40-50 ha). However, localized schemes can also be taken up for the benefit of a single hamlet or a village. In either case the demarcation of area should be based on the following broad criteria:

- Where ground water levels are declining due to over-exploitation

- Where substantial part of the aquifer has already been desaturated i.e. regeneration of water in wells and hand pumps is slow after some water has been drawn
- Where availability of water from wells and hand pumps is inadequate during the lean months
- Where ground water quality is poor and there is no alternative source of water

2.2 SOURCES OF WATER FOR RECHARGE

Before undertaking a recharge scheme, it is important to first assess the availability of adequate water for recharge. Following are the main sources, which need to be identified and assessed for adequacy:

- Precipitation (rainfall) over the demarcated area
- Large roof areas from where rainwater can be collected and diverted for recharge
- Canals from large reservoirs from which water can be made available for recharge
- Natural streams from which surplus water can be diverted for recharge, without Violating the rights of other users
- Properly treated municipal and industrial wastewaters. This water should be used only after ascertaining its quality

“In situ” precipitation is available at every location but may or may not be adequate for the recharge purposes. In such cases water from other sources may be transmitted to the recharge site. Assessment of the available sources of water would require consideration of the following factors:

- Available quantity of water
- Time for which the water would be available
- Quality of water and the pretreatment required

Conveyance system required to bring the water to the recharge site

2.3 INFILTRATION CAPACITY OF SOIL

Infiltration capacity of soil is an important factor that governs the rate of saturation of the vadose zone and thereby the efficacy or otherwise of a recharge scheme. Infiltration capacity of different soil types are done by field-tests by State Agriculture Departments and/ or the Land Use Survey Organizations. This data/ information together with maps showing infiltration rates is usually available in their departmental reports published periodically and are available with the District Agriculture Officer. At the district level, this information is available in the departmental reports of the Central and State Ground Water Boards.

2.4 AQUIFER SUITABILITY

This depends mainly on storage coefficient, availability of storage space and permeability. Very high permeability results in loss of recharged water due to sub-surface drainage where as low permeability reduces recharge rate. In order to have good recharge rate and to retain the recharged water for sufficient period for its use during lean period, moderate permeability is needed. Older alluvium, buried channels, alluvial fans, dune sands, glacial outwash etc. are the favorable places for recharge. In hard rock areas, fractured, weathered and cavernous rocks are capable of allowing high intake of water. The basaltic rocks i.e. those formed by lava flows, usually have large local pockets, which can take recharge water.

2.5 HYDRO-METEOROLOGICAL STUDIES

These studies are undertaken to understand the rainfall pattern and evaporation losses and thereby to determine the amount of water that would be available from a given catchment and the size of storages to be built. The main factors to be considered are:

- Minimum annual rainfall during the previous 10 years
- Number of rainy spells in a rainy season and duration of each spell
- Amount of rainfall in each rainy spell
- Rainfall intensity (maximum) 3 hourly, 6 hourly etc. as may be relevant for a region. As a general guide, the one, which causes significant runoff and local flooding, should be adopted.

This information/ data is usually readily available in District Statistical Reports published by the District Statistical Organization. However, the most important source is the India Meteorological Department. For the purpose of rainwater harvesting only readily available secondary data is adequate. The alternative sources of this data are the reports of major, medium or minor irrigation projects, which have been recently completed in the region or are under construction or are planned.

2.6 QUALITY OF SOURCE WATER

Chemicals and Salts

Problems which arise as a result of recharge to ground water are mainly related to the quality of raw waters that are available for recharge and which generally require some sort of treatment before being used in recharge installations. They are also related to the changes in the soil structure and the biological phenomena, which take place when infiltration begins, thereby causing environmental concerns. The chemical and bacteriological analysis of source water and that of ground water is therefore essential.

Sediment Load

A major requirement for waters that are to be used in recharge projects is that they be silt free. Silt may be defined as the content of undissolved solid matter, usually measured in mg/l, which settles in stagnant water or in flowing water with velocities, which do not exceed 0.1 m/hr.

2.7 PREVENTION OF CLOGGING OF SOIL PORES

This is one of the important considerations in planning an artificial recharge scheme. The usual methods to minimize the clogging are:

- Periodical removing of the mud-cake and dicing or scraping of the surface layer
- Installation of a filter on the surface, the permeability of which is lower than that of the natural strata (the filter must be removed and renewed periodically)
- Addition of organic matter or chemicals to the uppermost layer
- Cultivation of certain plant-covers, notably certain kinds of grass
- Providing inverted filter consisting of fine sand, coarse sand and gravel at the bottom of infiltration pits/ trenches are very effective

Clogging by biological activity depends upon the mineralogical and organic composition of the water and basin floor and upon the grain-size and permeability of the floor. The only feasible method of treatment developed so far consists in thoroughly drying the ground under the basin.

2.8 HYDRO CHEMISTRY

Quality of water is more important than its quantity. For determination of physiochemical parameters, 20 samples were collected from different wells. Various physical characteristics viz., pH, EC, TDS and the concentrations of major cations and anions ie ca, Mg, Na, K, CO3, HCO3, Cl and SO4 have been determined. Major part of the area possesses ground water suitable for domestic and most suitable for agriculture. However, ground water in some areas in unsuitable due to medium salinity. Low pH of the lake may be due to the excessive use of acid producing fertilizers. Evaluation of ground water quality for Agriculture use and drinking water purpose were carried out. Thematic maps depicting the spatial variation of various hydro chemical parameters were prepared. The major part of the area possesses ground water suitable for domestic, agriculture and industrial use.

2.9 WATERSHED MANAGEMENT

A watershed is an area of land where all of the water that is under it or drains off of it goes into the same place. The importance of healthy watersheds is explained by John Wesley Powell, scientist geographer “that area of land, a bounded hydrologic system, within which all living things are inextricably linked by their common water course and where, as humans settled, simple logic demanded that they become part of a community”. Our study area is divided in to 10 zones and by demarcating the individual blocks to identify the potential flow of water which is affordable for recharging the lake.

III METHODS OF AUGMENTATION

These can be broadly classified as:

- Spreading Method
    - Spreading within channel
    - Spreading stream water through a network of ditches and furrows
    - Ponding over large area
        - (a) Along stream channel viz. Check Dams/ Nala Bunds
        - (b) Vast open terrain of a drainage basin viz. Percolation Tanks
        - (c) Modification of village tanks as recharge structures.

- Recharge Shafts
    - Vertical Shafts
    - Lateral Shafts
- Injection Wells
- Induced Recharge
- Improved Land and Watershed Management
    - Contour Bunding
    - Contour Trenching
    - Bench Terracing
    - Gully Plugging

3.1 CHANNEL SPREADING

This involves constructing small ‘L’ shaped bunds within a stream channel so that water moves along a longer path thereby improving natural recharge. This method is useful where a small flowing channel flows through a relatively wide valley. However this is not useful where rivers/ streams are prone to flash floods and the bunds (levees) may be destroyed.

3.2 DITCH AND FURROW METHOD

In areas with irregular topography, shallow, flat-bottomed and closely spaced ditches or furrows provide maximum water contact area for recharge water from source stream or canal. This technique requires less soil preparation than the recharge basins and is less sensitive to silting. Typical plan or series of ditches originating from a supply ditch and trending down the topographic slope towards the stream. Generally three patterns of ditch and furrow system are adopted.

3.3 CHECK DAMS

Check dam is a small, often temporary, dam constructed across a swale, drainage ditch, or waterway to counteract erosion by reducing water flow velocity. Check dams themselves are not a type of new technology; rather, they are an ancient technique dating all the way back to the second century A.D. Check dams are typically, not always, implemented as a system, consisting of several check dams situated at regular intervals across the area of interest

3.4 PERCOLATION TANKS (PT)/ SPREADING BASIN

These are the most prevalent structures in India to recharge the ground water reservoir both in alluvial as well as hard rock formations. The efficacy and feasibility of these structures is more in hard rock formation where the rocks are highly fractured and weathered.. The percolation tanks are however also feasible in mountain fronts occupied by talus scree deposits..

3.5 MODIFICATION OF VILLAGE TANKS AS RECHARGE STRUCTURES

The existing village tanks, which are often silted up or damaged, can be modified to serve as recharge structure. In general no “Cut Off Trench” (COT) and Waste Weir is provided for village tanks. A village tanks can be converted into a recharge structure by desilting its bed and providing a COT on the upstream end of the bund. Several such tanks are available which can be modified for enhancing ground water recharge.

3.6 RECHARGE OF DUG WELLS AND HAND PUMPS

In alluvial as well as hard rock areas, there are thousands of dug wells, which have either gone dry, or the water levels have declined considerably. These dug wells can be used as structures to recharge the ground water reservoir. Storm water, tank water, canal water etc. can be diverted into these structures to directly recharge the dried aquifer. By doing so the soil moisture losses during the normal process of artificial recharge, are reduced. The recharge water is guided through a pipe to the bottom of well, below the water level to avoid scouring of bottom and entrapment of air bubbles in the aquifer. The quality of source water including the silt content should be such that the quality of ground water reservoir is not deteriorated. Schematic diagrams of dug well recharge In urban and rural areas, the roof top rainwater can be conserved and used for recharge of ground water. This approach requires connecting the outlet pipe from rooftop to divert the water to either existing wells/ tube wells/ bore wells or specially designed wells. The urban housing complexes or institutional buildings having large roof areas can be utilized for harvesting roof top rainwater for recharge purposes.

3.7 RECHARGE SHAFT

These are the most efficient and cost effective structures to recharge the aquifer directly. These can be constructed in areas where source of water is available either for some time or perennially. Following are the site characteristics and design guidelines:

(i) To be dug manually if the strata is of non-caving nature.

(ii) If the strata is caving, proper permeable lining in the form of open work, boulder lining should be provided.

(iii) The diameter of shaft should normally be more than 2 m to accommodate more water and to avoid eddies in the well.

(iv) In the areas where source water is having silt, the shaft should be filled with boulder, gravel and sand to form an inverted filter. The upper-most sandy layer has to be removed and cleaned periodically. A filter should also be provided before the source water enters the shaft.

(v) When water is put into the recharge shaft directly through pipes, air bubbles are also sucked into the shaft through the pipe, which can choke the aquifer. The injection pipe should therefore be lowered below the water level.

3.8 ARTIFICIAL RECHARGE THROUGH INJECTION WELLS

Injection wells are structures similar to a tube well but with the purpose of augmenting the ground water storage of a confined aquifer by pumping in treated surface water under pressure The injection wells are advantageous when land is scarce.

3.9 INDUCED RECHARGE

It is an indirect method of artificial recharge involving pumping from aquifer, hydraulically connected with surface water, to induce recharge to the ground water reservoir. When the cone of depression intercepts river recharge boundary a hydraulic connection gets established with surface source, which starts providing part of the pumpage yield. In such methods, there is actually no artificial build up of ground water storage but only passage of surface water to the pump through an aquifer. In this sense, it is more a pumpage augmentation rather than artificial recharge measure. In hard rock areas the abandoned channels often provide good sites for induced recharge. Check weir in stream channel, at location up stream of the channel bifurcation, can help in high infiltration from surface reservoir to the abandoned channel when heavy pumping is carried out in wells located in the buried channel.

3.10 SITE CHARACTERISTICS AND DESIGN GUIDELINES

A collection well is a large diameter (4 to 8 m) well from which laterals are driven/ drilled near the bottom at one or two levels into permeable strata. The central well is a vertical concrete cassion in pre-cast rings, (wall thickness 0.45 m) sunk upto the bottom of aquifer horizon. The bottom of cassion is sealed by thick concrete plugs. Slotted steel pipes, 9 mm thick, 15 to 50 cm in diameter having open area above 15% and a tapered leading are driven laterally through portholes at appropriate places in the cassion. The successive slotted pipes are welded and driven using special hydraulic jacks installed at the bottom of the cassion. The number of laterals is usually less than 16, thus permitting minimum angle of 22°30”, between two laterals. The maximum length of lateral reported is 132 m and the total length of laterals from 120 to 900 m depending upon requirement of yield. The laterals are developed by flushing and if entrance velocity of water is kept less than 6-9 mm/sec, these do not get filled by sand. The effective radius of a collector well is 75 to 85% of the individual lateral length.

IV. CONCLUSION

Conventional method of augmentation was used to measure the quality and quantity of water in the Panamarathupatti Lake. It has been found that water can be used for domestic purpose and to some extent for agricultural purposes. Based on the findings, this study also identified sites for replenishing groundwater for suitable development, suitable policy intervention by the state and local people’s cooperation are essential for protecting the lake from water pollution and increasing water resources and these will ensure sustainable development in the study area. The method recharge is very useful for block wise ground water exploitation and recharge.

REFERENCES

[1]. Ambroggi, R.P. 1977. Underground Reservoirs to Control the Water Cycle, Scientific American, 236(5):21-27.
[2]. Asano, T. 1985. Artificial Recharge of Groundwater. Butterworth Publishers, Boston, 767 pp.

[3]. CGWB (Central Ground Water Board) 1994. Manual on Artificial Recharge of Ground Water. Technical Series-M, No. 3. Ministry of Water Resources, Government of India, 215 pp.

[4]. Helweg, O.J. and G. Smith 1978. Appropriate Technology for Artificial Aquifers. Groundwater, 16(3):144-148.

[5]. Huisman, L. and T.N. Olsthoorn 1983. Artificial Groundwater Recharge. Pitman Publishing Inc., Massachusetts, 320 pp.

[6]. Oaksford, E.T. 1985. Artificial Recharge: Methods, Hydraulics, and Monitoring, In: Artificial Recharge of Groundwater, T. Asamo, editor. Butterworth Publishers, Boston, pp. 69-127.

[7]. Rushton, K.R. and P.N. Phadtare 1989. Artificial Recharge Pilot Projects in Gujarat, India, In: Groundwater Management: Quantity and Quality, IAHS Publication No. 188, pp. 533-545.

[8]. Todd, D.K. 1980. Groundwater Hydrology. Second Edition. John Wiley & Sons, New York, 535 pp.

[9]. Widstrand, C. (Editor) 1978. The Social and Ecological Effects of Water Development in Developing Countries. Pergamon Press, New York.

[10]. Manual on Artificial Recharge of Ground Water 1994. Technical Series – M, No. 3, Central Ground Water Board, Faridabad, March 1994, 215 p.

[11]. National Drinking Water Mission and Department of Rural Development 1989. Rain Water Harvesting. Government of India, New Delhi.

[12]. Nayantara Nanda Kumar and Niranjan Aiyagari 1997. Artificial Recharge of Groundwater. http://www.cee.vt.edu/program_areas/environmental/teach/gwprimer/recharge/recharge.html

[13]. O'Hare, M.P., Fairchild, D.M., Hajali, P.A., Canter, L.W. 1986. Artificial Recharge of Groundwater. Proceedings of the Second International Symposium on Artificial Recharge of Groundwater.

[14]. Phillips, Steven P. The Role of Saturated Flow in Artificial Recharge Projects. U.S. Geological Survey, Placer Hall, 6000 J Street, Sacramento, California 95819-6129.

[15]. Sophocleous, M.A. and J. A. Schloss. Estimated Annual Groundwater Recharge. http://www.kgs.ukans.edu/HighPlains/atlas/atrch.htm

[16]. Subramani.T, Sivakumar.C.T, Kathirvel.C, Sekar.S," Identification Of Ground Water Potential Zones In Tamil Nadu By Remote Sensing And GIS Technique" International Journal of Engineering Research and Applications , Vol. 4 , Issue 12(Version 3), pp.127-138, 2014.

[17]. Subramani.T , Vishnumanoj.V, "Land Use and Land Cover Change Detection and Urban Sprawl Analysis of Panamarathupatti Lake, Salem", International Journal of Engineering Research and Applications, Vol. 4, Issue 6(Version 2), pp.117-127, 2014.

[18]. Subramani, T. "Study of Pollution Prevention Strategies For Reclamation of Ooty Lake" International Journal of Engineering Research and Applications, Vol.2, Issue.3, pp 783-791, 2012.

[19]. Subramani.T, Prasath.K, Velmurugan.P, Baskaran.V, "Impacts of Irrigation and Drought on Salem Ground Water", International Journal of Engineering Research and Applications, Vol. 4, Issue 6(Version 3), pp.117-122, 2014.

[20]. Subramani.T , Someswari.P, "Identification And Analysis Of Pollution In Thirumani Muthar River Using Remote Sensing", International Journal of Engineering Research and Applications, Vol. 4, Issue 6(Version 2), pp.198-207, 2014.

OPEN ACCESS

International
Journal
Of Modern Engineering Research (IJMER)

On Characterizations of NANO RGB-Closed Sets in NANO Topological Spaces

Dhanis Arul Mary A[1], Dr. I. Arockiarani[2]

[1,2]*Department of Mathematics, Nirmala College for Women, Coimbatore, Tamilnadu, India*

ABSTRACT: *The purpose of this paper is to establish and derive the theorems which exhibit the characterization of nano rgb-closed sets in nano topological space and obtain some of their interesting properties. We also use this notion to consider new weak form of continuities with these sets.*

2010 AMS classification: 54A05, 54C10.

Keywords: *Nano Rgb-closed, nano rgb-open, nano rgb-continuity, nano rgb-irresoluteness.*

I. INTRODUCTION

Levine [9] introduced the concept of generalized closed sets as a generalization of closed sets in topological spaces. This concept was found to be useful to develope many results in general topology. The notion of nano topology was introduced by Lellis Thivagar [11] which was defined in terms of approximations and boundary region of a subset of an universe using an equivalence relation on it. He also established the weak forms of nano open sets namely nano α -open sets, nano semi open sets and nano pre open sets [11]. Extensive research on generalizing closedness in nano topological spaces was done in recent years by many mathematicians [5, 6, 16].

The aim of this paper is to continue the study of nano generalized closed sets in nano topological spaces. In particular, we present the notion of nano regular generalized b-closed sets (briefly, nano rgb-closed sets) and obtain their characterizations with counter examples. Also we establish various forms of continuities associated to nano regular generalized closed sets.

II. PRELIMINARIES

Definition 2.1[17]: Let U be a non-empty finite set of objects called the universe and R be an equivalence relation on U named as the indiscernibility relation. Then U is divided into disjoint equivalence classes. Elements belonging to the same equivalence class are said to be indiscernible with one another. The pair (U, R) is said to be the approximation space. Let $X \subseteq U$

1. The lower approximation of X with respect to R is the set of all objects, which can be for certainly classified as X with respect to R and it is denoted by $L_R(X)$. That is

$L_R(X) = \bigcup_{x \in U} \{R(x) : R(x) \subseteq X\}$, where R(x) denotes the equivalence class determined by $x \in U$.

2. The upper approximation of X with respect to R is the set of all objects, which can be possibly classified as X with respect to R and it is denoted by $U_R(X)$. That is

$$U_R(X) = \bigcup_{x \in U} \{R(x) : R(x) \cap X \neq \phi\}$$

3. The boundary region of X with respect to R is the set of all objects, which can be classified neither as X nor as not-X with respect to R and it is denoted by $B_R(X)$. That is

$B_R(X) = U_R(X) - L_R(X)$.

Definition 2.2[11]: Let U be non-empty, finite universe of objects and R be an equivalence relation on U. Let $X \subseteq U$. Let $\tau_R(X) = \{U, \phi, L_R(X), U_R(X), B_R(X)\}$. Then $\tau_R(X)$ is a topology on U, called as the nano topology with respect to X. Elements of the nano topology are known as the nano-open sets in U and $(U, \tau_R(X))$ is called the nano topological space. $[\tau_R(X)]^c$ is called as the dual nano topology of $\tau_R(X)$. Elements of $[\tau_R(X)]^c$ are called as nano closed sets.

Definition 2.3[12]: If $\tau_R(X)$ is the nano topology on U with respect to X, then the set $B = \{U, L_R(X), B_R(X)\}$ is the basis for $\tau_R(X)$.

Definition 2.4[12]: If $(U, \tau_R(X))$ is a nano topological space with respect to X where $X \subseteq U$ and if $A \subseteq U$, then the nano interior of A is defined as the union of all nano-open subsets of A and it is denoted by Nint(A).

That is, Nint(A) is the largest nano open subset of A. The nano closure of A is defined as the intersection of all nano closed sets containing A and is denoted by Ncl(A). That is, Ncl(A) is the smallest nano closed set containing A.

Definition 2.5[11]: Let $(U, \tau_R(X))$ be a nano topological space and A⊆U. Then A is said to be

(i) nano semi-open if A $\subseteq$ Ncl(Nint(A))
(ii) nano pre-open if A $\subseteq$ Nint(Ncl(A))
(iii) nano α -open if A $\subseteq$ Nint(Ncl(Nint(A)))
(iv) nano semi pre-open if A $\subseteq$ Ncl(Nint(Ncl(A)))
(v) nano b-open if A $\subset$Ncl(NintA) $\cup$ Nint(NclA).

NSO(U, X), NPO(U, X), NαO(U, X), NSPO(U, X) and NBO(U, X) respectively denote the families of all nano semi-open, nano pre-open, nano α-open, nano semi pre-open and nano b- open subsets of U.

Let $(U, \tau_R(X))$ be a nano topological space and A $\subseteq$ U. A is said to be nano semi closed, nano pre-closed, nano α-closed, nano semi pre closed and nano b-closed if its complement is respectively nano semi-open, nano pre-open, nano α –open, nano semi pre open and nano regular open.

Definition 2.6: A subset A of a nano topological space $(U, \tau_R(X))$is called

(1) nano generalized closed (briefly, nano g-closed)[5], if Ncl(A) $\subseteq$ G whenever A $\subseteq$ G and G is nano open in U.
(2) nano semi-generalized closed (briefly, nano sg-closed)[6], if Nscl(A) $\subseteq$ G whenever A $\subseteq$ G and G is nano semi-open in U.
(3) nano α -generalized closed (briefly, nano α g-closed)[16], if N α cl(A) $\subseteq$ G whenever A $\subseteq$ G and G is nano open in U.
(4) nano generalized α -closed (briefly, nano g α -closed)[16], if N α cl(A) $\subseteq$ G whenever A $\subseteq$ G and G is nano α -open in U.

Definition 2.7[12]: Let $(U, \tau_R(X))$ and $(V, \tau_{R'}(Y))$ be nano topological spaces. Then a mapping $f : (U, \tau_R(X)) \rightarrow (V, \tau_{R'}(Y))$ is said to be

(i) nano continuous if f^{-1}(B) is nano open in U for every nano-open set B in V.
(ii) nano α- continuous if f^{-1}(B) is nano α-open in U for every nano-open set B in V.
(iii) nano semi-continuous if f^{-1}(B) is nano semi-open in U for every nano-open set B in V.
(iv) nano pre-continuous if f^{-1}(B) is nano pre-open in U for every nano-open set B in V.

III. Nano RGB-closed sets

In this section, we investigate the class of nano regular generalized b-closed sets and study some of their characterizations.

Definition 3.1: A subset A of a nano topological space $(U, \tau_R(X))$ is said to be nano regular generalized closed sets (briefly Nrgb-closed) if Nbcl(A) $\subseteq$ G whenever A $\subseteq$ G and G is regular open in U.

The collection of all nano rgb-closed subsets of U is denoted by NrgbC(U, X).

Theorem 3.1: Every nano b-closed set is nano rgb-closed.

Proof: If A is nano b-closed in U and G is nano regular open in U such that A $\subseteq$ G, Nbcl(A) = A $\subseteq$ G. Therefore A is nano rgb-closed.

Remark 3.1: Converse of the above theorem need not be true which can be seen from the following example.

Example 3.1: Let U = {a, b, c, d} with U/R = {{a}, {c}, {b, d}} and X = {a, b}. Then the nano topology is defined as $\tau_R(X)$ = {U, ϕ, {a}, {b, d}, {a, b, d}}. Here the sets {a, b}, {a, d} are nano rgb-closed but not nano b-closed.

The following theorem can also be proved in a similar way.

Theorem 3.2: Let $(U, \tau_R(X))$ be a nano topological space and A$\subseteq$U, then every nano closed, nano regular closed, nano α -closed , nano semi-closed, nano pre closed, nano g-closed, nano gb-closed, nano rg-closed, nano sg-closed, nano gs-closed, nano α g-closed, nano g α -closed sets are nano rgb-closed.

Remark 3.2: However the converse of the above theorem need not be true can be seen from the following example.

Example 3.1 shows that the sets {b}, {d} are nano rgb-closed but not nano closed and nano rg-closed, the sets {a}, {b} are nano rgb-closed but not nano regular closed, the sets {a}, {b, d} are nano rgb-closed but not nano pre-closed, the sets {a, c}, {a, c, d} are nano rgb-closed but not nano gb-closed, the sets {a, c}, {a, d} are nano rgb-closed but not nano α g-closed and {a, d}, {a, b, d} are nano rgb-closed but not nano g α -closed.

Example 3.2: Let U = {a, b, c, d} with U/R = {{a}, {c}, {b, d}} and X = {b, d}. Then the nano topology is defined as $\tau_R(X)$ = {U, ϕ, {b, d}}. Here the sets {b}, {d} are nano rgb-closed but not nano gs-closed and the sets {a, b}, {a, d} are nano rgb-closed but not nano sg-closed.

Example 3.3: Let U = {x, y, z} with U/R = {{x}, {y, z}} and X = {x, z}. Then the nano topology is defined as $\tau_R(X)$ = {U, ϕ, {x}, {y, z}}. Here the sets {y}, {z} are nano rgb-closed but not nano α -closed and the sets {x, y}, {x, z} are nano rgb-closed but not nano semi closed.

Example 3.4: Let U = {a, b, c, d} with U/R = {{a, c}, {b}, {d}} and X = {a, d}. Then the nano topology is defined as $\tau_R(X)$ = {U, ϕ, {d}, {a, c}, {a, c, d}}. Here the sets {c}, {d} are nano rgb-closed but not nano g-closed.
We have the following implications for properties of subsets but none of its reverse implication is true.

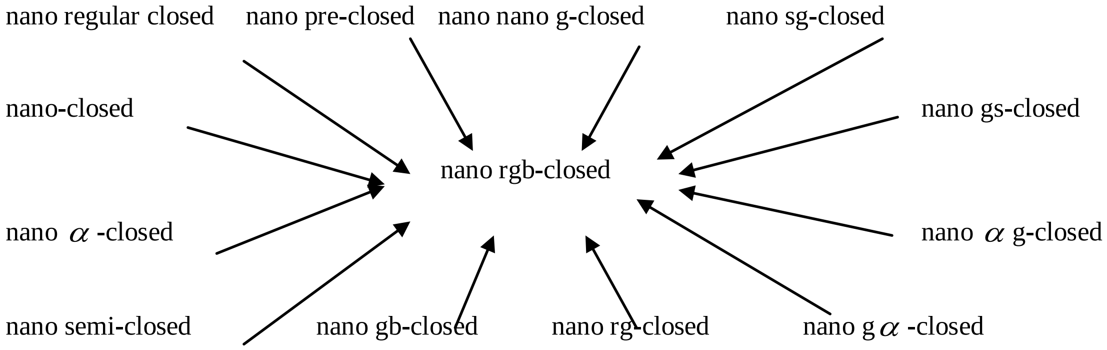

Theorem 3.3: A set A is nano rgb-closed in (U, X). Then Nbcl(A)-A has no non-empty nano regular-closed set.
Proof: Let A be nano rgb-closed in (U, X), and F be nano regular-closed subset of Nbcl(A)-A. That is, F $\subseteq$ Nbcl(A)-A. which implies F $\subseteq$ Nbcl(A) $\cap$ A^c. Then F $\subseteq$ Nbcl(A) and F $\subseteq A^c$. F $\subseteq A^c$ implies A $\subseteq F^c$ where F is a nano regular-open set. Since A is nano rgb-closed, Nbcl(A) $\subseteq$ F^c. That is, F $\subseteq$ $[\text{Nbcl(A)}]^c$. Thus, F $\subseteq$ Nbcl(A) $\cap$ $[\text{Nbcl(A)}]^c$ = ϕ. Therefore F = ϕ.

Theorem 3.4: Let A be nano rgb-closed set. Then A is nano b-closed if and only if Nbcl(A)-A is nano regular closed.
Proof: Let A be nano rgb-closed set. If A is nano b-closed, then we have Nbcl(A)-A = ϕ , which is a nano regular closed set. Conversely, let Nbcl(A)-A be nano regular-closed. Then by Theorem 3.3, Nbcl(A)-A does not contain any non-empty nano regular closed set. Thus, Nbcl(A)-A = ϕ . That is, Nbcl(A) = A. Therefore A is nano b-closed.

Theorem 3.5: Let A be nano regular open nano rgb-closed set. Then, A $\cap$ F is nano rgb-closed whenever F $\in$ NbC(U, X).
Proof: Let A be nano regular open and nano rgb-closed, then Nbcl(A) $\subseteq$ A, but A $\subseteq$ Nbcl(A). Thus, A is nano b-closed in U. Hence A $\cap$ F is nano b- closed in U which implies that A $\cap$ F is nano rbg-closed in U.

Theorem 3.6: Let B $\subseteq$ A $\subseteq$ U where A is a nano rgb-closed and nano regular open set. Then B is nano rgb-closed relative to A if and only if B is nano rgb-closed in U.

Proof: We first note that since $B \subseteq A$ and A is both a nano rgb-closed and nano regular open set, then Nbcl(A) $\subseteq$ A and thus Nbcl(B) $\subseteq$ Nbcl(A) $\subseteq$ A. Now from the fact that $A \cap$ Nbcl(B) = Nbcl_A(B), we have Nbcl(B) = Nbcl_A(B) $\subseteq$ A. If B is nano rgb-closed relative to A and G is nano regular open subset of U such that $B \subseteq G$, then $B = B \cap A \subseteq G \cap A$ where $G \cap A$ is nano regular open in A. Hence as B is nano rgb-closed relative to A, Nbcl(B) = Nbcl_A(B) $\subseteq G \cap A \subseteq G$. Therefore B is nano rgb-closed in U.

Conversely if B is nano rgb-closed in U and G is an nano regular open subset of A such that $B \subseteq G$, then $G = N \cap A$ for some nano regular open subset N of U. As $B \subseteq N$ and B is nano rgb-closed in U, Nbcl(B) $\subseteq$ N . Thus Nbcl_A(B) = Nbcl(B) $\cap A \subseteq N \cap A = G$. Therefore B is nano rgb-closed relative to A.

Theorem 3.7: If A is nano rgb-closed set and B is any set such that $A \subseteq B \subseteq$ Nbcl(A), then B is nano rgb-closed set.

Proof: Let $B \subseteq G$, where G is a nano regular open set. Since A is nano rgb-closed and $A \subseteq G$, then Nbcl(A) $\subseteq$ G and Nbcl(B) $\subseteq$ Nbcl(Nbcl(A)) = Nbcl(A) $\subseteq$ G. Therefore, Nbcl(B) $\subseteq$ G and hence B is a nano rgb-closed set.

Theorem 3.8: If A and B are nano rgb-closed sets, then $A \cup B$ is nano rgb-closed.

Proof: Let G be a nano regular open set in U such that $A \cup B \subseteq G$. Then, A and B $\subseteq$ G. Since A and B are nano rgb-closed and G is a nano regular open set containing A and B we have Nbcl(A) $\subseteq$ G and Nbcl(B) $\subseteq$ G. Therefore, Nbcl($A \cup B$) = Nbcl(A) $\cup$ Nbcl(B) $\subseteq$ G. That is Nbcl($A \cup B$) $\subseteq$ G. Hence $A \cup B$ is nano rgb-closed.

Remark 3.3: Intersection of two nano rgb-closed sets need not be nano rgb-closed which is shown by the following example.

Example 3.5: Let U = {a, b, c, d} with U/R = {{a, d},{b}, {c}} and X = {a, c}. Then the nano topology is defined as $\tau_R(X)$= {U, ϕ, {c}, {a, d}, {a, c, d}}. Here the sets {a, c}, {c, d} are nano rgb-closed but {a, c} $\cap$ {c, d} = {c} is not nano rgb-closed set.

Theorem 3.9: Let U and V be two nano topological spaces, $A \subseteq V \subseteq U$, and A be nano rgb-closed in U. Then A is nano rgb-closed in V.

Proof: Let G_1 be nano regular open relative to V such that $A \subseteq G_1$. Then $G_1 = V \cap G$, where G is nano regular open in U and $A \subseteq V \cap G$. Therefore $A \subseteq G$. That is G is nano regular open set containing A. Since A is nano rgb-closed in U, Nbcl(A) $\subseteq$ G. Therefore $V \cap$ Nbcl(A) $\subseteq V \cap G$. That is Nbcl_V(A) $\subseteq G_1$ for every nano regular open set G_1in V such that $A \subseteq G_1$. Hence A is nano rgb-closed relative to V.

Definition 3.2: A subset A of a nano topological space U is called nano regular generalized b-open (simply Nrgb-open) if A^c is nano rgb-closed.

The collection of all nano rgb-open subsets of U is denoted by NrgbO(U, X).

Example 3.6: Let U = {a, b, c, d} with U/R = {{a, d}, {b}, {c}} and X = {a, c}. Then the nano topology is defined as $\tau_R(X)$= {U, ϕ, {c}, {a, d}, {a, c, d}}. Let A = {a, c, d}, then A^c = {b} is nano rgb-closed, since U is the only nano regular open set containing A^c. Therefore A is nano rgb-open. If A = {a, b, d}, then A^c = {c} is not nano rgb-closed, since Nbcl(A^c) = Nbcl({c}) = {b, c} and {b, c} $\not\subseteq$ {c}, a regular open set such that $A^c \subseteq G$. Therefore A is not nano rgb-open.

Remark 3.4: $x \in$Nrgbcl(A) if and only if $G \cap A \neq \phi$ for every rgb-open set containing x.

Remark 3.5: For subsets A, B of a nano topological space $(U, \tau_R(X))$

(i) U – Nrgbint(A) = Nrgbcl(U-A)
(ii) U – Nrgbcl(A) = Nrgbint(U-A)

Theorem 3.10: Every nano b-open set nano rgb- open.

Proof follows from the Theorem 3.1**.**

Theorem 3.11: A subset $A \subseteq U$ is nano rgb-open if and only if F $\subseteq$ Nbint(A) whenever F is nano regular closed set and F $\subseteq$ A.

Proof: Let A be nano rgb-open set and suppose F $\subseteq$ A where F is nano regular closed. Then U-A is a nano rgb-closed set contained in the nano regular open set U-F. Hence Nbcl(U-A) $\subseteq$ U-F and U-Nbint(A) $\subseteq$ U-F. Thus F $\subseteq$ Nbint(A). Conversely, if F is a nano regular closed set with F $\subseteq$ Nbint(A) and F $\subseteq$ A, then U-Nbint(A) $\subseteq$ U-F. Thus Nbcl(U-A) $\subseteq$ U-F. Hence U-A is a nano rgb-closed set and A is a nano rgb-open set.

Theorem 3.12: If A and B are nano rgb-open, then A $\cap$ B is nano rgb-open.

Proof: Let A and B are nano rgb-open sets, then A^c and B^c are nano rgb-closed. Hence $A^c \cup B^c (A \cap B)^c$ is nano rgb-closed and thus A $\cap$ B is nano rgb-open.

Remark 3.6: The Union of nano rgb-open sets need not be rgb-open which is proved from the following example.

Example 3.7: Let U = {a, b, c, d} with U/R = {{a, d}, {b}, {c}} and X = {a, c}. Then the nano topology is defined as $\tau_R(X)$ = {U, ϕ, {c}, {a, d}, {a, c, d}}. Here the sets {d}, {a, b} are nano rgb-open sets but {d} $\cup$ {a, b} = {a, b, d} is not nano rgb-open.

Theorem 3.15: If Nbint(A) $\subseteq$ B $\subseteq$ A and if A is nano rgb-open then B is also nano rgb-open.

Proof: Let Nbint(A) $\subseteq$ B $\subseteq$ A, then $A^c \subseteq B^c \subseteq$ Nbcl(A^c) where A^c is nano rgb-closed set and hence B^c is also nano rgb-closed by Theorem 3.7. Therefore B is nano rgb-open.

IV. nano rgb-continuous and rgb-irresolute function

In this section we define nano rgb-continuous function and study some of their characterizations.

Definition 4.1: Let $(U, \tau_R(X))$ and $(V, \tau_{R'}(X))$ be nano topological spaces. Then a mapping $f : (U, \tau_R(X)) \to (V, \tau_{R'}(Y))$ is said to be nano regular generalized b-continuous (nano rgb-continuous) if the inverse image of every closed set in V is nano rgb-closed in U.

Remark 4.1: Since the complement of nano rgb-closed set is nano rgb-open, f is nano rgb-continuous if and only if the inverse image of every nano open set in V is nano rgb-open in U.

Theorem 4.1: Let $(U, \tau_R(X))$ and $(V, \tau_{R'}(Y))$ be nano topological spaces and a mapping $f : (U, \tau_R(X)) \to (V, \tau_{R'}(Y))$. Then, every nano b-continuous, nano continuous, nano α-continuous, nano semi continuous, nano pre continuous, nano g-continuous, nano sg-continuous functions are nano rgb-continuous.

Proof follows from the definition.

Remark 4.2: The converse of the above theorem need not be true which can be seen from the following examples.

Example 4.1: Let U = {a, b, c, d} with U/R = {{a, c}, {b}, {d}} and X = {a, d}. Then the nano topology is defined as $\tau_R(X)$ = {U, ϕ, {d}, {a, c}, {a, c, d}}. Let V = {x, y, z, w} with V/R' = {{x}, {y, z}, {w}}. Then $\tau_R(X)$ = {V, ϕ, {x}, {x, y, z}, {y, z}}.Define $f : U \to V$ as f(a) = x, f(b)= w, f(c) = y and f(d) = z. Then f is nano rgb-continuous but f is not nano continuous and nano semi continuous since $f^{-1}(\{x, w\})$ = {a, b} and $f^{-1}(\{y, z, w\})$ = {b, c, d} which are not nano closed and nano semi closed in U whereas {x, w}, {y, z, w} are nano closed in V. Thus a nano rgb-continuous function is not nano continuous and nano semi continuous.

Example 4.2: Let U = {a, b, c, d} with U/R = {{a, c}, {b}, {d}} and X = {a, d}. Then the nano topology is defined as $\tau_R(X)$ = {U, ϕ, {d}, {a, c}, {a, c, d}}. Let V = {x, y, z, w} with V/R' = {{x}, {y, z}, {w}}. Then $\tau_{R'}(Y)$ = {V, ϕ, {x}, {x, y, z}, {y, z}}.Define $f : U \to V$ as f(a) = w, f(b)= x, f(c) = y and f(d) = z. Then f is nano rgb-continuous but f is not nano b-continuous, g-continuous and nano pre continuous since $f^{-1}(\{y, z, w\})$ = {a, c, d} is not nano b-closed, nano g-closed and nano pre-closed in U. Thus a nano rgb-continuous function is not nano b-continuous, nano g-continuous and nano pre continuous.

Example 4.3: Let U = {a, b, c, d} with U/R = {{a}, {c}, {b, d}} and X = {b, d}. Then the nano topology is defined as $\tau_R(X)$= {U, ϕ, {b, d}. Let V = {x, y, z, w} with V/R' = {{x}, {y, z}, {w}}. Then $\tau_{R'}(Y)$ = {V, ϕ, {x}, {x, y, z}, {y, z}}.Define $f: U \to V$ as f(a) = x, f(b)= w, f(c) = y and f(d) = z. Then f is nano rgb-continuous but f is not nano sg-continuous since $f^{-1}(\{x, w\})$ = {a, b} and $f^{-1}(\{w\})$ = {b} which are not nano sg-closed in U whereas {x, w}, {w} are nano closed in V. Thus a nano rgb-continuous function is not nano sg-continuous.

The above results can be summarized in the following diagram.

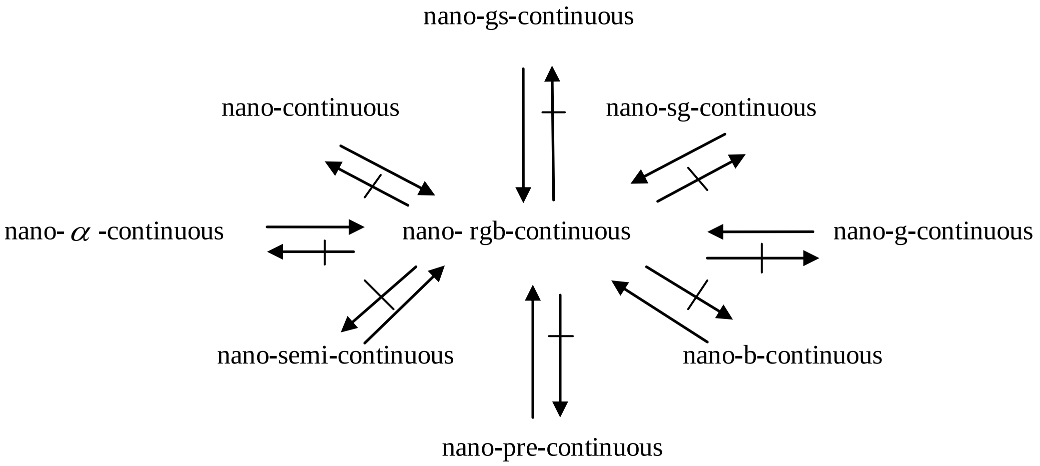

Theorem 4.2: A function $f:(U,\tau_R(X)) \to (V,\tau_{R'}(Y))$ is nano rgb-continuous if and only if the inverse image of every nano closed set in V is nano rgb-closed in U.

Proof: Let f be nano rgb-continuous and F be nano closed in V. That is, V-F is nano open in V. Since f is nano rgb- continuous, $f^{-1}(V-F)$ is nano rgb-open in U. That is, $U - f^{-1}(F)$ is nano rgb-open in U. Therefore, $f^{-1}(F)$ is nano rgb-closed in U. Thus, the inverse image of every nano closed set in V is nano rgb-closed in U, if f is nano rgb-continuous on U. Conversely, let the inverse image of every nano closed be nano rgb-closed. Let G be nano open in V. Then V-G is nano closed in V. Then $f^{-1}(V-G)$ is nano rgb-closed in U. That is, $U - f^{-1}(G)$ is nano rgb-closed in U. Therefore, $f^{-1}(G)$ is nano rgb-open in U. Thus, the inverse image of every nano open set in V is nano rgb-open in U. That is f is nano rgb-continuous on U.

In the following theorem, we establish a characterization of nano rgb-continuous functions in terms of nano rgb-closure.

Theorem 4.3: A function $f:(U,\tau_R(X)) \to (V,\tau_{R'}(Y))$ is nano rgb-continuous if and only if $f(Nrgbcl(A)) \subseteq Ncl(f(A))$ for every subset A of U.

Proof: Let f be nano rgb-continuous and A ⊆ U. Then f(A) ⊆ V. Since f is nano rgb-continuous and $Ncl(f(A))$ is nano closed in V, $f^{-1}(Ncl(f(A)))$ is nano rgb -closed in U. Since f(A) ⊆ $Ncl(f(A))$, $f^{-1}(f(A))$ ⊆ $f^{-1}(Ncl(f(A)))$, then $Nrgbcl(A)$ ⊆ $Nrgbcl[f^{-1}(Ncl(f(A)))]$ = $f^{-1}(Ncl(f(A)))$. Thus, $Nrgbcl(A)$ ⊆ $f^{-1}(Ncl(f(A)))$. Therefore, $f(Nrgbcl(A))$ ⊆ $Ncl(f(A))$ for every subset A of U. Conversely, let $f(Nrgbcl(A)) \subseteq Ncl(f(A))$ for every subset A of U. If F is nano closed inV, since $f^{-1}(F)$ ⊆U, $f(Nrgbcl(f^{-1}(F)))$ ⊆ $Ncl(f(f^{-1}(F)))$ = $Ncl(F)$= F. That is, $f(Nrgbcl(f^{-1}(F)))$ ⊆ F. Thus $Nrgbcl(f^{-1}(F))$ ⊆ $f^{-1}(F)$. But $f^{-1}(F)$ ⊆ $Nrgbcl(f^{-1}(F))$. Hence, $Nrgbcl(f^{-1}(F))$ = $f^{-1}(F)$ Therefore, $f^{-1}(F)$ is nano rgb-closed in U for every nano closed set F in V. That is, f is nano rgb-continuous.

Remark 4.3: If $f:\left(U,\tau_R(X)\right)\rightarrow\left(V,\tau_{R'}(Y)\right)$ is nano b-continuous, then $f(Nrgbcl(A))$ is not necessarily equal to $Ncl(f(A))$.

Example 4.4: Let U = {a, b, c, d} with U/R = {{a, c}, {b}, {d}} and X = {a, d}. Then the nano topology is defined as $\tau_R(X)$ = {U, ϕ, {d}, {a, c}, {a, c, d}}. Let V = {x, y, z, w} with V/R' = {{x}, {y, z}, {w}}. Then $\tau_R(X)$ = {V, ϕ, {x}, {x, y, z}, {y, z}}.Define $f:U\rightarrow V$ as f(a) = x, f(b)= w, f(c) = y and f(d) = z. Then f is nano rgb-continuous. Let A = {c} $\subseteq$ V. Then $f(Nrgbcl(A))$ = f({c}) = {y}. But, $Ncl(f(A))$ = Ncl({y}) = {y, z, w}. Thus, $f(Nrgbcl(A)) \neq Ncl(f(A))$, even though f is nano b-continuous.

In the following theorem, we characterize nano rgb-continuous functions in terms of inverse image of nano closure.

Theorem 4.4: A function $f:\left(U,\tau_R(X)\right)\rightarrow\left(V,\tau_{R'}(Y)\right)$ is nano rgb-continuous if and only if $Nrgbclf^{-1}(B)) \subseteq f^{-1}(Ncl(B))$.

Proof: If f is nano rgb-continuous and B$\subseteq$V, then $Ncl(B)$ is nano closed in V and hence $f^{-1}(Ncl(B))$ is nano rgb-closed in U. Therefore, $Nrgbcl[f^{-1}(Ncl(B))]$ = $f^{-1}(Ncl(B))$. Since B $\subseteq$ $Ncl(B)$, $f^{-1}(B)$ $\subseteq$ $f^{-1}(Ncl(B))$. Therefore, $Nrgbcl(f^{-1}(B)) \subseteq Nrgbcl[f^{-1}(Ncl(B))]$ = $f^{-1}(Ncl(B))$. That is, $Nrgbclf^{-1}(B)) \subseteq f^{-1}(Ncl(B))$. Conversely, let $Nrgbclf^{-1}(B))$ $\subseteq$ $f^{-1}(Ncl(B))$ for every subset B of V. If B is nano closed in V, then $Ncl(B)$= B. By assumption, $Nrgbclf^{-1}(B))$ $\subseteq$ $f^{-1}(Ncl(B))$ = $f^{-1}(B)$. Thus $Nrgbclf^{-1}(B))$ $\subseteq$ $f^{-1}(B)$. But $f^{-1}(B)$ $\subseteq$ $Nrgbclf^{-1}(B))$. Therefore $Nrgbclf^{-1}(B))$ = $f^{-1}(B)$. That is, $f^{-1}(B)$ is nano rgb-closed in U for every nano closed set B in V. Therefore f is nano rgb-continuous on U.

The following theorem establishes nano rgb-continuous functions in terms of inverse image of nano rgb-interior of a subset of V.

Theorem 4.5: A function $f:\left(U,\tau_R(X)\right)\rightarrow\left(V,\tau_{R'}(Y)\right)$ is nano rgb-continuous on U if and only if $f^{-1}(N\operatorname{int}(B))$ $\subseteq$ $Nrgb\operatorname{int}(f^{-1}(B))$ for every subset B of V.

Proof: If f is nano rgb-continuous and B $\subseteq$V, then $N\operatorname{int}(B)$ is nano open in V and hence $f^{-1}(N\operatorname{int}(B))$ is nano rgb-open in U. Therefore, $Nrgb\operatorname{int}[f^{-1}(N\operatorname{int}(B))]$ = $f^{-1}(N\operatorname{int}(B))$. Also $N\operatorname{int}(B)$ $\subseteq$B implies that $f^{-1}(N\operatorname{int}(B))$ $\subseteq$ $f^{-1}(B)$. Therefore, $Nrgb\operatorname{int}[f^{-1}(N\operatorname{int}(B))]$ $\subseteq$ $Nrgb\operatorname{int}(f^{-1}(B))$. That is, $f^{-1}(N\operatorname{int}(B))$ $\subseteq$ $Nrgb\operatorname{int}(f^{-1}(B))$. Conversely, let $f^{-1}(N\operatorname{int}(B))$ $\subseteq$ $Nrgb\operatorname{int}(f^{-1}(B))$ for every B $\subseteq$V. If B is nano-open in V, then $N\operatorname{int}(B)$ = B. By assumption, $f^{-1}(N\operatorname{int}(B))$ $\subseteq$ $Nrgb\operatorname{int}(f^{-1}(B))$. Thus, $f^{-1}(B)$ $\subseteq$ $Nrgb\operatorname{int}(f^{-1}(B))$. But $Nrgb\operatorname{int}(f^{-1}(B))$ $\subseteq$ $f^{-1}(B)$. Therefore, $f^{-1}(B)$ = $Nrgb\operatorname{int}(f^{-1}(B))$. That is, $f^{-1}(B)$ is nano rgb-open in U for every nano open set B in V. Therefore, f is nano rgb-continuous on U.

Remark 4.4: Equality of the above theorems 4.4 and 4.5 does not hold in general can be seen from the following example.

Example 4.5: Let U = {a, b, c, d} with U/R = {{a, c}, {b}, {d}} and X = {a, d}. Then the nano topology is defined as $\tau_R(X)$ = {U, ϕ, {d}, {a, c}, {a, c, d}}. Let V = {x, y, z, w} with V/R' = {{x}, {y, z}, {w}}. Then $\tau_R(X)$ = {V, ϕ, {x}, {x, y, z}, {y, z}}.Define $f:U\rightarrow V$ as f(a) = x, f(b)= w, f(c) = y and f(d) = z. Then f is nano rgb-continuous.

(i) Let B = {z} $\subseteq$ V. Then $f^{-1}(Ncl(B))$ = $f^{-1}(y,z,w)$ = {b, c, d} and $Nrgbclf^{-1}(B))$ = $Nrgbclf^{-1}(B))$ = {d}. Therefore $Nrgbclf^{-1}(B)) \neq f^{-1}(Ncl(B))$.

(ii) Let B = {x, w}$\subseteq$V. Then $f^{-1}(N\operatorname{int}(B))$ = $f^{-1}(N\operatorname{int}(\{x,w\}))$ = {a, b} and

$Nrgb\text{int}(f^{-1}(B)) = Nrgb\text{int}(f^{-1}(\{x, w\})) = \phi$. Therefore $f^{-1}(N\text{int}(B)) \neq Nrgb\text{int}(f^{-1}(B))$.

Theorem 4.6: If $(U, \tau_R(X))$ and $(V, \tau_{R'}(Y))$ are nano topological spaces with respect to X $\subseteq$ U and Y $\subseteq$ V respectively, then any function $f : U \to V$, the following conditions are equivalent:

(a) $f : (U, \tau_R(X)) \to (V, \tau_{R'}(Y))$ is nano rgb-continuous.

(b) $f(Nrgbcl(A)) \subseteq Ncl(f(A))$ for every subset A of U.

(c) $Nrgbclf^{-1}(B)) \subseteq f^{-1}(Ncl(B))$ for every subset B of V.

Proof follows from the theorems 4.2, 4.3, 4.4.

Definition 4.2: Let $(U, \tau_R(X))$ and $(V, \tau_{R'}(Y))$ be two nano topological spaces. Then a function $f : U \to V$ is said to be nano regular generalized b-irresolute (nano rgb- irresolute) if the inverse image of every nano rgb-closed set in V is nano rgb-closed in U.

Example 4.4: Let U = {a, b, c, d} with U/R = {{a, c}, {b}, {d}} and X = {a, d}. Then the nano topology is defined as $\tau_R(X)$ = {U, ϕ, {d}, {a, c}, {a, c, d}}. Let V = {x, y, z, w} with V/R' = {{x}, {y, z}, {w}}. Then $\tau_{R'}(Y)$ = {V, ϕ, {x}, {x, y, z}, {y, z}}.Define $f : U \to V$ as f(a) = x, f(b)= w, f(c) = y and f(d) = z. Then f is nano rgb-irresolute since the inverse image of every nano rgb-closed set in V is nano rgb-closed in U.

Theorem 4.7: A function $f : U \to V$ is nano rgb-irresolute if and only if for every nano rgb-open set F in V, $f^{-1}(F)$ is nano rgb-open in U.

Proof follows from the fact that the complement of a nano rgb-open set is nano rgb-closed and vice versa.

Theorem 4.8: A function $f : U \to V$ is nano rgb-irresolute, then f is nano rgb-continuous.

Proof: Since every nano closed set is nano rgb closed, the inverse image of every nano closed set in V is nano rgb closed in U, whenever the inverse image of every nano rgb-closed set is nano rgb-closed. Therefore, any nano rgb-irresolute function is nano rgb-continuous.

Remark 4.5: The converse of the above theorem need not be true shown in the following example.

Example 4.7: Let U = {a, b, c, d} with U/R = {{b}, {c}, {a, d}} and X = {a, c}. Then the nano topology is defined as $\tau_R(X)$ = {U, ϕ, {c}, {a, d}, {a, c, d}}. Let V = {x, y, z, w} with V/R' = {{y}, {w}, {x, z}}. Then $\tau_{R'}(Y)$ = {V, ϕ, {z}, {x, z}, {x, z, w}}.Define $f : U \to V$ as f(a) = x, f(b)= y, f(c) = z and f(d) = w. Then f is nano rgb-continuous. But f is not nano rgb-irresolute, since $f^{-1}(\{z\})$ = {c} which is not nano rgb-closed in V whereas {z} is nano rgb-closed in V. Thus a nano rgb-continuous function is not nano rgb-irresolute.

Theorem 4.9: If $f : U \to V$ is nano rgb-irresolute and $g : V \to W$ is nano rgb-continuous, then $g \circ f : U \to W$ is nano rgb-continuous.

Theorem 4.10: If $f : U \to V$ is nano rgb-continuous and $g : V \to W$ is nano continuous, then $g \circ f : U \to W$ is nano rgb-continuous.

The proof of the theorems 4.9 and 4.10 are obvious.

Theorem 4.11: If $f : U \to V$ is nano rgb-irresolute and $g : V \to W$ is nano b-continuous, then $g \circ f : U \to W$ is nano rgb-continuous.

Proof: Let G be nano open in W. Then $g^{-1}(G)$ is nano b- open in V, since g is nano b-continuous. Thus $g^{-1}(G)$ is nano rgb-open in V, since every nano b-open is nano rgb-open. Then $f^{-1}(g^{-1}(G)$ =

$(g \circ f)^{-1}(G)$ is nano rgb-open in U and hence $g \circ f$ is nano rgb-continuous. Similarly we can prove the following theorem.

Theorem 4.12: If $f : U \to V$ is nano rgb-irresolute and $g : V \to W$ is nano α -continuous, then $g \circ f : U \to W$ is nano rgb-continuous.

Theorem 4.13: If $f : U \to V$ is nano rgb-irresolute and $g : V \to W$ is nano semi-continuous, then $g \circ f : U \to W$ is nano rgb-continuous.

Theorem 4.14: If $f : U \to V$ is nano rgb-irresolute and $g : V \to W$ is nano pre-continuous, then $g \circ f : U \to W$ is nano rgb-continuous.

Theorem 4.15: If $f : U \to V$ is nano rgb-irresolute and $g : V \to W$ is nano g-continuous, then $g \circ f : U \to W$ is nano rgb-continuous.

Proof of the above theorems follows from the definition.

Theorem 4.16: Let $(U, \tau_R(X)), (V, \tau_{R'}(Y)), (W, \tau_{R''}(Z))$ be nano topological spaces. If $f : U \to V$ and $g : V \to W$ are nano rgb-irresolute, then $g \circ f : U \to W$ is nano rgb-irresolute.

Proof: Let G $\subseteq$ W is nano rgb-open, then $g^{-1}(G)$ is nano rgb-open in V, since g is nano rgb-irresolute. Since f is nano rgb-irresolute, $f^{-1}(g^{-1}(G)$ is nano rgb-open in U. Thus $(g \circ f)^{-1}(G)$ is nano rgb-open in U. Therefore, $g \circ f$ is nano rgb-irresolute.

REFERENCES

[1] D. Andrijević - Semi preopen sets, Mat. Vesnik, 38(1986), no. 1, 24-32.

[2] D. Andrijević, On b-open sets, Mat. Vesnik 48 (1996), no. 1-2, 59-64.

[3] Ahmad Al-Omari and Mohd. Salmi Md. Noorani, On Generalized b-closed sets, Bull. Malays. Math. Sci. Soc. (2)32(1)(2009), 19-30.

[4] P. Bhattacharryya and B. K. Lahiri, semi generalized closed sets in topology, Indian J. Math. 29(1987), (1988), no.3, 375-382.

[5] Bhuvaneswari and Mythili Gnanapriya K, Nano generalized closed sets in nano topological spaces,International Journal of Scientific and Research Publications, (2014).

[6] Bhuvaneswari K, Ezhilarasi, On nano semi- generalized and generalized- semi closed sets in nano topological spaces, International Journal of Mathematics and Computer Applications Research, (2014), 117-124.

[7] E. Ekici and Caldas, Slightly γ -continuous functions, Bol. Soc. Parana. Mat. (3) 22 (2004), no. 2, 63-74.

[8] M. Ganster and M. Steiner, On b τ -closed sets, Appl. Gen. Topol. 8 (2007), no. 2, 243-247.

[9] N. Levine, Generalized closed sets in topology, Rend. Circ. Mat. Palermo (2) 19 (1970), 89- 96.

[10] N. Levine, semi open sets and semi continuity in topological spaces, Amer, Math. Monthly 70(1963), 36- 41.

[11] M. Lellis Thivagar and Carmel Richard, On nano forms of weakly open sets, International Journal of Mathematics and statistics Invention, (2013), 31-37.

[12] Lellis Thivagar. M and Carmel Richard “On Nano Continuity”, Mathematical theory and modeling, (2013), no.7, 32-37.

[13] A. S. Mashhour, M. E. Abd El-Monsef and S. N. El-Deep, On pre continuous and weak pre-continuous mappings, Proc. Math. Phys. Soc. Egypt No. 53 (1982), 47-53 (1983).

[14] H. Maki, R. Devi and K. Balachandran, Associated topologies of generalized α -closed sets and α -generalized closed sets, Mem. Fac. Sci. Kochi Univ. Ser. A Math. 15 (1994), 51-63.

[15] O. Njastad, On some classes of nearly open sets, Pacic J. Math. 15 (1965), 961-970.

[16] Thanga Nachiyar R, Bhuvaneswari K, “On nano generalized α -closed sets and nano α - generalized closed sets in nano topological spaces ”, International Journal of Engineering Trends and Technology, (2014), no.6.

[17] Z. Pawlak (1982) “Rough Sets”, International Journal of Information and Computer Sciences, 11(1982), 341-356.

OPEN ACCESS

International
Journal
Of Modern Engineering Research (IJMER)

Effect of Air Entrainment on Compressive Strength, Density, and Ingredients of Concrete

Mohammed Abas Abdela Salem[1], R. K. Pandey[2]

[1,2]*(Department of Civil Engineering, Department of Civil Engineering, Department of Construction Technology, Sam Higginbotom Institute of Agriculture Technology & Sciences)*

***(Department of Civil Engineering, Sam Higginbotom Institute of Agriculture Technology & Sciences)*

ABSTRACT: *The micro air bubbles in concrete mix act as fine aggregates which lead to reduction of the aggregates. The reduction of fine aggregates will cause reduction of water required for concrete mix without impairing the strength of concrete mix. This reduction has to be considered in designing an air entrained concrete mix. Theoretical (equations) and experimental study have been carried out to study the effect of air entrainment on compressive strength, density and ingredients of fresh concrete mix. During all the study, water cement ratio (w/c) was maintained constant at 0.5 to study the affection of air entrainment (a %) on concrete mix. The results have shown substantial decreasing in cement, water, aggregates and concrete density followed with decreasing in compressive strength of concrete. The results of this study has given more promising to use it as a guide for concrete mix design to choose the most appropriate concrete mix design economically.*

Keywords: *About five key words in alphabetical order, separated by comma.*

I. INTRODUCTION

Air entrained concrete consider one of the important discovery made in concrete technology. Since 1930 after the recognition of the merits of air entrained concrete, the use of such concrete increases all over the world especially in United States and Canada [1]. About 85 percent of the concrete manufacture in America contains air entraining agent. The air entraining agent consider as fifth ingredient in concrete making technology.

Air entrained concrete is made either by using air entraining cement or by mixing a small quantity of air entraining agent. These airs entraining agent produce millions of micro air bubbles inside the concrete mix acting as flexible ball bearings. The micro air bubbles of size ranging from 5 microns to 80 microns distribute in the entire mass of concrete resulting in modification of the properties of it regarding workability, segregation, bleeding and finishing quality [3].

Since the air bubbles form in water, the lower w/c ratio of the paste the hard to entrain air in the paste. On the other hand, the higher w/c ratio of the paste, the small air voids can easily become large ones and then escape from the paste. It has been reported that increasing of w/c ratio leads to increases in the spacing in hardened concrete and the air void system become worse [4].

The characteristics and grading of aggregates have also significant influence on air entrainment. In mortar and concrete, the fine aggregates can form a space to hold the air bubbles and prevent them from escaping. Furthermore, aggregate with a sharp shape, like crushed stone, will entrain less air than gravel. The sharper the aggregate is the harder for the air bubbles to attach on it [5].

Entrained air has major impact on water-cement ratio. Air entrained concrete can have lower water-cement ratios than non-air-entrained concrete; this minimize the reductions in strength that generally accompany and related to air entrainment [6].

II. METHODOLOGY (STUDY METHOD)

The methodology for studying the effect of air entrained on concrete mix is based on theoretical equations. These equations were derived from required water absorption and from volumetric equation which widely used in concrete mix design with some assumptions. By using these equations, verity of concrete proportions data can be generated. The theoretical results of concrete proportions data was carried out experimentally to perform concrete mixes design and to plot the relationship between the air entrainment and concrete compressive strength. By using this relationship, a guideline for a variety of concrete compressive strength will all of concrete proportions can be presented. The following is the assumptions and the equations used in this study.

1.1 Assumptions:

- $\boldsymbol{\rho}_c$ = (Specific gravity of cement) = 3.1.
- W_c = (The rate of required water to cement for complete paste hydration) = 0.23
- $\boldsymbol{\rho}_A$ = (Specific gravity of aggregates) = 2.7
- W_{An} = (Max absorbed water required by weight of aggregates) = 2%
- W_A = (available water for aggregates absorption and concrete workability) = 0.04
- C/W = (the rate cement to water) = 2.0
- a = (Air entrainment as percentage) = 0 – 8%

1.2 Equations:

- $\frac{C}{\rho_C} + \frac{A}{\rho_A} + W + a = 1000$ (volumetric equation) where
  C = cement, A = Aggregates, W = water

- $W = C * W_C + A * W_A$ (water absorption equation)
  By combining the previous equations we get

- $\frac{C}{\rho_C} + \frac{A}{\rho_A} + C * W_C + A * W_A + a = 1000$
  From the above three equations, we get

- $C = \frac{(1000 - a\% * 1000) * W_A}{(0.553 + b) * w_A + (\frac{1}{\rho_A} * b)}$

- $A = \frac{(1000 - a\% * 1000) - C * (\frac{1}{\rho_C} + W_C)}{\frac{1}{\rho_A} + W_A}$ (where $b = \frac{W}{C} - 0.23$)

III. STUDY PROGRAMS

1. Theoretical study

By using the previous equations and assumptions with verity values of air entrainment, a Table with variable concrete proportions data can be generated as follows.

Table (1) Generated Densities and Proportions of Concrete Mix Based On Air Entrainment

Air Entrainment %	Cement (kg/m^3)	Water (dm^3/m^3)	Aggregates (kg/m^3)	Density (kg/m^3)
0	301	150	2031	2483
1	298	149	2011	2458
2	295	147	1991	2433
3	292	146	1971	2409
4	289	144	1950	2383
5	286	143	1930	2359
6	283	141	1910	2334
7	280	140	1889	2309
8	277	138	1869	2284

2. Experimental study

From the previous Table, twenty four specimens were prepared based on different air entrainment values (a %) to perform compressive strength tests procedure as follows.

- Twenty four concrete specimens with variable (a %) values were prepared (Table (1))
- Cubic moulds were filled in 3 layers, each approximately 1/3 of the height of the moulds
- Each layer was stroked 25 times by the stroking rod all over the cross section of the layer
- After the top layer was stroked, a trowel and stroking rod used to smooth the concrete surface level
- The specimens were cured in water tank for 28 days
- Compressive strength studies were carried out on the specimens using compressive strength machine
- A Table (1) contains all the compressive strength values of the concrete mixes were presented

Table (2) Realtionship between Air Entrainment, Compressive Strength, Density, and the Proportions Of Concrete Mix

Air Entrainment (%)	Cement (Kg/m$^{3)}$	Water (Kg/m$^{3)}$	Aggregates (Kg/m$^{3)}$	Density (Kg/m$^{3)}$	Compressive Strength (kg/cm$^{2)}$
0	301	150	2031	2438	300
1	298	149	2011	2458	275
2	295	147	1991	2433	253
3	292	146	1971	2409	234
4	289	144	1950	2383	216
5	286	143	1930	2359	200
6	283	141	1910	2334	186
7	280	140	1889	2309	173
8	277	138	1869	2284	161

IV. RESULTS AND DISCUSSION

From the Table (1) the increasing in air content can decrease all the proportions of concrete by variable values. This influence on concrete ingredients can be plotted as graphs from which a guideline for air entrainment can be presented. Figure (1) shows the effect of air entrainment on cement content per cubic meter in concrete mix. Figure (2) shows the influence of air entrainment on water content in fresh concrete mix while Figure (3) and Figure (4) illustrate the relationship between entrained air with aggregates and density of concrete respectively. Figure (5) illustrate the significance of reduction especially in higher strength mixes. All the reduction of proportions of concrete caused by increasing of air content can be graphed as shown below.

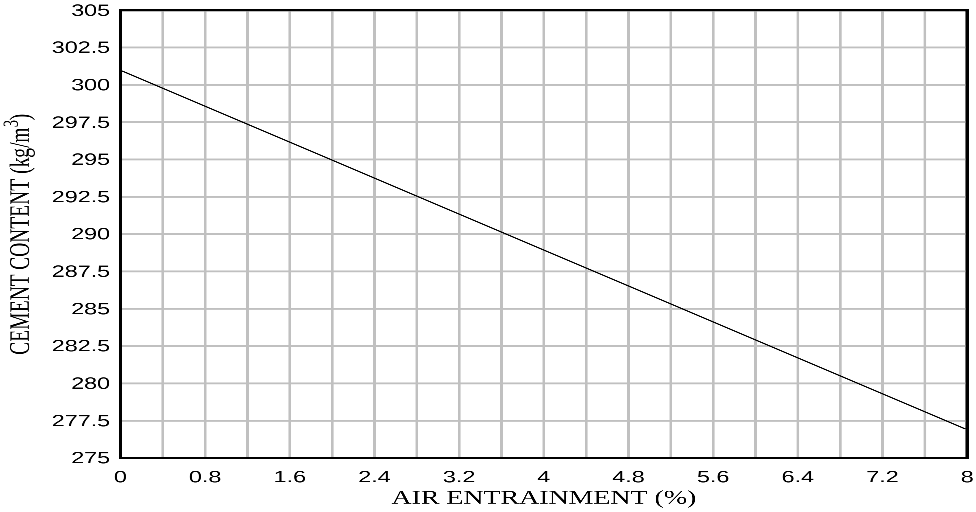

FIGURE (1) EFFECT OF AIR ENTRAINMENT ON CEMENT CONTENT OF CONCRETE MIX

FIGURE (2) EFFECT OF AIR ENTRAINMENT ON WATER CONTENT OF CONCRETE MIX

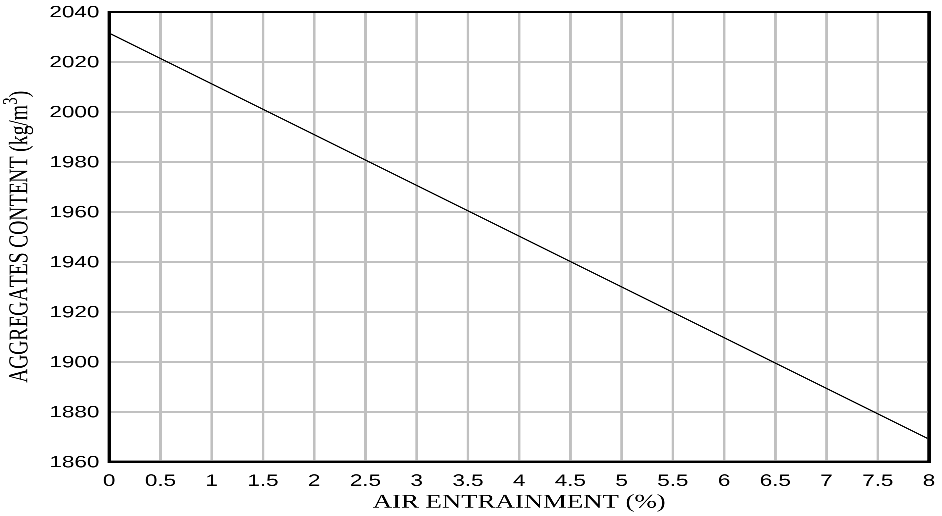

FIGURE (3) EFFECT OF AIR ENTRAINMENT ON AGGREGATES CONTENT OF CONCRETE MIX

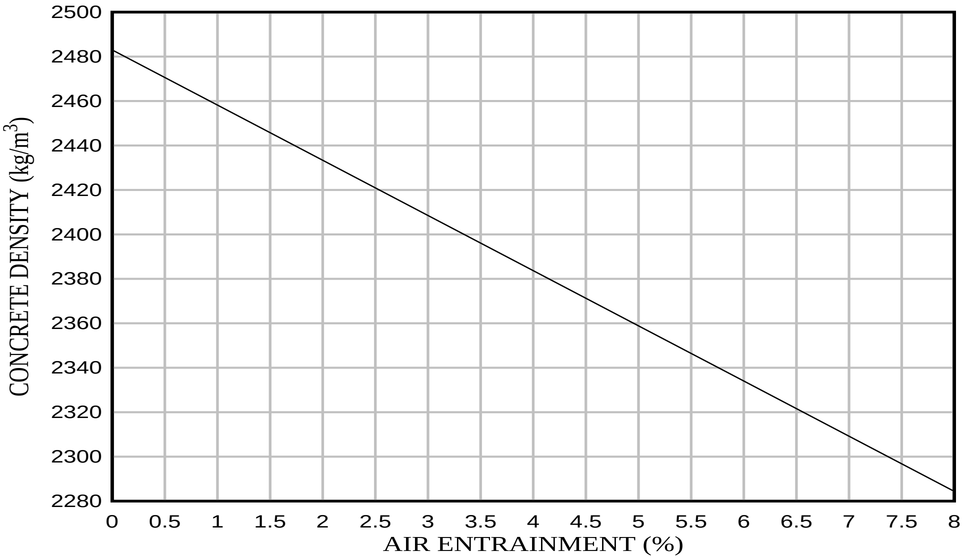

FIGURE (4) EFFECT OF AIR ENTRAINMENT ON DENSITY OF CONCRETE IN CONCRETE MIX

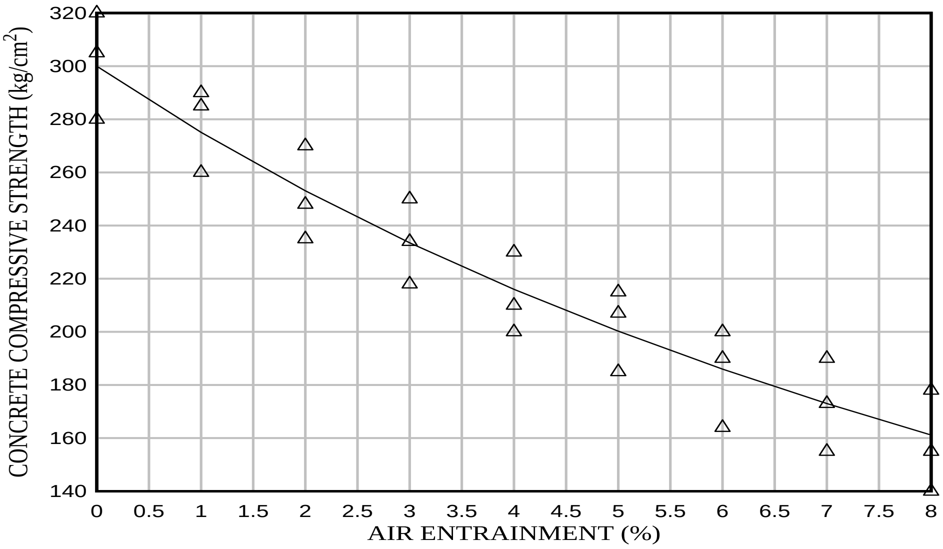

FIGURE (5) EFFECT OF AIR ENTRAINMENT ON COMPRESSIVE STRENGTH OF CONCRETE IN CONCRETE MIX

From the previous Table and Figures, effect of air entrainment on ingredients of concrete mix is clearly causing reduction on these components. The reduction value is variable for each component by each percent increasing in air entrainment.

- Reduction in aggregates content by 20.25 kg/m^3 weight for each percent increasing in air entrainment
- Reduction in water content by 1.5 kg/m^3 weight for each percent increasing in air entrainment
- Reduction in concrete density by 24.875kg/m^3 weight for each percent increasing in air entrainment
- The cement content in the concrete mix is reduced by 3 kg/m^3 for each percent increasing in air entrainment
- Reduction in concrete compressive strength by 12.5kg/m3 weight for each percent in air entrainment
- Reduction in strength become more significant in higher strength mixes
- The workability and the slump of the concrete remain without any impairing due to the increasing of air entrainment since C/W and W_A were constant during all the testing calculations.

V. SUMMARY AND CONCLUSION

It has been studied the effect of air entrained on aggregates, water, and cement content in fresh concrete mix. It was noticed that the air bubbles which generated by using either special type of cement or by using an air entrainment agent distributed in the entire mass of the concrete acting as flexible ball bearings. These flexible balls act as a fine aggregate as well which cause reduction in the aggregates followed by reduction in the water and cement content as result of this reduction. The workability (slump test) in concrete mix remains without changing due to the increasing of air entrainment since C/W and W_A are constant. The conclusion of this study can be summarized as following.

- The air entrainment is necessary in concrete mix design and it can consider fifth proportion.
- The air entrainment can reduce the ingredients of concrete without any effect in the workability of the concrete mix which mean more economical concrete mix can be achieved by using air entrainment agent whoever decreasing of concrete compressive strength by increasing of air entrainment should be considered.
- The reduction of cement due to the increasing of air entrainment in the concrete mix result in a lower heat of hydration in mass concrete (dams as example). The decrease in temperature due to the hydration process result in reduction in cracking and any undesirable internal stresses.

REFERENCES

[1] K. H. Khyat, (2000). Optimization and Performance of the Air-Entrained, *International Journal of ACI Material Journal, Vol. 97, No. 5, pp, 526-535 (2000)*

[2] H. Kamal, Khyat and Joseph Assaad, (2002). Air-Void Stability in Self-Consolidation Concrete, *International Journal of ACI Material Journal, Vol. 99, No. 4, pp, 408-416 (2002)*

[3] S. Lausten, (2011). *Engineered Air-Entrainment for Concrete*, doctoral thesis., Technical University of Denmark, Lyngby, Denmark, (2011)

[4] Yan Shang, Changwen Miao, Jiaping Lui and Qianping, (2010). Influencing Factors of Air Void Characteristics in Hardened Concrete, 2nd *International Symposium of Service Life Design for Infrastructure, pp, 817-824 (2010)*

[5] V. H. Dodson, (1990), *Concrete Admixture*, Van Nostrand Reinhold, New York, (1990).

[6] W. A. Cordon, (1946), Entrained Air-A Factor in the Design of Concrete Mixes, *Materials Laboratories Report No C-310,* Research and Geology Division, Bureau of Reclamation, Denver, March 15, 1946.

OPEN ACCESS

International Journal Of Modern Engineering Research (IJMER)

Static Analysis of a Pyro Turbine by using CFD

P.V.S.R. Vinay Kumar. K[1], M. Sri Rama Murthy[2], Dr. P.V.V. Rama Rao[3], Chandra Rao. Ch[4]
[1]PG Student, [2]Associate Professor, [3]Professor, [4]Assistant Professor
[1, 2, 4] Department of Mechanical Engineering, Sir C.R.Reddy College of Engineering, Eluru,
[3] Department of Electrical & Electronics Engineering, Shri Vishnu Engineering College for Women, Bhimavaram

ABSTRACT: *This paper aims to develop a standard design procedure for pyro turbine that can be manufactured locally in developing countries with very low head, steady power (200W to 1 kW with no discharge regulation), low cost and isolated network operation. The present research work has been carried out to modify the original blade material i.e. AK Stainless Steel 340 with different blade material ASME Stainless Steel SA516 Gr. 70 to withstand turbulence at the site which significantly affected the turbine operation. For this, a solid 3D model of turbine is generated through Catia V5. Static analysis by using CFD for original blade material is done Further static analysis by using CFD is done to the modified blade material for turbulence which shows that turbulence was successfully withstanded and had withstanded the high Pressure and Von-Mises Stress as well as minimum .deformation The results obtained by comparing original and modified blade materials are within the limits. The design is safe.*

Keywords: *Ansys (Static), Catia, Pyro Hydro Turbine, Turbulence, Von-misses Stress*

I. INTRODUCTION

Climatic changes all over the world are believed to be due to the excessive use of conventional (fossil) energy sources [1]. It is felt essential to draw attention towards the application of renewable energy sources which seem to be the most suitable future fuel. Importance of small hydroelectric power plants have increased manifold to meet the fast increasing electrical energy demand as well as to develop rural electrification for smaller and remote villages that cannot afford a larger hydropower project. This case study of design process is a critical process to understand the effectiveness of design methods which were implemented by human designers to overcome design fixations [2]. Even though the power generated is less than 5kW, but the benefit gain from this energy is the ability to raise the standard living of residents in remote areas [3]. Similar studies and tests on a series of Hydro – Turbine design models are conducted in rural parts where the national grid is inaccessible and reiterated that impulse forces at specific time instances i.e. peak hours cannot be replaced or replicate upon each other [4]. Due to improper blade profile in the existing blade design, the required power enhancement is not achieved [5]. In developing countries like India, Nepal, Vietnam etc. energy savings, high power consumption as well as power generation are of very much concern. So they are opting for Offline Grid system, Stand-alone Systems etc. At present scenarios, their daunting problem of concern is the turbulence. With this background, an attempt has been made to reduce turbulence by modifying original blade material.

II. PYRO HYDRO TURBINE

The factors given in the below table 1 determine the type of hydro power scheme to be used:

Table 1: Power Output Classification of Hydro Power Scheme

Classification	Power Output, P
Pyro	10W to 200W
Pico	0.2KW to 5 KW
Micro	5-100KW
Mini	100KW- 1MW
Small	1-10 MW
Medium	0-100 MW
Large	>100KW

Figure 1: Profile of Pyro Hydro Turbine

III. MATERIALS AND METHODS

The material used to fabricate a turbine blade should have fine grain structure with particle size, excellent formability, good weldability, uniform surface, maximum thickness (205mm), high Brinell hardness (x100 – 4.15), high tensile strength (485MPa-620MPa), corrosion resistance, sturdy construction and temperature resistance. This ensures that the turbines will function at their best efficiency for the expected life span on the pyro turbine. With the above background, ASME Stainless steel SA516 Gr.70 (Gr.70 stands for increasing tensile strength levels of 55, 60, 65, 70) used for present research so that the turbulence will be minimized. Mechanical properties are shown in below Table 2:

Table 2: Mechanical Properties of Original (AK Stainless Steel 340) and Modified blade material (ASME Stainless Steel SA516 Gr. 70)

Sl. No	**Mechanical Properties**	**Original blade material(AK Stainless Steel 340)**	**Modified blade material (ASME Stainless Steel SA516 Gr.70)**
1	Thickness (mm)	134	205
2	Brinell Hardness(BHN)	3x100	4.15 x 100
3	Tensile Strength(MPa)	325	485 – 620
4	Yield Strength(MPa)	241	260

IV. STATIC ANALYSIS

4.1 Static Analysis for Catia model of pyro turbine for original and modified blade material at 1200 Rpm
Original blade material Total pressure = 5.07e5 Pascal = 0.507 Mpa
Pressure on each blade = 0.507/12 = 0.0422MPa = 4.2 e -002
Modified blade material Total pressure = 1.28e6 Pascal = 1.28MPa
Pressure on each blade = 1.28/12 = 0.106 Mpa

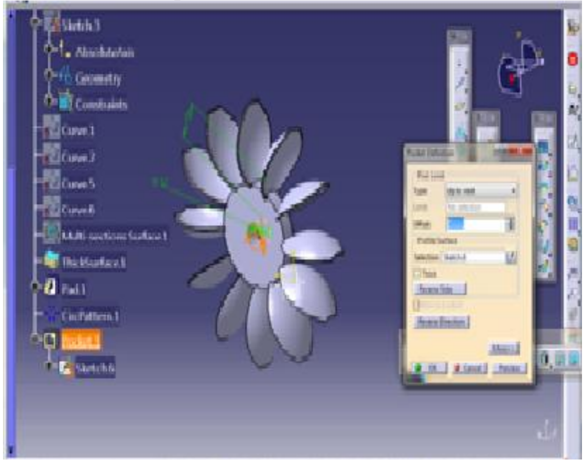

Figure 2: Catia model of Actual turbine of AK Stainless Steel 340

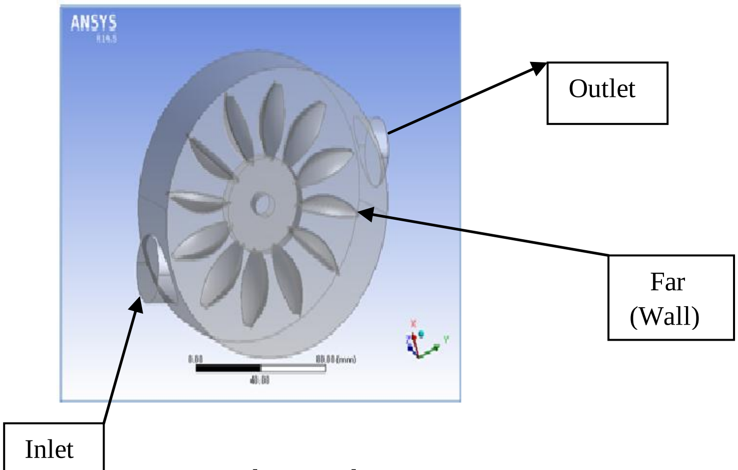

Fig 3: Boundary Conditions

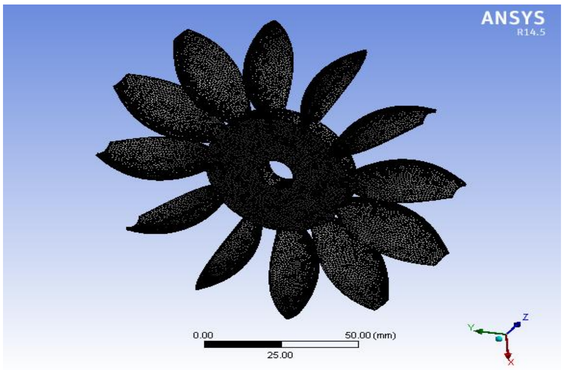

Fig 4: Original Solid meshed File

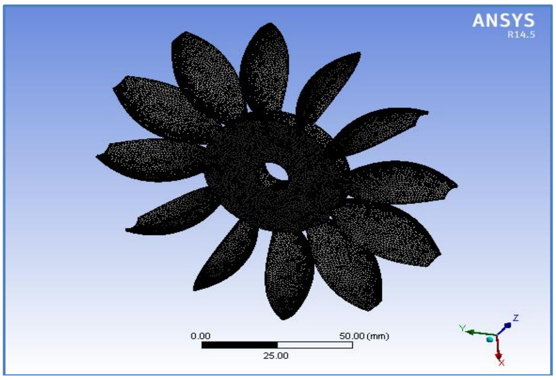

Fig 5**:** Modified Meshed File

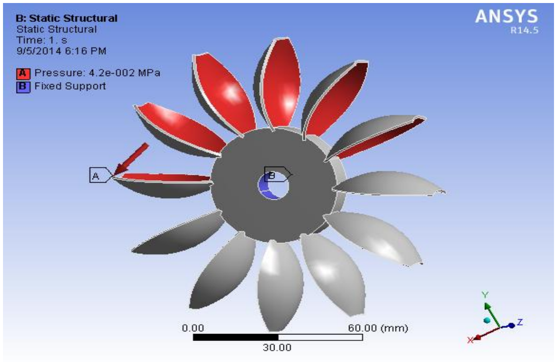

Fig 6: Original Fluid pressure applied on all Blades

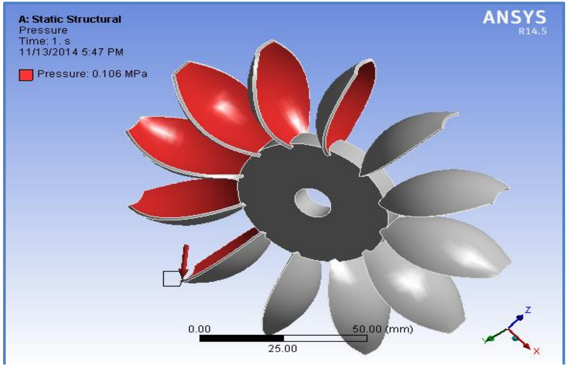

Fig 7: Modified Static pressure applied on all Blades

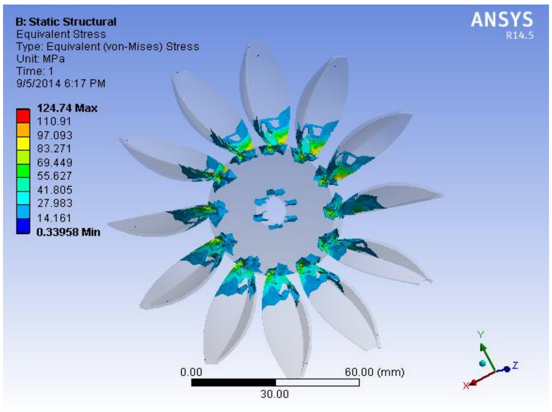

Fig 8: Original Equivalent Von-Mises stress

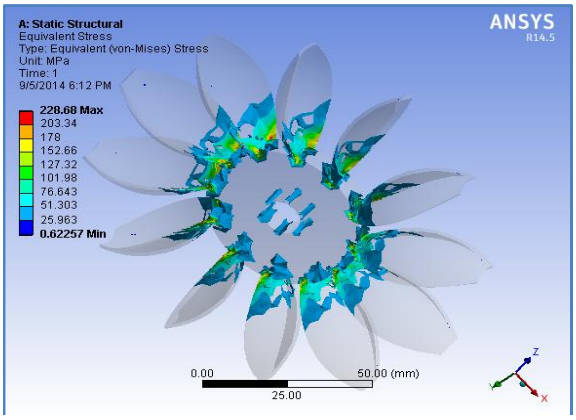

Fig 9: Modified Equivalent Von-Mises stress

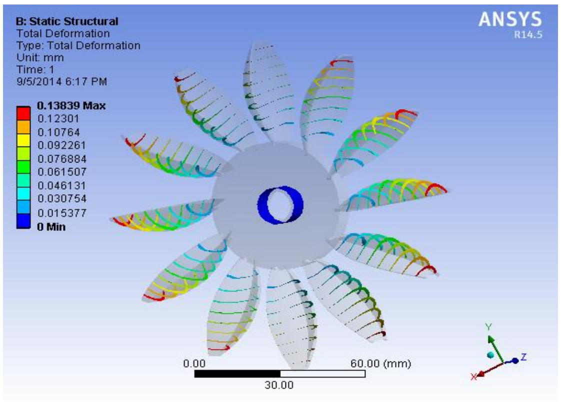

Fig 10: Original Total deformation

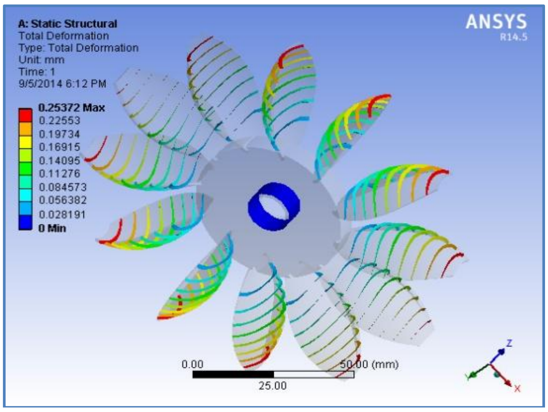

Fig 11: Modified Total deformation

V. RESULTS AND DISCUSSIONS

Table 2: Static Analysis Results

Material	**Applied Pressure for each blade(MPa)**	**Equivalent Von-Mises stress (MPa)**	**Total Deformation (mm)**
AK Stainless Steel 340	0.0422	124.74	0.13839
ASME Stainless Steel SA516 Gr.70	0.1066	228.68	0.25372

4.1 Comparison of Speed with respect to Pressure, Von-Mises Stress and Deformation

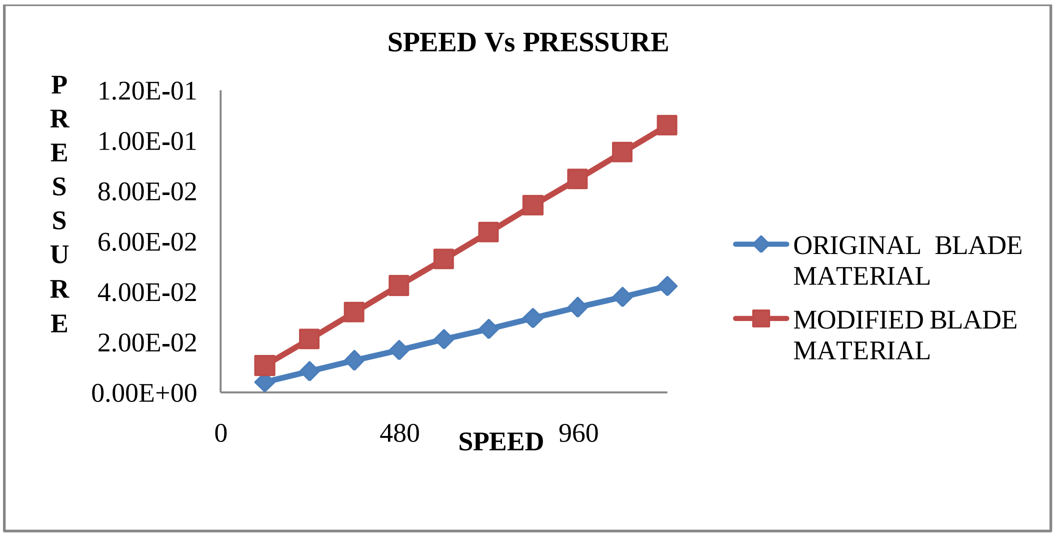

Fig 12: Speed Vs Pressure

Figure 12 represents behaviour of the exerted fluid pressure being applied on all blades for original and modified blade material at speeds 120,480, 960 and 1200 rpm. It can be observed that the exerted fluid pressure for the above said speeds are at 0.00422MPa-0.01688 MPa -0.03376 MPa -0.0422 Mpa and 0.01066 MPa -0.0424 MPa -0.0848 MPa -0.1066 Mpa. The exerted pressure on both blade materials substantially increases with the increase in speed and minimum at 120 rpm of 0.0422 Mpa and maximum at 1200rpm of 0.1066MPa.The effect of turbulence found to be increasing gradually with the increasing speeds. This behaviour can be correlated to turbulence effect with an expected positive result that it withstands higher turbulence and pressure of 0.1066MPa.

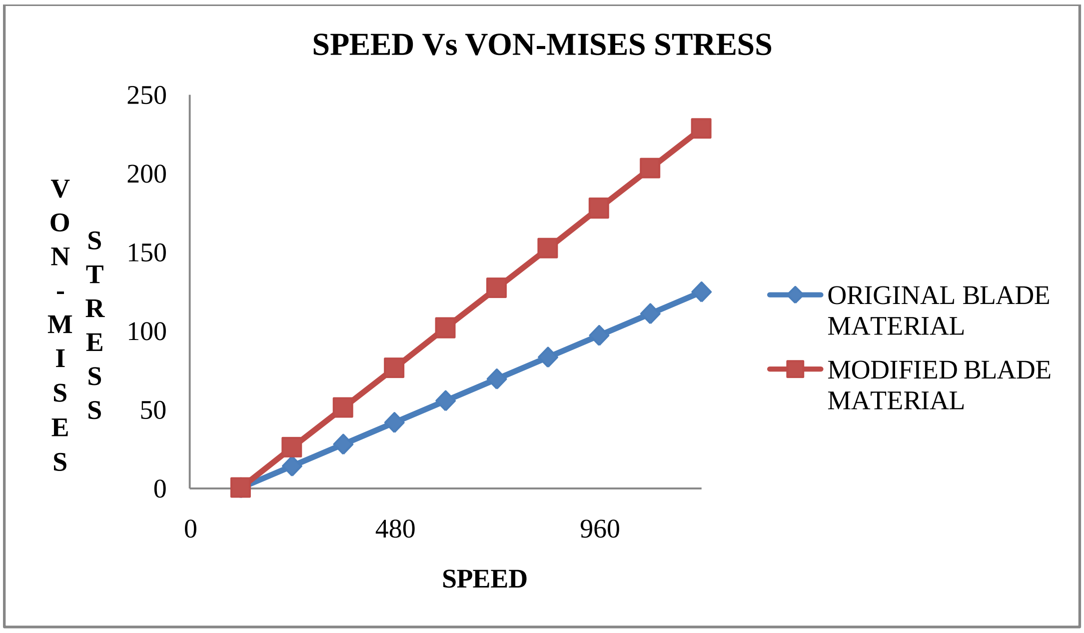

Fig 13: Speed Vs Von-Mises Stress

From fig. 13, it can be observed that the Von-Mises Stress for the above said speeds are at 0.33958MPa-41.805MPa -97.093MPa -124.74Mpa and 0.62257MPa -76.643MPa -178MPa -228.68MPa. The Von-Mises Stress on both blade materials drastically increases with the increase in turbulence as well as speed and minimum at 120 rpm of 0.33958MPa and reached maximum at 1200rpm of 228.68MPa. A drastic increment in Von-Mises Stress has been observed for modified blade material and the maximum value obtained is 228.68Mpa with an aspiring result that it withstands higher turbulence and maximum Von-Mises Stress. This can be highlighted as a good ductile and weldability behaviour.

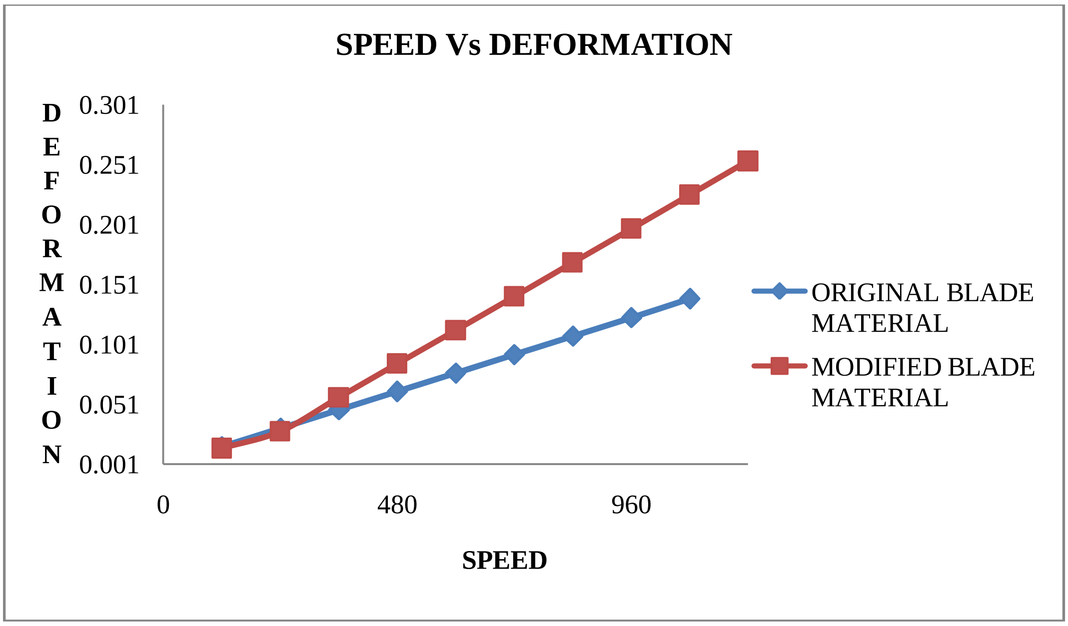

Fig 14: Speed Vs Deformation

From fig. 14, by comparing deformation behaviour for original and modified blade material at speeds 120rpm, 480rpm, 960rpm and 1200rpm of pyro turbine the deformations obtained are 0.0mm-0.046131mm -0.10764 mm -0.1389 mm and 0.0 mm -0.084573 mm -0.19734 mm -0.25372 mm. The deformation on both original and modified blade material gradually increases which is minimum at 120 rpm of 0.33958MPa and maximum at 1200rpm of 228.68MPa. The effect of deformation is found to be nominal. This can be attributed to be a safe design.

VI. CONCLUSION

After comparing the Static Analysis results with respect of original and modified blade materials being used, the following conclusions are made.

i. Observed that the turbulence was effectively tackled.
ii. Modifications are incorporated successfully with respect to inlet nozzle.
iii. Compared the Pressure, Von-Mises stress and Total deformation for original and modified materials of blade and concluded that ASME Stainless Steel SA516 Gr. 70 is the best suited blade material for safe design as it is withstanding the huge turbulence and is within the analysis range.

Acknowledgement

The authors gratefully acknowledge the support of Department of Science & Technology and Power and Energy Research Center, Shri Vishnu Engineering College for Women to undertake this project work

REFERENCES

[1] P.P. Sharma, S. Chatterji and Balwinder Singh, “Matlab Based Simulation of Components of Small Hydro-Power Plants” VSRD International Journal of Electrical, Electronics & Communication Engineering, Vol. 3 Issue 8, (2013), pp 372-380.

[2] J.S.Linsey, I.Tseng, K.Fusss, et al., “A Study of Design Fixation, Its Mitigaion and Perception in Engineering Design Faculty”, Journal of Mechanical Design, 132,041003, (2010), Pages: 01-12.

[3] Urvin Rameshbhai Patel, Devendra A Patel and Manish S Maisuria Vol. 3, No. 3, July, 2014 “Analyse the Effect of Mass Flow Rate on the Efficiency of Pico Turbine & Validate with Experimental Results” International Journal of Mechanical Engineering & Robotic Research 2014

[4] Patrick Ho-Yan (2012), “Design of a Low Head Pico Hydro Turbine for Rural Electrification in Cameroon”, A Thesis presented to the University of Guelph, Ontario, Canada, April, 2012

[5] Sushant Waghin, Dhananjay Panchagade, **“**Analyzing Effect of Impeller Width on Mass Flow Rate of Centrifugal Blower using CFD”**,** International Journal of Electrical, Electronics & Communication Engineering, Vol. 3 Issue 8, (2013), pp 372-380.

[6] Sam Y. Zamrik, Ph.D. ASME President 2007-2008, “2028 Vision for Mechanical Engineering: A report of the Global Summit on the Future of Mechanical Engineering “, July (2008), ASME, Three Park Avenue, New York, NY 10016, USA

[7] J H Park, N J Lee, J V Wata, Y C Hwang, Y T Kim and Y H Lee, “Analysis of a pico tubular-type hydro turbine performance by runner blade shape using CFD” ,26th IAHR Symposium on Hydraulic Machinery and Systems IOP Publishing, IOP Conf. Series: Earth and Environmental Science **15** (2012) 042031doi:10.1088/1755-1315/15/4/042031

[8] Sourabh Khurana, Varun Goel and Anoop Kumar, “FEM Analysis of Turgo Impulse Turbine Blade”, Walailak Journal of Science & technology 2013; 10(4): 363-368 http://wjst.wu.ac.th

[9] R.G. Simpson, A.A. Williams, “Application of computational fluid dynamics to the design of pico propeller turbines” Nottingham Trent University, *Proceedings of the International Conference on Renewable Energy for Developing Countries - 2006*

[10] K.P. V. S. R. Vinay Kumar et.al., Certain Aspects of Framework for Handling Design Nonlinearity, *38th National Systems Conference Real Time Systems - Modeling, Analysis and Control JNTU College of Engineering Hyderabad (Autonomous), Hyderabad , Telangana, 5-7 November -2014*